12th Human Amyloid Imaging

January 17-19, 2018
Miami, Florida

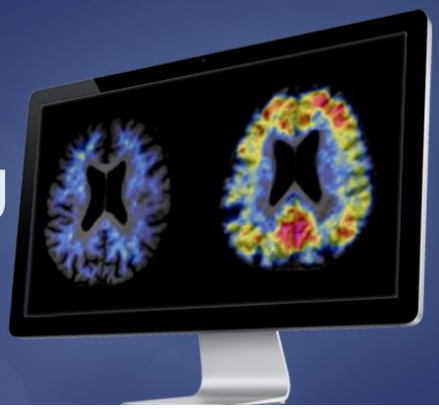

Co-Organizers:
Keith A. Johnson, MD ● William J. Jagust, MD ● William E. Klunk, MD, PhD ● Chester A. Mathis, PhD

Conference Program and Abstracts

www.worldeventsforum.com/hai

TABLE OF CONTENTS

HAI 2018 PROGRAM AT-A-GLANCE

Wednesday, January 17, 2018

11:45 am - 12:00 pm	**WELCOME NOTES**	Keith Johnson
12:00 pm - 02:00 pm	**Session 1: METHODS AND ANALYSIS**	CHAIRS: Bradley Christian | Sandra Sanabria
02:00 pm - 03:30 pm	**POSTER SESSION 1**	
03:30 pm - 05:00 pm	**Session 2: NEW TRACERS**	CHAIRS: Roger Gunn | Chester Mathis
05:00 pm - 06:30 pm	**Session 3: MK-6240**	CHAIRS: Robert Koeppe | Julie Price
06:30 pm - 08:30 pm	Welcome Reception	

Thursday, January 18, 2018

07:30 am - 08:30 am	Breakfast *(Starlight Ballroom, 18th Floor—access only with an HAI badge)*	
08:30 am - 10:15 am	**Session 4: PATHOLOGICAL CORRELATES**	CHAIRS: Milos Ikonomovic | Melissa Murray
10:15 am - 11:00 am	**POSTER SESSION 2A**	
11:00 am - 11:45 am	**KEYNOTE LECTURE**	William Seeley
11:45 am - 01:30 pm	**Session 5: GENETICALLY DETERMINED AD**	CHAIRS: William Klunk | Eric McDade
01:30 pm - 02:45 pm	Lunch *(Starlight Ballroom, 18th Floor)*	
02:45 pm - 04:45 pm	**Session 6: AMYLOID AND TAU: CORRELATIONS WITH PATIENT CHARACTERISTICS AND CSF**	CHAIRS: Oskar Hansson | Agneta Nordberg
04:45 pm - 04:50 pm	**TAU CONSORTIUM ANNOUNCEMENT**	
04:50 pm - 05:35 pm	**POSTER SESSION 2B**	
05:35 pm - 07:30 pm	Network Reception	

Friday, January 19, 2018

07:30 am - 08:30 am	Breakfast *(Starlight Ballroom, 18th Floor—access only with an HAI badge)*	
08:30 am - 09:45 am	**Session 7: STAGING AND LONGITUDINAL STUDIES**	CHAIRS: Keith Johnson | Reisa Sperling
10:15 am - 11:00 am	**POSTER SESSION 3A**	
11:00 am - 12:45 pm	**Session 8: APPLICATIONS IN CLINICAL POPULATIONS**	CHAIRS: Rik Ossenkoppele | Gil Rabinovici
12:45 pm - 02:00 pm	Lunch *(Starlight Ballroom, 18th Floor)*	
02:00 pm - 02:45 pm	**KEYNOTE LECTURE**	Peter Davies
02:45 pm - 04:15 pm	**Session 9: EARLY DETECTION AND PREDICTION**	CHAIRS: William Jagust | Elizabeth Mormino
04:15 pm - 05:00 pm	**POSTER SESSION 3B**	
05:00 pm - 06:05 pm	**Session 10: AD—VASCULAR INTERACTIONS**	CHAIRS: Tammie Benzinger | Sylvia Villeneuve
06:05 pm - 06:15 pm	**AWARDS CEREMONY**	
06:15 pm	Closing Notes	Keith Johnson

HAI 2018 PROGRAM

Wednesday, January 17, 2018		
11:45 am - 12:00 pm	Welcome Notes	**Keith Johnson**, *Massachusetts General Hospital, Boston, MA, US*
12:00 - 2:00	**Session 1: METHODS AND ANALYSIS**	CHAIRS: **Bradley Christian**, *University of Wisconsin-Madison, Madison, WI, US* **Sandra Sanabria**, *Genentech, South San Francisco, CA, US*
12:00	Serial measurements with Rousset-Style (GTM) PVC are less precise than with traditional approaches	**Christopher Schwarz**, *Mayo Clinic, Rochester, MN, US*
12:15	Modeling amyloid, tau, and cortical thickness changes across the Alzheimer's disease spectrum	**Jungho Cha**, *University of California, San Francisco, CA, US*
12:30	Amyloid load - a more sensitive outcome measure for quantifying amyloid-β	**Roger Gunn**, *Invicro, London, United Kingdom*
12:45	Data-driven tau-PET covariance networks enhance associations with cognition in Alzheimer's disease	**Jacob Vogel**, *Montreal Neurological Institute, Montreal, QC, Canada*
01:00	Regional tau elevation patterns in clinically normal adults using sparse k-means clustering	**Kirsten Moody**, *Massachusetts General Hospital, Harvard Medical School, Boston, MA, US*
01:15	Evaluation of visual interpretation methods for tau PET imaging	**Ida Sonni**, *University of California, Berkeley, CA, US*
01:30	Discussion	
02:00 - 3:30	**POSTER SESSION 1**	**Posters 1—49**
03:30 - 5:00	**Session 2: NEW TRACERS**	CHAIRS: **Chester Mathis**, *University of Pittsburgh, Pittsburgh, PA, US* **Roger Gunn**, *Invicro, London, UK*
03:30	PET imaging of synaptic density in Alzheimer's disease	**Ming-Kai Chen**, *Yale University School of Medicine, New Haven, CT, US*
03:45	Characterizing the relationship of [18F]GTP1 (Genentech tau probe 1) PET imaging with Alzheimer's disease pathophysiology	**Sandra Sanabria**, *Genentech, Inc., South San Francisco, CA, US*
04:00	A head-to-head comparison between [11C]PBB3 and [18F]PM-PBB3 in patients with AD and non-AD tauopathy	**Manabu Kubota**, *National Institute of Radiological Sciences, Chiba, Japan*
04:15	Clinical evaluation of 18F-PI-2620, a next generation tau PET agent in subjects with Alzheimer's disease and Progressive Supranuclear Palsy	**Andrew Stephens**, *Piramal Imaging, Berlin, Germany*
04:30	Discussion	
05:00 - 6:30	**Session 3: MK-6240**	CHAIRS: **Julie Price**, *Massachusetts General Hospital, Boston, MA, US* **Robert Koeppe**, *University of Michigan, Ann Arbor, MI, US*
05:00	Clinical validation of the novel PET tracer [18F]MK6240 for in vivo quantification of neurofibrillary tangles	**Pedro Rosa-Neto**, *McGill University, Montreal, QC, Canada*
05:15	Test-retest characterization and pharmacokinetic properties of [18F]MK-6240	**Cristian Salinas**, *Biogen, Cambridge, MA, US*
05:30	In vivo observations and quantification of tau with [F-18]MK-6240 PET from young controls to Alzheimer's disease	**Tobey Betthauser**, *University of Wisconsin-Madison, Madison, WI, US*
05:45	Tau imaging in Alzheimer's disease with 18F-MK6240, a second generation selective tau tracer	**Christopher Rowe**, *Austin Health, Melbourne, Australia*
06:00	Discussion	
06:30 - 8:30	**Welcome Reception**	

Thursday, January 18, 2018

07:30 – 08:30	Breakfast *(Starlight Ballroom, 18th Floor)*	
08:30 - 10:15	**Session 4: PATHOLOGICAL CORRELATES**	CHAIRS: **Melissa Murray**, *Mayo Clinic, Jacksonville, FL, US* **Milos Ikonomovic**, *University of Pittsburgh, Pittsburgh, PA, US*
08:30	Autoradiographic Evaluation of MK-6240 compared to AV-1451	**Val Lowe**, *Mayo Clinic, Rochester, MN, US*
08:45	In vivo and in vitro [18F]MK6240 show neurofibrillary tangles deposition heterogeneity in individuals with a wide range of cognitive symptoms	**Tharick Pascoal**, *McGill University, Montreal, QC, Canada*
09:00	Multi-site study of PiB-PET imaging using the Centiloid method: relationships to pathological measures of β-amyloid pathology	**Renaud La Joie**, *University of California, San Francisco, CA, US*
09:15	[F-18]-AV-1451 binding profile in Chronic Traumatic Encephalopathy: a postmortem case series	**Cinthya Aguero Murillo**, *Massachusetts General Hospital, Boston, MA, US*
09:30	Neuropathological and biochemical correlates of tau and amyloid PET imaging in two autopsy brains	**Milos Ikonomovic**, *University of Pittsburgh, Pittsburgh, PA, US*
09:45	Discussion	
10:15 - 11:00	**POSTER SESSION 2A**	**Posters 50—99**
11:00 - 11:30	**KEYNOTE: Network-based neurodegeneration**	**William Seeley**, *University of California, San Francisco, CA, US*
11:30	Keynote Discussion	
11:45 am – 01:30 pm	**Session 5: GENETICALLY DETERMINED AD**	CHAIRS: **Eric McDade**, *Washington University in Saint Louis, St. Louis, MO, US* **William Klunk**, *University of Pittsburgh, Pittsburgh, PA, US*
11:45	Genetic and environmental factors are differentially related to Aβ burden in the presymptomatic phase of autosomal dominant and sporadic Alzheimer's disease	**Julie Gonneaud**, *McGill University, Montreal, QC, Canada*
12:00	In vivo measurements of cortical thickness, amyloid and tau pathology, and episodic memory in preclinical autosomal dominant Alzheimer's disease	**Yakeel Quiroz**, *Massachusetts General Hospital, Harvard Medical School, Boston, MA, US*
12:15	Comparison of striatal longitudinal changes in amyloid deposition in non-demented elderly and Down syndrome	**Dana Tudorascu**, *University of Pittsburgh, Pittsburgh, PA, US*
12:30	[F-18]AV-1451 PET in non-demented adults with Down Syndrome is related to both amyloid and age	**Ann Cohen**, *University of Pittsburgh, Pittsburgh, PA, US*
12:45	Baseline amyloid PET and longitudinal change in non-amyloid biomarkers from the DIAN Study	**Eric McDade**, *Washington University in Saint Louis, St. Louis, MO, US*
01:00	Discussion	
01:30	Lunch break *(Starlight Ballroom, 18th Floor)*	
02:45 - 04:45	**Session 6: AMYLOID & TAU: CORRELATIONS WITH PATIENT CHARACTERISTICS AND CSF**	CHAIRS: **Oskar Hansson**, *Lund University, Lund, Sweden* **Agneta Nordberg**, *Karolinska Institute, Stockholm, Sweden*
02:45	Genotype-dependent longitudinal trajectories of brain metabolism and cognition in autosomal dominant AD	**Elena Rodriguez-Vieitez**, *Karolinska Institute, Stockholm, Sweden*
03:00	Coupling between amyloid and tau occurs at a younger age in APOE E4 carriers than in non-carriers	**Heidi Jacobs**, *Massachusetts General Hospital, Harvard Medical School, Boston, US*
03:15	Greater tau load and reduced cortical thickness in the parietal cortex of APOE ε4 negative AD patients	**Niklas Mattsson**, *Lund University, Lund, Sweden*

Thursday, January 18, 2018		
03:30	Sex-specific effects on cognitive decline in preclinical Alzheimer's disease: findings from ADNI, AIBL and HABS	**Rachel Buckley**, *Massachusetts General Hospital, Harvard Medical School, Boston, MA, US*
03:45	Distinct information from CSF tau and AV1451 PET measures in nondemented individuals	**Elizabeth Mormino**, *Stanford University, Stanford, CA, US*
04:00	Abnormal CSF Aβ changes do not reliably precede florbetapir-PET increases in Aβ-negative normals followed longitudinally	**Susan Landau**, *University of California, Berkeley, CA, US*
04:15	Discussion	
04:45	**TAU CONSORTIUM ANNOUNCEMENT**	
04:50 - 05:35	**POSTER SESSION 2B**	**Posters 50—99**
05:35 - 07:30	Network Reception	

Friday, January 19, 2018		
07:30 - 08:30	Breakfast *(Starlight Ballroom, 18th Floor)*	
08:30 - 10:15	**Session 7: STAGING AND LONGITUDINAL STUDIES**	CHAIRS: **Keith Johnson**, *Massachusetts General Hospital, Boston, MA, US* **Reisa Sperling,** *Brigham and Women's Hospital, Boston, MA, US*
08:30	Longitudinal tau-PET in aging and Alzheimer's disease	**Clifford Jack**, *Mayo Clinic, Rochester, MN, US*
08:45	Longitudinal [18F]-AV-1451 tau-PET scans in healthy older adults and Alzheimer's disease	**Theresa Harrison**, *University of California, Berkeley, CA, US*
09:00	"Where matters most": Regional amyloid deposition predict progression from preclinical to prodromal stages of Alzheimer's disease	**Gerard Bischof**, *University Hospital Cologne, Cologne, Germany*
09:15	In-vivo staging of regional amyloid deposition: evidence for validity and clinical significance from two independent cohort studies	**Michel Grothe**, *German Center for Neurodegenerative Diseases (DZNE), Rostock, Germany*
09:30	Predictors of regional AV1451 uptake in non-demented older adults	**Murat Bilgel**, *National Institute on Aging, Baltimore, MD, US*
09:45	Discussion	
10:15 - 11:00	**POSTER SESSION 3A**	**Posters 100-149**
11:00 am - 12:45 pm	Session 8: **APPLICATIONS IN CLINICAL POPULATIONS**	CHAIRS: **Gil Rabinovici**, *University of California, San Francisco, CA, US* **Rik Ossenkoppele**, *VU University Medical Center, Amsterdam, Netherlands*
11:00	Impact of the appropriate use criteria: effect of amyloid imaging on diagnosis and patient management in an unselected memory clinic cohort: the ABIDE project	**Arno de Wilde**, *VU University Medical Center, Amsterdam, Netherlands*
11:15	The influence of age at onset on regional [18F]AV-1451 uptake in atypical Alzheimer's disease	**Jennifer Whitwell**, *Mayo Clinic, Rochester, MN, US*
11:30	Hemispheric asymmetry on structural MRI, [18F]AV-1451-PET, and [11C]PIB-PET across clinical phenotypes of Alzheimer's disease	**Adrienne Visani**, *University of California, San Francisco, CA, US*

Friday, January 19, 2018		
11:45	Detection of tau pathology in Gerstmann-Sträussler-Scheinker Disease (PRNP F198S) by [18F]Flortaucipir PET	**Shannon Risacher**, *Indiana University School of Medicine, Indianapolis, IN, US*
12:00 pm	FDG-PET in tau-negative amnestic dementia resembles that of autopsy proven hippocampal sclerosis	**Hugo Botha**, *Mayo Clinic, Rochester, MN, US*
12:15	Discussion	
12:45	Lunch *(Starlight Ballroom, 18th Floor)*	
02:00 - 02:30	**KEYNOTE: Molecular, temporal and spatial aspects of tau pathology**	**Peter Davies**, *Northwell Health, Great Neck, NY, US*
02:30	Discussion	
02:45 - 04:15	**Session 9: EARLY DETECTION & PREDICTION**	CHAIRS: **William Jagust**, *University of California, Berkeley, CA, US* **Elizabeth Mormino**, *Standford University, Stanford, CA, US*
02:45	Early detection of longitudinal amyloid-related cognitive decline in middle-aged and initially amyloid-negative adults	**Michelle Farrell**, *University of Texas at Dallas, Dallas, TX, US*
03:00	Prediction of incident sporadic Alzheimer dementia: longitudinal biomarkers and clinical changes	**Beau Ances**, *Washington University in Saint Louis, St. Louis, MO, US*
03:15	Multiple brain markers contribute to risk of progression on the Clinical Dementia Rating Scale in clinically normal older adults	**Taylor Neal**, *Massachusetts General Hospital, Boston, MA, US*
03:30	Low levels of brain beta-amyloid predict tau deposition and memory decline in aging	**Stephanie Leal**, *University of California, Berkeley, CA, US*
03:45 pm	Discussion	
04:15 - 05:00	**POSTER SESSION 3B**	**Posters 100-149**
05:00 - 06:05	**Session 10: AD—VASCULAR INTERACTIONS**	CHAIRS: **Tammie Benzinger**, *Washington University in Saint Louis, St. Louis, MO, US* **Sylvia Villeneuve**, *McGill University, Montreal, QC, Canada*
05:00	Amyloid deposition, small-vessel disease accrual and neurodegeneration, and progression to Mild Cognitive Impairment (MCI) in cognitively normal older adults	**Neelesh Nadkarni**, *University of Pittsburgh, Pittsburgh, PA, US*
05:15	The association of mid- and late-life systemic inflammation with brain amyloid deposition: atherosclerosis risk in communities-PET Study	**Keenan Walker**, *Johns Hopkins University, Baltimore, MD, US*
05:30	β-amyloid burden and vascular risk interact to predict neocortical tau PET signal in clinically normal older individuals	**Jennifer Rabin**, *Massachusetts General Hospital, Boston, MA, US*
05:45	Discussion	
06:05	**AWARDS CEREMONY**	
06:15	Closing Notes	**Keith Johnson**, *Massachusetts General Hospital, Boston, MA, US*

PODIUM and POSTER PRESENTER INDEX

POSTER INDEX (by presenter's last name)

Board #	Poster Title	Authors	Presenter
WEDNESDAY – POSTER SESSION 1			
13	Explaining [18F]-AV-1451 variability in healthy controls across the lifespan	Baker | Harrison | Maass | La Joie | Jagust	**Baker, Suzanne**
38	A more accurate alternative to SUVR for quantifying binding rate-of-change in serial PET	Becker | Price | Johnson	**Becker, J. Alex**
31	Optimal time window for [18F]-AV-1451 binding quantification in AD using SUVr	Wimberley | Lagarde | Olivieri | Kuhnast | Caillé | Gervais | Sarazin | Bottlaender	**Bottlaender, Michel**
19	Assessment of centiloid scaling values in test-retest evaluation using multiple image quantification software platforms	Battle | Buckley | Pillay	**Buckley, Christopher**
09	Novel alpha-synuclein positron emission tomography (PET) tracers for the diagnosis of Parkinson's disease	Capotosti | Tsika | Molette | Ravache | Vokali | Rodriguez | Davranche | Darmency | Purohit | Paterson | Kroth | Stoehr | Lowe | Pfeifer | Muhs	**Capotosti, Francesca**
37	Preliminary report on the associations between CSF T-tau and P-tau with [18F]MK6240 binding	Chamoun | Kang | Pascoal | Mathotaarachchi | Benedet | Shin | Therriault | Bouhachi | Hsiao | Massarweh | Chartrand | Soucy | Gauthier | Rosa-Neto	**Chamoun, Mira**
40	Initial evaluation of correspondence between tau PET ligand [F-18]MK6240 and cognitive status	Clark | Betthauser | Christian | Poetter | Sanson | Oh | Johnson	**Clark, Lindsay**
06	Comparison of parametric methods for visual assessment of [18F]Flutemetamol amyloid PET images in a cognitively healthy elderly population	Collij | Konijnenberg | Reimand | ten Kate | den Braber | Lopes Alves | Zwan | Yaqub | van Assema | Wink | Boomsma | Lammerstma | Scheltens | Visser | Barkhof | van Berckel	**Collij, Lyduine**
30	Simplified non-invasive tracer kinetic analysis for 18F-Florbetaben PET using a dual time-window acquisition protocol	De Santi | Barthel | Bullich | Koglin | Becker | Jovalekic | Stephens | Sabri	**De Santi, Susan**
16	Longitudinal tau quantitation with anatomically-guided PET image deblurring	Tabassum | Li | Becker | El Fakhri | Johnson | Dutta	**Dutta, Joyita**
14	Centiloid validation of multi-atlas PET-SUVR analysis in the multi-tracer AMYPAD study	Grecchi | Foley | Wolz | Gispert | Hill	**Grecchi, Elisabetta**
20	Optimized coffee-break protocol for quantitative [18F]flutemetamol studies	Heeman | Yaqub | Heurling | Lopes Alves | Gispert | Foley | Lammertsma | AMYPAD Consortium	**Heeman, Fiona**
12	A theoretical and empirical investigation of imperfect reference regions	Heurling | Smith | Strandberg | Ohlsson | Hansson | Schöll	**Heurling, Kerstin**
04	Optimal reference region analysis for [18F]MK6240 based on full kinetic modeling	Kang | Pascoal | Chamoun | Mathotaarachchi | Shin | Benedet | Therriault | Savard | Knight | Hsiao | Bouhachi | Massarweh | Chakravarty | Chartrand | Bennacef | Ng | Soucy | Gauthier | Rosa-Neto	**Kang, Min Su**
23	Methodologic considerations for calculating standard uptake value ratio amyloid reduction in the Gantenerumab open label extension studies	Klein | Delmar | Abi-Saab | Andjelkovic | Milosavljevic-Ristic | Seibyl | Marek | Martenyi | Baudler | Fontoura | Doody	**Klein, Gregory**
34	Development of thiophene-based optical ligands that selectively detect tau pathology in Alzheimer's disease	Shirani | Appelqvist | Bäck | Klingstedt | Cairns | Svensson | Nilsson	**Klingstedt, Therése**
41	Low-dose NeuroPET scans for longitudinal PET: a feasibility study with Flortaucipir	Lois | Grogg | Schultz | Price | Johnson	**Lois, Cristina**
27	The impact of PET reconstruction method on measured amyloid SUVR	Matthews | Andrews | Smith	**Matthews, Dawn**
39	Structure-binding relationship of quinoline derivatives on monoamine oxidase B	Okamura | Harada | Furumoto | Arai | Yanai | Kudo	**Okamura, Nobuyuki**
25	Prediction of cognitive decline by 18F-AV45 PET normalized to subcortical white matter reference region	Ottoy | Niemantsverdriet | Verhaeghe | De Roeck | Struyfs | Somers | wyffels | Van den Bossche | Van Mossevelde | Ceyssens | Stroobants | Bjerke | Engelborghs | Staelens	**Ottoy, Julie**

Board #	Poster Title	Authors	Presenter
WEDNESDAY – POSTER SESSION 1			
36	Voxel-wise determination of thresholds and accuracy of [18F]AV1451 and [18F]MK6240 ligands for neurofibrillary tangles	Pascoal | Mathotaarachchi | Chamoun | Kang | Therriault | Struyfs | Ng | Savard | Shin | Knight | Benedet | Massarweh | Chakravarty | Soucy | Chartrand | Gauthier | Rosa-Neto	**Pascoal, Tharick**
32	Amyloid tracer harmonization using a bootstrapped non-linear mapping	Properzi | Buckkley | Mormino | Price | Sperling | Johnson | Schultz1	**Properzi, Michael**
10	Performance of supratentorial white matter reference regions for longitudinal quantification of [18F]flutemetamol PET scans	Salvadó | Foley | Grecchi | Cardoso | Lopes-Alves | Markiewicz | Falcon | Battle | Lammertsma | Schmidt | Barkhof | Molinuevo | Gispert | AMYPAD Consortium	**Salvadó, Gemma**
08	Optimal centiloid transformations when using measurement methods differing in acquisition parameters and in quantification software	Schwarz | Tosakulwong | Senjem | Gunter | Therneau | Vemuri | Lowe | Jack	**Schwarz, Christopher**
22	Reduced acquisition time PET quantification applied to [18F]-florbetapir	Scott | Jiao | Melbourne | Markiewicz | Schott | Hutton | Ourselin	**Scott, Catherine J**
15	PET scanner variance in multi-center clinical trials using the Hoffman Phantom	Adamczuk | Pannetier | Pham | Gorman | Runkle | Scott | Suhy	**Scott, David**
29	Longitudinal change in brain perfusion in cognitively normal elderly subjects measured by early frames Florbetapir F 18 PET	Shcherbinin | Schwarz | Su | Charil | Hornbeck | Christensen | Eads | Benzinger | Sims	**Shcherbinin, Sergey**
07	Validation of a new semi-quantitative tau-PET analysis without image intensity normalization	Shokouhi | Kang | Gwirtsman	**Shokouhi, Sepi**
24	A non-invasive optical retinal imaging method to predict cerebral amyloid PET status	Soucy | Chevrefils | Sylvestre | Arbour | Rhéaume | Beaulieu | Rosa-Neto | Mathotaarachchi | Nasreddine | Gauthier | Lesage	**Soucy, Jean-Paul**
26	Centiloid analysis in cross-sectional and longitudinal PiB PET studies	Su | Flores | Hornbeck | Speidel | Vlassenko | Gordon | Koeppe | Mintun | Klunk | Xiong | Morris | Benzinger	**Su, Yi**
21	Characterization of [3H]SIL26 binding to alpha-synuclein fibrils	Svensson | Paslawski | Svenningsson | Sohn | Strom | Sandell	**Svensson, Samuel**
33	In vivo assessment of several 18F SV2A PET tracers	Carroll | Alagille | Tress | Mistico | Constantinescu | Sandiego | Papin | Gouasmat | Zheng | Marek | Seibyl | Barret | Tamagnan	**Tamagnan, Gilles**
17	Tau and alpha synuclein selective binding compounds derived from Aprinoia Therapeutics' PM-PBB3 binding-site focused compound collection	Tempest | Jang | Tai | Higuchi | Ono | Shimada | Suhara | Zhang | Tamagnan | Carroll | Marek | Seibyl | Alagille | Barret	**Tempest, Paul**
03	Regional distribution, asymmetry, and clinical correlates of tau uptake on [18f]av-1451 PET in atypical Alzheimer's disease	Tetzloff | Graff-Radford | Tosakulwong | Martin | Machulda | Duffy | Clark | Senjem | Spychalla | Drubach | Jack Jr. | Lowe | Josephs | Whitwell	**Tetzloff, Katerina**
35	Unbiased assessment of global amyloid load as determined by Voxel-wise receiver operating characteristic analysis	Therriault | Pascoal | Mathotaarachchi | Alves | Collij | Kang | Savard | Benedet | Knight | Ng | Shin | Chamoun | Massarweh | Soucy | Gauthier | Rosa-Neto	**Therriault, Joseph**
01	Differing patterns of [18F]AV-1451 uptake in primary progressive apraxia of speech and agrammatic primary progressive aphasia	Utianski | Schwarz | Duffy | Clark | Machulda | Senjem | Jack | Lowe | Whitwell | Josephs	**Utianski, Rene**
11	Parametric imaging of [18F]florbetapir: a test-retest study in healthy subjects and patients with Alzheimer's disease	Verfaillie | Golla | van der Weijden | Timmers | Schober | Schuit | Windhorst | Scheltens | van der Flier | Lammertsma | van Berckel | Boellaard	**Verfaillie, Sander**
05	Sleep efficiency moderates the relationship between beta-amyloid and memory retention	Wilckens | Tudorascu | Snitz | Price | Aizenstein | Lopez | Erickson | Lopresti | Laymon | Minhas | Mathis | Buysse | Klunk | Cohen	**Wilckens, Kristine**
42	Parametric methods for [18F]flortaucipir PET	Wolters | Golla | Timmers | Ossenkoppele | van der Weijden | Scheltens | Schwarte | Mintun | Devous | Schuit | Windhorst | Lammertsma | Yaqub | van Berckel | Boellaard	**Wolters, Emma**

Board #	Poster Title	Authors	Presenter
WEDNESDAY – POSTER SESSION 1			
43	Improved quantification of [18F]flortaucipir uptake in the hippocampus after partial volume correction	Wolters | Golla | Timmers | Ossenkoppele | van der Weijden | Scheltens | Schwarte | Mintun | Devous | Schuit | Windhorst | Barkhof | Yaqub | Lammertsma | Boellaard | van Berckel	**Wolters, Emma**
44	Amyloid deposition is associated with different patterns of hippocampal connectivity in men versus women	Wu | Thurston | Tudorascu | Karim | Mathis | Lopresti | Kamboh | Cohen | Snitz | Klunk | Aizenstein	**Wu, Minjie**
18	Noise reduction algorithm for amyloid image preserving image resolution — quantitative evaluation using clinical images	Yamada | Kimura | Fuji | Watanabe | Nagaoka | Nemoto | Hanaoka | Kaida | Hosokawa | Ishii	**Yamada, Takahiro**
28	Head-to-head comparison of 11C-PBR28 and 18F-GE180 for the quantification of TSPO in the human brain	Zanotti Fregonara | Pascual | Rizzo | Yu | Pal | Beers | Carter | Appel | Atassi | Masdeu	**Zanotti Fregonara, Paolo**
02	PBR-28 binding is elevated in Alzheimer's disease but not in suspected non-AD pathophysiology	Zou | Razlighi | Klein | Polly | Stern | Kreisl	**Zou, James**

Board #	Poster Title	Authors	Presenter
THURSDAY – POSTER SESSIONS 2A AND 2B			
79	The relationship between amyloid deposition and both global and hippocampal atrophy	Allison | Berman | Clark | Christian | Betthauser | Oh | Asthana | Bendlin | Johnson	**Allison, Samantha**
69	Relationships between [11C]PiB positivity and an imaging marker of cerebrovascular pathology positivity	Berman | Allison | Christian | Betthauser | Oh | Asthana | Carlsson | Bendlin | Johnson	**Berman, Sara**
54	[18F]MK-6240 autoradiography in AD, PSP, and CBD	Betthauser | Runde | Johnson | Salamat | Roy | Christian	**Betthauser, Tobey**
93	Human testing of non-selective alpha-synuclein PET tracers	Borroni | Honer | Gobbi | Mathis | Klunk | Kotzbauer | Tu | Mach | Mitchell | Marek | Eberling	**Borroni, Edilio**
84	Increased central arterial stiffening relates to CSF markers of tau aggregation and neurodegeneration in the oldest-old	Cambronero | Liu | Moore | Babicz | Hohman | Gifford | Bell | Acosta | Terry | Nair | Wang | Carr | Blennow | Zetterberg | Jefferson	**Cambronero, Francis**
71	Amyloid imaging in hereditary cerebral amyloid angiopathy: detection and progression of pure vascular amyloid caused by APP E693Q	Schultz | Kloet | Sohrabi | Chatterjee | Gardnener | Taddei | Benzinger | Fagan | Sperling | Johnson | Bateman | Gurol | van Buchem | Martins | Chhatwal | Greenberg	**Chhatwal, Jasmeer**
65	[18F]AV-1451 tau PET imaging in MAPT 10+16 mutation carriers	Clarke | Jiao | Dick | Convery | Koriath | Woollacott | Weston | Gunn | Rabiner | Rossor | Warren | Fox | Ourselin | Bocchetta | Rohrer	**Clarke, Mica**
85	Alterations in memory self-appraisal are associated with elevated tau deposition in normal older adults	d'Oleire Uquillas | Schultz | Jacobs | Hanseeuw | Buckley | Pascual-Leone | Sperling | Johnson | Vannini	**d'Oleire Uquillas, Federico**
60	Trajectories of fiber tract impairment in autosomal dominant Alzheimer's disease	Araque Caballero | Benzinger | Suarez-Calvet | Levin | Morris | Bateman | Haass | Ewers	**Ewers, Michael**
76	How useful is amyloid PET in clinical diagnosis? A systematic review and meta-analysis	Fantoni | Chalkidou | O'Brien | Farrar | Hammers	**Farrar, Gill**
87	Increasing Aβ is associated with nonlinear change in BOLD modulation to difficulty in cognitively normal middle-aged and older adults: further evidence from an n-back task	Foster | M. Kennedy | Rodrigue	**Foster, Chris**
61	The BDNF Val66Met SNP is related to hippocampal connectivity and cognitive decline in autosomal dominant Alzheimer's disease	Franzmeier | Ren | Levin | Bateman | Morri | Benzinger | Ewers	**Franzmeier, Nicolai**
62	Tau accumulation and memory decline are more closely related to striatal than cortical amyloidosis in individuals with early-onset autosomal dominant Alzheimer's disease	Hanseeuw | Lopera | Sperling | Norton | Guzman-Velez | Baena | Schultz | Gatchel | Jin | Chen | Reiman | Johnson | Quiroz	**Hanseeuw, Bernard**

Board #	Poster Title	Authors	Presenter
THURSDAY – POSTER SESSIONS 2A AND 2B			
55	Imaging-autopsy correlation of 18F-THK5351 in typical and atypical cases of progressive supranuclear palsy	Harada | Ishiki | Kai | Furukawa | Furumoto | Tashiro | Kitamoto | Kudo | Yanai | Arai | Okamura	**Harada, Ryuichi**
58	Confocal analysis of fluorescent signal derived from CN-Flutemetamol-labeled diffuse and neuritic plaques in Alzheimer's disease	Ikonomovic | Buckley | Abrahamson | Mathis | Klunk | Farrar	**Ikonomovic, Milos**
51	Potential use of 18F-THK5351 PET to identify gliosis: Wallerian degeneration of the pyramidal tract after a cerebral infarction	Ishibashi | Kameyama | Tago | Toyohara | Ishii	**Ishibashi, Kenji**
70	[18F]Fluorotaucipir binding in patients with cerebral amyloid angiopathy without hemorrhage and mild cognitive symptoms	Jin | Benson | Schultz | Becker | Charidimou | Fotiadis | Katz | Luner | Moody | Sanchez | Sperling | Xiong | Viswanathan | Johnson	**Jin, David**
57	Structure and distribution of amyloid beta	Joseph | Sparling | Stys	**Joseph, Jeffrey**
92	Age-related change of THK-5351 PET in amyloid-negative and non-demented elderly subjects	Kato | Iwata | Kizawa | Fukaya | Kuratsubo | Kimiura | Okamura | Yanai | Ito | Nakamura | Study Group	**Kato, Takashi**
88	Co-existence of deleterious and neuroprotective interaction between amyloid and neuroinflammation in late stage Alzheimer's disease	Knight | Kang | Parent | Pascoal | Mathotaarachchi | Therriault | Benedet | Camoun | Aliaga | Zimmer | Shin | Aliaga | Kostikov | Soucy | Gauthier | Cuello | Rosa-Neto	**Knight, Ashley**
80	AV1451-PET measurements show substantial overlap across diagnostic groups and amyloid status	Landau | Korman | Jagust	**Landau, Susan**
63	Tau pathology in Down syndrome	Lemoine | Bharani | Hamlett | Perez | Mufson | Poon | Simic | Nordberg | Granholm	**Lemoine, Laetitia**
68	CYP2C19 effects in brain amyloid load and hippocampus' functional integrity	Lessa Benedet | Iturria-Medina | Savard | Kang | Mathotaarachchi | A. Pascoal | Therriault | Shin | Gauthier | C. Evans | Labbe | Rosa-Neto	**Lessa Benedet, Andrea**
64	Singular Value Decomposition (SVD) identification of PiB and FDG topographies in Dominantly Inherited Alzheimer's Network (DIAN)	Loe | Brier | McCarthy | Stern | Kuffner | Morris | Bateman | Benzinger | Ances	**Loe, Maren**
81	Shrinking cortex and tau burden in the aphasic variant of Alzheimer's disease	Martersteck | Sridhar | Rainford | Mesulam | Rogalski	**Martersteck, Adam**
86	Segregation of tau deposits across clinical stages provides the basis for pathophysiological staging in AD	Mathotaarachchi | A. Pascoal | L. Benedet | Shin | Kang | Struyfs | Therriault | Chamoun | Ng | Savard | Knight | Gauthier | Rosa-Neto	**Mathotaa-rachchi, Sulantha**
59	Comparison of Down syndrome PiB PET templates for MRI-less PET quantification	Minhas | Laymon | Tudorascu | Lao | Campbell | Yu | Lopresti | Mathis | Klunk | Handen | Christian | Cohen	**Minhas, Davneet**
75	In pre-clinical AD, subjective cognitive decline is associated with brain hyperactivation in conflict monitoring/control regions	Mizuno | Karim | Rangarajan | Klunk | Aizenstein | Snitz	**Mizuno, Akiko**
90	18F-AV-1451 uptake on tau PET differs between dementia with Lewy bodies and posterior cortical atrophy	Nedelska | Josephs | Graff-radford | Przybelski | Lesnick | Boeve | Lowe | Drubach | Knopman | Petersen | Jack, Jr. | Whitwell | Kantarci	**Nedelska, Zuzana**
78	Quantifying stages of subtle memory impairment in clinically normal older adults	Papp | Mormino | Grober | Sperling | Johnson | Rentz	**Papp, Kate**
89	Amyloid and tau deposition determine cognitive impairment through epigenetic changes in individuals across the AD spectrum	Pascoal | Shin | Kang | Ng | Benedet | Mathotaarachchi | Therriault | Chamoun | Massarweh | Knight | Soucy | Gauthier | Rosa-Neto	**Pascoal, Tharick**
74	Amyloid network topology characterizes the progression of Alzheimer's disease during the pre-dementia stages	Pereira | Strandberg | Palmqvist | Volpe | van Westen | Westman | Hansson	**Pereira, Joana**
73	Flortaucipir PET imaging and neuropsychological performances dissociate dorsal and ventral stream dysfunction in Posterior Cortical Atrophy	Putcha | Collins | Wong | Dickerson | McGinnis	**Putcha, Deepti**

Board #	Poster Title	Authors	Presenter
THURSDAY – POSTER SESSIONS 2A AND 2B			
72	Midlife insulin resistance and APOE genotype are associated with late-life brain amyloid accumulation	Rinne | Ekblad | Johansson | Helin | Viitanen | Laine | Puukka | Jula	**Rinne, Juha**
91	Finding ground zero: identifying the medial temporal origin of tau deposition during life	Sanchez | Augustinack | Becker | Jacobs | Jin | Katz | Luner | Moody | Rentz | Sperling | Price | Johnson	**Sanchez, Justin**
66	Longitudinal change of functional connectivity in the DIAN cohort: functional connectivity as a longitudinal biomarker in autosomal dominant AD	Schultz | Sperling | Buckley | Johnson | Benzinger | Ances | Morris | Buckles | Xiong | McDade | Cairns | Marcus | Fulbright | Jack | Ringman | Farlow | Kinnunen | Fox | Masters | Schofield | Salloway | Levin | Bateman | Chhatwal	**Schultz, Aaron**
50	Quantitative thresholding of [18F]Florbetapir brain uptake using Thal phases of Abeta deposition relate to clinical stages of disease	Seneca | Burger | Florea	**Seneca, Nicholas**
83	Cognition and [18F]-Florbetaben PET imaging of amyloid in Parkinson's disease	Stark | Melzer | Keenan | Myall | Kaur | Livingston | Horne | Marsh | Grenfell | Young | MacAskill | Dalrymple-Alford | Anderson	**Stark, Megan**
52	Preclinical evaluation of 18F-THK5351 off-target binding to melanin-containing cells	Tago | Toyohara | Harada | Furumoto | Okamura | Kudo | Takahashi-Fujigasaki | Murayama | Ishii	**Tago, Tetsuro**
53	To tau or to MAO-B? Most of the 18F-THK5351 signal is blocked by selegiline	Villemagne | Doré | Okamura | Baxendale | Harada | Mulligan | Furumoto | Salvado | Yanai | Masters | Rowe	**Villemagne, Victor**
82	Cross-sectional associations between tau pathology burden measured by [18F]GTP1 PET imaging and cognition in AD adjusting for amyloid PET and cortical atrophy	Ward | Manser | Teng | Sanabria-Bohorquez | Ray | Baker | Kerchner | Weimer	**Ward, Michael**
77	[18F]AV-1451 binds to an unidentified white matter target in semantic dementia	Whitwell | Martin | Schwarz | Duffy | Clark | Machulda | Botha | Graff-Radford | Jones | Utianski | Knopman | Petersen | Lowe | Jack | Josephs	**Whitwell, Jennifer**
67	An UNC5C locus is associated with susceptibility to cognitive decline and hippocampal neurodegeneration in clinically normal older adults	Yang | Chhatwal | Papp | Rabin | Hanseeuw | Mormino | Buckley | Schultz | Properzi | Hedden | Marshall | Rentz | Johnson | De Jager | Sperling	**Yang, Hyun-Sik**
56	Relationship of basal ganglia mineralization to "off-target" AV-1451 binding in Down syndrome	Zammit | Laymon | Minhas | Tudorescu | Lopresti | Mathis | Sabbagh | Zaman | Klunk | Handen | Christian | Cohen	**Zammit, Matthew**

Board #	Poster Title	Authors	Presenter
FRIDAY – POSTER SESSIONS 3A AND 3B			
115	[18F] AV-1451 uptake in corticobasal syndrome: the influence of beta-amyloid and clinical presentation	Ali | Whitwell | Martin | Senjen | Knopman | Jack | Lowe | Petersen | Boeve | Josephs	**Ali, Farwa**
116	Tau positron emission tomography is not elevated in HIV infected individuals	Ances | Beaumont | Cooley | Strain | Morris | Benzinger	**Ances, Beau**
141	Longitudinal relationships between brain amyloid deposition and glucose metabolism across the Alzheimer's disease spectrum	Bejanin | Arenaza-Urquijo | De Flores | Tomadesso | Chételat	**Bejanin, Alexandre**
104	Assessing the impact of beta-amyloid deposition in progressive supranuclear palsy	Boland | Ahlskog, PhD, MD | Tosakulwong, BS | Senjem, MS | Spychalla, BS | Petersen, MD | Jack Jr, MD | Lowe, MD | Josephs, MD, MST, MSc | Whitwell, PhD	**Boland, Sarah**
102	Application of the PredictND decision support system to cross-sectional imaging and psychometric data from an aMCI to probable AD three year outcomes clinical study	Buckley | Moreland | Urhemaa | van Gils | Wolber | lotjonen	**Buckley, Christopher**
121	Cerebrospinal fluid ratio of phosphorylated tau protein to beta-amyloid peptide 42 may improve the prediction of amyloid PET positivity: data from the Czech Brain Ageing Study	Cerman | Laczo | Vyhnalek | Sheradova | Ferda | Belohlavek | Hort	**Cerman, Jiri**

Board #	Poster Title	Authors	Presenter
FRIDAY – POSTER SESSIONS 3A AND 3B			
113	Twelve-month glucose metabolism declines in an empirically pre-defined statistical region-of-interest in amyloid-positive persons with Alzheimer's dementia and Mild Cognitive Impairment: updated ADNI findings	Chen | Lee | Kuang | Luo | Devadas | Thiyyagura | Chen | Bauer | Weiner | Jagust | Van Dyck | Reiman	**Chen, Kewei**
111	Effects of amyloid deposition and hippocampal activation on subjective memory complaints	Chen | Jingting | Farrell | Park	**Chen, Xi**
105	Flortaucipir imaging in primary progressive aphasia predicts variability in language impairment	Collins | Quimby | Makaretz | Sweeney | Wong | McGinnis | Dickerson	**Collins, Jessica**
112	Thresholds for amyloid positivity among normal, MCI and mild dementia subjects using [F-18] Florbetaben	Duara | Loewenstein | Lizzaraga | Adjouadi | Barker | Greig-Custo | Penate | Hanson | Marsiske | Vaillancourt | DeKosky | Golde	**Duara, Ranjan**
117	Left frontal hub connectivity delays cognitive decline in autosomal dominant and sporadic Alzheimer's disease	Franzmeier | Duezel | Jessen | Benzinger | Levin | Fagan | Morris | Bateman | Ewers	**Franzmeier, Nicolai**
136	[18F]-THK5351 binding patterns are associated with language deficits in primary progressive aphasia	Gabel | Schaeverbeke | Meersmans | Bruffaerts | Van Bouwel | Dries | Peeters | Van Laere | Dupont | Vandenberghe	**Gabel, Silvy**
109	Is there a local neurotoxic effect of regional amyloid deposits? A network-domain specific study of florbetapir-PET – cognition associations	Grothe | Sorg | Teipel	**Grothe, Michel**
118	Sex and e4 genotype influence the longitudinal association between amyloid and tau pathology in clinically normal older adults	Hanseeuw | Buckley | Mormino | Jacobs | Chhatwal | Gomez | Johnson | Sperling	**Hanseeuw, Bernard**
132	The BioFINDER-2 study: a longitudinal investigation on the role of Tau and amyloid on cognitive function using 18F-RO6958948 and 18-Flutemetamol PET tracers	Hansson | Mattsson | Smith | Schöll | Klein | Farrar | Borroni | Coloma | Palmqvist | Stomrud	**Hansson, Oskar**
131	Multiple brain markers contribute to age-related changes in cognition	Hedden | Nierle | Perea | Rabin | Buckley | Schultz | Johnson | Sperling	**Hedden, Trey**
125	Tau pathology networks associated with functional connectivity networks and disease progression in Alzheimer's disease	Hönig | Bischof | Seemiller | Hammes | Fink | van Eimeren | Drzezga	**Hönig, Merle**
139	Long-term clinical stability in amyloid-positive subjects is predicted by negative FDG-PET scan	Iaccarino | Sala | Perani	**Iaccarino, Leonardo**
128	Nucleus basalis of Meynert volume predicts early tau pathology and memory performance when amyloid levels are elevated in cognitively normal older individuals	Jacobs | Hanseeuw | Schultz | Papp | Rentz | Sperling | Johnson	**Jacobs, Heidi**
127	Tau aggregates imaged with 18F-Flortaucipir PET contribute to core clinical features of the Lewy body dementias	Katz | Ye | Shirvan | Schultz | Makaretz | Dickerson | Sperling | Growdon | Johnson | Gomperts	**Katz, Samantha**
135	Effects of amyloid, tau, and hippocampal volume on normal and fast gait speeds in cognitively normal older adults: results from the Harvard Aging Brain study	Kirn | Buckley | Hanseeuw | Klein | Properzi | Sperling | Johnson	**Kirn, Dylan**
106	[18F]flutemetamol amyloid binding potential in relation to memory in cognitively normal subjects aged 80 years and older	Legdeur | Buslenko | Konijnenberg | ten Kate | Badissi | Tomassen | den Braber | Yaqub | Boomsma | Lammertsma | Maier | Scheltens | van Berckel | Visser	**Legdeur, Nienke**
123	18F-AV1451 tau PET in patients at risk for chronic traumatic encephalopathy	Lesman-Segev | La Joie | Tsai | Bourakova | Visani | Ayakta | P O'Neil | Maass | Baker | Perry | Kramer | Miller | Jagust | Rabinovici	**Lesman-Segev, Orit**
124	Longitudinal [18F]THK5317 and [18F]FDG PET in relation to novel CSF tau fragments in Alzheimer's disease and related primary tauopathies	Leuzy | Chiotis | Cicognola | Saint-Aubert | Zetterberg | Blennow | Höglund | Nordberg	**Leuzy, Antoine**

Board #	Poster Title	Authors	Presenter
FRIDAY – POSTER SESSIONS 3A AND 3B			
110	A similar prevalence and magnitude of amyloid positivity between cognitively normal elderly Japanese and Americans	Yu | Lopresti | Ihara | Cui | Aizenstein | Dodge | Minhas | Lopez | Klunk | Mathis | Kuller | Miyamoto | Sekikawa	**Lopresti, Brian**
138	Tau deposition in relation to verbal and phonemic fluency in the Framingham Heart Study	Luner | Jacobs | Papp | Becker | Beiser | Daniluk | Himali | Jin | Katz | Killiany | Moody | Pase | Peets | Raman | Sanchez | Satizabal | Schafer | Seshadri | Johnson	**Luner, Evelyn**
134	Effects of tau and amyloid deposition on domain-specific memory function in old age	Maass | Berron | Harrison | Baker | Mellinger | Swinnerton | Bell | Duezel | Jagust	**Maass, Anne**
100	Cross-sectional and longitudinal atrophy is preferentially associated with tau rather than Aβ PET pathology	McCullough | Gordon | Mishra | Blazey | Su | Christensen | Dincer | Jackson | Hornbeck | Morris | Ances | Benzinger	**McCullough, Austin**
129	Increased GM regions in association with SUVR are candidate to predict convergence to Preclinical AD	Monté-Rubio | Rodriguez-Gomez | Sanabria | Alegret | Perez-Cordon | Lomeña | Pavia | Gismondi | Bullich | Vivas-Larruy | Gomez-Chiari | Ruiz-Laza | Tárraga | Boada	**Monté-Rubio, Gemma**
140	Associations between tau, Aβ and cortical thickness with cognition in Alzheimer's disease	Ossenkoppele | Smith | Ohlsson | Mattsson | Strandberg | Palmqvist | Hansson	**Ossenkoppele, Rik**
120	Evidence for neuroinflammation in semantic dementia	Pascual | Zanotti-Fregonara | Pal | Rockers | Funk | Yu | Roman | Schultz | Masdeu	**Pascual, Belen**
137	Personality traits and neuropsychiatric factors are related to increased amyloid deposition in cognitively normal older adults	Pichet Binette | Vachon-Presseau | Gonneaud | Marchant | Bellec | Breitner | Villeneuve | Research Group	**Pichet Binette, Alexa**
114	Flortaucipir PET measurements and relationships with cognitive impairment	Protas | Ghisays | Luo | DeMarco | Thiyyagura | Devadas | Bauer | Landau | Weiner | Jagust | Reiman | Chen	**Protas, Hillary**
119	The DCTclockTM test captures subtle cognitive changes and biomarker evidence of preclinical Alzheimer's disease	Rentz | Papp | Orlovsky | Souillard-Mandar | Penney | Davis | Johnson	**Rentz, Dorene**
108	[18F]Flutemetamol imaging in the ALFA project: Cognitively healthy subjects enriched for Alzheimer's disease genetic risk factors	Salvadó | Brugulat | Falcon | Pavia | Lomeña | Molinuevo | Gispert	**Salvadó, Gemma**
103	Tau pathology detected by [18F]GTP1 negatively correlates with cortical volume in Alzheimer's disease	Ray | Baker | Manser | Ward | Teng | Weimer | Sanabria Bohórquez	**Sanabria Bohórquez, Sandra**
130	Distinct [18F]-THK5351 binding patterns in primary progressive aphasia variants	Schaeverbeke | Gabel | Bruffaerts | Meersmans | Van Bouwel | Dries | Peeters | Van Laere | Dupont | Vandenberghe	**Schaeverbeke, Jolien**
133	PiB PET as a biomarker for white matter integrity in aging and dementia	Su | Wang | Flores | Wang | Beau | Morris | Benzinger	**Su, Yi**
101	[18F]Florbetapir binding potential in relation to cognition in subjective cognitive decline	Timmers | Verfaillie | Wesselman | Slot | Prins | van der Weijden | Yaqub | Lammertsma | Boellaard | Ossenkoppele | van der Flier | van Berckel	**Timmers, Tessa**
126	Characterizing regional β-amyloid burden by magnetic susceptibility	Unschuld | van Bergen | Li | Quevenco | Gietl | Treyer | Meyer | Buck | Kaufmann | Nitsch | van Zijl | Hock	**Unschuld, Paul**
107	Amyloid-β load is related to worries in individuals with subjective cognitive decline	Verfaillie | Timmers | Slot | van der Weijden | Wesselman | Prins | Sikkes | Lammertsma | Scheltens | Ossenkoppele | van Berckel | van der Flier	**Verfaillie, Sander**
122	Relationships between self-reported sleep, tau, and Aβ in healthy older adults	Winer | Maass | Harrison | Mellinger | Baker | Walker | Jagust	**Winer, Joseph**

POSTER INDEX (by board number)

Board #	Poster Title	Authors	Presenter
WEDNESDAY – POSTER SESSION 1			
01	Differing patterns of [18F]AV-1451 uptake in primary progressive apraxia of speech and agrammatic primary progressive aphasia	Utianski | Schwarz | Duffy | Clark | Machulda | Senjem | Jack | Lowe | Whitwell | Josephs	**Utianski, Rene**
02	PBR-28 binding is elevated in Alzheimer's disease but not in suspected non-AD pathophysiology	Zou | Razlighi | Klein | Polly | Stern | Kreisl	**Zou, James**
03	Regional distribution, asymmetry, and clinical correlates of tau uptake on [18f]av-1451 PET in atypical Alzheimer's Disease	Tetzloff | Graff-Radford | Tosakulwong | Martin | Machulda | Duffy | Clark | Senjem | Spychalla | Drubach | Jack Jr. | Lowe | Josephs | Whitwell	**Tetzloff, Katerina**
04	Optimal reference region analysis for [18F]MK6240 based on full kinetic modeling	Kang | Pascoal | Chamoun | Mathotaarachchi | Shin | Benedet | Therriault | Savard | Knight | Hsiao | Bouhachi | Massarweh | Chakravarty | Chartrand | Bennacef | Ng | Soucy | Gauthier | Rosa-Neto	**Kang, Min Su**
05	Sleep efficiency moderates the relationship between beta-amyloid and memory retention	Wilckens | Tudorascu | Snitz | Price | Aizenstein | Lopez | Erickson | Lopresti | Laymon | Minhas | Mathis | Buysse | Klunk | Cohen	**Wilckens, Kristine**
06	Comparison of parametric methods for visual assessment of [18F]Flutemetamol amyloid PET images in a cognitively healthy elderly population	Collij | Konijnenberg | Reimand | ten Kate | den Braber | Lopes Alves | Zwan | Yaqub | van Assema | Wink | Boomsma | Lammerstma | Scheltens | Visser | Barkhof | van Berckel	**Collij, Lyduine**
07	Validation of a new semi-quantitative tau-PET analysis without image intensity normalization	Shokouhi | Kang | Gwirtsman	**Shokouhi, Sepi**
08	Optimal centiloid transformations when using measurement methods differing in acquisition parameters and in quantification software	Schwarz | Tosakulwong | Senjem | Gunter | Therneau | Vemuri | Lowe | Jack	**Schwarz, Christopher**
09	Novel alpha-synuclein positron emission tomography (PET) tracers for the diagnosis of Parkinson's disease	Capotosti | Tsika | Molette | Ravache | Vokali | Rodriguez | Davranche | Darmency | Purohit | Paterson | Kroth | Stoehr | Lowe | Pfeifer | Muhs	**Capotosti, Francesca**
10	Performance of supratentorial white matter reference regions for longitudinal quantification of [18F]flutemetamol PET scans	Salvadó | Foley | Grecchi | Cardoso | Lopes-Alves | Markiewicz | Falcon | Battle | Lammertsma | Schmidt | Barkhof | Molinuevo | Gispert | AMYPAD Consortium	**Salvadó, Gemma**
11	Parametric imaging of [18F]florbetapir: a test-retest study in healthy subjects and patients with Alzheimer's disease	Verfaillie | Golla | van der Weijden | Timmers | Schober | Schuit | Windhorst | Scheltens | van der Flier | Lammertsma | van Berckel | Boellaard	**Verfaillie, Sander**
12	A theoretical and empirical investigation of imperfect reference regions	Heurling | Smith | Strandberg | Ohlsson | Hansson | Schöll	**Heurling, Kerstin**
13	Explaining [18F]-AV-1451 variability in healthy controls across the lifespan	Baker | Harrison | Maass | La Joie | Jagust	**Baker, Suzanne**
14	Centiloid validation of multi-atlas PET-SUVR analysis in the multi-tracer AMYPAD study	Grecchi | Foley | Wolz | Gispert | Hill	**Grecchi, Elisabetta**
15	PET scanner variance in multi-center clinical trials using the Hoffman Phantom	Adamczuk | Pannetier | Pham | Gorman | Runkle | Scott | Suhy	**Scott, David**
16	Longitudinal tau quantitation with anatomically-guided PET image deblurring	Tabassum | Li | Becker | El Fakhri | Johnson | Dutta	**Dutta, Joyita**
17	Tau and alpha synuclein selective binding compounds derived from Aprinoia Therapeutic's PM-PBB3 binding-site focused compound collection	Tempest | Jang | Tai | Higuchi | Ono | Shimada | Suhara | Zhang | Tamagnan | Carroll | Marek | Seibyl | Alagille | Barret	**Tempest, Paul**
18	Noise reduction algorithm for amyloid image preserving image resolution — quantitative evaluation using clinical images	Yamada | Kimura | Fuji | Watanabe | Nagaoka | Nemoto | Hanaoka | Kaida | Hosokawa | Ishii	**Yamada, Takahiro**
19	Assessment of centiloid scaling values in test-retest evaluation using multiple image quantification software platforms	Battle | Buckley | Pillay	**Buckley, Christopher**

Board #	Poster Title	Authors	Presenter
WEDNESDAY – POSTER SESSION 1			
20	Optimized coffee-break protocol for quantitative [18F]flutemetamol studies	Heeman | Yaqub | Heurling | Lopes Alves | Gispert | Foley | Lammertsma | AMYPAD Consortium	**Heeman, Fiona**
21	Characterization of [3H]SIL26 binding to alpha-synuclein fibrils	Svensson | Paslawski | Svenningsson | Sohn | Strom | Sandell	**Svensson, Samuel**
22	Reduced acquisition time PET quantification applied to [18F]-florbetapir	Scott | Jiao | Melbourne | Markiewicz | Schott | Hutton | Ourselin	**Scott, Catherine**
23	Methodologic considerations for calculating standard uptake value ratio amyloid reduction in the Gantenerumab open label extension studies	Klein | Delmar | Abi-Saab | Andjelkovic | Milosavljevic-Ristic | Seibyl | Marek | Martenyi | Baudler | Fontoura | Doody	**Klein, Gregory**
24	A non-invasive optical retinal imaging method to predict cerebral amyloid PET status	Soucy | Chevrefils | Sylvestre | Arbour | Rhéaume | Beaulieu | Rosa-Neto | Mathotaarachchi | Nasreddine | Gauthier | Lesage	**Soucy, Jean-Paul**
25	Prediction of cognitive decline by 18F-AV45 PET normalized to subcortical white matter reference region	Ottoy | Niemantsverdriet | Verhaeghe | De Roeck | Struyfs | Somers | wyffels | Van den Bossche | Van Mossevelde | Ceyssens | Stroobants | Bjerke | Engelborghs | Staelens	**Ottoy, Julie**
26	Centiloid analysis in cross-sectional and longitudinal PiB PET studies	Su | Flores | Hornbeck | Speidel | Vlassenko | Gordon | Koeppe | Mintun | Klunk | Xiong | Morris | Benzinger	**Su, Yi**
27	The impact of PET reconstruction method on measured amyloid SUVR	Matthews | Andrews | Smith	**Matthews, Dawn**
28	Head-to-head comparison of 11C-PBR28 and 18F-GE180 for the quantification of TSPO in the human brain	Zanotti Fregonara | Pascual | Rizzo | Yu | Pal | Beers | Carter | Appel | Atassi | Masdeu	**Zanotti Fregonara, Paolo**
29	Longitudinal change in brain perfusion in cognitively normal elderly subjects measured by early frames Florbetapir F 18 PET	Shcherbinin | Schwarz | Su | Charil | Hornbeck | Christensen | Eads | Benzinger | Sims	**Shcherbinin, Sergey**
30	Simplified non-invasive tracer kinetic analysis for 18F-Florbetaben PET using a dual time-window acquisition protocol	De Santi | Barthel | Bullich | Koglin | Becker | Jovalekic | Stephens | Sabri	**De Santi, Susan**
31	Optimal time window for [18F]-AV-1451 binding quantification in AD using SUVr	Wimberley | Lagarde | Olivieri | Kuhnast | Caillé | Gervais | Sarazin | Bottlaender	**Bottlaender, Michel**
32	Amyloid tracer harmonization using a bootstrapped non-linear mapping	Properzi | Buckkley | Mormino | Price | Sperling | Johnson | Schultz1	**Properzi, Michael**
33	In vivo assessment of several 18F SV2A PET tracers	Carroll | Alagille | Tress | Mistico | Constantinescu | Sandiego | Papin | Gouasmat | Zheng | Marek | Seibyl | Barret | Tamagnan	**Tamagnan, Gilles**
34	Development of thiophene-based optical ligands that selectively detect tau pathology in Alzheimer's disease	Shirani | Appelqvist | Bäck | Klingstedt | Cairns | Svensson | Nilsson	**Klingstedt, Therése**
35	Unbiased assessment of global amyloid load as determined by Voxel-wise receiver operating characteristic analysis	Therriault | Pascoal | Mathotaarachchi | Alves | Collij | Kang | Savard | Benedet | Knight | Ng | Shin | Chamoun | Massarweh | Soucy | Gauthier | Rosa-Neto	**Therriault, Joseph**
36	Voxel-wise determination of thresholds and accuracy of [18F]AV1451 and [18F]MK6240 ligands for neurofibrillary tangles	Pascoal | Mathotaarachchi | Chamoun | Kang | Therriault | Struyfs | Ng | Savard | Shin | Knight | Benedet | Massarweh | Chakravarty | Soucy | Chartrand | Gauthier | Rosa-Neto	**Pascoal, Tharick**
37	Preliminary report on the associations between CSF T-tau and P-tau with [18F]MK6240 binding	Chamoun | Kang | Pascoal | Mathotaarachchi | Benedet | Shin | Therriault | Bouhachi | Hsiao | Massarweh | Chartrand | Soucy | Gauthier | Rosa-Neto	**Chamoun, Mira**
38	A more accurate alternative to SUVR for quantifying binding rate-of-change in serial PET	Becker | Price | Johnson	**Becker, J. Alex**
39	Structure-binding relationship of quinoline derivatives on monoamine oxidase B	Okamura | Harada | Furumoto | Arai | Yanai | Kudo	**Okamura, Nobuyuki**
40	Initial evaluation of correspondence between tau PET ligand [F-18]MK6240 and cognitive status	Clark | Betthauser | Christian | Poetter | Sanson | Oh | Johnson	**Clark, Lindsay**

Board #	Poster Title	Authors	Presenter
WEDNESDAY – POSTER SESSION 1			
41	Low-dose NeuroPET scans for longitudinal PET: a feasibility study with Flortaucipir	Lois | Grogg | Schultz | Price | Johnson	**Lois, Cristina**
42	Parametric methods for [18F]flortaucipir PET	Wolters | Golla | Timmers | Ossenkoppele | van der Weijden | Scheltens | Schwarte | Mintun | Devous | Schuit | Windhorst | Lammertsma | Yaqub | van Berckel | Boellaard	**Wolters, Emma**
43	Improved quantification of [18F]flortaucipir uptake in the hippocampus after partial volume correction	Wolters | Golla | Timmers | Ossenkoppele | van der Weijden | Scheltens | Schwarte | Mintun | Devous | Schuit | Windhorst | Barkhof | Yaqub | Lammertsma | Boellaard | van Berckel	**Wolters, Emma**
44	Amyloid deposition is associated with different patterns of hippocampal connectivity in men versus women	Wu | Thurston | Tudorascu | Karim | Mathis | Lopresti | Kamboh | Cohen | Snitz | Klunk | Aizenstein	**Wu, Minjie**

Board #	Poster Title	Authors	Presenter
THURSDAY – POSTER SESSIONS 2A AND 2B			
50	Quantitative thresholding of [18F]Florbetapir brain uptake using Thal phases of Abeta deposition relate to clinical stages of disease	Seneca | Burger | Florea	**Seneca, Nicholas**
51	Potential use of 18F-THK5351 PET to identify gliosis: Wallerian degeneration of the pyramidal tract after a cerebral infarction	Ishibashi | Kameyama | Tago | Toyohara | Ishii	**Ishibashi, Kenji**
52	Preclinical evaluation of 18F-THK5351 off-target binding to melanin-containing cells	Tago | Toyohara | Harada | Furumoto | Okamura | Kudo | Takahashi-Fujigasaki | Murayama | Ishii	**Tago, Tetsuro**
53	To tau or to MAO-B? Most of the 18F-THK5351 signal is blocked by selegiline	Villemagne | Doré | Okamura | Baxendale | Harada | Mulligan | Furumoto | Salvado | Yanai | Masters | Rowe	**Villemagne, Victor**
54	[18F]MK-6240 autoradiography in AD, PSP, and CBD	Betthauser | Runde | Johnson | Salamat | Roy | Christian	**Betthauser, Tobey**
55	Imaging-autopsy correlation of 18F-THK5351 in typical and atypical cases of progressive supranuclear palsy	Harada | Ishiki | Kai | Furukawa | Furumoto | Tashiro | Kitamoto | Kudo | Yanai | Arai | Okamura	**Harada, Ryuichi**
56	Relationship of basal ganglia mineralization to "off-target" AV-1451 binding in Down syndrome	Zammit | Laymon | Minhas | Tudorescu | Lopresti | Mathis | Sabbagh | Zaman | Klunk | Handen | Christian | Cohen	**Zammit, Matthew**
57	Structure and distribution of amyloid beta	Joseph | Sparling | Stys	**Joseph, Jeffrey**
58	Confocal analysis of fluorescent signal derived from CN-Flutemetamol-labeled diffuse and neuritic plaques in Alzheimer's disease	Ikonomovic | Buckley | Abrahamson | Mathis | Klunk | Farrar	**Ikonomovic, Milos**
59	Comparison of Down syndrome PiB PET templates for MRI-less PET quantification	Minhas | Laymon | Tudorascu | Lao | Campbell | Yu | Lopresti | Mathis | Klunk | Handen | Christian | Cohen	**Minhas, Davneet**
60	Trajectories of fiber tract impairment in autosomal dominant Alzheimer's disease	Araque Caballero | Benzinger | Suarez-Calvet | Levin | Morris | Bateman | Haass | Ewers	**Ewers, Michael**
61	The BDNF Val66Met SNP is related to hippocampal connectivity and cognitive decline in autosomal dominant Alzheimer's disease	Franzmeier | Ren | Levin | Bateman | Morri | Benzinger | Ewers	**Franzmeier, Nicolai**
62	Tau accumulation and memory decline are more closely related to striatal than cortical amyloidosis in individuals with early-onset autosomal dominant Alzheimer's disease	Hanseeuw | Lopera | Sperling | Norton | Guzman-Velez | Baena | Schultz | Gatchel | Jin | Chen | Reiman | Johnson | Quiroz	**Hanseeuw, Bernard**
63	Tau pathology in Down syndrome	Lemoine | Bharani | Hamlett | Perez | Mufson | Poon | Simic | Nordberg | Granholm	**Lemoine, Laetitia**

Board #	Poster Title	Authors	Presenter
THURSDAY – POSTER SESSIONS 2A AND 2B			
64	Singular Value Decomposition (SVD) identification of PiB and FDG topographies in Dominantly Inherited Alzheimer's Network (DIAN)	Loe | Brier | McCarthy | Stern | Kuffner | Morris | Bateman | Benzinger | Ances	**Loe, Maren**
65	[18F]AV-1451 tau PET imaging in MAPT 10+16 mutation carriers	Clarke | Jiao | Dick | Convery | Koriath | Woollacott | Weston | Gunn | Rabiner | Rossor | Warren | Fox | Ourselin | Bocchetta | Rohrer	**Clarke, Mica**
66	Longitudinal change of functional connectivity in the DIAN cohort: functional connectivity as a longitudinal biomarker in autosomal dominant AD	Schultz | Sperling | Buckley | Johnson | Benzinger | Ances | Morris | Buckles | Xiong | McDade | Cairns | Marcus | Fulbright | Jack | Ringman | Farlow | Kinnunen | Fox | Masters | Schofield | Salloway | Levin | Bateman | Chhatwal	**Schultz, Aaron**
67	An UNC5C locus is associated with susceptibility to cognitive decline and hippocampal neurodegeneration in clinically normal older adults	Yang | Chhatwal | Papp | Rabin | Hanseeuw | Mormino | Buckley | Schultz | Properzi | Hedden | Marshall | Rentz | Johnson | De Jager | Sperling	**Yang, Hyun-Sik**
68	CYP2C19 effects in brain amyloid load and hippocampus' functional integrity	Lessa Benedet | Iturria-Medina | Savard | Kang | Mathotaarachchi | A. Pascoal | Therriault | Shin | Gauthier | C. Evans | Labbe | Rosa-Neto	**Lessa Benedet, Andrea**
69	Relationships between [11C]PiB positivity and an imaging marker of cerebrovascular pathology positivity	Berman | Allison | Christian | Betthauser | Oh | Asthana | Carlsson | Bendlin | Johnson	**Berman, Sara**
70	[18F]Fluorotaucipir binding in patients with cerebral amyloid angiopathy without hemorrhage and mild cognitive symptoms	Jin | Benson | Schultz | Becker | Charidimou | Fotiadis | Katz | Luner | Moody | Sanchez | Sperling | Xiong | Viswanathan | Johnson	**Jin, David**
71	Amyloid imaging in hereditary cerebral amyloid angiopathy: detection and progression of pure vascular amyloid caused by APP E693Q	Schultz | Kloet | Sohrabi | Chatterjee | Gardnener | Taddei | Benzinger | Fagan | Sperling | Johnson | Bateman | Gurol | van Buchem | Martins | Chhatwal | Greenberg	**Chhatwal, Jasmeer**
72	Midlife insulin resistance and APOE genotype are associated with late-life brain amyloid accumulation	Rinne | Ekblad | Johansson | Helin | Viitanen | Laine | Puukka | Jula	**Rinne, Juha**
73	Flortaucipir PET imaging and neuropsychological performances dissociate dorsal and ventral stream dysfunction in Posterior Cortical Atrophy	Putcha | Collins | Wong | Dickerson | McGinnis	**Putcha, Deepti**
74	Amyloid network topology characterizes the progression of Alzheimer's disease during the pre-dementia stages	Pereira | Strandberg | Palmqvist | Volpe | van Westen | Westman | Hansson	**Pereira, Joana**
75	In pre-clinical AD, subjective cognitive decline is associated with brain hyperactivation in conflict monitoring/control regions	Mizuno | Karim | Rangarajan | Klunk | Aizenstein | Snitz	**Mizuno, Akiko**
76	How useful is amyloid PET in clinical diagnosis? A systematic review and meta-analysis	Fantoni | Chalkidou | O'Brien | Farrar | Hammers	**Farrar, Gill**
77	[18F]AV-1451 binds to an unidentified white matter target in semantic dementia	Whitwell | Martin | Schwarz | Duffy | Clark | Machulda | Botha | Graff-Radford | Jones | Utianski | Knopman | Petersen | Lowe | Jack | Josephs	**Whitwell, Jennifer**
78	Quantifying stages of subtle memory impairment in clinically normal older adults	Papp | Mormino | Grober | Sperling | Johnson | Rentz	**Papp, Kate**
79	The relationship between amyloid deposition and both global and hippocampal atrophy	Allison | Berman | Clark | Christian | Betthauser | Oh | Asthana | Bendlin | Johnson	**Allison, Samantha**
80	AV1451-PET measurements show substantial overlap across diagnostic groups and amyloid status	Landau | Korman | Jagust	**Landau, Susan**
81	Shrinking cortex and tau burden in the aphasic variant of Alzheimer's disease	Martersteck | Sridhar | Rainford | Mesulam | Rogalski	**Martersteck, Adam**
82	Cross-sectional associations between tau pathology burden measured by [18F]GTP1 PET imaging and cognition in AD adjusting for amyloid PET and cortical atrophy	Ward | Manser | Teng | Sanabria-Bohorquez | Ray | Baker | Kerchner | Weimer	**Ward, Michael**

Board #	Poster Title	Authors	Presenter
THURSDAY – POSTER SESSIONS 2A AND 2B			
83	Cognition and [18F]-Florbetaben PET imaging of amyloid in Parkinson's disease	Stark | Melzer | Keenan | Myall | Kaur | Livingston | Horne | Marsh | Grenfell | Young | MacAskill | Dalrymple-Alford | Anderson	**Stark, Megan**
84	Increased central arterial stiffening relates to CSF markers of tau aggregation and neurodegeneration in the oldest-old	Cambronero | Liu | Moore | Babicz | Hohman | Gifford | Bell | Acosta | Terry | Nair | Wang | Carr | Blennow | Zetterberg | Jefferson	**Cambronero, Francis**
85	Alterations in memory self-appraisal are associated with elevated tau deposition in normal older adults	d'Oleire Uquillas | Schultz | Jacobs | Hanseeuw | Buckley | Pascual-Leone | Sperling | Johnson | Vannini	**d'Oleire Uquillas, Federico**
86	Segregation of tau deposits across clinical stages provides the basis for pathophysiological staging in AD	Mathotaarachchi | A. Pascoal | L. Benedet | Shin | Kang | Struyfs | Therriault | Chamoun | Ng | Savard | Knight | Gauthier | Rosa-Neto	**Mathotaa-rachchi, Sulantha**
87	Increasing Aβ is associated with nonlinear change in BOLD modulation to difficulty in cognitively normal middle-aged and older adults: further evidence from an n-back task	Foster | M. Kennedy | Rodrigue	**Foster, Chris**
88	Co-existence of deleterious and neuroprotective interaction between amyloid and neuroinflammation in late stage Alzheimer's disease	Knight | Kang | Parent | Pascoal | Mathotaarachchi | Therriault | Benedet | Camoun | Aliaga | Zimmer | Shin | Aliaga | Kostikov | Soucy | Gauthier | Cuello | Rosa-Neto	**Knight, Ashley**
89	Amyloid and tau deposition determine cognitive impairment through epigenetic changes in individuals across the AD spectrum	Pascoal | Shin | Kang | Ng | Benedet | Mathotaarachchi | Therriault | Chamoun | Massarweh | Knight | Soucy | Gauthier | Rosa-Neto	**Pascoal, Tharick**
90	18F-AV-1451 uptake on tau PET differs between dementia with Lewy bodies and posterior cortical atrophy	Nedelska | Josephs | Graff-radford | Przybelski | Lesnick | Boeve | Lowe | Drubach | Knopman | Petersen | Jack, Jr. | Whitwell | Kantarci	**Nedelska, Zuzana**
91	Finding ground zero: identifying the medial temporal origin of tau deposition during life	Sanchez | Augustinack | Becker | Jacobs | Jin | Katz | Luner | Moody | Rentz | Sperling | Price | Johnson	**Sanchez, Justin**
92	Age-related change of THK-5351 PET in amyloid-negative and non-demented elderly subjects	Kato | Iwata | Kizawa | Fukaya | Kuratsubo | Kimiura | Okamura | Yanai | Ito | Nakamura | Study Group	**Kato, Takashi**
93	Human testing of non-selective alpha-synuclein PET tracers	Borroni | Honer | Gobbi | Mathis | Klunk | Kotzbauer | Tu | Mach | Mitchell | Marek | Eberling	**Borroni, Edilio**

Board #	Poster Title	Authors	Presenter
FRIDAY – POSTER SESSIONS 3A AND 3B			
100	Cross-sectional and longitudinal atrophy is preferentially associated with tau rather than Aβ PET pathology	McCullough | Gordon | Mishra | Blazey | Su | Christensen | Dincer | Jackson | Hornbeck | Morris | Ances | Benzinger	**McCullough, Austin**
101	[18F]Florbetapir binding potential in relation to cognition in subjective cognitive decline	Timmers | Verfaillie | Wesselman | Slot | Prins | van der Weijden | Yaqub | Lammertsma | Boellaard | Ossenkoppele | van der Flier | van Berckel	**Timmers, Tessa**
102	Application of the PredictND decision support system to cross-sectional imaging and psychometric data from an aMCI to probable AD three year outcomes clinical study	Buckley | Moreland | Urhemaa | van Gils | Wolber | lotjonen	**Buckley, Christopher**
103	Tau pathology detected by [18F]GTP1 negatively correlates with cortical volume in Alzheimer's disease	Ray | Baker | Manser | Ward | Teng | Weimer | Sanabria Bohórquez	**Sanabria Bohórquez, Sandra**
104	Assessing the impact of beta-amyloid deposition in progressive supranuclear palsy	Boland | Ahlskog, PhD, MD | Tosakulwong, BS | Senjem, MS | Spychalla, BS | Petersen, MD | Jack Jr, MD | Lowe, MD | Josephs, MD, MST, MSc | Whitwell, PhD	**Boland, Sarah**
105	Flortaucipir imaging in primary progressive aphasia predicts variability in language impairment	Collins | Quimby | Makaretz | Sweeney | Wong | McGinnis | Dickerson	**Collins, Jessica**

Board #	Poster Title	Authors	Presenter
FRIDAY – POSTER SESSIONS 3A AND 3B			
106	[18F]flutemetamol amyloid binding potential in relation to memory in cognitively normal subjects aged 80 years and older	Legdeur | Buslenko | Konijnenberg | ten Kate | Badissi | Tomassen | den Braber | Yaqub | Boomsma | Lammertsma | Maier | Scheltens | van Berckel | Visser	**Legdeur, Nienke**
107	Amyloid-β load is related to worries in individuals with subjective cognitive decline	Verfaillie | Timmers | Slot | van der Weijden | Wesselman | Prins | Sikkes | Lammertsma | Scheltens | Ossenkoppele | van Berckel | van der Flier	**Verfaillie, Sander**
108	[18F]Flutemetamol imaging in the ALFA project: Cognitively healthy subjects enriched for Alzheimer's disease genetic risk factors	Salvadó | Brugulat | Falcon | Pavia | Lomeña | Molinuevo | Gispert	**Salvadó, Gemma**
109	Is there a local neurotoxic effect of regional amyloid deposits? A network-domain specific study of florbetapir-PET – cognition associations	Grothe | Sorg | Teipel	**Grothe, Michel**
110	A similar prevalence and magnitude of amyloid positivity between cognitively normal elderly Japanese and Americans	Yu | Lopresti | Ihara | Cui | Aizenstein | Dodge | Minhas | Lopez | Klunk | Mathis | Kuller | Miyamoto | Sekikawa	**Lopresti, Brian**
111	Effects of amyloid deposition and hippocampal activation on subjective memory complaints	Chen | Jingting | Farrell | Park	**Chen, Xi**
112	Thresholds for amyloid positivity among normal, MCI and mild dementia subjects using [F-18] Florbetaben	Duara | Loewenstein | Lizzaraga | Adjouadi | Barker | Greig-Custo | Penate | Hanson | Marsiske | Vaillancourt | DeKosky | Golde	**Duara, Ranjan**
113	Twelve-month glucose metabolism declines in an empirically pre-defined statistical region-of-interest in amyloid-positive persons with Alzheimer's dementia and Mild Cognitive Impairment: updated ADNI findings	Chen | Lee | Kuang | Luo | Devadas | Thiyyagura | Chen | Bauer | Weiner | Jagust | Van Dyck | Reiman	**Chen, Kewei**
114	Flortaucipir PET measurements and relationships with cognitive impairment	Protas | Ghisays | Luo | DeMarco | Thiyyagura | Devadas | Bauer | Landau | Weiner | Jagust | Reiman | Chen	**Protas, Hillary**
116	Tau positron emission tomography is not elevated in HIV infected individuals	Ances | Beaumont | Cooley | Strain | Morris | Benzinger	**Ances, Beau**
115	[18F] AV-1451 uptake in corticobasal syndrome: the influence of beta-amyloid and clinical presentation	Ali | Whitwell | Martin | Senjen | Knopman | Jack | Lowe | Petersen | Boeve | Josephs	**Ali, Farwa**
117	Left frontal hub connectivity delays cognitive decline in autosomal dominant and sporadic Alzheimer's disease	Franzmeier | Duezel | Jessen | Benzinger | Levin | Fagan | Morris | Bateman | Ewers	**Franzmeier, Nicolai**
118	Sex and e4 genotype influence the longitudinal association between amyloid and tau pathology in clinically normal older adults	Hanseeuw | Buckley | Mormino | Jacobs | Chhatwal | Gomez | Johnson | Sperling	**Hanseeuw, Bernard**
119	The DCTclockTM test captures subtle cognitive changes and biomarker evidence of preclinical Alzheimer's disease	Rentz | Papp | Orlovsky | Souillard-Mandar | Penney | Davis | Johnson	**Rentz, Dorene**
120	Evidence for neuroinflammation in semantic dementia	Pascual | Zanotti-Fregonara | Pal | Rockers | Funk | Yu | Roman | Schultz | Masdeu	**Pascual, Belen**
121	Cerebrospinal fluid ratio of phosphorylated tau protein to beta-amyloid peptide 42 may improve the prediction of amyloid PET positivity: data from the Czech Brain Ageing Study	Cerman | Laczo | Vyhnalek | Sheradova | Ferda | Belohlavek | Hort	**Cerman, Jiri**
122	Relationships between self-reported sleep, tau, and Aβ in healthy older adults	Winer | Maass | Harrison | Mellinger | Baker | Walker | Jagust	**Winer, Joseph**
123	18F-AV1451 tau PET in patients at risk for chronic traumatic encephalopathy	Lesman-Segev | La Joie | Tsai | Bourakova | Visani | Ayakta | P O'Neil | Maass | Baker | Perry | Kramer | Miller | Jagust | Rabinovici	**Lesman-Segev, Orit**
124	Longitudinal [18F]THK5317 and [18F]FDG PET in relation to novel CSF tau fragments in Alzheimer's disease and related primary tauopathies	Leuzy | Chiotis | Cicognola | Saint-Aubert | Zetterberg | Blennow | Höglund | Nordberg	**Leuzy, Antoine**

Board #	Poster Title	Authors	Presenter
FRIDAY – POSTER SESSIONS 3A AND 3B			
125	Tau pathology networks associated with functional connectivity networks and disease progression in Alzheimer's disease	Hönig | Bischof | Seemiller | Hammes | Fink | van Eimeren | Drzezga	**Hönig, Merle**
126	Characterizing regional β-amyloid burden by magnetic susceptibility	Unschuld | van Bergen | Li | Quevenco | Gietl | Treyer | Meyer | Buck | Kaufmann | Nitsch | van Zijl | Hock	**Unschuld, Paul G.**
127	Tau aggregates imaged with 18F-Flortaucipir PET contribute to core clinical features of the Lewy body dementias	Katz | Ye | Shirvan | Schultz | Makaretz | Dickerson | Sperling | Growdon | Johnson | Gomperts	**Katz, Samantha**
128	Nucleus basalis of Meynert volume predicts early tau pathology and memory performance when amyloid levels are elevated in cognitively normal older individuals	Jacobs | Hanseeuw | Schultz | Papp | Rentz | Sperling | Johnson	**Jacobs, Heidi**
129	Increased GM regions in association with SUVR are candidate to predict convergence to Preclinical AD	Monté-Rubio | Rodriguez-Gomez | Sanabria | Alegret | Perez-Cordon | Lomeña | Pavia | Gismondi | Bullich | Vivas-Larruy | Gomez-Chiari | Ruiz-Laza | Tárraga | Boada	**Monté-Rubio, Gemma**
130	Distinct [18F]-THK5351 binding patterns in primary progressive aphasia variants	Schaeverbeke | Gabel | Bruffaerts | Meersmans | Van Bouwel | Dries | Peeters | Van Laere | Dupont | Vandenberghe	**Schaeverbeke, Jolien**
131	Multiple brain markers contribute to age-related changes in cognition	Hedden | Nierle | Perea | Rabin | Buckley | Schultz | Johnson | Sperling	**Hedden, Trey**
132	The BioFINDER-2 study: a longitudinal investigation on the role of tau and amyloid on cognitive function using 18F-RO6958948 and 18-Flutemetamol PET tracers	Hansson | Mattsson | Smith | Schöll | Klein | Farrar | Borroni | Coloma | Palmqvist | Stomrud	**Hansson, Oskar**
133	PiB PET as a biomarker for white matter integrity in aging and dementia	Su | Wang | Flores | Wang | Beau | Morris | Benzinger	**Su, Yi**
134	Effects of tau and amyloid deposition on domain-specific memory function in old age	Maass | Berron | Harrison | Baker | Mellinger | Swinnerton | Bell | Duezel | Jagust	**Maass, Anne**
135	Effects of amyloid, tau, and hippocampal volume on normal and fast gait speeds in cognitively normal older adults: results from the Harvard Aging Brain study	Kirn | Buckley | Hanseeuw | Klein | Properzi | Sperling | Johnson	**Kirn, Dylan**
136	[18F]-THK5351 binding patterns are associated with language deficits in primary progressive aphasia	Gabel | Schaeverbeke | Meersmans | Bruffaerts | Van Bouwel | Dries | Peeters | Van Laere | Dupont | Vandenberghe	**Gabel, Silvy**
137	Personality traits and neuropsychiatric factors are related to increased amyloid deposition in cognitively normal older adults	Pichet Binette | Vachon-Presseau | Gonneaud | Marchant | Bellec | Breitner | Villeneuve | Research Group	**Pichet Binette, Alexa**
138	Tau deposition in relation to verbal and phonemic fluency in the Framingham Heart Study	Luner | Jacobs | Papp | Becker | Beiser | Daniluk | Himali | Jin | Katz | Killiany | Moody | Pase | Peets | Raman | Sanchez | Satizabal | Schafer | Seshadri | Johnson	**Luner, Evelyn**
139	Long-term clinical stability in amyloid-positive subjects is predicted by negative FDG-PET scan	Iaccarino | Sala | Perani	**Iaccarino, Leonardo**
140	Associations between tau, Aβ and cortical thickness with cognition in Alzheimer's disease	Ossenkoppele | Smith | Ohlsson | Mattsson | Strandberg | Palmqvist | Hansson	**Ossenkoppele, Rik**
141	Longitudinal relationships between brain amyloid deposition and glucose metabolism across the Alzheimer's disease spectrum	Bejanin | Arenaza-Urquijo | De Flores | Tomadesso | Chételat	**Bejanin, Alexandre**

HAI 2018 ABSTRACTS

Wednesday, January 17, 2018 - 12:00 pm - 02:00 pm

Podium Session

Session 1: Methods and Analysis

CHAIRS: Bradley Christian, Sandra Sanabria

Wednesday, January 17, 2018		
12:00 - 02:00	**Session 1: METHODS AND ANALYSIS**	CHAIRS: Bradley Christian | Sandra Sanabria
12:00	Serial measurements with Rousset-Style (GTM) PVC are less precise than with traditional approaches	**Schwarz** | Gunter | Lowe | Weigand | Vemuri | Senjem | Petersen | Knopman | Jack
12:15	Modeling amyloid, tau, and cortical thickness changes across the Alzheimer's disease spectrum	**Cha** | Park | Lee | Baker | Visani | Bourakova | Pham | Janabi | O'Neil | Miller | Jagust | Rabinovici
12:30	Amyloid load - a more sensitive outcome measure for quantifying amyloid-β	Whittington | **Gunn**
12:45	Data-driven tau-PET covariance networks enhance associations with cognition in Alzheimer's disease	**Vogel** | Mattsson | Iturria-Medina | Strandberg | Schöll | Danserau | Villeneuve | van der Flier | Scheltens | Bellec | Evans | Hansson | Ossenkoppele
01:00	Regional tau elevation patterns in clinically normal adults using sparse k-means clustering	**Moody** | Gonzalez | Mowrey | Rentz | Satizabel | Pase | Beiser | Jin | Katz | Himali | Luner | Daniluk | Schafer | Peets | Sanchez | Killiany | DeCarli | Sperling | Seshadri | Price | Johnson
01:15	Evaluation of visual interpretation methods for tau PET imaging	**Sonni** | Maass | Korman | Baker | Landau | Jagust
01:30	Discussion	

Serial measurements with Rousset-Style (GTM) PVC are less precise than with traditional approaches

Christopher Schwarz, Jeffrey Gunter, Val Lowe, Stephen Weigand, Prashanthi Vemuri, Matthew Senjem, Ronald Petersen, David Knopman, Clifford Jack

Mayo Clinic, Rochester, MN, US

Background: Rousset-style partial volume correction (PVC) using a geometric transfer matrix (GTM) has recently surged in popularity for tau PET analysis. This rise has been fueled by: 1) the need to correct for bleed-in of nearby off-target binding, and other neighboring areas, when measuring uptake in small regions e.g. hippocampus, and 2) its inclusion as the default method in PETSurfer (FreeSurfer 6.0). Here, we compare the reliability of GTM PVC, 2-compartment (Meltzer-style) PVC, and no PVC for longitudinal PET measurements.

Methods: Although tau PET has popularized GTM PVC, at present we have limited serial tau data. Therefore, we performed this comparison in Mayo Clinic subjects (n=301) each with 3 pairs (within 3 years) of PiB PET and MRI scans. We measured SUVR in a composite cortical region using each PVC option with four different pipelines: 1) a previously-described in-house cross-sectional SPM12/ANTs-based pipeline; 2) a previously-described in-house SPM12/ANTs-based pipeline for simultaneous cross-timepoint analysis; 3) PETSurfer using cross-sectional FreeSurfer 6.0; 4) PETSurfer using longitudinal FreeSurfer 6.0. An 8mm PSF was assumed. We used a linear mixed-effects model to compute the within-subject coefficient of variation (σ_error/mean) for serial measurements from each method.

Conclusions: Measurements using GTM PVC had significantly more unexplained within-subject variability (σ_error/mean ≈15-25%) than those using 2-compartment or no PVC (≈5-15%) (Figure 1). This imprecision was consistent across two separate implementations of GTM PVC (in-house and FreeSurfer), and was not reduced by pipelines designed specifically to stabilize serial measurements, or by using WM-based reference regions. These numbers are concerning when compared to the average annual increase in PET signal for AD dementia subjects, which has been estimated as approximately 4% with PiB (amyloid), and approximately 5% with AV1451 (tau). Based on this data, we do not recommend using GTM PVC for serial analysis.

Figure 1: Imprecision in PiB PET SUVR when using each combination of measurement pipeline, PVC, and reference region. Imprecision was measured as the within-subject coefficient of variation (σ_{error}/mean) from a linear mixed-effects model using 3 timepoints of PiB PET scans (n=301 subjects) with corresponding MRI. Imprecision when using GTM PVC was consistently significantly larger than when using 2-compartment PVC or no PVC.

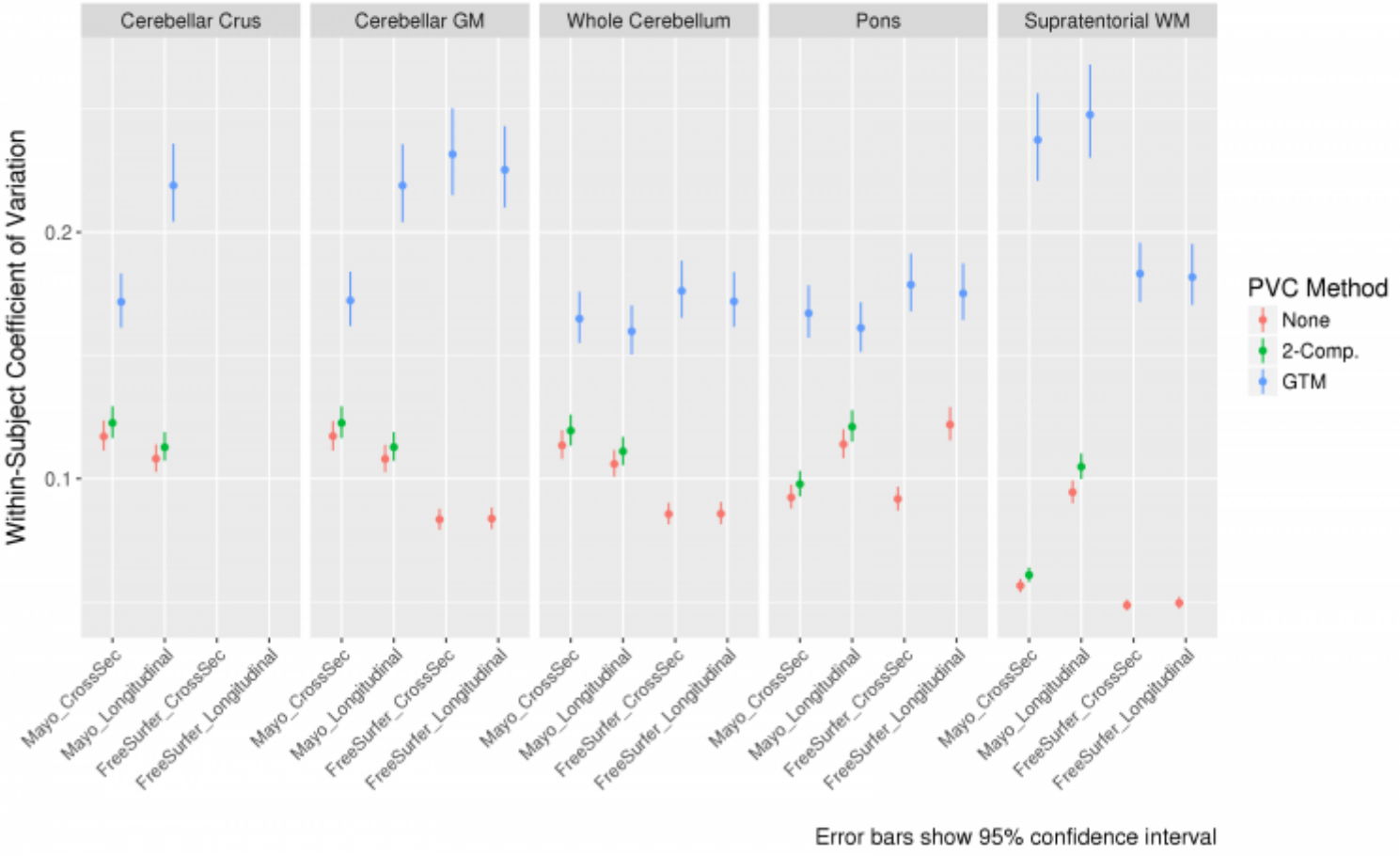

Keywords: Serial processing, methods, Partial Volume Correction, GTM, PVC

Modeling amyloid, tau, and cortical thickness changes across the Alzheimer's disease spectrum

Jungho Cha[1], Yeong-Hun Park[2], Jong-Min Lee[2], Suzanne Baker[3,4], Adrienne Visani[1], Viktoriya Bourakova[1], Julie Pham[1], Mustafa Janabi[3], James O'Neil[3], Bruce Miller[1], William Jagust[3,4], Gil Rabinovici[1]

[1]*Memory and Aging Center, Department of Neurology, University of California, San Francisco, San Francisco, CA, US*
[2]*Department of Biomedical Engineering, Hanyang University, Seoul, South Korea*
[3]*Molecular Biophysics and Integrated Bioimaging, Lawrence Berkeley National Laboratory, Berkeley, CA, US*
[4]*Helen Wills Neuroscience Institute, University of California, Berkeley, Berkeley, CA, US*

Objective: To apply and compare linear and logistic regression approaches to modeling progression of amyloid, tau, and neurodegeneration across the AD spectrum using cross-sectional data.

Methods: [^{11}C]PiB-, [^{18}F]AV1451-PET, and 3T T1-weighted MRI were obtained for 110 subjects, including 49 cognitively normal controls (NC, 33PiB-,and 16PiB+), and 61 PiB+ patients (12MCI,and 49AD)(Table1). MRIs were processed with the CIVET-pipeline. PiB 0-90min DVR and AV1451 80-100min SUVR images were created using cerebellar gray matter for PiB (PiB+=cortical DVR>1.065), and inferior cerebellar gray matter for AV1451. Images were mapped onto CIVET-derived cortical surfaces and smoothed. We modeled global measures of each modality using both linear and logistic models, applying both diagnosis and MMSE as proxies for disease progression. Akaike Information Criterion (AIC) was used to determine the relative likelihood that biomarker progression best fit logistic or linear models. To adjust for effects of age, sex, and education, we repeated all models using W-scores (based on PiB-NC) each biomarker. Each estimated model of biomarker was normalized for easier comparison.

Table 1. Demographics of subjects.

	Normal Controls (PiB-)	Normal Controls (PiB+)	MCI	AD
n	33	16	12	49
Age (years)	76.73±7.21	78.94±3.13	62.17±8.31	63.78±8.56
Sex (m/f)	14/19	7/9	5/7	18/31
Education (years)	16.67±1.81	16.44±2.00	18.00±3.30	17.18±2.71
MMSE	28.70±1.33	28.31±1.35	27.3±3.14	21.57±5.24
PiB DVR	1.00±0.04	1.41±0.25	1.57±0.27	1.68±0.19

Data are presented as mean±SD. MCI=mild cognitive impairment, AD=Alzheimer's disease, MMSE=Mini-Mental State Examination, DVR= Distribution volume ratios.

Results: PiB appeared to reach early saturation at the control phase, while AV1451 plateaued at MCI/earlyAD and cortical thickness appeared more dynamic through later stages of AD(Figure1). W-scores provided similar results(Figure2). AIC determined a high probability for a sigmoid model for PiB (probability=100%) and AV1451 (97%), but probabilities of sigmoid vs. linear models were similar for cortical thickness (52% and 48%)(Table2).

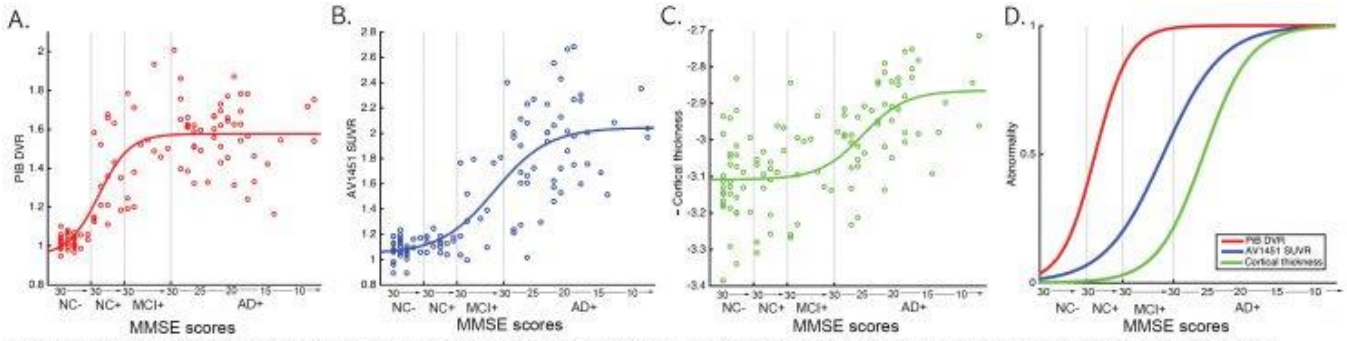

Figure 1. Data-driven biomarker plots of (A) PiB DVR, (B) AV1451 SUVR, (C) inverse cortical thickness, and (D) normalized three measures, based on the abnormality, against diagnosis and MMSE scores. All of the results were calculated for the NC- to AD+ clinical transition.

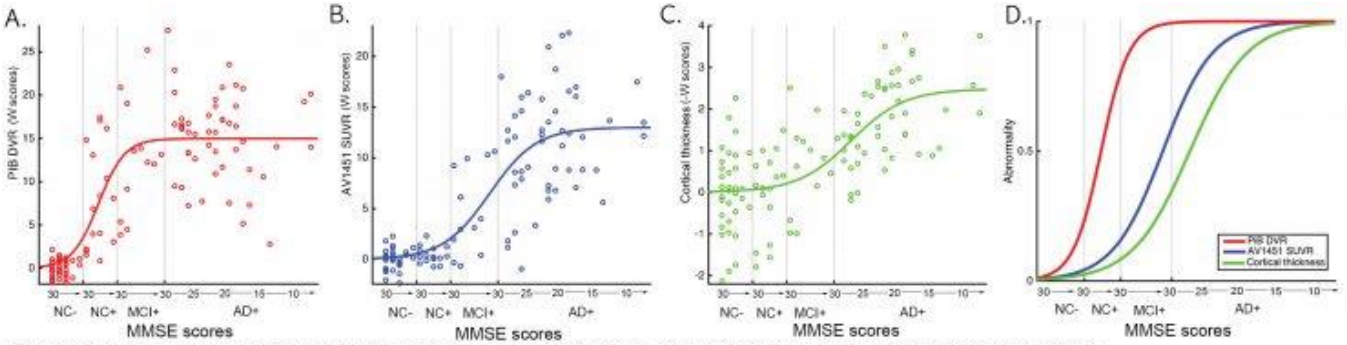

Figure 2. Data-driven biomarker plots of W scores using (A) PiB DVR, (B) AV1451 SUVR, (C) inverse cortical thickness, and (D) normalized three measures, based on the abnormality, against diagnosis and MMSE scores. All of the results were calculated for the NC- to AD+ clinical transition.

Table 2. Akaike information criterion (AIC) for sigmoid and linear model. The probabilities are based on the differences of AIC scores.

	PiB DVR	AV1451 SUVR	Cortical thickness
Raw values			
AIC (Sigmoid)	-398.86	-281.97	-478.88
AIC (Linear)	-354.44	-275.02	-478.73
Probability (%) (Sigmoid vs Linear)	100 vs 0	97 vs 3	52 vs 48
W scores			
AIC (Sigmoid)	342.61	296.88	-4.6258
AIC (Linear)	379.19	304.62	-5.3818
Probability (%) (Sigmoid vs Linear)	100 vs 0	98 vs 2	41 vs 59

Conclusions: Our results suggest global cortical PiB and AV1451 follow sigmoidal patterns over the course of AD, while cortical thickness remains dynamic at the symptomatic stage and may follow either a sigmoid or linear pattern. AV1451 appears to increase after PiB reaches a plateau, but precedes changes in cortical thickness. These results, which need to be confirmed with longitudinal data, are consistent with AD being an amyloid-facilitated tauopathy, which in turn leads to neuronal loss.

Keywords: Biomarker Plot, linear and logistic regression, PiB-PET, AV1451-PET, Cortical thickness

Amyloid load - a more sensitive outcome measure for quantifying amyloid-β

Alex Whittington[1], Roger N. Gunn[1,2]

[1]*In Vicro, London, United Kingdom*
[2]*Imperial College London, London, United Kingdom*

Introduction: The global amyloid-β (Aβ) burden in Alzheimer's disease (AD) is routinely quantified from static Aβ PET scans using the mean cortical standardized uptake value ratio (SUVr). We introduce a novel outcome measure amyloid load ($A\beta_L$) together with an algorithm to calculate it and investigate whether $A\beta_L$ provides an increase in power over SUVr.

Methods: Previous spatiotemporal modelling of Aβ accumulation in AD using a logistic growth model with [^{18}F]-AV45 data allowed us to estimate two canonical images in MNI152 space for Aβ carrying capacity (***K***) and non-specific binding (***NS***)[1]. $A\beta_L$ is calculated from a static ***SUVr*** image using these canonical images and an image based regression according to the to $IQ_{A\beta}$ algorithm which is deduced from the prior logistic growth modelling[1];

$$\mathbf{SUVr}=A\beta_L\mathbf{K}+ns\mathbf{NS}$$

$A\beta_L$ was calculated for both cross-sectional and longitudinal ADNI [^{18}F]-AV45 PET data. The cross-sectional ADNI data consisted of 769 scans from four groups (HC=211, EMCI=223, LMCI=203, AD=132). The longitudinal data consisted of 147 scans from EMCI subjects that received two-year follow-up scans (1.96±(0.12)years).

Results: In the cross-sectional analysis, $A\beta_L$ produced greater effect sizes (hedges g) between all ADNI classifications than mean cortical SUVr (Figure 1) with the mean increase being 56%. In the longitudinal analysis, the effect size between baseline and follow-up was 0.35 using mean cortical SUVr and 0.49 using $A\beta_L$ (Figure 2). For a clinical trial of an anti-Aβ therapeutic with N=100 subjects (50 placebo and 50 drug), this would result in $A\beta_L$ having a substantial increase in power to detect changes in the Aβ burden (Figure 3).

Conclusions: $A\beta_L$, as calculated by the $IQ_{A\beta}$ algorithm, is a novel outcome measure with increased sensitivity for measuring Aβ burden and offers increased power for subject classification and clinical trials assessing anti-Aβ therapeutics

1.Whittington,A., Sharp,D. & Gunn,R.N. *J Nucl Med*(In press)

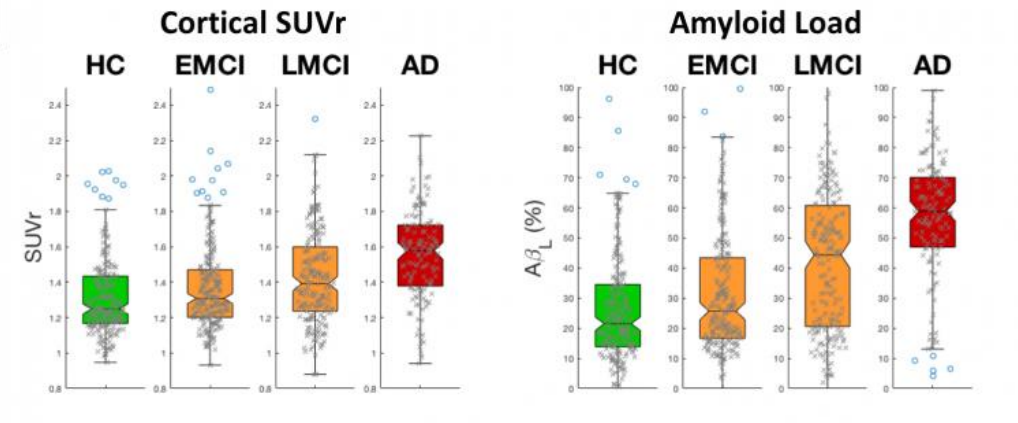

	EMCI	LMCI	AD
Effect size vs HC	0.21	0.43	0.97
Effect size vs EMCI		0.23	0.77
Effect size vs LMCI			0.50

	EMCI	LMCI	AD
Effect size vs HC	0.24	0.71	1.51
Effect size vs EMCI		0.49	1.24
Effect size vs LMCI			0.64

Figure 1

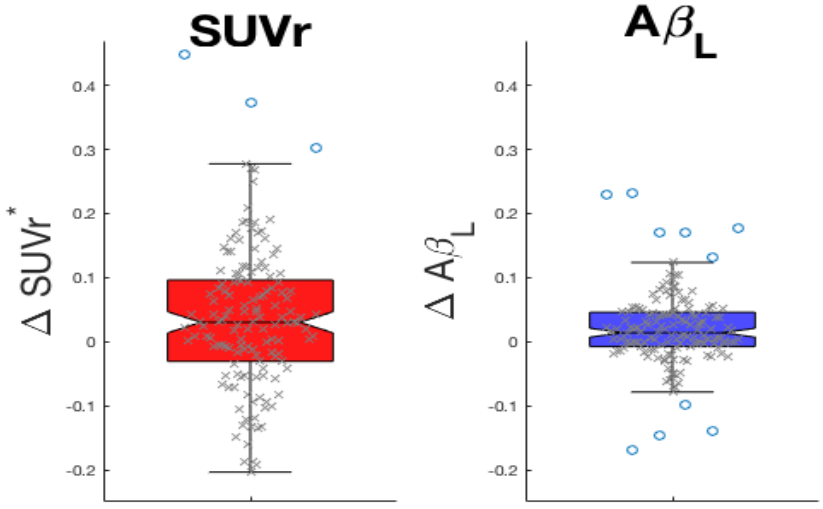

Figure 2

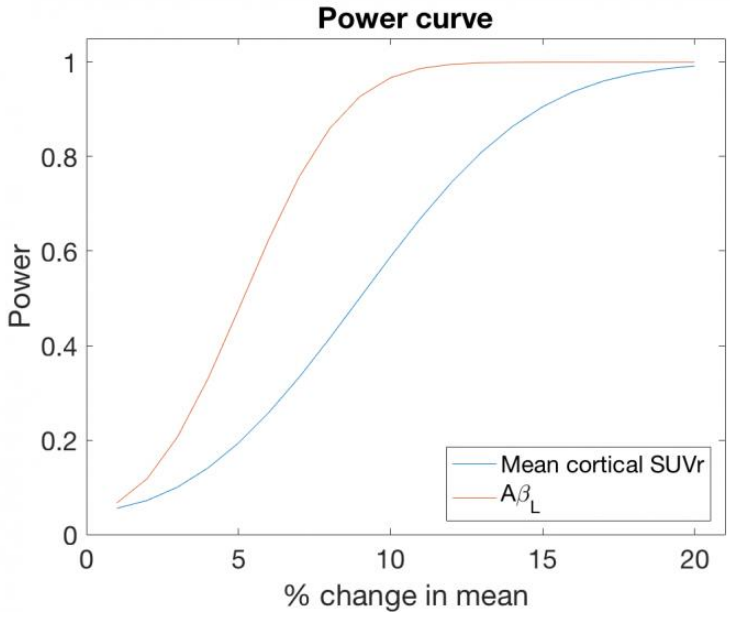

Figure 3

Keywords: Amyloid Load, Static Amyloid-β PET

Data-driven tau-PET covariance networks enhance associations with cognition in Alzheimer's disease

Jacob Vogel[1,2], Niklas Mattsson[3,4,5], Yasser Iturria-Medina[1], T. Olof Strandberg[3], Michael Schöll[3,6], Christian Danserau[9], Sylvia Villeneuve[1,9], Wiesje van der Flier[2,10], Philip Scheltens[2], Pierre Bellec[7,8], Alan Evans[1], Oskar Hansson[3,4], Rik Ossenkoppele[2,3]

[1]*Montreal Neurological Institute, Montreal, QC, Canada*
[2]*Alzheimer Center and Department of Neurology, VU University medical center, Amsterdam, Netherlands*
[3]*Clinical Memory Research Unit, Lund University, Lund, Sweden*
[4]*Memory Clinic, Skåne University Hospital, Lund, Sweden*
[5]*Department of Neurology, Skåne University Hospital, Lund, Sweden*
[6]*Wallenberg Centre for Molecular and Translational Medicine, University of Gothenburg, Gothenburg, Sweden*
[7]*Department of Computer Science and Operations research, Université de Montréal, Montreal, QC, Canada*
[8]*Centre de Recherche de l'Institut Universitaire de Gériatrie de Montréal, Montreal, QC, Canada*
[9]*Department of Psychiatry, McGill University, Montreal, QC, Canada*
[10]*Department of Epidemiology and Biostatistics, VU University medical center, Amsterdam, Netherlands*

Previous PET studies have quantified filamentous tau pathology using regions-of-interest (ROIs) based on observations of the topographical distribution of neurofibrillary tangles in post-mortem tissue. An alternative approach for neuroimaging studies could be to select ROIs using data-driven methodologies, thereby taking advantage of the abundance of information contained in neuroimaging data. The present study employs an unsupervised data-driven method to identify spatial patterns of tau-PET distribution, and to compare these patterns to previously published "pathology-driven" ROIs. Tau-PET patterns were identified from a discovery sample comprised of 123 subjects from the Swedish BioFINDER study, including normal controls (n=55) and patients with mild cognitive impairment (MCI; n=21) or Alzheimer's disease (AD) dementia (n=47), who underwent [^{18}F]AV1451 PET scanning. Associations with cognition were tested in a separate sample from ADNI (43 controls, 37 MCI, 10 AD dementia). BioFINDER [^{18}F]AV1451 images were entered into a voxelwise clustering algorithm, which resulted in five clusters (Fig.1): 1) an "off-target" cluster encompassing the subcortex and hippocampus, and clusters comprising 2) frontal, 3) medial/inferior temporal, 4) temporo-parietal and 5) unimodal sensory regions. Mean [^{18}F]AV1451 uptake in the data-driven, and the previously published pathology-driven ROIs, was extracted from ADNI [^{18}F]AV1451 scans. Linear models compared [^{18}F]AV1451 signal across all 40 regions to Mini-Mental State Examination (MMSE) scores, adjusting for age, sex and education. Significant relationships emerged in two ROIs: the data-driven temporo-parietal and medial/inferior temporal clusters (Fig.2). Inputting all regions plus demographics (43 features total) into a feature selection routine (LASSO) resulted in selection of three ROIs (data-driven temporo-parietal and subcortical clusters, and a late-stage pathological region) and education, which together explained 25% of variance in MMSE scores (Fig.3). These results generalized to other tests of global cognition. Our findings suggest that hypothesis-free, data-derived ROIs may offer enhanced utility compared to theory-driven ROIs, by utilizing information specific to tau-PET signal.

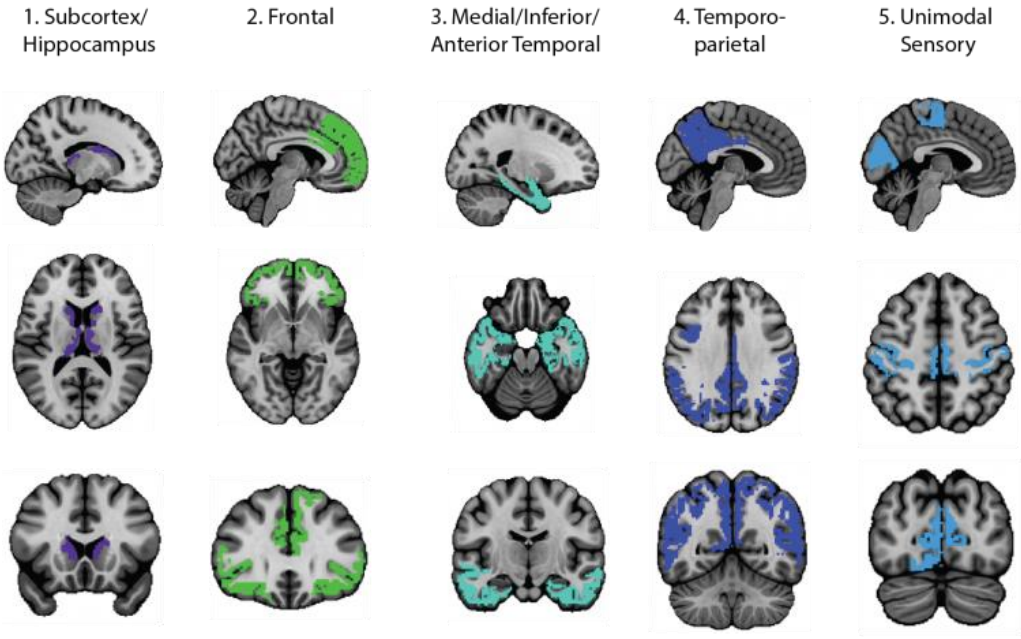

A clustering algorithm called Bootstrap Analysis of Stable Clusters (Bellec et al., 2010, Neuroimage) was used to identify spatial patterns of tau covariance across subjects. The algorithm identified five clusters, pictured.

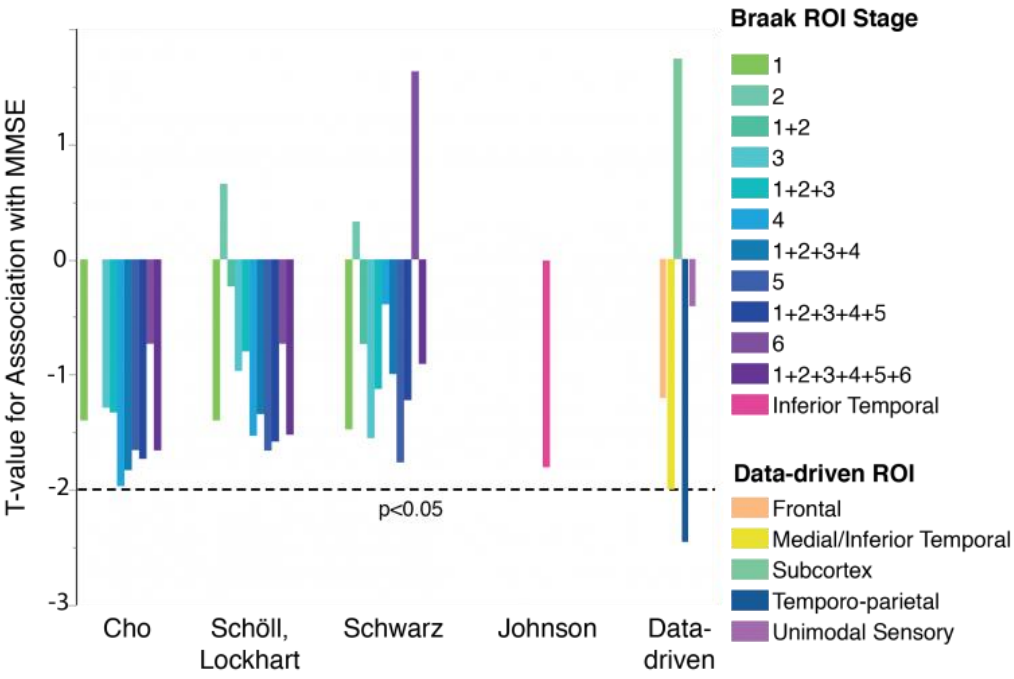

Fig.2. General linear models adjusting for age, sex and education were run between AV1451 in each of 40 ROIs and MMSE. ROIs were Braak stage ROIs from three studies, Schöll, Lockhart et al., 2016 Neuron; Cho et al., 2016 *Ann. Neurol.*; Schwarz et al., 2016 *Brain*; as well as the data-driven ROIs from Fig.1, and the bilateral inferior temporal lobe ROI used in Johnson et al., *Ann. Neurol.* The data-driven ROIs improved correlations with MMSE compared to previously published ROIs.

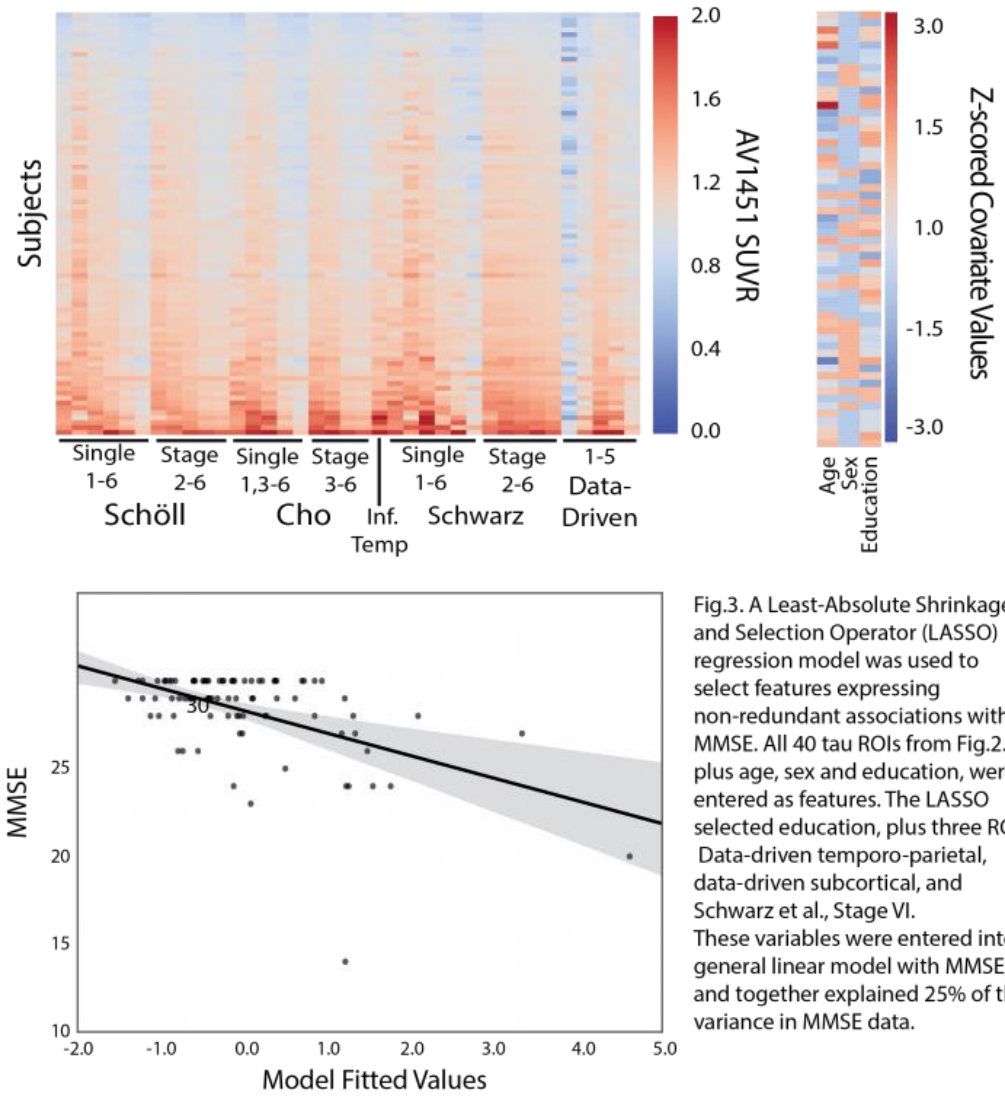

Fig.3. A Least-Absolute Shrinkage and Selection Operator (LASSO) regression model was used to select features expressing non-redundant associations with MMSE. All 40 tau ROIs from Fig.2., plus age, sex and education, were entered as features. The LASSO selected education, plus three ROIs: Data-driven temporo-parietal, data-driven subcortical, and Schwarz et al., Stage VI. These variables were entered into a general linear model with MMSE, and together explained 25% of the variance in MMSE data.

Keywords: Tau-PET, AV1451, cognition, machine learning

Regional tau elevation patterns in clinically normal adults using sparse k-means clustering

Kirsten Moody[1], Ivan Gonzalez[1], Wenzhu Mowrey[3], Dorene Rentz[1,2], Claudia Satizabel[4,5], Matthew Pase[4,6], Alexa Beiser[4,7], David Jin[1], Samantha Katz[1], Jayandra J. Himali[4,5], Evelyn Luner[1], Daniel Daniluk[4], Collin Schafer[4], Bryanne Peets[4], Justin Sanchez[1], Ronald Killiany[8], Charles DeCarli[9], Reisa Sperling[1,2], Sudha Seshadri[4], Julie Price[1], Keith Johnson[1,2]

[1]Departments of Neurology, Radiology, and the Athinoula A. Martinos Center for Biomedical Imaging, Massachusetts General Hospital, Harvard Medical School, Boston, MA, US
[2]Center for Alzheimer's Research and Treatment, Department of Neurology, Brigham and Women's Hospital, Harvard Medical School, Boston, MA, US
[3]Department of Epidemiology and Population Health, Albert Einstein College of Medicine, Bronx, NY, US
[4]The Framingham Heart Study, Framingham, MA, US
[5]Department of Neurology, Boston University School of Medicine, Boston, MA, US
[6]Centre for Human Psychopharmacology, Swinburne University of Technology, Hawthorn, Australia
[7]Department of Biostatistics, Boston University School of Public Health, Boston, MA, US
[8]Center for Biomedical Imaging, Boston University School of Medicine, Boston, MA, US
[9]University of California at Davis, Sacramento, CA, US

Objectives: Temporal lobe tau deposition has been postulated as a critical accompaniment of cognitive impairment in AD, but is elevated in as many as 40% of clinically normal (CN) older individuals at autopsy (Braak III+, CDR-SB=0, mean age=87; NACC, Serrano-Pozo 2013).

We applied sparse k-means clustering (SKM) to temporal lobe tau PET measures to define tight-clusters (high- versus low-tau) among CN adults and identified regions contributing most to clustering. We also assessed associations of these tau clusters with age and amyloidosis.

Methods: CN participants (Table 1) in the Harvard Aging Brain Study (HABS) and Framingham Heart Study (FHS) underwent [^{11}C]PiB amyloid and [^{18}F]Flortaucipir (FTP) tau PET at Massachusetts General Hospital (HABS vs. FHS MMSE p=0.9276). FTP SUVR was measured (cerebellum reference) in eight FreeSurfer regions: superior-temporal sulcus; entorhinal; fusiform; temporal pole; and inferior, superior, middle temporal and parahippocampal cortices. SKM with 2 clusters, 2000 resamples, and tight-clusters were defined to include participants at 95% confidence.

Results: Cluster 1, "low-tau", was identified in 196/292 (67%), Cluster 2, "high-tau", in 32/292 (11%); and 64/292 (22%) unassigned at 95% confidence level. Regional SKM weights were highest for entorhinal, second highest for fusiform, and least for middle temporal cortex. Tau SUVR was age related in the low-tau [20-92y], but not the high-tau group (Figure 1). Low-tau participants were more likely than high-tau to be male and have low-amyloid (Table 1; Figure 2).

Conclusions: SKM identified the relative importance of different temporal regions for clustering of CNs into high- and low-tau groups. Two SKM clusters were identified in 78% of clinically normal individuals aged 20-92y. Age related tauopathy is evident in the low-tau group, along with low-amyloid burden, suggesting that the cluster includes those with incipient tauopathy. The high-tau cluster has more heterogeneous levels of tau at high-amyloid burden and greater age.

Table 1: Characteristics of the total sample and tight-clusters

	Total Sample	Cluster 1 Low Tau	Cluster 2 High Tau
N	292	196	32
†Age, y **	68 ± 14 [20,92]	65 ± 13 [20,92]	80 ± 6 [69,90]
Male, n (%) **	139 (48)	95 (48)	10 (31)
†Years of Education*	16 ± 2.8 [6,21]	16 ± 3.3 [6,21]	17 ± 2.7 [9,20]
†Baseline MMSE*	29 ± 1.0 [25,30]	29 ± 1.0 [25,30]	29 ± 1.2 [26,30]
High Amyloid, %	24	13	66

†mean+sd; [range]
significance between clusters * p<0.05, ** p<0.01
MMSE=mini-mental state exam

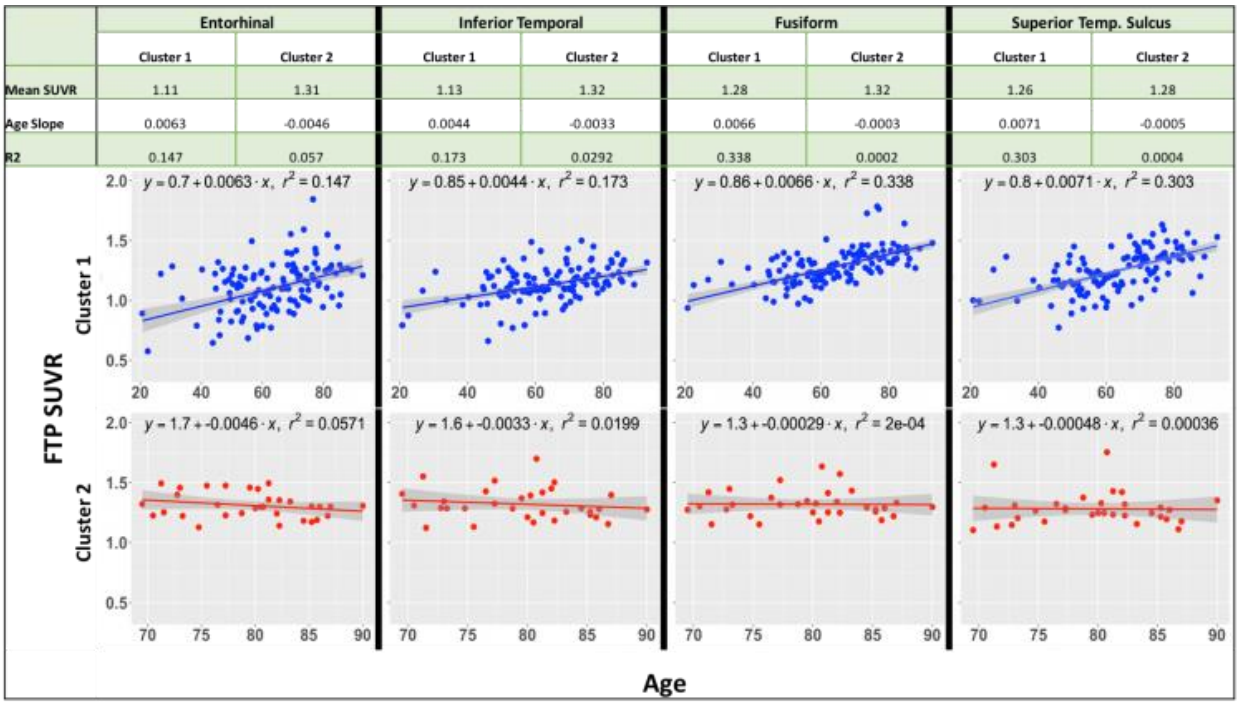

Figure 1: Regional average tau SUVR, SUVR-Age Slope, and correlation R2 of average SUVR and age between clusters. The entorhinal and inferior temporal average SUVR values are significantly different between Cluster 1 and 2 (p<.001). Fusiform and superior temporal sulcus are the regions that had the highest correlation with age in Cluster 1 (R^2=0.338 and 0.303, respectively), but failed to be correlated in Cluster 2 (R^2<.001). Cluster 1 (blue) ranges from 20-92 years and Cluster 2 (red) ranges from 69-90 years.

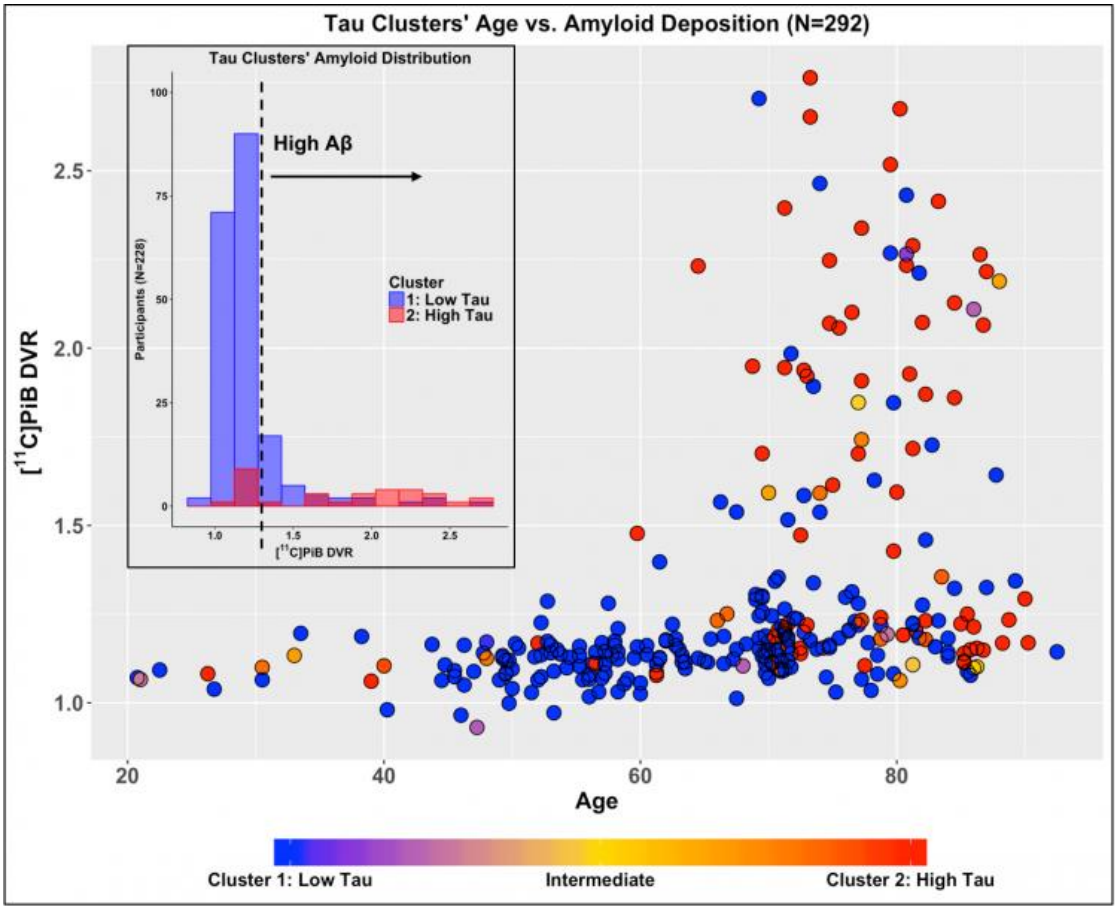

Figure 2: Relationships between tau clusters, amyloidosis, and age. Scatterplot shows amyloid deposition as a function of age by the spectrum of clusters. The color scale indicates the 95% confidence level from SKM analysis: low tau (blue) is Cluster 1, N=196; high tau (red) is Cluster 2, N=32; and the intermediate (gold) are not associated with a tight-cluster, N=64. The histogram (inset) shows the distribution of amyloid based on participant PiB load of those in tight-clusters (N=228). High amyloid (Aβ) is represented as PiB DVR > 1.3. DVR = distribution volume ratio

Keywords: Tau-PET, Flortaucipir, clinically normal, cluster analysis, SKM

Evaluation of visual interpretation methods for tau PET imaging

Ida Sonni[1], Anne Maass[2], Deniz Korman[1], Suzanne L. Baker[2], Susan M. Landau[2], William J. Jagust[1,2]

[1]Molecular Biophysics and Integrated Bioimaging, Lawrence Berkeley National Lab, Berkeley, CA, US
[2]Helen Wills Neuroscience Institute, University of California, Berkeley, Berkeley, CA, US

Aim: We sought to identify an accurate visual interpretation method for the qualitative evaluation of ^{18}F-AV-1451 tau PET scans.

Materials and methods: We studied a heterogeneous sample of 60 subjects (32 cognitively normal older adults, 14 MCI subjects, 14 AD patients) scanned with ^{18}F-AV-1451 PET. A nuclear medicine physician interpreted all the tau PET SUVR images qualitatively using 3 rating scales. Two rating scales evaluated ^{18}F-AV-1451 uptake in 7 cortical regions (medial, inferior and lateral temporal, medial and lateral parietal, frontal and occipital) either by presence/absence of uptake or on a gradient from 0 to 2. The third rating scale assessed ^{18}F-AV-1451 uptake in 3 regions corresponding to the Braak stages (Braak I/II, III/IV and V/VI). The results of the visual interpretation were compared to the average global tau deposition and correlated to amyloid status and clinical diagnosis. The rating scale providing best correlations with global tau quantification was further validated with qualitative and quantitative analysis of 200 additional scans of patients across the disease spectrum.

Results: Final scores of all visual rating scales were significantly and strongly associated with quantification of global ^{18}F-AV-1451 uptake. The strongest correlation was found with the scale allowing differentiation between mild and intense uptake across the 7 cortical regions (correlation coefficient =0.875, Table 1). As expected, the mean values of the visual rating scores within each diagnostic category were lower for the amyloid negative subjects than for the amyloid positive. The mean visual scores showed an increasing trend directly correlated to diagnosis, with controls having the lowest, MCI an intermediate, and AD the highest values (Table 2).

Conclusion: Our data show that visual rating scales strongly correlate with tau SUVR quantification, particularly when allowing differentiation between mild and intense uptake. This is a promising alternative approach to tau measurement in clinical settings.

Table 1: Spearman's rank Correlation

Spearman's rho	Global Tau SUVR	Scale 0 to 7	Scale 0 to 14	Braak Stages
Global Tau SUVR	1.000	.749**	.875**	.815**
Scale 0 to 7	.749**	1.000	.902**	.922**
Scale 0 to 14	.875**	.902**	1.000	.906**
Braak Stages	.815**	.922**	.906**	1.000
**. Correlation is significant at the 0.01 level (1-tailed).				

Table 2: Descriptive Statistics

Visual Rating Scale 0 to 14				
Diagnosis		**Mean**	**Std. Deviation**	**N**
Control	Amyloid -	3.08	3.28	13
	Amyloid +	5.16	4.41	19
	Total	4.31	4.07	32
MCI	Amyloid -	0.00	0.00	4
	Amyloid +	7.6	6.45	10
	Total	5.43	6.44	14
AD	Amyloid +	13.5	1.4	14
	Total	13.5	1.4	14
Total	Amyloid -	2.35	3.14	17
	Amyloid +	8.44	5.61	43
	Total	6.72	5.72	60

Keywords: Visual interpretation, Tau PET, AV-1451

Wednesday, January 17, 2018 - 02:00 pm - 03:30 pm

Poster Session 1

Board #	Poster Title	Authors	Presenter
WEDNESDAY – POSTER SESSION 1			
13	Explaining [18F]-AV-1451 variability in healthy controls across the lifespan	Baker | Harrison | Maass | La Joie | Jagust	**Baker, Suzanne**
38	A more accurate alternative to SUVR for quantifying binding rate-of-change in serial PET	Becker | Price | Johnson	**Becker, J. Alex**
31	Optimal time window for [18F]-AV-1451 binding quantification in AD using SUVr	Wimberley | Lagarde | Olivieri | Kuhnast | Caillé | Gervais | Sarazin | Bottlaender	**Bottlaender, Michel**
19	Assessment of centiloid scaling values in test-retest evaluation using multiple image quantification software platforms	Battle | Buckley | Pillay	**Buckley, Christopher**
09	Novel alpha-synuclein positron emission tomography (PET) tracers for the diagnosis of Parkinson's disease	Capotosti | Tsika | Molette | Ravache | Vokali | Rodriguez | Davranche | Darmency | Purohit | Paterson | Kroth | Stoehr | Lowe | Pfeifer | Muhs	**Capotosti, Francesca**
37	Preliminary report on the associations between CSF T-tau and P-tau with [18F]MK6240 binding	Chamoun | Kang | Pascoal | Mathotaarachchi | Benedet | Shin | Therriault | Bouhachi | Hsiao | Massarweh | Chartrand | Soucy | Gauthier | Rosa-Neto	**Chamoun, Mira**
40	Initial evaluation of correspondence between tau PET ligand [F-18]MK6240 and cognitive status	Clark | Betthauser | Christian | Poetter | Sanson | Oh | Johnson	**Clark, Lindsay**
06	Comparison of parametric methods for visual assessment of [18F]Flutemetamol amyloid PET images in a cognitively healthy elderly population	Collij | Konijnenberg | Reimand | ten Kate | den Braber | Lopes Alves | Zwan | Yaqub | van Assema | Wink | Boomsma | Lammerstma | Scheltens | Visser | Barkhof | van Berckel	**Collij, Lyduine**
30	Simplified non-invasive tracer kinetic analysis for 18F-Florbetaben PET using a dual time-window acquisition protocol	De Santi | Barthel | Bullich | Koglin | Becker | Jovalekic | Stephens | Sabri	**De Santi, Susan**
16	Longitudinal tau quantitation with anatomically-guided PET image deblurring	Tabassum | Li | Becker | El Fakhri | Johnson | Dutta	**Dutta, Joyita**
14	Centiloid validation of multi-atlas PET-SUVR analysis in the multi-tracer AMYPAD study	Grecchi | Foley | Wolz | Gispert | Hill	**Grecchi, Elisabetta**
20	Optimized coffee-break protocol for quantitative [18F]flutemetamol studies	Heeman | Yaqub | Heurling | Lopes Alves | Gispert | Foley | Lammertsma | AMYPAD Consortium	**Heeman, Fiona**
12	A theoretical and empirical investigation of imperfect reference regions	Heurling | Smith | Strandberg | Ohlsson | Hansson | Schöll	**Heurling, Kerstin**
04	Optimal reference region analysis for [18F]MK6240 based on full kinetic modeling	Kang | Pascoal | Chamoun | Mathotaarachchi | Shin | Benedet | Therriault | Savard | Knight | Hsiao | Bouhachi | Massarweh | Chakravarty | Chartrand | Bennacef | Ng | Soucy | Gauthier | Rosa-Neto	**Kang, Min Su**
23	Methodologic considerations for calculating standard uptake value ratio amyloid reduction in the Gantenerumab open label extension studies	Klein | Delmar | Abi-Saab | Andjelkovic | Milosavljevic-Ristic | Seibyl | Marek | Martenyi | Baudler | Fontoura | Doody	**Klein, Gregory**
34	Development of thiophene-based optical ligands that selectively detect tau pathology in Alzheimer's disease	Shirani | Appelqvist | Bäck | Klingstedt | Cairns | Svensson | Nilsson	**Klingstedt, Therése**
41	Low-dose NeuroPET scans for longitudinal PET: a feasibility study with Flortaucipir	Lois | Grogg | Schultz | Price | Johnson	**Lois, Cristina**
27	The impact of PET reconstruction method on measured amyloid SUVR	Matthews | Andrews | Smith	**Matthews, Dawn**
39	Structure-binding relationship of quinoline derivatives on monoamine oxidase B	Okamura | Harada | Furumoto | Arai | Yanai | Kudo	**Okamura, Nobuyuki**

Board #	Poster Title	Authors	Presenter
WEDNESDAY – POSTER SESSION 1			
25	Prediction of cognitive decline by 18F-AV45 PET normalized to subcortical white matter reference region	Ottoy | Niemantsverdriet | Verhaeghe | De Roeck | Struyfs | Somers | wyffels | Van den Bossche | Van Mossevelde | Ceyssens | Stroobants | Bjerke | Engelborghs | Staelens	**Ottoy, Julie**
36	Voxel-wise determination of thresholds and accuracy of [18F]AV1451 and [18F]MK6240 ligands for neurofibrillary tangles	Pascoal | Mathotaarachchi | Chamoun | Kang | Therriault | Struyfs | Ng | Savard | Shin | Knight | Benedet | Massarweh | Chakravarty | Soucy | Chartrand | Gauthier | Rosa-Neto	**Pascoal, Tharick**
32	Amyloid tracer harmonization using a bootstrapped non-linear mapping	Properzi | Buckkley | Mormino | Price | Sperling | Johnson | Schultz1	**Properzi, Michael**
10	Performance of supratentorial white matter reference regions for longitudinal quantification of [18F]flutemetamol PET scans	Salvadó | Foley | Grecchi | Cardoso | Lopes-Alves | Markiewicz | Falcon | Battle | Lammertsma | Schmidt | Barkhof | Molinuevo | Gispert | AMYPAD Consortium	**Salvadó, Gemma**
08	Optimal centiloid transformations when using measurement methods differing in acquisition parameters and in quantification software	Schwarz | Tosakulwong | Senjem | Gunter | Therneau | Vemuri | Lowe | Jack	**Schwarz, Christopher**
22	Reduced acquisition time PET quantification applied to [18F]-florbetapir	Scott | Jiao | Melbourne | Markiewicz | Schott | Hutton | Ourselin	**Scott, Catherine**
15	PET scanner variance in multi-center clinical trials using the Hoffman Phantom	Adamczuk | Pannetier | Pham | Gorman | Runkle | Scott | Suhy	**Scott, David**
29	Longitudinal change in brain perfusion in cognitively normal elderly subjects measured by early frames Florbetapir F 18 PET	Shcherbinin | Schwarz | Su | Charil | Hornbeck | Christensen | Eads | Benzinger | Sims	**Shcherbinin, Sergey**
07	Validation of a new semi-quantitative tau-PET analysis without image intensity normalization	Shokouhi | Kang | Gwirtsman	**Shokouhi, Sepi**
04	The correlation of amyloid peptides with FDG PET scan in diagnosis of Alzheimer's disease	Soni | Medhi | Modi | Goyal | Mohanty | Singh | V Y | Jangir | Sarma	**Soni, Hariom**
24	A non-invasive optical retinal imaging method to predict cerebral amyloid PET status	Soucy | Chevrefils | Sylvestre | Arbour | Rhéaume | Beaulieu | Rosa-Neto | Mathotaarachchi | Nasreddine | Gauthier | Lesage	**Soucy, Jean-Paul**
26	Centiloid analysis in cross-sectional and longitudinal PiB PET studies	Su | Flores | Hornbeck | Speidel | Vlassenko | Gordon | Koeppe | Mintun | Klunk | Xiong | Morris | Benzinger	**Su, Yi**
21	Characterization of [3H]SIL26 binding to alpha-synuclein fibrils	Svensson | Paslawski | Svenningsson | Sohn | Strom | Sandell	**Svensson, Samuel**
33	In vivo assessment of several 18F SV2A PET tracers	Carroll | Alagille | Tress | Mistico | Constantinescu | Sandiego | Papin | Gouasmat | Zheng | Marek | Seibyl | Barret | Tamagnan	**Tamagnan, Gilles**
17	Tau and alpha synuclein selective binding compounds derived from Aprinoia Therapeutics' PM-PBB3 binding-site focused compound collection	Tempest | Jang | Tai | Higuchi | Ono | Shimada | Suhara | Zhang | Tamagnan | Carroll | Marek | Seibyl | Alagille | Barret	**Tempest, Paul**
03	Regional distribution, asymmetry, and clinical correlates of tau uptake on [18f]av-1451 PET in atypical Alzheimer's disease	Tetzloff | Graff-Radford | Tosakulwong | Martin | Machulda | Duffy | Clark | Senjem | Spychalla | Drubach | Jack Jr. | Lowe | Josephs | Whitwell	**Tetzloff, Katerina**
35	Unbiased assessment of global amyloid load as determined by Voxel-wise receiver operating characteristic analysis	Therriault | Pascoal | Mathotaarachchi | Alves | Collij | Kang | Savard | Benedet | Knight | Ng | Shin | Chamoun | Massarweh | Soucy | Gauthier | Rosa-Neto	**Therriault, Joseph**
01	Differing patterns of [18F]AV-1451 uptake in primary progressive apraxia of speech and agrammatic primary progressive aphasia	Utianski | Schwarz | Duffy | Clark | Machulda | Senjem | Jack | Lowe | Whitwell | Josephs	**Utianski, Rene**
11	Parametric imaging of [18F]florbetapir: a test-retest study in healthy subjects and patients with Alzheimer's disease	Verfaillie | Golla | van der Weijden | Timmers | Schober | Schuit | Windhorst | Scheltens | van der Flier | Lammertsma | van Berckel | Boellaard	**Verfaillie, Sander**
05	Sleep efficiency moderates the relationship between beta-amyloid and memory retention	Wilckens | Tudorascu | Snitz | Price | Aizenstein | Lopez | Erickson | Lopresti | Laymon | Minhas | Mathis | Buysse | Klunk | Cohen	**Wilckens, Kristine**

Board #	Poster Title	Authors	Presenter
WEDNESDAY – POSTER SESSION 1			
42	Parametric methods for [18F]flortaucipir PET	Wolters | Golla | Timmers | Ossenkoppele | van der Weijden | Scheltens | Schwarte | Mintun | Devous | Schuit | Windhorst | Lammertsma | Yaqub | van Berckel | Boellaard	**Wolters, Emma**
43	Improved quantification of [18F]flortaucipir uptake in the hippocampus after partial volume correction	Wolters | Golla | Timmers | Ossenkoppele | van der Weijden | Scheltens | Schwarte | Mintun | Devous | Schuit | Windhorst | Barkhof | Yaqub | Lammertsma | Boellaard | van Berckel	**Wolters, Emma**
44	Amyloid deposition is associated with different patterns of hippocampal connectivity in men versus women	Wu | Thurston | Tudorascu | Karim | Mathis | Lopresti | Kamboh | Cohen | Snitz | Klunk | Aizenstein	**Wu, Minjie**
18	Noise reduction algorithm for amyloid image preserving image resolution — quantitative evaluation using clinical images	Yamada | Kimura | Fuji | Watanabe | Nagaoka | Nemoto | Hanaoka | Kaida | Hosokawa | Ishii	**Yamada, Takahiro**
28	Head-to-head comparison of 11C-PBR28 and 18F-GE180 for the quantification of TSPO in the human brain	Zanotti Fregonara | Pascual | Rizzo | Yu | Pal | Beers | Carter | Appel | Atassi | Masdeu	**Zanotti Fregonara, Paolo**
02	PBR-28 binding is elevated in Alzheimer's disease but not in suspected non-AD pathophysiology	Zou | Razlighi | Klein | Polly | Stern | Kreisl	**Zou, James**

P1: Differing patterns of [18F]AV-1451 uptake in primary progressive apraxia of speech and agrammatic primary progressive aphasia

Rene Utianski, Christopher Schwarz, Joseph Duffy, Heather Clark, Mary Machulda, Matthew Senjem, Clifford Jack, Val Lowe, Jennifer Whitwell, Keith Josephs

Mayo Clinic, Rochester, MN, US

Background: Recent research demonstrated elevated [18F]AV-1451 uptake in supplementary and superior premotor cortices in patients with primary progressive apraxia of speech (PPAOS) when compared to healthy controls. In this follow-up study, we compare patterns of tau tracer uptake in patients with PPAOS to a group of patients with agrammatic variant of primary progressive aphasia (agPPA), a disorder of language, given that some patients with agPPA have apraxia of speech.

Aim: The goal of the current study was to investigate differences in tau tracer uptake patterns in patients with PPAOS and agPPA.

Methods: Eleven patients with PPAOS and nine patients with agPPA (without AOS) underwent tau-PET imaging with [18F]AV-1451 and amyloid-PET imaging using Pittsburgh Compound B (PiB). Uptake of [18F]AV-1451 was assessed as cortical to cerebellar crus ratios (SUVr) in cortical regions of interest measured using the MCALT atlas, and compared voxel-wise in SPM12. A global PiB ratio>1.42 was deemed amyloid positive. Each patient was age- and sex-matched to three controls.

Results: Regions of abnormal [18F]AV-1451 tracer uptake differed between patients with agPPA and PPAOS. Greater tau tracer uptake was present in regions of the language network (e.g. left Broca's and Wernicke's areas and angular gyrus) in agPPA patients compared to both matched controls and PPAOS patients. Tau tracer uptake was never greater in controls or PPAOS patients than in agPPA patients. Seven PPAOS and seven agPPA patients were PiB negative although PiB status did not appear to affect tracer uptake in either group.

Conclusions: This study demonstrates [18F]AV-1451 tracer uptake in patients with agPPA in regions known to be involved with language processing. The patterns of tau tracer uptake differed between PPAOS, a motor speech disorder, and agPPA, a disorder of language, supporting an association of area of tau tracer uptake and clinical presentation.

Figure 1. Partial volume corrected (PVC) tau-PET SUVrs (x-axis) and the associated top 20 AUROCS (y-axis), ranked from highest to lowest AUROC (value listed in each panel). * denotes AUROC values whose 95% confidence interval excluded 0.5.

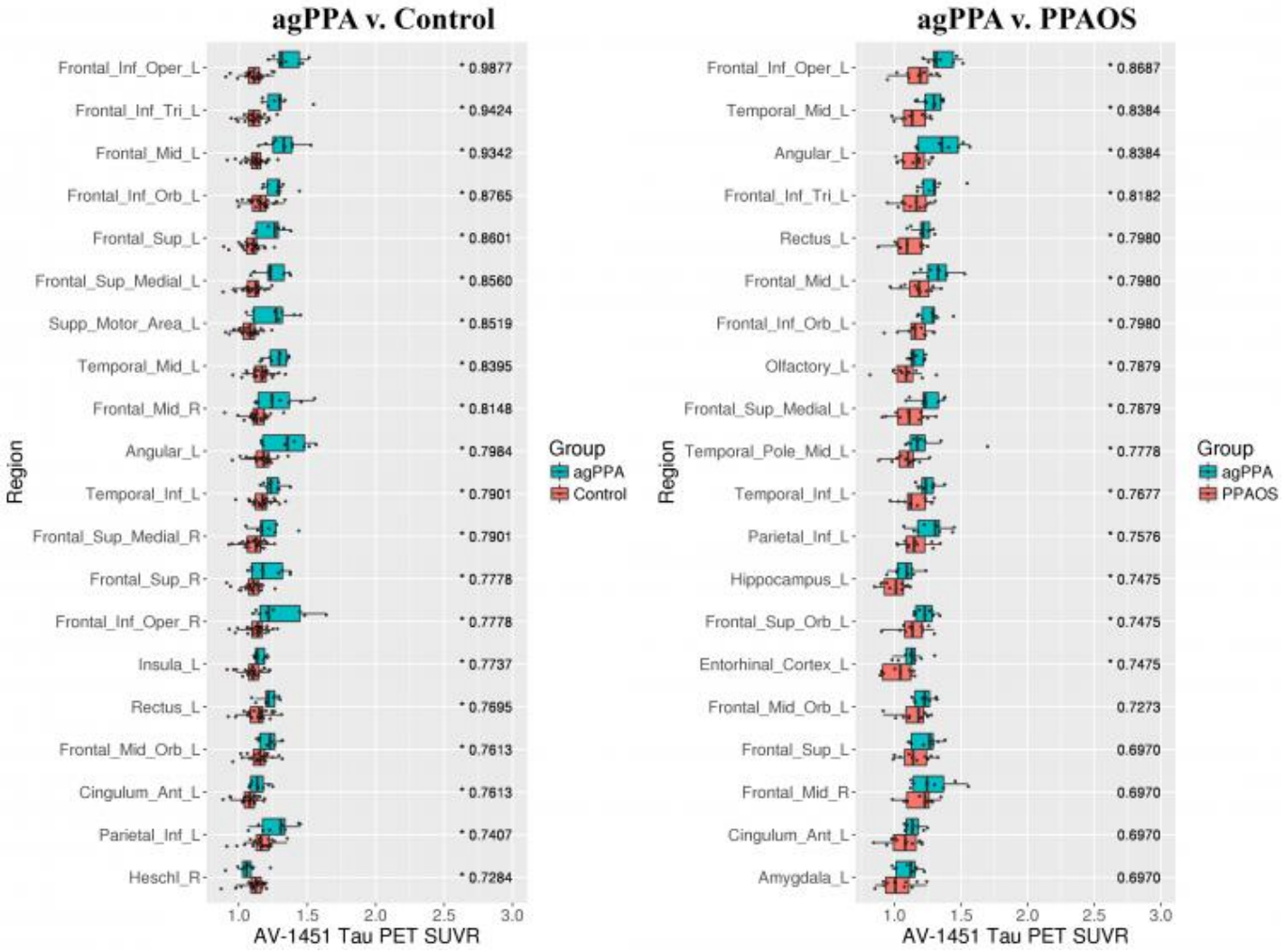

Figure 2. Regions where partial volume-corrected AV-1451 Tau PET SUVr was significantly (FDR-corrected p<0.05, extent >50 voxels) larger in agPPA than in PPAOS, displayed on a semitransparent 3D brain render.

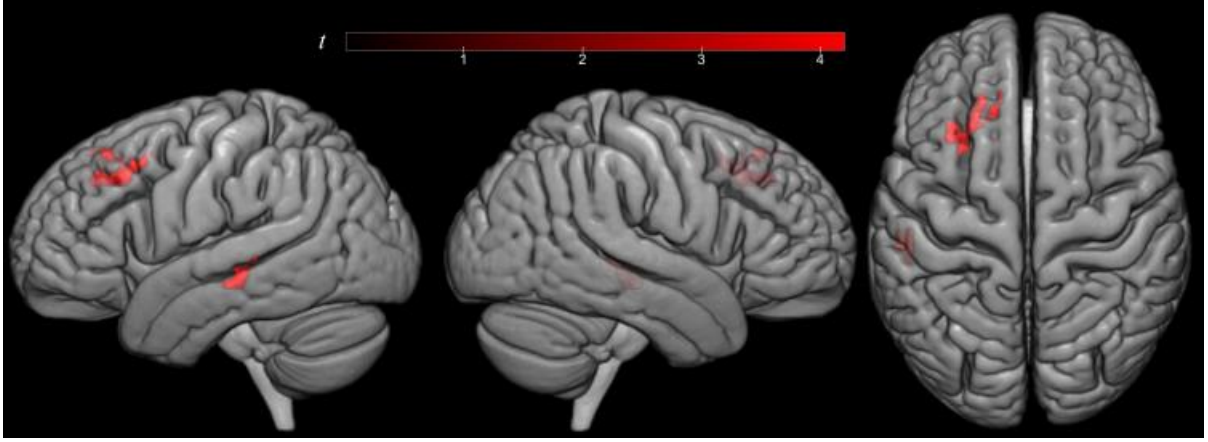

Figure 3. Regions where partial volume-corrected AV-1451 Tau PET SUVr was significantly (FDR-corrected p<0.05, extent >50 voxels) larger in agPPA than in controls, displayed on a semitransparent 3D brain render.

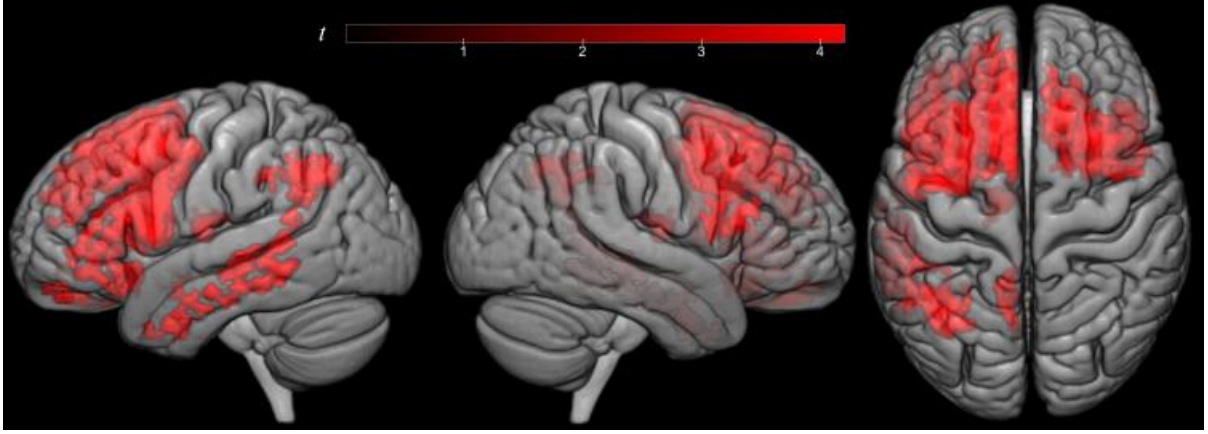

Keywords: primary progressive aphasia, primary progressive apraxia of speech, amyloid imaging, tau imaging

P2: PBR-28 binding is elevated in Alzheimer's disease but not in suspected non-AD pathophysiology

James Zou, Qolamreza Razlighi, Julia Klein, Krista Polly, Yaakov Stern, William Kreisl

Columbia University Taub Institute for Research on Alzheimer's Disease and the Aging Brain, New York, NY, US

Background: It remains unclear if neuroinflammation is a primary contributor to Alzheimer's disease (AD) or a nonspecific response to neurodegeneration. We sought to determine if the amount of 18 kDa translocator protein (TSPO) – a microglial activation marker – differed between cognitively impaired patients with biomarker evidence of AD and impaired patients with suspected non-AD pathophysiology.

Methods: Eighteen patients meeting clinical criteria for amnestic mild cognitive impairment (MCI) or mild AD who had evidence of hippocampal atrophy on MRI underwent florbetaben PET to determine amyloid status. Fifteen amyloid-negative controls were also included. ^{11}C-PBR-28 PET images were acquired 60-90 minutes post-injection. Scans were corrected for partial volume effects and gray matter regions were extracted using the Hammers atlas in PMOD. Standardized uptake value ratios were calculated using cerebellar gray matter as a "pseudo-reference" region. TSPO genotyping was performed.

Results: Among cognitively impaired patients, 12 were amyloid-positive and 6 were amyloid-negative (Table 1). ^{11}C-PBR-28 binding in amyloid-positive patients was greater than controls in prefrontal cortex, middle and inferior temporal gyrus, superior temporal gyrus, medial temporal cortex, posterior cingulate gyrus, superior parietal lobule and inferior parietal lobule ($P < 0.003$). ^{11}C-PBR28 binding in amyloid-positive patients was greater than amyloid-negative patients in posterior cingulate ($P = 0.001$), superior parietal lobule ($P = 0.01$), and inferior parietal lobule ($P < 0.05$). No difference in ^{11}C-PBR28 binding was seen between amyloid-negative patients and controls in any region.

Conclusion: Among patients meeting clinical criteria for amnestic MCI or mild AD, those who are amyloid-positive on PET have greater TSPO binding than those who are amyloid-negative, despite hippocampal atrophy in both groups. This suggest that microglial activation is not simply a response to neurodegeneration but is associated with cerebral amyloidosis. Neuroinflammation may therefore play a stronger role in AD than in non-AD pathologies that also cause hippocampal atrophy and memory impairment.

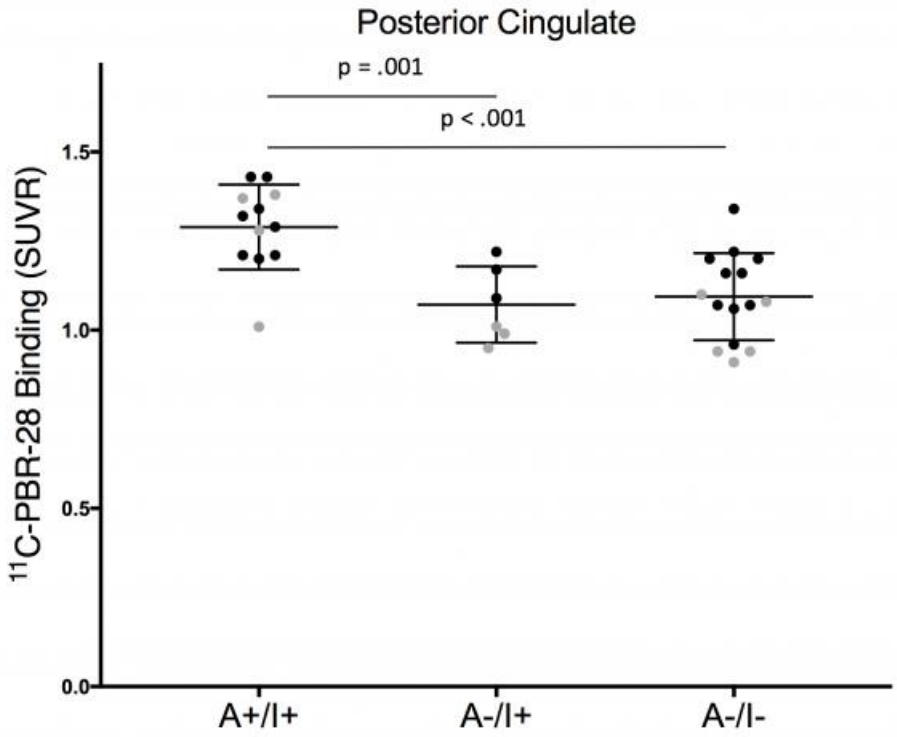

Figure 1: ^{11}C-PBR28 binding is increased in amyloid-positive cognitively-impaired subjects (A+/I+), with no difference between amyloid-negative impaired subjects (A-/I+) and amyloid-negative controls (A-/I-). High affinity and Mixed affinity TSPO binders are represented by black and grey respectively. Error bars denote mean ± SD.

Table 1: Clinical characteristics of study subjects.

Profile	Age	Sex (Male/female)	Years of education	TSPO genotype (HAB/MAB)	MMSE*	SRT-DR (z-score)**
Amyloid (+) Impaired	65.0 ± 8.7	11/1	17.8 ± 1.5	8/4	24.1 ± 4.3†	-2.6 ± 1.3††
Amyloid (-) Impaired	71.7 ± 8.5	3/3	15.2 ± 3.3	3/3	27 ± 4.0	-1.9 ± 0.74††
Amyloid (-) Control	67.3 ± 3.9	4/11	15.7 ± 2.8	10/5	29.4 ± 0.8	0.77 ± 0.99

MMSE = Mini Mental State Exam, SRT-DR = Selective Reminding Test – Delayed Recall, HAB = high affinity binder, MAB = mixed affinity binder.
* Data missing for 2 amyloid (-) controls
** Data missing for 1 amyloid (+) impaired subject who could not complete testing
† $P = 0.001$ *vs.* amyloid (-) controls
†† $P < 0.001$ *vs.* amyloid (-) controls

Keywords: Alzheimer's Disease, Neuroinflammation, Suspected Non-AD pathophysiology (SNAP), [11C]-PBR-28

P3: Regional distribution, asymmetry, and clinical correlates of tau uptake on [18f]av-1451 PET in atypical Alzheimer's disease

Katerina Tetzloff, Jonathan Graff-Radford, Nirubol Tosakulwong, Peter Martin, Mary Machulda, Joseph Duffy, Heather Clark, Matthew Senjem, Anthony Spychalla, Daniel Drubach, Clifford Jack Jr., Val Lowe, Keith Josephs, Jennifer Whitwell

Mayo Clinic, Rochester, MN, US

Introduction: Alzheimer's disease (AD) can have multiple clinical presentations, which pathological studies suggest result from differences in the regional distribution of tau pathology. Positron emission tomography (PET) ligands that can detect tau proteins in vivo provide the opportunity to investigate the biological mechanisms underlying atypical presentations of AD. We aimed to assess regional patterns of tau uptake on [18F]AV-1451 PET imaging in two atypical AD variants, posterior cortical atrophy (PCA) and logopenic progressive aphasia (lvPPA).

Methods: Twenty-five atypical AD subjects that showed beta-amyloid deposition on PET were included in the study (12 PCA, 13 lvPPA) and were age and gender-matched to 56 controls. All subjects underwent [18F]AV-1451 PET and 3T volumetric MRI. Group comparisons of tau uptake were performed using both voxel- and region-level analyses. The degree of lobar tau asymmetry was also calculated. Regional tau uptake was correlated both to age and performance on clinical evaluations.

Results: Both PCA and lvPPA showed diffuse tau uptake throughout all cortical regions (Figure). However, PCA showed greater tau uptake in occipital regions compared to lvPPA (Figure), and there was some evidence in the region-level analysis that lvPPA showed increased uptake in left superior frontal lobe and temporal pole compared to PCA. Tau deposition in lvPPA showed a predominant left-sided asymmetry, while deposition in PCA was more bilateral with a tendency towards right-sided asymmetry. Younger subjects showed significantly greater tau uptake in frontal and parietal lobes. Tau uptake in left frontal and temporal lobes correlated with performance on sentence repetition, and uptake in the right occipital lobe correlated to severity of simultanagnosia and visuoperceptual impairment.

Conclusions: Tau deposition, as measured by [18F]AV-1451 PET imaging, is closely related to clinical presentation in the atypical AD variants of PCA and lvPPA, with age being a significant factor in determining the degree of cortical tau deposition.

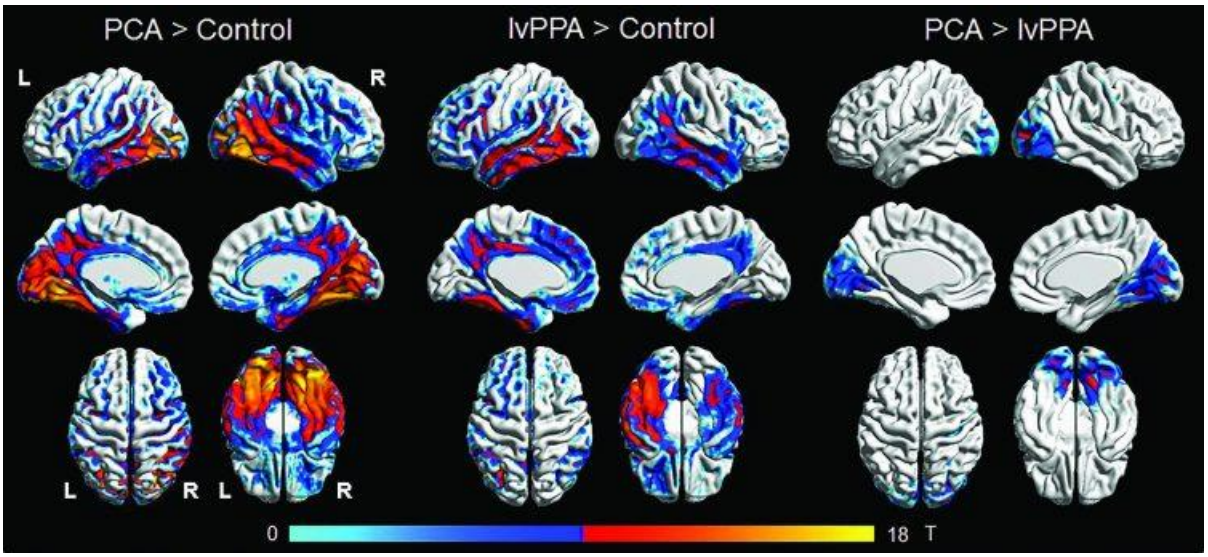

Keywords: tau, positron emission tomography, neuroimaging, dementia, aphasia

P4: Optimal Reference region analysis for [18F]MK6240 based on full kinetic modeling

Min Su Kang[1,2], Tharick A. Pascoal[1,2], Mira Chamoun[1,2], Sulantha Mathotaarachchi[1,2], Monica Shin[1,2], Andrea Benedet[1,2], Joseph Therriault[1,2], Melissa Savard[1,2], Ashley Knight[1,2], Chris Hsiao[3], Reda Bouhachi[3], Gassan Massarweh[3], Mallar Chakravarty[2], Daniel Chartrand[3], Idriss bennacef[4], Kok Pin Ng[1,2], Jean-Paul Soucy[3], Serge Gauthier[2], Pedro Rosa-Neto[1,2]

[1]Translational Neuroimaging laboratory - McGill Centre for Studying in Aging, Montreal, QC, Canada
[2]Brain Imaging Centre – Douglas Research Centre, Montreal, QC, Canada
[3]McConnell Brain Imaging Centre – McGill University, Montreal, QC, Canada
[4]3Translational Biomarkers, Merck & Co., Inc., West Point, PA, US

Background: There has been unmet needs for in vivo imaging techniques to accurately quantify the neurofibrillary tangles (NFT) in the brain. A novel positron emission tomography (PET) tracer, [^{18}F]MK6240, has been introduced to specifically bind to NFT with no off-target binding in the in vitro assays. Here, we conducted 3 hours scans with full quantification, including arterial input with metabolite correction as a gold standard, to assess and validate the reference tissue methods.

Methods: Total 5 patients underwent 3 hours PET scans in HRRT with continuous arterial sampling using Twilite. We collected 8 blood samples to calculate the parent fraction and metabolite level throughout the scan. The target regional [^{18}F]MK6240 were quantified with 2 Tissue Compartment Model (2TCM) VT while non-target regions were quantified with Logan VT. Then, the nondisplacable (ND) binding compartments from 2TCM in the targets were compared to Logan VT in the non-targets to assess the level of ND binding. Also, 2TCM VT in the targets were associated with Logan reference region method (DVR) to validate the reference tissue method. Last, the stability of the reference regional signals was assessed based on the mean square error.

Results: Out of 7 potential reference regions investigated (cerebellar grey, cerebellar vermis, pons, striatum, white matter, Cerebellar grey&Pons, Cerebellar Vermis&Pons), striatum and white matter showed significantly different level of ND binding compared to the target ND binding. Furthermore, cerebellar grey, cerebellar vermis, and pons showed significant correlation between VT and DVR in the targets. Although Pons was the only region preferably fitted 1TCM than 2TCM, the cerebellar grey demonstrated the most stable signal with the least mean square error value.

Conclusion: Our study suggests that Pons fits the reference region profile. However, cerebellar grey may be optimal for the quantification of [^{18}F]MK6240 in daily practice given high variability of Pons signal.

Keywords: tau, PET, reference region, kinetic modeling, Imaging

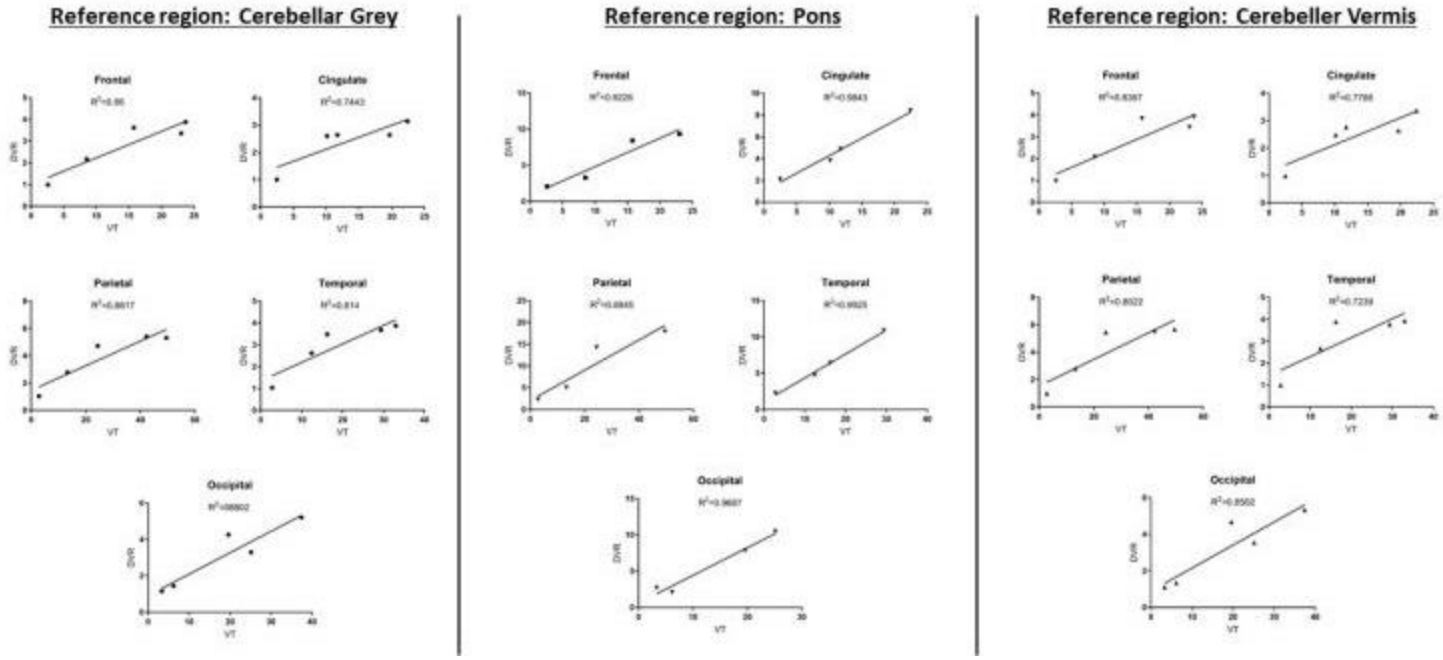
Reference region: Cerebellar Grey
Reference region: Pons
Reference region: Cerebeller Vermis
Frontal
Cingulate
Parietal
Temporal
Occipital
DVR
VT

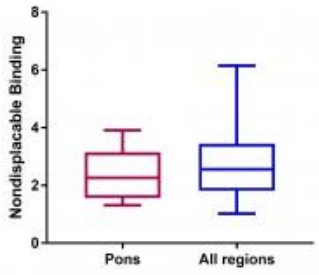
Nondisplacable Binding
Pons
All regions

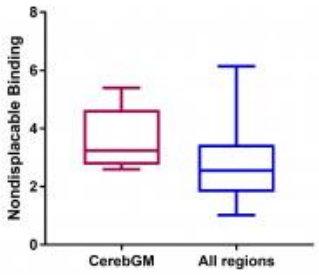
Nondisplacable Binding
CerebGM
All regions

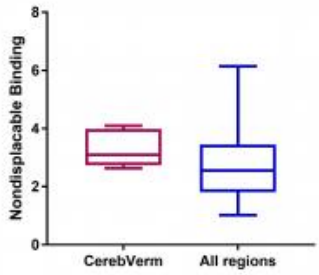
Nondisplacable Binding
CerebVerm
All regions

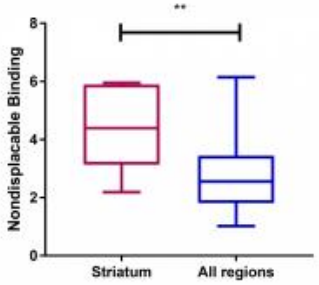
**
Nondisplacable Binding
Striatum
All regions

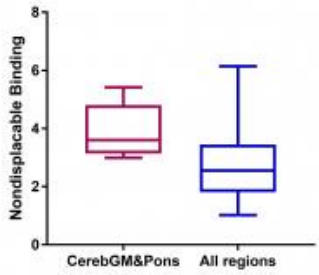
Nondisplacable Binding
CerebGM&Pons
All regions

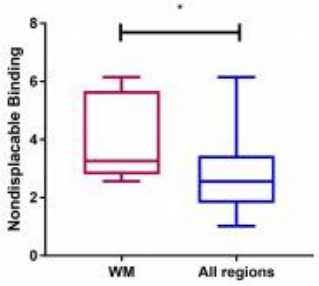
*
Nondisplacable Binding
WM
All regions

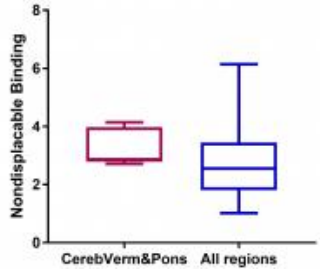
Nondisplacable Binding
CerebVerm&Pons
All regions

P5: Sleep efficiency moderates the relationship between beta-amyloid and memory retention

Kristine Wilckens[1], Dana Tudorascu[1], Beth Snitz[1], Julie Price[2], Howard Aizenstein[1], Oscar Lopez[1], Kirk Erickson[1], Brian Lopresti[1], Charles Laymon[1], Davneet Minhas[1], Chester Mathis[1], Daniel Buysse[1], William Klunk[1], Ann Cohen[1]

[1]*University of Pittsburgh, Pittsburgh, PA, US*
[2]*Massachusetts General Hospital, Charlestown, MA, US*

Introduction: Amyloid-β (Aβ) accumulation is a marker of Alzheimer's disease, but presence of Aβ is not sufficient to bring about symptoms of cognitive impairment. Modifiable health factors, including sleep health, cognitive activity, and physical fitness are hypothesized to mitigate progression of cognitive decline and neurodegeneration with aging. Specifically, measures of sleep efficiency such as wake after sleep onset are consistently associated with cognitive performance in older adults.

Objectives: Here we assessed whether wake after sleep onset moderated the relationship between Aβ deposition and neuropsychological performance assessed with memory recall using the Rey-Osterrieth Complex Figure task, switching using the Trail-making task, and FAS verbal fluency.

Methods: Participants were 41 older adults (28 cognitively healthy and 13 cognitively impaired) ages 68-100, mean = 86.32. Aβ was assessed with a global measure of Pittsburgh Compound B (PiB). A hierarchical linear regression model with each neuropsychological measure as the dependent variable, and wake after sleep onset and Aβ and their interaction as the independent variables was performed.

Results: Wake after sleep onset significantly moderated the relationship between amyloid deposition and immediate ($\beta = 0.42$, $p = 0.01$) and delayed memory recall ($\beta = 0.47$, $p = 0.002$) corrected for multiple comparisons: among individuals with higher Aβ, less wake after sleep onset was associated with better memory recall. There were no moderating associations for switching or verbal fluency, p's > 0.30. These results support the general hypothesis that sleep relates to cognitive function, and specifically suggest that higher sleep efficiency mitigates the association between Aβ and memory recall. Future work should evaluate the potential protective role of sleep efficiency in memory impairment and progression of Alzheimer's disease.

Keywords: amyloid-β, sleep, neuropsychological performance, mild cognitive impairment, preclinical Alzheimer's disease

P6: Comparison of parametric methods for visual assessment of [18F]Flutemetamol amyloid PET images in a cognitively healthy elderly population

Lyduine E. Collij[1], Elles Konijnenberg[2], Juhan Reimand[3], Mara ten Kate[2], Anouk den Braber[2,4], Isadora Lopes Alves[1], Marissa Zwan[2], Maqsood M. Yaqub[1], Danielle M.E. van Assema[1], Alle Meije Wink[1], Dorret I. Boomsma[2], Adriaan A Lammerstma[1], Philip Scheltens[2], Pieter Jelle Visser[2], Frederik Barkhof[1,5], Bart N.M. van Berckel[1]

[1]*Department of Radiology and Nuclear Medicine, VU University Medical Center, Amsterdam, Netherlands*
[2]*Alzheimer Center, VU University Medical Center, Amsterdam, Netherlands*
[3]*Centre of Radiology, North Estonia Medical Centre, Tallinn, Estonia*
[4]*Dept. of Biological Psychology, VU University, Amsterdam, Netherlands*
[5]*Institute of Neurology and Healthcare Engineering, University College London, London, United Kingdom*

Background: Reliable *in-vivo* identification of amyloid pathology in the cognitively healthy elderly population is of utmost importance, considering the shift in research focus to this population. Visual interpretation of semi-quantitative standardized uptake value ratios (SUVr) images is thought to be sufficient for this purpose. However, SUVr overestimates amyloid burden and shows lower inter-reader agreement compared to fully quantitative non-displaceable binding potentials (BP_{ND}).

Objective: Compare two methods for visual assessment of [^{18}F]flutemetamol images in a cognitively healthy elderly population.

Methods: Dynamic [^{18}F]flutemetamol scanning was performed in 190 participants (mean age 70.44 ± 7.56 ys, 59.5% female, mean MMSE score 29 ± 1.13). BP_{ND} and SUVr images with cerebellar grey matter as a reference region were generated. Images were visually assessed by 3 independent readers. Inter-reader agreement was calculated using Fleiss Kappa.

Results: Inter-reader agreement was moderate for SUVr images (Fleiss $\kappa = .57$) and good for BP_{ND} images (Fleiss $\kappa = .77$). Discordant reads were observed in 35 cases (18.4%) using SUVr and in 15 cases (7.9%) using BP_{ND}, of which 9 cases were overlapping (**Figure 1**). (Semi-)quantitative SUVr and BP_{ND} values showed a strong correlation ($\rho = .83$, $p < .01$). Concordant positive cases had a significantly higher SUVr and BP_{ND} value than concordant negative cases ($p < .01$).
Based on the concordant cohort (N = 149), the cut-off for SUVr was calculated at 1.52 and for BP_{ND} at .26. Nearly all SUVr discordant cases were below these cut-off values for both SUVr and BP_{ND} (**Figure 2A**). The BP_{ND} visual read was in accordance with the quantitative value for the cases with discordant inter-method visual read, while SUVr was not (**Figure 2B**).

Conclusion: The differences in inter-reader agreement support the use BP_{ND} parametric images for visual assessment of [^{18}F]flutemetamol in a population with low amyloid burden.

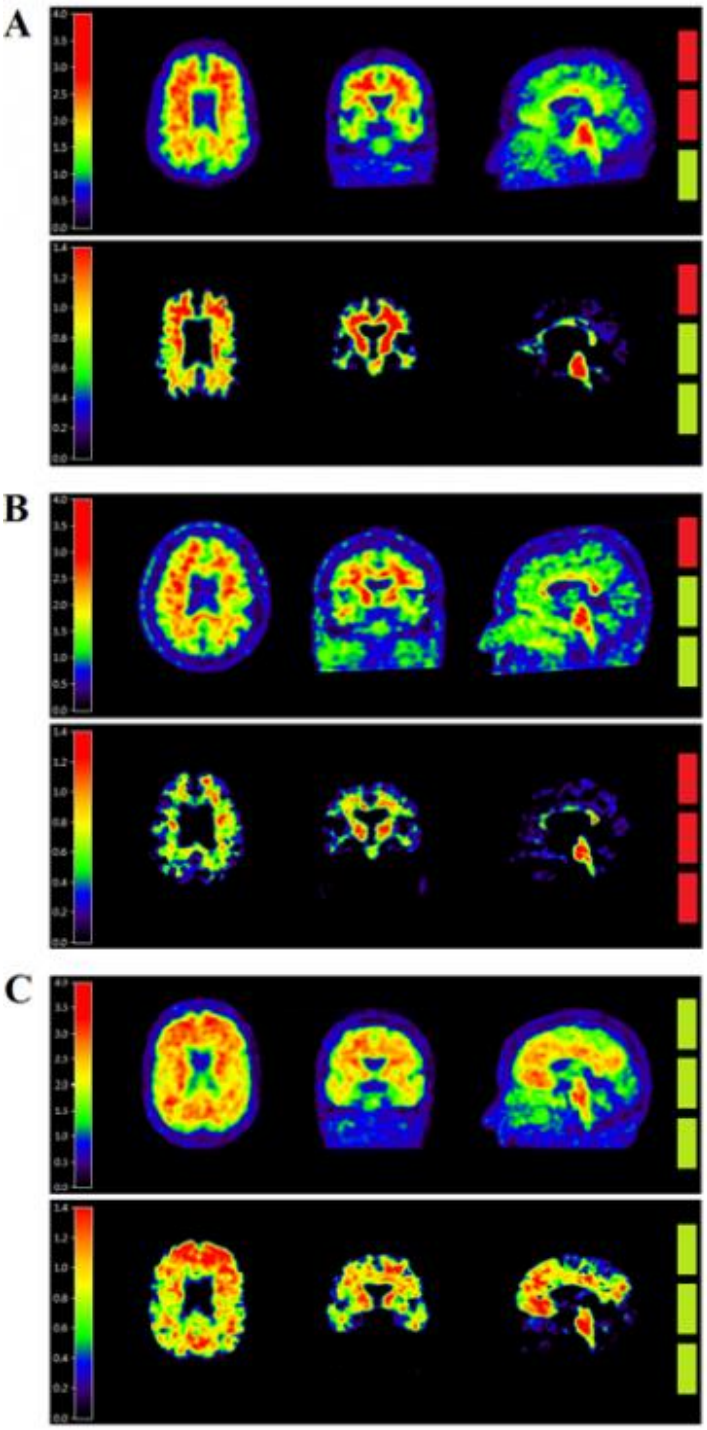

Figure 1.Examples visual read

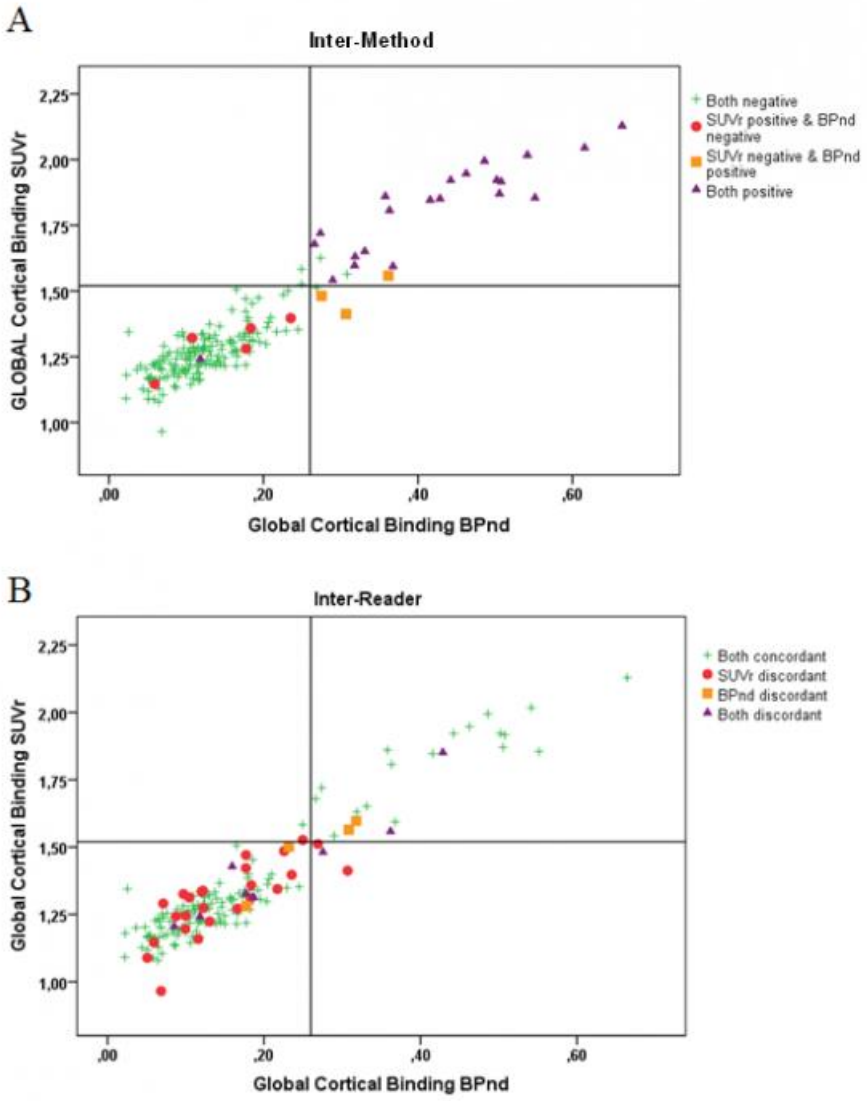

Keywords: flutemetamol, visual assessment, inter-reader agreement, BPnd parametric images

P7: Validation of a new semi-quantitative tau-PET analysis without image intensity normalization

Sepi Shokouhi[1], Hakmook Kang[2], Harry Gwirtsman[3]

[1]*Vanderbilt University Institute of Imaging Science, Nashville, TN, US*
[2]*Vanderbilt University Medical Center, Biostatistics, Nashville, TN, US*
[3]*Vanderbilt University Medical Center, Psychiatry, Nashville, TN, US*

The selection of an appropriate tau-PET reference region for image intensity normalization can be a challenge in several tauopathies, including progressive supranuclear palsy, and chronic traumatic encephalopathy. This study implements a novel image analysis approach, the weighted two-point correlation function (wS2), on tau-PET without requiring intensity normalization. As a way of validation, we applied this method to normalized and non-normalized ADNI PET images of 43 cognitively normal subjects to test whether the wS2 outcome is unaffected by the normalization process. We also determined the association between wS2 and subjects' CSF Aβ, tau, ptau, and cognition. Methods: We first sampled randomly distributed voxel-pairs (events) on each subject's 18F-AV1451 image. All events were weighted based on the intensity ratios between the sampled voxel-pairs and parsed by their corresponding distances to obtain the wS2 curves.

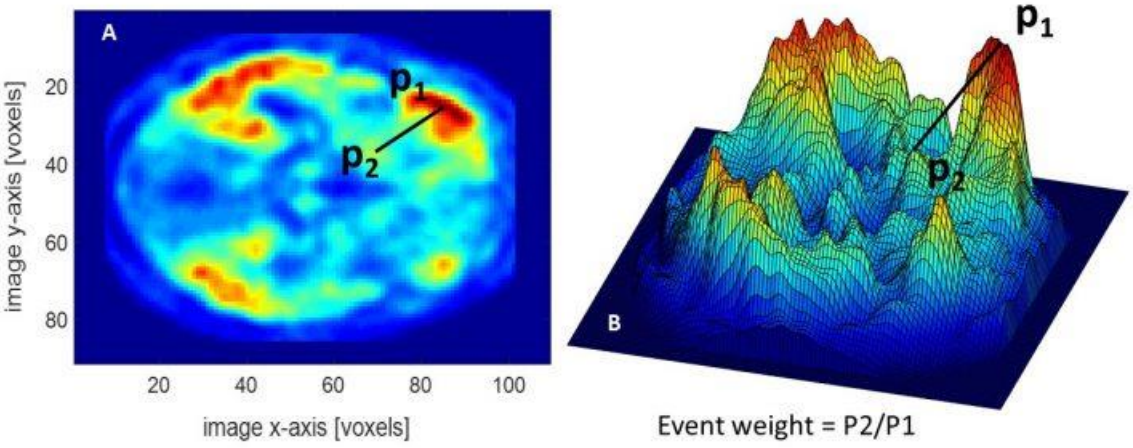

Figure 1: Illustration of a randomly sampled event in wS2 calculation. Figure 1.B shows the locations of the two sampled voxels in surface plot to highlight their corresponding slope. For each event, the weighting function was calculated as the ratio between the intensities of the two voxels.

The linear slopes were calculated on the wS2 log-plots and served as the outcome of this analysis. A linear regression was used to determine the associations between wS2 slopes and other biomarkers, and to help find the optimal range of sampled voxel-pair distances. While events at close distances are potentially affected by PET resolution limits, those at far distances may not correlate with changes in tau-pathology. Results: the wS2 outcomes of normalized and non-normalized images were the same. The associations between wS2 slopes, MMSE ($P<0.005$, $R=0.32$) and CSF-Aβ ($P<0.04$, $R=0.43$) were significant for all voxel-pair distances in ranges between 8-40 mm. However, the association to CSF-tau ($P=0.09$, $R=0.29$) and CSF-ptau ($P=0.08$, $R=0.2$) reached only marginal significance at 8-20 mm voxel-pair distances.

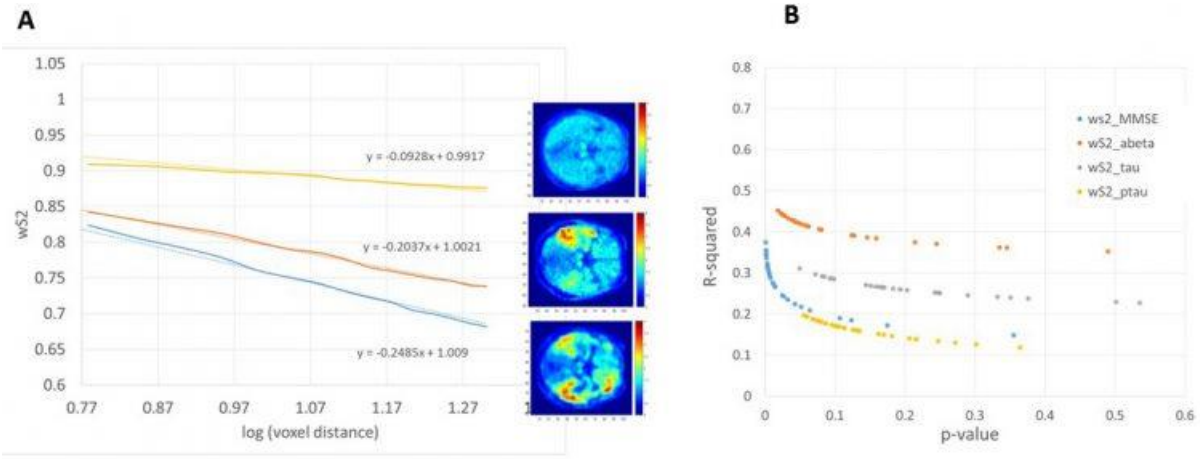

Figure 2: weighted two-point correlation (wS2) curves of three sample AV-1451 images (A). The linear slope was used as the outcome of the analysis. The association between ws2 outcome and MMSE scores, CSF Aβ,tau, and ptau for different ranges of voxel distances are shown in Figure 2.B.

For comparison, the global and regional ROIs provided similar associations to MMSE (P<0.01, R=0.28,0.2) and CSF-Aβ (P<0.06, R=0.42,0.47) but no significant correlation to tau and ptau. Conclusion: We validated a new tau-PET biomarker for potential future applications in tauopathies that pose a challenge for PET intensity normalization.

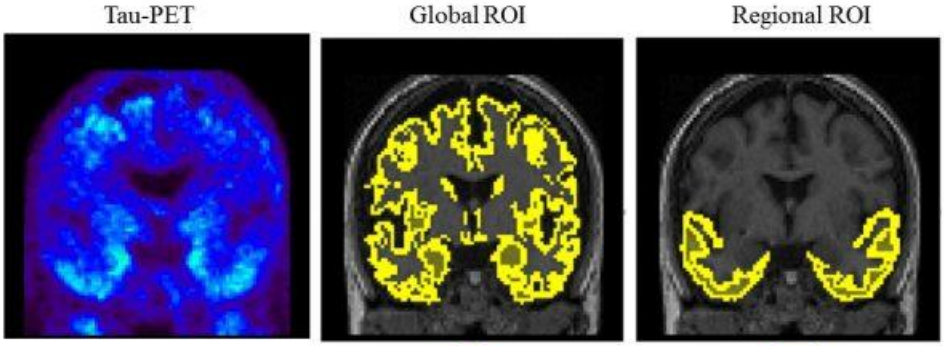

outcome	R-squared	P-value
MMSE	0.28	0.001
CSF-Aβ	0.42	0.006
CSF-tau	0.12	0.9
CSF-ptau	0	0.44

TABLE I

outcome	R-squared	P-value
MMSE	0.19	0.01
CSF-Aβ	0.47	0.001
CSF-tau	0.12	0.7
CSF-ptau	0.01	0.3

TABLE II

Figure 3: Global and regional ROIs were applied on AV-1451 images. The regional ROI included medial temporal lobe, transentorhinal cortex, fusiform gyrus, superior temporal gyrus following Schwarz et al. 2016. Associations between SUVR values and other biomarkers are presented in TABLES I & II.

Keywords: tau-PET, two-point correlation

P8: Optimal centiloid transformations when using measurement methods differing in acquisition parameters and in quantification software

Christopher Schwarz, Nirubol Tosakulwong, Matthew Senjem, Jeffrey Gunter, Terry Therneau, Prashanthi Vemuri, Val Lowe, Clifford Jack

Mayo Clinic, Rochester, MN, US

Background: The Centiloid scale provides a data transformation approach to standardize amyloid PET measurements for direct comparisons across sites and studies using different acquisition and/or quantification methods. Its authors recommend that sites using a method other than the "standard Centiloid method" perform a series of linear regressions to transform between each differing methodological variable separately, and then use the composite of these transforms to transform unscaled SUVR values into standard Centiloid units.

Methods: Our site uses PiB images acquired from 40-60 minutes post-injection (vs. 50-70 minutes used for the Centiloid method), and in-house image quantification software. According to the Centiloid approach, transforming our data requires the composite of two "level-2" transformations: one for the difference in acquisition times and one for the difference in quantification software (Figure 1). To optimize our approach, we calculated values for the standard Centiloid PiB dataset and performed our site's transformations in three ways: 1) the recommended 2-step linear-regression approach, 2) a single linear regression directly between the methods, and 3) a single Deming regression directly between the methods. For each transformation approach, we compared the transformed values with the reference values for same data, to determine which had the smallest mean difference i.e. best transformation accuracy.

Conclusions: All transformation approaches produced values that were within acceptable tolerance (within 2% of reference values) (Table 1). However, the one-step linear regression approach had the smallest differences, and we therefore considered it the most optimal. This data suggests that a one-step direct approach may produce slightly smaller errors, potentially due to fewer regression steps, than the standard two-step approach. Using this more optimized approach to calculate transformations may increase the precision of values reported in Centiloid units, thus improving the power of multi-site studies and meta-analyses.

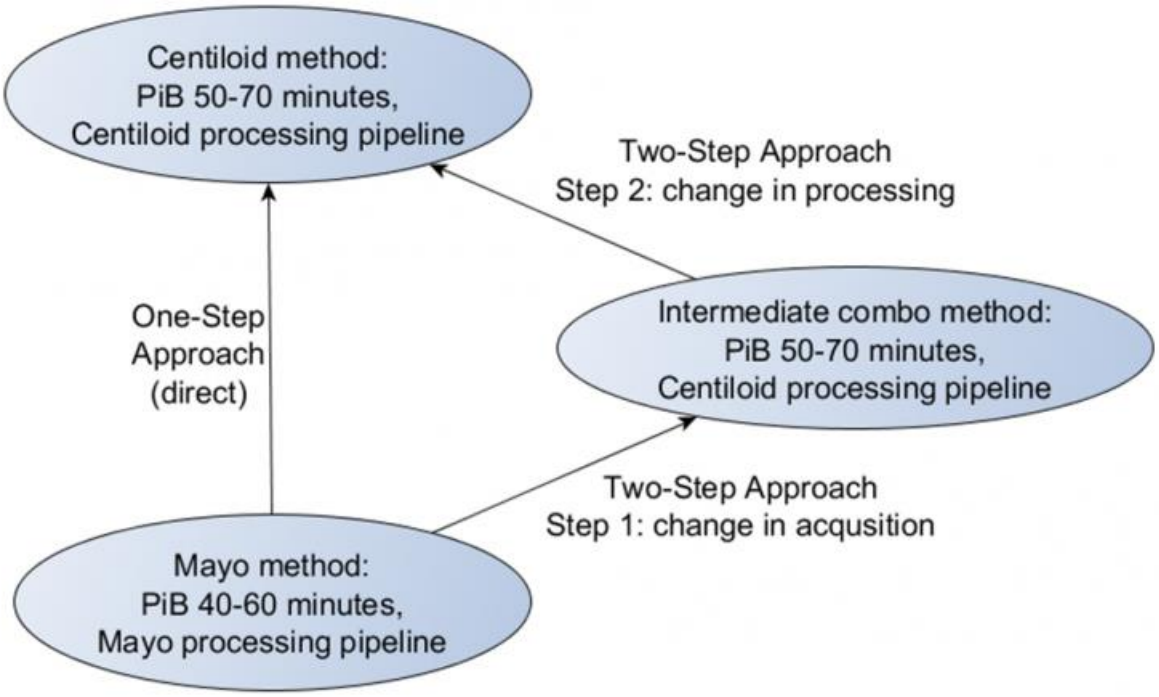

Figure 1: Illustration of the one-step and two-step approaches for Centiloid transformations, which we compare in this work.

	Young Controls group		AD group	
	Mean (SUVR)	Mean % Diff from Reference Values (SUVR)	Mean (SUVR)	Mean % Diff from Reference Values (SUVR)
Reference Values	1.0095	0.00%	2.0761	0.00%
1-Step Linear	1.0098	**0.03%**	2.0759	**-0.01%**
1-Step Deming	1.0172	0.76%	2.0703	-0.28%
2-Step Linear	1.0057	-0.38%	2.0790	0.14%

Table 1: Differences between the transformed SUVR values, from each of the tested transformation methods, and the published reference values.

Keywords: centiloid, PiB, regression, statistical methods, centiloid level-2 transforms

P9: Novel alpha-synuclein positron emission tomography (PET) tracers for the diagnosis of Parkinson's disease

Francesca Capotosti[1], Elpida Tsika[1], Jerome Molette[1], Myriam Ravache[1], Efthymia Vokali[1], Patrick Rodriguez[1], Aurelien Davranche[1], Vincent Darmency[1], Ajay Purohit[2], David Paterson[2], Heiko Kroth[1], Jan Stoehr[1], David Lowe[1], Andrea Pfeifer[1], Andreas Muhs[1]

[1]*AC Immune, Lausanne, Switzerland*
[2]*Biogen, Cambridge, MA, US*

Objectives: The accumulation of aggregated alpha-synuclein in form of Lewy bodies and Lewy neurites is the pathognomonic signature in patients with Parkinson's disease (PD) and other synucleinopathies. Currently, the diagnosis of PD and other synucleinopathies is solely based on the clinical evaluation of symptoms, indicating a strong unmet clinical need. The direct association between progressive formation of alpha-synuclein inclusions and severity of clinical symptoms supports the development of PET tracers for non-invasive examination of low-density alpha-synuclein aggregates in the human brain. Ultimately a PET tracer for alpha-synuclein will not only improve the diagnosis of PD but will also provide a biomarker for disease progression and will be useful in the evaluation of the efficacy of therapies aiming to reduce alpha-synuclein levels in the brain.

Methods: We designed and screened biochemically and *in vivo* low-molecular-weight compounds, with CNS-PET imaging properties that selectively bind to brain-derived pathological alpha-synuclein. Binding affinity and selectivity over other proteins pathological aggregates were evaluated by fluorescence staining, radiobinding assay, as well as autoradiography with ^{3}H compounds on human PD and Alzheimer's disease (AD) samples. Several ^{18}F radiolabeled compounds were, tested in rodent models for brain penetration and their general pharmacokinetic (PK) profile.

Results: Compounds derived from several different chemical series showed binding to Lewy bodies and Lewy neurites in human PD brain sections with (low) nanomolar affinities. These compounds were selective for alpha-synuclein aggregates over amyloid-beta aggregates as measured by autoradiography and radiobinding assays using AD patient-derived samples. Furthermore, PK profiling in rodents with ^{18}F radiolabeled compounds showed good and fast brain uptake as well as rapid washout.

Conclusions: We identified several compounds with potential for high affinity and selectivity for human PD-derived alpha-synuclein aggregates. Brain uptake and PK profiles are supportive for their further development as PET ligands to allow the direct imaging and possible diagnosis of synucleinopathies in humans.

Keywords: alpha-synuclein, PET, Parkinson's disease

P10: Performance of supratentorial white matter reference regions for longitudinal quantification of [18F]flutemetamol PET scans

Gemma Salvadó[1], Cristopher Foley[2], Elisabetta Grecchi[3], M. Jorge Cardoso[4], Isadora Lopes-Alves[5], Pawel Markiewicz[4], Carles Falcon[1], M Battle[2], Adriaan A. Lammertsma[5], Mark E. Schmidt[6], Frederik Barkhof[4,5], José Luís Molinuevo[1], Juan Domingo Gispert[1], on behalf of AMYPAD Consortium[7]

[1]*Barcelonabeta Brain Research Center, Barcelona, Spain*
[2]*GE Healthcare, Amersham, United Kingdom*
[3]*IXICO, London, United Kingdom*
[4]*University College London, London, United Kingdom*
[5]*VU Medical Center, Amsterdam, Netherlands*
[6]*Janssen Pharmaceutica, Beerse, Belgium*
[7]*Amyloid Imaging to prevent Alzheimer's Disease (AMYPAD) Consortium, Amsterdam, Netherlands*

Objective: To compare the performance of different supratentorial white matter (sWM) reference regions (RR) with that of Centiloid standard RRs [1] for quantification of longitudinal amyloid (Aβ) PET data.

Methods: Longitudinal MRI and [^{18}F]flutemetamol PET images (577±55 days apart) were acquired from 125 subjects in the AIBL study [2]. Centiloid standard method was used to determine SUVr values in the target VOI, with two pipelines: applying it to both time points independently (*cross-sectional*) and to averaged image pairs (*longitudinal*).

Tested sWM RRs included atlas-based, subject-specific, and the four standard Centiloid RRs, with a total of 17 RRs. sWM in MNI were derived from the Harvard-Oxford atlas (HO), in-house from UCL and from the Neuromorphometrics labels (SPM) with successive one-voxel erosions (up to 5). The rest were obtained from individual subject tissue segmentations with successive erosions (0-4).

Three figures of merit were calculated: 1) Effect size of longitudinal change (Cohen's d) tested in individuals with intermediate Centiloid values (20<CL<50), 2) Plausibility defined as the percentage of all subjects with non-negative Aβ changes, and 3) *Long-time* test-retest variation (lt-TRT) in stable participants, defined as either positives (CL>50) or negatives (CL<20) with changes below 0.04 in SUVr [3].

Results: The longitudinal performance of the sWM RRs was comparable across the two pipelines. sWM outperformed standard Centiloid RRs in all figures of merit. Full results are shown in figures 1 and 2.

Conclusion: Atlas-based sWM, which allow an easier automation, can be used as RR without losing performance compared with that of subject-specific, both approaches improving Centiloid standard RRs performance in [18F]flutemetamol longitudinal studies.

Acknowledgements: Authors would like to acknowledge Dr. Christopher Rowe on behalf of AIBL for sharing [^{18}F]flutemetamol PET scans with the AMYPAD consortium.

References:

[1] Klunk W. et al., Alzheimer's & Dementia (2014)

[2] Ellis K.A. et al., International Psychogeriatrics (2009)

[3] Jack C. Jr. et al., Neurology (2013)

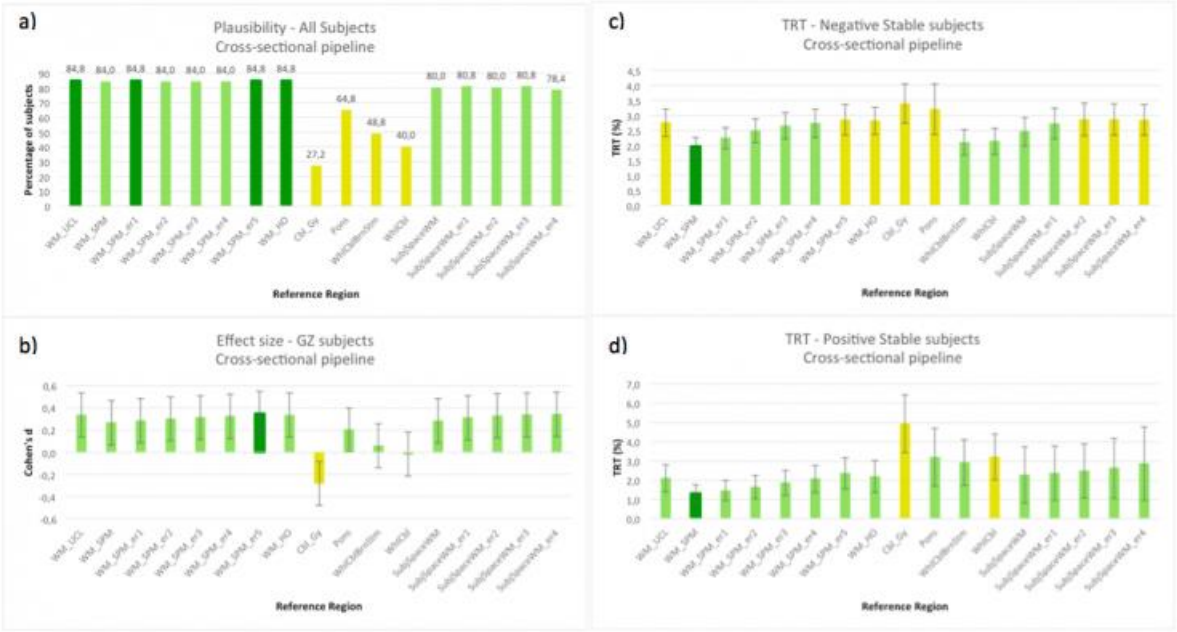

Figure 1: Mean and 95%CI results for the *cross-sectional* pipeline of: (a) plausibility for all subjects, as percentage of subjects whose Aβ-load did not decrease on the follow-up; (b) effect size of longitudinal change for gray zone subjects; and long-time test-retest for both negative stable (c) and positive stable (d) subjects. Dark green columns represent the best results for each figure of merit, light green are those that are statistical comparable (overlapping CI) to the best result and, finally, reference regions that are statistically worse (non-overlapping CI) than the best result are depicted in yellow. WM: white matter; SPM: Neuromorphometrics labels of SPM; er: erode; HO: Harvard-Oxford atlas; CblGy: cerebellum gray; WhlCblBrnStm: whole cerebellum and brainstem; WhlCbl: whole cerebellum; SubjSpace: subject space.

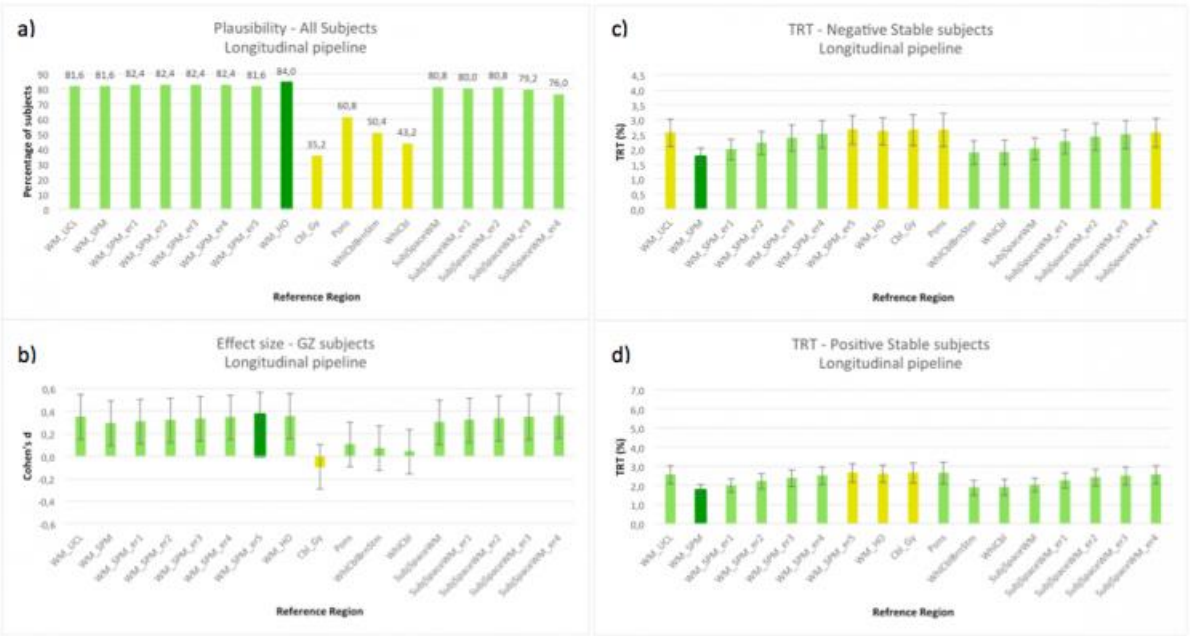

Figure 2: Mean and 95%CI results for the *longitudinal* pipeline of: (a) plausibility for all subjects, as percentage of subjects whose Aβ-load did not decrease on the follow-up; (b) effect size of longitudinal change for gray zone subjects; and long-time test-retest for both negative stable (c) and positive stable (d) subjects. Dark green columns represent the best results for each figure of merit, light green are those that are statistical comparable (overlapping CI) to the best result and, finally, reference regions that are statistically worse (non-overlapping CI) than the best result are depicted in yellow. WM: white matter; SPM: Neuromorphometrics labels of SPM; er: erode; HO: Harvard-Oxford atlas; CblGy: cerebellum gray; WhlCblBrnStm: whole cerebellum and brainstem; WhlCbl: whole cerebellum; SubjSpace: subject space.

Reference region	Cross-sectional pipeline	Longitudinal pipeline
WM UCL	✖	✖
WM SPM	✔	✔
WM SPM erode 1	✔	✔
WM SPM erode 2	✔	✔
WM SPM erode 3	✔	✔
WM SPM erode 4	✔	✔
WM SPM erode 5	✖	✖
WM Harvard-Oxford atlas	✖	✖
Cerebellum gray	✖	✖
Pons	✖	✖
Whole cerebellum and brainstem	✖	✖
Whole cerebellum	✖	✖
Subject space WM	✔	✔
Subject space WM erode 1	✔	✔
Subject space WM erode 2	✖	✔
Subject space WM erode 3	✖	✔
Subject space WM erode 4	✖	✖

Table 1: Summary of reference regions performance for *cross-sectional* and *longitudinal* pipelines. Green check marks represent statistical good performance in all four figures of merit and red crosses depict a statistical worse performance in at least one figure of merit.

Keywords: Reference region, Longitudinal, Centiloid, flutemetamol, AIBL

P11: Parametric imaging of [18F]florbetapir: a test-retest study in healthy subjects and patients with Alzheimer's disease

Sander C.J. Verfaillie[1,2], Sandeep S.V. Golla[2], Chris W.J. van der Weijden[2], Tessa Timmers[1,2], Patrick Schober[3], Robert C. Schuit[2], Albert D. Windhorst[2], Philip Scheltens[1], Wiesje M. van der Flier[1], Adriaan A. Lammertsma[2], Bart N.M. van Berckel[2], Ronald Boellaard[2]

[1]Neurology & Alzheimer Center, VU University Medical Center, Amsterdam, Netherlands
[2]Radiology & Nuclear Medicine, VU University Medical Center, Amsterdam, Netherlands
[3]Anaesthesiology, VU University Medical Center, Amsterdam, Netherlands

Background: Accumulation of amyloid beta (Aβ) is one of the pathological hallmarks of Alzheimer's disease (AD), which can be visualized using [^{18}F]florbetapir positron emission tomography (PET). Accurate quantification of Aβ is important for monitoring disease progression and response to disease-modifying therapies. The aim of this study was to evaluate various parametric methods for voxel-by-voxel quantification of [^{18}F]florbetapir binding and to assess their test-retest (TRT) reliability.

Methods: Eight AD patients (age: 67±6) and eight controls (age: 63±4) were included. Two 90 minutes dynamic PET scans (Philips Ingenuity PET/CT), including arterial sampling, were acquired (~4 weeks apart) after a bolus injection of 293±15MBq [^{18}F]florbetapir (specific activity: 4µg/mL). Parametric images were generated using several linearization and basis function approaches (reference region: cerebellum grey matter). Logan and Spectral Analysis (SA) were used to generate volume of distribution (V_T) images. Receptor parametric mapping (RPM), simplified reference tissue model (SRTM2), reference Logan (RLogan) and standardized uptake value ratios ($SUV_{r(50-70)}$) were used to obtain binding potential (BP_{ND}) or $SUV_{r(50-70)}$ images. BP_{ND} and V_T were compared with corresponding estimates from the plasma input two-tissue compartment (2T4k_V_B) model. TRT values (%) were obtained for both optimal parametric and $SUV_{r(50-70)}$ images.

Results: RPM (BP_{ND}+1) showed the least bias (r^2=0.92; slope=0.91) compared to 2T4k_V_B derived values. In addition, Logan (r^2=0.94; slope=0.85) and RLogan (r^2=0.92; slope=0.88), and SRTM2 (r^2=0.92; slope=0.88) correlated well with their 2T4k_V_B counterparts. Relatively lower correlations were obtained for SUVr (r^2=0.74; slope=0.90) and SA (r^2=0.60; slope=0.81) with 2T4k_V_B DVR and V_T values. RPM (BP_{ND}+1) and $SUV_{r(50-70)}$ showed a TRT variation of 4.2% (controls: 2.6%, AD: 5.4%) and 8.8% (controls: 8.8%, AD: 8.9%), respectively.

Conclusions: RPM was the parametric method of choice for [^{18}F]florbetapir, combining the highest accuracy (lowest bias) with the best TRT reliability. Performance of the semi-quantitative SUVr approach was substantially poorer, especially with regards to TRT variability.

Keywords: quantitative amyloid imaging, florbetapir, parametric imaging, test-retest

P12: A theoretical and empirical investigation of imperfect reference regions

Kerstin Heurling[1], Ruben Smith[2,3], Olof T Strandberg[3], Tomas Ohlsson[4], Oskar Hansson[3,5], Michael Schöll[1,3]

[1]*Wallenberg Centre for Molecular and Translational Medicine and the Department of Psychiatry and Neurochemistry, University of Gothenburg, Gothenburg, Sweden*
[2]*Department of Neurology, Lund University, Skåne University Hospital, Lund, Sweden*
[3]*Clinical Memory Research Unit, Department of Clinical Sciences, Lund University, Malmö/Lund, Sweden*
[4]*Department of Radiation Physics, Skåne University Hospital, Lund, Sweden*
[5]*Memory Clinic, Skåne University Hospital, Lund, Sweden*

Background: The definition of a reference region (RR) states no specific or displaceable binding and non-displaceable binding unaffected by demographics that is similar to that of the target region. Regional increased retention of [^{18}F]AV-1451 has previously been reported in superior lobules I-VI of the cerebellar grey RR (SUIT cerebellum atlas)[1]. In this study we investigated factors relevant in the influence of imperfect RRs, and applied on the uptake of [^{18}F]AV-1451 in clinical data.

Methods: The theoretical influence of heterogeneity properties in a RR was investigated algebraically.

[^{18}F]AV-1451 80-100 min uptake in cerebellar grey lobules (excluding vermis) and its effect on SUVR were assessed in six patients with Alzheimer's disease (AD) and four elderly healthy controls (HC) (BioFINDER cohort).

Results: The influence of imperfect RRs, defined as a multiple of the true SUVR, depends on the uptake in the imperfect subregion expressed as a multiple of the assumed true RR uptake ($m_{Conc}=Conc_{imperfect}/Conc_{true}$), and the relative size of the subregion exhibiting imperfection ($\%Vol=Vol_{imperfect}/Vol_{whole}$). The relationship is as follows:

$M_{SUVR}=(1+\%Vol(m_{Conc}-1))^{-1}$ (Figure 1)

Within the BioFINDER cohort, the cerebellum lobules I-VI constituted 31.4±2.9% of the RR, with no difference between AD and HC (Table 1). Uptake was 14% higher in the superior portions compared to the rest of cerebellar grey among AD subjects, but no difference was observed in HC. Inclusion of cerebellum subregions I-VI in the RR yields an average 4.3% decrease in SUVR among AD subjects ($p>0.01$), but no effect on SUVR among the HCs.

Conclusions: Impact of including imperfections in a RR is related to the relative size and magnitude of uptake of the imperfect subregion. We observed higher uptake in the superior portions of the cerebellar grey in the AD group. However, impact on target region SUVR was small.

1. Baker S, Maass A, Landau S, et al. HAI 2017.

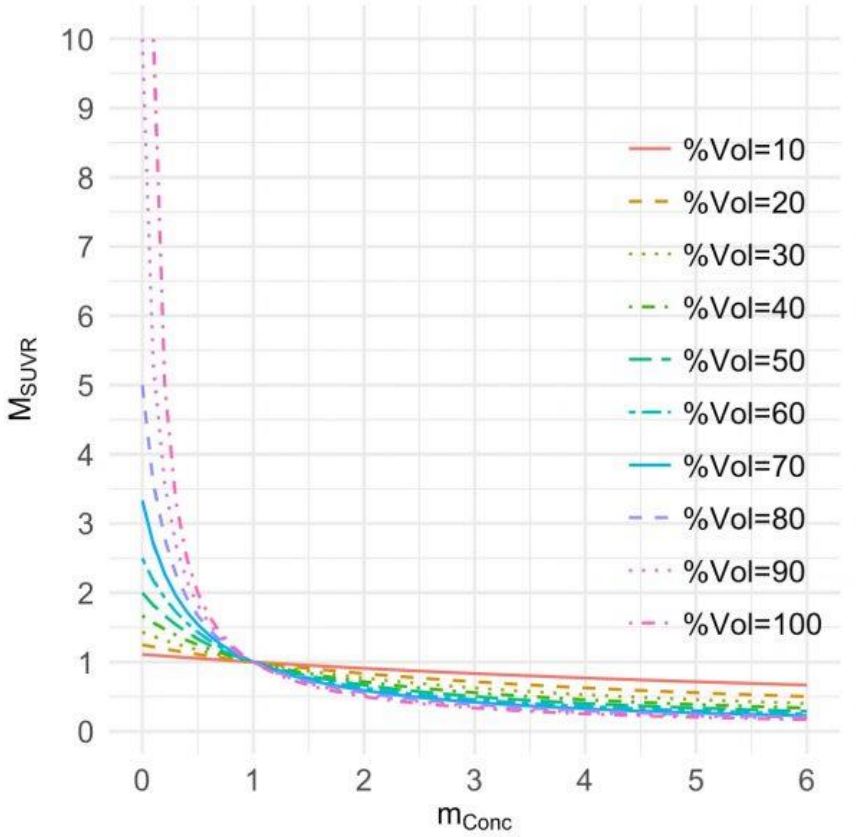

Figure 1. The theoretical effect on SUVR by an imperfection within the reference region is related to two factors: the magnitude of the imperfect uptake (decreased: $m_{Conc}<1$, increased: $m_{Conc}>1$) and the relative size of subregion to the whole reference region (%Vol). M_{SUVR} represents the multiple of the true SUVR, i.e. $M_{SUVR}=2$ indicates an estimated SUVR twice the true SUVR

Table 1. Parameters estimated in the superior subregions of the cerebellar grey across six AD and four HC subjects. m_{Conc} is magnitude of the imperfect uptake, %Vol is the relative size of subregion to the whole reference region, M_{SUVR} represents the multiple of the true SUVR. Change in SUVR is presented as the percent increase or decrease relative to the true SUVR

Cerebellar subregion	% Vol	m_{Conc}	M_{SUVR}	Change in SUVR (%)
I-IV AD	5.0±0.7	1.11±0.04*††	0.995±0.002††§§	-0.5±0.17††§§
I-IV HC	5.6±0.7	0.96±0.05	1.002±0.003	0.2±0.27
V AD	7.6±1.0	1.15±0.09*†	0.989±0.007†§§	-1.1±0.69†§§
V HC	9.2±1.4	1.00±0.06	1.000±0.005	0.1±0.51
IV AD	19.3±2.0	1.15±0.11*†	0.972±0.020†§	-2.8±1.96†§
IV HC	15.8±2.6	1.01±0.03	0.998±0.005	-0.2±0.53
I-VI AD	31.9±2.5	1.14±0.09*†	0.957±0.025†§§	-4.3±2.54†§§
I-VI HC	30.6±3.9	1.00±0.04	1.001±0.013	0.1±1.28

* Regional uptake>Uptake in rest of reference region ($p<0.05$) using pairwise Students t-test
† AD≠HC ($p<0.05$) using Student's two-sample t-test, †† AD≠HC ($p<0.001$) using Student's two-sample t-test
§ $M_{SUVR} \neq 1$, Change in SUVR ≠ 0 ($p<0.05$), §§ $M_{SUVR} \neq 1$, Change in SUVR ≠ 0 ($p<0.01$)

Keywords: reference regions, SUVR, method validation, AV-1451

P13: Explaining [18F]-AV-1451 variability in healthy controls across the lifespan

Suzanne Baker[1], Theresa Harrison[2], Anne Maass[2,3], Renaud La Joie[4], William Jagust[1,2]

[1]*Lawrence Berkeley National Laboratory, Berkeley, CA, US*
[2]*Helen Wills Neuroscience Institute, UC Berkeley, Berkeley, CA, US*
[3]*Center for Neurodegenerative Diseases, Magdeburg, Germany*
[4]*Memory and Aging Center, UCSF, San Francisco, CA, US*

Background: Detection of the earliest stages of tau accumulation is important for studying aging and AD, and is affected by the signal to noise ratio of the tracer. [18F]-AV1451 is successful at differentiating healthy controls from subjects with AD, however it shows substantial variability in healthy controls, especially subjects younger than 40, where little to no tau accumulation is expected (Figure 1).

Methods: In a cohort of healthy controls (n=69; age=20-93; M/F 34/35) who were PIB negative (DVR<1.065), we analyzed [18F]-AV1451 SUVRs 80-100 min post-injection and [11C]-PIB SUVRs 50-70 min post-injection. The analyses were done with and without partial volume correction (PVC; Rousset method, same in [11C]-PIB and [18F]AV-1451); reference region was inferior cerebellar gray. Linear models were used on PVC data to explore relationships between cortical uptake, age, thalamus, putamen, pallidum, caudate, and hemispheric and cerebellar white matter.

Results: Adjusted r2 and $p<0.0001$ are reported. Significant [18F]-AV1451 correlations were found between age and putamen (r2=0.722), caudate (r2=0.591) and pallidum (r2=0.586), not with white matter of thalamus. All white matter regions were correlated with each other and with thalamus (r2>0.65). Non-PVC correlations between cerebellar white and cortex were r2=0.274 for [11C]-PIB and r2=0.65 for [18F]-AV1451. Figure 2 shows that white matter correlation with cortex was removed after PVC in [11C]-PIB but not in [18F]-AV1451, suggesting that the [18F]-AV1451 correlation stems from non-specific binding in both gray and white matter, not only partial volume effects. Figure 3 shows the r2 between cortical regions and non-specific binding regions in [18F]-AV1451. 67.4% of the variability in whole cortex is explained by non-specific binding in the putamen and thalamus.

Conclusions: Non-specific binding of [18F]-AV1451 in cortex appears to reflect an age-related phenomenon (putamen) and a non-age related phenomenon (white matter/thalamus). These factors may reduce signal to noise at low levels of tracer binding.

Figure 1: Variability in [18F]-AV1451 in [11C]-PIB negative healthy controls

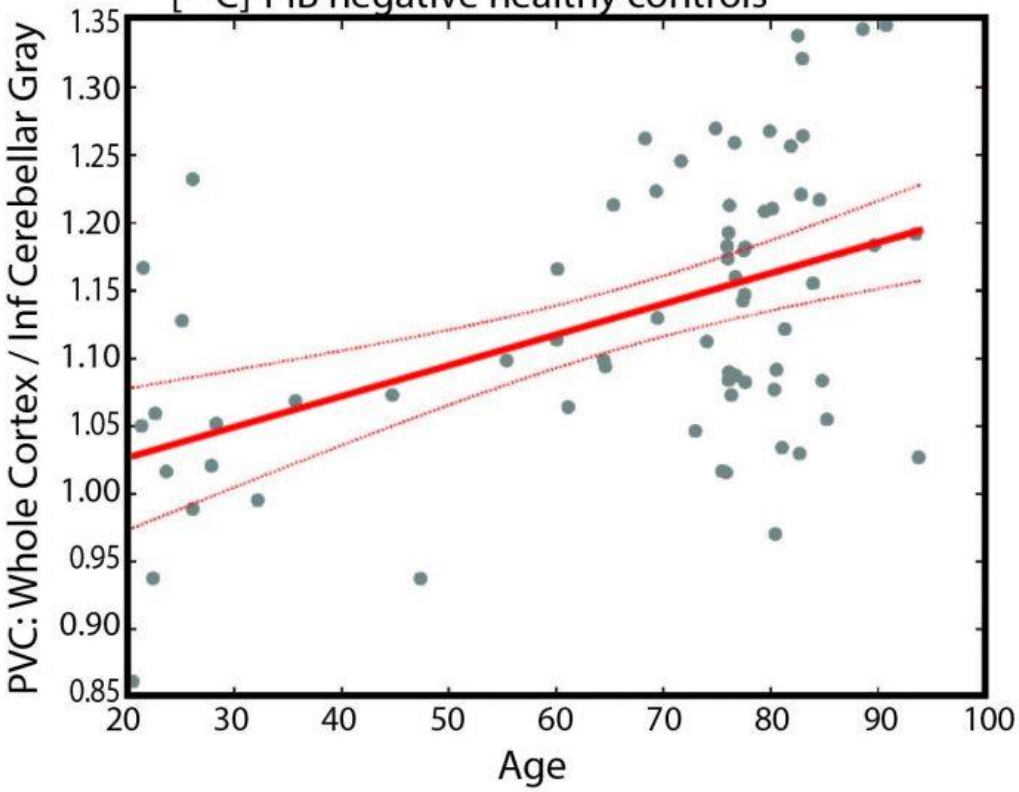

Figure 2

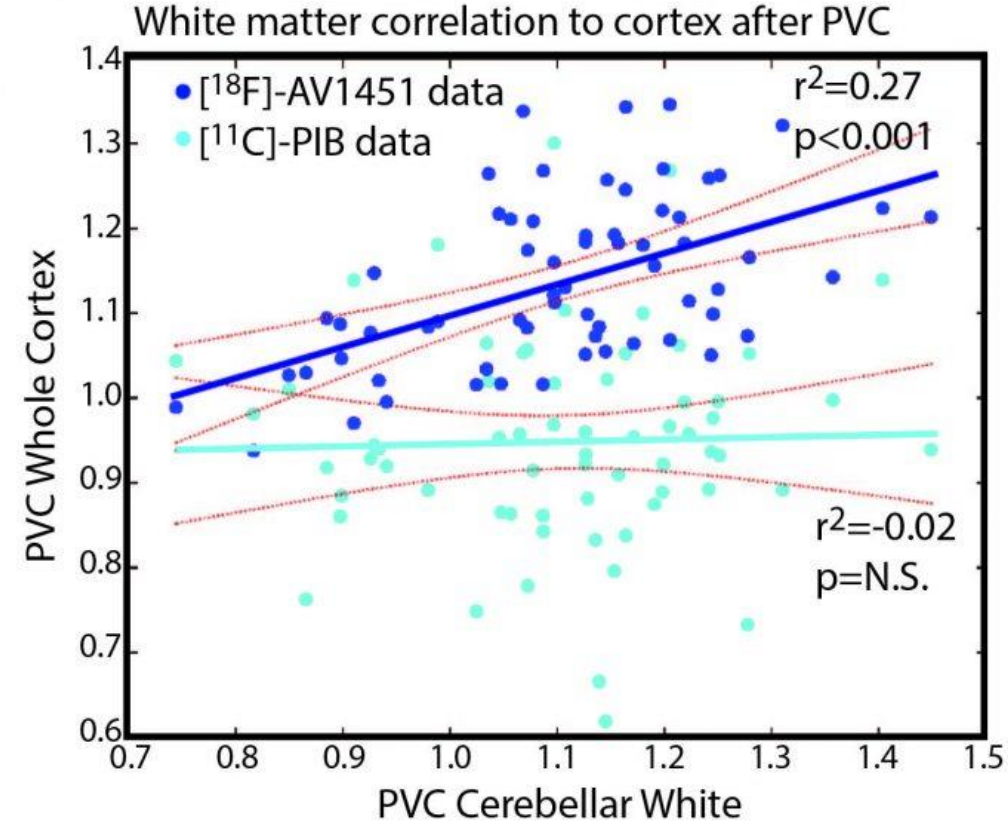

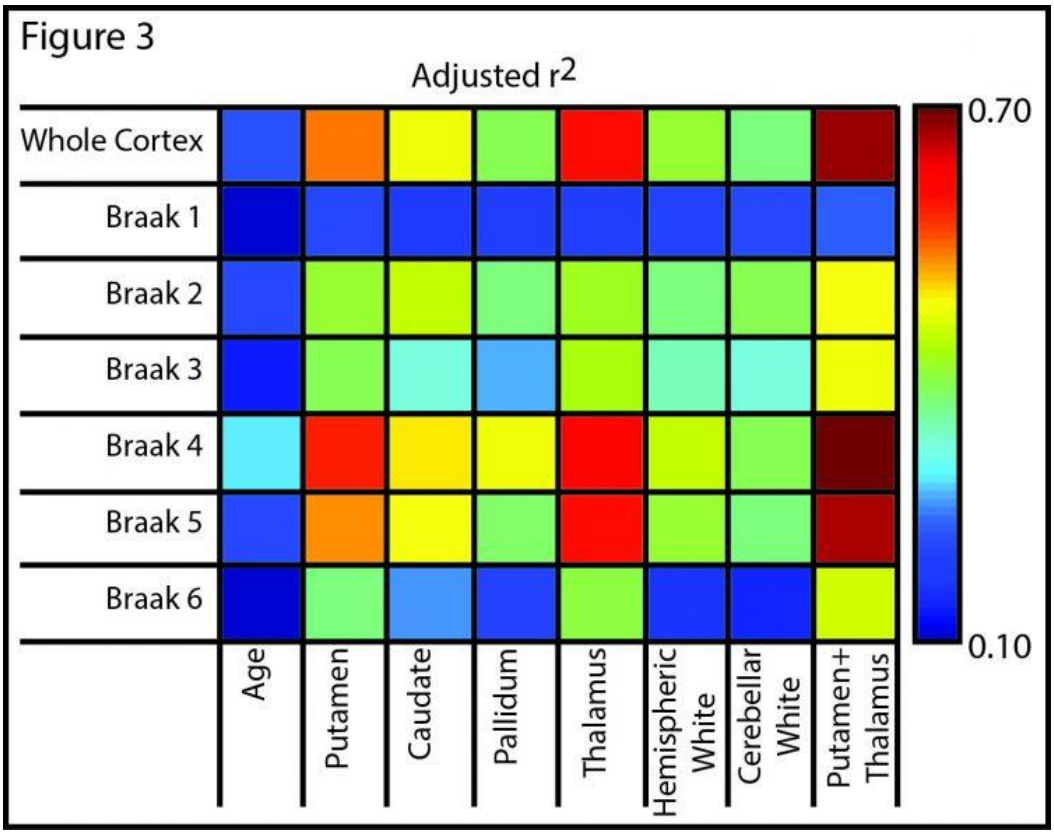

Keywords: AV1451, non-specific binding, healthy controls

P14: Centiloid validation of multi-atlas PET-SUVR analysis in the multi-tracer AMYPAD study

Elisabetta Grecchi[1], Christopher Foley[2], Robin Wolz[1], Juan D. Gispert[3], Derek Hill[1]

[1]*IXICO, London, United Kingdom*
[2]*GE Healthcare, Amersham, United Kingdom*
[3]*Barcelonabeta Brain Research Center, Barcelona, Spain*

Background: Utilization of a standardized quantitative imaging analysis scale, Centiloid, for comparing β-amyloid imaging tracers in Alzheimer's disease (AD) is within the objectives of the AMYPAD study (http://amypad.eu/). A total of 6000 scans will be collected across ~20 European PET centers using the Florbetaben and Flutemetamol amyloid tracers. The utilization of the Centiloid scale will allow to compare the quantitative expression of Aß burden across all subjects. This work validated the AMYPAD SUVR quantification workflow to produce a standardized Florbetaben and Flutemetamol Centiloid conversion. The analysis workflow is a multi-atlas SUVR PET analysis operating in subject native space using subject specific brain segmentation (LEAP).

Method: Using Centiloid Volume of Interest (VOI) regions and 4 subject-specific reference regions (grey/whole cerebellum, pons, whole cerebellum + brain stem), three different databases were processed using the LEAP-SUVR analysis: (1) GAAIN PIB images (YC=35,AD=45), (2) PIB and FBB images (YC=10,HE=5,MCI=9,FTD=2,AD=7), (3) PIB and FLUT images (YC=24,HE=10,MCI=20,AD=20). All PIB data were used to calibrate LEAP-SUVR against the GAAIN SPM analysis using all 4 reference regions (analysis A). Using linear regression, FBB-SUVR and FLUT-SUVR were converted into PIB-like SUVRs that were then converted into Centiloid using equations from analysis A (analysis B). The combination of analysis A and B allowed to generate the final transformation of LEAP-SUVR into Centiloids (one transformation for each reference region).

Results: Strong correlation between SPM and LEAP-SUVR was observed (Figure 1). Eight different conversion equations were computed (FBB and FLUT for 4 reference regions). Converting SUVR values into Centiloid, resulted in comparable mean values for an AD population (Figure 2).

Conclusions: Robust and reliable Centiloid estimates can be obtained for FBB and FLUT using the AMYPAD LEAP-SUVR method. The LEAP-SUVR Centiloid conversion will allow multi-tracer and multi-reference region comparison over a wide range of regions of interest in a 6000 subjects database.

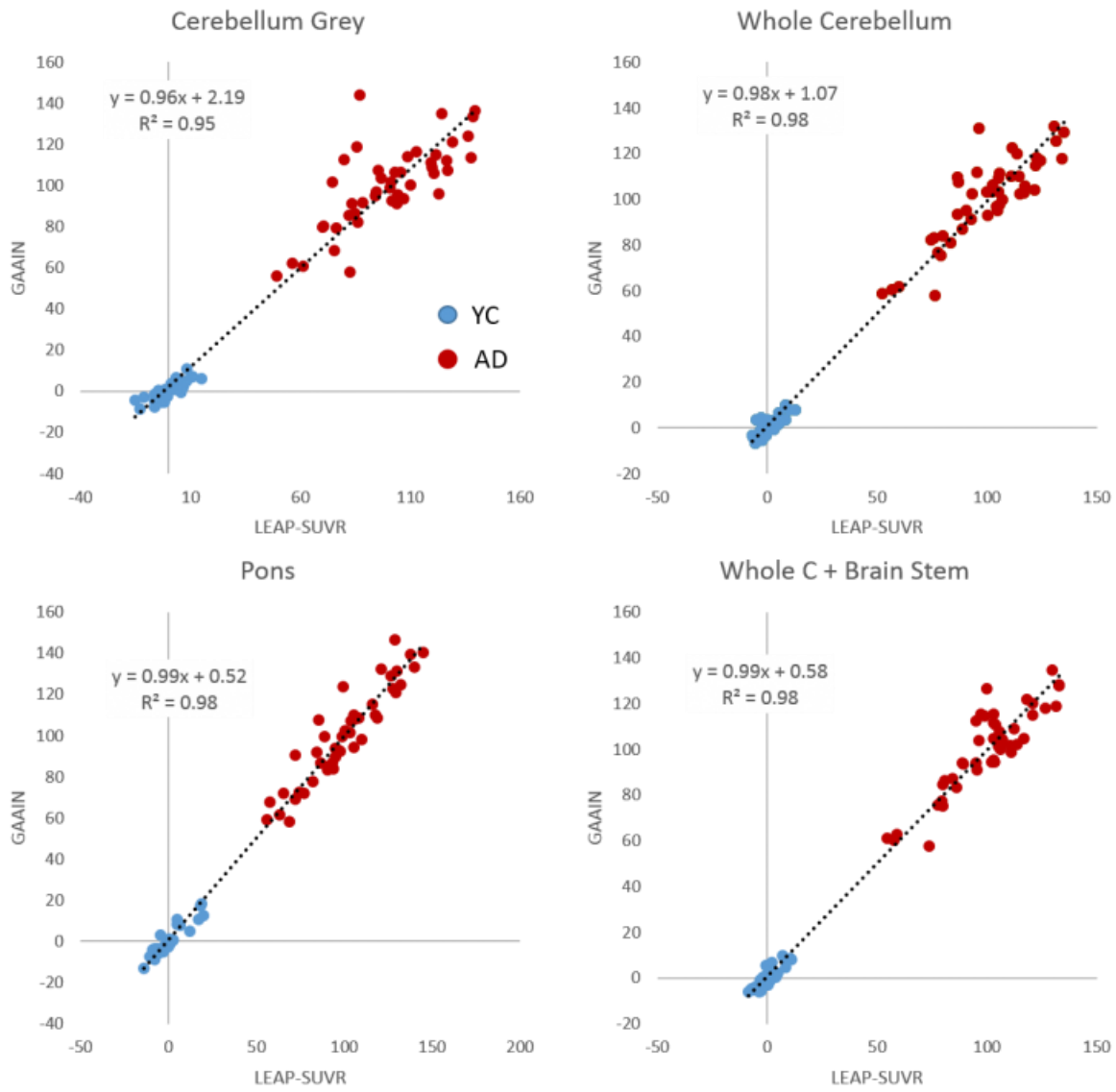

AD

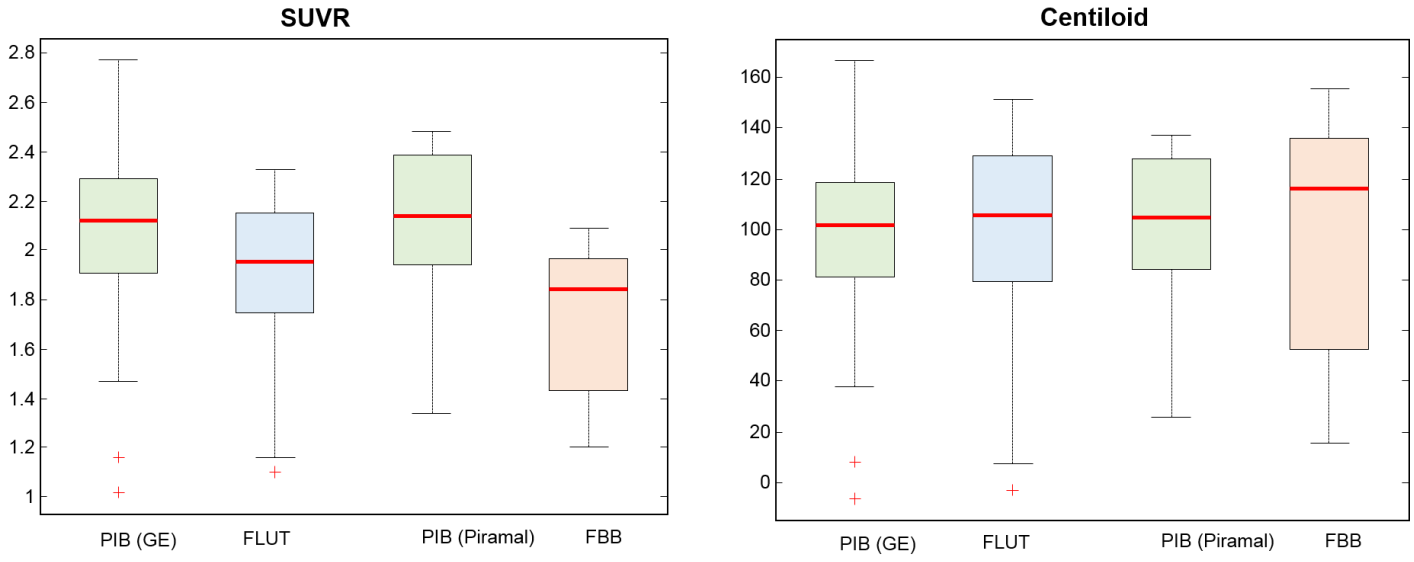

Keywords: AMYPAD, Centiloid, Amyloid PET, Alzheimer's disease

P15: PET scanner variance in multi-center clinical trials using the Hoffman Phantom

Katarzyna Adamczuk[1], Nicolas Pannetier[1], Ha Pham[1], Beth Gorman[2], Maureen Runkle[2], David Scott[1], Joyce Suhy[1]

[1]*Bioclinica, Newark, CA, US*
[2]*Bioclinica, Philadelphia, PA, US*

Background: In longitudinal clinical trials changes to the imaging equipment affect the stability of quantitative measurement. It is especially impactful when the effect on quantitative measurement is similar in magnitude to the effect of prospective therapy. The main objective of this work is to measure scanner performance using the Hoffman phantom and to estimate inter and intra PET scanner variability.

Methods: Hoffman phantom scans were acquired on 4 different models for each of 3 manufacturers. Models were matched within manufacturer for attenuation, scatter and random corrections, dynamic acquisition and iterative reconstruction. Intra- and inter-model variance was estimated.

Hoffman phantoms were prepared by mixing 0.5-0.6 mCi 18F-FDG solution in the phantom, and imaging immediately using 4x5 min acquisition. Frames were averaged and co-registered to the digital reference. Once co-registered, effective spatial resolution was determined by fitting in-plane and axial Gaussian smoothing parameters to best match the digital reference to the source phantom data. Intensity of the source data was normalized to the digital reference using a grey matter region. Once co-registered, smoothed and intensity normalized, a difference image was computed. Scanner spatial resolution, axial uniformity, and grey-to-white matter contrast were calculated.

Results & Conclusion: Scanner resolution improves with newer models and is different among manufactures. Although, some models do not fit to this pattern. Models also differ in image intensity and sensitivity. More so between than within manufacturers. Data suggests that higher resolution contributes to larger differences in intensity between the source and the reference phantom images. Lower image resolution contributes to lower grey to white matter ratio and therefore may impede visual interpretation of acquired images for the worst performing cameras. Scanner models differ largely between manufacturers and to considerable extent within manufacturer. Longitudinal clinical trials must pay particular attention to scanner selection and risk of potential scanner change.

Keywords: longitudinal clinical trials, Hoffman phantom, scanner variability, FDG, tau, amyloid

P16: Longitudinal tau quantitation with anatomically-guided PET image deblurring

Ruchira Tabassum[1], Quanzheng Li[2], Alex Becker[2], Georges El Fakhri[2], Keith Johnson[2], Joyita Dutta[1,2]

[1]*University of Massachusetts Lowell, Lowell, MA, US*
[2]*Massachusetts General Hospital, Boston, MA, US*

Objectives: PET imaging of tau neurofibrillary pathology has emerged as a major component of image-based biomarker development for aging and Alzheimer's disease. In order to improve tau PET accuracy, we evaluated an image deblurring technique that utilizes anatomical information to correct for partial volume effects, and investigated its impact on region-of-interest (ROI) analysis for longitudinal [18F] Flortaucipir datasets.

Methods: The deblurring technique is based on deconvolution of PET data with the actual spatially variant point spread function (PSF) of the scanner and an MR-based information theoretic framework that minimizes the joint entropy between the PET image and a T1-weighted high-resolution MR image. Deblurring was performed on two time points of serial [18F] Flortaucipir PET data acquired in 13 Harvard Aging Brain Study participants over 3 years.

Results: We computed mean standardized uptake value ratios (SUVRs) corresponding to the following 6 ROIs: inferior temporal cortex (ITC), fusiform gyrus (FG), posterior cingulate (PC), parahippocampal gyrus (PHG), entorhinal cortex (EC), and hippocampus (H). Transverse slices from a subject showing the MR, ROI masks, and original and deblurred PET images at two time points are shown in Fig. 1. As shown in Fig. 2, the ROI mean SUVRs in the deblurred images showed consistent improvement relative to those for the original images of 13 subjects acquired at two different time points separated by about 3 years. The difference images across the two time points exhibited prominent improvements in SUVR changes over time as a result of deblurring. As shown in Fig. 3, for the six ROIs, the percentage mean observed changes over 3 years were: 2.7% (ITC), 13.8% (FG), 22.7% (PC), 22.7% (PHG), 23.0% (EC), and 6.2% (H).

Conclusion: Accurate measurement of the PET PSF and MR-based priors led to enhanced image contrast. This translated into a marked improved in computed longitudinal SUVR change for each ROI.

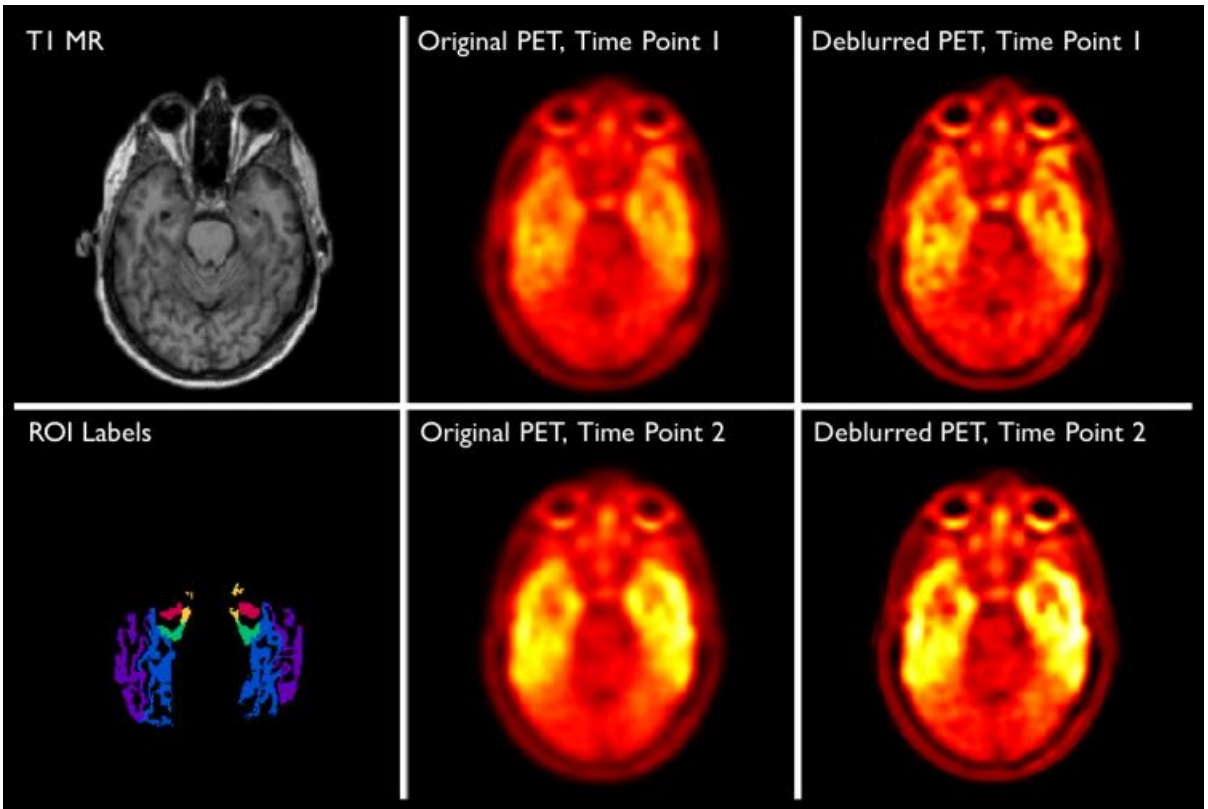

Fig. 1: Transverse slices from a subject showing the MR, ROI masks, and original and deblurred PET images at two time points. The ROI labels include inferior temporal cortex (ITC), fusiform gyrus (FG), posterior cingulate (PC, not visible in the displayed slice), parahippocampal gyrus (PHG), entorhinal cortex (EC), and hippocampus (H).

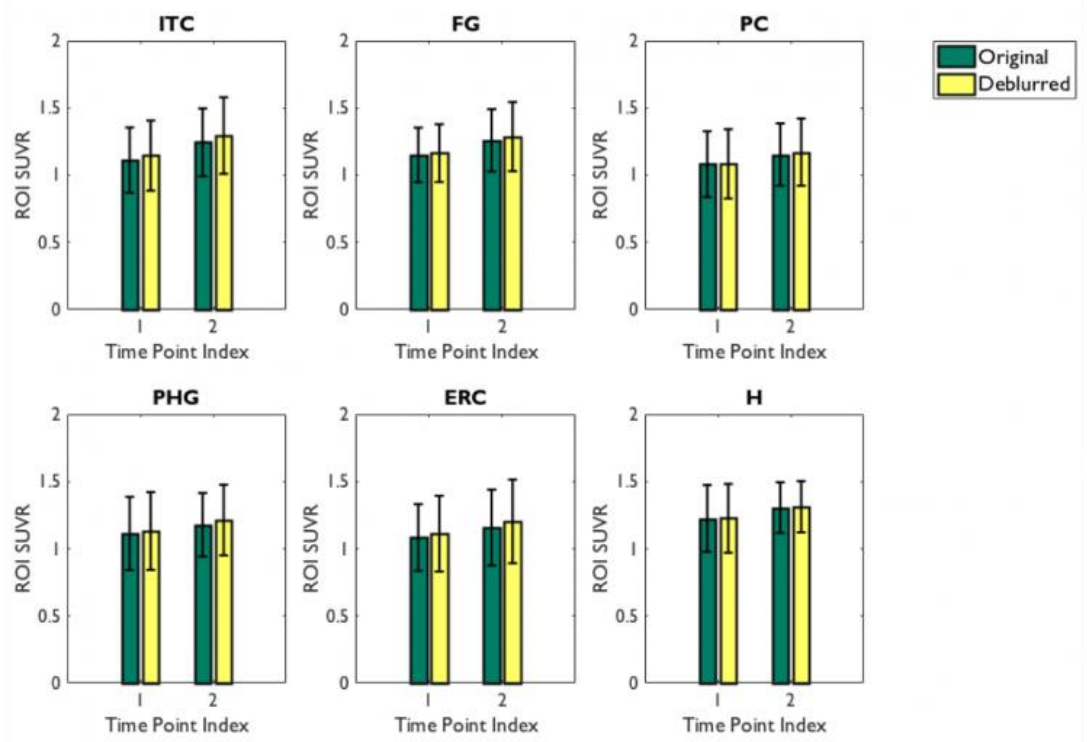

Fig. 2: Mean ROI values for the original and deblurred PET images for 6 regions of interest (ROIs): inferior temporal cortex (ITC), fusiform gyrus (FG), posterior cingulate (PC), parahippocampal gyrus (PHG), entorhinal cortex (EC), and hippocampus (H).

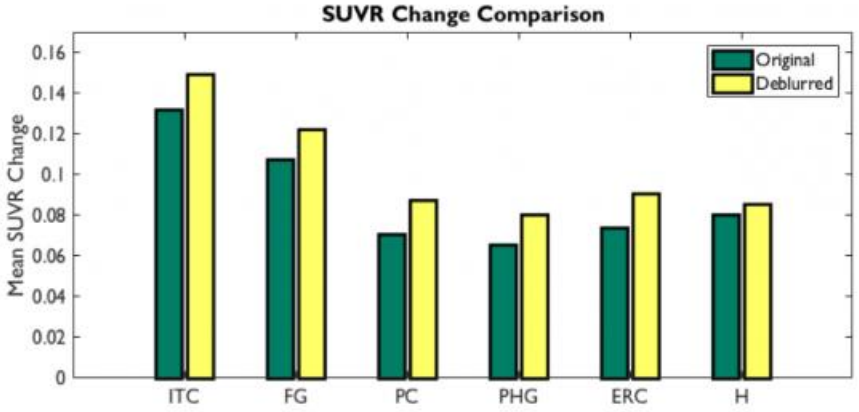

Fig. 3: Mean ROI change across two time points separated by 3 years for the original and deblurred PET images for 6 regions of interest (ROIs): inferior temporal cortex (ITC), fusiform gyrus (FG), posterior cingulate (PC), parahippocampal gyrus (PHG), entorhinal cortex (EC), and hippocampus (H).

Keywords: PET, partial volume correction, tau quantitation, Alzheimer's disease

P17: Tau and alpha synuclein selective binding compounds derived from Aprinoia Therapeutics' PM-PBB3 binding-site focused compound collection

Paul Tempest[1], Ming-Kuei Jang[1], Chin-Yin Tai[1], Makoto Higuchi[2], Maiko Ono[2], Hitoshi Shimada[2], Tetsuya Suhara[2], Ming-Rong Zhang[2], Gilles Tamagnan[3], Vincent Carroll[3], Ken Marek[3], John Seibyl[3], David Alagille[3], Oliver Barret[3]

[1]*Aprinoia Therapeutics, Taipei, Taiwan*
[2]*National Institute for Quantum Science and Radiological Science and Technology (QST), Chiba, Japan*
[3]*Invicro, New Haven, CT, US*

Tau and alpha synuclein selective binding compounds derived from Aprinoia Therapeutics' PM-PBB3 binding-site focused compound collection

18F-PM-PBB3 is unique among known Tau imaging agents as it has been shown to be useful for PET imaging of Tau in both (3R) AD and (4R) PSP patients. Aprinoia, in collaborating with QST, have initiated global clinical studies with 18F-PM-PBB3 in the US, China, Japan and Taiwan. Aprinoia's development of the next generation PM-PBB3 binding-site focused tracer has led to the generation of a ~1000 compound CNS-biased collection. This collection has been screened against other protein aggregates and targets to generate new leads.

Alpha-synuclein is an important marker in PD. Screening Aprinoia's compound collection against in vitro generated aSyn aggregates has resulted in several lead compounds that show selectivity for aSyn over Tau.

Our goal is to provide a single imaging compound able to image multi-isoforms of Tau across various tauopathies. Additionally, we hope to leverage our compound collection to generate tracers for other protein aggregates such as alpha-synuclein, TDP-43 etc to help facilitate diagnosis, track progression and assist clinical trials.

Keywords: tau, alpha-synuclein, PET, PM-PBB3

P18: Noise reduction algorithm for amyloid image preserving image resolution — quantitative evaluation using clinical images

Takahiro Yamada[1], Yuichi Kimura[1], Kosuke Fuji[1], Shogo Watanabe[1], Takashi Nagaoka[1], Mitsutaka Nemoto[2], Kohei Hanaoka[3], Hayato Kaida[4], Chisa Hosokawa[4], Kazunari Ishii[3,4]

[1]*Graduate School of Biology-Oriented Science and Technology, Kindai University, Wakayama, Japan*
[2]*Faculty of Biology-Oriented Science and Technology, Kindai University, Wakayama, Japan*
[3]*Division of PET Molecular Imaging, Kindai University Hospital, Osaka, Japan*
[4]*Department of Radiology, Faculty of Medicine, Kindai University, Osaka, Japan*

Introduction: Detecting a small and thin accumulation of amyloid β (Aβ) is helpful for a study on Alzheimer's disease (AD) and the early diagnosis, but it is difficult due to the noise in *BP*ND image. A conventional noise reduction algorithm uses a spatial information in PET image, averaging neighboring voxels, but it makes a small Aβ accumulation undetectable. We have proposed a new noise reduction algorithm for amyloid image named CAKS in HAI2017. CAKS gathers such voxels that have similar kinetics (Kimura, *NeuroImage*, 1999). In HAI2018, we evaluate the performance using clinical PiB images.

Method: CAKS is applied to 85 images PiB, and our neuroradiologists diagnose Aβ deposition both of original *BP*ND and CAKS-applied images. As presented in Table 1, there are 42 positive cases, 33 negative cases, and 10 equivocal cases. *BP*ND images are computed using LGA with a reference region and $t^* = 30$ [min]. In order to investigate the development of the contrast between gray and white matter, ROI are placed in the left and right frontal lobes and the posterior cingulate gyrus, and their neighboring white matter.

Results: The typical *BP*ND image of negative case is presented in Fig. 1. CAKS reduces the noise, and the boundary white matter is preserved. The contrast is significantly improved by 2.4 times as much (one-tailed test of Wilcoxon signed-rank test, $p < 0.01$). The diagnosis to six equivocal cases change to positive cases with CAKS; and the negative cases change to positive cases.

Discussion: We conclude that CAKS is applicable to an amyloid imaging.

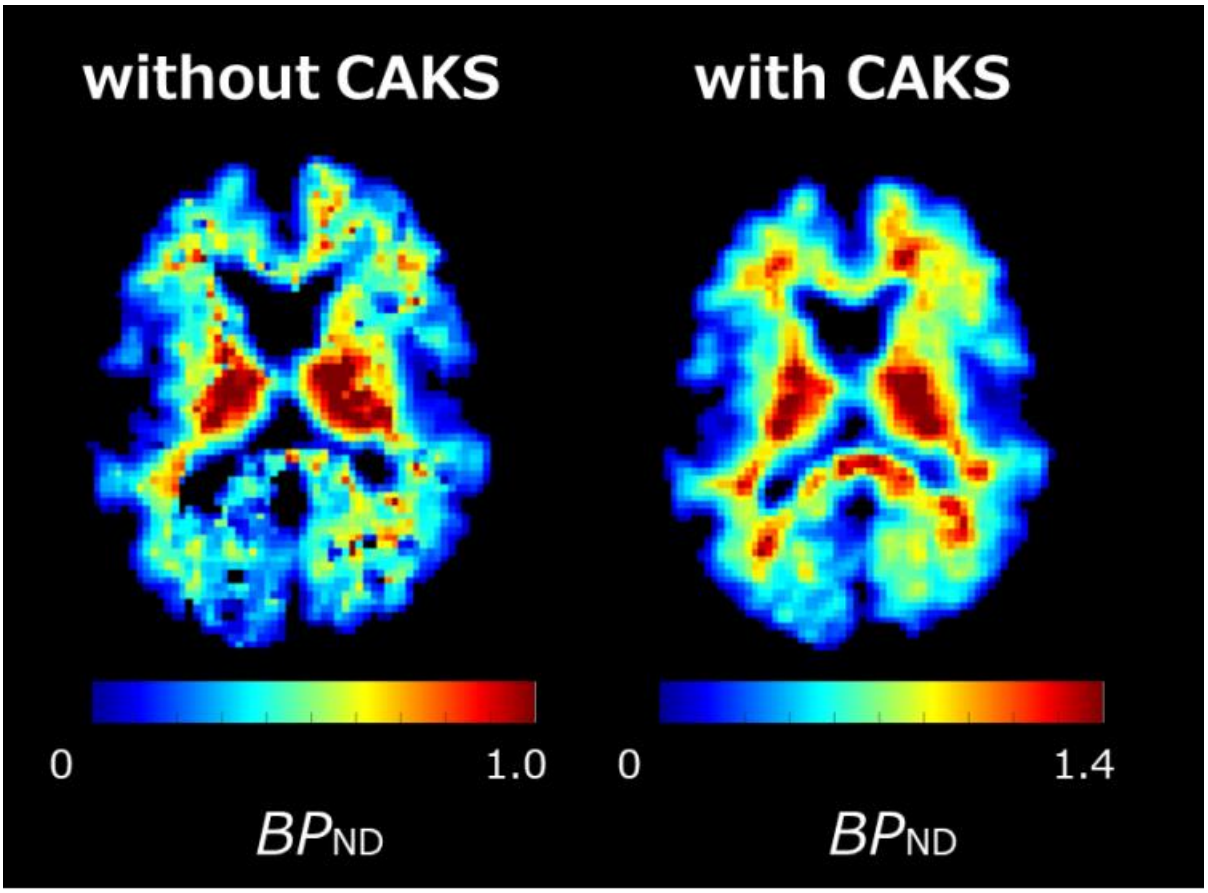

Fig. 1. images of an Aβ negative case. CAKS can improve image quality without loss of image resolution.

	original diagnosis		
	positive	negative	equivocal
n	42	33	10
change to positive		**1**	**6**
change to negative	0		0
change to equivocal	0	0	

Table 1. Changes of diagnosis by CAKS.

Keywords: PET, noise reduction, kinetic analysis, algorithm

P19: Assessment of centiloid scaling values in test-retest evaluation using multiple image quantification software platforms

Mark Battle, Christopher Buckley, Lovena Pillay

GE Healthcare, Amersham, United Kingdom

Introduction: Centiloid scaling offers a standardized, quantitative imaging analysis method for measuring uptake of β-amyloid imaging PET tracers in Alzheimer's disease (AD)[1,2]. We previously reported data showing the value of Centiloid scaling for [^{18}F]flutemetamol subjects, utilising SPM8 and PMOD generate Standard Uptake Value ratio (SUVr) values that were scaled to a [^{11}C]PiB-equivalent before conversion to Centiloid[3].

SUVr analysis has been shown to be a simple and robust method of quantitative image evaluation, both in terms of Test-Retest variability and ability to determine effects between groups[4]. SUVr values can be used to provide an approximation of the distribution volume ratio (DVR).

Here, we investigate the robustness of Centiloid pipelines in subjects using Test-Retest [^{18}F]flutemetamol scans, and comparing the Centiloid values.

Methods: Centiloid Volume of Interest (VOI) regions were applied to [^{18}F]flutemetamol PET data, processed following the methods described by Klunk *et.al.*[2]. [^{18}F]flutemetamol images for 10 AD subjects, with retest scans acquired within one week of test scan, were processed using 3 different process pipelines; SPM8, PMOD and FSL. SUVr and Centiloid values for the VOI regions were calculated, and these are presented with the SUVr-1 for the same images.

Results: The average Test and Retest SUVr values were 1.8±0.2 for each pipeline for both scans. When converted to Centiloid values, the average values for test (T) and retest (R) were; PMOD T: 89.9±20.5, R: 100.5±21.1, SPM8 T: 96.4±21.2, R: 97.7±21.3, FSL T: 100.0±25.4, R: 100.3±25.3.

Conclusions: For [^{18}]flutemetamol, using Centiloids to determine the Test-Retest difference, gave an average of approximately 3% between Test and Retest values. This is comparable with the difference in estimated binding potential (SUVr-1), indicating Centiloid shows a close association. Different image processing pipelines did not produce any significantly different results, showing that Centiloid scaling is robust and can be applied to compare results from across platforms.

Keywords: Centiloid, [18F]flutemetamol, PMOD, FSL, Test-Retest

P20: Optimized coffee-break protocol for quantitative [18F]flutemetamol studies

Fiona Heeman[1], Maqsood Yaqub[1], Kerstin Heurling[2], Isadora Lopes Alves[1], Juan Domingo Gispert[3], Christopher Foley[4], Adriaan A. Lammertsma[1], on behalf of the AMYPAD Consortium[5]

[1]*Department of Radiology & Nuclear Medicine, Amsterdam Neuroscience, VU University Medical Center, Amsterdam, Netherlands*
[2]*Wallenberg Centre for Molecular and Translational Medicine and the Department of Psychiatry and Neurochemistry, University of Gothenburg, Gothenburg, Sweden*
[3]*Barcelonaβeta Brain Research Center, Pasqual Maragall Foundation, Barcelona, Spain*
[4]*GE Healthcare, Amersham, United Kingdom*
[5]*Amyloid imaging to prevent Alzheimer's disease (AMYPAD) Consortium, Amsterdam, Netherlands*

Introduction: [^{18}F]flutemetamol is a validated PET tracer for imaging amyloid beta accumulation in the brain. For diagnostic purposes, a static scan, acquired 90-110 minutes after injection, is sufficient. For monitoring disease progression and treatment response, however, quantification using a 110 minutes dynamic scan, starting at tracer injection, may be required for a higher sensitivity in measuring changes. A disadvantage is the long scanning time, which may cause discomfort to patients. This can be reduced by using a "coffee-break" protocol, in which a patient is only scanned during the early and late phases after tracer injection, providing a rest period. The aim of this simulation study was to define the optimal [^{18}F]flutemetamol coffee-break, optimizing patient comfort, whilst maintaining quantitative accuracy.

Methods: Based on kinetic parameters derived from clinical data, 110 minutes time-activity curves (TACs) were simulated for various levels of amyloid load, using the simplified reference tissue model (SRTM) (Table 1). Next, different levels of noise (COV) were added to the TACs, to represent voxel and region level data. Coffee-breaks, ranging from 80 (i.e. 10-90) to 0 (i.e. 90-90=full data set) minutes, were removed from these TACs. Finally, resulting TACs were fitted using SRTM to obtain the non-displaceable binding potentials (BP_{ND}), which were compared with corresponding values for the full data set.

Results: Longer coffee-breaks were associated with larger absolute errors in BP_{ND}, especially for the longest coffee-break (10-90 minutes), where a significant bias was seen, even without adding noise to the data (Fig.1). For higher noise levels, absolute errors also started to increase for other coffee-break intervals (Fig.1).

Conclusion: A 30-90 minute coffee-break appeared to be the optimal trade-off between absolute errors and patient comfort. In addition, it allows for interleaved scanning protocols (i.e. scanning the first part of a second patient during the coffee-break of the first patient), thereby optimizing scanner time and tracer usage.

Table 1
Kinetic parameters used in the simulations

	R1	K2	BP_{ND}
TR_I	0.827	0.080	0.107
TR_II	0.827	0.080	0.211
TR_III	0.827	0.080	0.315
TR_IV	0.827	0.080	0.453

TR = target region

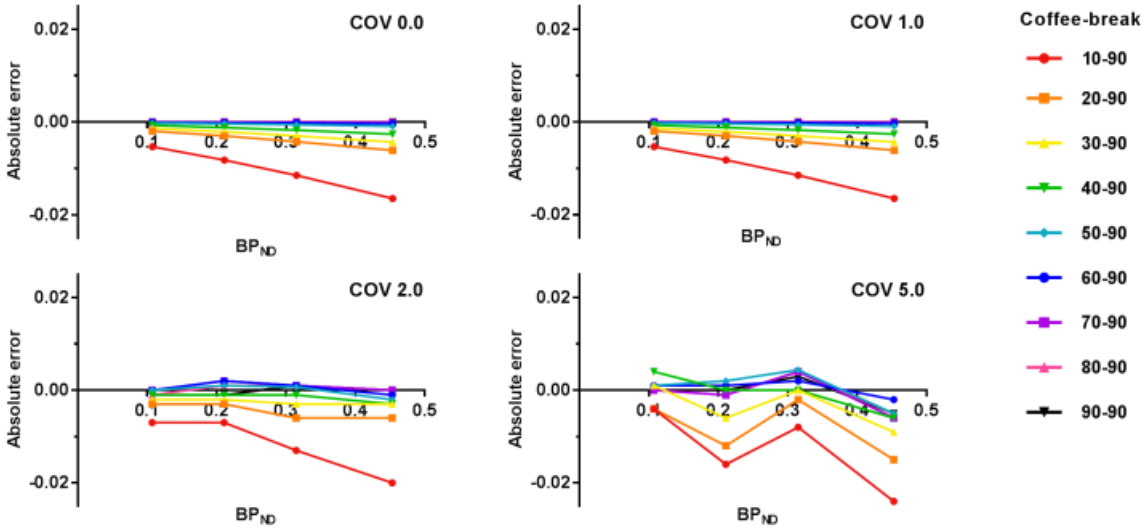

Figure 1. Absolute errors in SRTM derived BP_{ND} for simulated TACs with different coffee-break protocols. COV = coefficient of variance (noise level)

Keywords: [18F]flutemetamol, coffee-break protocol, quantification, simulation

P21: Characterization of [3H]SIL26 binding to alpha-synuclein fibrils

Samuel Svensson[1], Wojciech Paslawski[2], Per Svenningsson[2], Dan Sohn[3], Peter Strom[3], Johan Sandell[3]

[1]*CBD Solutions, Center for Molecular Medicine, Stockholm, Sweden*
[2]*Department of Clinical Neuroscience, Karolinska Institutet, Stockholm, Sweden*
[3]*Novandi Chemistry AB, Biovation Park Telge, Sodertalje, Sweden*

α-Synuclein (α-Syn) forms highly ordered insoluble amyloid aggregates, which are stabilized by beta sheet protein structure (fibrils). α-Syn fibrils accumulate intracellularly as cytoplasmic (Lewy bodies) and as Lewy neuritic inclusions. α-Syn are also present in Aß plaques in AD, which might be indicative of an interactive mechanism between these proteins. Moreover, 50% of LDB patients develop Aß plaques and neurofibrillary tangles in addition to Lewy bodies suggesting that these pathologies may act synergistically. Furthermore, α-Syn fibrils are pathological hallmarks in PD, PD with dementia (PDD), Dementia with Lewy bodies (DLB) and multiple system atrophy (MSA). MSA is a more aggressive disorder than PD also has a higher α-syn load. In MSA, α-syn is predominantly found in glia. Considering the need of high binding selectivity over Aβ and tau fibrils. the development of a PET radioligand for α-syn is a major challenge. It has been reported that the radioligand [^{125}I]SIL23 binds both to recombinant α-syn fibrils and to tissue samples from α-syn mouse models in vitro. However, [123I]SIL23 has failed as an in vivo α-syn imaging agent. In the present study we have in vitro characterized radioligand binding of [^{3}H]SIL26 to recombinant α-syn fibrils. [^{3}H]SIL26 (36Ci/mmol) is a tritium labeled analogue of SIL23 and is commercially available through Novandi Chemistry AB. ^{3}H-SIL26 was found to bind to α-Syn fibrils at nM affinity and our data suggest that this ligand can be used in screening assays to identify new lead compounds for α-Syn PET tracers. To search for new lead compounds suitable as α-Syn PET tracers we now aim to screen a chemical library of unique amyloid binding compounds, which have previously been developed by CBD Solutions and collaborators. These compounds are structurally not related to SIL23/SIL26.

Keywords: alpha-synuclein, fibrils, positron emission tomography

P22: Reduced acquisition time PET quantification applied to [18F]-florbetapir

Catherine J Scott[1], Jieqing Jiao[1], Andrew Melbourne[1], Pawel J Markiewicz[1], Jonathan M Schott[2], Brian F Hutton[3,4], Sebastien Ourselin[1,2]

[1]*Translational Imaging Group, CMIC, University College London, London, United Kingdom*
[2]*Dementia Research Centre, Institute of Neurology, University College London, London, United Kingdom*
[3]*Institute of Nuclear Medicine, University College London, London, United Kingdom*
[4]*Centre for Medical Radiation Physics, University of Wollongong, NSW, Australia*

Introduction: Dynamic PET with pharmacokinetic modelling is a quantitative technique, however long acquisition times mean that SUVR is commonly used, despite its sensitivity to blood flow changes confounding longitudinal studies. We have proposed a novel method to incorporate cerebral blood flow (CBF) information from arterial spin labelling (ASL) MRI into the pharmacokinetic modelling to halve the acquisition time from 60 to 30 minutes. This method exploits the simultaneous acquisition of PET and MRI data using a PET/MRI scanner.

Aim: To perform sensitivity analysis for [^{18}F]-florbetapir data to assess the influence of errors in tracer delivery (R_1) estimation from ASL on the estimate of amyloid burden (BP_{ND}).

Methods: This methodology adapts the simplified reference tissue model (SRTM) for reduced acquisition time and was applied to 32 subjects from Insight46, a neuroimaging sub-study of the Medical Research Council National Survey of Health and Development. Linear regression was used to derive R_1 from ASL-CBF on a leave-one-out basis. Errors in R_1 estimation were calculated on a regional and voxelwise level and used for the sensitivity analysis. Sensitivity analysis was performed on 16 simulated time-activity-curves, at 15 noise levels (0.5-30%, 200 realizations per level).

Results: Fig.1 shows the sensitivity analysis, where regional BP_{ND} mean absolute error is below 0.1, which is a negligible change in amyloid burden. However, for voxelwise analysis, the higher error in R_1 estimation due to ASL artefacts, combined with greater noise in the PET, result in a clinically notable error level. This is reflected in the real data in fig.2 and fig.3.

Conclusions: The proposed method accounts for blood flow so is suitable for regional longitudinal analysis of [^{18}F]-florbetapir data, however improved R_1 estimation is required for voxelwise analysis. This methodology always outperforms SUVR and can be applied to other tracers in amyloid and tau imaging where SRTM is used.

	% noise in PET data														
% R1 error	0.5	0.7	0.9	1.2	1.6	2.2	2.9	3.9	5.2	7.0	9.3	12.5	16.7	22.4	30.0
1.5 (r)	0.0188	0.0220	0.0279	0.0370	0.0472	0.0585	0.0685	0.0795	0.0953	0.1056	0.1227	0.1364	0.1493	0.1510	0.1510
21.0 (v)	0.0791	0.0805	0.0821	0.0856	0.0888	0.0937	0.0974	0.1027	0.1127	0.1196	0.1343	0.1448	0.1562	0.1578	0.1578
Scale:	Regional level (r)							Voxel level (v)				Noisy voxel level			

Fig.1: Sensitivity analysis showing mean absolute error in amyloid burden estimation (BP_{ND}) for simulated data fitted using the proposed method on 30 minutes of PET data plus R_1 derived from ASL, compared to the gold standard 60 minutes of PET data. The different noise percentages represent different size regions of interest from regions, to voxels, to low signal voxels (noise in real data used here did not exceed 8% for single voxels). Two different percentage errors in R_1 estimation were simulated based on the errors found in real data, where there was a 1.5% error for regional analysis and 21% error for voxelwise analysis.

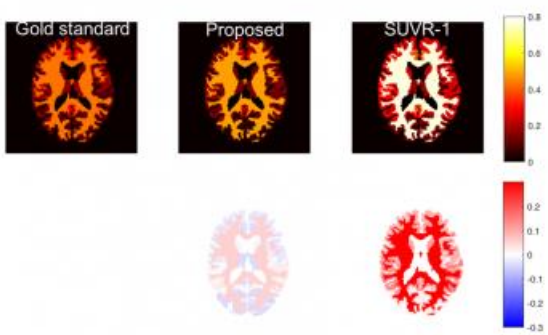

Fig.2: Regional analysis on an example subject. *[Top row]* estimation of amyloid burden (BP_{ND}), *[bottom row]* error compared to gold standard. This shows that the proposed method provides an accurate estimate of amyloid burden whereas SUVR greatly overestimates it.

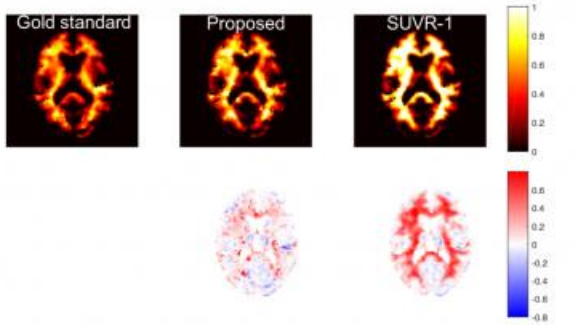

Fig.3: Voxelwise analysis on an example subject. *[Top row]* estimation of amyloid burden (BP_{ND}), *[bottom row]* error compared to gold standard. This shows that the proposed method is similar to the gold standard, but artefacts in the ASL data have made the estimation noisier. However, it outperforms SUVR which greatly overestimates amyloid burden.

Keywords: kinetic modelling, reduced acquisition time, blood flow, florbetapir, quantification

P23: Methodologic considerations for calculating standard uptake value ratio amyloid reduction in the Gantenerumab open label extension studies

Gregory Klein[1], Paul Delmar[2], Danielle Abi-Saab[2], Mirjana Andjelkovic[2], Smiljana Milosavljevic-Ristic[2], John Seibyl[3], Ken Marek[3], Ferenc Martenyi[2], Monika Baudler[2], Paulo Fontoura[2], Rachelle Doody[2]

[1]*Hoffman La Roche, Basel, Switzerland*
[2]*Roche/Genentech Product Development, Neuroscience, Basel, Switzerland*
[3]*InviCRO, LLC., Boston, MA, US*

Background: Gantenerumab is a fully human monoclonal antibody currently under evaluation at titrated doses up to 1200 mg SC monthly in the Scarlet RoAD (SR, NCT01224106) and Marguerite RoAD (MR, NCT02051608) open label extension (OLE) studies. The molecule has demonstrated high levels of florbetapir PET amyloid reduction, measured by standard uptake value ratio (SUVR) methods using a cerebellar grey reference region. Prior analyses of florbetapir ADNI data have shown higher longitudinal effect sizes using white matter reference regions compared to cerebellar regions. Here we report the effect size of different amyloid PET SUVR quantification methods and reference regions in the gantenerumab studies.

Methods: Template-space and native-space Freesurfer methods were used to compute SUVR measures of OLE baseline and OLE week 52 data. Analysis was restricted to the MR patients due to large variability of dosing and pre-OLE characteristics in the SR OLE study. Percentage of patients at week 52 below the amyloid positivity threshold and longitudinal effect size for patients meeting a high-dose criteria (≥ 6 doses at 900-1200 mg) were calculated for SUVR methods using cerebellar grey, whole cerebellum, pons, and subcortical white matter reference regions. Correlation of SUVR with total gantenerumab dosing was also calculated.

Results: Consistent, high reductions of SUVR to below the amyloid positivity threshold were seen for the 31 patients fulfilling the high dose criteria, regardless of reference region used. Longitudinal effect size and correlation with total gantenerumab dosing was largest for the pons reference region. A white matter reference was inferior to whole cerebellum and pons in both the template- and native-space approaches.

Conclusions: Optimal reference regions may be different for interventional studies compared to observational studies. Pons or whole cerebellar reference regions appear superior in an SUVR analysis to cerebellar grey or white matter for longitudinal studies of gantenrumab.

Keywords: gantenerumab, SUVR, amyloid, reference region

P24: A non-invasive optical retinal imaging method to predict cerebral amyloid PET status

Jean-Paul Soucy[1], Claudia Chevrefils[2], Jean-Philippe Sylvestre[2], Jean Daniel Arbour[3], Marc-André Rhéaume[3], Sylvain Beaulieu[4], Pedro Rosa-Neto[1,5,6], Sulantha S. Mathotaarachchi[1,5], Ziad S. Nasreddine[7], Serge Gauthier[6], Frédéric Lesage[8]

[1]*McConnell Brain Imaging Centre, Montreal Neurological Institute, McGill University, Montreal, QC, Canada*
[2]*Optina Diagnostics, Montreal, QC, Canada*
[3]*Clinique ophtalmologique 2121, Montreal, QC, Canada*
[4]*Département de médecine nucléaire, Hôpital Maisonneuve-Rosemont, Montreal, QC, Canada*
[5]*Translational Neuroimaging Laboratory, McGill Centre for Studies in Aging, Douglas Mental Health University Institute, Montreal, QC, Canada*
[6]*Alzheimer's Disease Research Unit, The McGill University Research Centre for Studies in Aging, Montreal, McGill University, Montreal, QC, Canada*
[7]*MoCA Clinic and Institute, Greenfield Park, QC, Canada*
[8]*École Polytechnique de Montréal, Institut de génie biomédical, Département de Génie électrique, Montreal, QC, Canada*

Background: There is a clear shift in clinical studies evaluating disease-modifying treatments for Alzheimer's disease (AD) towards recruiting amyloid positive subjects at the earliest stages of, or even before, cognitive impairment. A screening approach identifying such target populations could dramatically impact clinical trials by greatly reducing the cost associated with cerebral PET amyloid imaging. In this pilot study, a non-invasive retina (an optically accessible extension of the central nervous system) imaging approach with the Metabolic Hyperspectral Retinal Camera (MHRC) is evaluated as a proxy to identify biomarkers which correlate with the cerebral load of amyloid plaques.

Methods: The cohort (n=25) included probable AD (n=11) and age-matched controls (60 to 85 years) with no concomitant retinal diseases or significant ocular media opacity. Hyperspectral retinal measurements were obtained in the spectral range 450-900 nm (Figure 1). Image analysis based on textures on the spatial/spectral dimensions in segmented areas along the retinal vasculature was used to extract 16 statistical measures (Figure 2). A classifier was trained, using 61 datasets (1-3 per subject), to establish the predictive value of those texture features based on the cerebral amyloid status determined with ^{18}F-Florbetaben PET (SUVR). A leave-one-out approach was used to determine the sensitivity and specificity values of the method.

Results: Consistent with literature reports, 3 of 11 clinically probable AD cases were amyloid negative, while 3 of the 14 cognitively normal were amyloid positive. Excellent retinal scanning correspondence with PET amyloid status was achieved, independently of cognition, with estimated sensitivity and specificity values of 85% and 97%, respectively.

Conclusions: The developed machine learning approach, based on hyperspectral retinal imaging, shows promise in predicting cerebral amyloid PET status and could serve as a screening tool to identify subjects in the early stages of the AD continuum, for instance in a drug development context.

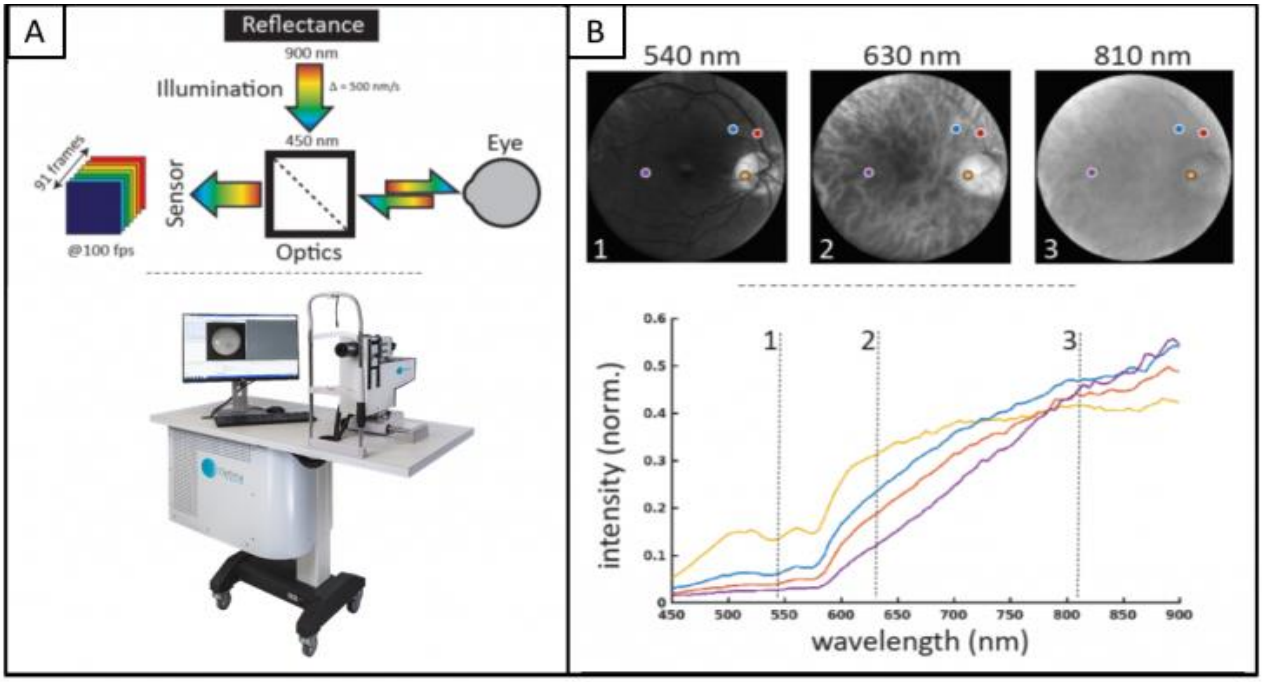

Figure 1. A) Schematic of the Reflectance mode and photograph of the MHRC. Using a scientific CMOS camera and fast wavelength selection from a supercontinuum laser, one can acquire images of the retina in a series of wavelengths delivering a dataset with spectral information at each pixel. B) Images at different wavelengths and different points chosen in tissue, over vessels and in the optic nerve show varying spectral characteristics used to discriminate properties of the retina.

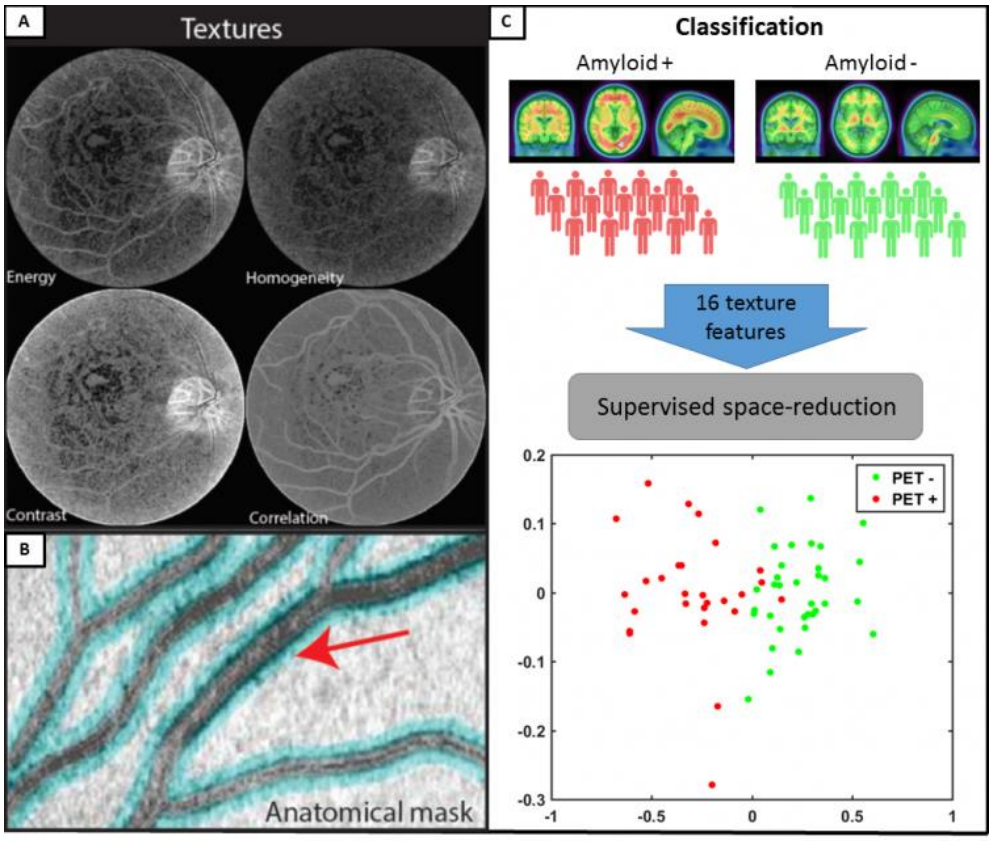

Figure 2. Process used to classify amyloid positive and negative subjects based on hyperspectral retinal images. Spatial/spectral texture maps are built (A) and 16 texture features are extracted around vessels (B) using an anatomical mask from vascular segmentation. Supervised classification of the retinal texture features based on the PET amyloid status leads to excellent discrimination of the amyloid positive and negative subjects when the first two components are kept (C).

Keywords: Amyloid, Retina, Hyperspectral imaging, PET, Screening

P25: Prediction of cognitive decline by 18F-AV45 PET normalized to subcortical white matter reference region

Julie Ottoy[1], Ellis Niemantsverdriet[2], Jeroen Verhaeghe[1], Ellen De Roeck[2], Hanne Struyfs[2], Charisse Somers[2], Leonie wyffels[3], Tobi Van den Bossche[2], Sara Van Mossevelde[2], Sarah Ceyssens[3], Sigrid Stroobants[3], Maria Bjerke[2], Sebastiaan Engelborghs[2], Steven Staelens[1]

[1]*Molecular Imaging Center Antwerp, University of Antwerp, Antwerp, Belgium*
[2]*Reference Center for Biological Markers of Dementia (BIODEM), University of Antwerp, Antwerp, Belgium*
[3]*Department of Nuclear Medicine, Antwerp University Hospital, Antwerp, Belgium*

Background: This study aimed to investigate the association between amyloid-beta (Aβ) plaque load and cognition, and their changes over a 12-month period in healthy controls (HC), MCI and AD dementia. The impact of reference tissue selection on these associations was evaluated.

Methods: Aβ-burden was quantified with positron emission tomography (PET) using 18F-AV45 SUVR in the frontal, parietal, temporal, and precuneus gray matter, normalized to either cerebellar gray ($SUVR_{CB}$) or subcortical white matter ($SUVR_{WM}$). Change in SUVR between baseline and follow-up (ΔSUVR) was defined as $100*(SUVR_{follow\text{-}up}–SUVR_{baseline})/SUVR_{baseline}$. Cognitive measures included MMSE and RBANS scores. The clinical diagnosis was made by consensus of an expert panel (not biomarker-based). Associations between Aβ-PET and cognition were investigated using ANCOVA corrected for gender, age, *APOE-ε*4, education, baseline diagnosis, and time between PET scans.

Results: Higher baseline $SUVR_{WM}$ was associated with lower $\Delta SUVR_{WM}$ (e.g. frontal: p=0.006; MCI: n=19, AD: n=4), indicating that amyloid reaches a plateau (Fig.1). There was no such association for reference CB. The number of subjects in whom SUVR contra-intuitively decreased over time (ΔSUVR<0) was less for reference WM compared to CB (e.g. frontal: 9% versus 35%, Fig.1 and Fig.2). At baseline and for all cortical target regions, higher $SUVR_{CB\_or\_WM}$ was significantly associated with lower cognitive performance (immediate and delayed recall; HC: n=11, MCI: n=38, AD: n=13). In this respect, lower p-values were reached for WM than CB normalization (immediate: p=0.0004 vs p=0.005; delayed: p=0.024 vs p=0.046). In addition, higher baseline $SUVR_{WM}$ and lower $\Delta SUVR_{WM}$ was significantly associated with more cognitive decline (resp. Δdelayed (HC: n=10, MCI: n=28, AD: n=8) and Δimmediate recall (MCI: n=19, AD: n=3)). There was no such association for reference CB.

Conclusion: Cortical $SUVR_{WM}$ was stronger associated with cognition than $SUVR_{CB}$. Higher baseline $SUVR_{WM}$ was associated with higher change in cognitive impairment and lower change in amyloid over time.

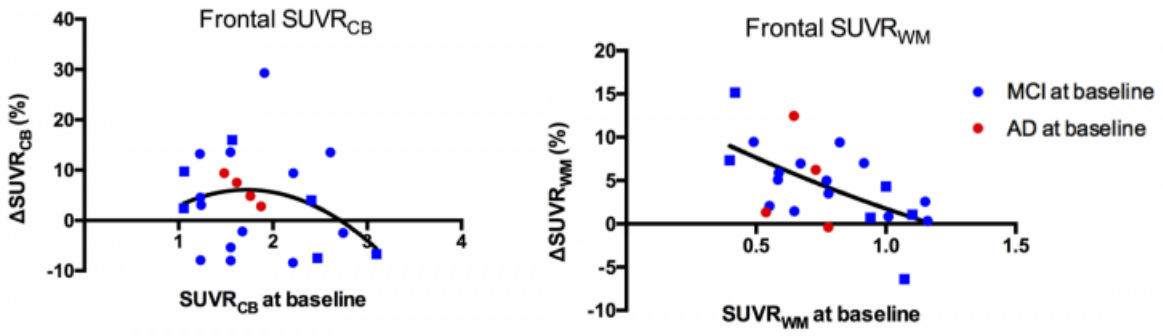

Fig. 1: Frontal lobe ΔSUVR versus SUVR at baseline, normalized to either CB (SUVR$_{CB}$, left) or WM (SUVR$_{WM}$, right). Blue squares indicate the MCI subjects who converted to AD dementia after 1 year follow-up.

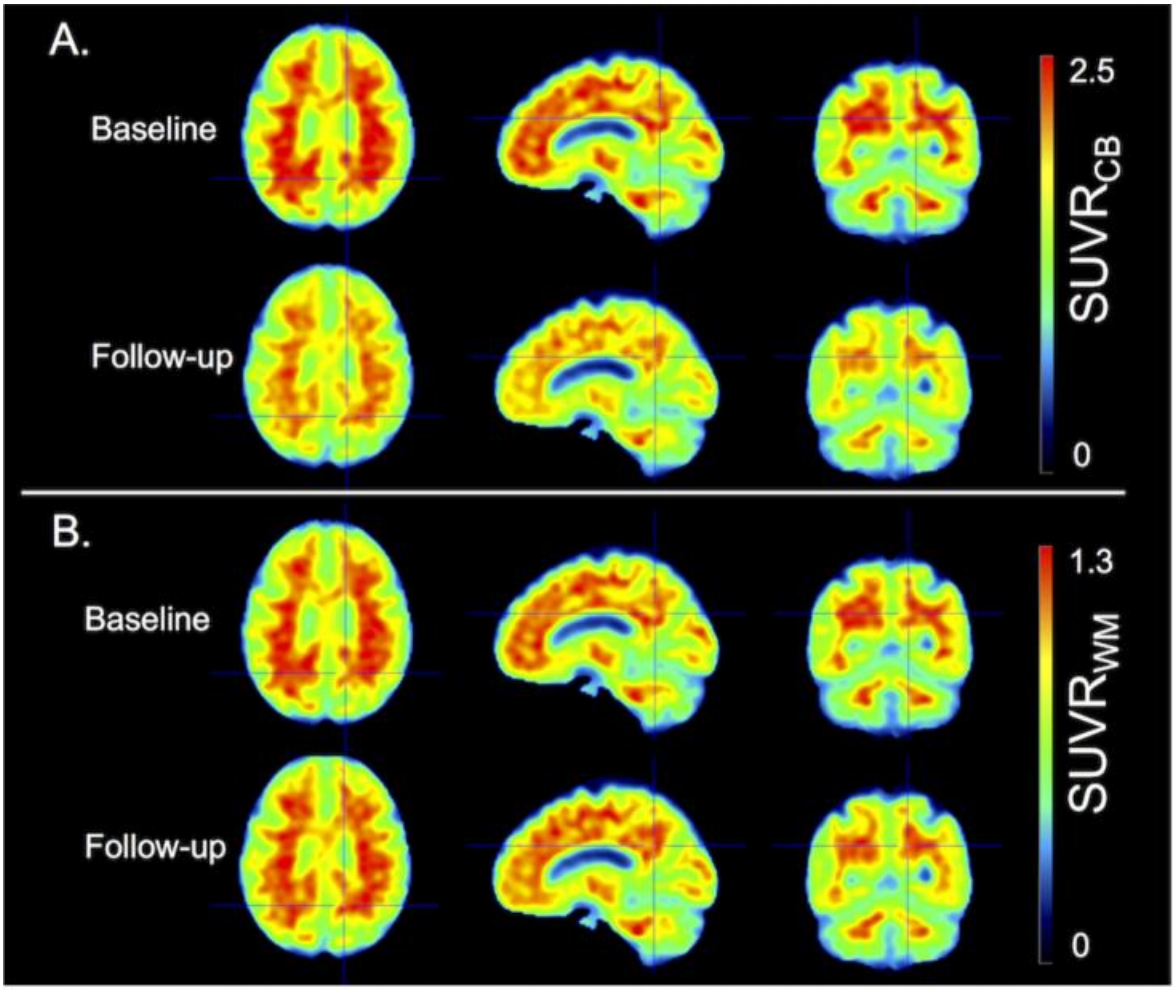

Fig. 2: Illustration in one MCI subject, showing unexpected decline in SUVR$_{CB}$ (panel A) from baseline towards follow-up, whereas SUVR$_{WM}$ (panel B) was stable or slightly increased depending on the brain region.

Keywords: Alzheimer's disease, 18F-florbetapir, PET, reference region, biomarkers

P26: Centiloid analysis in cross-sectional and longitudinal PiB PET studies

Yi Su[1,3], Shaney Flores[1], Russ Hornbeck[1], Benjamin Speidel[5], Andrei Vlassenko[1,3], Brian Gordon[1,3], Robert Koeppe[6], Mark Mintun[7], William Klunk[8], Chengjie Xiong[3,4], John Morris[2,3], Tammie Benzinger[1,3]

[1]*Department of Radiology, Washington University School of Medicine, St. Louis, MO, US*
[2]*Department of Neurology, Washington University School of Medicine, St. Louis, MO, US*
[3]*Knight Alzheimer Disease Research Center, Washington University School of Medicine, St., MO, US*
[4]*Division of Biostatistics, Washington University School of Medicine, St. Louis, MO, US*
[5]*Department of Radiology and Biomedical Imaging, University of California, San Francisco, CA, US*
[6]*Department of Radiology, University of Michigan, Ann Arbor, MI, US*
[7]*Avid Radiopharmaceuticals, Philadelphia, PA, US*
[8]*Department of Neurology, University of Pittsburgh, Pittsburgh, PA, US*

Background: The Centiloid approach is proposed to standardize amyloid PET quantification from different groups and using different methods or different tracers. It is unclear how well this approach can harmonize amyloid burden measurements derived from different underlying quantification methods. In this study, we assess the variability of the amyloid burden measurements in the Centiloid scale using cross-sectional and longitudinal imaging data.

Methods: [^{11}C]-Pittsburgh compound B (PiB) imaging data from the Global Alzheimer's Association Information Network (GAAIN) and Knight Alzheimer Disease Research Center (ADRC) were analyzed using different quantification techniques and converted to the Centiloid scale. The inter- and intra-individual variabilities of amyloid burden measurements were assessed in participants with minimal amyloid burden. Effect size and sample size estimation were also performed based on the variability of amyloid burden measurements and annual rate of amyloid accumulation.

Results: The Centiloid approach normalizes amyloid burden measurements derived from different quantification techniques into a common comparable Centiloid scale. However, inter- and intra- individual variabilities of amyloid burden measurements in the Centiloid scale is dependent upon the underlying quantification techniques. Partial volume correction reduces the measurement variabilities ($p<0.05$). The largest effect size in annual amyloid burden change was achieved when brainstem was used as the reference region for standard uptake value ratios with partial volume corrected data. The estimated sample size required in hypothetical clinical trials was also smallest using Centiloid measurements obtained using this approach (N=17).

Conclusion: As a simple scaling method, the Centiloid process can provide a degree of standardization across different quantification techniques, but it does not affect the variability inherent in a technique prior to standardization. Thus, the differences across techniques in sensitivity to amyloid burden changes in longitudinal studies remains after scaling. When possible, common processing techniques should be used for analysis of data across multiple projects and centers.

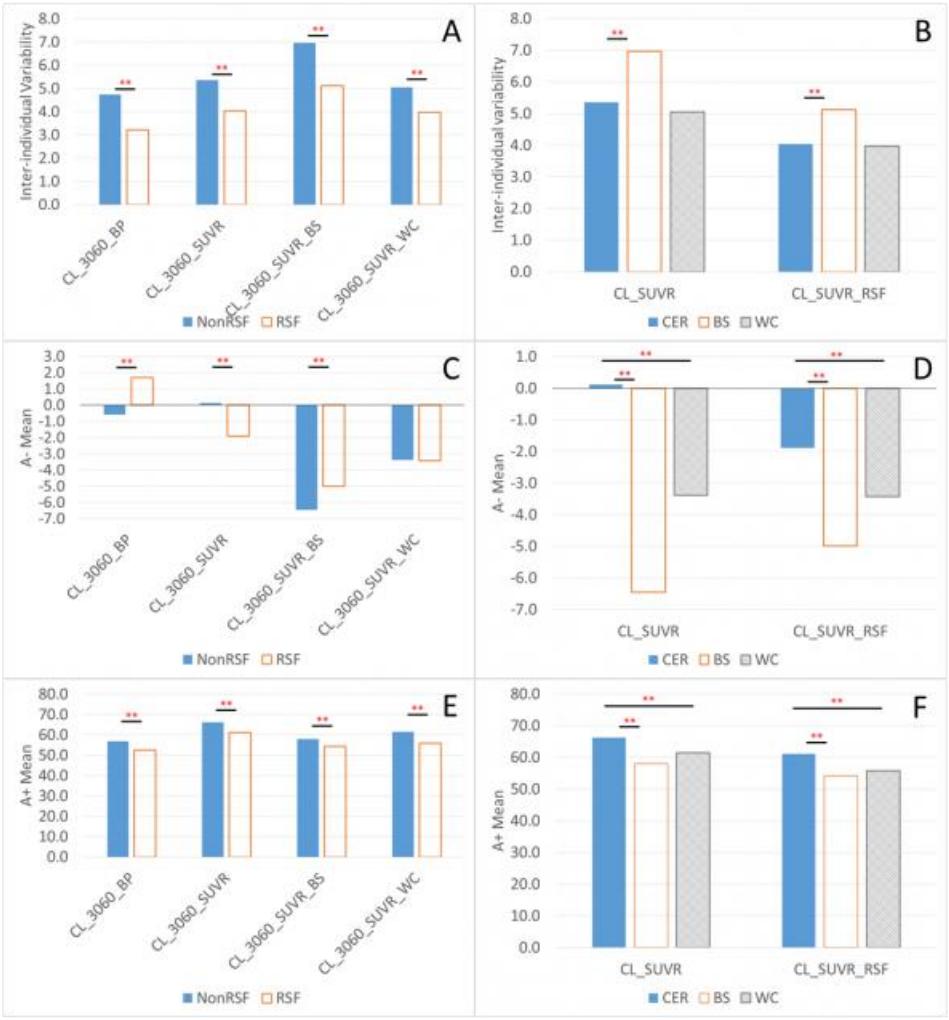

Figure 1. Comparison of inter-individual variability of measured amyloid burden (A, B), mean amyloid burden in people with minimal amyloid burden (C, D), and in people with substantial amyloid (E, F), for different quantification methods, i.e. with or without partial volume correction (A, C, E), and using different reference region (B, D, F). RSF: Regional spread function based partial volume correction; NonRSF: without partial volume correction; **significant difference ($p<0.0005$) that survives Bonferroni correction for multiple comparisons.

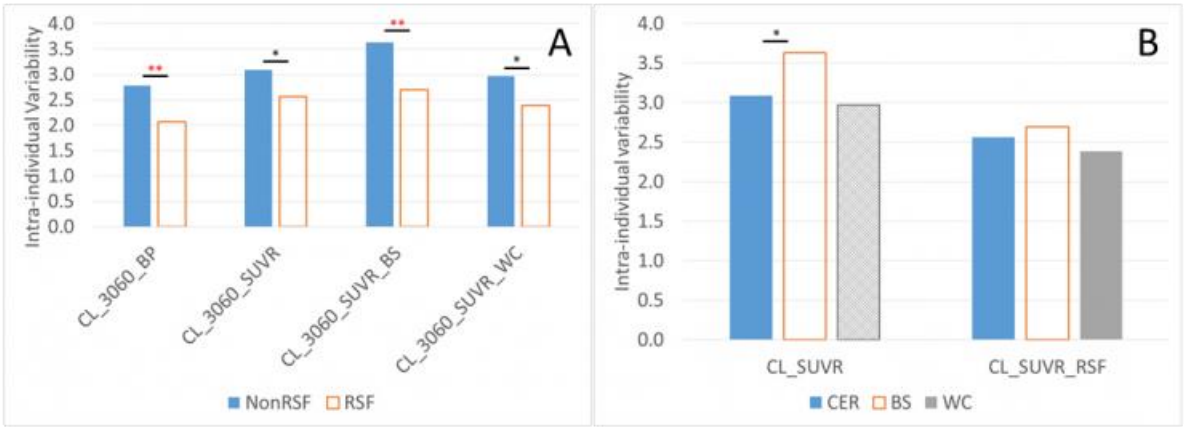

Figure 2. Comparison of intra-individual varability of amyloid burden measurements for quantification methods with and without partial volume correction (A), and using different reference region (B). RSF: Regional spread function based partial volume correction; NonRSF: without partial volume correction; **significant difference ($p<0.0005$) that survives Bonferroni correction for multiple comparisons. *significant difference ($p<0.05$) that does not survive Bonferroni correction.

	CL_3060_BP	CL_3060_ BP_RSF	CL_3060_ SUVR	CL_3060_ SUVR_RSF	CL_3060_ SUVR_BS	CL_3060_ SUVR_RSF _BS	CL_3060_ SUVR_WC	CL_3060_ SUVR_RSF _WC
Intra-individual variability	2.8	2.1	3.1	2.6	3.6	2.7	3.0	2.4
Annualized rate of change in A+ group	3.5	3.7	3.9	4.4	5.1	5.2	4.0	4.3
Effect size of annual change	1.3	1.8	1.2	1.7	1.4	1.9	1.3	1.8
Sample Size (50% reduction in rate)	51	31	70	45	30	17	58	31
p-values								
longitudinal change in A+ group	2.15E-12	9.41E-17	4.21E-10	2.67E-13	1.99E-16	1.05E-22	1.95E-11	9.09E-17
test of intra-individual variability								
RSFvsNonRSF		7.61E-05		1.27E-02		6.88E-05		3.28E-03
BSvsCER					3.10E-02	5.14E-01		
WCvsCER							5.88E-01	3.21E-01
SUVRvsBP			1.51E-01	3.62E-03				

Figure 3. Summary of Centiloid analysis results in the longitudinal Knight ADRC cohort. The default reference region is cerebellar cortex. CL: Centloid value; BP: binding potential; RSF: regional spread function based partial volume correction; SUVR: standard uptake value ratio; BS: brainstem as the reference region; WC: whole cerebellum as the reference region.

Keywords: PET, PiB, amyloid imaging, Centiloid

P27: The impact of PET reconstruction method on measured amyloid SUVR

Dawn Matthews[1], Randolph Andrews[1], Anne Smith[2]

[1]*ADM Diagnostics, Northbrook, IL, US*
[2]*Siemens Medical Solutions USA, Inc., Knoxville, TN, US*

Background: The measurement of amyloid PET Standardized Uptake Value Ratio (SUVR) can be effected by numerous technical factors. Since typical annual rates of amyloid accumulation are in the 1 to 3% range, even small variations can significantly increase the number of subjects required to detect a change in burden due to disease or to treatment intervention. We systematically evaluated the impact of image reconstruction method and parameters upon amyloid SUVR, and whether certain regions were most susceptible to reconstruction method variability.

Methods: The florbetapir PET scans of fifteen subjects (2 HC, 7 MCI, 6 early AD) imaged from 50 to 70 minutes post-tracer injection on a Siemens mCT scanner were reconstructed using several different methods and parameters. Methods evaluated were Filtered Back Projection, OSEM, and OSEM with Point Spread Function (OSEM+PSF). Smoothing of 0mm, 3mm, and 5mm FWHM, and voxel sizes of 2mmx2mmx2mm and 1mmx1mmx2mm were compared. OSEM permutations of 2, 4, and 6 iterations were also compared. Intensities were measured for two sets of target regions of interest (ROIs), the first based upon the AAL atlas and the second using Freesurfer segmentation. Reference regions included whole cerebellum, cerebellar cortex, brainstem, pons, and white matter. Multivariate machine learning approaches were applied to identify voxel-based differences between methods.

Results: Reconstruction parameters impacted SUVR. Cortical average SUVR (reference whole cerebellum) deviations were within +/- 4% from the OSEM 4i24s 5mm values used as a reference point. However, individual regions showed large changes in individual subjects, often exceeding +/-15%. Regions most impacted were cingulate, frontal and temporal pole. The brainstem was consistently the most variable across reconstruction methods, followed by pons. Whole cerebellum and white matter were least variable.

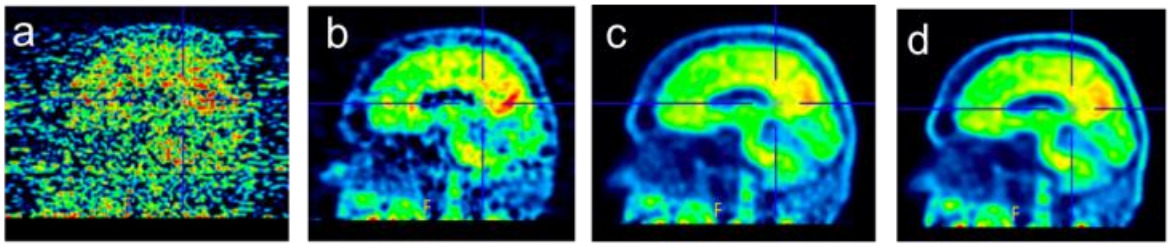

Figure 1. Florbetapir image reconstructed using (a) FBP 0mm smooth; (b) FBP 5mm; (c) OSEM 4i24s 5mm; (d) OSEM+PSF 4i24s 5mm.

Conclusions: Image reconstruction can impact amyloid SUVR, particularly on a regional and individual level, and method consistency is thus important in longitudinal clinical trials.

Keywords: amyloid, reconstruction, variability

P28: Head-to-head comparison of 11C-PBR28 and 18F-GE180 for the quantification of TSPO in the human brain

Paolo Zanotti Fregonara[1], Belen Pascual[1], Gaia Rizzo[2], Meixiang Yu[1], Neha Pal[1], David Beers[1], Randall Carter[3], Stanley Appel[1], Nazem Atassi[4], Joseph Masdeu[1]

[1]Nantz National Alzheimer Center and Houston Methodist Neurological Institute, and Weill Cornell Medicine, Houston, TX, US
[2]Imanova Ltd., Centre for Imaging Sciences, Hammersmith Hospital, London, United Kingdom
[3]GE Global Research, Schenectady, NY, US
[4]Neurological Clinical Research Institute, Massachusetts General Hospital, Boston, MA, US

Introduction: ^{18}F-GE180 is a new positron emission tomography (PET) tracer to quantify the translocator protein TSPO, a biomarker for inflammation. The aim of this study was to compare head-to-head ^{18}F-GE180 to the well-established TSPO tracer ^{11}C-PBR28, by scanning with either tracer during the same day in the same subjects.

Methods: Five subjects underwent a 90-minute PET scan with ^{11}C-PBR28 in the morning and ^{18}F-GE180 in the afternoon. A metabolite-corrected arterial input function was obtained in each subject for both tracers, and the brain uptake was quantified with a two-tissue compartmental model.

Results: The rate of metabolism of ^{18}F-GE180 in arterial blood was slower than that of ^{11}C-PBR28 (the percentages of unmetabolized parent in plasma at 90 minutes were 74.9 ± 4.15% and 11.2 ± 1.90%, respectively). The plasma free fraction was similar for both tracers: 3.5% ± 1.1 for ^{18}F-GE180 and 4.1% ± 1.1 for ^{11}C-PBR28. The average total volume of distribution (V_T) of ^{18}F-GE180 was about 20 times smaller than that of ^{11}C-PBR28 (0.15 ± 0.03 mL/cm^3 for ^{18}F-GE180 and 3.27 ± 0.66 mL/cm^3 for ^{11}C-PBR28). ^{18}F-GE180 was characterized by a poor transfer from the vascular compartment to the brain (K_1 was about ten times smaller than that of ^{11}C-PBR28). Moreover, kinetic modeling was more difficult with ^{18}F-GE180, as its V_T values were identified with a lower precision than those of ^{11}C-PBR28 and outlying values were more frequent.

Conclusion: The V_T of ^{18}F-GE180 is about 20 times smaller than that of ^{11}C-PBR28, due to a low penetration in the brain from the vascular compartment. In addition, kinetic modeling of ^{18}F-GE180 is more challenging than with ^{11}C-PBR28. Therefore, compared to ^{11}C-PBR28, ^{18}F-GE180 has unfavorable characteristics for TSPO imaging.

Keywords: 11C-PBR28, 18F-GE180, neuroinflammation, TSPO

P29: Longitudinal change in brain perfusion in cognitively normal elderly subjects measured by early frames Florbetapir F 18 PET

Sergey Shcherbinin[1], Adam Schwarz[1], Yi Su[2], Arnaud Charil[1], Russ Hornbeck[2], Jon Christensen[2], Jennifer Eads[1], Tammie Benzinger[2], John Sims[1]

[1]*Eli Lilly and Company, Indianapolis, IN, US*
[2]*Washington University in St. Louis, School of Medicine, Saint Louis, MO, US*

Background: Existing cross-sectional data support the potential utility of using the early frames of florbetapir F 18 PET scans as a biomarker of brain perfusion, but its longitudinal performance characteristics remain unknown. We report initial findings on longitudinal change in perfusion derived from early-frames florbetapir scans in cognitively normal older individuals.

Methods: We examined longitudinal (follow-up period [mean±SD] 2.0±0.9 years) changes in dynamic 0-70 minute florbetapir images for N=41 cognitively normal participants (22 female / 19 male, age 67.5±8.0, MMSE 29.3±1.0) from the Knight Alzheimer's Disease Research Center Memory and Aging Projects. Elevated amyloid level was defined as >19 centiloids (Jack CR *et al*, 2017) on the 50-70 minute images. Perfusion was derived from 0-5 minute images and quantified as the mean signal in a composite (temporal, parietal and cingulate) region of interest with two reference regions, pSUVR-cortex and pSUVR-pons.

Results: The mean longitudinal change was -0.5% using pSUVR-cortex and -1.3% and using pSUVR-pons, with the majority of individual changes being <±5% (Figure). The mean pSUVR-cortex change for individuals with elevated amyloid levels (N=18) was -0.012±0.016 (14/18 showing a perfusion decrease) compared with 0.000±0.025 for those without elevated amyloid (N=23; 11/23 showing a perfusion decrease). Moreover, 56% of participants with pSUVR-cortex that decreased over time (compared with 25% of participants with increased pSUVR-cortex) had elevated amyloid level at baseline. Results with pSUVR-pons were similar, although the spread of perfusion measurements was greater.

Conclusions: Preliminary analysis of 41 longitudinal dynamic florbetapir images revealed small (although mirroring the reduction seen in FDG (Landau SM *et al*, 2011)) changes in perfusion over the approximately 2-year follow-up period. Importantly, the test-retest characteristics of these measures remain to be assessed. The current observations further encourage examination of early-frames florbetapir scans as a potential surrogate for measuring the progression of neurodegeneration in longitudinal studies.

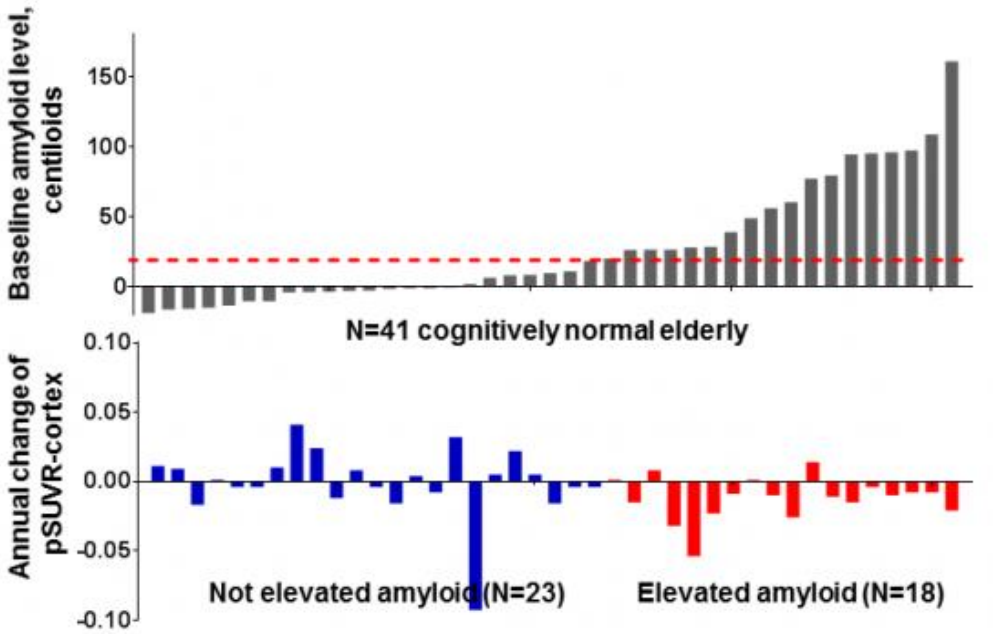

	Not elevated amyloid level, [mean ± SD]	Elevated amyloid level, [mean ± SD]
Age, years	65.2 ± 8.1	70.4 ± 7.1
% female	N=12 (52%)	N=10 (56%)
% ApoE carriers	N=4 (17%)	N=9 (50%)
MMSE	29.3 ± 1.0	29.4 ± 1.0
Amyloid level, centiloids	-2.5 ± 9.9	65.0 ± 38.7
Baseline pSUVR-pons	1.19 ± 0.09	1.25 ± 0.11
Baseline pSUVR-cortex	1.03 ± 0.05	1.06 ± 0.05
Annual change pSUVR-pons	-0.003 ± 0.035	-0.033 ± 0.060
Annual change pSUVR-cortex	0.000 ± 0.025	-0.012 ± 0.016
% decreased pSUVR-pons	N=12 (52.2%)	N=13 (72.2%)
% decreased pSUVR-cortex	N=11 (47.8%)	N=14 (77.8%)

Keywords: florbetapir perfusion longitudinal progression biomarker

P30: Simplified non-invasive tracer kinetic analysis for 18F-Florbetaben PET using a dual time-window acquisition protocol

Susan De Santi[1], Henryk Barthel[2], Santiago Bullich[3], Norman Koglin[3], Georg Becker[2], Aleksandar Jovalekic[3], Andrew Stephens[3], Osama Sabri[2]

[1]*Piramal Imaging, Boston, MA, US*
[2]*University of Leipzig, Leipzig, Germany*
[3]*Piramal Imaging GmbH, Berlin, Germany*

Background: Accurate quantitation of amyloid-beta (Aß) plaque load using positron-emission-tomography (PET) is important for monitoring Aß accumulation and response to therapy. A standardized uptake value ratios (SUVR) approach is found to be suitable in most clinical research settings, but might introduce a bias due to radiotracer clearance or cerebral blood flow (CBF) changes over time. The objectives of this work were: (1) to validate a non-invasive kinetic modeling method for 18F-florbetaben PET using a simplified acquisition protocol and (2) to assess the influence of CBF changes and radiotracer clearance on SUVRs and non-invasive kinetic modeling data.

Methods: Data from twenty subjects (10 probable AD, 10 age-matched healthy volunteers) scanned dynamically for 140 min were used. Arterial samples were collected during scanning and corrected for metabolites. The binding potential (BP_{ND}) was compared to the SUVR and to non-invasive tracer kinetic methods (simplified reference tissue model (SRTM), and multilinear reference tissue model (MRTM2)) and different shortened or interrupted acquisition approaches were compared. Simulations were carried out to assess the effect of CBF and radiotracer clearance changes.

Results: A 0-30 and 120-140 min dual time-window acquisition protocol provided the best compromise between patient comfort and quantification accuracy. By that, excellent agreement was found between BP_{ND} obtained using full and two time-window (2TW) acquisition protocols ($BP_{ND,2TW}$= 0.01+ 1.00x$BP_{ND,FULL}$, R^2=0.97 (MRTM2); $BP_{ND,2TW}$= 0.05+ 0.92x$BP_{ND,FULL}$, R^2=0.93 (SRTM)). Simulations showed a limited impact of CBF and radiotracer clearance changes on MRTM2 parameters and SUVRs.

Conclusion: This study demonstrates accurate non-invasive kinetic modeling of 18F-florbetaben PET data using a simplified dual time-window dynamic acquisition protocol, thus providing a good compromise between quantification accuracy, scan duration and patient burden. In cases, where maximum quantification accuracy is needed, a dynamic scan protocol may be beneficial.

Keywords: PET, amyloid, modeling, florbetaben

P31: Optimal time window for [18F]-AV-1451 binding quantification in AD using SUVr

Catriona Wimberley[1], Julien Lagarde[1,2], Pauline Olivieri[1,2], Bertrand Kuhnast[1], Fabien Caillé[1], Philippe Gervais[1], Marie Sarazin[1,2], Michel Bottlaender[1,3]

[1]UMR 1023 IMIV, Service Hospitalier Frédéric Joliot, CEA, Inserm, Université Paris Sud, CNRS, Université Paris-Saclay, Orsay, France
[2]Unit of Neurology of Memory and Language, Université Paris Descartes, Sorbonne Paris Cité, INSERM UMR S894, Centre Hospitalier Sainte Anne, Paris, France
[3]UNIACT, Neurospin, CEA, Gif-sur-Yvette, France

Brain tau aggregate can be assessed with [^{18}F]-AV-1451 PET. The SUV ratio of [^{18}F]-AV-1451 has been shown to be correlated with binding parameters estimated from compartmental modelling. Usually, a time window earlier than 130 min is used, when the SUVr is not at equilibrium introducing a bias. The later time points are more likely to be in equilibrium but are often disregarded due to higher noise. The aim of this work was to denoise the images and to compare SUVr at the early and late acquisition windows.

Five amyloid-positive (PIB-index >1.45) Alzheimer patients and 5 amyloid-negative age-matched healthy volunteers were included. [^{18}F]-AV-1451 was synthesized on site with precursor supplied by Avid Radiopharmaceuticals (Philadelphia, USA). PET scans were performed on a HRRT camera (Siemens) for two acquisition windows (70-120 and 180-220 min after 370 MBq tracer injection) and images were reconstructed using OSEM with PSF correction. The images were denoised using a principal components analysis. SUVr was calculated for original and denoised images. Regional SUVr from early and late acquisition windows were compared.

In healthy controls, the SUVr appears stable between the 2 windows (mean regional increase: 6.2±5.7%). In AD patients, SUVr increase during the early acquisition window, and were higher at the later acquisition window (180-220 min), but are more stable within the window. The % difference of SUVr value between the two acquisition windows depended on the late SUVr value: the higher the late SUVr, the larger the % difference (Fig 3).

The SUVr from early time windows are underestimated when compared to the more stable SUVr at the late windows. This underestimation is not linear: the higher the late SUVr, the higher the loss of values at early times. The use of denoising allows the use of the late time window for a more reliable SUVr estimation.

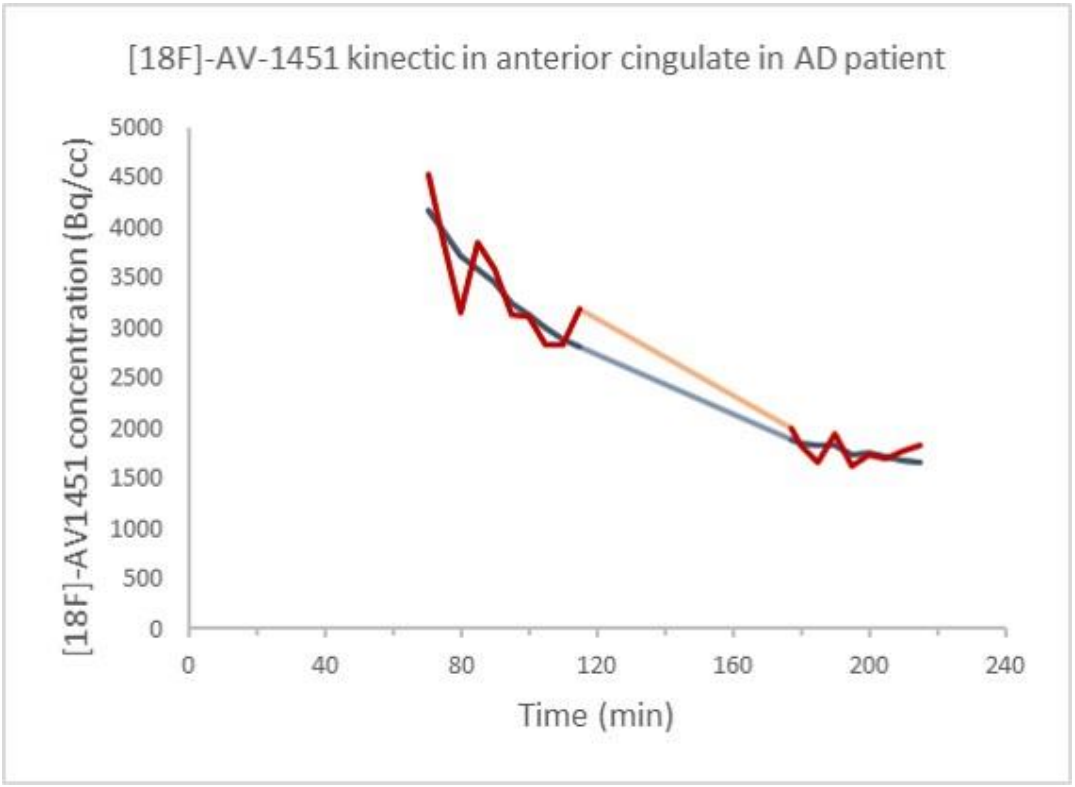
[18F]-AV-1451 kinectic in anterior cingulate in AD patient
[18F]-AV1451 concentration (Bq/cc)
5000
4500
4000
3500
3000
2500
2000
1500
1000
500
0
0
40
80
120
160
200
240
Time (min)

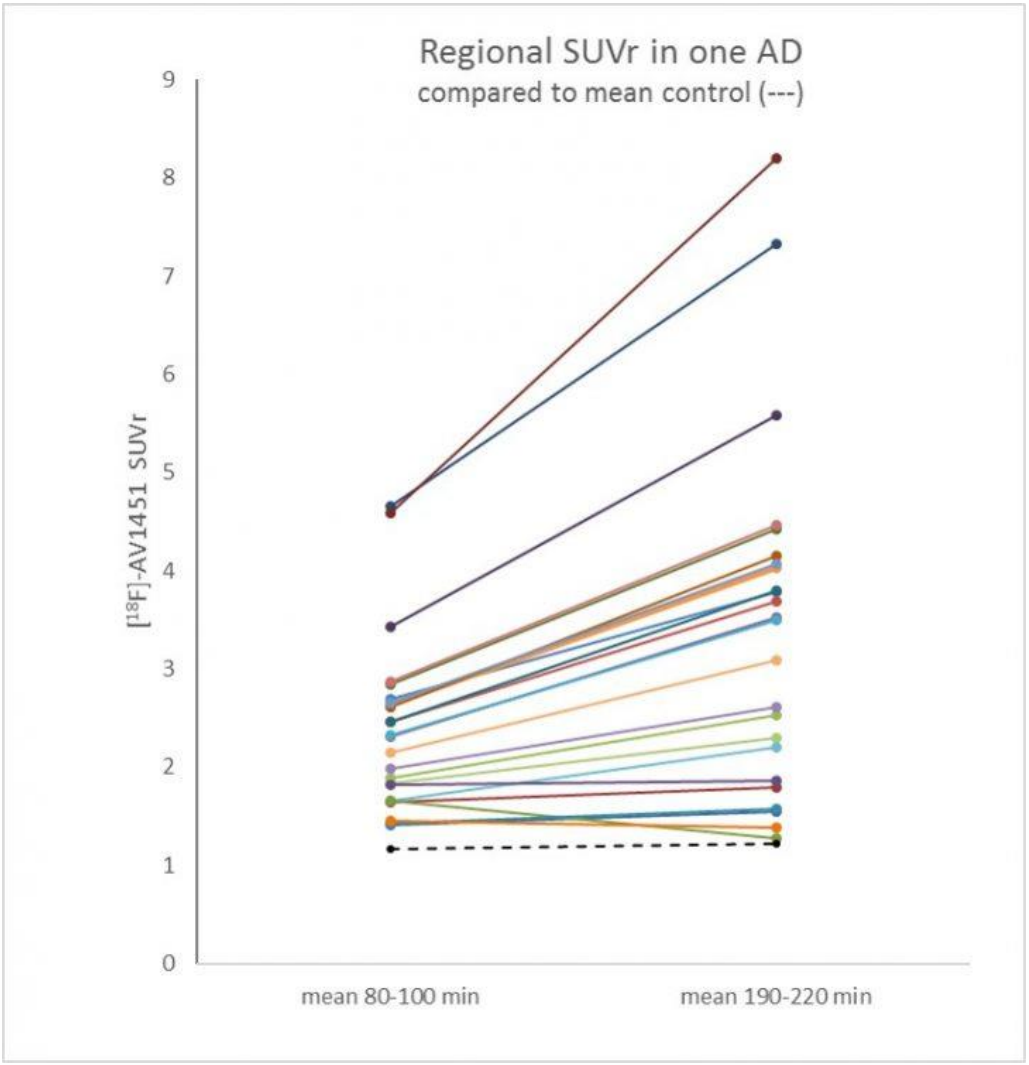
Regional SUVr in one AD
compared to mean control (---)
[18F]-AV1451 SUVr
9
8
7
6
5
4
3
2
1
0
mean 80-100 min
mean 190-220 min

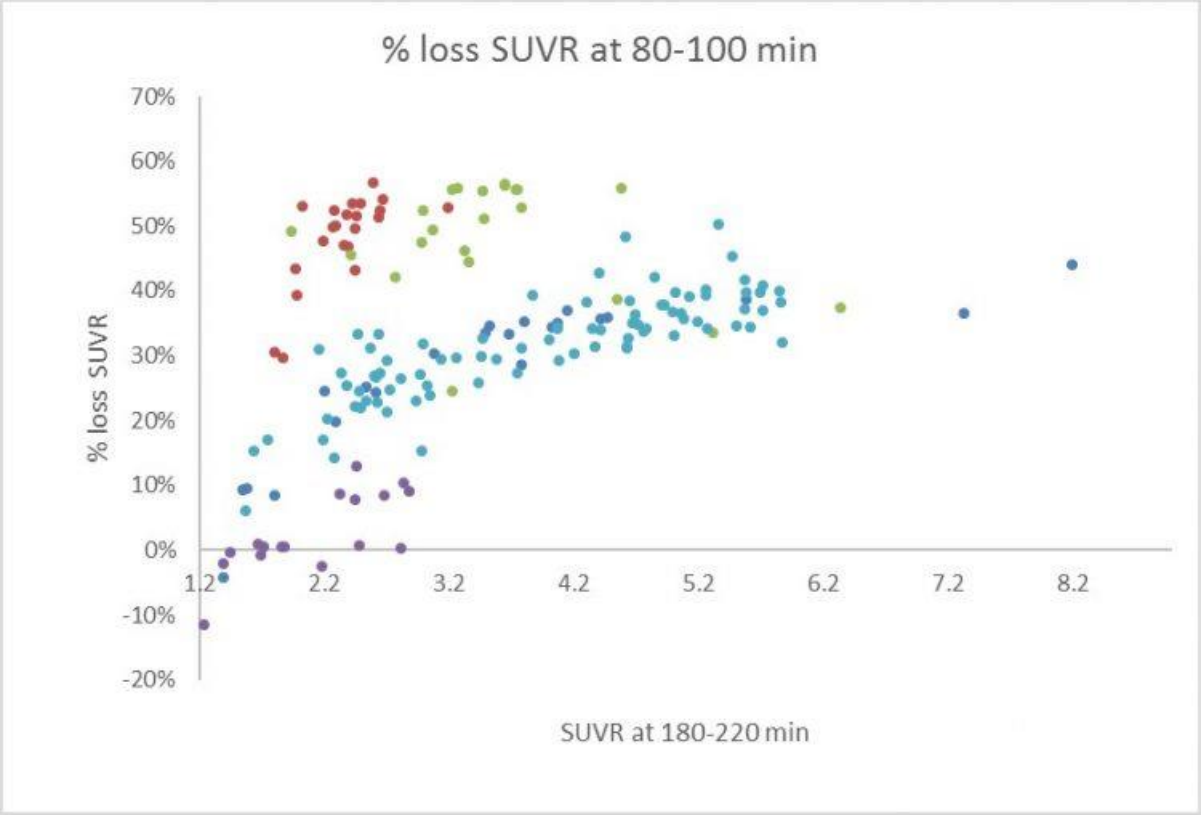

Keywords: Tau, AV-1451, PET, Denoising, SUVr

P32: Amyloid tracer harmonization using a bootstrapped non-linear mapping

Michael Properzi[1], Rachel Buckkley[1,4,5,6], Elizabeth Mormino[7], Julie Price[2,4], Reisa Sperling[1,3,4], Keith Johnson[2,4], Aaron Schultz1[1,4]

[1]*Department of Neurology, Massachusetts General Hospital, Boston, MA, US*
[2]*Department of Radiology, Massachusetts General Hospital, Boston, MA, US*
[3]*Department of Neurology, Brigham and Women's Hospital, Boston, MA, US*
[4]*Harvard Medical School, Boston, MA, US*
[5]*Florey Institutes of Neuroscience and Mental Health, Melbourne, Australia*
[6]*Melbourne School of Psychological Science, Melbourne, Australia*
[7]*Stanford University, Stanford, CA, US*

Introduction: There is an increasing drive to merge large, amyloid-PET datasets in order to address more complex research questions, inform AD clinical trials, and translate results between amyloid radiotracers. An impediment to comparisons between amyloid-PET radiotracers are differences in dynamic range, sensitivity, and scaling. We present a bootstrapped non-linear mapping (BNLM) approach that allows direct comparison between Ab-PET datasets using different tracers (Pittsburgh Compound-B (PiB) and Florbetapir (FBP)).

Methods: We utilize baseline Ab-PET datasets of clinically-normal participants from ADNI (FBP), AIBL (PIB), and HABS (PIB). Summary measures were computed via a PET-template pipeline as SUVrs using a cortical composite (FLR) with a whole-cerebellum reference region. Cross-sample mapping was performed via 10,000 bootstrapped samples of PiB and FBP matched for age, sex and apolipoprotein e4 (APOEe4) status. A transfer function for each bootstrapped sample was generated via smoothed cumulative distribution functions. An SUVr equivalency map and confidence intervals were extracted across these 10,000 fits using sliding-window PCA.

Results: We compared BNLM with a reference method that linearly transforms PiB to FBP data. Figure 2 shows the effect of the transformations, and highlights the improvement of the distributional scales after non-linear transformation in comparison with a linear method. Non-linearly transformed PiB data was not significantly different from raw FBP data when tested using a two sample KS-test (KS=0.06,p=0.416). By contrast, linearly transformed data showed significant differences (KS=0.11,p=0.01). We confirmed the applicability of this method on an out of sample AIBL FBP dataset.

Discussion: Our non-linear transformation method allows for more direct comparisons between PET radiotracers. It has the advantage of accounting for underlying demographic differences and thus avoiding the introduction of systematic cohort biases. Future work will assess the sensitivity of our method to reproduce in-cohort classifications of high/low amyloid post-transformation, and its applicability to other radiotracers.

Keywords: Amyloid, Cross-Tracer, Non-Linear

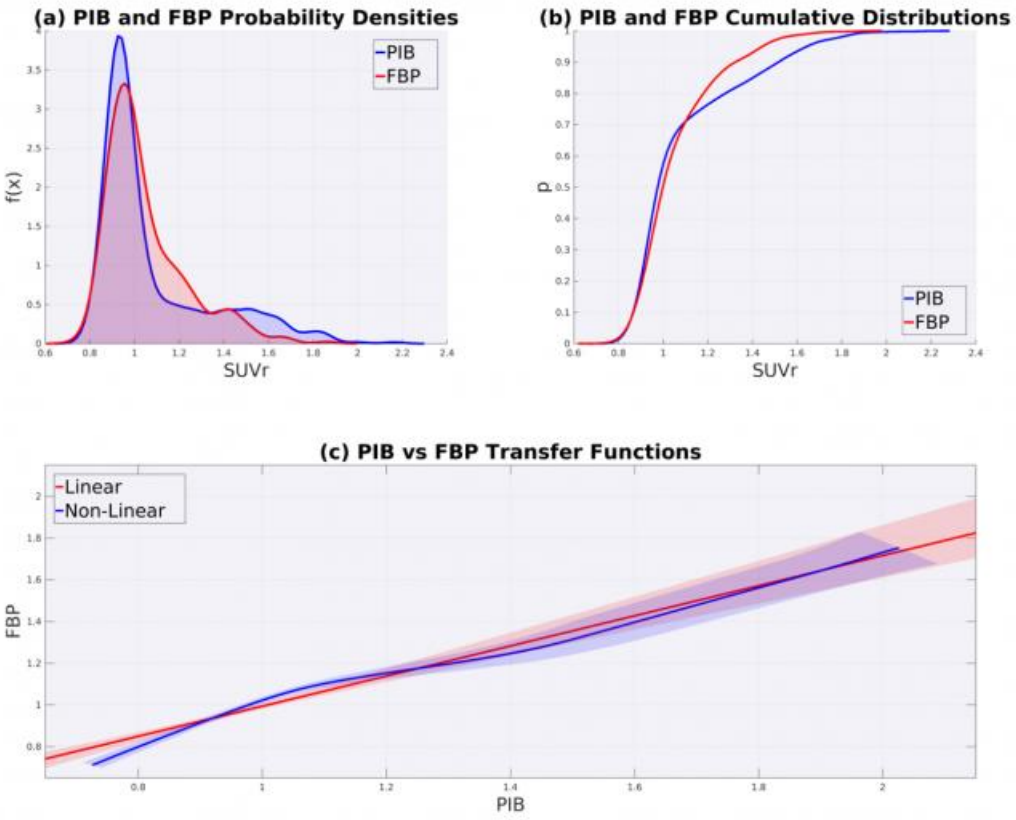

Figure 1: (a) & (b) PIB and FBP distributions exhibit a non-linear relationship in scale. (c) Transfer functions created from 10,000 matched sub-samples.

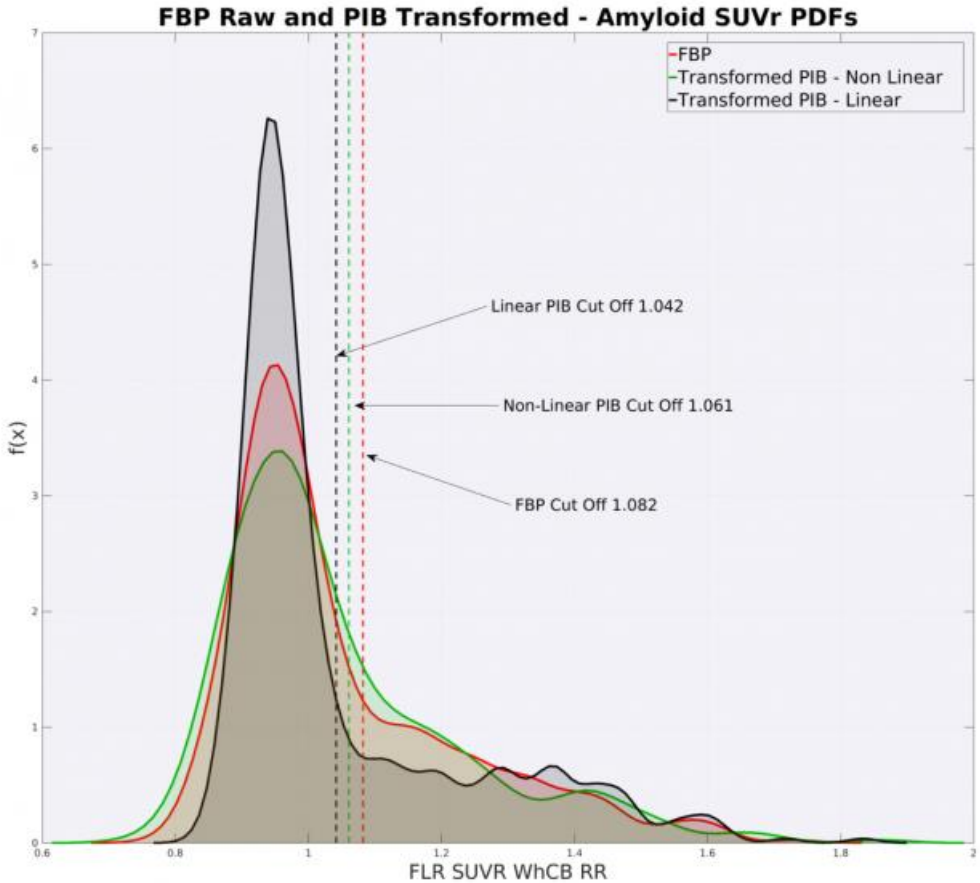

Figure 2: Comparison of PIB data transformed using linear and non-linear methods. PIB Distributional scaling is parsimonious with raw FBP data after non-linear transformation.

P33: In vivo assessment of several 18F SV2A PET tracers

Vincent Carroll, David Alagille, Cedric Tress, Laetitia Mistico, Cristian Constantinescu, Christine Sandiego, Caroline Papin, Alexandra Gouasmat, MingQiang Zheng, Ken Marek, John P. Seibyl, Olivier Barret, Gilles D. Tamagnan

Invicro, New Haven, CT, US

Objective: Synaptic vesicle glycoprotein 2A (SV2A) could serve as a biomarker of synaptic density and PET imaging targeting SV2A could provide a tool to assess progression of neurodegenerative diseases. Data using two SV2A tracers, 11C-UCB-J and 18F-UCB-H has been reported. In initial human studies, 11C-UCB-J showed promising results demonstrating reduction of signal in Alzheimer's disease and Parkinson disease subjects compared to healthy volunteers. It would be very desirable to develop an 18F SV2A tracer to facilitate production of radiopharmaceutical for multi-center imaging studies. We have screened several 18F derivatives of UCB-J in rhesus or cynomolgus macaques to identify an 18F PET tracer with a signal at least comparable to 11C-UCB-J.

Methods: 18F-UCB-J, 18F-UCB-H and five 18F derivatives were administered in non-human primates (166 ± 44 MBq) and imaging was carried out over 2 hours. Blood samples were taken at different time points to evaluate the metabolism of the different tracers by HPLC. The tracer uptake and distribution was assessed prior to and following blockade using Levetiracetam (30mg/kg).

Results: All compounds displayed very good brain penetrance with a maximum SUV of 5-8 within 10 min of injection. 18F-UCB-J showed high consistency compared to literature results with 11C-UCB-J. 18F-UCB-H R-isomer displayed higher signal compared to the racemate, as recently reported in the literature, but showed sub-optimal signal compared to 18F-UCB-J. MNI-1038 showed uptake and distribution consistent with UCB-J. Pre-block of MNI-1038 with Levetiracetam showed robust occupancy across all cortical regions sampled, and similar to that reported with 11C-UCB-J. MNI-1038 also showed similar metabolism to UCB-J, with a free fraction of ~40%. All other 18F derivatives showed results similar or lower than 18F-UCB-H.

Conclusions: Screening of five 18F derivatives of UCB-J allowed identification of an 18F tracer exhibiting characteristics consistent with 11C-UCB-J, and with similar Levetiracetam occupancy as that measured with 11C-UCB-J.

Keywords: SV2A, biomarker, Alzheimer's, Parkinson's, neurodegeneration

P34: Development of thiophene-based optical ligands that selectively detect tau pathology in Alzheimer's disease

Hamid Shirani[1], Hanna Appelqvist[1], Marcus Bäck[1], Therése Klingstedt[1], Nigel Cairns[2], Samuel Svensson[1,3], K. Peter R. Nilsson[1]

[1]*Linköping University, Linköping, Sweden*
[2]*Washington University School of Medicine, St Louis, MO, US*
[3]*CBD Solutions, Stockholm, Sweden*

Background and Aim: Luminescent conjugated oligothiophenes (LCOs) are optical probes that bind to protein aggregates and fluoresce with high intensity. They have been used to study misfolded proteins *in vitro* and *in vivo*, and detect a wider range of protein aggregates in comparison to conventional amyloid dyes[1]. We recently reported how to structurally transform an LCO from being a general protein aggregate ligand to a probe that was selective for Aβ aggregates in Alzheimer's disease (AD, Fig 1, q-FTAA-CN)[2]. In this project, our aim was to further utilize the versatility of LCOs to identify thiophene-based tau selective ligands.

Methods: A library of structurally diverse ligands was synthesized to be able to identify the optimal design for achieving selective binding to tau aggregates. The ligands were hybrids of LCOs and different chemical compounds joined together with or without a vinyl linker. The evaluation of the ligands was performed on post-mortem brain sections from AD patients using antibodies directed against Aβ or tau to assess protein specificity[3].

Results: The staining experiments revealed that linking thiophenes with a benzothiazole motif resulted in ligands highly selective for tau in AD. The so called bi-thiophene-vinyl-benzothiazole (bTVBT) probes could be used to detect all types of tau pathologies in AD brain, whereas no labelling of Aβ aggregates could be seen (Fig 1, bTVBT2). The bTVBTs fluoresced very intense when binding and allowed visualization of also very small tau positive neurites.

Conclusion: In conclusion, we have identified thiophene-based ligands that are selective for tau aggregates in human AD brain. The next step is to introduce a radioactive isotope in the probe structure to trace their binding to tau in living subjects using positron emission tomography.

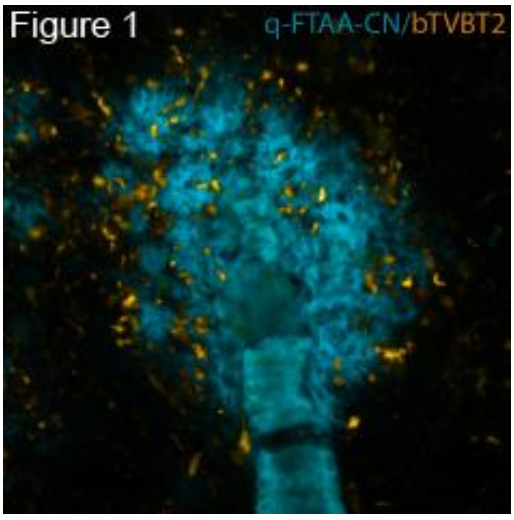

1. Klingstedt T et al. (2011) *Org Biomol Chem*, 9(24)
2. Bäck et al. (2016) *Chemistry*, 22(51)
3. Shirani et al. (2017) *Chemistry*, doi: 10.1002/chem.201703846

Keywords: Alzheimer´s disease, protein aggregates, tau aggregates, fluorescent ligands, amyloid-beta

P35: Unbiased assessment of global amyloid load as determined by Voxel-wise receiver operating characteristic analysis

Joseph Therriault[1], Tharick Pascoal[1], Sulantha Mathotaarachchi[1], Isadora Alves[2], Lyduine Collij[2], Min Su Kang[1], Melissa Savard[1], Andrea Benedet[1], Ashley Knight[1], Kokpin Ng[3], Monica Shin[1], Mira Chamoun[1], Gassan Massarweh[4], Jean-Paul Soucy[4], Serge Gauthier[1,4], Pedro Rosa-Neto[1,4]

[1]Translational Neuroimaging Laboratory, McGill University Research Centre for Studies in Aging, Montreal, Canada, Montreal, QC, Canada
[2]Dept of Radiology & Nuclear Medicine, VUMC, Amsterdam, Netherlands
[3]Department of Neurology, National Neuroscience Institute, Singapore, Singapore
[4]Department of Neurology, McGill University, Montreal, QC, Canada

Aims: Recent efforts have focused on characterizing individuals as amyloid positive or negative in order to enrich disease-modifying clinical trials. However, current Aβ dichotomizations ignore the regional distribution of amyloid pathology, which may have important implications for clinical progression. In this study, we investigated the regional patterns of amyloid deposition that can optimally differentiate between AD patients and controls.

Methods: We assessed cognitively normal (n=302), and AD (n=224) individuals who underwent [^{18}F]Florbetapir PET, cognitively normal (n = 26) and AD (n = 35) individuals scanned with [^{11}C]PiB and cognitively normal (n = 30) and AD (n = 30) scanned with [^{18}F]Flutafuranol. To identify the brain regions that optimally differentiate controls from AD patients, we conducted a ROC curve in every brain voxel. Then, parametric maps of area under the curve were generated for each amyloid imaging agent (Figure 1). Area under the curve values were highest in clusters in the precuneus, posterior cingulate, lateral temporal, and medial prefrontal cortices, as well as the striatum. Next, to determine if amyloid burden in these structures is related to outcome measures related to disease severity, we conducted linear regressions assessing the relationship between amyloid burden from AD signature regions and the standard neocortical composite mask and brain metabolism as assessed by [^{18}F]FDG uptake in MCI (n = 390). We compared the slopes and adjusted R^2 of each model.

Results: In MCI, we observed stronger relationships between brain metabolism and amyloid in AD signature regions (adj R^2=0.27, p=6.74^{-5}) than with global amyloid burden (adj R^2=0.25, p=0.005) (Figure 2).

Conclusion: Our results suggest that the optimization of masks as proposed here may increase the sensitivity to detect amyloid-related metabolic or cognitive dysfunction in clinical trials.

Figure 1

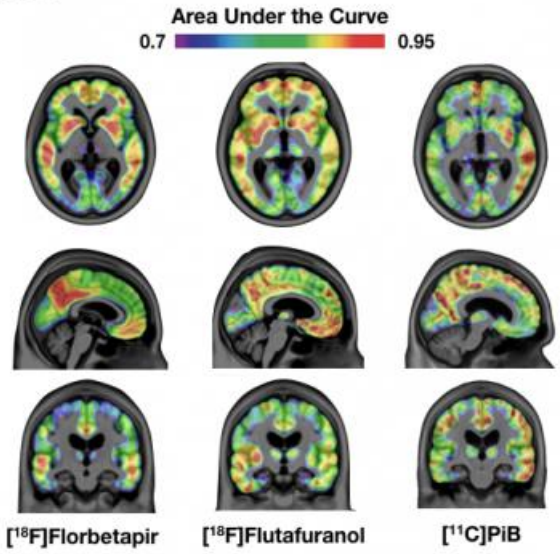

Figure 2

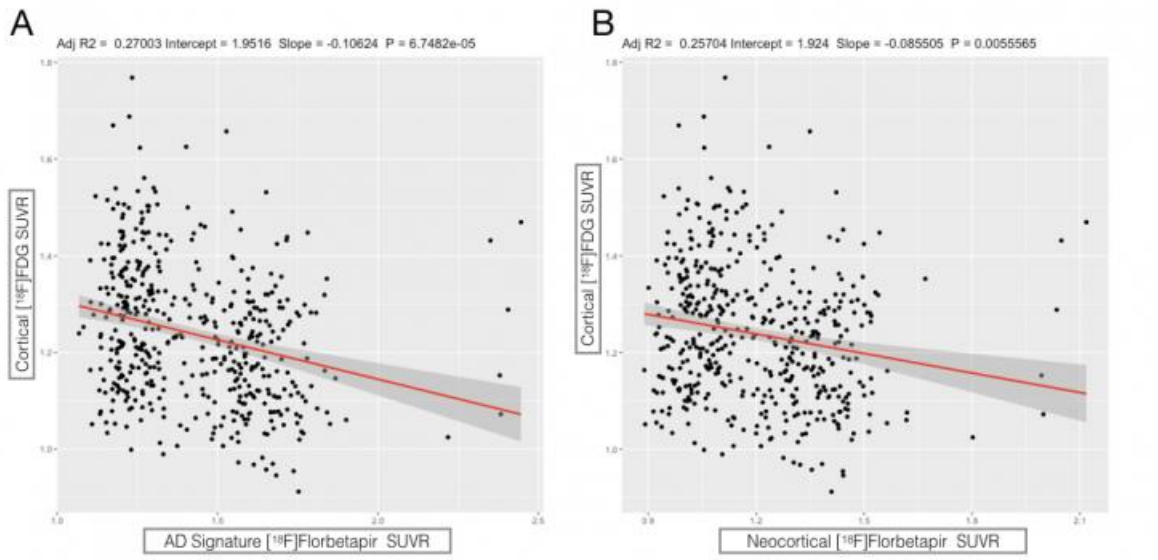

Keywords: ROC Curve, Metabolism, Default Mode Network, Amyloid, Vulnerability

P36: Voxel-wise determination of thresholds and accuracy of [18F]AV1451 and [18F]MK6240 ligands for neurofibrillary tangles

Tharick Pascoal, Sulantha Mathotaarachchi, Mira Chamoun, Min Su Kang, Joseph Therriault, Hanne Struyfs, Kok Pin Ng, Melissa Savard, Monica Shin, Ashley Knight, Andrea Benedet, Gassan Massarweh, Mallar Chakravarty, Jean-Paul Soucy, Daniel Chartrand, Serge Gauthier, Pedro Rosa-Neto

McGill University, Montreal, QC, Canada

Objective: To examine the voxel-wise sensitivity, specificity, area under the curve (AUC), and thresholds of neurofibrillary tangle deposition with the PET ligands [^{18}F]AV1451 and [^{18}F]MK6240.

Method: We assessed 95 cognitively normal and 17 AD individuals from ADNI cohort who underwent [^{18}F]AV1451 at baseline. We imaged 15 cognitively normal (age=68.5 (7.6), MMSE=29.1 (1.3)) and 22 AD (age=70.2 (10.9) MMSE = 19 (7.8)) individuals with [^{18}F]MK6240. [^{18}F]AV1451 and [^{18}F]MK6240 standardized uptake value ratios (SUVR) were processed using cerebellum grey matter as reference region and calculated at 75-105 and 90-110 minutes, respectively. Receiver operating characteristic curves, contrasting controls with AD, assessed the least distance from point to the curve at every brain voxel, which provided the ligand uptake value with the best trade-off between sensitivity and specificity for AD. Finally, we generated a voxel-wise sensitivity, specificity, AUC, and thresholds parametric images.

Results: For [^{18}F]AV1451, the highest cutoff values were found in the striatum reaching a SUVR of 1.5. For [^{18}F]MK6240, the highest cutoff values were found in the temporal lobe, precuneus, and posterior cingulate cortices with SUVR values reaching 2 in some voxels. Remarkably, the regions with the highest AUC for a diagnostic of dementia using both ligands were found in the precuneus, posterior cingulate, frontal, and medial and basal temporal cortices (Fig.1). The highest AUC using [^{18}F]MK6240 was found in posterior cingulate cortex (PCC) with values of 0.95. The highest AUC using [^{18}F]AV1451 reached 0.9 and was found in the entorhinal cortex.

Conclusions: These results highlight that the tau accumulation associated with a diagnosis of AD occurs predominantly in brain's circuits early described by histopathological studies. These regional thresholds have the potential to be used in clinical trials for the enrolment of individuals with tau abnormalities.

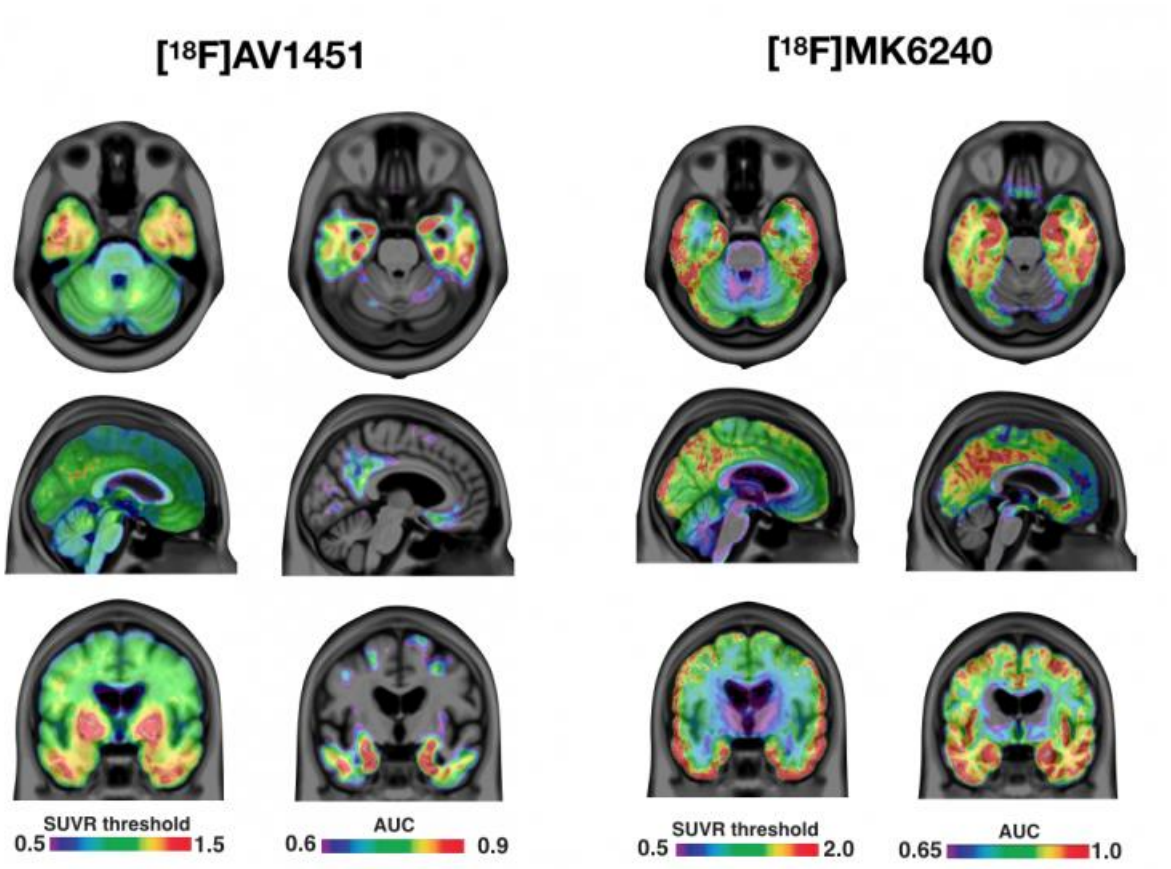

Keywords: Tau imaging, Alzheimer's disease

P37: Preliminary report on the associations between CSF T-tau and P-tau with [18F]MK6240 binding

Mira Chamoun[1], Min Su Kang[1,2], Tharick A. Pascoal[1], Sulantha Mathotaarachchi[1], Andréa L. Benedet[1,3], Monica Shin[1], Joseph Therriault[1], Reda Bouhachi[6], Chris Hsiao[6], Gassan Massarweh[6], Daniel Chartrand[6], Jean-Paul Soucy[6], Serge Gauthier[4], Pedro Rosa-Neto[1,4,5,6]

[1]*Translational Neuroimaging Laboratory, McGill University Research Centre for Studies in Aging, Montreal, QC, Canada*
[2]*Douglas Hospital Research Centre, McGill University, Montreal, QC, Canada*
[3]*CAPES Foundation, Ministry of Education of Brazil, Brasília, Brazil*
[4]*Alzheimer's Disease Research Unit, McGill University Research Centre for Studies in Aging, Montreal, QC, Canada*
[5]*Department of Neurology and Neurosurgery, McGill University, Montreal, QC, Canada*
[6]*Montreal Neurological Institute, Montreal, QC, Canada*

Rationale: While amyloid load and CSF Aβ1-42 reveal a non-linear association with various amyloid imaging agents, previous studies comparing CSF tau and imaging tau load measured with [^{18}F]AV-14-51 have revealed significant associations in various cortical regions. Here, we tested the association between cerebrospinal fluid (CSF) total-tau (T-tau) and phosphorylated-tau (P-tau) with the novel tau imaging agent [^{18}F]MK6240. We tested the linearity of these associations as well as its distribution in the brain.

Methods: We conducted an observational study in healthy elderly controls and patients with various dementias. All patients had CSF measurement of Aβ and tau and PET Aβ ([^{18}F]NAV4669) and tau ([^{18}F]MK6240) ligands at baseline. [^{18}F]NAV4669 and [^{18}F]MK6240 binding outcomes were calculated using $SUVR_{40\text{-}70}$ $SUVR_{90\text{-}110}$, respectively using the cerebellum as reference region.

Results: We scanned 9 individuals AD (N=5; MMSE=17.2±7), MCI (N=1;MMSE=26), FTD (N=2; MMSE=29.5±1), CN (N=1, MMSE=29); aged 56 to 70 yo. All participants had complete cognitive assessments. We observed that CSF T-tau and P-tau were highly correlated with [^{18}F]MK6240 uptake in the mesial temporal structures. The region with the highest correlation was the entorhinal cortex (T-tau: $R= 0.91$, $p < 0.001$; P-tau: $R= 0.78$, $p < 0.001$).

Conclusion: The associations between CSF T-tau or P-tau with [18F]MK6240 support the concept that pair helical filament availability and monomeric forms of CSF p-tau and t-tau similarly reflects the tau pathology in vivo.

Keywords: CSF, T-tau, P-tau, [18F]MK6240, correlation

P38: A more accurate alternative to SUVR for quantifying binding rate-of-change in serial PET

J. Alex Becker, Julie Price, Keith Johnson

Massachusetts General Hospital, Boston, MA, US

Introduction: Traditional methods of PET quantification are limited to the analysis of isolated cross-sectional PET time-points, and do not leverage the richer structure inherent in intra-subject PET data. Moreover, PET data gathered in therapeutic or observational studies are often quantified by the SUVR, which suffers from bias when applied to either cross-sectional or serial data. We have developed a comprehensive reference-tissue-based modeling approach for serial PET that encompasses all tissue regions at all time-points, in order to improve accuracy of estimates of binding rates-of-change compared to SUVR-based measures.

Methods: (Model) We specialized our model to apply to "late-time-dynamic" PET data (4-6 5-minute frames acquired ~80 minutes post-injection) typical for AD PET investigations that include [18F]Flortaucipir (FTP) tau imaging. Kinetics of 32 Freesurfer-defined cortical ROIs were approximated by 1-tissue compartment models with effective efflux rates depending on tracer binding potential (BP) and reference tissue BP was fixed at 0. BP was assumed to vary linearly over time and BP rates-of-change were simultaneously estimated for all ROI. (Simulations) To assess accuracy and precision of estimated BP rates, computer simulations were performed by calculating synthetic serial PET TACs based on an FTP plasma input function and kinetic rate parameters (K1-k4) derived from a 3 time-point serial PiB study of an elderly normal control subject.

Results: The mean of 500 SUVR-based rate-of-change estimates in 32 ROIs (Fig 1, red triangles) were increasingly biased as the true rate-of-change increased (median bias: 24% of true rate). BP rates-of-change estimated by the new model (black circles), showed less bias and no trend in bias over this range (median: 1.2%).

Conclusions: Our results indicate that a model of serial PET that exploits the commonalities in the kinetics across ROIs and over time yields estimates of binding rates-of-change with reduced bias compared to SUVR-based estimates.

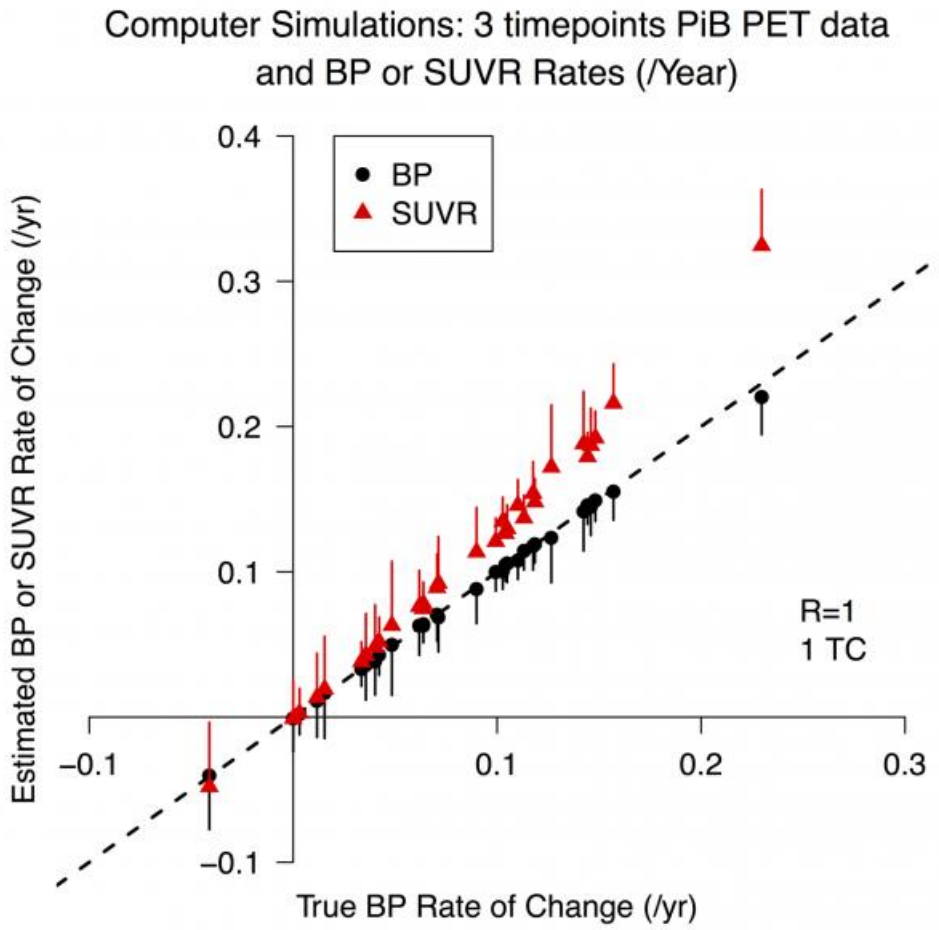

Figure 1. Bias of binding rates-of-change estimated from serial LTD PET by SUVR (red) increases with increasing true rate, compared to rates estimated with the proposed model (black). Accuracy and precision of binding rates-of-change for 32 Freesurfer cortical ROIs, estimated over 500 simulation replications. Points show average, and bars SD of the distribution of replication estimates: BP rate-of-change estimates (black), SUVR rate (red), versus ground-truth BP rate-of-change used to generate the replications (x-axis); line of identity is dashed.

Keywords: Kinetic modeling, serial PET

P39: Structure-binding relationship of quinoline derivatives on monoamine oxidase B

Nobuyuki Okamura[1,2,3], Ryuichi Harada[2], Shozo Furumoto[3], Hiroyuki Arai[4], Kazuhiko Yanai[2,3], Yukitsuka Kudo[4]

[1]*Faculty of Medicine, Tohoku Medical and Pharmaceutical University, Sendai, Japan*
[2]*Department of Pharmacology, Tohoku University School of Medicine, Sendai, Japan*
[3]*Cyclotron and Radioisotope Center, Tohoku University, Sendai, Japan*
[4]*Institute of Development, Aging and Cancer, Tohoku University, Sendai, Japan*

Background: Several quinoline derivatives have been developed as tau PET tracers. However, recent studies have demonstrated high off-target binding of THK5351 to monoamine oxidase B (MAO-B). MAO-B would be a promising target of PET imaging for monitoring neuroinflammatory change after several disease conditions such as trauma, infection, ischemia, stroke, and neurodegenerative disease. To clarify the chemical structure that is responsible for the binding to MAO-B, we measured the binding affinity of these derivatives for recombinant MAO-B and human brain samples.

Methods: Binding affinity to recombinant MAO-B was evaluated by in vitro competitive binding assay of ^{3}H-THK5351 with test compounds. Ki values were calculated using GraphPad Prism software. Binding affinity to MAO-B and PHF-tau was also evaluated by in vitro autoradiography using frozen brain tissues from the hippocampus, striatum and frontal cortex of normal controls and Alzheimer's disease. Blocking studies were conducted using MAO-B inhibitor lazabemide.

Results: High binding affinity (Ki < 10 nM) to recombinant MAO-B was observed in THK5351 (Ki = 4.9 nM), THK5105 (Ki = 5.8 nM) and other quinoline derivatives having fluoro-2-propanol structure. These compounds also bound to MAO-B in human brain sections with high affinity. In contrast, the binding affinity to MAO-B was low in BF-158 (Ki = 187.3 nM) and other quinoline derivatives without fluoro-2-propanol structure. We identified the compounds that can selectively bind to MAO-B or PHF-tau in human brain samples.

Conclusions: Fluoro-2-propanol structure of quinoline derivatives is responsible for the binding to MAO-B. These findings will help in the development of novel radiotracers for MAO-B or PHF-tau.

Keywords: monoamine oxidase, tau, PET, Alzheimer's disease

P40: Initial evaluation of correspondence between tau PET ligand [F-18]MK6240 and cognitive status

Lindsay Clark[1,2], Tobey Betthauser[1], Bradley Christian[1], Jennifer Poetter[1], Leah Sanson[1], Jennifer Oh[1], Sterling Johnson[1,2]

[1]*University of Wisconsin School of Medicine & Public Health, Madison, WI, US*
[2]*William S Middleton Veterans Memorial Hospital, Madison, WI, US*

Objective: Evaluate the correspondence between MK-6240 tau tracer distribution and cognitive status, beta-amyloid burden, and cognitive performance.

Methods: 22 participants recruited from longitudinal parent studies (3 younger controls (YC), 9 older controls (OC), 3 with clinical diagnoses of mild cognitive impairment (MCI), 7 with clinical diagnoses of dementia) underwent T1-weighted MRI and dynamic [C-11]PiB and [F-18]MK-6240 PET scans (Siemens ECAT HR+) to assess beta-amyloid and tau burden, respectively, and neuropsychological testing. Reconstructed PET images were interframe realigned, coregistered to T1w MRI, and parametric DVR (PiB, HYPR denoising, Logan graphical analysis) and SUVR (MK-6240, 70-90 min) images were generated using a cerebellar GM reference region. Regional values were extracted using GM-restricted AAL ROIs inverse warped to native T1 space. Parametric images were normalized to MNI space and individuals were visually grouped as PiB+ or PiB- and according to Braak tau stages. Bivariate correlations evaluated associations among regional SUVR and memory performance.

Results: 7 participants (32%) exhibited amyloid and tau spatial patterns consistent with Alzheimer's disease; of these, 5 were clinically diagnosed with dementia (5 of 7 in dementia group) and 2 were OC (2 of 9 OC; see Table). All 7 participants were classified as PiB+. Fifteen participants exhibited minimal MK-6240 specific binding including all 3 YC, 7 of 9 OC, all 3 MCI, and 2 of 7 clinical dementia. Only 3 of these 15 were classified as PiB+. Greater MK-6240 uptake in temporal lobe regions correlated with poorer episodic memory performance (r's = -0.47 – -0.52, p's < .05; see Figure).

Conclusions: In this pilot sample of 22 participants, greater MK-6240 distribution corresponded with dementia diagnosis, amyloid positivity, and poorer memory performance. Data collection is ongoing and future analyses will continue to investigate these relationships in a larger sample.

	Braak 0	Braak I/II	Braak III/IV	Braak V/VI
N (YC / OC / MCI / DEM)	3 / 7 / 3 / 2	0 / 0 / 0 / 1	0 / 2 / 0 / 0	0 / 0 / 0 / 4
PiB +	3 (20%)	1 (100%)	2 (100%)	4 (100%)

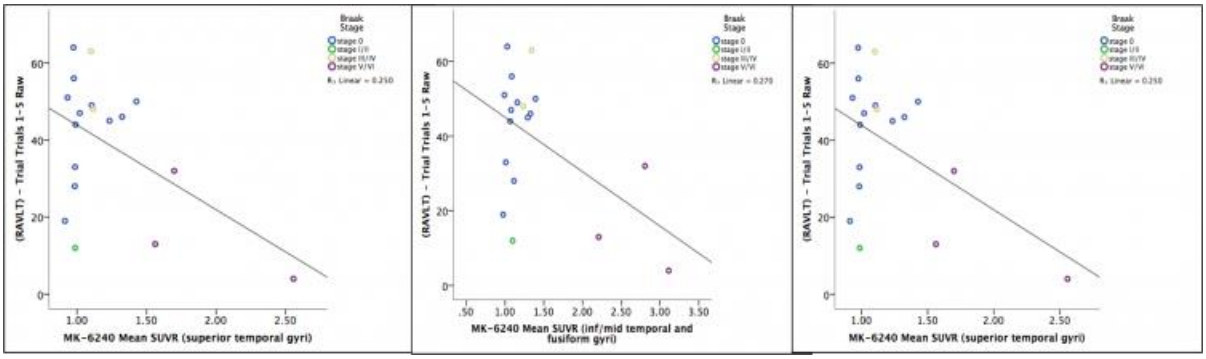

Keywords: tau PET, amyloid PET, neuropsychology, dementia

P41: Low-dose NeuroPET scans for longitudinal PET: a feasibility study with Flortaucipir

Cristina Lois[1], Kira Grogg[1], Aaron Schultz[2], Julie C. Price[2], Keith A. Johnson[1]

[1]Gordon Center for Medical Imaging, Division of Nuclear Medicine and Molecular Imaging, Department of Radiology, Massachusetts General Hospital / Harvard Medical School, Boston, MA, US
[2]Athinoula A. Martinos Center for Biomedical Research, Department of Radiology, Massachusetts General Hospital / Harvard Medical School, Boston, MA, US

Introduction: Longitudinal PET studies have the potential to follow disease progression and assess treatment efficacy. Several PET radio tracers can provide information about amyloid and tau load, metabolism, and neuroinflammation in AD. However, radiation exposure limits the number of PET scans an individual may undergo. Therefore, high-sensitivity scanners that enable repeat low-dose imaging are needed to acquire rich longitudinal data.

Objective: Evaluate the feasibility of low-dose PET imaging using the high-sensitivity brain PET/CT NeuroPET [1].

Methods: Nine subjects (1 AD, 1 MCI, 7 controls) underwent two low-dose (4.5±0.8 mCi) Flortaucipir (FTP) PET scans within 6 months on the NeuroPET. Regional SUVR values were compared with values measured using a HR+ tomograph [2]. Measurement repeatability was examined by comparing SUVR values obtained at both time points in control subjects.

Results: Low-dose NeuroPET images yielded FTP distribution patterns consistent with known retention patterns in AD and controls. SUVR values were consistent with published values and measurement repeatability was good (7±5%). Subject positioning was sometimes challenging resulting in inadequate brain coverage, which was addressed with minor hardware modifications. Image reconstruction often required manual intervention, limiting its usefulness for large multi-center efforts.

Conclusions: NeuroPET provided SUVR values and patterns of uptake consistent with published FTP results using half of the typically injected dose. NeuroPET is a feasible system for pilot studies, but unpractical for large studies requiring high throughput, routine imaging, and multi-center standardization.

[1] Grogg et al.J Nucl Med. 2016 57(4).

[2] Johnson et al. Ann Neurol. 2016, 79(1).

Subject	Age at Baseline	Dose at Baseline (mCi)	Dose at Follow-up (mCi)
AD	72	3.99	5.19
MCI	74	4.19	5.29
Control 1	79	2.01	4.27
Control 2	61	5.37	5.06
Control 3	74	4.31	4.86
Control 4	76	3.91	5.15
Control 5	63	4.29	5.37
Control 6	45	3.98	5.29
Control 7	64	4.31	---

Table 1. Subject demographics.

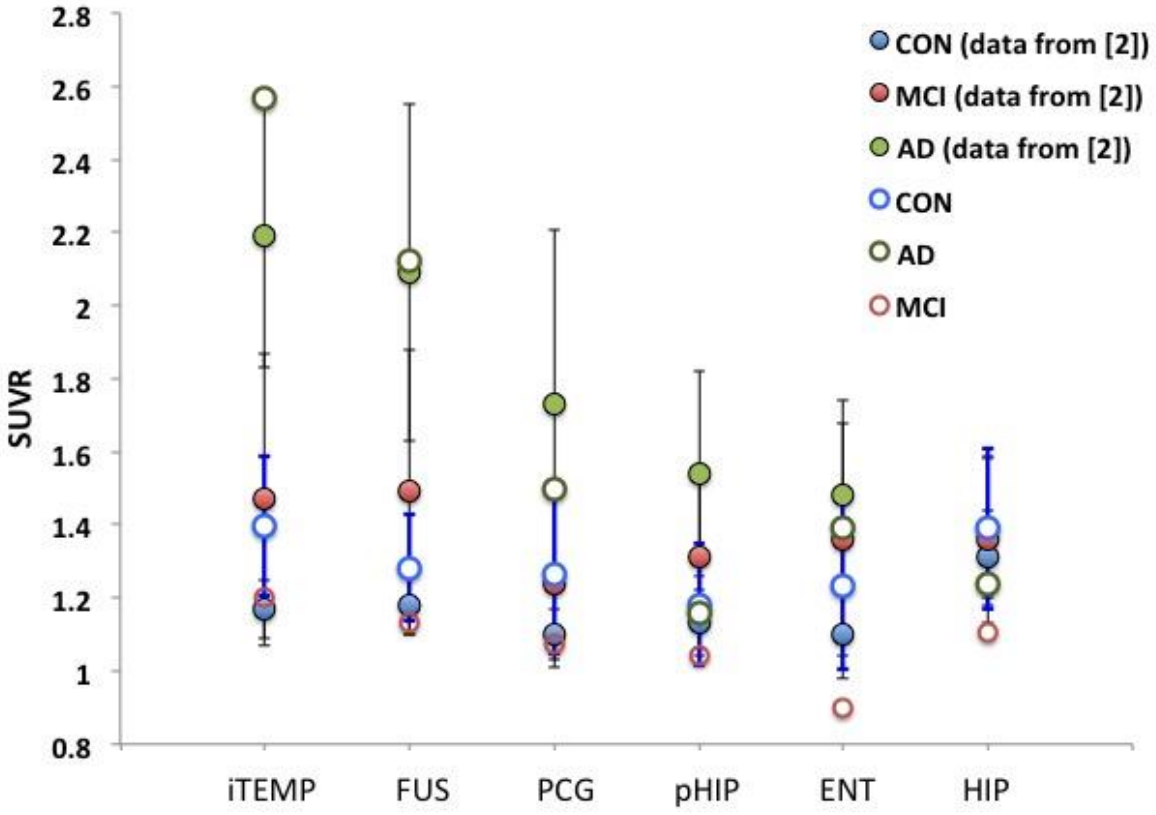

Fig.1. FTP regional SUVRs obtained in NeuroPET (inferior temporal (iTEMP), fusiform (FUS), posterior cingulate (PCG), parahippocampal (pHIP), entorhinal (ENT), and hippocampus (HIP)). Data measured in the HR+ [2] is plotted for reference.

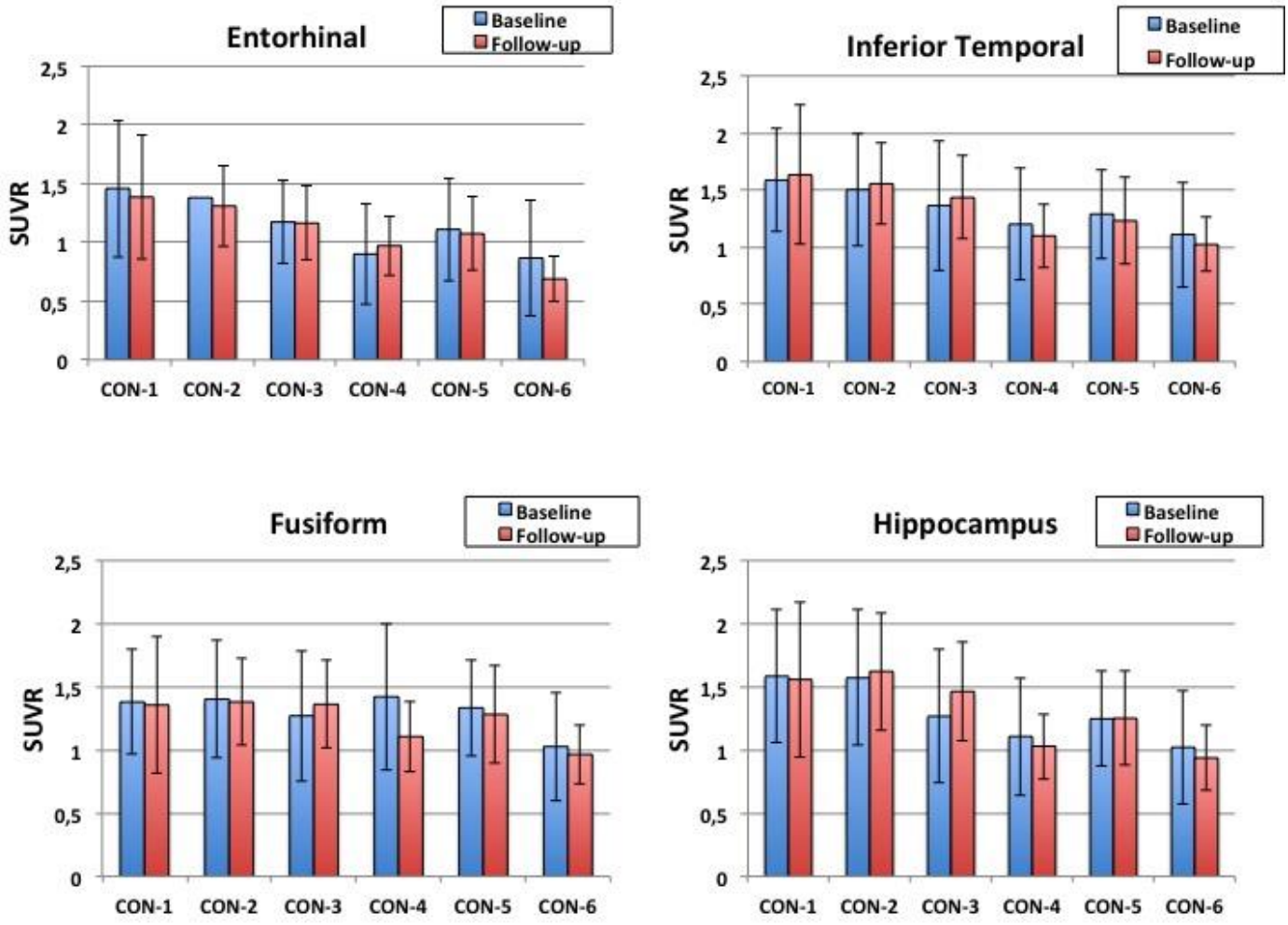

Fig.2 FTP SUVRs at baseline and 6 months follow-up for our control subjects illustrate the good measurement repeatability.

Keywords: Flortaucipir, low-dose PET, NeuroPET

P42: Parametric methods for [18F]flortaucipir PET

Emma E Wolters[1,2], Sandeep SV Golla[1], Tessa Timmers[1,2], Rik Ossenkoppele[1,2], Chris WJ van der Weijden[1], Philip Scheltens[2], Lothar Schwarte[3], Mark A Mintun[4], Michael Devous[4], Robert C Schuit[1], Albert D Windhorst[1], Adriaan A Lammertsma[1], Maqsood Yaqub[1], Bart NM van Berckel[1], Ronald Boellaard[1]

[1]*Department of Radiology & Nuclear Medicine, Amsterdam Neuroscience, VU University Medical Center, Amsterdam, Netherlands*
[2]*Department of Neurology & Alzheimer Center, Amsterdam Neuroscience, VU University Medical Center, Amsterdam, Netherlands*
[3]*Department of Anesthesiology, Amsterdam Neuroscience, VU University Medical Center, Amsterdam, Netherlands*
[4]*Avid Radiopharmaceuticals (a wholly owned subsidiary of Eli Lilly and Company), Philadelphia, OR, US*

Background: [^{18}F]flortaucipir is a promising positron emission tomography (PET) tau tracer to visualize in vivo tau binding in Alzheimer's disease (AD). The purpose of the present study was to evaluate the performance of several parametric methods, as well as standardized uptake values ratios (SUVr), to obtain quantitatively accurate parametric images of [^{18}F]flortaucipir.

Methods: Dynamic PET scans of 130 minutes duration, including arterial sampling, were performed in 10 AD patients and 10 controls (C). Parametric images were generated using a variety of methods. Plasma input based Logan and Spectral Analysis (SA) were used to generate volume of distribution (V_T) images. Reference Logan (RLogan), multilinear reference tissue models (MRTM), receptor parametric mapping (RPM), and simplified reference tissue model 2 (SRTM2) were used to obtain binding potential (BP_{ND}) images. Parametric regional BP_{ND} and V_T values were compared with respective values derived from a reversible two tissue plasma input compartment model. Performance of SUVr was assessed by comparing values with corresponding indirect BP_{ND} (distribution volume ratio (DVR)) obtained using non-linear regression (NLR).

Results: Plasma input Logan (r^2=0.95; slope=0.80) and SA (r^2=0.92; slope=0.99) estimated V_T well. Rlogan (r^2=0.93; slope=0.79), RPM (r^2=0.95; slope=0.98) and SRTM2 (r^2=0.95; slope=0.96) correlated well with NLR derived DVR. Although SUVr obtained using a 80-100 min scan duration correlated well with DVR (r^2=0.91; slope=1.09) and SRTM derived BP_{ND} (r^2=0.83; slope=0.90), bias of SUVr appeared to depend on uptake time and underlying level of specific binding(Figure 1-2).

Conclusions: RPM and SA provide the most accurate parametric BP_{ND} and V_T images, respectively, and are the recommended methods for voxel level parametric kinetic analysis. Individual SUVr values appear biased when compared with DVR and this bias varies with uptake time and actual DVR value(Figure 1-2).While preliminary, this bias suggests that SUVr should be used with caution, especially in longitudinal studies where changes in specific binding can be expected.

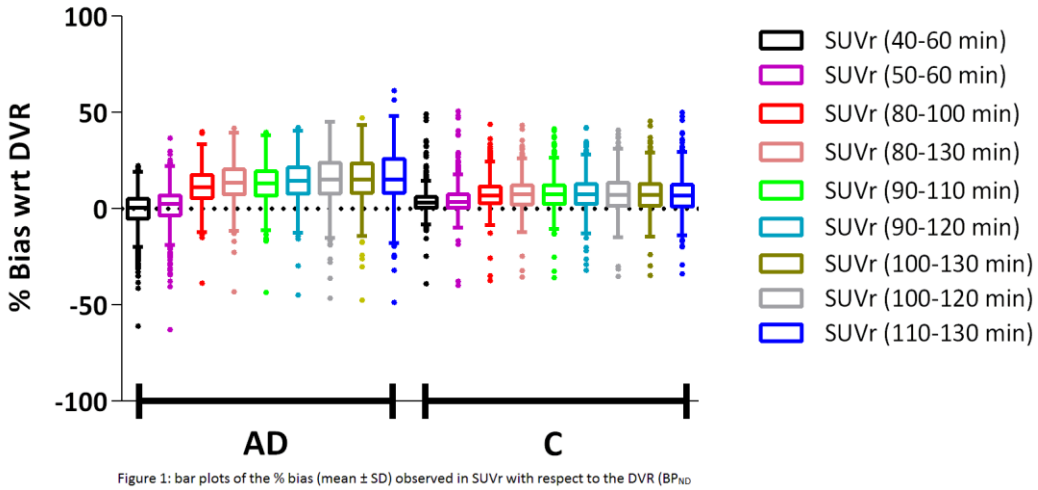

Figure 1: bar plots of the % bias (mean ± SD) observed in SUVr with respect to the DVR (BP_{ND}

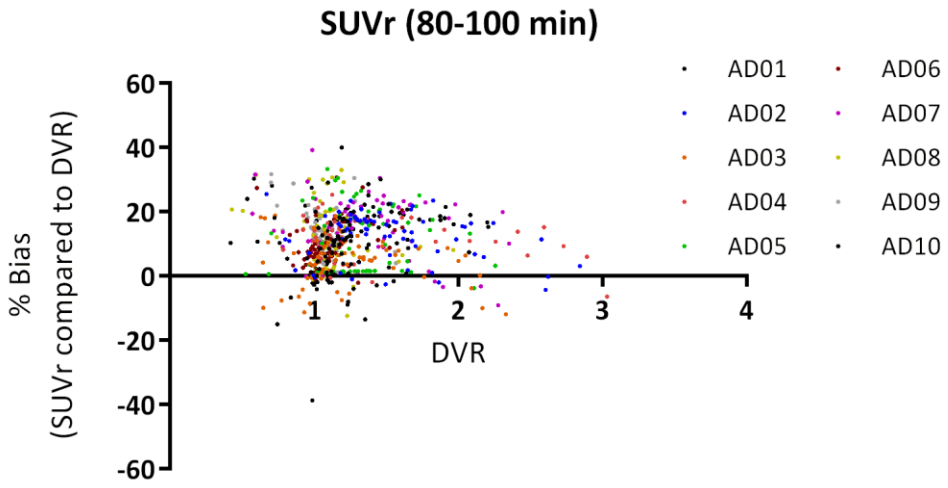

Figure 2: Scatter plot of the observed bias (%) in SUVr obtained using 80 to 100 min scan duration with respect to DVR (BP_{ND} + 1).

Keywords: PET,[18F] flortaucipir, parametric imaging, Alzheimer's disease

P43: Improved quantification of [18F]flortaucipir uptake in the hippocampus after partial volume correction

Emma E Wolters[1,2], Sandeep SV Golla[1], Tessa Timmers[1,2], Rik Ossenkoppele[1,2], Chris WJ van der Weijden[1], Philip Scheltens[2], Lothar Schwarte[3], Mark A Mintun[4], Michael Devous[4], Robert C Schuit[1], Albert D Windhorst[1], Frederik Barkhof[1,5], Maqsood Yaqub[1], Adriaan A Lammertsma[1], Ronald Boellaard[1], Bart NM van Berckel[1]

[1]*Department of Radiology & Nuclear Medicine, Amsterdam Neuroscience, VU University Medical Center, Amsterdam, Netherlands*
[2]*Department of Neurology & Alzheimer Center, Amsterdam Neuroscience, VU University Medical Center, Amsterdam, Netherlands*
[3]*Department of Anaesthesiology, Amsterdam Neuroscience, VU University Medical Center, Amsterdam, Netherlands*
[4]*Avid Radiopharmaceuticals (a wholly owned subsidiary of Eli Lilly and Company), Philadelphia, PA, US*
[5]*Institutes of Neurology & Healthcare Engineering, UCL, London, United Kingdom*

Background: In Alzheimer's Disease (AD), the hippocampus is among the earliest brain regions affected by tau pathology. Given the close proximity of the hippocampus to the choroid plexus (CP), off-target binding in the CP may cause spill-in of [^{18}F]flortaucipir activity, which subsequently will lead to inaccurate quantification of tau binding. The purpose of this study was to assess the impact of CP activity on quantification of hippocampus uptake and to correct for this spill-in using partial volume correction (PVC).

Methods: 130 minutes dynamic PET scans, including arterial sampling, were performed in 10 AD patients and 10 controls. A combination of HYPR denoising and Van cittert iterative deconvolution was used to generate PVC PET images[1]. Regions of interest (ROI) were defined for the hippocampus by 1) using T1 weighted MRI, Hammers template[2] and PVElab[3] (complete ROI), 2) an eroded hippocampal ROI (eroded ROI), to correct for spill-in from the CP. The CP was drawn manually on PVC PET images and MRI flair. Hippocampal distribution volume (V_T) for complete and eroded ROI with/without PVC were correlated with CP V_T.

Results: For controls, the relationship between hippocampus and CP uptake was significantly reduced after using both an optimized ROI and PVC (r^2= 0.59, slope= 0.80 versus r^2= 0.15, slope= 0.15; p for interaction <0.05) (figure 1). A similar, even stronger, trend was observed for AD patients indicating that the dependence of hippocampus V_T on CP uptake can be decreased by PVC and VOI adjustment regardless of subject group (p <0.01) (figure 2).

Conclusion: After PVC and optimized hippocampus ROI, only a weak correlation remained between the hippocampal and CP V_T. The proposed PVC method significantly improves accuracy of hippocampal V_T values and should be used for investigating the relation between *in vivo* tau binding in the hippocampus and both clinical and pathophysiological markers of AD.

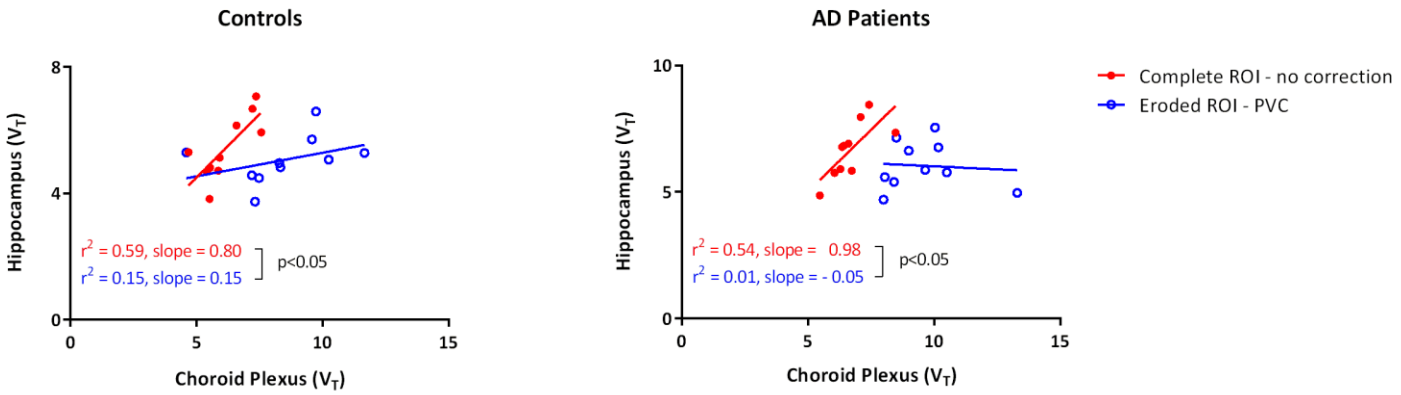

Figure 1: Scatter plots illustrating the relationship between Hippocampus V_T and Choroid plexus V_T compared before and, after both PVC and eroded hippocampus ROI for AD patients and controls.

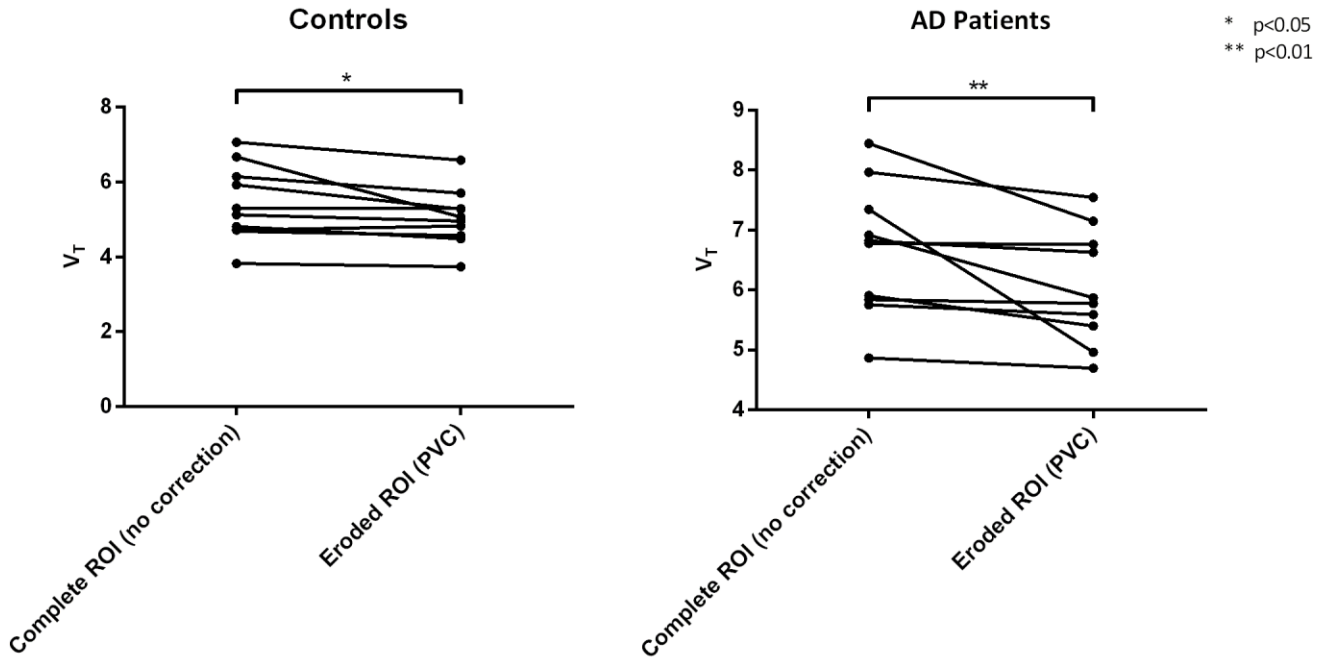

Figure 2: Spaghetti plots of Hippocampus V_T before and, after both PVC and eroded hippocampus ROI within AD patients and controls.

Keywords: [18F]Flortaucipir, Alzheimer's disease, quantification, hippocampus, partial volume correction

P44: Amyloid deposition is associated with different patterns of hippocampal connectivity in men versus women

Minjie Wu[1], Rebecca Thurston[1,2], Dana Tudorascu[3], Helmet Karim[1], Chester Mathis[4], Brian Lopresti[4], M. Ilyas Kamboh[5], Ann Cohen[1], Beth Snitz[6], William Klunk[1], Howard Aizenstein[1,7]

[1]*Department of Psychiatry, University of Pittsburgh, Pittsburgh, PA, US*
[2]*Departments of Epidemiology and Psychology, University of Pittsburgh, Pittsburgh, PA, US*
[3]*Departments of Medicine and Biostatistics, University of Pittsburgh, Pittsburgh, PA, US*
[4]*Department of Radiology , University of Pittsburgh, Pittsburgh, PA, US*
[5]*Department of Human Genetics, University of Pittsburgh, Pittsburgh, PA, US*
[6]*Department of Neurology, University of Pittsburgh, Pittsburgh, PA, US*
[7]*Department of Bioengineering, University of Pittsburgh, Pittsburgh, PA, US*

Compared to men, women are disproportionately affected by Alzheimer's disease (AD) and have an accelerated trajectory of cognitive decline and disease progression. Growing evidence suggests that biological factors other than longevity also contribute to gender differences in AD. This study investigated whether older men and women with normal cognition differ in hippocampal functional connectivity based on burden of AD-related pathologies (N=61, 41 females, 65–93 years old). Brain Aβ load was measured with PET imaging using Pittsburgh Compound-B. Hippocampal functional connectivity was assessed during a face-name associative memory task and during resting state. We found men and women showed different associations between Aβ load and hippocampal functional connectivity (Fig. 1A, corrected $p<0.05$). During associative encoding, in men greater Aβ burden was accompanied by greater connectivity between the hippocampus and prefrontal regions, whereas in women hippocampal connectivity did not vary by amyloid burden (Fig. 1B). Higher functional connectivity represents more synchronized hippocampal-prefrontal activations, suggesting an efficient compensatory response to Aβ deposition in men. Lack of an Aβ-related change in hippocampal connectivity may indicate a diminished compensatory response in women. These findings were further verified with resting-state fMRI data acquired on the same participants. Intrinsic hippocampal-prefrontal connectivity was positively correlated with Aβ load in men and was negatively correlated with Aβ load in women (Fig. 1C). This validation further strengthens our findings, showing that gender-divergent changes of hippocampal connectivity are present regardless of whether the memory system is explicitly on-line. These converging results indicate that cognitively normal older men and women may have different neural system changes related to Aβ deposition, which may contribute to the gender-specific AD risk. Diminished neural compensation may underlie connectivity differences and explain the accelerated trajectory of cognitive decline and AD progression in women.

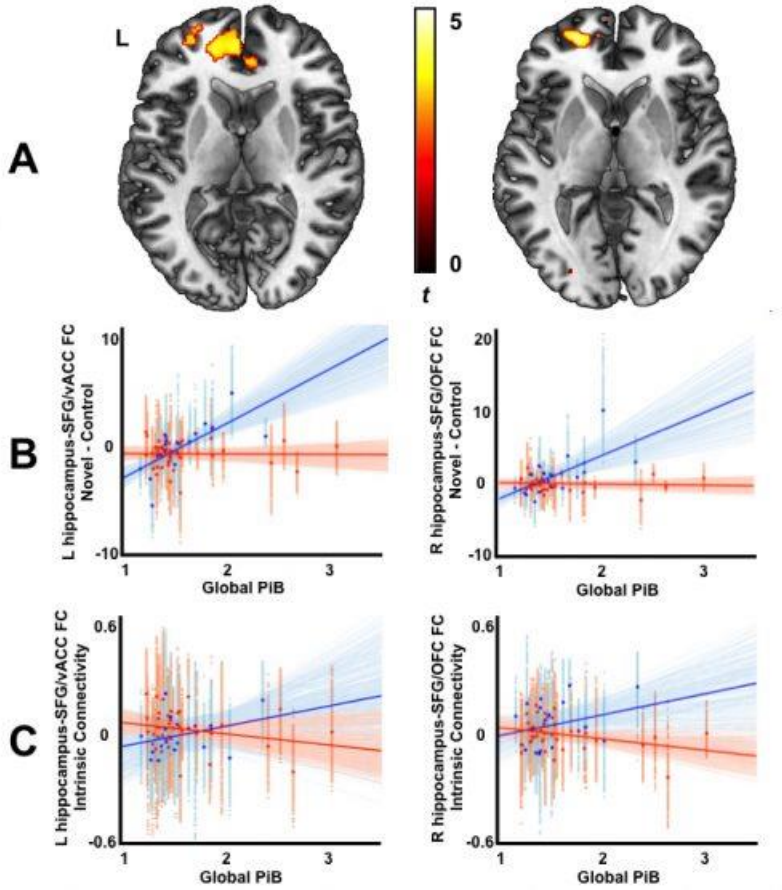

Fig. 1. Gender differences in brain Aβ-related hippocampal functional connectivity (blue: men, red: women).

Keywords: Alzheimer's disease, gender, beta-amyloid, functional connectivity, neural compensation

Wednesday, January 17, 2018 - 03:30 pm - 05:00 pm

Podium Session

Session 2: New Tracers

CHAIRS: Roger Gunn, Chester Mathis

Wednesday, January 17, 2018		
03:30 - 05:00	**Session 2: NEW TRACERS**	CHAIRS: Roger Gunn | Chester Mathis
03:30	PET imaging of synaptic density in Alzheimer's disease	**Chen** | Mecca | Naganawa | Finnema | Toyonaga | Lin | McDonald | Michalak | Nabulsi | Huang | Arnsten | Carson | van Dyck
03:45	Characterizing the relationship of [18F]GTP1 (Genentech tau probe 1) PET imaging with Alzheimer's disease pathophysiology	**Sanabria Bohórquez** | Baker | Ray | Manser | Ward | Teng | Wildsmith | Höglund | Blennow | Marik | Ayalon | Kerchner | Weimer
04:00	A head-to-head comparison between [11C]PBB3 and [18F]PM-PBB3 in patients with AD and non-AD tauopathy	**Kubota** | Shimada | Tagai | Kitamura | Ono | Kimura | Ichise | Shinotoh | Takahata | Yamamoto | Sano | Seki | Tempest | Jang | Seibyl | Barret | Alagille | Marek | Zhang | Suhara | Higuchi
04:15	Clinical evaluation of 18F-PI-2620, a next generation tau PET agent in subjects with Alzheimer’s Disease and progressive supranuclear palsy	**Stephens** | Seibyl | Mueller | Barret | Berndt | Madonia | Alagille | Schieferstein | Kroth | Bullich | Pfeifer | Muhs | Tamagnan | Marek | Dinkelborg
04:30	Discussion	

PET imaging of synaptic density in Alzheimer's disease

Ming-Kai Chen, Adam Mecca, Mika Naganawa, Sjoerd Finnema, Takuya Toyonaga, Shu-fei Lin, Julia McDonald, Hannah Michalak, Nabeel Nabulsi, Yiyun Huang, Amy Arnsten, Richard Carson, Christopher van Dyck

Yale University School of Medicine, New Haven, CT, US

Background: Synaptic loss is well established as the major structural correlate of cognitive impairment in Alzheimer's disease (AD). The ability to image synaptic density *in vivo* would accelerate the development of disease-modifying treatments for AD. One suitable target is the synaptic vesicle glycoprotein 2A (SV2A), an essential vesicle membrane protein ubiquitously expressed in virtually all synapses. *In vivo* SV2A positron emission tomography (PET) imaging could provide a highly informative indicator for synaptic density in AD. ^{11}C-UCB-J was demonstrated as an excellent PET tracer for quantitative measurement of SV2A in our first-in-human PET studies in healthy participants.

Methods: We compared ^{11}C-UCB-J binding in 10 AD and 11 cognitively normal (CN) participants. AD participants were all confirmed Aβ+ by ^{11}C-Pittsburgh Compound B (^{11}C-PiB) PET spanned the disease stages from amnestic mild cognitive impairment (MCI, n=5) to mild dementia (n=5). CN participants were all confirmed Aβ–. Participants received high resolution PET imaging after injection of ^{11}C-UCB-J (493 ± 224 MBq). We measured volume of distribution (*VT*) and binding potential (*BPND*) of ^{11}C-UCB-J for SV2A specific binding in brain regions of interest (ROIs).

Findings: AD participants compared to CN participants demonstrated significant reduction (41%) in hippocampal SV2A binding as assessed by ^{11}C-UCB-J *BPND* (P = 0.005) and 28% reduction measured by *VT* (P = 0.011). These reductions persisted after correction for tissue loss, i.e., partial volume correction (*BPND*: P = 0.020, *VT*: P = 0.056). Exploratory analyses of other brain ROIs and statistical parametric mapping (SPM) also revealed reductions in entorhinal cortex. Hippocampal SV2A binding was correlated with a composite episodic memory score in the overall sample.

Interpretation: ^{11}C-UCB-J PET may provide a direct measure of synaptic density in AD and therefore holds promise as an *in vivo* biomarker and outcome measure for trials of disease-modifying therapies—particularly those that target the preservation and restoration of synapses in AD.

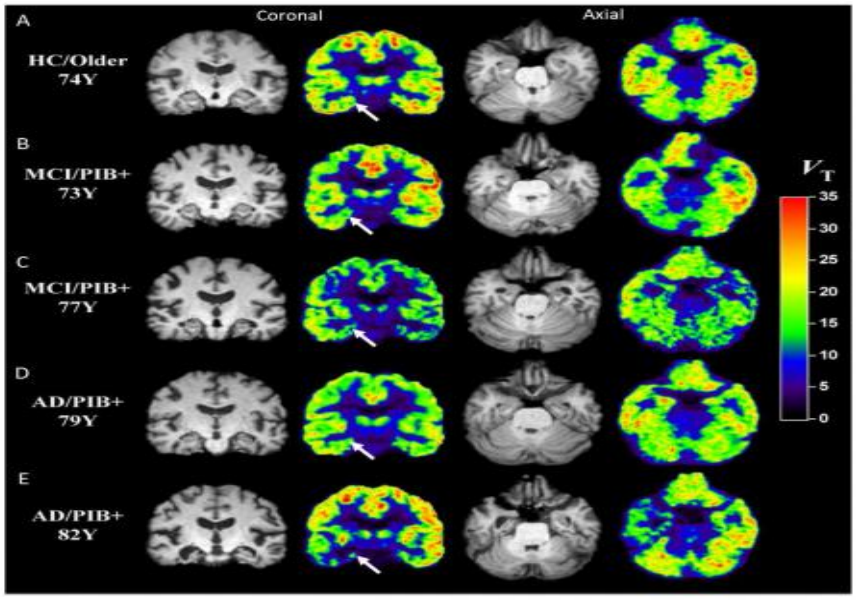

Figure 1. Representative coronal and axial images of ^{11}C-UCB-J parametric PET (V_T) and MRI scans in CN (A), MCI (B, C), and mild AD dementia (D, E). The CN had a negative ^{11}C-PiB scan and all AD had positive ^{11}C-PiB scans. The pseudo-color in PET images represents the intensity of UCB-J binding (V_T) with reference value displayed on the color bar. Evident reduction of ^{11}C-UCB-J binding in the hippocampus of AD was noted as compared to CN (see arrow for the region of right hippocampus). Various degrees of reduction can be visualized in the temporoparietal cortex of MCI (B, C) and mild AD dementia (D) and right temporal cortex of participant E.

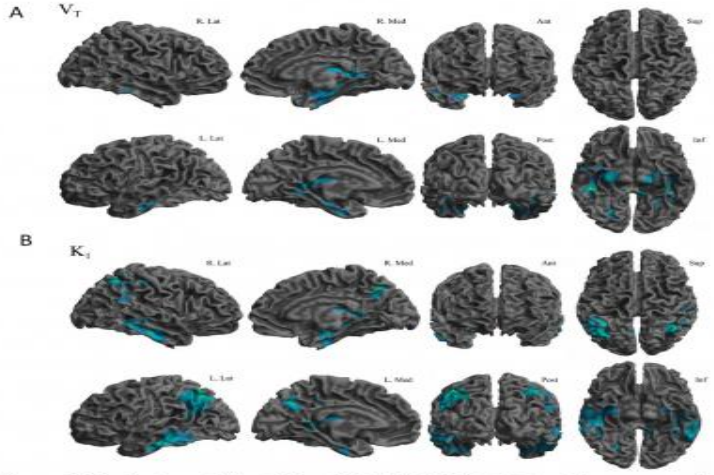

Figure 2. Voxelwise analysis of V_T and $K1$ with SPM in AD (n = 9) as compared to CN (n = 8). (A) Blue-green color indicates the brain regions with statistically significant reduction of V_T in AD as compared to CN, as rendering on the surfaces of brain at different projections. Statistically significant reduction of ^{11}C-UCB-J binding in the hippocampus was consistent with the findings from ROI analysis. (B) Blue-green color indicated statistically significant reduction of K_1 in AD as compared to CN, as rendering on the surfaces of brain at different projections. There was a broader regional reduction of K_1 in temporoparietal cortices of AD as compared to CN. The findings were consistent with the results from ROI analysis. Of note, the pattern of regional K_1 reduction in AD was highly similar to the classic clinical features of FDG PET in AD.

Keywords: Synaptic density, SV2A, hippocampus, PET, AD

Characterizing the relationship of [18F]GTP1 (Genentech tau probe 1) PET imaging with Alzheimer's disease pathophysiology

Sandra Sanabria Bohórquez[1], Suzanne Baker[1], Rebecca Ray[1], Paul Manser[1], Michael Ward[1], Edmond Teng[1], Kristin Wildsmith[1], Kina Höglund[2], Kaj Blennow[2], Jan Marik[1], Gai Ayalon[1], Geoffrey A. Kerchner[1], Robby Weimer[1]

[1]Genentech, Inc., South San Francisco, CA, US
[2]Department of Psychiatry & Neurochemistry, The Sahlgrenska Academy, University of Gothenburg, Mölndal, Sweden

Objective: In Alzheimer's disease (AD), the density and extent of brain tau pathology postmortem has been shown to correlate with cognitive dysfunction and atrophy. We examined the associations between the cross-sectional [^{18}F]GTP1 PET evaluation of tau pathology with cognitive, cortical atrophy and CSF biomarker in AD.

Methods: [^{18}F]GTP1 and Amyvid PET imaging, MRI, CSF and neurocognitive measures were collected from subjects participating in [^{18}F]GTP1 reproducibility and natural history studies. Analyses included amyloid (Aβ) negative (n=7) and Aβ-positive (n=8) healthy volunteers (HV), and Aβ-positive prodromal (n=18), mild (n=21) and moderate (n=17) AD subjects. [^{18}F]GTP1 SUVR (calculated using cerebellum gray) was measured in the whole cortical gray matter (WCG), *in vivo* Braak regions (Schöll et al., Neuron 2016) and the AD meta-ROI proposed by Jack et al. (Alzheimer's & Dementia 2017). CSF biomarkers were analyzed via immunoassay.

Results: [^{18}F]GTP1 SUVR and CSF mid-domain tau levels generally increased with disease severity. In Aβ+ HV and AD subjects, the lowest [^{18}F]GTP1 uptake was observed in Braak 5/6. Similar uptake was observed across all Braak regions in Aβ- HV. The effect size between HV and AD was largest in the AD meta-ROI (Hedge's=1.44) and lowest in Braak 5/6 (Hedge's=0.80). [^{18}F]GTP1 SUVR negatively correlated with cortical volume; the strongest correlations were observed in the AD meta-ROI (r=-0.56) followed by WCG and Braak 1/2 and 3/4 (r=-0.44). Partial correlation analyses show significant correlations of WCG [^{18}F]GTP1 SUVR with cognitive measures, after adjustment for composite amyloid SUVR. CSF mid-domain tau levels were moderately correlated with [^{18}F]GTP1 SUVR in the AD meta-ROI. Further analyses of the relationships between [^{18}F]GTP1 SUVR and CSF biomarkers, cognition, and atrophy are ongoing.

Conclusion: Tau pathology detected by [^{18}F]GTP1 correlates with key aspects of AD pathophysiology. Ongoing analysis of longitudinal data will provide further insights in changes due to normal aging and disease progression.

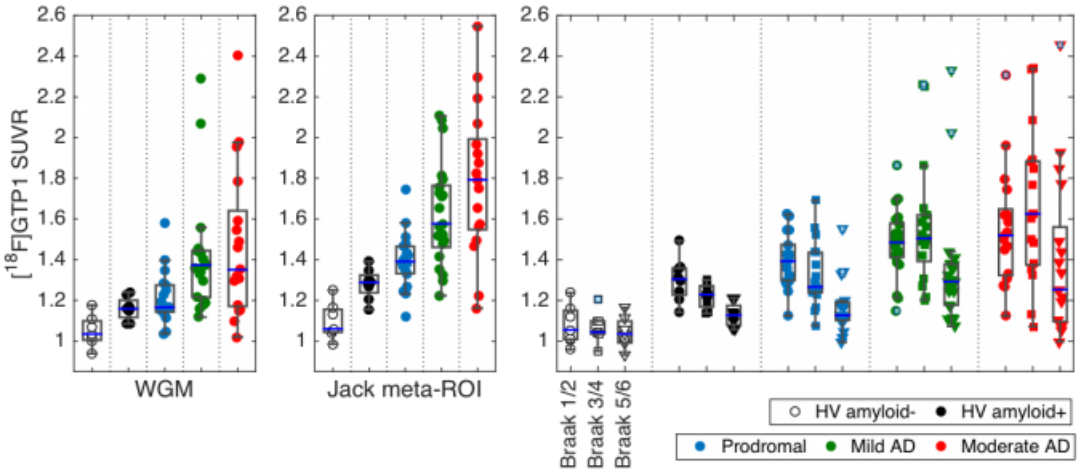

Figure 1. Regional [^{18}F]GTP1 SUVR measures in WGM, *in vivo* Braak regions and AD meta-ROI

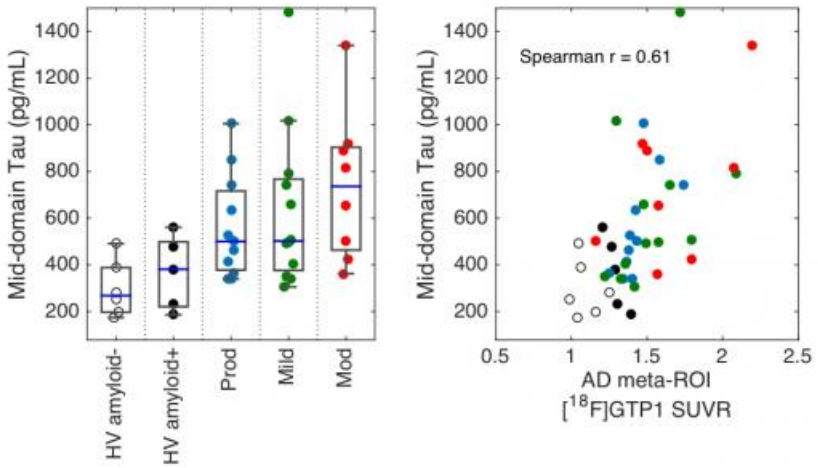

Figure 2. Mid-domain tau concentrations and correlation with AD meta-ROI [^{18}F]GTP1 SUVR

Keywords: Tau imaging, [18F]GTP1, Alzheimer's disease

A head-to-head comparison between [11C]PBB3 and [18F]PM-PBB3 in patients with AD and non-AD tauopathy

Manabu Kubota[1], Hitoshi Shimada[1], Kenji Tagai[1], Soichiro Kitamura[1], Maiko Ono[1], Yasuyuki Kimura[1,2], Masanori Ichise[1], Hitoshi Shinotoh[1,3], Keisuke Takahata[1], Yasuharu Yamamoto[1], Yasunori Sano[1], Chie Seki[1], Paul Tempest[4], Ming-Kuei Jang[4], John Seibyl[5], Olivier Barret[5], David Alagille[5], Kenneth Marek[5], Ming-Rong Zhang[1], Tetsuya Suhara[1], Makoto Higuchi[1]

[1]*National Institute of Radiological Sciences, National Institutes for Quantum and Radiological Science and Technology, Chiba, Japan*
[2]*Center for Development of Advanced Medicine for Dementia, National Center for Geriatrics and Gerontology, Obu, Japan*
[3]*Neurology Chiba clinic, Chiba, Japan*
[4]*Aprinoia Therapeutics, Taipei, Taiwan*
[5]*MNI, New Haven, CT, US*

Background: We recently developed a novel fluorinated tau PET ligand, [^{18}F]PM-PBB3, to improve characteristics of [^{11}C]PBB3. Our preclinical evidence suggested that [^{18}F]PM-PBB3 could capture tau deposits in living brains with high contrast and favorable kinetics. Here, we conducted a head-to-head comparison between PET data obtained using [^{11}C]PBB3 and [^{18}F]PM-PBB3 in patients with Alzheimer's disease (AD) and non-AD tauopathy.

Methods: Patients with AD and progressive supranuclear palsy (PSP), and healthy controls (HCs) underwent three PET scans with [^{11}C]PiB, [^{11}C]PBB3, and [^{18}F]PM-PBB3. In the scan with [^{18}F]PM-PBB3, arterial blood sampling was performed to determine binding potential (BP_{ND}) of the radioligand based on a compartment model. We also calculated BP_{ND} by a reference tissue model and standardized uptake value ratio (SUVR) using the cerebellum gray matter as reference. These estimates were compared to SUVR values of [^{11}C]PBB3 in each subject.

Results: The BP_{ND} values of [^{18}F]PM-PBB3 by a reference tissue model and SUVR were in good agreement with those by a compartment model. Compared to [^{11}C]PBB3, the peak brain radioactivity and contrast for tau lesions yielded by [^{18}F]PM-PBB3 were almost double of those produced by [^{11}C]PBB3. Unlike [^{11}C]PBB3, [^{18}F]PM-PBB3 showed minimal off-site binding in the brain parenchyma including the striatum. Binding of [^{18}F]PM-PBB3 in the brainstem was not evident in AD patients and HCs, but was prominent in PSP patients, resulting in a vivid contrast between PSP patients and the other subjects.

Conclusion: The current results indicate that [^{18}F]PM-PBB3 would be a promising PET ligand to quantify tau accumulation in AD and PSP patients with suitable kinetics and high contrast. The wide dynamic range and minimal parenchymal off-site binding of [^{18}F]PM-PBB3 would allow its application to differentiations among AD, non-AD tauopathies and HC by both visual inspection and quantitative assessments on an individual basis in a clinical workup.

Keywords: tau, [18F]PM-PBB3, PET, Alzheimer's disease, Progressive supranuclear palsy

Clinical evaluation of 18F-PI-2620, a next generation tau PET agent in subjects with Alzheimer's Disease and progressive supranuclear palsy

Andrew Stephens[1], John Seibyl[2], Andre Mueller[1], Olivier Barret[2], Mathias Berndt[1], Jennifer Madonia[2], David Alagille[2], Hanno Schieferstein[1], Heiko Kroth[3], Santiago Bullich[1], Andrea Pfeifer[3], Andreas Muhs[3], Gilles Tamagnan[2], Ken Marek[2], Ludger Dinkelborg[1]

[1]*Piramal Imaging, Berlin, Germany*
[2]*Invicro, New Haven, CT, US*
[3]*AC Immune SA, Lausanne, Switzerland*

Background: Intracellular tau deposition is a key pathologic feature of Alzheimer's disease (AD) and other neurodegenerative disorders. Several tau PET-probes have been developed for *in vivo* detection of brain tau load, although quantification is challenging due to high off target binding and slow brain-kinetics. ^{18}F-PI-2620 is a novel tau PET-tracer with a high binding-affinity for aggregated tau. Preclinically, ^{18}F-PI-2620 binds to both tau isoforms and is able to depict tau-deposits in AD brain sections from different Braak stages, as well as deposits in PSP. The clinical data reported here assesses the potential of ^{18}F-PI-2620 to visualize tau in subjects with AD and PSP, in comparison with non-demented controls (NDCs).

Methods: In an ongoing clinical imaging study, participants diagnosed with mild AD, non-AD tauopathies, or NDCs undergo dynamic PET imaging for 180 min. Some subjects are undergoing repeated scanning within 30 days after the initial PET scan including full arterial blood sampling.

Results: Imaging data show robust brain uptake and fast wash-out in non-target regions with peak SUVs > 4. There was no increased uptake seen in choroid plexus, basal ganglia, striatum, amygdala, meninges or other regions noted in first generation tau agents. In AD, focal asymmetric uptake was evident in temporal and parietal lobes, precuneus, and cingulate. SUVr time curves demonstrate a plateau at 60-90 min p.i. with resultant SUVrs of up to 4 in abnormal regions, whilst NDCs demonstrated lower SUVrs (1.0-1.2) in comparable brain regions. Importantly, PSP subjects demonstrated focal increased uptake in the globus pallidus and substantia nigra. Initial pharmacokinetic modeling indicates that SUVr from 60-90 min could be a good proxy for DVR, although pending full validation.

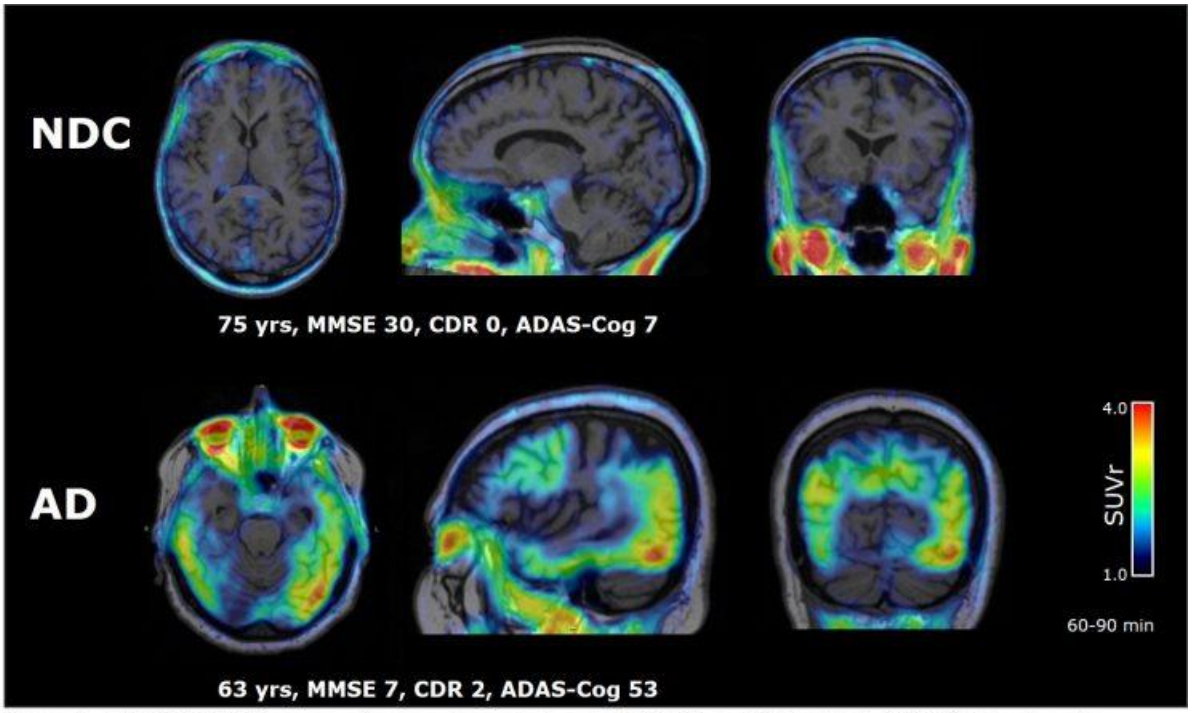

Figure 1. PI-2620 SUVr images of a non-demented control (NDC) and AD subject (60-90 min p.i. using cerebellar cortex as reference region)

Conclusion: ^{18}F-PI-2620 PET data in AD, PSP and NDC demonstrate favorable kinetics and high target specificity with low nonspecific binding and high signal in regions of expected tau pathology.

Keywords: tau, PET, AD, PSP, PI-2620

Wednesday, January 17, 2018 - 05:00 pm - 06:30 pm

Podium Session

Session 3: MK-6240

CHAIRS: Robert Koeppe, Julie Price

Wednesday, January 17, 2018		
05:00 pm - 06:30 pm	**Session 3: MK-6240**	CHAIRS: Robert Koeppe | Julie Price
05:00	Clinical validation of the novel PET tracer [18F]MK6240 for in vivo quantification of neurofibrillary tangles	Pascoal | Kang | Shin | Mathotaarachchi | Therriault | Ng | Lessa | Chamound | Savard | Knight | Bouhachi | Hsiao | Chartrand | Massarweh | Chakravarty | Bennacef | Soucy | Gauthier | **Rosa-Neto**
05:15	Test-retest characterization and pharmacokinetic properties of [18F]MK-6240	**Salinas** | Lohith | Purohit | Bennacef | Struyk | Sur | Barret | Constantinescu | Madonia | Marek | Hiatt | Martarello | Beaver
05:30	In vivo observations and quantification of tau with [F-18]MK-6240 PET from young controls to Alzheimer's disease	**Betthauser** | Murali | Barnhart | Stone | Rowley | Johnson | Christian
05:45	Tau imaging in Alzheimer's disease with 18F-MK6240, a second generation selective tau tracer	**Rowe** | Doré | Mulligan | Tyrrell | Lamb | Bourgeat | Cummins | Mito | Salvado | Masters | Villemagne
06:00	Discussion	

Clinical validation of the novel PET tracer [18F]MK6240 for in vivo quantification of neurofibrillary tangles

Tharick Pascoal[1], Min Su Kang[1], Monica Shin[1], Sulantha Mathotaarachchi[1], Joseph Therriault[1], Kok Pin Ng[1], Andrea Lessa[1], Mira Chamound[1], Melissa Savard[1], Ashley Knight[1], Reda Bouhachi[1], Chris Hsiao[1], Daniel Chartrand[1], Gassan Massarweh[1], Mallar Chakravarty[1], Idriss bennacef[2], Jean-Paul Soucy[1], Serge Gauthier[1], Pedro Rosa-Neto[1]

[1]*McGill University, Montreal, QC, Canada*
[2]*Translational Biomarkers, Merck & Co., Inc., West Point, Pennsylvania, West Point, PA, US*

Objective: To examine the kinetics of the novel positron emission tomography (PET) tracer for neurofibrillary tangles [^{18}F]MK6240 in human individuals.

Methods: Sixteen individuals (4 AD, 3 MCIs, 5 healthy elderly, and 3 healthy young (<25 y.o)) underwent 180 minutes dynamic examination with a HRRT PET scanner using the tracer [^{18}F]MK6240. Arterial sampling with metabolite corrections was performed in 6 participants. Compartmental modelling and several simplified quantitative approaches were performed. Clinical assessments, MRIs, and amyloid-PET scans were performed in all participants.

Results: [^{18}F]MK6240 appeared rapidly in the brain with a radioactivity peak between 2-5 minutes. AD and MCI participants, showed a slower clearance in regions expected to contain tangles, whereas in young and elderly controls, the radioactivity was low following a uniform rapid washout across all brain regions(Fig.1). Parent compound showed a rapid washout complicating accurate measurement in later time points, and one metabolite was detected(Fig.2). Binding in cerebellum, pons, striatum, and white matter was low and similar between individuals with different diagnostics showing potential to be used as reference region(Fig.3). Specific and total/non-displaceable binding reached the equilibrium between 60-70, and 80-90 minutes after injection in target regions, respectively. Reversible 2-tissue-compartment model described well the time–activity curves. Distribution volume ratio using simplified reference tissue model and reference Logan were highly correlated with standardized uptake value ratios(SUVR) measured after the ligand reaches the equilibrium at 90 minutes(slope~=0.95,R>0.98). SUVRs using the cerebellum gray matter calculated at 90-110 minutes were lower in controls than in MCIs or AD(Fig.4). There was a negligible difference in binding between young and elderly healthy individuals across all brain.

Discussion: [^{18}F]MK6240 was well tolerated, non-invasive quantitative approaches such as SUVR provided valid estimates of neurofibrillary tangles and well discriminated MCI and AD participants from controls. is a promising tracer with the potential to the evaluation of disease-modifying interventions and diagnostic use.

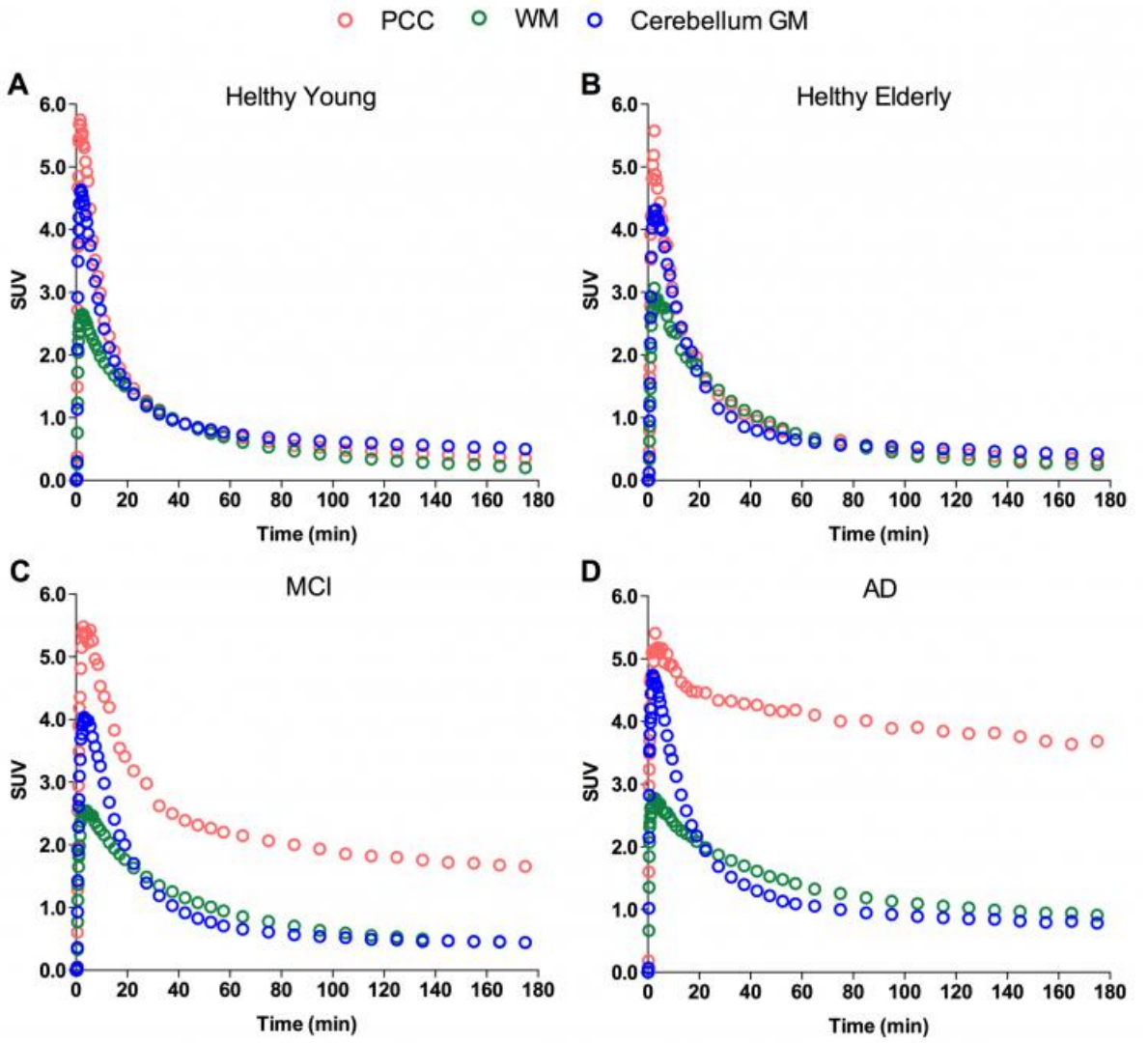
PCC
WM
Cerebellum GM
A
Helthy Young
B
Helthy Elderly
C
MCI
D
AD
SUV
Time (min)

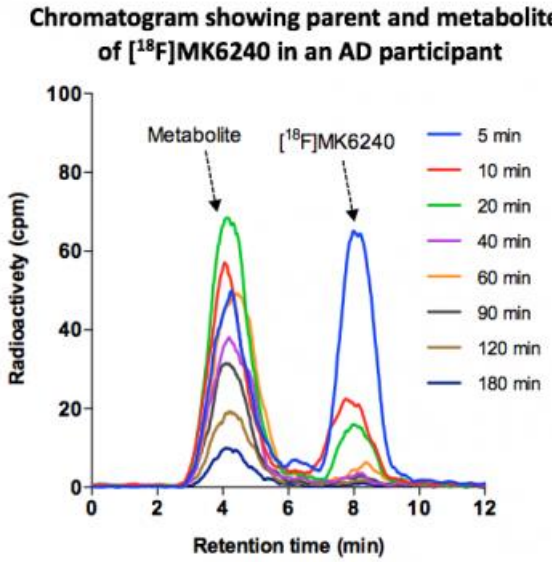
Chromatogram showing parent and metabolites of [18F]MK6240 in an AD participant
Metabolite
[18F]MK6240
5 min
10 min
20 min
40 min
60 min
90 min
120 min
180 min
Radioactivety (cpm)
Retention time (min)

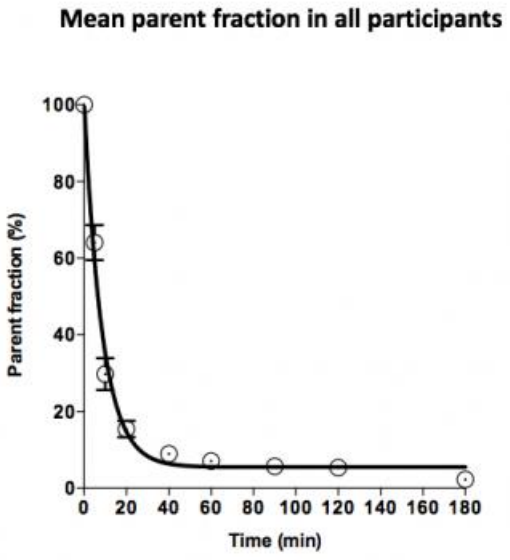
Mean parent fraction in all participants
Parent fraction (%)
Time (min)

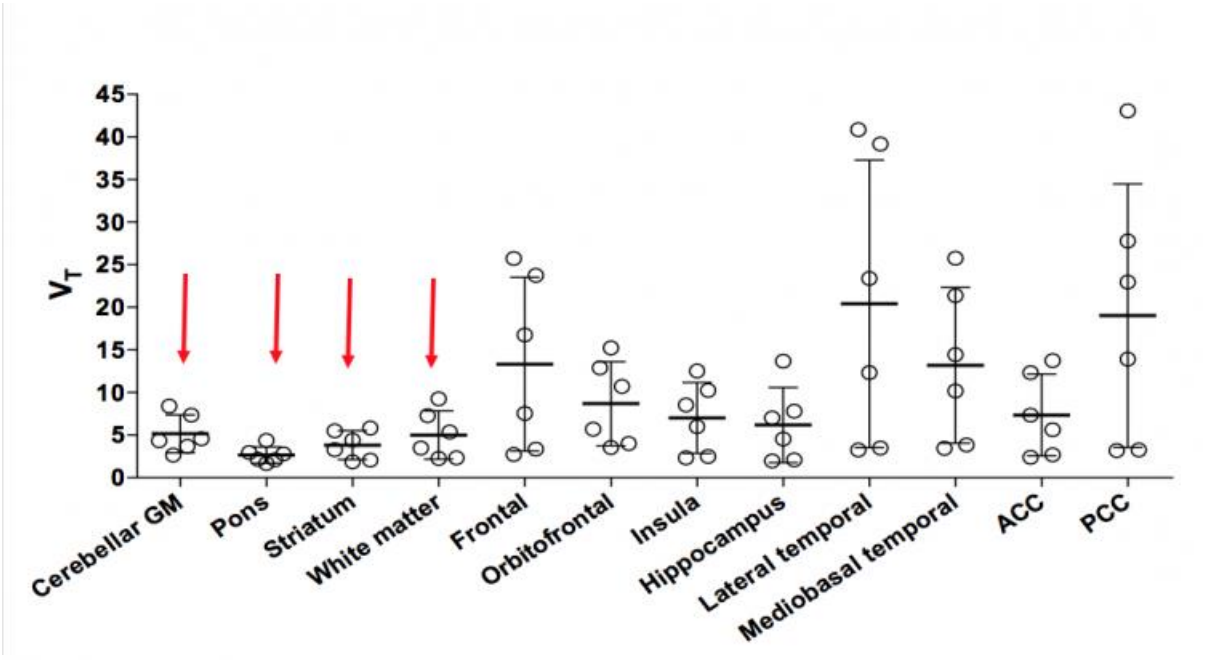

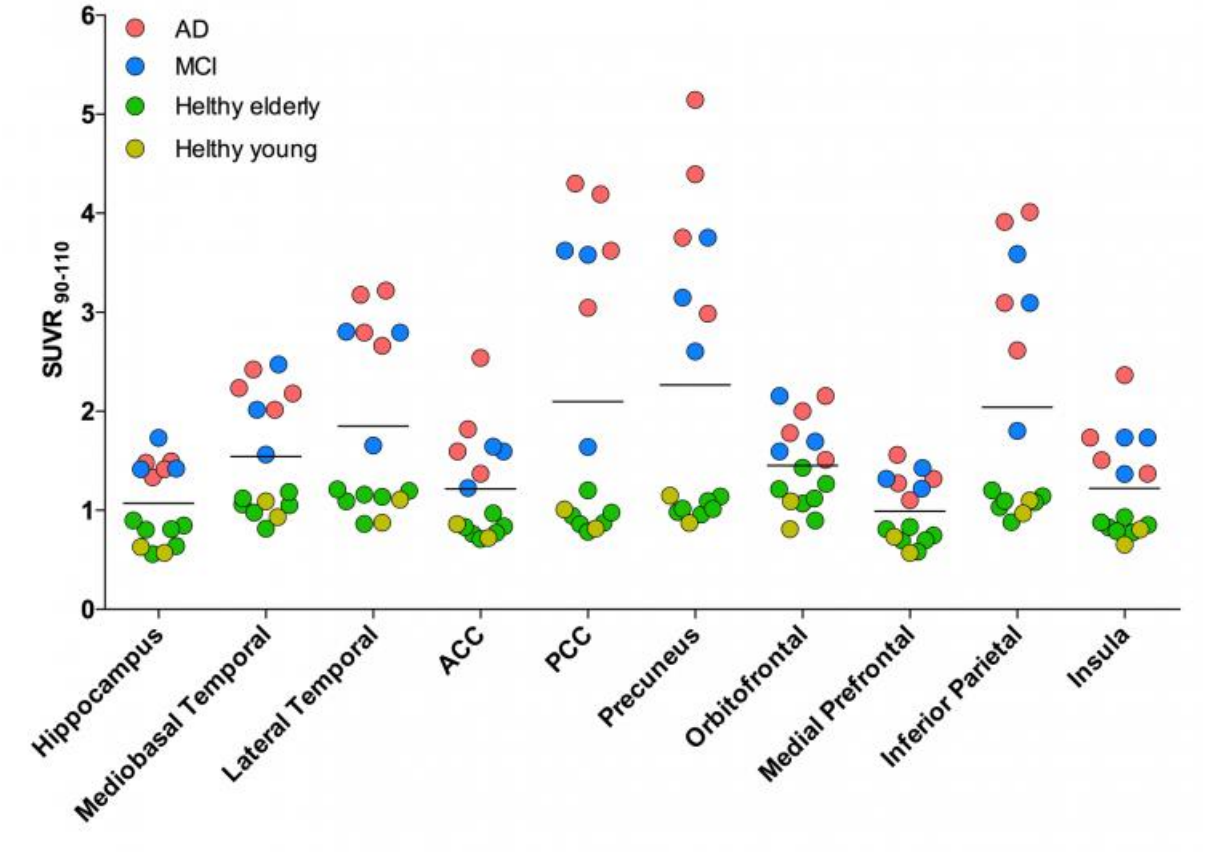

Keywords: Tau image, Alzheimer's disease, [18F]MK6240

Test-retest characterization and pharmacokinetic properties of [18F]MK-6240

Cristian Salinas[1], Talakad Lohith[2], Ajay Purohit[1], Idriss Bennacef[2], Arie Struyk[2], Cyrille Sur[2], Olivier Barret[3], Cristian Constantinescu[3], Jennifer Madonia[3], Kenneth Marek[3], Rick Hiatt[4], Laurent Martarello[1], John Beaver[1]

[1]*Biogen, Cambridge, MA, US*
[2]*Merck & Co, West Point, PA, US*
[3]*InviCRO, Boston, MA, US*
[4]*Cerveau Technologies, Boston, MA, US*

Abstract: MK-6240 is a promising tool for clinical assessment in patients with Alzheimer's disease. The regional distribution, test–retest variability and tracer uptake correlation with clinical endpoints were measured as important steps towards the characterization of [18F]-MK-6240 as a clinical imaging biomarker for neurofibrillary tangles (NFT).

Methods: Two high specific activity [18F]MK-6240 (PET studies were performed in normal control (n=3) and in amyloid positive (Florbetapir) Alzheimer's disease subjects (n=9, MMSE 9-24, age=64±8y) on two separate days (~14 days apart). Each subject underwent dynamic PET scanning for a 3 hour period post-injection, with a short standardized break. Arterial blood samples were collected to generate a plasma input function corrected for radiometabolites. Regional specific binding was assessed by volumes of distribution (VTs, 2TC), SRTM derived BPNDs and standardized uptake value ratios (SUVRs).

Results: Intravenous administration of [18F]MK-6240 was well tolerated. [18F]MK-6240 rapidly partitioned into brain, and its distribution pattern was consistent with NFT pathology in AD. [18F]MK-6240 exhibited fast plasma metabolism (<10% parent after 30 minutes). SUVR curves (using cerebellar grey-matter as reference) in NFT associated regions were high in AD (>2-3). In contrast a uniform distribution (~1) was consistently observed in healthy subjects. SUVRs (90-120 minutes) showed an average TRT variability ≤7% and high correlation with clinical measurements of disease stage. A strong linear correlation between SUVR and BPND was observed. Correlation between VT and SUVR was variable across subjects. Further investigation revealed that VT estimations were sensitive to small variations in terminal parent fraction measurements, potentially contributing to the observed variability.

Conclusion: Further investigation is needed to understand the factors contributing to VTs variability and to establish the true relationship between VT and SUVR outcomes. The good correlation between regional uptake, NFT distribution and clinical scores is a good evidence of [18F]MK-6240 suitability to assess tau deposition in AD patients.

Keywords: [18F]MK-6240, Tau PET, Test-Retest

In vivo observations and quantification of tau with [F-18]MK-6240 PET from young controls to Alzheimer's disease

Tobey Betthauser, Dhanabalan Murali, Todd Barnhart, Charles Stone, Howard Rowley, Sterling Johnson, Bradley Christian

University of Wisconsin-Madison School of Medicine and Public Health, Madison, WI, US

Objectives: This work investigates the in vivo kinetics and binding of tau radioligand [^{18}F]MK-6240 in subjects with a range of cognitive states.

Methods: Twenty-two participants (3 young controls (24-45yrs), 6 older controls (64-71yrs), 5 cognitive decliners, 1 aMCI, 7 probable AD) underwent T1-w MRI and [^{18}F]MK-6240 PET scans. MK-6240 PET time series were acquired (Siemens ECAT HR+) for up to 120 min following 10 mCi injection. Reconstructed PET data were interframe realigned, coregistered to T1 MRI, and time-activity curves (TACs) were extracted for GM restricted AAL ROIs inverse warped into native T1 space. Regional kinetics were assessed by comparing standard uptake values (SUVs) and target-to-reference (TTR) ratios with the inferior cerebellar GM as reference region. Multiple time graphical analysis (Logan) was investigated for distribution volume ratio (DVR) estimation. Various 20-minute SUVR windows were compared to DVR estimates by linear regression. SUVR images were used to identify patterns of tau and potential off-target binding.

Results: SUV TACs indicated good brain penetrance (SUV_{max} 2-4 following bolus) with the inferior cerebellum and pons revealing no regions of focal uptake. TTR TACs plateaued around 70-minutes, although neocortical regions in AD cases were still increasing at 90 minutes. Stable DVR estimates were achieved by 90 minutes post-injection in high DVR (>4.0) regions. Regression of SUVR on DVR indicated strong correlation ($R^2 \geq 0.98$) with a slope of 1.1 for SUVR 70-90 minutes post-injection. MK-6240 SUVR images (70-90 min) recapitulated Braak staging in most subjects. Regions with off-target binding included the nasal sinus and red nucleus in most subjects, sporadically and to varying degrees in the meninges and superior anterior vermis, and focal hemangiomas in two subjects.

Conclusions: These preliminary data indicate favorable in vivo kinetics and high specific binding of MK6240 for tau PET imaging and support additional investigations into its use for longitudinal studies of tau burden.

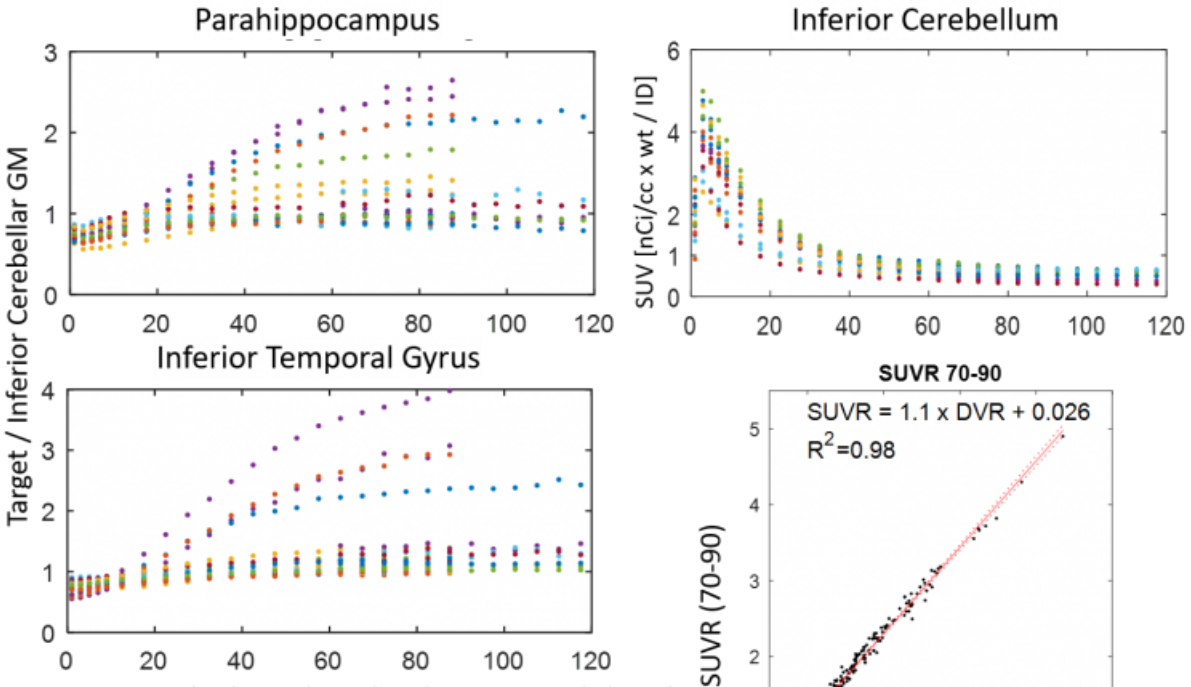

Figure 1: Standard uptake value (SUV, top right) and target-to-reference ratio (left) time-activity curves for [^{18}F]MK-6240 from 0-120 minutes. Linear regression for ROIs with distribution volume ratios (DVR) >1.2 with standard uptake value ratios (SUVR, 10-90 min) indicated strong correlation (bottom right).

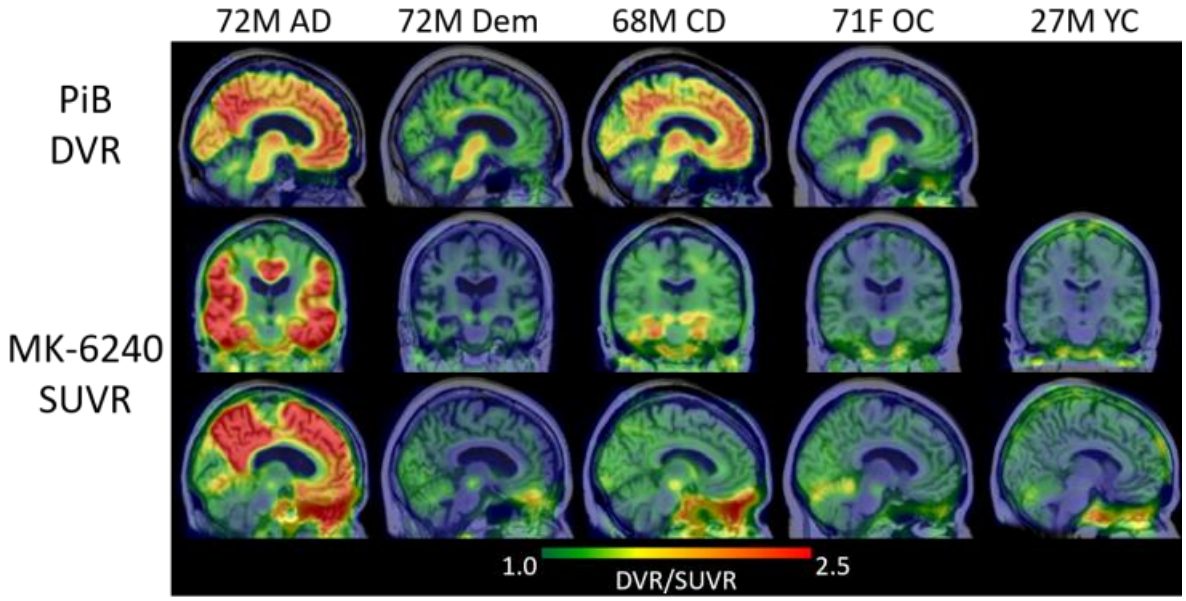

Figure 2: Composite image of [^{11}C]PiB DVR and [^{18}F]MK-6240 SUVR (70-90 min) images. AD = AD dementia, Dem = non-AD dementia, CD = longitudinal cognitive decliner, OC = older control, YC = young control

Keywords: tau, MK-6240, Alzheimer's

Tau imaging in Alzheimer's disease with 18F-MK6240, a second generation selective tau tracer

Christopher C Rowe[1,3], Vincent Doré[1,2], Rachel Mulligan[1], Regan Tyrrell[1], Fiona Lamb[1], Pierrick Bourgeat[2], Tia L Cummins[1,3], Remika Mito[3], Olivier Salvado[2], Colin L Masters[3], Victor L Villemagne[1,3]

[1]*Department of Molecular Imaging & Therapy, Austin Health, Melbourne, Australia*
[2]*CSIRO e-Health Research Centre, Brisbane, Australia*
[3]*The Florey Institute of Neuroscience and Mental Health, The University of Melbourne, Melbourne, Australia*

Background: Some first-generation tau tracers have been shown to either present "off-target" binding or lack of selectivity for tau. We evaluated the ability of ^{18}F-MK6240, a second-generation selective tau tracer, to detect and measure global and regional tau burden in the brain.

Methods: Eight probable Alzheimer's disease (AD), 3 mild cognitive impairment (MCI), 5 non-AD dementia (nADD), and 6 healthy elderly controls (HC), underwent Aβ-amyloid imaging with ^{18}F-NAV4694 and 120-min dynamic tau imaging with ^{18}F-MK6240. Global and regional ^{18}F-MK6240 binding was assessed using Distribution Volume Ratios (DVR) and standardized uptake value ratios (SUVR) at 70-90 and 90-120 min post injection, calculated using the cerebellar cortex as reference region.

Findings: One AD participant had both low Aβ and tau tracer retention. Six of the 7 remaining Aβ+AD patients showed high ^{18}F-MK6240 binding, greater in the temporoparietal and posterior-cingulate than in frontal cortex. Tracer retention in HC and nADD was very low. No "off-target" binding in choroid plexus or basal ganglia was observed. Significantly higher DVR_{CbCtx} was observed in Aβ+AD compared to HC in mesial temporal (Me, 1.26±0.28vs.0.80±0.05, *p=0.02*), temporoparietal (Te) 1.54±0.58vs.0.88±0.05, *p=0.02*), and rest of neocortex (R) (1.30±0.45vs.0.78±0.04, *p=0.02*). Similar differences were observed with $SUVR_{CbCtx}$ at 70-90 min: Me (2.02±1.00vs.0.87±0.08, *p=0.04*), Te (2.56±1.86vs.0.96±0.07, *p=0.03*), and R (2.01±1.44vs.0.88±0.11, *p=0.04*), and at 90-120 time windows: Me (1.91±0.93vs.0.85±0.16, *p=0.04*), Te (2.60±1.84vs.0.93±0.10, *p=0.04*), and R (2.10±1.45vs.0.82±0.09, *p=0.04*) time windows. There was high agreement between regional DVR_{CbCtx} and $SUVR_{CbCtx}$ at 70-90 min (r=0.93, *p<0.0001*; r=0.94, *p<0.0001*; and r=0.93, *p<0.0001*, for Me, Te and R, respectively) and at 90-120 min (r=0.88, *p<0.0001*; r=0.90, p<*0.0001*; and r=0.89, p<*0.0001*, for Me, Te and R, respectively. Identical interpretation resulted from visual inspection of 70-90 and 90-120 min images.

Interpretation: ^{18}F-MK6240 PET discriminates well between AD and HC, and should facilitate integration of tau imaging into clinical practice and therapeutic trials.

Keywords: Tau imaging, Alzheimer's disease, Positron emission tomography

Thursday, January 18, 2018 - 08:30 am - 10:15 am

Podium Session

Session 4: Pathological Correlates

CHAIRS: Milos Ikonomovic, Melissa Murray

Thursday, January 18, 2018		
08:30 - 10:15	**Session 4: PATHOLOGICAL CORRELATES**	CHAIRS: Milos Ikonomovic | Melissa Murray
08:30	Autoradiographic Evaluation of MK-6240 compared to AV-1451	**Lowe** | Bruinsma | Sarma | Curran | Min | Fang | Pandey | Bennacef | Serie | Jones | Josephs | Parisi | Knopman | Boeve | Kantarci | Jack | Dickson | Petersen | Murray
08:45	In vivo and in vitro [18F]MK6240 show neurofibrillary tangles deposition heterogeneity in individuals with a wide range of cognitive symptoms	**Pascoal** | Chamoun | Shin | Mathotaarachchi | Kang | Therriault | Savard | Benedet | Knight | Chakravarty | Massarweh | bennacef | Soucy | Gauthier | Rosa-Neto
09:00	Multi-site study of PiB-PET imaging using the Centiloid method: relationships to pathological measures of β-amyloid pathology	**La Joie** | Ayakta | Borys | Boxer | deCarli | Dore | Grinberg | Huang | Jack | Jin | Klunk | Ikonomovic | Lockhart | Lowe | Masters | Miller | Mungas | Murray | O'Neil | Olichney | Petersen | Reed | Rowe | Seeley | Vemuri | Villemagne | Jagust | Rabinovici
09:15	[F-18]-AV-1451 binding profile in Chronic Traumatic Encephalopathy: a postmortem case series	Marquié | **Aguero** | Siao Tick Chong | Ramanan | Sáez-Calveras | Verwer | Kim | Bennett | Silva Amaral | Johnson | Frosch | Alvarez | McKee | Normandin | Gómez-Isla
09:30	Neuropathological and biochemical correlates of tau and amyloid PET imaging in two autopsy brains	**Ikonomovic** | Abrahamson | Kofler | Price | Becker | Mathis | Lopez | Klunk
09:45	Discussion	

Autoradiographic evaluation of MK-6240 compared to AV-1451

Val Lowe[1], Tyler Bruinsma[1], Vidur Sarma[1], Geoffrey Curran[1], Hoon-Ki Min[1], Ping Fang[1], Mukesh Pandey[1], Idress Bennacef[2], Amanda Serie[3], David Jones[1], Keith Josephs[1], Joseph Parisi[1], David Knopman[1], Bradley Boeve[1], Kejal Kantarci[1], Clifford Jack[1], Dennis Dickson[3], Ronald Petersen[1], Melissa Murray[3]

[1]*Mayo Clinic, Rochester, MN, US*
[2]*Merck & Co., Inc., Kenilworth, NJ, US*
[3]*Mayo Clinic, Jacksonville, FL, US*

Background: Several tau-PET imaging radiotracers have been developed. Comparing the characteristics of these different radiotracers is important to better understand future applications. We therefore compared the binding of MK-6240 to AV-1451 PET in the same brain tissue samples in a wide range of tau pathologies.

Methods: Brain tissue sections (n=60) were obtained from our research brain bank from multiple different pathologies (normal, n=1; pathologic aging (PA, Braak ≤3), n=1; AD, n=4; FTD-TDP, n=3; AGD, n=2; CBD, n=3; PSP n=3; Pick's, n=3; PART, n=1; MAPT N297K, n=3; MAPT R406W, n=1 and MAPT P301L, n=1). Adjacent sections were incubated with [18F]AV-1451 and [18F]MK-6240 using identical methods. Self-blocking with each respective cold tau-PET agent was performed. Adjacent sections were also stained with PHF-1 and CP-13 for visual comparison.

Results: Both AV-1451 and MK-6240 showed binding to AD-tau (3R+4R) with MK-6240 showing less intense binding in some sections on visual comparison (9/11 AD sections) (Figure 1). The binding of MK-6240 was similar to AV-1451 in sole 3R and sole 4R tau cases in which both were poor. Comparisons of "off-target" binding showed similar findings, similar uptake was seen in the MAPT R406W case, and both radiotracers had discordant uptake with CP13 in "early" tau seen in pathological aging.

Conclusions: Minimally reduced binding of MK-6240 vs. AV-1451 in some AD cases may result in lower MK-6240 signal in AD dementia clinical imaging. The significance of this finding needs to be verified with *in vivo* imaging. Mild MK-6240 binding in non-AD tau cases, similar to AV-1451, was generally seen and argues for similar clinical imaging characteristics. Both radiotracers may have limited ability to detect early tau deposition as defined by IHC for early sites of phosphorylation.

Figure 1. Autoradiography findings of AV-1451 (left) and MK-6240 (middle) in a posterior hippocampal section of AD-type tau (respective blocking studies are shown below each) are shown. Minimally less binding is seen with MK-6240 in IHC positive regions (red arrows) as compared to AV-1451.

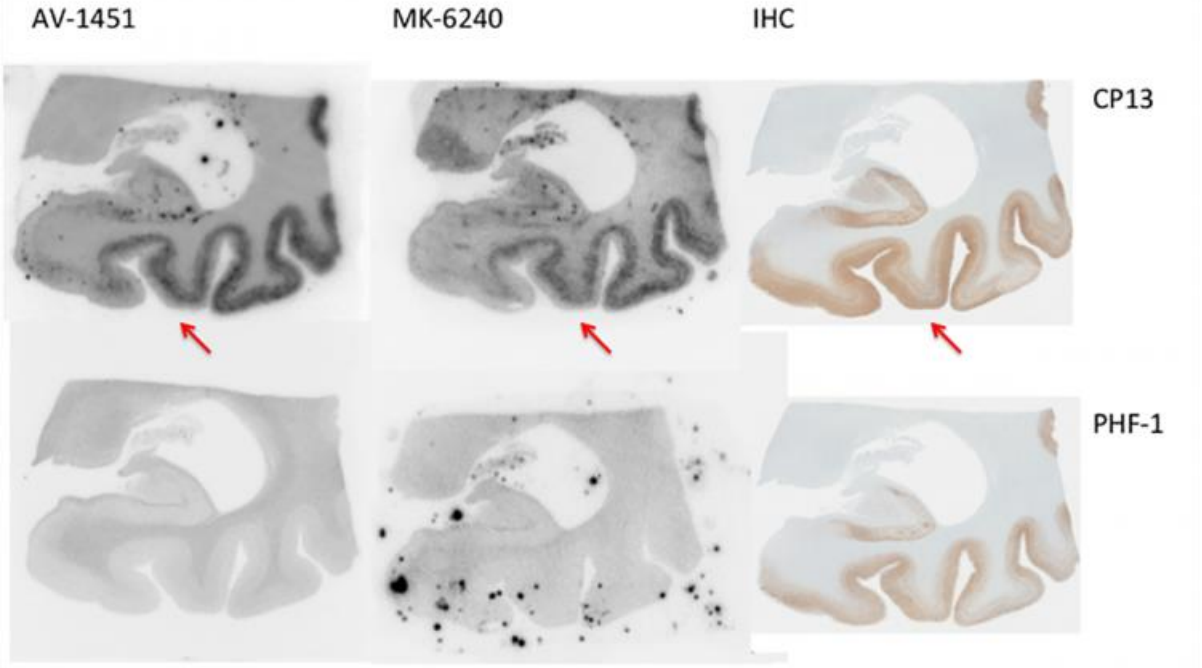

Keywords: Tau-PET, AV-1451, MK-6240,

In vivo and in vitro [18F]MK6240 show neurofibrillary tangles deposition heterogeneity in individuals with a wide range of cognitive symptoms

Tharick Pascoal[1], Mira Chamoun[1], Monica Shin[1], Sulantha Mathotaarachchi[1], Min Su Kang[1], Joseph Therriault[1], Melissa Savard[1], Andrea Benedet[1], Ashley Knight[1], Mallar Chakravarty[1], Gassan Massarweh[1], Idriss bennacef[2], Jean-Paul Soucy[1], Serge Gauthier[1], Pedro Rosa-Neto[1]

[1]*McGill University, Montreal, QC, Canada*
[2]*Translational Biomarkers, Merck & Co., Inc., West Point, Pennsylvania, West Point, PA, US*

Objective: To assess the patterns of neurofibrillary tangles deposition with [^{18}F]MK6240 in individuals with a wide range of cognitive profiles.

Methods: Sixth one individuals (18 healthy elderlies (age = 69.6 (6.9)), 10 MCIs (age= 68.3 (6.2)), 13 typical AD (age = 76.3 (9.9)), 14 atypical AD (age =60.8 (5.87)), 3 young (age= 23 (1.4)), 2 FTD MAPT mutation (age=60.3 (8.4)), and 1 sporadic FTD (age= 70)) underwent PET scans with [^{18}F]MK6240 and [^{18}F]NAV4694, as well as MRI and cognitive assessments. In vitro autoradiography was performed in tissues of controls and AD individuals with [^{18}F]MK6240. [^{18}F]MK6240 and [^{18}F]NAV4694 standardized uptake value ratios (SUVR) used the cerebellum grey matter as reference region and were calculated at 90-110 and 40-70 minutes, respectively.

Results: We found a high heterogeneity and a broad dynamical range of [^{18}F]MK6240 uptake across the population. [^{18}F]MK6240 was able to discriminate controls, MCI, and AD individuals (Fig.1). Autoradiography showed high binding in regions expected to have neurofibrillary tangles in AD patients, whereas the binding in elderly controls was negligible. We identified amyloid positive and tau negative individuals (Fig.2) as well as amyloid negative and tau positive ones (Fig.3). Out of 18 healthy elderlies, one individual was clearly [^{18}F]MK6240 positive with pattern similar to AD patients (Fig.4). Individuals with the clinical diagnostic of posterior cortical atrophy showed tau deposition predominantly in the posterior part of the brain. Relative [^{18}F]MK6240 uptake in tau negative individuals was observed in regions including substantia nigra, retina, choroid plexus, and meninges. Among young individuals the highest binding was found in the retina and meninges.

Discussion: There were no clinically detectable pharmacologic or side effects attributed to the [^{18}F]MK6240 uptake in our population. Different from other available PET ligands, [^{18}F]MK6240 showed negligible binding in most of cognitively normal elderly individuals. [^{18}F]MK6240 was able to discriminate controls, MCI, and AD individuals.

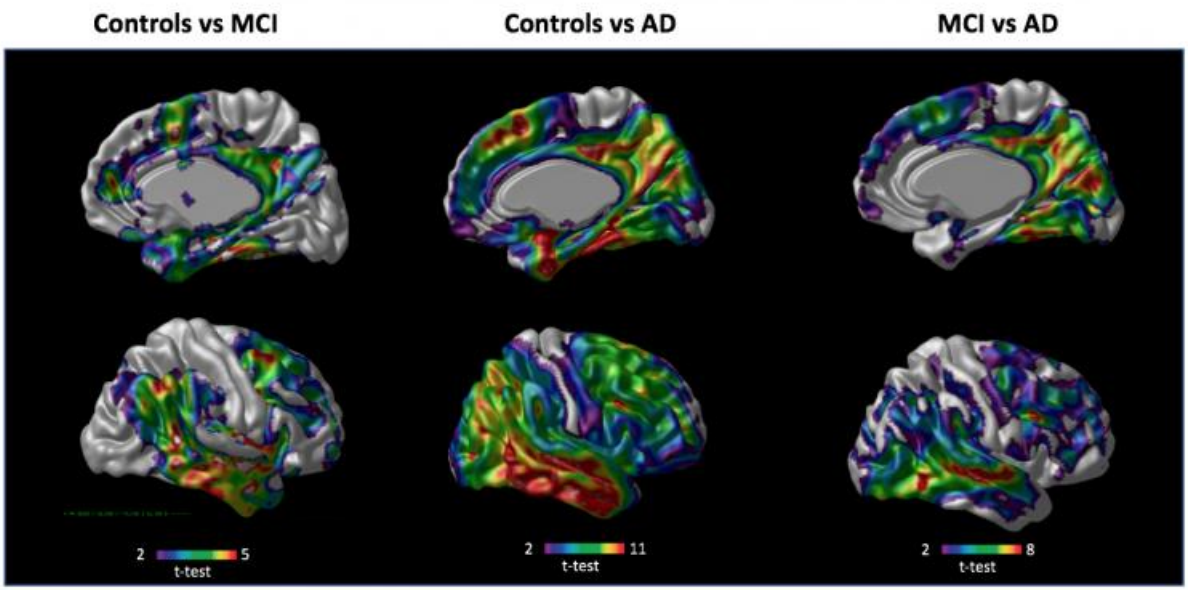
Controls vs MCI
Controls vs AD
MCI vs AD
2
5
t-test
2
11
t-test
2
8
t-test

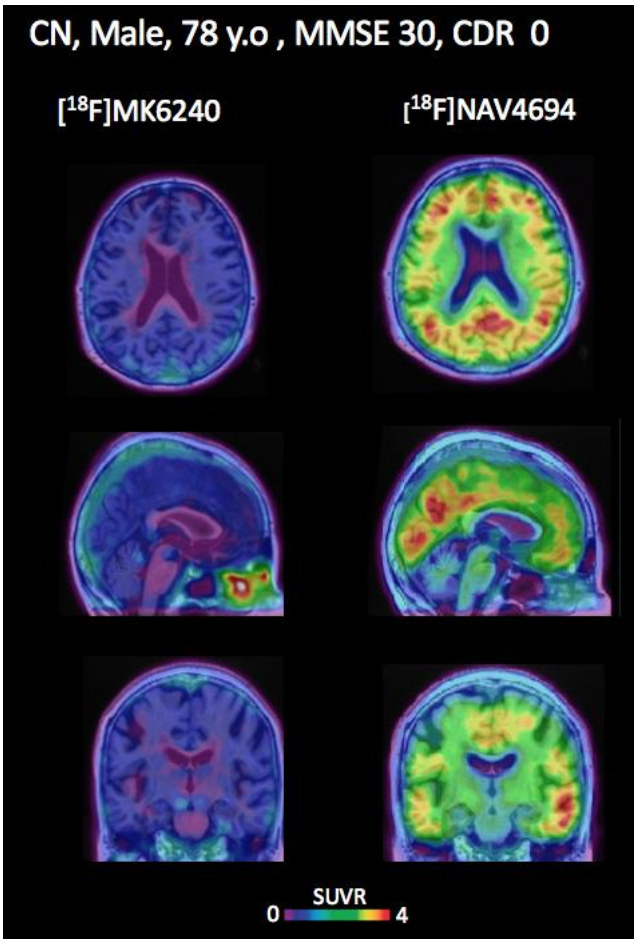
CN, Male, 78 y.o , MMSE 30, CDR 0
[18F]MK6240
[18F]NAV4694
SUVR
0
4

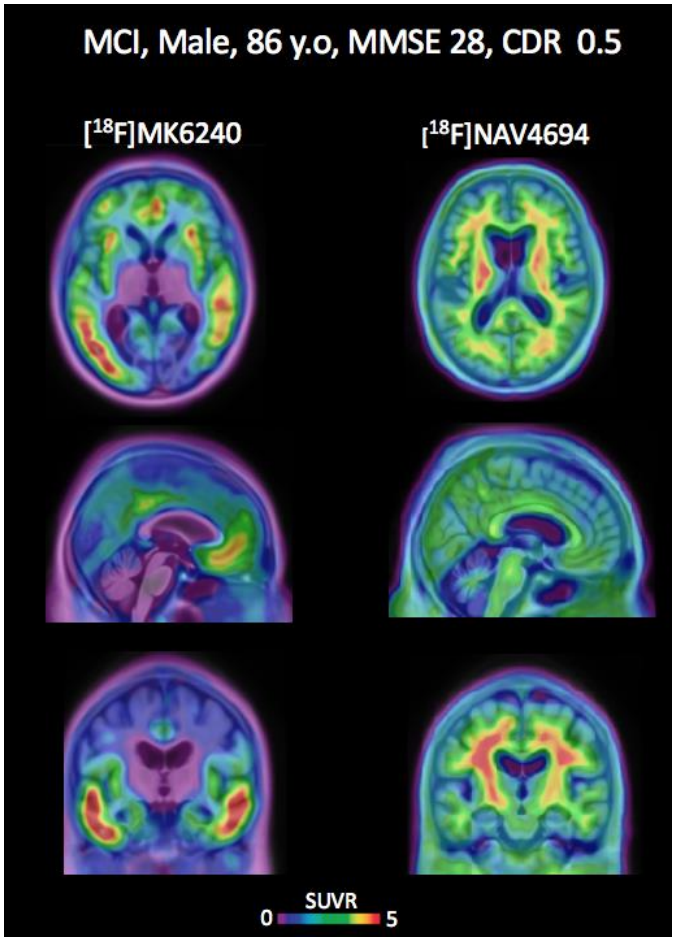
MCI, Male, 86 y.o, MMSE 28, CDR 0.5
[18F]MK6240
[18F]NAV4694
SUVR
0
5

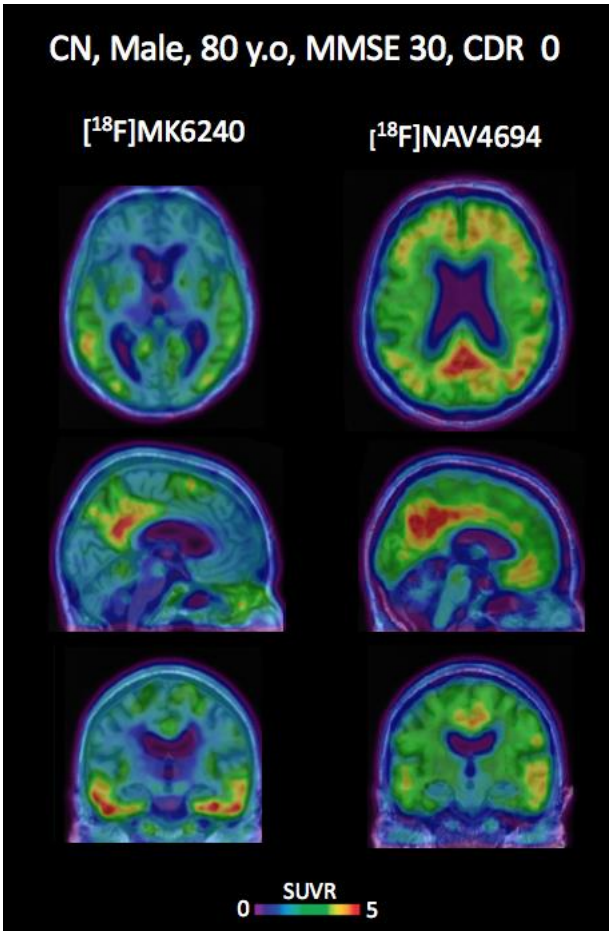

Keywords: Tau imaging, Neurodegenerative diseases, [18F]MK6240

Multi-site study of PiB-PET imaging using the Centiloid method: relationships to pathological measures of β-amyloid pathology

Renaud La Joie[1], Nagehan Ayakta[1], Ewa Borys[2], Adam L Boxer[1], Charles deCarli[2], Vincent Dore[3], Lea T Grinberg[1], Eric J Huang[1], Clifford R Jack[4], Lee-Way Jin[2], William E Klunk[5], Milos D Ikonomovic[5], Samuel N Lockhart[6], Val L Lowe[4], Colin L Masters[7], Bruce L Miller[1], Daniel M Mungas[2], Melissa E Murray[8], Jim O'Neil[9], John M Olichney[2], Ronald C Petersen[4], Bruce R Reed[2], Christopher C Rowe[3], William W Seeley[1], Prashanti Vemuri[4], Victor L Villemagne[3,7], William J Jagust[6,9], Gil D Rabinovici[1,6,9]

[1]*University of California, San Francisco, San Francisco, CA, US*
[2]*University of California, Davis, Davis, CA, US*
[3]*Centre for PET, Austin Health, Melbourne, Australia*
[4]*Mayo Clinic, Rochester, MN, US*
[5]*University of Pittsburgh, Pittsburgh, PA, US*
[6]*University of California, Berkeley, Berkeley, CA, US*
[7]*The Florey Institute of Neuroscience and Mental Health, Melbourne, Australia*
[8]*Mayo Clinic, Jacksonville, FL, US*
[9]*Lawrence Berkeley National Laboratory, Berkeley, CA, US*

Introduction: The Centiloid project provides a framework to process Aβ-PET data, enabling participating groups to quantify PET with a unified scale. We aimed to apply the Centiloid method to a large, multi-site cohort of patients with antemortem [11C]PiB-PET and available autopsy data, in order to characterize the relationships between Centiloid values (CLs) and underlying Aβ pathology.

Methods: We first validated implementation of the standard Centiloid pipeline using the [11C]PiB-Centiloid dataset available on www.gaain.org (Fig1a). We then analyzed a heterogeneous group of 179 participants from 4 centers, encompassing a broad range of clinical diagnoses and autopsy findings (Table 1). 50-70 min PET data from UCSF/UCD, UPitt and AIBL were preprocessed at UCSF while Mayo data was preprocessed on site (Fig1b). Statistical analyses were conducted to assess the relationships between resulting CLs and pathological measures of β-amyloid pathology (CERAD score and Thal phase). Receiver Operating Curve (ROC) analyses were run to determine an optimal Centiloid threshold distinguishing absent to sparse from moderate to frequent CERAD scores.

Results: CLs ranged from -26 to 169 and followed a bimodal distribution (Fig2a). Median CLs increased with CERAD score, although significant overlap was observed (Fig2b). Results were highly comparable across centers: the median CLs for participants with no versus frequent neuritic plaques were -3 versus 95 for UCSF/UCD, -3 versus 97 for UPitt, and -1 versus 91 for Mayo. CLs also increased with Thal phases in a non-linear fashion, with detectable PET binding increasing around Phase 2/3 (Fig2c). The area under the ROC for distinguishing CERAD absent-sparse from moderate-to-frequent was .91 (95%CI: .86-.95); Youden's index identified an optimal threshold of 12 CL (89% Sensitivity, 86% Specificity, 88% accuracy).

Conclusion: We demonstrated the feasibility and robustness of the Centiloid method for multi-site studies, and provided a pathology-based CL threshold to determine Aβ positivity.

	Total	UCSF/UCD	UPitt	Mayo	AIBL	Group comparison
n	179	73	32	69	5	
Clinical Diagnosis (%) HC / MCI / AD / non-AD	12 / 15 / 35 / 37	3 / 8 / 27 / 62	9 / 16 / 59 / 16	23 / 23 / 30 / 23	20 / 0 / 60 / 20	$\chi^2_{(6)} = 43.76$, $p < .001$
Male / Female (%)	117 / 62	60 / 40	72 / 28	70 / 30	40 / 60	$\chi^2_{(2)} = 1.95$, $p = .37$
Education	15.3 (2.9)	15.8 (2.8)	15.4 (3.1)	14.8 (2.7)	12.0 (3.0)	$F_{(2,168)} = 2.29$, $p = .11$, $\eta^2 = .03$
Age at PET	73.0 (11.7)	67.0 (9.0)	74.1 (14.9)	78.5 (9.5)	75.2 (14.7)	$F_{(2,171)} = 22.13$, $p < .001$, $\eta^2 = .21$
MMSE at PET	21.3 (7.1)	22.0 (6.8)	19.8 (7.4)	21.4 (7.2)	19.4 (8.0)	$F_{(2,165)} = 1.09$, $p = .34$, $\eta^2 = .01$
CDR at PET	1.1 (0.8)	1.1 (0.8)	1.6 (0.9)	0.8 (0.7)	1.4 (1.4)	$F_{(2,161)} = 9.03$, $p < .001$, $\eta^2 = .10$
PET to death (years)	3.3 (2.1)	3.7 (2.4)	3.8 (2.1)	2.5 (1.5)	2.8 (1.4)	$F_{(2,171)} = 7.54$, $p < .001$, $\eta^2 = .08$
CERAD Score (%) none / spar / mod / freq	23 / 10 / 21 / 46	40 / 8 / 7 / 45	13 / 3 / 9 / 75	12 / 13 / 41 / 35	0 / 40 / 20 / 40	$H_{(2)} = 11.4$, $p = .003$
Thal Phase (%) 0 / 1 / 2 / 3 / 4 / 5	10 / 8 / 12 / 18 17 / 35	27 / 14 / 11 / 9 7 / 32	6 / 3 / 3 /13 13 / 63	0 / 6 / 14 / 28 29 / 23	0 / 0 / 40 / 20 0 / 40	$H_{(2)} = 16.0$, $p < .001$
ApoE (%) ε4 carriers / non-carriers	40 / 60	30 / 70	36 / 64	51 / 49	60 / 40	$\chi^2_{(2)} = 6.7$, $p = .04$

Table 1. Description of study participants.
For continuous variable, mean (standard deviation) are represented. For ordinal and categorical variables, we indicated the percentage of each bin within each sample. Due to the small sample size from AIBL, group comparisons focused on UCSF/UCD, UPitt and Mayo participants; ANOVAs were used for continuous variables, Kruskal-Wallis tests for ordinal variables (CERAD and Thal), and Chi-square for categorical variables (sex, clinical diagnosis, ApoE status).

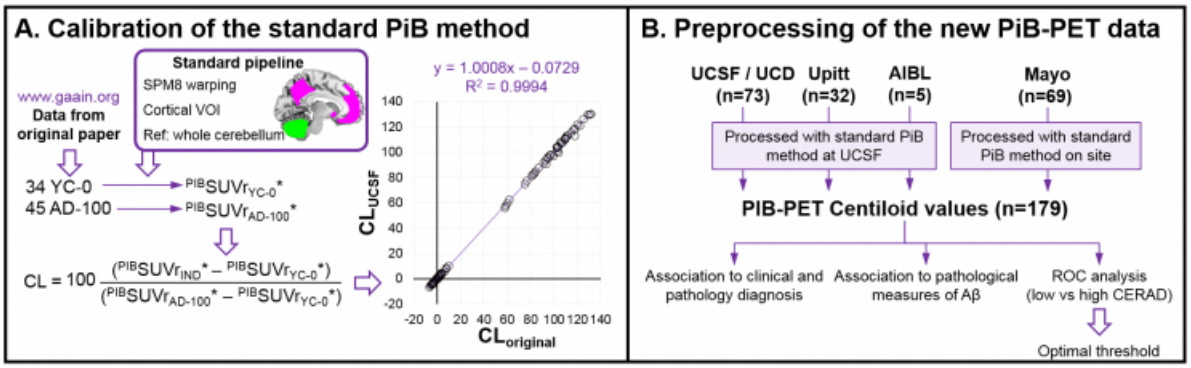

Figure 1. Calibration of the standard centiloid pipeline and outline of present study analyses

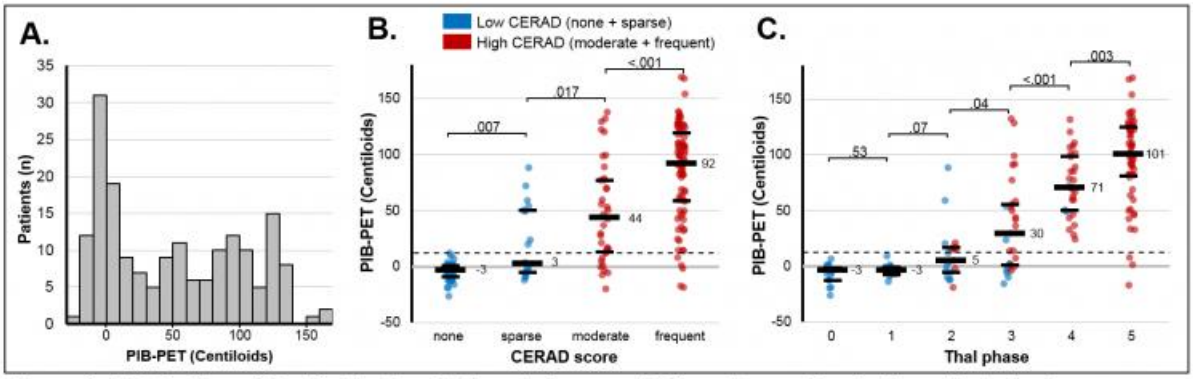

Figure 2. Distribution of Centiloid values in the whole group (left), and according to the pathological measures of β-amyloid pathology (middle and right).
Scatter plots show individual data points, as well as medians (large black line), and 1st and 3rd quartiles (small black lines) within each group; medians values are also indicated. After Kruskall Wallis tests showed significant ($p<.001$) effect of group, pairwise group comparisons were conducted using Mann-Whitney tests; corresponding p-values are shown on the plot. For the sake of clarity, we only showed the output of Mann-Whitney tests between contiguous groups, but all the other contrasts were significant ($p<0.05$). The dotted line indicates the threshold of 12CL identified by the ROC analysis (see text).

Keywords: centiloid, pathology, CERAD, Thal, threshold

[F-18]-AV-1451 binding profile in Chronic Traumatic Encephalopathy: a postmortem case series

Marta Marquié[1,2], Cinthya Aguero[1,2], Michael Siao Tick Chong[1,2], Prianca Ramanan[1,2], Nil Sáez-Calveras[1,2], Eline Verwer[3], Sally Ji Who Kim[3], Rachel Bennett[1,2], Ana Claudia Silva Amaral[1,2], Keith Johnson[1,3], Matthew Frosch[1,4], Victor Alvarez[5], Ann McKee[5], Marc Normandin[3], Teresa Gómez-Isla[1,2]

[1]*Massachusetts Alzheimer's Disease Research Center, Charlestown, MA, US*
[2]*Department of Neurology, Massachusetts General Hospital, Boston, MA, US*
[3]*Department of Radiology, Massachusetts General Hospital, Boston, MA, US*
[4]*Department of Pathology, Massachusetts General Hospital, Boston, MA, US*
[5]*Department of Pathology, Boston University School of Medicine, Boston, MA, US*

Introduction: Chronic traumatic encephalopathy (CTE) is a tauopathy associated to repetitive head trauma. To date, there are no validated in vivo biomarkers of CTE and definite diagnosis can only be done at postmortem. Recent studies have shown that PET tracer AV-1451 (Flortaucipir) exhibits high binding affinity for paired helical filament-tau aggregates in Alzheimer's brains (AD) but relatively low affinity for tau lesions in other tauopathies like FTLD-tau, PSP or CBD. Little is known, however, about the binding profile of this ligand in CTE.

Objective: To study the binding properties of [F-18]-AV-1451 on pathologically confirmed CTE postmortem brain samples.

Methods: We performed [F-18]-AV-1451 phosphor screen and high resolution autoradiography, quantitative tau measurements (immunohistochemistry and Western blotting), and tau seeding activity assays in brain blocks containing hippocampus, superior temporal cortex, superior frontal cortex, inferior parietal cortex and occipital cortex from 5 CTE cases: stage II-III (n=1), stage III (n=3), stage IV (n=1). No substantial concomitant AD pathology, with the exception of moderate diffuse plaques in one case, was detected.

Results: Despite the presence of abundant tau aggregates in multiple regions in all CTE brains, only very faint or no [F-18]-AV-1451 binding signal could be detected by autoradiography. The only exception was the presence of a strong signal confined to the region of the choroid plexus and the cortical surface in 3 cases. Tau immunostaining and Thio-S staining ruled out the presence of tau aggregates in those regions. High resolution nuclear emulsion revealed the presence of extracutaneous leptomeningeal melanocytes as the substrate of that signal (off-target binding). Levels of abnormally hyperphosphorylated tau species, as reported by Western Blot, and tau seeding activity were found to be substantially lower in CTE when compared to AD tissue.

Conclusion: AV-1451 may have limited utility for in vivo selective and reliable detection of tau aggregates in CTE.

Keywords: chronic traumatic encephalopathy, [F-18]-AV-1451, Flortaucipir, tau, PET

Neuropathological and biochemical correlates of tau and amyloid PET imaging in two autopsy brains

Milos Ikonomovic, Eric Abrahamson, Julia Kofler, Julie Price, Carl Becker, Chester Mathis, Oscar Lopez, William Klunk

University of Pittsburgh, Pittsburgh, PA, US

Objectives: Correlation analyses of Tau and beta-amyloid (Aβ) PET with region-matched postmortem Tau and Aβ pathology by quantitative immunohistochemistry and biochemistry.

Methods: [F-18]AV-1451 and [C-11]PiB PET scans were obtained in a 93 y.o. male with probable AD (Case#1) and a 91 y.o. cognitively normal female (Case#2). Atrophy-corrected SUVR values were correlated with postmortem Aβ and Tau or p-Tau measures by histology in the fixed left hemisphere (LH), and by quantitative ELISA in the frozen right hemisphere (RH), across 25 ROIs at the AC-PC axial plane and two additional ROIs in the hippocampus and precuneus.

Results: Neuropathology diagnosis in Case#1 (A2, B3, C2) reflected moderate Aβ and advanced Tau pathology, and in Case#2 (A3, B2, C2) advanced Aβ and minimal neocortical Tau pathology. Both subjects were [C-11]PiB PET positive, with GLB6 values 2.16 (Case#1) and 2.25 (Case#2). The LH histological analyses showed that in both cases, [C-11]PiB correlated with Aβ, but not Tau pathology. [F-18]AV-1451 correlated with Tau pathology (in part driven by the hippocampus ROI) and Aβ pathology in Case#1, but did not correlate with Tau or Aβ pathology in Case#2. In the RH from Case#1, [F-18]AV-1451 correlated with both Tau and Aβ concentration, and [C-11]PiB correlated with Aβ but not Tau concentration. In the RH from Case#2, [F-18]AV-1451 did not correlate with any post mortem ELISA measure, while [C-11]PiB correlated with both Aβ and Tau concentrations.

Conclusions: Correlations were seen between [F-18]AV-1451 PET and postmortem Tau pathology/concentrations in the probable AD case, in part driven by high Tau pathology and [F-18]AV-1451 retention in the hippocampus. Similar correlations were not seen in the cognitively normal control, possibly due to absent neocortical Tau and low Tau in the hippocampus. These results warrant additional studies in cases with moderate/severe neocortical Tau pathology.

We thank Avid Radiopharmaceuticals for providing [F-18]AV-1451 precursor.

Keywords: PET, tau, amyloid, imaging, Alzheimer's

Thursday, January 18, 2018 - 10:15 am - 11:00 am

Poster Session 2A *(2B will repeat at 4:50 pm)*

Board #	Poster Title	Authors	Presenter
THURSDAY, POSTER SESSIONS 2A AND 2B			
79	The relationship between amyloid deposition and both global and hippocampal atrophy	Allison | Berman | Clark | Christian | Betthauser | Oh | Asthana | Bendlin | Johnson	**Allison, Samantha**
69	Relationships between [11C]PiB positivity and an imaging marker of cerebrovascular pathology positivity	Berman | Allison | Christian | Betthauser | Oh | Asthana | Carlsson | Bendlin | Johnson	**Berman, Sara**
54	[18F]MK-6240 autoradiography in AD, PSP, and CBD	Betthauser | Runde | Johnson | Salamat | Roy | Christian	**Betthauser, Tobey**
93	Human testing of non-selective alpha-synuclein PET tracers	Borroni | Honer | Gobbi | Mathis | Klunk | Kotzbauer | Tu | Mach | Mitchell | Marek | Eberling	**Borroni, Edilio**
84	Increased central arterial stiffening relates to CSF markers of tau aggregation and neurodegeneration in the oldest-old	Cambronero | Liu | Moore | Babicz | Hohman | Gifford | Bell | Acosta | Terry | Nair | Wang | Carr | Blennow | Zetterberg | Jefferson	**Cambronero, Francis**
71	Amyloid imaging in hereditary cerebral amyloid angiopathy: detection and progression of pure vascular amyloid caused by APP E693Q	Schultz | Kloet | Sohrabi | Chatterjee | Gardnener | Taddei | Benzinger | Fagan | Sperling | Johnson | Bateman | Gurol | van Buchem | Martins | Chhatwal | Greenberg	**Chhatwal, Jasmeer**
65	[18F]AV-1451 tau PET imaging in MAPT 10+16 mutation carriers	Clarke | Jiao | Dick | Convery | Koriath | Woollacott | Weston | Gunn | Rabiner | Rossor | Warren | Fox | Ourselin | Bocchetta | Rohrer	**Clarke, Mica**
85	Alterations in memory self-appraisal are associated with elevated tau deposition in normal older adults	d'Oleire Uquillas | Schultz | Jacobs | Hanseeuw | Buckley | Pascual-Leone | Sperling | Johnson | Vannini	**d'Oleire Uquillas, Federico**
60	Trajectories of fiber tract impairment in autosomal dominant Alzheimer's disease	Araque Caballero | Benzinger | Suarez-Calvet | Levin | Morris | Bateman | Haass | Ewers	**Ewers, Michael**
76	How useful is amyloid PET in clinical diagnosis? A systematic review and meta-analysis	Fantoni | Chalkidou | O'Brien | Farrar | Hammers	**Farrar, Gill**
87	Increasing Aβ is associated with nonlinear change in BOLD modulation to difficulty in cognitively normal middle-aged and older adults: further evidence from an n-back task	Foster | M. Kennedy | Rodrigue	**Foster, Chris**
61	The BDNF Val66Met SNP is related to hippocampal connectivity and cognitive decline in autosomal dominant Alzheimer's disease	Franzmeier | Ren | Levin | Bateman | Morri | Benzinger | Ewers	**Franzmeier, Nicolai**
62	Tau accumulation and memory decline are more closely related to striatal than cortical amyloidosis in individuals with early-onset autosomal dominant Alzheimer's disease	Hanseeuw | Lopera | Sperling | Norton | Guzman-Velez | Baena | Schultz | Gatchel | Jin | Chen | Reiman | Johnson | Quiroz	**Hanseeuw, Bernard**
55	Imaging-autopsy correlation of 18F-THK5351 in typical and atypical cases of progressive supranuclear palsy	Harada | Ishiki | Kai | Furukawa | Furumoto | Tashiro | Kitamoto | Kudo | Yanai | Arai | Okamura	**Harada, Ryuichi**
58	Confocal analysis of fluorescent signal derived from CN-Flutemetamol-labeled diffuse and neuritic plaques in Alzheimer's disease	Ikonomovic | Buckley | Abrahamson | Mathis | Klunk | Farrar	**Ikonomovic, Milos**
51	Potential use of 18F-THK5351 PET to identify gliosis: Wallerian degeneration of the pyramidal tract after a cerebral infarction	Ishibashi | Kameyama | Tago | Toyohara | Ishii	**Ishibashi, Kenji**
70	[18F]Fluorotaucipir binding in patients with cerebral amyloid angiopathy without hemorrhage and mild cognitive symptoms	Jin | Benson | Schultz | Becker | Charidimou | Fotiadis | Katz | Luner | Moody | Sanchez | Sperling | Xiong | Viswanathan | Johnson	**Jin, David**

Board #	Poster Title	Authors	Presenter
THURSDAY, POSTER SESSIONS 2A AND 2B			
57	Structure and distribution of amyloid beta	Joseph | Sparling | Stys	**Joseph, Jeffrey T**
92	Age-related change of THK-5351 PET in amyloid-negative and non-demented elderly subjects	Kato | Iwata | Kizawa | Fukaya | Kuratsubo | Kimiura | Okamura | Yanai | Ito | Nakamura | Study Group	**Kato, Takashi**
88	Co-existence of deleterious and neuroprotective interaction between amyloid and neuroinflammation in late stage Alzheimer's disease	Knight | Kang | Parent | Pascoal | Mathotaarachchi | Therriault | Benedet | Camoun | Aliaga | Zimmer | Shin | Aliaga | Kostikov | Soucy | Gauthier | Cuello | Rosa-Neto	**Knight, Ashley**
80	AV1451-PET measurements show substantial overlap across diagnostic groups and amyloid status	Landau | Korman | Jagust	**Landau, Susan**
63	Tau pathology in Down syndrome	Lemoine | Bharani | Hamlett | Perez | Mufson | Poon | Simic | Nordberg | Granholm	**Lemoine, Laetitia**
68	CYP2C19 effects in brain amyloid load and hippocampus' functional integrity	Lessa Benedet | Iturria-Medina | Savard | Kang | Mathotaarachchi | A. Pascoal | Therriault | Shin | Gauthier | C. Evans | Labbe | Rosa-Neto	**Lessa Benedet, Andrea**
64	Singular Value Decomposition (SVD) identification of PiB and FDG topographies in Dominantly Inherited Alzheimer's Network (DIAN)	Loe | Brier | McCarthy | Stern | Kuffner | Morris | Bateman | Benzinger | Ances	**Loe, Maren**
81	Shrinking cortex and tau burden in the aphasic variant of Alzheimer's disease	Martersteck | Sridhar | Rainford | Mesulam | Rogalski	**Martersteck, Adam**
86	Segregation of tau deposits across clinical stages provides the basis for pathophysiological staging in AD	Mathotaarachchi | A. Pascoal | L. Benedet | Shin | Kang | Struyfs | Therriault | Chamoun | Ng | Savard | Knight | Gauthier | Rosa-Neto	**Mathotaa-rachchi, Sulantha**
59	Comparison of Down syndrome PiB PET templates for MRI-less PET quantification	Minhas | Laymon | Tudorascu | Lao | Campbell | Yu | Lopresti | Mathis | Klunk | Handen | Christian | Cohen	**Minhas, Davneet**
75	In pre-clinical AD, subjective cognitive decline is associated with brain hyperactivation in conflict monitoring/control regions	Mizuno | Karim | Rangarajan | Klunk | Aizenstein | Snitz	**Mizuno, Akiko**
90	18F-AV-1451 uptake on tau PET differs between dementia with Lewy bodies and posterior cortical atrophy	Nedelska | Josephs | Graff-radford | Przybelski | Lesnick | Boeve | Lowe | Drubach | Knopman | Petersen | Jack, Jr. | Whitwell | Kantarci	**Nedelska, Zuzana**
78	Quantifying stages of subtle memory impairment in clinically normal older adults	Papp | Mormino | Grober | Sperling | Johnson | Rentz	**Papp, Kate**
89	Amyloid and tau deposition determine cognitive impairment through epigenetic changes in individuals across the AD spectrum	Pascoal | Shin | Kang | Ng | Benedet | Mathotaarachchi | Therriault | Chamoun | Massarweh | Knight | Soucy | Gauthier | Rosa-Neto	**Pascoal, Tharick**
74	Amyloid network topology characterizes the progression of Alzheimer’s disease during the pre-dementia stages	Pereira | Strandberg | Palmqvist | Volpe | van Westen | Westman | Hansson	**Pereira, Joana**
73	Flortaucipir PET imaging and neuropsychological performances dissociate dorsal and ventral stream dysfunction in Posterior Cortical Atrophy	Putcha | Collins | Wong | Dickerson | McGinnis	**Putcha, Deepti**
72	Midlife insulin resistance and APOE genotype are associated with late-life brain amyloid accumulation	Rinne | Ekblad | Johansson | Helin | Viitanen | Laine | Puukka | Jula	**Rinne, Juha**
91	Finding ground zero: identifying the medial temporal origin of tau deposition during life	Sanchez | Augustinack | Becker | Jacobs | Jin | Katz | Luner | Moody | Rentz | Sperling | Price | Johnson	**Sanchez, Justin**
66	Longitudinal change of functional connectivity in the DIAN cohort: functional connectivity as a longitudinal biomarker in autosomal dominant AD	Schultz | Sperling | Buckley | Johnson | Benzinger | Ances | Morris | Buckles | Xiong | McDade | Cairns | Marcus | Fulbright | Jack | Ringman | Farlow | Kinnunen | Fox | Masters | Schofield | Salloway | Levin | Bateman | Chhatwal	**Schultz, Aaron**
50	Quantitative thresholding of [18F]Florbetapir brain uptake using Thal phases of Abeta deposition relate to clinical stages of disease	Seneca | Burger | Florea	**Seneca, Nicholas**

Board #	Poster Title	Authors	Presenter
THURSDAY, POSTER SESSIONS 2A AND 2B			
83	Cognition and [18F]-Florbetaben PET imaging of amyloid in Parkinson's disease	Stark | Melzer | Keenan | Myall | Kaur | Livingston | Horne | Marsh | Grenfell | Young | MacAskill | Dalrymple-Alford | Anderson	**Stark, Megan**
52	Preclinical evaluation of 18F-THK5351 off-target binding to melanin-containing cells	Tago | Toyohara | Harada | Furumoto | Okamura | Kudo | Takahashi-Fujigasaki | Murayama | Ishii	**Tago, Tetsuro**
53	To tau or to MAO-B? Most of the 18F-THK5351 signal is blocked by selegiline	Villemagne | Doré | Okamura | Baxendale | Harada | Mulligan | Furumoto | Salvado | Yanai | Masters | Rowe	**Villemagne, Victor**
82	Cross-sectional associations between tau pathology burden measured by [18F]GTP1 PET imaging and cognition in AD adjusting for amyloid PET and cortical atrophy	Ward | Manser | Teng | Sanabria-Bohorquez | Ray | Baker | Kerchner | Weimer	**Ward, Michael**
77	[18F]AV-1451 binds to an unidentified white matter target in semantic dementia	Whitwell | Martin | Schwarz | Duffy | Clark | Machulda | Botha | Graff-Radford | Jones | Utianski | Knopman | Petersen | Lowe | Jack | Josephs	**Whitwell, Jennifer**
67	An UNC5C locus is associated with susceptibility to cognitive decline and hippocampal neurodegeneration in clinically normal older adults	Yang | Chhatwal | Papp | Rabin | Hanseeuw | Mormino | Buckley | Schultz | Properzi | Hedden | Marshall | Rentz | Johnson | De Jager | Sperling	**Yang, Hyun-Sik**
56	Relationship of basal ganglia mineralization to "off-target" AV-1451 binding in Down syndrome	Zammit | Laymon | Minhas | Tudorescu | Lopresti | Mathis | Sabbagh | Zaman | Klunk | Handen | Christian | Cohen	**Zammit, Matthew**

P50: Quantitative thresholding of [18F]Florbetapir brain uptake using Thal phases of Abeta deposition relate to clinical stages of disease

Nicholas Seneca[1,2], Cyrill Burger[2], Ioana Florea[2]

[1]*Novartis Institutes for Biomedical Research (NIBR), Basel, Switzerland*
[2]*PMOD Technologies LLC., Zurich, Switzerland*

In vivo imaging of Aβ deposits using PET has allowed extrapolation of neuropathological assessments in living brain. However, the majority of imaging studies have used a cortical composite region of interest which focuses primarily on brain regions associated with Thal phase one of Aβ deposition [1]. Thus, the aim of our study was to measure Aβ deposits in brain regions associated with Thal phases and determine the relationship to clinical stages of disease. A total of 675 subjects from ADNI were included in the analysis. Pre-processed [^{18}F]Florbetapir baseline imaging studies and a reference region of white matter were used to calculate SUVr. A modified Hammers brain template was merged to reflect the brain regions associated with thal phases of Aβ deposition. A linear mixed effect model was applied between Thal phases, subjects and their interactions. Furthermore, a conditional inference tree was used to classify the imaging data into terminal nodes represented by groups of subjects. Patients with AD and MCI 'converters' had higher brain uptake in brain regions associated with Thal phases one to three compared to aged controls and MCI 'reverters'. Greater than 90% of all patients with AD and MCI 'converters' could be assigned using quantitative thresholds from Thal phases 1 to 5 (Figure 1).

In this study, patients with the highest Aβ deposition in brain were more clearly classified using these quantitative thresholds of [^{18}F]Florbetapir brain uptake in brain regions associated with all Thal phases of Aβ deposition besides phase four.

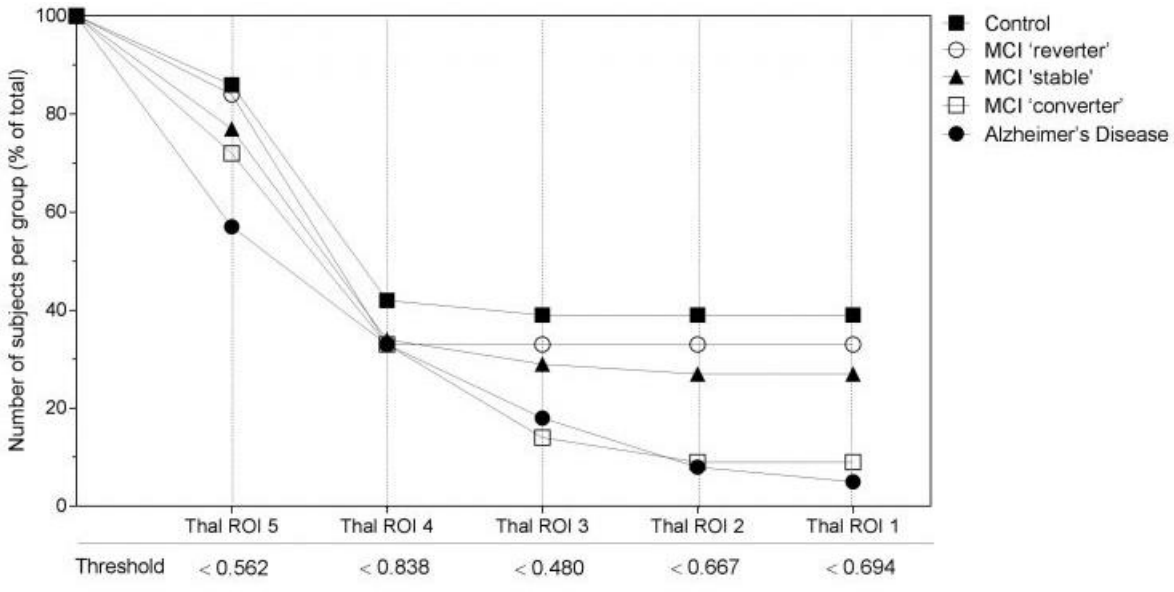

Figure 1. Results from conditional inference tree classifying the number of subjects per group (% of total) by using thresholds from brain uptakeof [^{18}F]Florbetapir in patients with Alzheimer's disease. More than 40% of patients with AD were identified including brain regions associated with Thal phase five. Furthermore, up to 95% of all AD patients were further identified with the inclusion of additional Thal brain regions in phase one to three.

Reference

1. Thal, D.R., et al., *Phases of A beta-deposition in the human brain and its relevance for the development of AD.* Neurology, 2002. **58**(12): p. 1791-800.

Keywords: Positron emission tomography; Thal phases; [18F]Florbetapir; Alzheimer's Disease; Aβ deposits

P51: Potential use of 18F-THK5351 PET to identify gliosis: Wallerian degeneration of the pyramidal tract after a cerebral infarction

Kenji Ishibashi[1], Masashi Kameyama[2], Tetsuro Tago[1], Jun Toyohara[1], Kenji Ishii[1]

[1]Research Team for Neuroimaging, Tokyo Metropolitan Institute of Gerontology, Tokyo, Japan
[2]Department of Nuclear medicine, Tokyo Metropolitan Geriatric Hospital, Tokyo, Japan

Background and aim: The radioligand, ^{18}F-THK5351, was initially developed to target tau aggregation present in neurofibrillary tangles[1]. However, ^{18}F-THK5351 was recently reported to bind to monoamine oxidase B (MAO-B) with a certain level of affinity[2, 3]. MAO-B is highly concentrated in astrocytes. MAO-B concentration increases during so-called "gliosis", which is a spectrum of changes in astrocytes that occur after brain injury. This suggests that ^{18}F-THK5351 concentrates in the lesion where gliosis occurs. We now present a case showing the potential use of ^{18}F-THK5351 PET to identify gliosis.

Case report: A 41-year-old man underwent ^{18}F-THK5351 PET two years after a right middle cerebral artery infarction. ^{18}F-THK5351 PET imaging revealed intense radioligand uptake along the ipsilateral pyramidal tract from the corona radiata to the medulla (Figure 1, arrows).

Discussion and conclusion: Wallerian degeneration of the pyramidal tract usually develops after a cerebral infarction including primary motor cortex. In the early stage, axonal swelling and breakdown of myelin sheath occur. In the later stage, the degenerated axons are replaced by gliosis, which is primarily the proliferation of astrocytes to form a scar. Hence, in this case, ^{18}F-THK5351 uptake may represent Wallerian degeneration of the ipsilateral pyramidal tract accompanied with gliosis by targeting MAO-B located in the lesions.

References

1. Tago T, et al. Structure-Activity Relationship of 2-Arylquinolines as PET Imaging Tracers for Tau Pathology in Alzheimer Disease. J Nucl Med. 2016.
2. Ng KP, et al. Monoamine oxidase B inhibitor, selegiline, reduces 18F-THK5351 uptake in the human brain. Alzheimer's research & therapy. 2017.
3. Harada R, et al. Correlations of 18F-THK5351 PET with post-mortem burden of tau and astrogliosis in Alzheimer's disease. J Nucl Med. 2017.

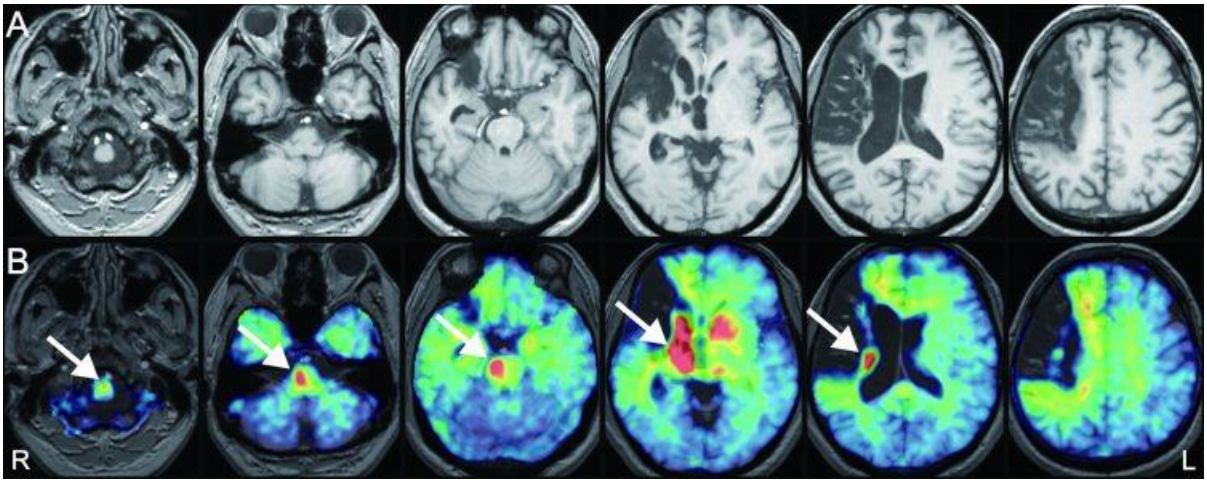

Figure 1
(A) MRI, (B) 18F-THK5351 images superimposed on MRI

Keywords: 18F-THK5351,Wallerian degeneration, pyramidal tract, cerebral infarction, gliosis

P52: Preclinical evaluation of 18F-THK5351 off-target binding to melanin-containing cells

Tetsuro Tago[1], Jun Toyohara[1], Ryuichi Harada[2], Shozo Furumoto[3], Nobuyuki Okamura[4], Yukitsuka Kudo[5], Junko Takahashi-Fujigasaki[6], Shigeo Murayama[6], Kenji Ishii[1]

[1]*Research Team for Neuroimaging, Tokyo Metropolitan Institute of Gerontology, Tokyo, Japan*
[2]*Department of Pharmacology, Tohoku University Graduate School of Medicine, Sendai, Japan*
[3]*Cyclotron and Radioisotope Center, Tohoku University, Sendai, Japan*
[4]*Division of Pharmacology, Tohoku Medical and Pharmaceutical University, Sendai, Japan*
[5]*Institute of Development, Aging and Cancer, Tohoku University, Sendai, Japan*
[6]*Department of Neuropathology, Tokyo Metropolitan Institute of Gerontology, Tokyo, Japan*

Objectives: "Off-target" binding of tau PET ligands is often observed in regions with melanin-containing cells (MCCs). In this study, several assays using ^{18}F-THK5351 as a representative positive control were performed to clarify the mechanism of off-target binding to MCCs.

Methods: Postmortem sections of the human midbrain and pons were used for ^{18}F-THK5351 autoradiography (ARG). Under small animal PET with C57BL/6 and B6 albino mice, ^{18}F-THK5351 binding in retinal pigment epithelium was assessed. Binding assays with ^{18}F-THK5351 were conducted using B16F10 murine melanoma cells and synthetic melanin pigment. Blocking activities of about two dozen compounds (e.g., tau ligands, amyloid ligands, monoamine oxidase B inhibitors, and tyrosinase inhibitors) against ^{18}F-THK5351 binding to B16F10 cells were determined for a structure-activity relationship study.

Results: ARG demonstrated ^{18}F-THK5351 specific binding in the substantia nigra and locus coeruleus. Accumulation of ^{18}F-THK5351 in the eyes was observed only in C57BL/6 mice (Fig. 1). Saturable binding was seen for ^{18}F-THK5351 to melanoma cells (K_{dHi} = 0.16 ± 0.09 μM, B_{maxHi} = 111 ± 51 pmol/mg protein), and ^{18}F-THK5351 binding was dose-dependently blocked by unlabeled THK5351, AV-1451, PBB3, and the lead compound of MK-6240 (Fig. 2, K_i = 0.22 ± 0.06 μM, 0.32 ± 0.25 μM, 1.41 ± 0.80 μM, and 1.57 ± 0.28 μM, respectively). Specific binding of ^{18}F-THK5351 to synthetic melanin was also confirmed. This structure-activity relationship study indicated that aromatic rings of compounds are important for the pi-stacking interaction with melanin structure. In addition, a certain aminopyridine group seemed to enhance the melanin-binding affinity of compounds.

Conclusion: Tau PET ligands appear to bind directly to melanin pigment in MCCs. These results will help accurate interpretation of PET images and facilitate future development of tau and α-synuclein ligands without off-target binding to melanin.

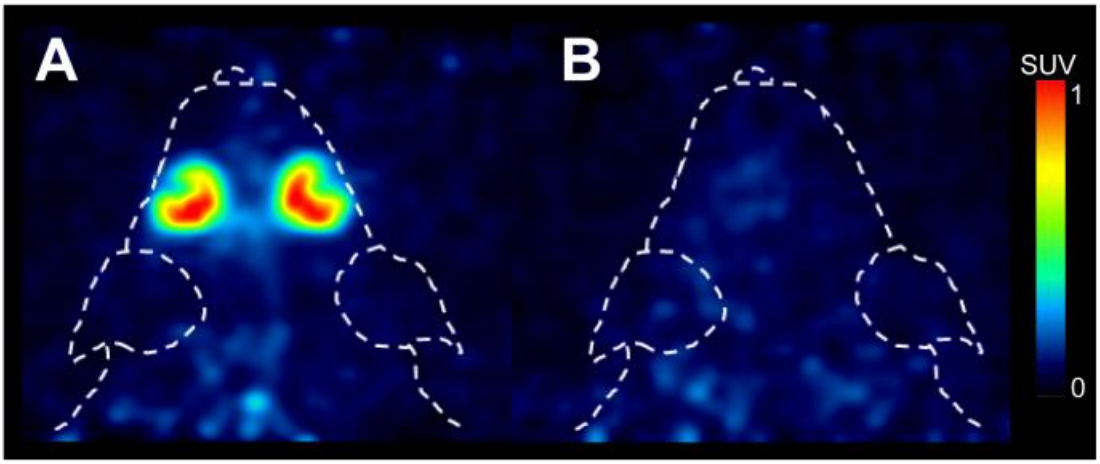

Figure 1. Images from ^{18}F-THK5351 PET of the heads of C57BL/6 (A) and B6 albino (B) mice.

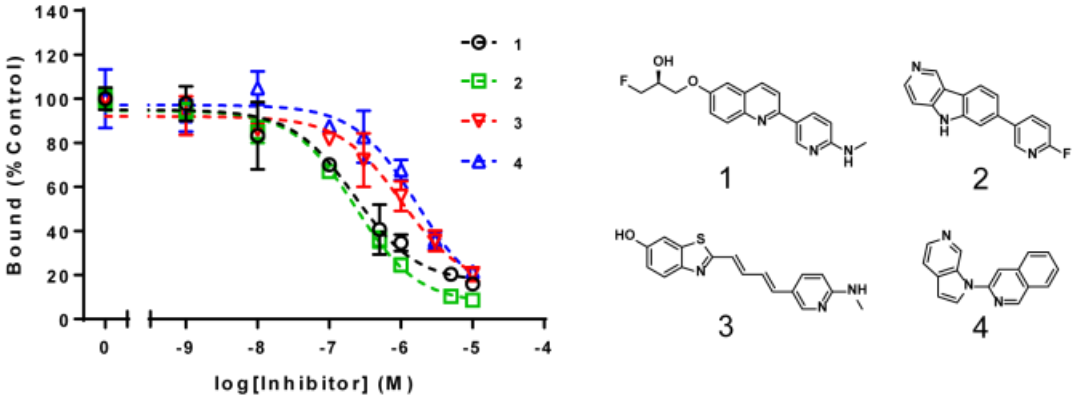

Figure 2. Competitive binding curves of compounds against ^{18}F-THK5351 binding to B16F10 cells.

Keywords: THK5351, tau, off-target binding, melanin

P53: To tau or to MAO-B? Most of the 18F-THK5351 signal is blocked by selegiline

Victor L Villemagne[1,2], Vincent Doré[1,3], Nobuyuki Okamura[4], David Baxendale[1], Ryuichi Harada[4], Rachel Mulligan[1], Shozo Furumoto[4], Olivier Salvado[3], Kazuhiko Yanai[4], Colin L Masters[2], Christopher C Rowe[1,2]

[1]Department of Molecular Imaging & Therapy, Austin Health, Melbourne, Australia
[2]The Florey Institute of Neuroscience and Mental Health, The University of Melbourne, Melbourne, Melbourne, Australia
[3]CSIRO e-Health Research Centre, Brisbane, Australia
[4]Department of Pharmacology, Tohoku University, Sendai, Japan

Background: It has been reported that ^{18}F-THK5351 binding in the brain of 5 mild cognitive impairment (MCI), two Alzheimer's disease (AD), and 1 PSP subjects, was reduced by ~36% in the cortex and by ~50% in the basal ganglia 1-hr after a single 10-mg oral dose of the monoamine oxidase B (MAO-B) inhibitor selegiline (Ng et al. AR&T, 2017). To explore if selegeline reduced ^{18}F-THK5351 signal in the absence of tau, we investigated the degree of signal reduction after a 5-day regimen of oral selegiline not only in AD patients, but also in non-AD dementia (nADD) and age-matched healthy controls (HC).

Methods: Ten participants (3 AD, 1 MCI, 4 HC and 2 nADD), underwent a ^{18}F-NAV4694 PET scan to ascertain Aβ-amyloidosis, a baseline ^{18}F-THK5351 scan, and a second ^{18}F-THK5351 scan after a 5-day of a 10-mg/d oral regimen of selegiline. Regional and global standardized uptake values (SUV), were generated for both NAV and THK studies.

Results: After the 5-day regimen of selegiline, the regional SUV were significantly reduced by 82% in the basal ganglia, by 72% in the mesial temporal cortex and by 65% in neocortical regions (Figure 1). Despite being the area with the lowest ^{18}F-THK5351 signal reduction, 55% of the cerebellar signal was reduced by selegiline. Interestingly, the same degree of regional signal reduction was observed in AD and HC participants.

Conclusions: Our results indicate that ~85% of the ^{18}F-THK5351 signal in the basal ganglia and 60-75% of the ^{18}F-THK5351 signal in cortical regions is reduced by selegiline. The fact that the same degree of signal reduction was observed in AD and HC participants, strongly suggests that the majority of ^{18}F-THK5351 retention is not due to binding to tau deposits. These findings clearly indicate ^{18}F-THK5351 should not be used to quantify tau deposits in the brain.

Figure 1. Effect of selegiline on regional ^{18}F-THK5351 retention
After a 5-day regimen of selegiline, the regional SUV were significantly reduced by 82% in the basal ganglia (striatum and thalamus), by 72% in the mesial temporal cortex and by 65% in neocortical regions.

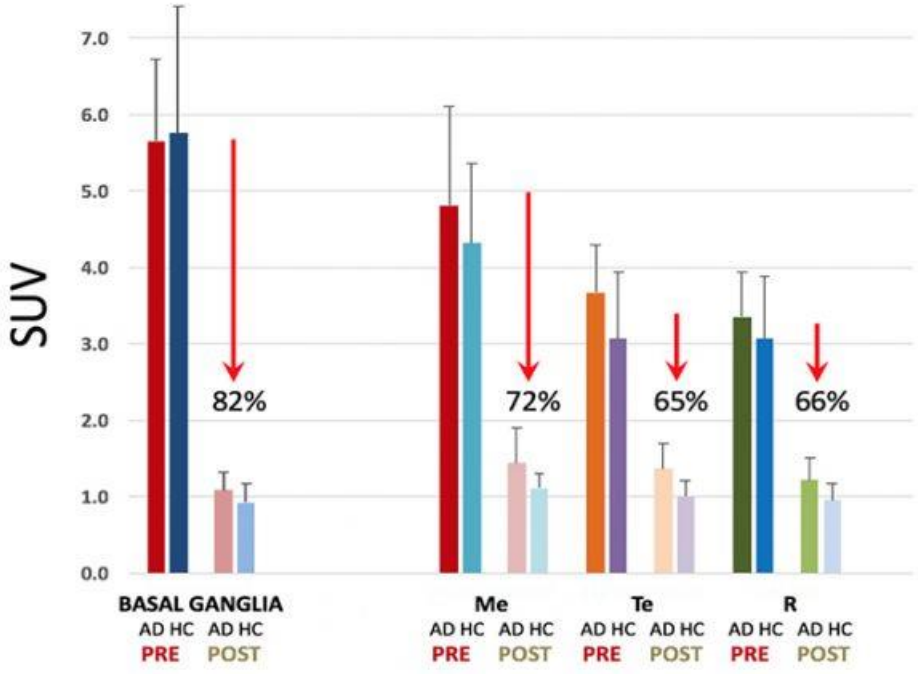

Abbreviations: ***AD****: Alzheimer's disease patients;* ***HC****: Healthy elderly controls;* ***Me*** *(Mesial-temporal) comprising entorhinal cortex, hippocampus, parahippocampus and amygdala;* ***Te*** *(Temporoparietal) comprising inferior and middle temporal, fusiform, supramarginal and angular gyri, orbitofrontal cortex, gyrus rectus, posterior cingulate/precuneus, superior and inferior parietal, and lateral occipital; and* ***R*** *(Rest of neocortex) comprising dorsolateral & ventrolateral prefrontal, superior temporal, and anterior cingulate.*

Keywords: Tau imaging, Alzheimer's disease, Positron emission tomography

P54: [18F]MK-6240 autoradiography in AD, PSP, and CBD

Tobey Betthauser, Rosie Runde, Sterling Johnson, M Shahriar Salamat, Subhojit Roy, Bradley Christian

University of Wisconsin-Madison School of Medicine and Public Health, Madison, WI, US

Objectives: This work investigates in vitro binding of [^{18}F]MK-6240 in AD, PSP, and CBD tauopathies using immunohistopathology and autoradiography.

Methods: Paraffin fixed tissue slices (8 μm) were selected from AD (x2, high and low Braak), PSP (x1), and CBD (x1) neuropathology confirmed cases. Slices from various brain regions (entorhinal and frontal cortex for AD; pons, medulla, and frontal cortex for PSP and CBD) were stained with AT-8, counter stained with 3,3'-diaminobenzidine (DAB), and images were acquired at x1 magnification. [^{18}F]MK-6240 (21±7 mCi/nmol) autoradiography was performed in adjacent slices with and without 600nM MK-6240 self-blocking. A high Braak AD control case was used to confirm labeling and blocking. Slices were equilibrated in 10x PBS for at least 30 min, incubated in labeling (0.3±0.1 nM [^{18}F]MK-6240) or blocking solution for one hour, rinsed with 50/50 EtOH/10x PBS for 2 min followed by 10x PBS for 2 min, air dried and exposed to a phosphor screen for one hour. After development, [^{18}F]MK-6240 autoradiographic images were compared to AT-8/DAB stains.

Results: Tau specific binding was observed in AD cases, including a case with low tau density (figure 1) confirmed with AT-8. Minimal specific binding was observed for PSP and CBD cases, with the exception of the frontal cortex in PSP, which showed a slight laminar pattern of reversible [^{18}F]MK-6240 binding that co-localized with AT-8 immunostaining.

Conclusions: Work is ongoing to perform anti-3R and anti-4R immunostaining in adjacent slices, and to perform autoradiography and immunostaining in fresh frozen tissues of PSP and CBD cases along with other non-AD tauopathies (e.g. CTE, TBI, Pick's Disease).

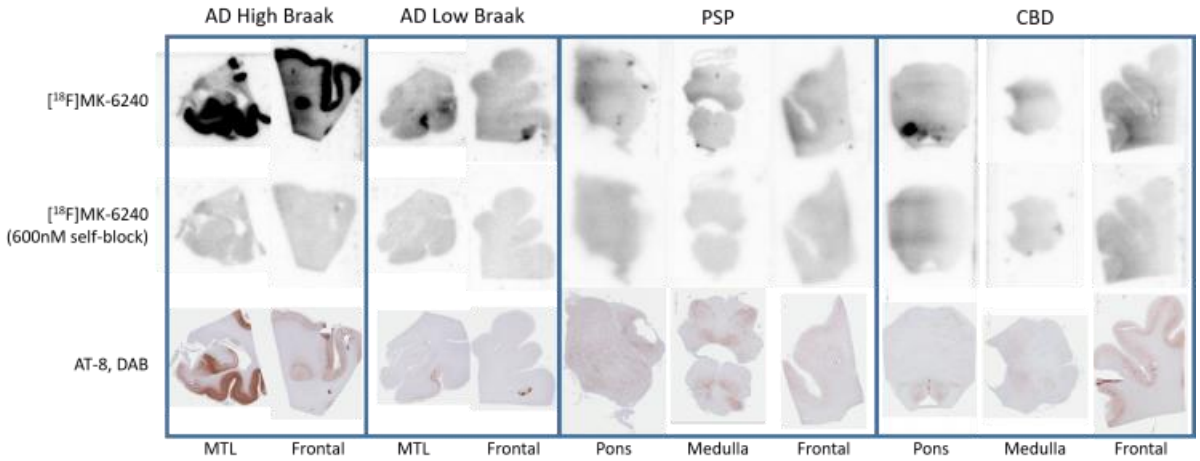

Keywords: MK-6240, tau, autoradiography

P55: Imaging-autopsy correlation of 18F-THK5351 in typical and atypical cases of progressive supranuclear palsy

Ryuichi Harada[1,2], Aiko Ishiki[2], Hideaki Kai[3], Katsutoshi Furukawa[2,5], Shozo Furumoto[4], Manabu Tashiro[4], Tetsuyuki Kitamoto[3], Yukitsuka Kudo[2], Kazuhiko Yanai[1,4], Hiroyuki Arai[2], Nobuyuki Okamura[4,5]

[1]*Department of Pharmacology, Tohoku University School of Medicine, Sendai, Japan*
[2]*Institute of Development, Aging and Cancer, Tohoku University, Sendai, Japan*
[3]*Department of Neurological Science, Tohoku University School of Medicine, S, Japan*
[4]*Cyclotron and Radioisotope Center, Tohoku University, S, Japan*
[5]*Tohoku Medical and Pharmaceutical University, Se, Japan*

Objectives: Previous studies have shown that ^{18}F-THK5351 PET detects monoamine oxidase B (MAO-B) with high affinity. The aim of study was to validate ^{18}F-THK5351 PET signal in autopsy-confirmed cases of typical and atypical progressive supranuclear palsy (PSP).

Methods: We performed postmortem examination of brain samples from two autopsy-confirmed PSP cases who underwent ^{18}F-THK5351 PET before death. Case 1 and 2 were clinically diagnosed as Richardson syndrome and progressive non-fluent aphasia, respectively. *In vitro* autoradiography of ^{3}H-THK5351 was performed using frozen brain sections. We quantitatively measured tau pathology and GFAP in autopsy brain sections and examined the correlation between tau, astrogliosis and ^{18}F-THK5351 retention.

Results: Both PSP cases were amyloid-negative, while significant ^{18}F-THK5351 retention was observed in the globus pallidus and midbrain. In case 2, who was clinically diagnosed as progressive non-fluent aphasia, additional ^{18}F-THK5351 retention was observed in the temporal cortex. In *in vitro* autoradiography, the specific THK5351 binding was detected in the area of antemortem ^{18}F-THK5351 retention, and these binding was completely displaced by MAO-B inhibitor lazabemide. Regional ^{18}F-THK5351 SUVR in ante-mortem PET image was significantly correlated with the density of astrogliosis as well as tau pathology at postmortem examination.

Conclusions: ^{18}F-THK5351 PET signals in PSP reflect reactive astrogliosis after tau accumulation.

Keywords: Tau, non-AD, progressive supranuclear palsy, imaging-autopsy

P56: Relationship of basal ganglia mineralization to "off-target" AV-1451 binding in Down syndrome

Matthew Zammit[1], Charles Laymon[2], Davneet Minhas[2], Dana Tudorescu[2], Brian Lopresti[2], Chester Mathis[2], Marwan Sabbagh[3], Shahid Zaman[4], William Klunk[2], Benjamin Handen[2], Bradley Christian[1], Ann Cohen[2]

[1]*University of Wisconsin-Madison School of Medicine, Madison, WI, US*
[2]*University of Pittsburgh School of Medicine, Pittsburgh, PA, US*
[3]*Barrow Neurological Institute, Phoenix, AZ, US*
[4]*University of Cambridge, Cambridge, United Kingdom*

[F-18]AV-1451 PET is the most widely used method to measure pathologic tau deposits associated with the pathophysiology of Alzheimer's disease (AD). It has been demonstrated that binding of [F-18]AV-1451 in the basal ganglia (BG) is likely "off-target", as it is observed in healthy elderly and is age related. Several groups have now suggested that mineralization within the BG is associated with [F-18]AV-1451. Further, mineralization within the BG has been reported pathologically in Down syndrome (DS).

Objective: To assess the relationship of [F-18]AV-1451 binding to mineralization within the basal ganglia.

Methods: 22 participants with DS (mean age 41.9 years) underwent [F-18]AV-1451 PET and MRI (including FLAIR and SWI sequences). [F-18]AV-1451 80-100 min summed images were created and warped to a common space via FreeSurfer, an ROI was created in the region of BG most commonly associated with mineralization. Images were converted to SUVR by normalization to FreeSurfer cerebellar gray matter. MRI FLAIR and SWI images were rated for mineralization using a 4-point rating scale (Penke et al., 2012) and the relationship between mineralization rating and [F-18]AV-1451 SUVR in the BG was explored using Spearman correlations.

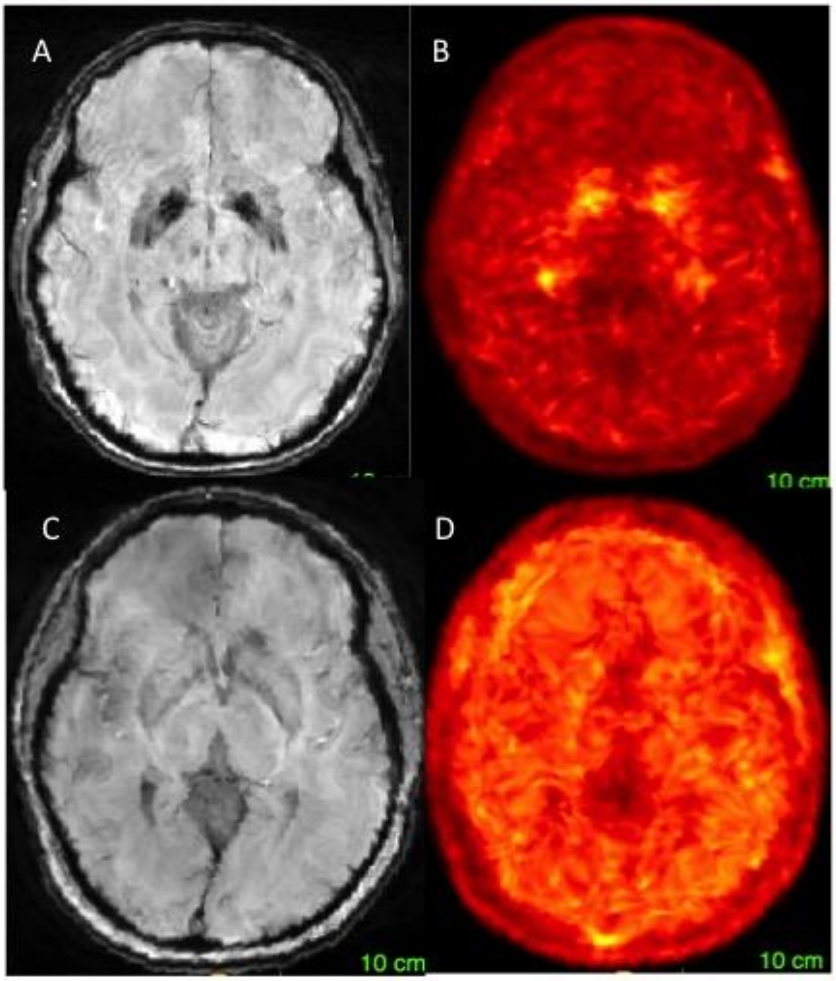

Results: A significant relationship was observed between [F-18]AV-1451 uptake in BG and mineralization rating ($r=0.75$, $p<0.0001$). A significant relationship was also observed between [F-18]AV-1451 in BG and age, as well as, between mineralization and age. Figure 1 demonstrates [F-18]AV-1451 uptake in a DS participant with significant mineralization (A-B) and without significant mineralization (C-D).

Discussion: Participants with DS demonstrate significant age and mineralization related "off-target" binding of [F-18]AV-1451. Ongoing studies, will explore this relationship in other regions of significant mineralization, including midbrain regions. These data suggest that due to the early appearance of mineralization in DS, this may be an ideal cohort to study "off-target" binding of [F-18]AV-1451 in the basal ganglia.

Keywords: AV-1451, tau, down syndrome

P57: Structure and distribution of amyloid beta

Jeffrey T Joseph, Joseph Sparling, Peter K Stys

University of Calgary, Calgary, AB, Canada

Introduction: Amyloid beta (Abeta) is a major constituent of amyloid plaques and is required for diagnosis of Alzheimer disease (AD). However, its accumulation in cortex is heterogeneous and it accumulates outside the cortex in regions that do not undergo degeneration in AD.

Methods: Examine the deposition of Abeta in cortical layers and basal ganglia, and contrast that with tau deposition. Examine the structure of amyloid in plaques with fluorescent amyloid imaging and fluorescent emission spectroscopy using conformation-sensitive amyloid probes.

Results: Unlike neocortex, Abeta deposition is minimal in the hippocampus in early stages of Alzheimer disease (AD) and only in later stages becomes deposited in Ammon's horn (CA) (fig. 1).

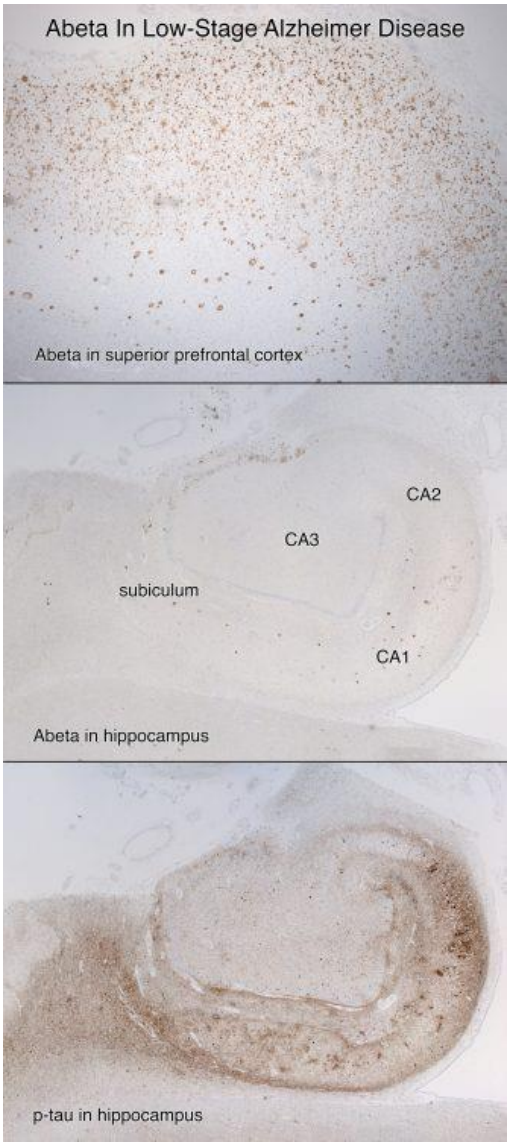

Its distribution changes in different cortical layers, with mostly diffuse amyloid plaques in granular layers and neuritic amyloid plaques with phosphorylated tau-positive (p-tau) neurites in layer 3 and 5-6. This contrasts with Lewy body disease, which can have abundant diffuse plaques without forming neuritic plaques. In the caudate nucleus in AD, deposition of both Abeta in diffuse plaques and p-tau can be extensive; however, these deposits are not associated with neuritic amyloid plaques (fig. 2).

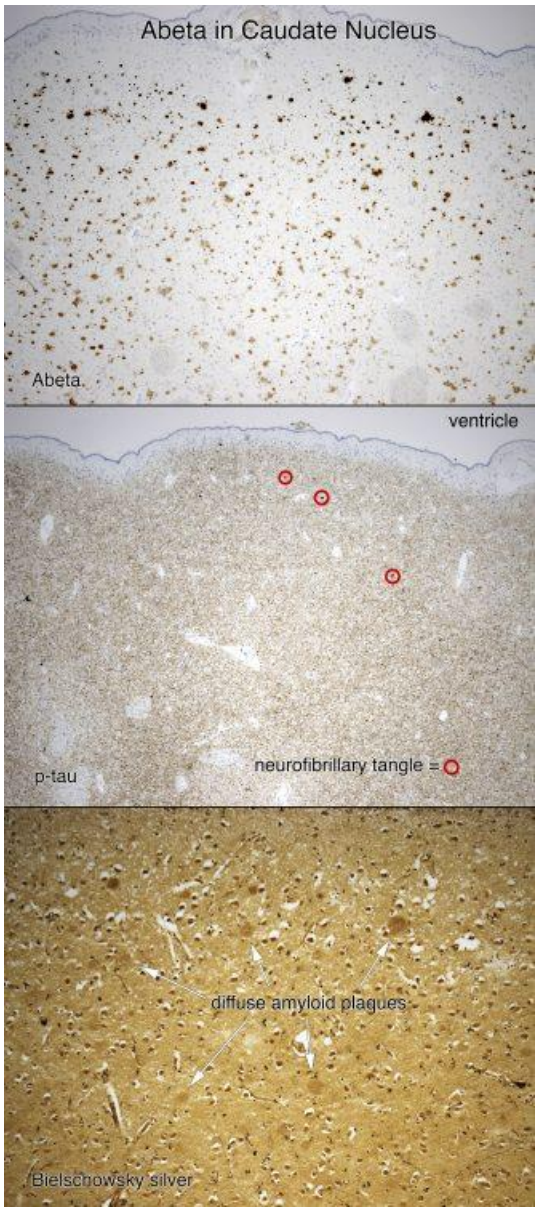

Fluorescent imaging and fluorescent emission spectroscopy of amyloid plaques in AD demonstrates that the amyloid core is structurally distinct from the amyloid rim in neuritic amyloid plaques (fig. 3).

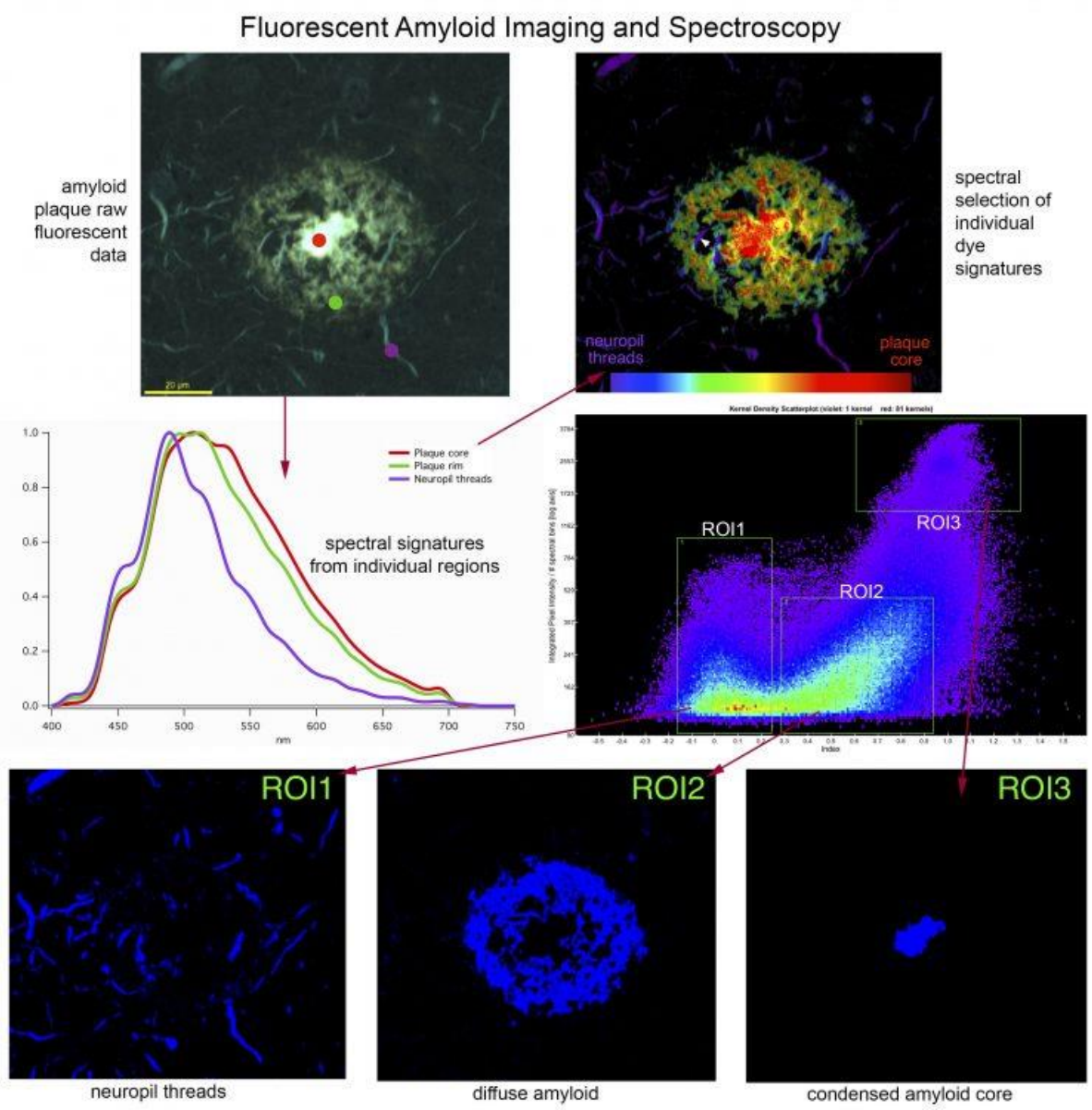

Conclusions:

1. Abeta deposition is frequently present in cognitively normal elderly individuals, in Lewy body disease, and is required in AD.

2. Abeta deposition occurs in the hippocampus only in later stages of AD.

3. The morphology of amyloid plaques changes in different cortical layers.

4. The conformation of amyloid beta within neuritic amyloid plaques is different in the periphery versus the compact central core.

5. Abeta deposition occurs in the basal ganglia in AD and can co-occur with abundant p-tau but does not form neuritic amyloid plaques.

Keywords: amyloid beta, conformation, Alzheimer's disease

P58: Confocal analysis of fluorescent signal derived from CN-Flutemetamol-labeled diffuse and neuritic plaques in Alzheimer's disease

Milos Ikonomovic[1], Christopher Buckley[2], Eric Abrahamson[5], Chester Mathis[4], William Klunk[3], Gill Farrar[2]

[1]*ADRC, University of Pittsburgh, Pittsburgh, PA, US*
[2]*GE Healthcare Life Sciences, Amersham, United Kingdom*
[3]*Department of Psychiatry, University of Pittsburgh, Pittsburgh, PA, US*
[4]*Department of Radiology, University of Pittsburgh, Pittsburgh, PA, US*
[5]*ADRC, University of Pittsburgh, Pittsburgh, PA, US*

Background: Specificity and sensitivity of Flutemetamol (Vizamyl) PET are high for detecting neuritic amyloid-beta plaques (NP). Somel false-positive results from the Flutemetamol clinical-pathological study, and high Flutemetamol retention in AD striatum, indicate that this radiotracer detects both NP and diffuse plaques (DP). Flutemetamol fluorescent derivative CN-Flutemetamol labels most morphological plaque types, with the amyloid core of NP exhibiting the brightest fluorescence. The current histopathology study uses Flutemetamol derivative CN-Flutemetamol to explore quantitatively Flutemetamol fluorescence in NP and DP.

Methods: 160 microns thick frontal cortex tissue sections from a typical AD case were processed using CN-Flutemetamol (1 µM) and analyzed imaged using a DSU spinning disk confocal microscope. This procedure allowed confocal image stacks to be taken throughout the entire volume of NP. Similar stack volumes were acquired through DP.

Results: On average, amyloid cores of NP comprised <75% of total NP volume, but had fluorescent intensity density measurements an order of magnitude larger than fluorescent density measurements in the surrounding corona of NP and in the entire DP (Figure 1).

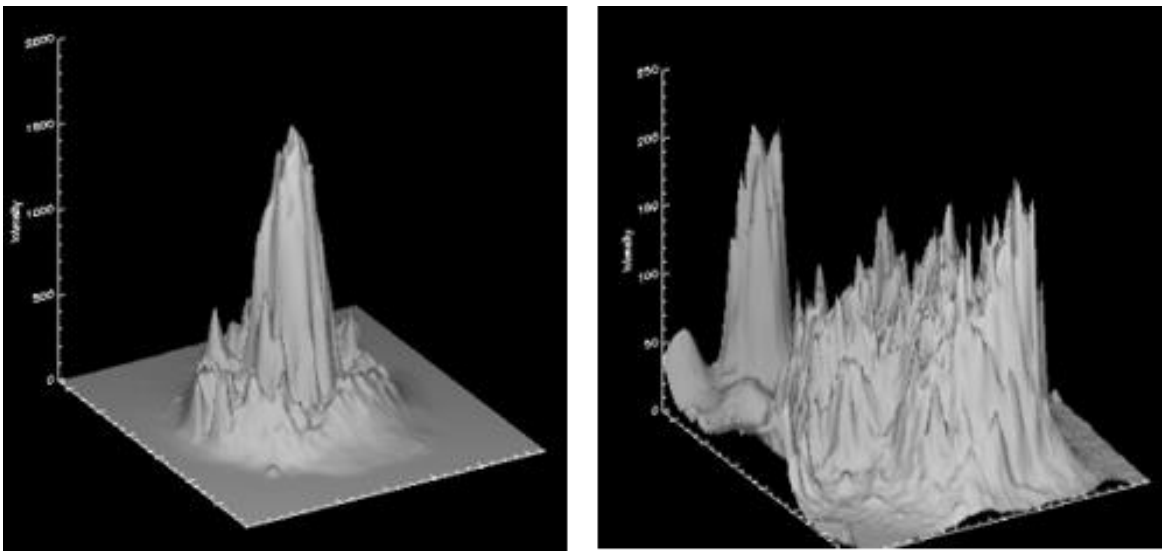

Figure 1. Surface plots illustrating CN-Flute intensity density measurements from a plane through the center of a cored NP (left) and a DP (right).

Discussion: The contribution of cored NP and DP to Flutemetamol retention in vivo likely depends on the size and density of individual plaques; in areas of mixed pathology large swaths of diffuse plaques could yield Flutemetamol retention levels comparable to those detected in the much smaller volumes of amyloid core in NP. In the caudate, the exceptionally high density of DP, as well as differences in striatal vasculature and white matter tracts (compared to neocortex) could be responsible for the high retention observed in this region in AD.

Keywords: Flutemetamol

P59: Comparison of Down syndrome PiB PET templates for MRI-less PET quantification

Davneet Minhas[1], Charles Laymon[1], Dana Tudorascu[2], Patrick Lao[4], Elizabeth Campbell[1], Zheming Yu[1], Brian Lopresti[1], Chester Mathis[1], William Klunk[3], Benjamin Handen[3], Bradley Christian[4], Ann Cohen[3]

[1]*Department of Radiology, University of Pittsburgh, Pittsburgh, PA, US*
[2]*Department of Medicine, University of Pittsburgh, Pittsburgh, PA, US*
[3]*Department of Psychiatry, University of Pittsburgh, Pittsburgh, PA, US*
[4]*Department of Medical Physics, University of Wisconsin, Madison, WI, US*

Background: Amyloid-beta accumulation in Down syndrome (DS) is an ongoing area of investigation. However, many factors including atypical DS brain morphology and motion artifacts can confound MRI-based techniques.

Objective: To develop and assess DS-population [^{11}C]PiB PET templates for accurate regional quantification in the absence of MRI.

Methods: [^{11}C]PiB and T1 MRI images were acquired in 80 DS subjects. MRIs were processed using FreeSurfer, and parcellations were visually inspected and manually edited where appropriate. Nine subjects failed parcellation and were excluded.

Global SUVR was assessed using a composite cortical grey matter (GM) FreeSurfer region and cerebellar GM as reference. Subjects were classified as [^{11}C]PiB-positive (PiB+) or [^{11}C]PiB-negative (PiB-) using a cutoff of 1.35.

MRIs were segmented and non-linearly registered via DARTEL (SPM12) to generate a DS-specific tissue probability template. Subject-specific DARTEL flow fields were applied to native-space FreeSurfer parcellations and [^{11}C]PiB images, to generate an average DS-specific FreeSurfer atlas and two [^{11}C]PiB templates: (1) an average template of all [^{11}C]PiB images (T_{DS}), and (2) an adaptive template (T_A) where: $T_A = w*T_{pos} + (1-w)*T_{neg}$; T_{pos} = average PiB+ image; T_{neg} = average PiB- image; and w = subject-specific weight (0-1), optimized during subject-to-template registration (Bourgeat et al., 2015).

[^{11}C]PiB images were non-linearly registered to both templates independently using stereotactic normalization (SPM12). Global SUVRs were assessed using the DS-specific FreeSurfer atlas and correlated to native-space MRI-based FreeSurfer SUVRs.

Results: Of 71 subjects, 13 were PiB+ and 58 PiB-. Intraclass correlation coefficients relative to MRI-based FreeSurfer SUVRs were 0.88 (95% CI: 0.82,0.93) for the average template and 0.96 (95% CI: 0.94,0.98) for the adaptive template.

Discussion: Due to the greater number of PiB- subjects, the average template T_{DS} was biased towards PiB- and underestimated SUVR. The adaptive template T_A outperformed the average template T_{DS} with some bias still present. Thus, additional non-linear registration and template methods should be explored.

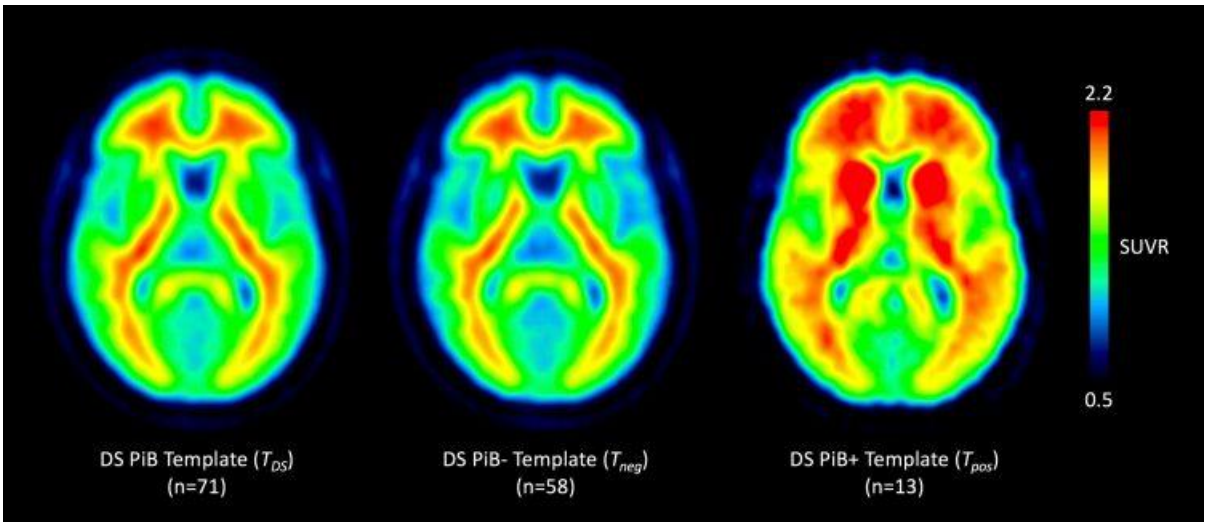

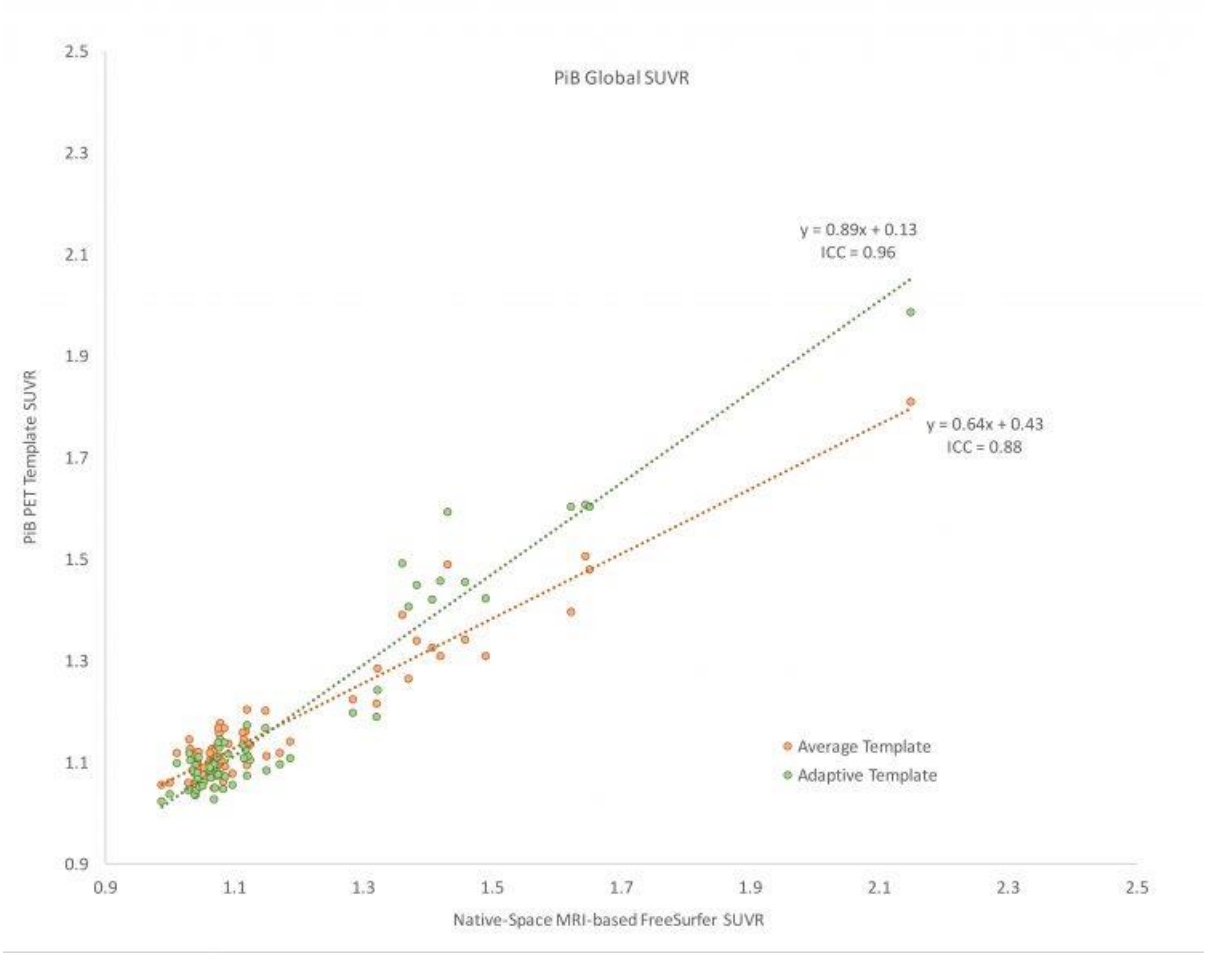

Keywords: PiB, PET, Down syndrome, template

P60: Trajectories of fiber tract impairment in autosomal dominant Alzheimer's disease

Miguel Araque Caballero[1], Tammie Benzinger[3], Marc Suarez-Calvet[2], Johannes Levin[2], John Morris[3], Randall Bateman[3], Christian Haass[2], Michael Ewers[1]

[1]*Institute for Stroke and Dementia Research (ISD), University Hospital LMU, Munich, Germany*
[2]*German Center for Neurodegenerative Diseases, Munich, Germany*
[3]*Department of Radiology, Washington University in St Louis, St. Louis, MI, US*

Background: White matter changes can be considered the "unsung hero" in Alzheimer's disease (AD), they are frequent but have not yet been adopted within common biomarker models of the pathological cascade in AD. Yet, fiber tract changes are associated with the decline of functional networks and cognition in AD. The objective of the current cross-sectional study in autosomal dominant AD (ADAD) was to assess the trajectories of fiber tract impairment as a function of estimated years from symptom onset (EYO).

Methods: DTI scans were obtained for 59 mutation carriers (MC) and 44 non-carriers (NC) from the Autosomal Dominant Alzheimer's Network (DIAN). The DTI scans were preprocessed, spatially normalized and skeletonized, using the Tract-Based Spatial Statistics (TBSS) toolbox of FSL. WMH segmentation was based on FLAIR images. John-Hopkins-Fiber-Tract-Atlas ROIs were superimposed onto the white matter skeleton for extraction of ROI-based mean diffusivity. In voxel-based and ROI-based non-parametric regression analyses, the interaction effect of mutation status (MC vs NC) x EYO onto mean diffusivity (MD) was tested ($p = 0.05$, family-wise error corrected).

Results: In the MC group, TBSS analysis revealed a significantly faster increase of MD primarily within the medial-frontal and posterior-parietal white matter. At the fiber tract level, MD of the forceps major and forceps minor were first elevated in MC at EYO [-10 to -5], followed at EYO [-5 to zero] by abnormalities in the superior-longitudinal fasciculus, inferior-fronto-occipital fasciculus, and anterior-thalamic radiation. These fiber tract alterations were observed within and outside WMH, and followed abnormal PIB-PET (EYO: -20 to -10) and CSF tau (EYO: -20 to -15), but co-occurred with grey matter (hippocampus) atrophy. Lower CSF Aß, higher CSF tau and CSF sTREM2 were associated with higher MD in MC.

Conclusion: Long-ranging fiber tracts connecting posterior parietal brain and midline brain regions are the first to be impaired a decade before dementia onset.

Keywords: DTI, fiber tract, vascular, autosomal dominant Alzheimer's disease, DIAN

P61: The BDNF Val66Met SNP is related to hippocampal connectivity and cognitive decline in autosomal dominant Alzheimer's disease

Nicolai Franzmeier[1], Jinyi Ren[1], Johannes Levin[2,3], Randall Bateman[4,5,6], John C Morri[4,5,6], Tammie Benzinger[4,5], Michael Ewers[1]

[1]*Institute for Stroke and Dementia Research, Ludwig Maximilians University, Munich, Germany*
[2]*German Center for Neurodegenerative Diseases, Munich, Germany*
[3]*Department of Neurology, Ludwig Maximilians University, Munich, Germany*
[4]*Department of Radiology, Washington University, St. Louis, MO, US*
[5]*Knight Alzheimer's Disease Research Center, Washington University, St. Louis, MO, US*
[6]*Hope Center for Neurological Disorders, Washington University, St. Louis, MO, US*

Background: The protein Brain derived neurotrophic factor (BDNF) is involved in neural plasticity and neurogenesis. The single nucleotide polymorphism (SNP) Val66MET in the gene encoding BDNF ($BDNF_{Val66Met}$) has been associated with worse hippocampal atrophy and episodic memory impairment in Alzheimer's disease (AD). However, whether the $BDNF_{Val66Me}$ is associated with altered functional networks, particularly those underlying memory in AD, is unclear.

Methods: We included 115 mutation carriers (MC) with autosomal dominant AD (ADAD) and 91 control non-carriers (NC) from the DIAN study. For each subject, we assessed seed-based resting-state connectivity of the left & right hippocampus (Hipp-L/Hipp-R). First, in order to test the $BDNF_{Val66Met}$ SNP effect on hippocampus connectivity in ADAD, we assessed in voxel-wise regression analysis the interaction $BDNF_{Val66Met}$ x estimated years from symptom onset (EYO) on Hipp-L/Hipp-R connectivity maps. The analyses were controlled for gender, education, and Hipp-L/Hipp-R grey matter volume. Next, cluster maps of significant $BDNF_{Val66Met}$ x EYO interaction were binarized and mean hippocampus connectivity within the cluster map was extracted. Lastly, we tested whether the mean hippocampus connectivity within the cluster maps was associated with delayed recall and MMSE.

Results: In MC but not NC, we found a significant interaction $BDNF_{Val66Met}$ x EYO on Hipp-R connectivity to a large cluster in the bilateral mediofrontal cortex (Figure 1A), where $BDNF_{Met}$-carriers exhibited a stronger decrease in connectivity compared to $BDNF_{Val}$-carriers (Figure 1B). In MC but not NC lower Hipp-R to mediofrontal connectivity was associated with lower memory ($p<0.05$, Figure 1C) and MMSE scores ($p<0.001$) with closer proximity to symptom onset (i.e. interaction EYO x Hipp-R connectivity).

Conclusions: In ADAD, $BDNF_{Met}$-carriage is associated with stronger hippocampal connectivity disruptions, which is associated with more severe cognitive impairment.

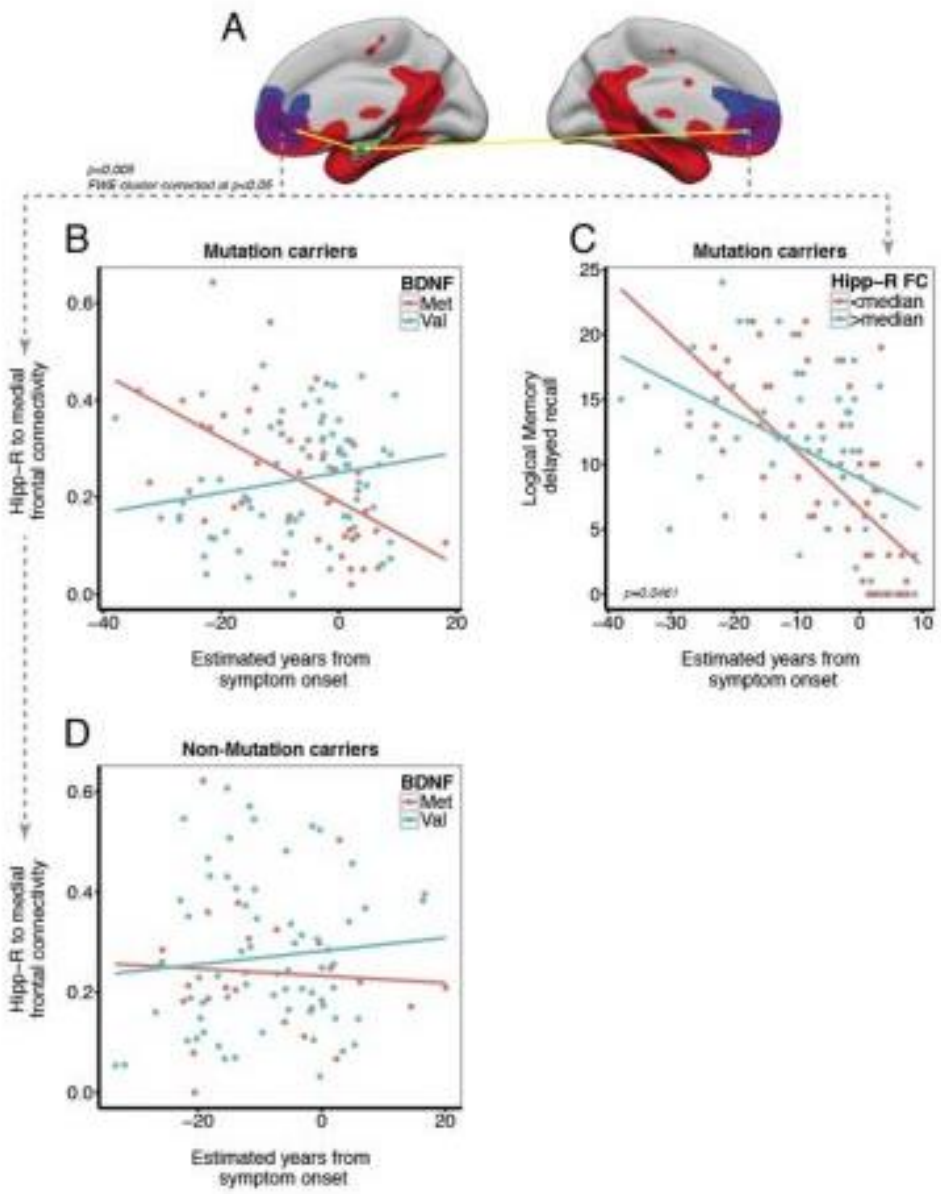

Figure 1: (A) Results of the voxel-wise interaction $BDNF_{Val66Met}$ x estimated years from symptom onset (EYO) on Hipp-R connectivity (see cyan ROI). Areas showing significant Hipp-R connectivity are displayed in red, the cluster showing a significant $BDNF_{Val66Met}$ intetraction is displayed in blue/purple. (B) Scatterplot illustrating the directionality of the voxel-wise interaction. (C) Significant interaction between Hipp-R connectivity and EYO on logical memory delayed recall. (D) Normal course of Hipp-R connectivity to the mediofrontal cortex for non-mutation carriers.

Keywords: BDNF, autosomal dominant Alzheimer's disease, Memory

P62: Tau accumulation and memory decline are more closely related to striatal than cortical amyloidosis in individuals with early-onset autosomal dominant Alzheimer's disease

Bernard Hanseeuw[1,2], Francisco Lopera[3], Reisa Sperling[1], Daniel Norton[1], Edmarie Guzman-Velez[1], Ana Baena[1], Aaron Schultz[1], Jennifer Gatchel[1], David Jin[1], Kewei Chen[4], Eric Reiman[4], Keith Johnson[1], Yakeel Quiroz[1]

[1]*Massachusetts General Hospital, Boston, MA, US*
[2]*Cliniques Universitaires Saint-Luc, Brussels, Belgium*
[3]*University of Antioquia, Medellin, Colombia*
[4]*Banner Alzheimer's Institute, Phoenix, AZ, US*

Background: To determine whether striatal amyloidosis can help predict disease progression in individuals at genetic risk for AD, we sought to examine the tau accumulation relationship with cortical and striatal amyloid, and with memory performance in non-demented individuals with autosomal dominant Alzheimer's disease (ADAD).

Methods: Twenty-five (13 carriers, 12 non-carriers, age range=28-55) non-demented individuals from the Colombian kindred (PSEN1 E280A mutation) were evaluated using PiB-PET, Flortaucipir-PET (FTP; tau), and memory testing (CERAD Word List Learning). PiB was measured in Freesurfer-defined neocortical and striatal (caudate/putamen) aggregates. FTP was measured in entorhinal and inferior temporal cortices.

Results: Fig.1: Compared to non-carriers, mutation carriers had an age-related increase in cortical (0.025±0.004 DVR/year, p<0.0001) and striatal (0.042±0.007 DVR/year, p<0.0001) PiB binding. The annual rate of PiB accumulation was marginally greater in striatum than cortex (0.017±0.009 DVR/year, p=0.06). FTP binding increased with age (entorhinal: 0.043±0.011 SUVr/year, p=0.0007; inferior temporal: 0.015±0.007 SUVr/year, p=0.04) and memory scores decreased with age (-0.38±0.09 items/year, p=0.0004).

Fig.2: In mutation carriers, PiB was associated with FTP binding in entorhinal (cortex: R^2=0.39, p=0.02; striatum: R^2=0.67, p=0.0007) and inferior temporal (cortex: R^2=0.34, p=0.04; striatum: R^2=0.47, p=0.01), and with worse memory (cortex: R^2=0.39, p=0.02; striatum: R^2=0.71, p=0.0003).

Fig.3: The difference between striatal and cortical PiB was associated with FTP binding in entorhinal (R^2=0.37, p=0.03) and inferior temporal (R^2=0.21, p=0.11), and with worse memory (R^2=0.41, p=0.02). These associations survived age-adjustment (entorhinal FTP: partial-R^2=0.26, p=0.09, memory: partial-R^2=0.35, p=0.04). Only striatal PiB was significant when both PiB regions competed to predict entorhinal FTP (cortex: +0.1±0.5SUVr/DVR, p=0.8; striatum: +0.9±0.3SUVr/DVR, p=0.017) or memory (cortex: -0.5±4.1 items/DVR, p=0.9; striatum: -8.6±2.6 items/DVR, p=0.009).

Conclusions: These findings suggest that striatal amyloid in preclinical ADAD may be more predictive of progression to dementia than cortical amyloid. This study provides insight into the role of striatal amyloid in the progression of AD, and informs the pre-symptomatic treatment trials targeting amyloid in this population.

Fig.1 Cortical and striatal PiB (amyloid), entorhinal FTP (tau), and memory scores as a function of age, in mutation carriers (red) and non-carriers (blue)

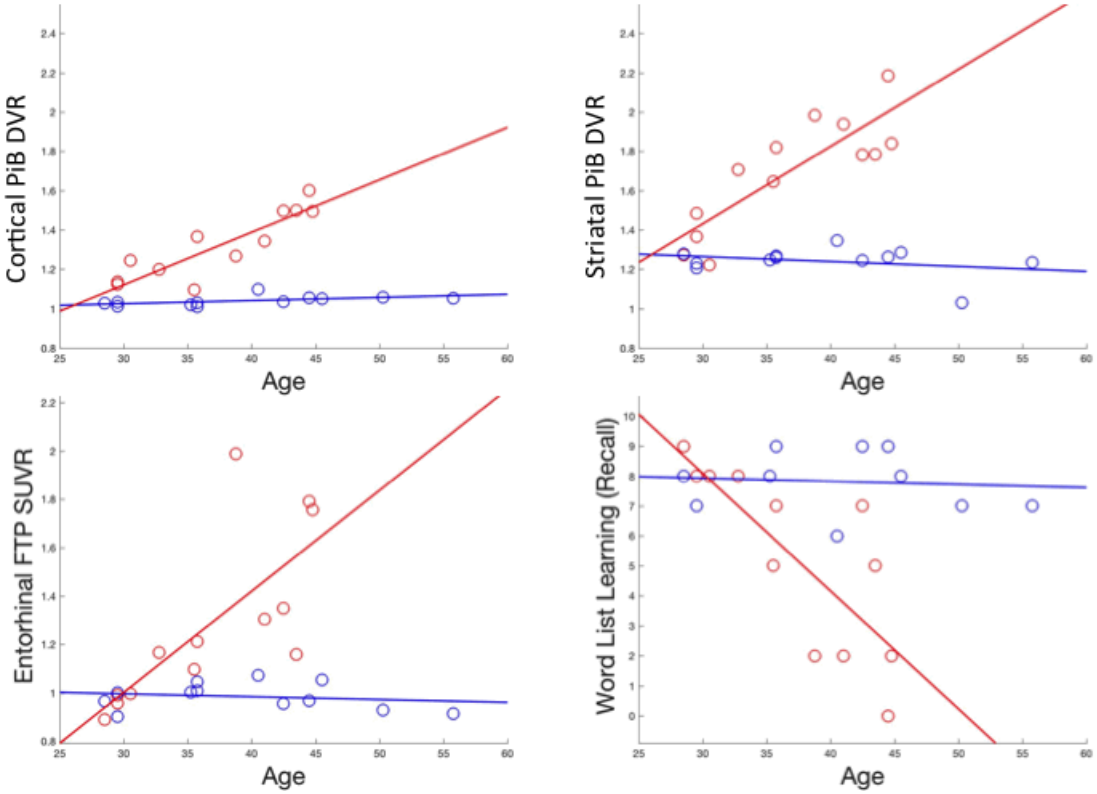

Fig.2. Associations between regional PiB measures, entorhinal FTP, and memory scores

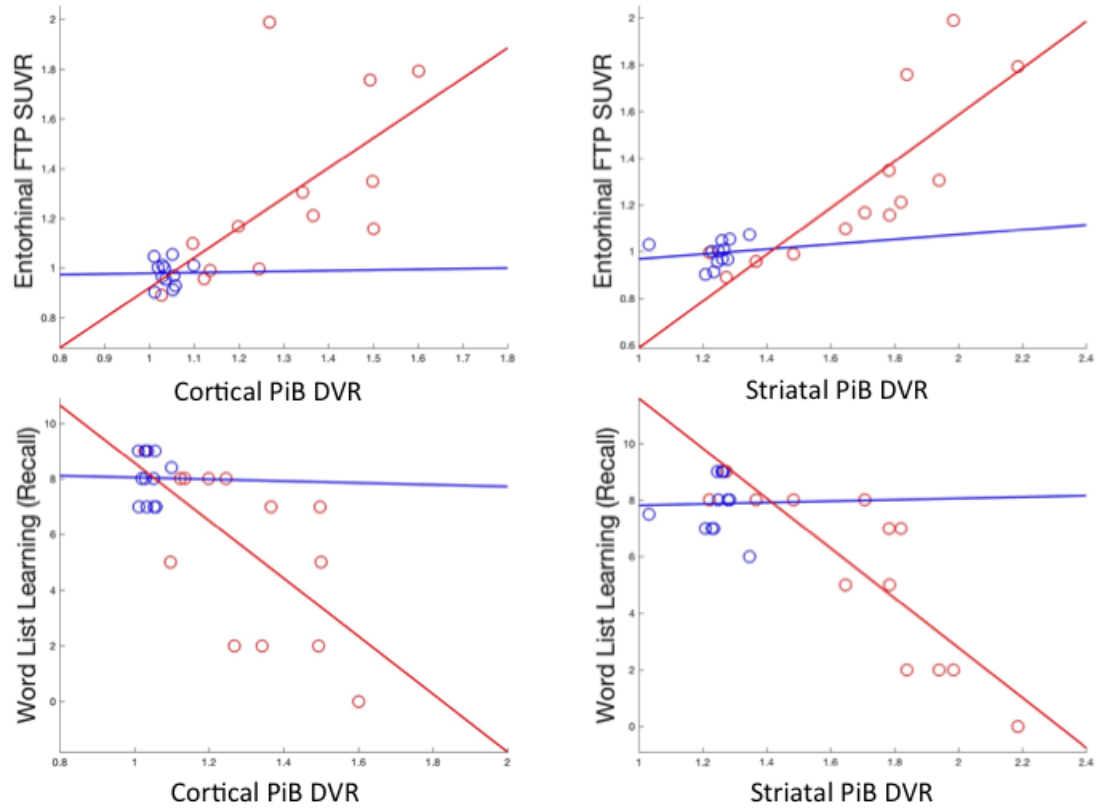

Fig.3. The difference between striatal and cortical PiB binding is associated with increase in entorhinal FTP binding and decrease in memory performance

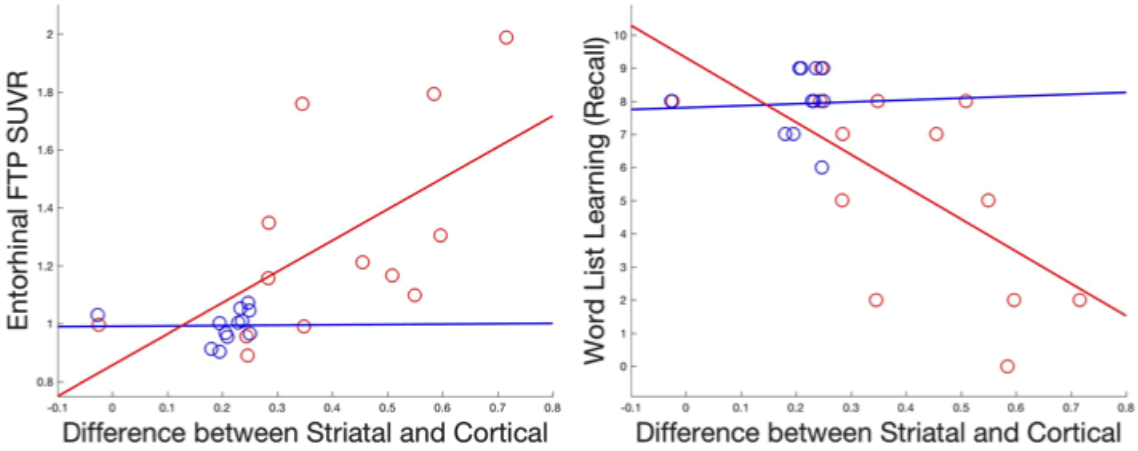

Keywords: Autosomal Dominant Alzheimer's Disease, Tau-PET imaging, PiB-PET imaging, striatum, memory

P63: Tau pathology in Down syndrome

Laetitia Lemoine[1], Krishna Bharani[2,3], Eric Hamlett[2,3], Sylvia Perez[4], Elliott Mufson[4], Wayne W. Poon[5], Goran Simic[6], Agneta Nordberg[1,7], Ann-Charlotte Granholm[2,3]

[1]*Department of Neurobiology, Care Sciences, and Society, Center for Alzheimer Research, Division of Translational Alzheimer Neurobiology, Karolinska Institutet, Stockholm, Sweden*
[2]*Knoebel Institute for Healthy Aging and the Department of Biological Sciences, University of Denver, Denver, CO, US*
[3]*Medical University of South Carolina, Charleston, SC, US*
[4]*Barrow Neurological Institute, Department of Neurobiology, Phoenix, AZ, US*
[5]*Institute for Memory Impairments and Neurological Disorders, University of California, Irvine, CA, US*
[6]*Department of Neuroscience, Croatian Institute for Brain Research, School of Medicine, University of Zagreb, Zagreb, Croatia*
[7]*Theme Aging, Karolinska University Hospital, Huddinge, Sweden*

Background: Down syndrome (DS) patients are at high-risk to develop Alzheimer's disease (AD) with an onset around 35 years of age, in part due to the presence of the triplication of chromosome 21 where the *APP* gene is located. Evaluation of autopsy cases revealed that at 35 years of age DS subjects display similar pathology to AD including amyloid plaques and tau containing neurofibrillary tangles (Hartley *et al.*, 2015). A recent study of exosomes purified from blood revealed increased levels of tau and amyloid-β (Aβ) in DS children as young as 8 years of age (Hamlett *et al.*, 2017). Moreover, abnormal tau phosphorylation has been observed in fetal tissue from DS (Milenkovic *et al.*, 2017). Our aim was to evaluate tau and amyloid deposition in fetal as well as adult DS postmortem cases in comparison to sporadic AD and healthy controls using both ^{3}H-THK5117 and ^{3}H-PIB autoradiography, in comparison with AT8 tau and Amylo-Glo fluorescent staining, respectively.

Methods: Autoradiography using ^{3}H-THK5117 and ^{3}H-PIB was performed on paraffin embedded hippocampal, temporal and frontal cortex sections from 3 fetal and 5 adult DS cases, 3 sporadic AD and 2 controls. Immunostaining using AT8 and Amylo-Glo staining was performed on adjacent sections.

Results: Both fetal and adult DS cases displayed ^{3}H-THK5117 and ^{3}H-PIB binding. ^{3}H-THK5117 binding was higher in adult DS cases in comparison to sporadic AD cases. ^{3}H-PIB binding was lower compared to ^{3}H-THK5117 in all adult cases. AT8 and Amylo-Glo staining corresponded, respectively to ^{3}H-THK5117 and ^{3}H-PIB binding, both in adult DS and AD cases.

Conclusion: In this study, we observed early and significant tau binding in DS cases. This study will allow new insights into tau pathology and could facilitate the understanding of neurofibrillary pathology in both DS cases as well as sporadic AD.

Keywords: Down syndrome, Autoradiography, THK5117, AT8, PIB

P64: Singular Value Decomposition (SVD) identification of PiB and FDG topographies in Dominantly Inherited Alzheimer's Network (DIAN)

Maren Loe, Matthew Brier, John McCarthy, Ari Stern, Todd Kuffner, John Morris, Randall Bateman, Tammie Benzinger, Beau Ances

Washington University in Saint Louis, Saint Louis, MO, US

Introduction: Amyloid deposition and hypometabolism are characteristic of Alzheimer's Disease (AD). Spatial and temporal patterns of pathological changes have previously been proposed with amyloid deposition and hypometabolic changes not independent processes. We explored the relationship of these biomarkers in DIAN, both cross-sectionally and longitudinally.

Methods: Amyloid PET (PiB) and glucose metabolism (FDG) were obtained from 308 DIAN participants (187 mutation positive (M+), 121 mutation negative (M-)). 152 participants (97 M+, 52 M-) had ≥ 2 scans. PiB and FDG were preprocessed using previously described methods. Analyses were conducted using SVD. This linear algebra technique, similar to principal component analysis, investigated the underling structure by estimating highly dimensional data sets as linear combinations of a set of components, or topographies. An ANOVA examined the effects of mutation status (M+ vs. M-) and estimated years to onset (EYO) on topographies.

Results: To reduce the dimensionality of our data set, SVD was performed for the cross-sectional and longitudinal cohorts separately. A total of three PiB and two FDG topographies (**Figure 1**) were identified. Using receiver operator curve (ROC) analyses the first and second PIB topographies were significantly more represented in the M+ compared to M- participants at 10-20 years prior to EYO. In contrast, the two FDG topographies separated M+ from M- after EYO (**Figure 2**). In the longitudinal cohort, each of the topographies was compared both within and across modalities. The topographies were stable across time and supported cross-sectional findings (**Figure 3**).

Conclusion: In the DIAN cohort, SVD identified that PiB and FDG changes occurred in different topographies at different times. Focal changes in amyloid (e.g. precuneus, basal ganglia, and frontal cortex) occurred prior to EYO. These results suggest a potential distinct spatial cascade of events occurs within DIAN.

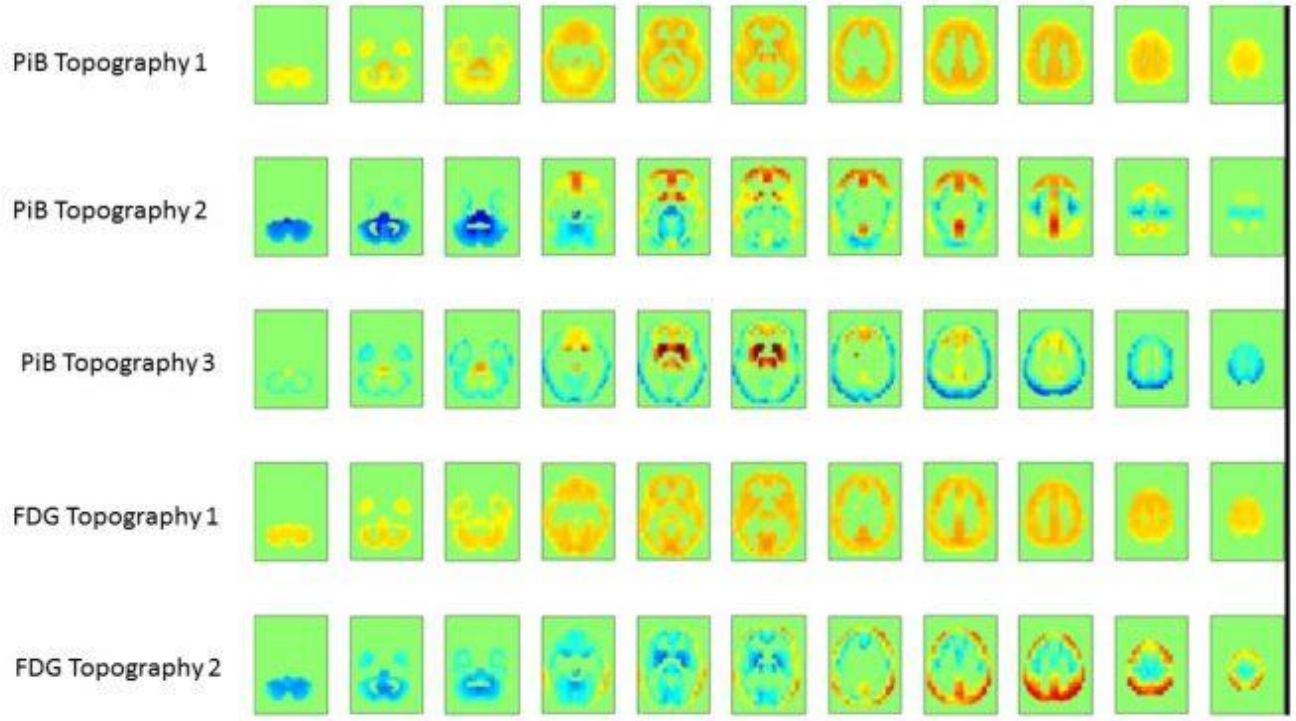

Figure 1.

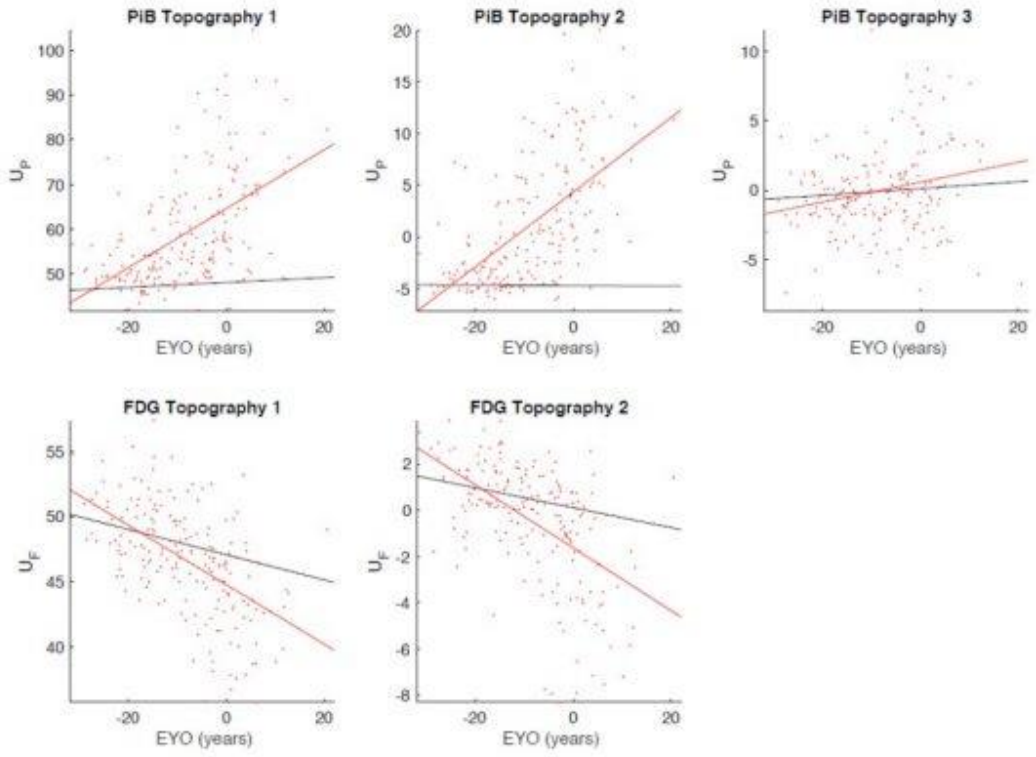

Figure 2.

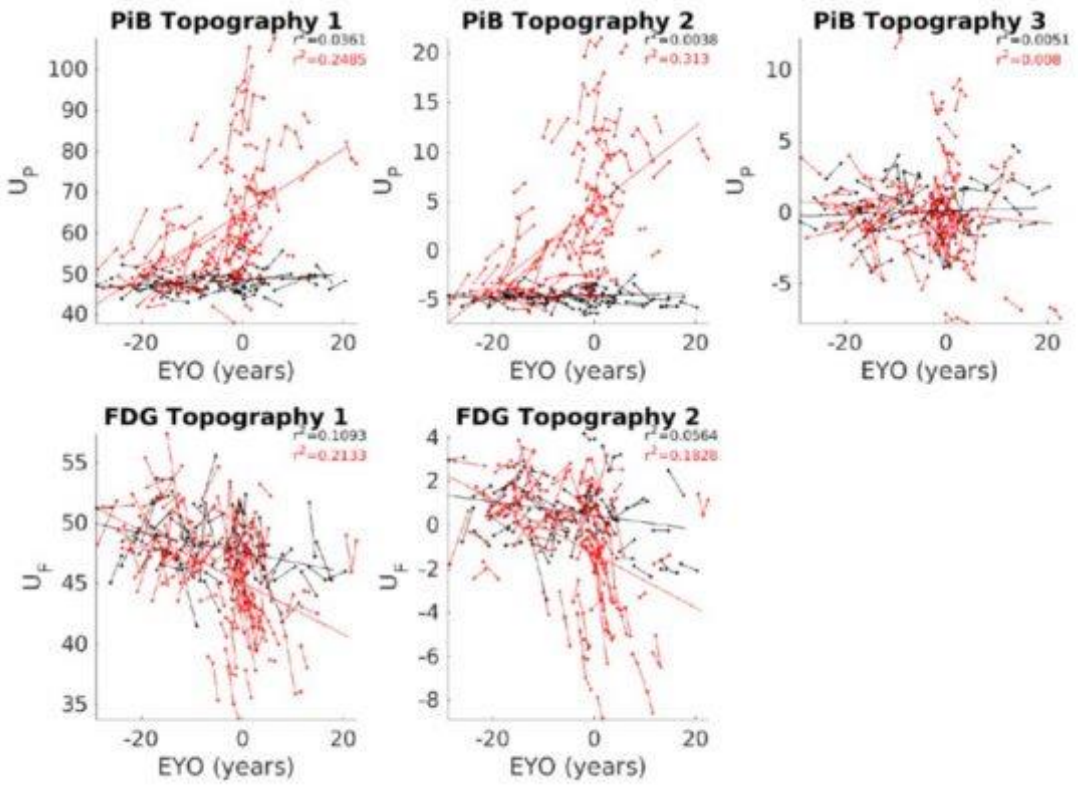

Figure 3.

Keywords: Autosomal dominant Alzheimer disease, amyloid, PIB, FDG, Singular Value Decomposition (SVD)

P65: [18F]AV-1451 tau PET imaging in MAPT 10+16 mutation carriers

Mica Clarke[1], Jieqing Jiao[1], Katrina Dick[1], Rhian Convery[1], Carolin Koriath[1], Ione Woollacott[1], Philip Weston[1], Roger Gunn[2], Ilan Rabiner[2], Martin Rossor[1], Jason Warren[1], Nick Fox[1], Sebastien Ourselin[1], Martina Bocchetta[1], Jonathan Rohrer[1]

[1]*University College London, London, United Kingdom*
[2]*Imanova, London, United Kingdom*

Tau pathology underlies about 50% of cases of frontotemporal dementia (FTD) but there are currently no *in vivo* biomarkers of tau. The [18F]AV-1451 ligand was developed for PET imaging of tau deposition but there have only been limited studies in FTD so far. We aimed to compare the distribution of [18F]AV-1451 tracer retention in carriers of the intronic 10+16 mutation in the *MAPT* gene (n=6, 2 symptomatic, 4 asymptomatic) with that of 6 age-matched healthy control participants. All participants were scanned on a Siemens Biograph 6 PET-CT scanner with Truepoint gantry. Dynamic PET data were acquired continuously following intravenous bolus injection of [18F]AV-1451 for 120 mins in 3D-mode. Dynamic images were reconstructed using a filtered back projection algorithm (direct inversion Fourier transform), with isotropic voxel size of 2 x 2 x 2 mm^3. Corrections for decay and random counts were performed, and attenuation and scatter were corrected based on a low-dose CT scan acquired preceding PET acquisition. Rigid head motion correction was performed to align the reconstructed dynamic PET frames using image registration for each scan. Frames affected by mismatched attenuation correction were identified by visual inspection and excluded from kinetic analysis. Standardized uptake value ratios (SUVR) were calculated using the cerebellum as a reference. Linear regression analyses revealed significant differences in mean SUVR between carriers and controls in frontal (p=0.04), parietal (p=0.01) and cingulate (p=0.02) cortices, as well as the caudate (p=0.02). Analyses also revealed an age-related increase in mean SUVR in controls as well as carriers, particularly in a number of subcortical regions. In summary, a number of areas show significantly increased [18F]AV-1451 binding in carriers compared with controls, suggesting this tracer would benefit from further study in a larger cohort.

Keywords: frontotemporal dementia, FTD, tau, [18F]AV-1451

P66: Longitudinal change of functional connectivity in the DIAN cohort: functional connectivity as a longitudinal biomarker in autosomal dominant AD

Aaron Schultz[1], Reisa Sperling[1], Rachel Buckley[1], Keith Johnson[1], Tammie Benzinger[2], Beau Ances[2], John Morris[2], Virginia Buckles[2], Chengjie Xiong[2], Eric McDade[2], Nigel Cairns[2], Daniel Marcus[2], Amanda Fulbright[2], Clifford Jack[3], John Ringman[5], Martin Farlow[4], Kirsi Kinnunen[6], Nick Fox[6], Colin Masters[7], Peter Schofield[8], Steve Salloway[9], Johannes Levin[10], Randall Bateman[2], Jasmeer Chhatwal[1]

[1]*MGH/HMS, Boston, MA, US*
[2]*Wash U, St. Louis, MO, US*
[3]*Mayo, Rochester, MN, US*
[4]*Indiana University - Purdue University, Indianapolis, IN, US*
[5]*USC, Los Angeles, CA, US*
[6]*University College London, London, United Kingdom*
[7]*University of Melbourne, Melbourne, Australia*
[8]*NeuRA, Sydney, Australia*
[9]*Butler University, Indianapolis, IN, US*
[10]*University of Munich, Munich, Germany*

Rationale: Cross-sectional differences in functional connectivity MRI (fcMRI) strength have been consistently observed across the spectrum of late-onset and autosomal dominant AD (ADAD). However, reports of longitudinal fcMRI have been rare, reflecting the need for analytic methods optimized to detect disease related changes over time. Leveraging the unique strengths of ADAD–including predictable age of onset, known amyloid pathology, and the relative absence of age-related network degradation - we describe an analytic method optimized to detect AD-related network degradation over longitudinal follow-up.

Methods: Template Based Rotation (TBR) was performed on 142 DIAN participants (86 mutation-carriers (M+), and 56 non-carriers (M-)) followed for 2.38±0.73 years. To minimize inter-session variability unrelated to disease progression, we 1) relied on the inherent signal/noise segregation of TBR, omitting explicit data cleaning strategies including temporal-filtering, motion, nuisance, and global signal regression; and 2) generated whole-network fcMRI measures via spatial-correlations (sTBR) between individual session maps and *a priori* templates. Linear mixed effect models controlling for movement, PiB-PET, and estimated-years-to-symptom-onset (EYO), including interactions with mutation-status, were used to assess change in fcMRI over time.

Results: Consistent with cross-sectional patterns, M+ showed significant longitudinal decreases in default/salience and control network connectivity ($p<0.001$); marginal changes in dorsal attention and motor networks ($p<0.062$); and no change in visual networks (Figure-1). The rate of fcMRI change was significantly greater in M+ vs. M- for the default/salience ($p=0.028$), left ($p = 0.007$) and right ($p<0.001$) control networks (Figure-2). No independent effect of amyloid burden (PiB-PET) was observed when controlling for mutation and EYO.

Conclusion: Longitudinal fcMRI changes in ADAD were observable with sTBR, and the pattern of longitudinal network degradation mirrored prior cross-sectional results. Though continued work is needed to

optimize metrics, sTBR differentiated longitudinal rates of change in M+ vs. M-, illustrating the feasibility of longitudinal connectivity analysis in multi-site clinical research.

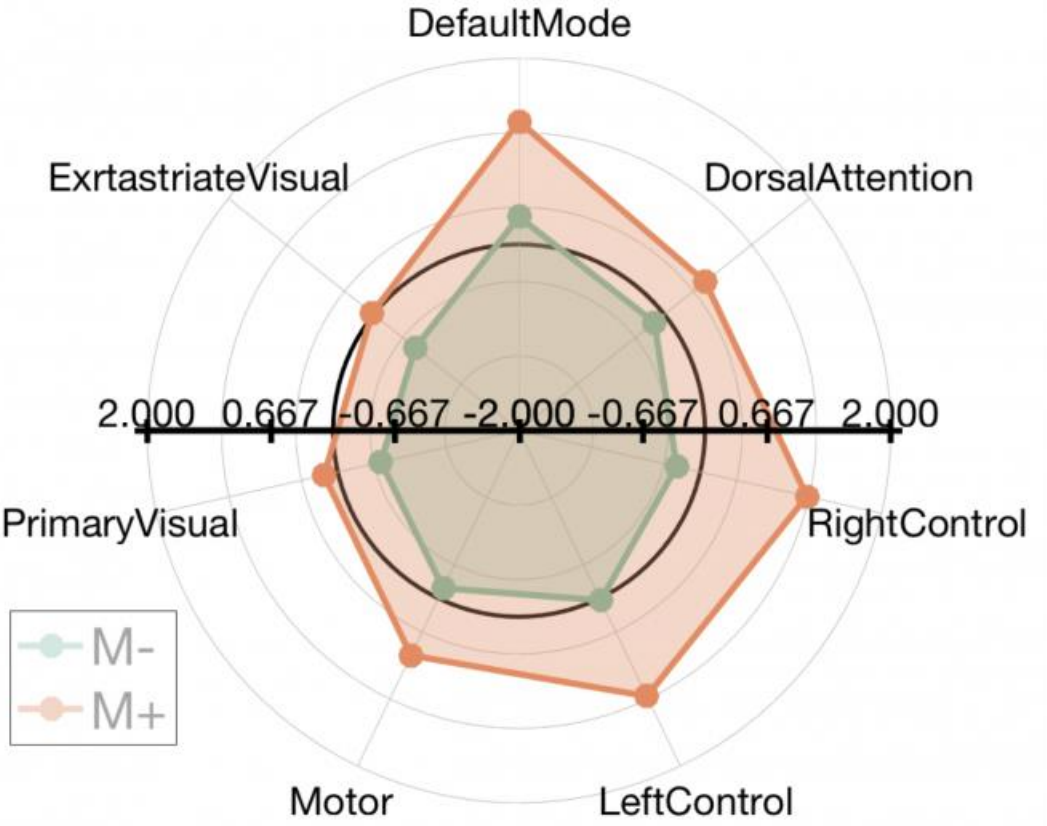

Figure 1: *Longitudinal rates of fcMRI change in ADAD mutation carriers (M+) and non-carriers (M-).* Rates of change in 6 cortical networks are depicted in the above spider plot, with M+ shown in orange, M- in green. The black circle represents a zero rate of change during the follow-up period. In M-, none of the examined networks showed a significant rate of change over time. In M+, the default/salience as well as the right and left frontoparietal control networks showed the greatest change over time, with marginal declines in dorsal attention and motor networks, and no change in visual networks observed.

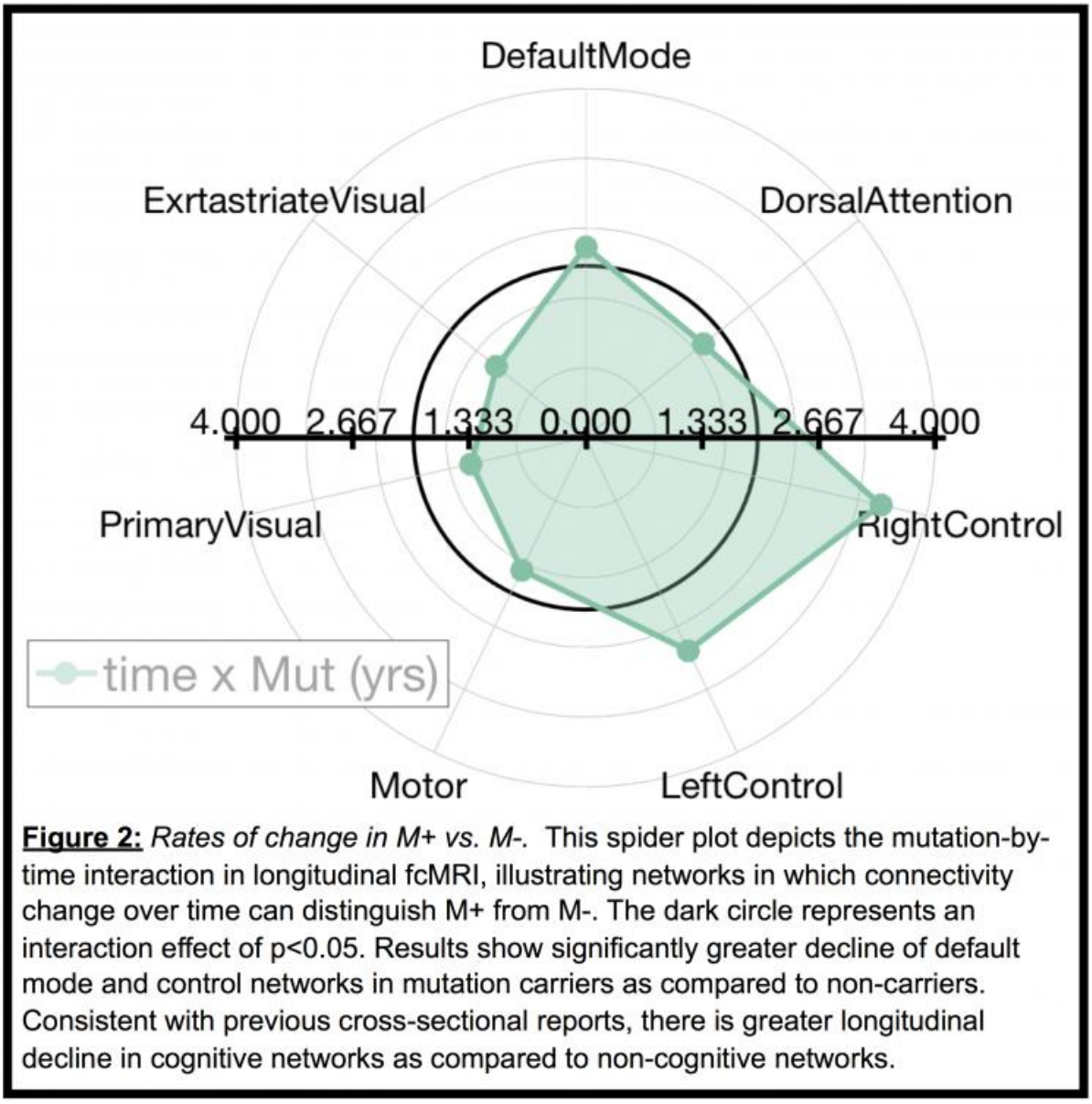

Figure 2: *Rates of change in M+ vs. M-.* This spider plot depicts the mutation-by-time interaction in longitudinal fcMRI, illustrating networks in which connectivity change over time can distinguish M+ from M-. The dark circle represents an interaction effect of $p<0.05$. Results show significantly greater decline of default mode and control networks in mutation carriers as compared to non-carriers. Consistent with previous cross-sectional reports, there is greater longitudinal decline in cognitive networks as compared to non-cognitive networks.

Keywords: functional connectivity, DIAN, longitudinal, ADAD, PiB

P67: An UNC5C locus is associated with susceptibility to cognitive decline and hippocampal neurodegeneration in clinically normal older adults

Hyun-Sik Yang[1,2], Jasmeer Chhatwal[1], Kathryn Papp[1,2], Jennifer Rabin[1], Bernard Hanseeuw[1], Elizabeth Mormino[1,3], Rachel Buckley[1], Aaron Schultz[1], Michael Properzi[1], Trey Hedden[1], Gad Marshall[1,2], Dorene Rentz[1,2], Keith Johnson[1,2], Philip De Jager[4], Reisa Sperling[1,2]

[1]*Massachusetts General Hospital, Boston, MA, US*
[2]*Brigham and Women's Hospital, Boston, MA, US*
[3]*Stanford Medical School, Palo Alto, CA, US*
[4]*Columbia University Medical Center, New York, NY, US*

Background: A recent genome-wide association study linked *UNC5C* rs3846455^{G} with cognitive susceptibility to neuropathologies, and *UNC5C* has been implicated in hippocampal neurodegeneration in animal models. We investigated the association of *UNC5C* rs3846455^{G} with cognitive decline and hippocampal atrophy in clinically normal older adults.

Methods: Study participants are from Harvard Aging Brain Study, a longitudinal cohort study of clinically normal older adults. We analyzed 211 participants with rs3846455 genotype, longitudinal Preclinical Alzheimer's Cognitive Composite (PACC), and longitudinal brain MRIs. We used linear regressions to test the association of rs3846455^{G} carrier status with baseline PACC, HVadj (bilateral hippocampal volume adjusted for intracranial volume), and Aβ (measured by Pittsburgh Compound B PET FLR DVR). Next, we used linear mixed effect models to examine the effect of rs3846455^{G} on longitudinal PACC and HVadj. Interaction between rs3846455^{G} and baseline Aβ was also examined to determine whether Aβ modifies the effect of rs3846455^{G} on longitudinal PACC or HVadj. Sex and baseline age were adjusted in all analyses, and years of education was also controlled when the analysis outcome was PACC.

Results: *UNC5C* rs3846455^{G} was not associated with baseline PACC, HVadj, or Aβ. However, rs3846455^{G} was associated with longitudinal decrease in PACC (β=-0.070, 95% CI -0.139 to 0.001, p=0.046) and longitudinal decline in HVadj (β=-60.6, 95% CI -99.5 to -60.6, p=0.0023). On interaction models, baseline Aβ accentuated the effect of rs3846455^{G} on longitudinal PACC decline (β=-0.53, p=0.0012), but did not significantly moderate the association of rs3846455^{G} with longitudinal HVadj (p=0.11).

Conclusion: *UNC5C* rs3846455^{G}, which does not have a direct association with Aβ, has a synergistic effect with Aβ on cognitive decline, and exacerbates age-related hippocampal atrophy in clinically normal older adults. Our results replicate a previous report associating rs3846455^{G} with cognitive susceptibility to neuropathology, and strengthen the evidence that *UNC5C* is implicated in hippocampal neurodegeneration.

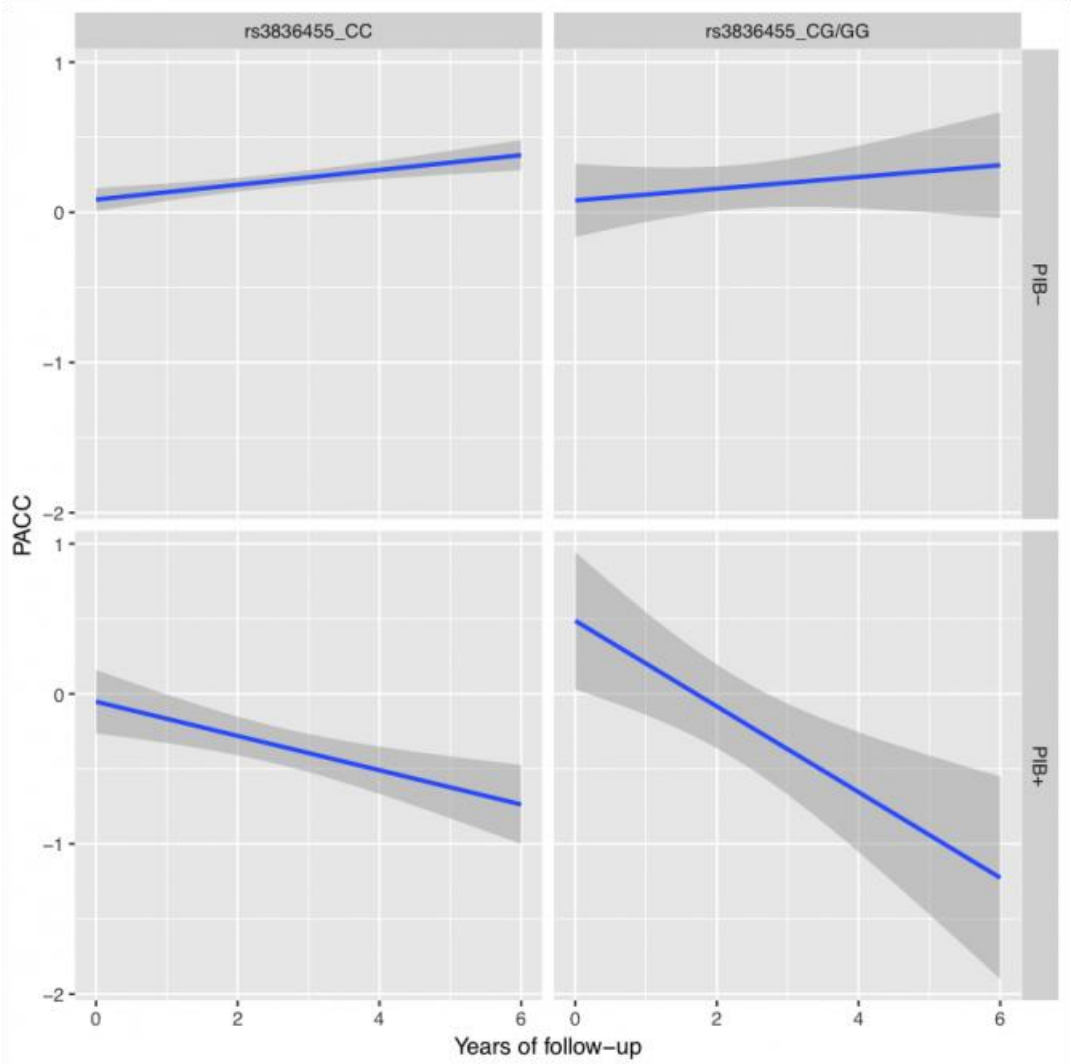

Figure 1. *UNC5C* rs3846455 genotype and longitudinal change in Preclinical Alzheimer's Cognitive Composite (PACC). rs3846455^{G} minor allele carriers (rs3846455^{CG} or rs3846455^{GG} genotype) had worse cognitive trajectory, especially in PIB+ group. PIB+ group was defined as participants with Pittsburgh Compound B PET FLR DVR > 1.186.

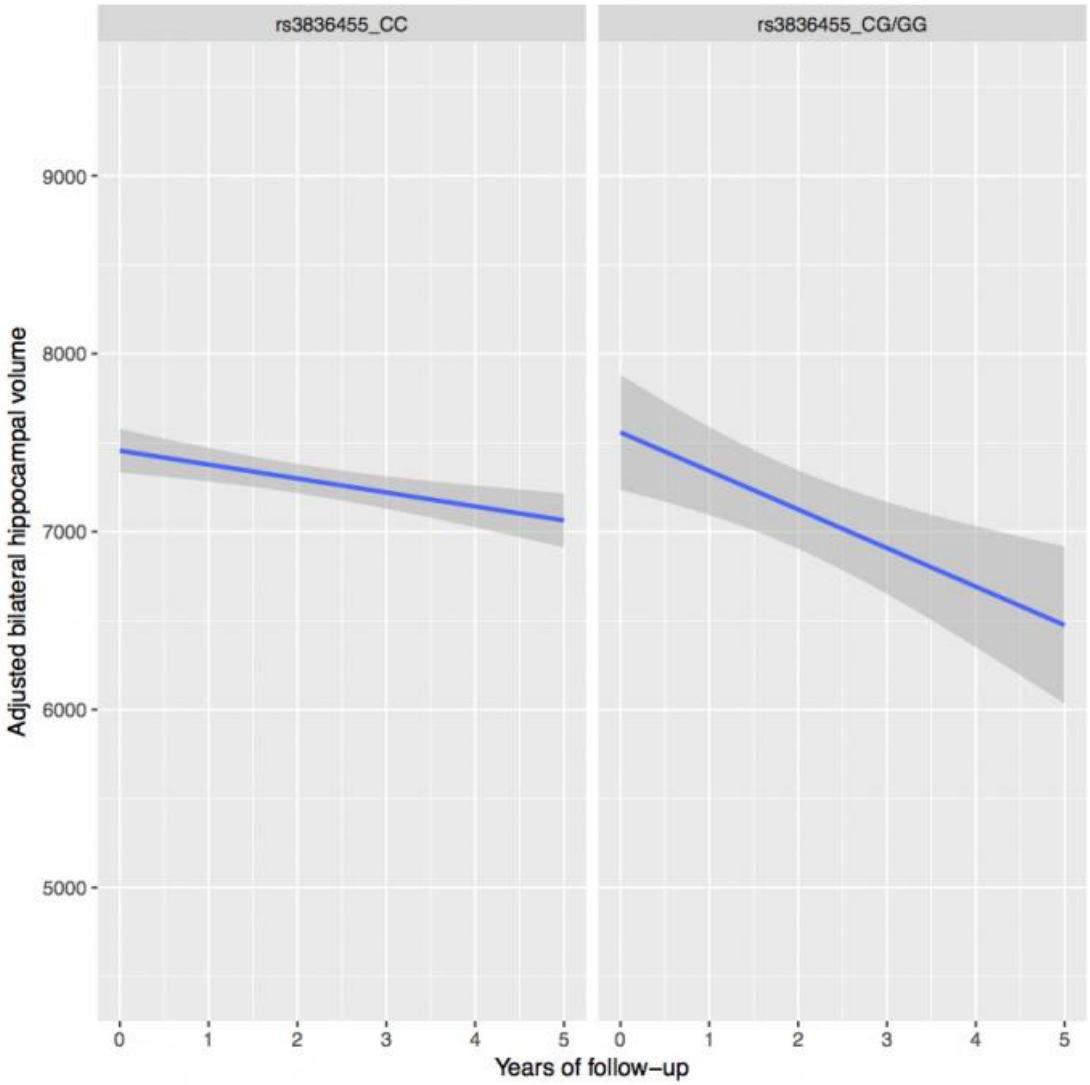

Figure 2. *UNC5C* rs3846455 genotype and longitudinal change in bilateral hippocampal volume adjusted for intracranial volume (HVadj). rs3846455^{G} minor allele carriers (rs3846455^{CG} or rs3846455^{GG} genotype) had more hippocampal atrophy over time.

Keywords: cognitive resilience, genetics, amyloid, neurodegeneration, clinically normal

P68: CYP2C19 effects in brain amyloid load and hippocampus' functional integrity

Andrea Lessa Benedet[1,2], Yasser Iturria-Medina[3,4], Mélissa Savard[1,5], Min-Su Kang[1,5], Sulantha Mathotaarachchi[1], Tharick A. Pascoal[1], Joseph Therriault[1], Monica Shin[1], Serge Gauthier[8], Alan C. Evans[3,4], Aurélie Labbe[7], Pedro Rosa-Neto[1,3,6,8]

[1]*Translational Neuroimaging Laboratory, McGill University Research Centre for Studies in Aging, Montreal, QC, Canada*
[2]*CAPES Foundation, Ministry of Education of Brazil, Brasilia, Brazil*
[3]*Montreal Neurological Institute, McGill University, Montreal, QC, Canada*
[4]*Ludmer Centre for NeuroInformatics and Mental Health, Montreal, QC, Canada*
[5]*Douglas Hospital Research Centre, McGill University, Montreal, QC, Canada*
[6]*Department of Neurology and Neurosurgery, McGill University, Montreal, QC, Canada*
[7]*Department of Decision Sciences, HEC Montreal, Montreal, QC, Canada*
[8]*Alzheimer's Disease Research Unit, McGill University Research Centre for Studies in Aging, Montreal, QC, Canada*

We have previously shown an association between *CYP2C19* polymorphism (rs4388808) and Aβ pathology–indexed *in vivo* and *post mortem*–, suggesting a protective effect of the minor allele (MA) on carriers as compared to non-carriers. Additionally, MA carriers presented better global cognition.

Objectives: Evaluate the effect of rs4388808 on amyloid load in the voxel level. Additionally, we aim to verify the effect of the SNP on hippocampal functional integrity over time.

Methods: The ADNI subjects used were genotyped using the Illumina-HumanOmni2.5 BeadChip. After QC, the SNP rs4388808 was recoded based on the dominant model. The amyloid load was indexed by [18F]florbetapir on 338 ADNI subjects. For the voxel-based analysis parametric images were obtained contrasting the SUVR between genotype groups, adjusting for age, gender, APOE-e4 and diagnose. After RFT correction for multiple comparisons, the T-value threshold of significance was $\leq$- 3.1 ($P \leq 0.001$).

To have a quantitative indicator of the hippocampus' functional integrity, we measured fractional amplitude of low-frequency fluctuation (fALFF) over time on 114 ADNI subjects. The subjects were then classified into AD spectrum–which includes AD and MCI–and controls. To access the change of fALFF over time, linear mixed models were then applied in rs4388808^{G} carriers and non-carriers of each group, being adjusted for gender, APOE-e4 and diagnose.

Results: The analysis showed that carriers of rs4388808^{G} had less [^{18}F]florbetapir binding in the frontal, posterior cingulate, and inferior temporal cortices (Figure 1). Only MA carriers in the AD spectrum group showed a significant change on hippocampal fALFF over time (p_{right}= 0.04; p_{left}= 0.06; $p_{bilateral}$= 0.04), presenting a positive slope (Figure 2).

Conclusion: The rs4388808^{G} carriers present less amyloid load in AD related regions. The rs4388808^{G} carriers in the AD spectrum present a positive change of hippocampal fALFF over time. Results may indicate a protective effect of the SNP, corroborating previous findings.

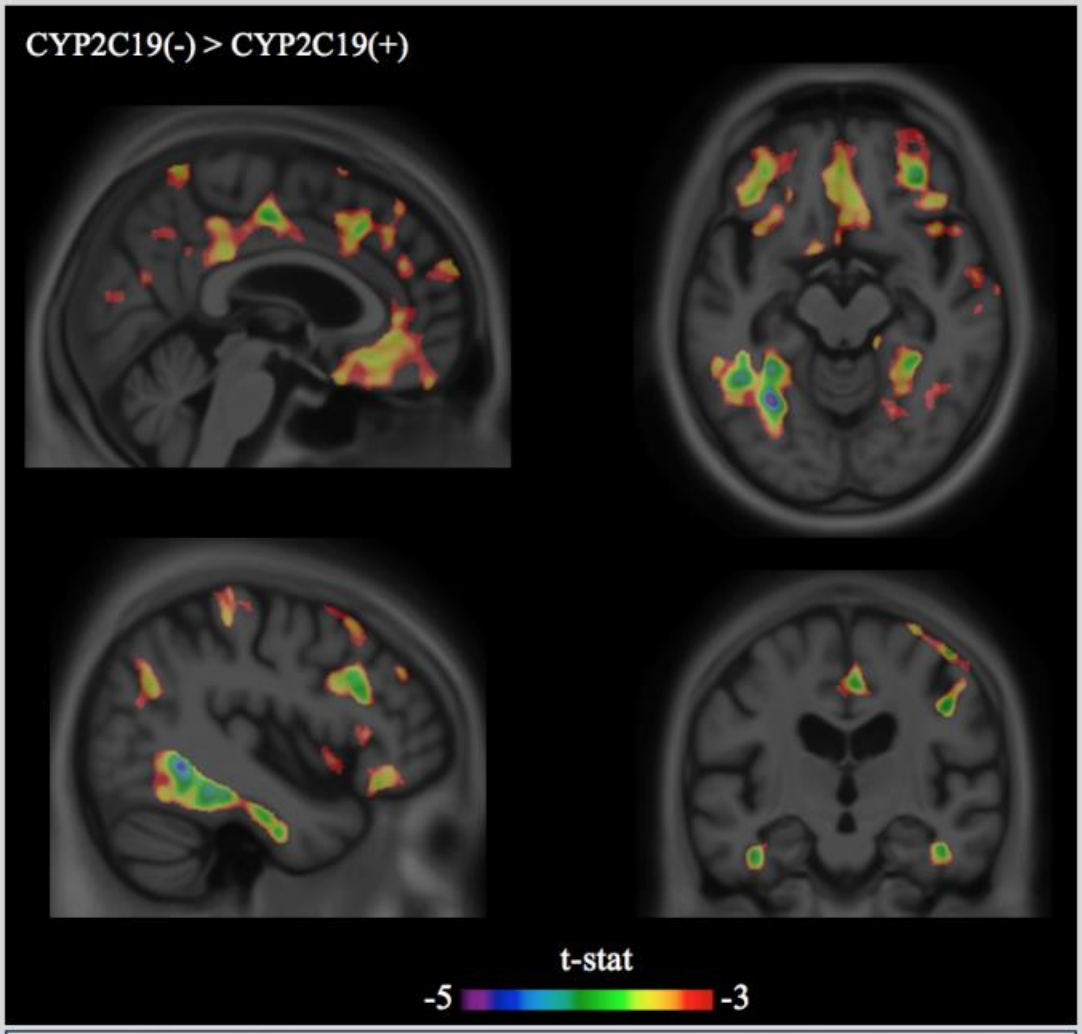

Figure 1. T-statistical parametric maps superimposed on an average structural MRI show brain regions with lower SUVR values in MA carriers (*CYP2C19* (+)) of the polymorphism in *CYP2C19*.

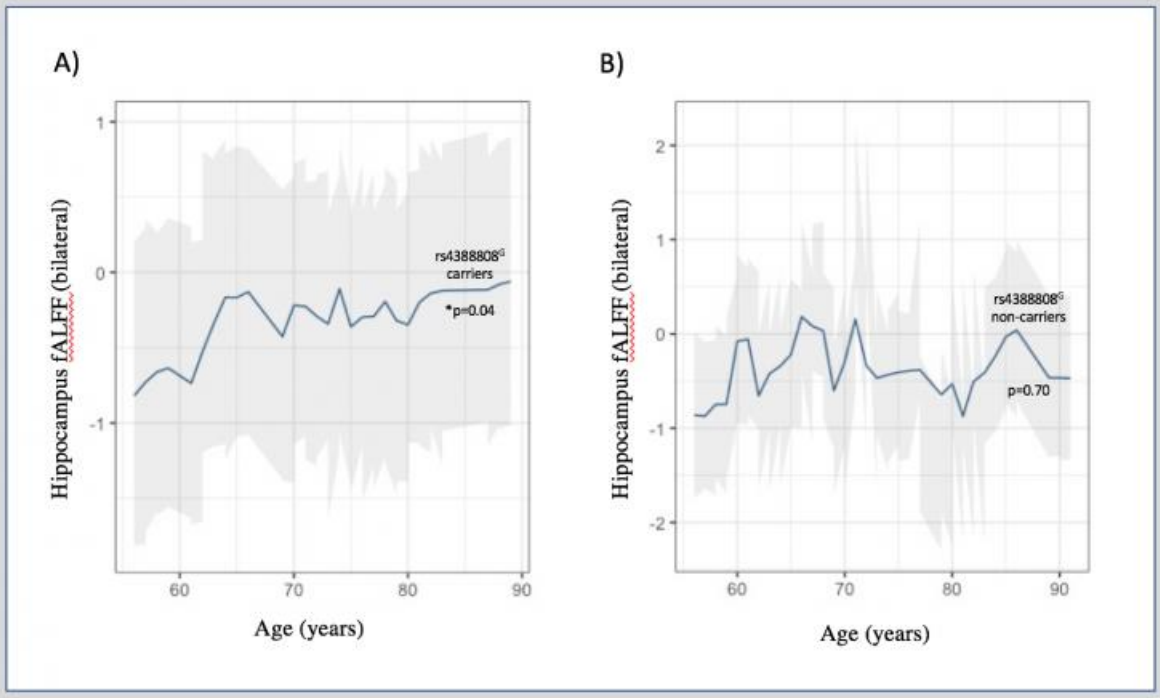

Figure 2. Fitted linear mixed models of hippocampus' fractional amplitude of low-frequency fluctuation (fALFF) over time in *CYP2C19* rs4388808^{G} carriers (A) and non-carriers (B).

Keywords: gene, CYP450, amyloid, hippocampus, fMRI

P69: Relationships between [11C]PiB positivity and an imaging marker of cerebrovascular pathology positivity

Sara Berman, Samantha Allison, Bradley Christian, Tobey Betthauser, Jennifer Oh, Sanjay Asthana, Cynthia Carlsson, Barbara Bendlin, Sterling Johnson

University of Wisconsin School of Medicine and Public Health, Madison, WI, US

Background: Although the majority of cases of clinical AD are found at autopsy to have significant concomitant vascular disease, the proposed ATN criteria do not include any measures of cerebrovascular disease, but they do encourage their development. We classify participants based on both amyloid and vascular positivity status.

Methods: We examined the distribution of white matter hyperintensity total lesion volume (WMH-TLV) using the T2-FLAIR MRI of n=856 cognitively normal (CN) subjects from the Wisconsin Alzheimer's Disease Research Center and Wisconsin Registry for Alzheimer's Prevention. A cutoff for elevated cerebrovascular disease as indexed by WMH-TLV was determined as 1.5 SD greater than the mean value. In the n=234 (65.4% female) participants with PET-PiB and FLAIR (CN (n=208), MCI (n=15), and AD (n=11)), we classified participants according to their amyloid (PiB-DVR ≥1.19) and vascular positivity status.

Results: The cutoff for WMH-TLV positivity was 45.635 ml; patients with a clinical diagnosis were more likely to be V+ (p=.002). WMH-TLV and PiB index were not correlated (Spearman's *rho* = .030, p = .65), nor were pulse pressure (PP) and PiB (Spearman's *rho* = .042, p=.52). 67.9% (159/234) of participants were A-/V-, 21.8% (51/234) were A+/V-, 6.4% (15/234) were A-/V+, and 3.8% (9/234) were A+/V+ when using WMH as the biomarker for V *(Figure 1).* 3.8% (6/159) of A-/V-, 23.5% (12/51) of A+/V-, 6.7% (1/15) of A-/V+, and 77.8% (7/9) of A+/V+ had a clinical diagnosis of MCI or dementia. Cognition also differed across biomarker groups *(Table 1).*

Discussion: Nonspecific metrics of vascular health, an imaging biomarker (WMH-TLV) and a common physical exam metric (PP), were not correlated with amyloid, suggesting independence of these pathologies. There were differences in cognition by A/V biomarker groups. Ischemic lesions may be only one facet of vascular pathology and study with more specific measures of cerebrovascular health are needed.

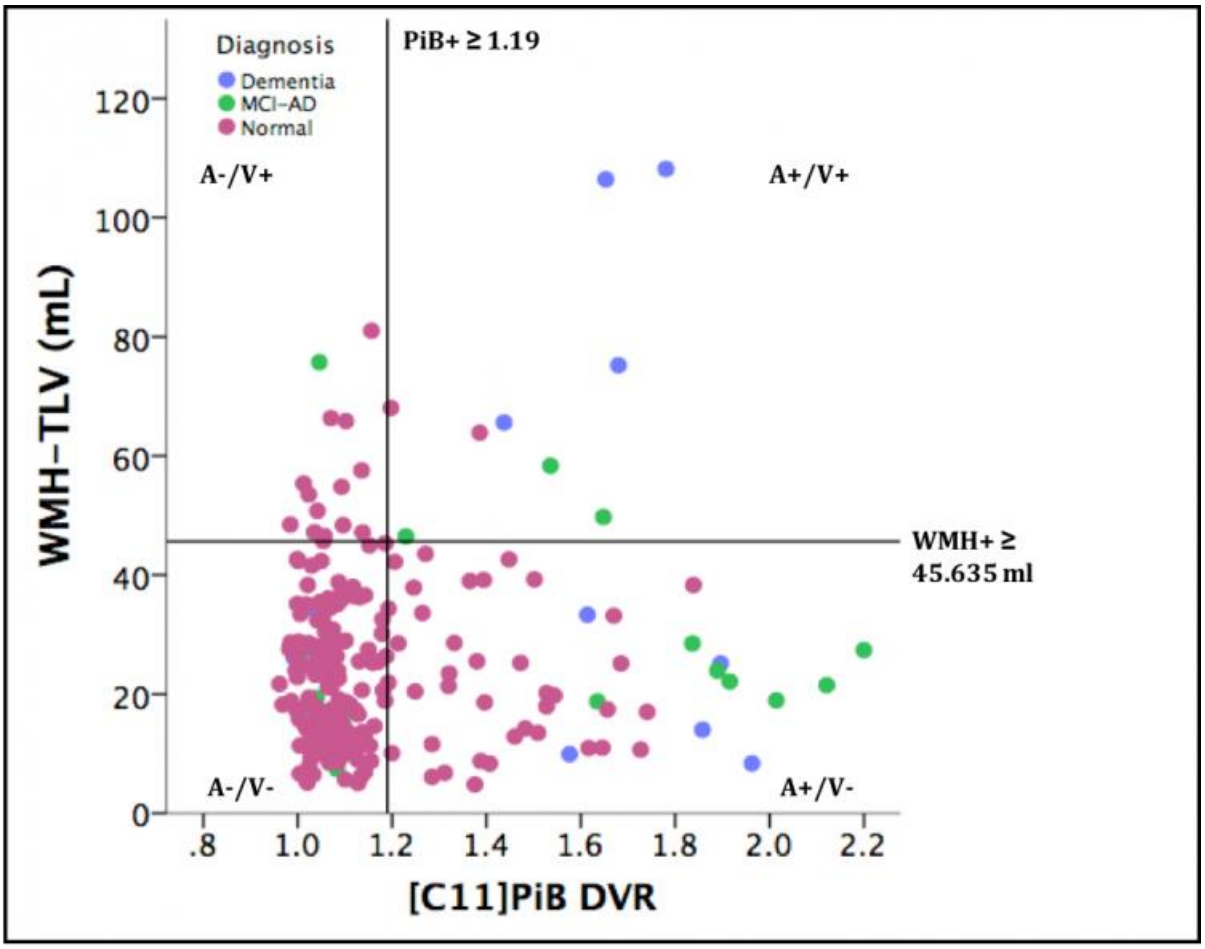

Figure 1: WMH-TLV, as measured via T2-FLAIR imaging, is on the y-axis, and PiB DVR is on the x-axis. Cutoffs for PiB positivity (≥ 1.19) and WMH (≥ 45.635 ml) are noted.

Table 1: Cognitive Performance Across Amyloid and Vascular Biomarker Groups – All Participants		
Cognitive Test	Pairwise Comparisons	Interval between PiB and Neuropsych Test (yrs) (mean: SD)
WAIS-DS (*p*<.001, n=227)	A+/V+ << A-/V- (p<.001) A+/V- << A-/V- (p=.001)	.37 (.43)
Animal Naming (*p*<.001, n=228)	A+/V+ << A-/V- (p<.001) A+/V+ << A+/V- (p=.009) A+/V+<< A-/V+ (p=.031)	.50 (.67)
RAVLT Long Delay (*p*<.001, n=233)	A+/V+ << A-/V- (p<.001) A+/V+ << A+/V- (p=.004)	.36 (.42)
Cognitive Performance Across Amyloid and Vascular Biomarker Groups – Cognitively Normal Subset		
WAIS-DS (*p*<.013, n=206)	A+/V- << A-/V- (uncorrected p=.018) A-/V+ << A-/V- (uncorrected p=.019)	.36 (.42)
Animal Naming (*p*=.217, n=203)	N/A	.51 (.70)
RAVLT Long Delay (*p*<.101, n=208)	N/A	.36 (.43)

X << Y indicates group X performed worse than group Y
***** Only participants with cognitive testing within 3 years of the PiB scan were included in cognition analyses, so n's for each analysis are noted**
*****Pairwise p values are adjusted for multiple comparisons by the Dunn-Bonferroni approach unless otherwise noted**
***** A+/V+ only had two cognitively normal subjects, so this cell was likely underpowered for analysis in the cognitively normal subset**
***** WAIS-DS (Weschler Adult Intelligence Scale- Digit Symbol); RAVLT (Rey Auditory Verbal Learning Test)**

Keywords: PiB, WMH, cerebrovascular, biomarker, amyloid

P70: [18F]Fluorotaucipir binding in patients with cerebral amyloid angiopathy without hemorrhage and mild cognitive symptoms

David Jin, Emily Benson, Aaron P. Schultz, J. Alex Becker, Andreas Charidimou, Panagiotis Fotiadis, Samantha R. Katz, Evelyn Luner, Kirsten Moody, Justin S. Sanchez, Reisa Sperling, Li Xiong, Anand Viswanathan, Keith Johnson

Departments of Radiology and Neurology, Massachusetts General Hospital, Boston, MA, US

Objective: Cerebral amyloid angiopathy (CAA) is a contributor of hemorrhagic stroke and vascular cognitive impairment in elderly patients without stroke. Previous reports indicate that amyloid PET can identify cerebrovascular b-amyloid in CAA patients. Whether amyloid related cerebrovascular dysfunction, tau pathology, or both lead to cognitive symptoms in CAA is unknown. Although neuritic amyloid plaque- related neurofibrillary pathology has been associated at autopsy with CAA severity (NACC data), tau deposition *in vivo* has not been assessed in sporadic CAA.

Methods: We acquired tau PET with 18F Flortaucipir (FTP) and amyloid PET with 11C PiB in 24 patients with a clinical diagnosis of CAA by the Boston Criteria and 78 control subjects from the Harvard Aging Brain Study (HABS) matched by age and cognitive performance on the MMSE. Tau deposition was measured with FTP (SUVR, cerebellar reference), sampled in Freesurfer regions of interest (ROI) defined by the intersection of individual native tissue probabilities and a probabilistic FS-GTM atlas, including geometric transform matrix partial volume correction. In addition to measuring SUVR in entorhinal and inferior temporal cortex, we also measured SUVR in volume-weighted ROI aggregates (frontal, temporal, parietal, and occipital).

Results: Mean FTP SUVRs were higher in CAA patients compared to controls in entorhinal cortex, inferior temporal gyrus, and frontal and temporal cortical aggregates (see figure). SUVRs in the occipital and parietal aggregates were not significantly elevated compared to controls.

Conclusions: The higher FTP SUVRs in CAA corroborates the autopsy findings of neurofibrillary pathology and demonstrate an *in vivo* method by which it can be evaluated in sporadic CAA. These results raise the possibility that degree of tau deposition could be used as a biomarker to predict cognitive impairment in patients with CAA.

	Control	CAA	% Elevation	* p <
Demographics				
Age, mean (SD)	75.3 (7.3)	76.0 (5.2)	-	-
Min	58.3	65.5		
Max	89	88.5		
Gender (%Female)	53.8%	54.2%	-	-
MMSE	27.5 (3.2)	26.3 (2.3)	-	-
ROI Aggregate Mean SUVR (SD)				
Frontal	1.12 (0.10)	1.20 (0.21)	6.76%	p<0.05
Temporal	1.23 (0.20)	1.38 (0.30)	12.21%	p<0.05
Occipital	1.12 (0.17)	1.14 (0.13)	1.34%	-
Parietal	1.13 (0.19)	1.19 (0.22)	5.86%	-
Key ROI SUVR (SD)				
Entorhinal	1.16 (0.22)	1.27 (0.24)	10.12%	p<0.05
Inferior temporal	1.31 (0.25)	1.50 (0.38)	14.00%	p<0.05

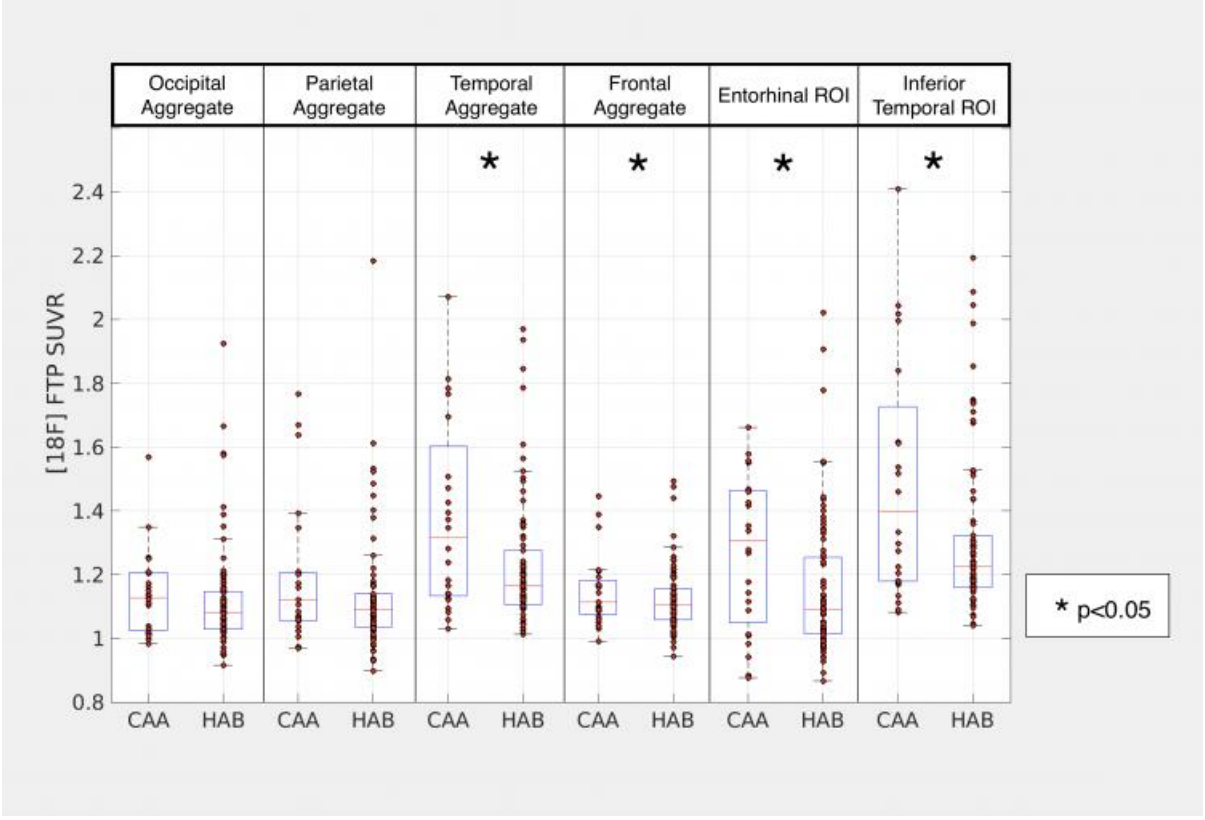

Keywords: Cerebral amyloid angiopathy, geometric transform matrix, FreeSurfer, region of interest analysis, Fluorotaucipir

P71: Amyloid imaging in hereditary cerebral amyloid angiopathy: detection and progression of pure vascular amyloid caused by APP E693Q

Aaron Schultz[1,3], Reina Kloet[4], Hamid Sohrabi[5], Pratishtha Chatterjee[5], Samantha Gardnener[5], Kevin Taddei[5], Tammie Benzinger[6], Anne Fagan[6], Reisa Sperling[1,2,3], Keith Johnson[1,2,3], Randall Bateman[6], M. Edip Gurol[2,3], Mark van Buchem[4], Ralph Martins[5], Jasmeer Chhatwal[1,2,3], Steven Greenberg[2,3]

[1]*Massachusetts General Hospital, Martinos Center for Biomedical Imaging, Boston, MA, US*
[2]*Brigham and Women's Hospital, Boston, MA, US*
[3]*Harvard Medical School, Boston, MA, US*
[4]*Leiden University Medical Center, Leiden, Netherlands*
[5]*Edith Cowan University, Joondalup, Australia*
[6]*Washington University School of Medicine, St. Louis, MO, US*

Rationale: Carriers of the APP E693Q ("Dutch") mutations have well-described deposition of fibrillar beta-amyloid pathology restricted to cerebral and leptomeningeal vessels leading to dominantly-inherited cerebral amyloid angiopathy (CAA). Bringing together imaging and CSF data from European and Australian APP E693Q carriers, we examined whether amyloid PET can be used to distinguish mutation carriers from non-carriers. We also assessed variations in amyloid burden with age, symptoms, and longitudinal PET in anticipation of potential treatment trials for this heretofore untested population.

Methods: Regional and global amyloid burden was assessed in 19 APP E693Q mutation carriers (M+) and 17 mutation non-carriers (M-) using PiB PET. Primary analyses examined mutation status by age interactions across a wide age-range in asymptomatic and symptomatic individuals (Figures 1-2). In a subset of 18 individuals (10 M+, 8 M-) imaged as part of the Dominantly Inherited Alzheimer's Network (DIAN), rates of change in amyloid PET were assessed in longitudinal data (mean follow-up 2.7y; Figure 3) using linear mixed effect models.

Results: Using a cortical composite of frontal, lateral, and retrosplenial regions (FLR), mutation carriers showed significantly increased overall PiB retention and steeper linear associations between PiB-PET and age than mutation non-carriers (mutation X age; $t(32)=4.34, p<0.001$). A similar effect was seen in available longitudinal data, with mutation carriers demonstrating faster fibrillar amyloid accumulation in the asymptomatic phase ($t(45)=3.26, p=0.006$; Figure 3). Intriguingly, while CSF Ab42 was similarly reduced across APP E693Q mutation carriers and ADAD mutation carriers from DIAN, amyloid PET signal was much lower in APP E693Q compared to ADAD mutation carriers.

Conclusion: APP E693Q mutation carriers with essentially pure CAA show elevated amyloid PET signal with age and higher longitudinal amyloid accumulation relative to mutation non-carriers. These findings support amyloid PET as a candidate biomarker in clinical trials for hereditary CAA.

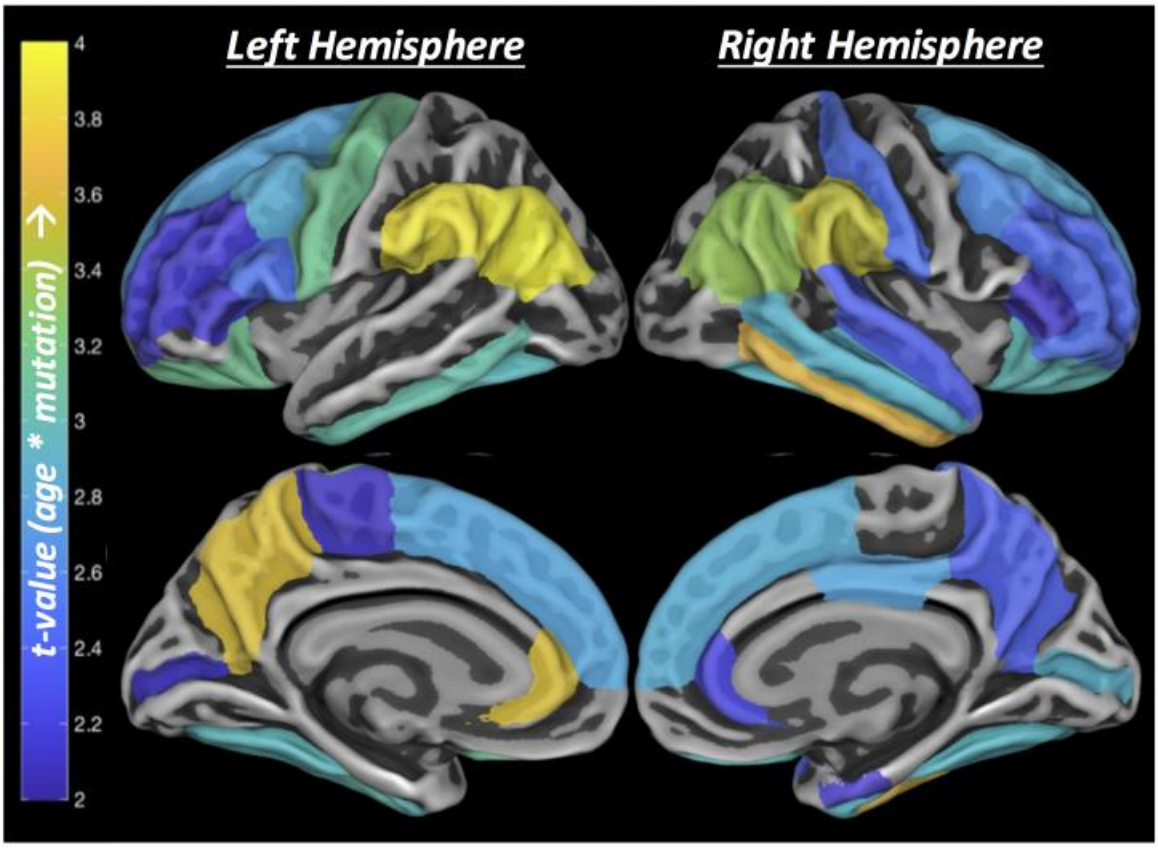

Figure 1: ***Temporal and Regional Patterns of Amyloid Deposition in APP E693Q carriers vs. non-carriers.*** APP E693Q carriers showed greater amyloid deposition with increasing age across a widespread set of FreeSurfer-segmented cortical ROIs (Only ROIs at $p \leq 0.05$ for age by mutation interaction are shown).

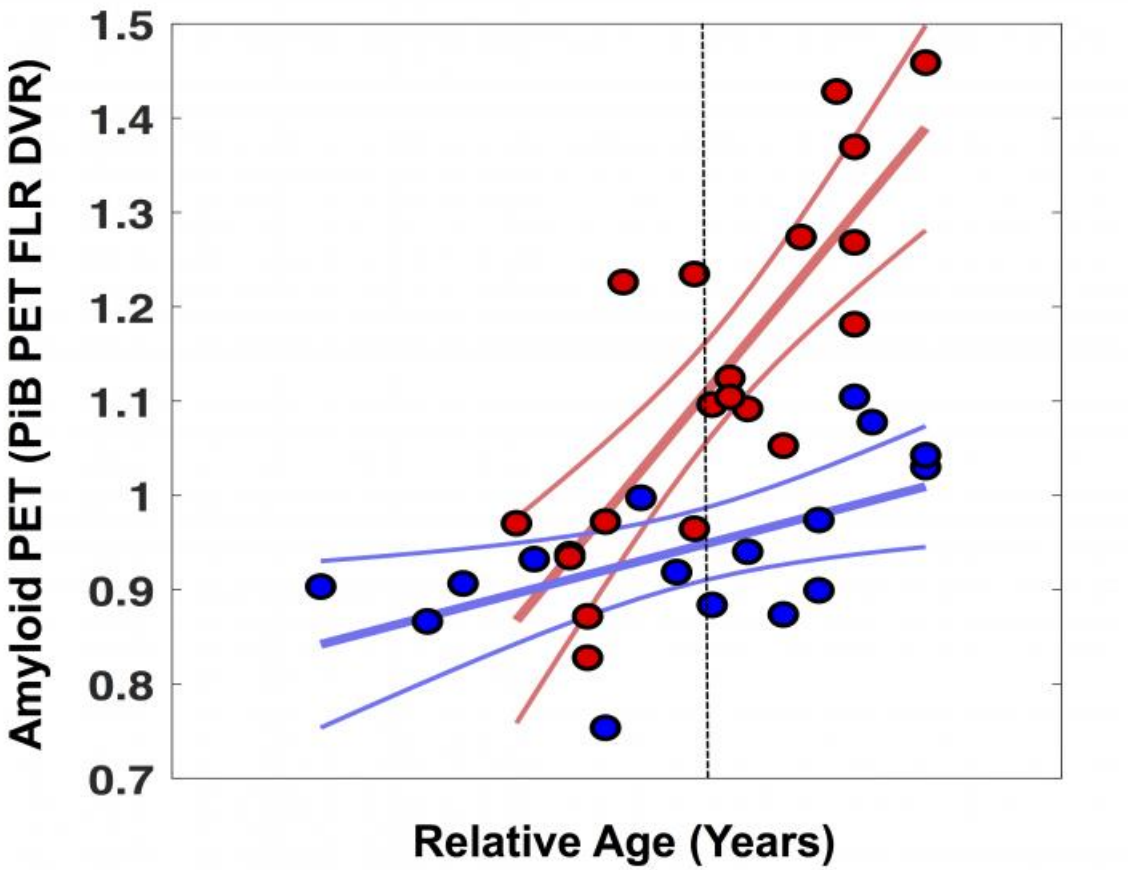

Figure 2: ***Age as a predictor of amyloid burden in cross-sectional data.*** Cortical composite PiB PET SUVRs were calculated for APP E693Q mutation carriers (red) and non-carriers (blue) and plotted against years of age (dashed line indicates mean age). APP E693Q carriers showed significantly greater amyloid burden with increasing age as compared to mutation non-carriers from the same families.

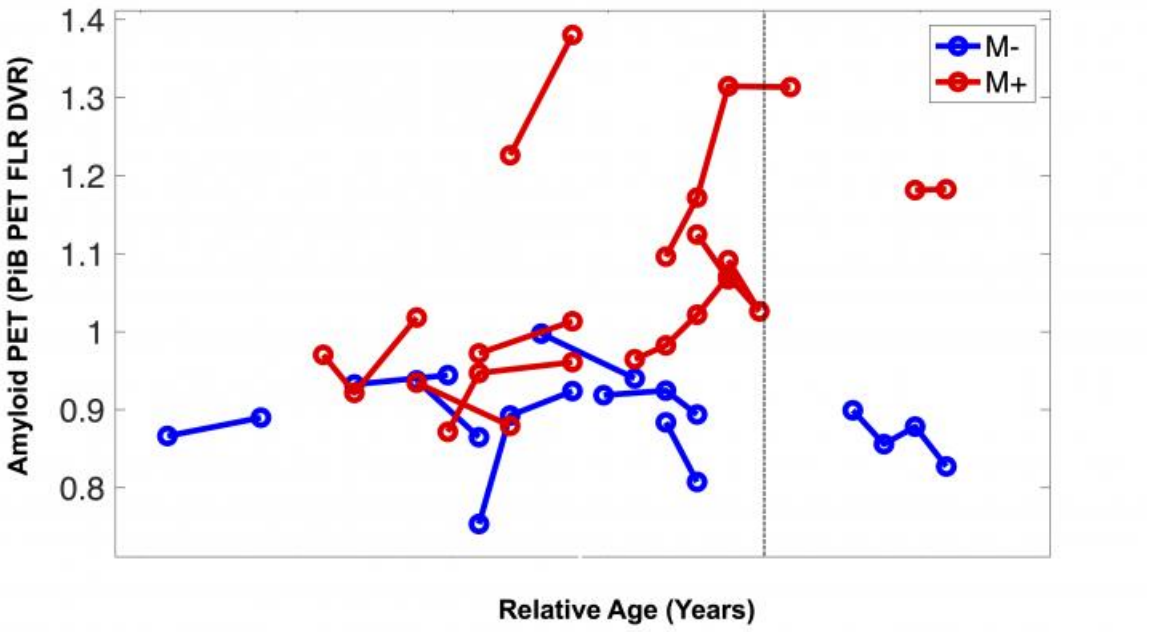

Figure 3: ***APP E693Q mutation carriers show significantly faster rates of longitudinal amyloid accumulation as compared to non-carriers.*** Longitudinal PiB PET data from asymptomatic APP E693Q Mutation carriers (M+; red) and non-carriers (M-; blue). The dashed line indicates the mean age of the sample.

Keywords: amyloid, APP, angiopathy, genetics

P72: Midlife insulin resistance and APOE genotype are associated with late-life brain amyloid accumulation

Juha Rinne[1,7], Laura Ekblad[1], Jarkko Johansson[1,2], Semi Helin[1], Matti Viitanen[3,4], Hanna Laine[3,5], Pauli Puukka[6], Antti Jula[6]

[1]*Turku PET Centre, University of Turku, Turku, FI*
[2]*Department of Radiation Sciences, Umeå University, Umeå, SE*
[3]*Turku City Hospital, University of Turku, Turku, Finland*
[4]*Clinical Geriatrics, Karolinska Institutet, Karolinska University Hospital, Huddinge, Sweden*
[5]*Department of Medicine, University of Turku, Turku University Hospital, Turku, Finland*
[6]*National Institute for Health and Welfare, Turku, Finland*
[7]*Division of Clinical Neurosciences, Turku University Hospital, Turku, Finland*

Objective: Is midlife insulin resistance an independent risk factor for brain amyloid accumulation in vivo after 15 years, and is this risk modulated by APOE ε4 genotype?

Methods: Altogether 60 non-demented elderly (mean age at baseline 55.4 and at follow-up 70.9 years, 55.5% women) from the Finnish population-based, nationwide Health2000 study with [11C]Pittsburgh compound B PET imaging. The participants were recruited according to their Homeostatic Model Assessment of Insulin resistance (HOMA-IR) values in the year 2000, and their APOE ε4 genotype. The exposure group (IR+, n=30) consisted of individuals with HOMA-IR >2.17 at baseline (highest tertile of the Health2000 study population), and the control group (IR-, n=30) of individuals with HOMA-IR <1.25 at baseline (lowest tertile). The groups were enriched for APOE ε4 carriers, resulting in 50% (n=15) APOE ε4 carriers in both groups. Analyses were performed with multivariate logistic and linear regression.

Results: 33.3% of the IR- group, and 60.0% of the IR+ group had an amyloid positive PET scan (odds ratio 3.0, p=0.04). The increased risk was seen both in carriers and non-carriers of APOE ε4 genotype. Higher midlife insulin resistance was associated with a greater brain amyloid burden (β=0.11, p=0.04, Table 1). Quantitative results are presented in Table 1. Poorer cognitive processing speed and executive functioning at follow-up was associated with higher HOMA-IR values (Table 2). Higher prefrontal and lateral temporal cortex PIB uptake was associated with slower processing speed in cognitive testing both in ROI-based (β= -0.96, p=<0.0001 for prefrontal and β= -1.25, p=<0.0001; adjusted for age, education and gender) and voxel-based correlation analyses (T=4.59, p <0.05, FWE corrected).

Conclusions: These results indicate that midlife insulin resistance is an independent risk factor for brain amyloid accumulation in non-demented elderly individuals and is associated with slower cognitive processing speed.

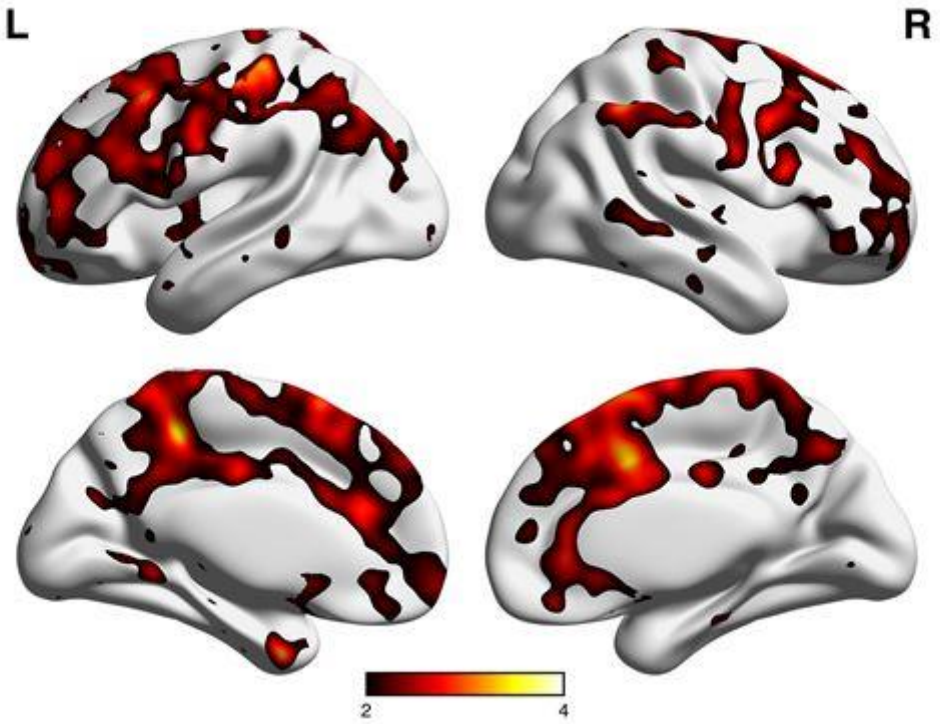

Voxel-by-voxel SPM analysis of [^{11}C]PIB uptake showing regions where individuals with insulin resistance 15 years before the PET scans had higher [^{11}C]PIB uptake than the control group. The color scale starts from the height threshold (T) 2.0, derived from SPM analysis adjusted for age, time from baseline to PIB scan, gender and years of education, and indicating difference between IR- and IR+ groups for all regions shown in color in the image, yellow being most significant ($p<0.025$ when $T=2.0$, uncorrected for multiple comparisons). N=60.

Table 1. PIB standardized uptake value ratios (SUVRs) in ROIs typical for amyloid accumulation in Alzheimer´s disease, according to the participants' HOMA-IR values at baseline in 2000.

Region of interest	*IR-*	*IR+*	*p-value[a]*	*p-value[b]*
PIB composite score	1.51±0.37	1.73±0.48	0.050	0.04
Parietal cortex	1.55±0.39	1.78±0.49	0.046	0.05
Prefrontal cortex	1.53±0.39	1.75±0.50	0.056	0.03
Lateral temporal cortex	1.34±0.27	1.48±0.41	0.10	0.10
Cingulum anterior	1.69±0.38	1.97±0.50	0.02	0.01
Cingulum posterior	1.76±0.46	2.02±0.52	0.04	0.04
Precuneus	1.73±0.50	2.06±0.65	0.03	0.04

The results are shown as unadjusted mean SUVR±SD. [a]*P*-values for unadjusted differences between individuals with and without insulin resistance at baseline in 2000, assessed with Student´s *t*-test. [b]analyses adjusted for age, time from baseline to PIB scan, sex, and years of formal education. The adjusted analyses are performed with multivariate linear regression analysis.

Table 2. Domain-spesific neuropsychological test scores according to insulin resistance (HOMA-IR) values at baseline in 2000.

z-score (mean [SD])	*IR-*	*IR+*	*P-value[a]*	*P-value[b]*	*P-value[c]*
Executive functions	0.32 (0.68)	-0.29 (0.67)	0.002	0.015	0.019
Processing speed	0.35 (0.65)	-0.32 (0.82)	0.001	0.009	0.006
Episodic memory	0.12 (1.0)	-0.13 (0.77)	0.28	0.89	0.70
Language	0.24 (0.77)	-0.10 (0.65)	0.09	0.35	0.37

Unadjusted p-values derived from analyses with Student´s two-sample *t*-test. Adjusted analyses were performed with multivariate linear regression analysis.
[a]unadjusted, [b]adjusted for level of education, [c]further adjusted for age and gender

Keywords: Alzheimer's disease, amyloid, insulin resistance, HOMA-IR, PET

P73: Flortaucipir PET imaging and neuropsychological performances dissociate dorsal and ventral stream dysfunction in Posterior Cortical Atrophy

Deepti Putcha, Jessica Collins, Bonnie Wong, Brad Dickerson, Scott McGinnis

Frontotemporal Disorders Unit, Department of Neurology, Massachusetts General Hospital and Harvard Medical School, Boston, MA, US

Background: Posterior cortical atrophy (PCA) is a neurodegenerative syndrome often arising from Alzheimer's disease pathology. Little is known regarding the topographical distribution of paired helical filament (PHF) tau in relation to cognitive deficits in this disorder. We sought to relate performances on tasks of visual/quantitative functions to tau deposition in regions of interest hypothesized to support these tasks.

Methods: Six individuals (mean age = 69.6 years, 4F/2M) diagnosed with PCA based on neurological and neuroimaging exams underwent neuropsychological evaluation and ^{18}F-FTP PET imaging. Bilateral FTP SUVR values were calculated in dorsal parietal regions, including the inferior parietal lobules (IPL), superior parietal lobules (SPL); a medial parietal region (isthmus cingulate); and a ventral stream region (inferior temporal gyrus; ITG). Spearman's rank order correlations determined the association between FTP binding in these regions and a measure of simultanagnosia (BORB Overlapping Figures), an auditory calculation task, and a single object identification task (BORB Foreshortened View).

Results: Poor performance on calculations was related to greater tau deposition in dominant (lh) dorsal stream parietal regions (IPL; r_s=-0.97, p=0.005 and SPL; r_s=-0.9, p=0.01; isthmus cingulate; r_s=-0.9, p=0.04) but not in non-dominant (rh) dorsal (p>0.8) or ventral regions (p<0.09). In contrast, poor performance on the BORB Foreshortened View task was related to greater tau deposition in a non-dominant ventral stream region (rhITG; r_s= -0.87, p=0.02), but not in a dominant ventral region (lhITG; p> 0.1) or any dorsal stream region (p>0.1). Poor performance on the BORB Overlapping Figures task was related to greater tau in a non-dominant dorsal medial region (rh isthmus cingulate, r_s= 0.9, p= 0.04), but not to any other region of interest (all p's >0.2).

Conclusions: These preliminary results support previously hypothesized (Crutch et al., 2017) syndromic variability within PCA, associated with tau deposition in dorsal parietal and ventral temporal brain regions.

Keywords: PCA, tau, Alzheimer's, cognition, visuospatial deficit

P74: Amyloid network topology characterizes the progression of Alzheimer's disease during the pre-dementia stages

Joana Pereira[1], Tor Olof Strandberg[2,3], Sebastian Palmqvist[2,4], Giovanni Volpe[5], Danielle van Westen[6,7], Eric Westman[1], Oskar Hansson[2,3]

[1]*Division of Clinical Geriatrics, Department of Neurobiology, Care Sciences and Society, Karolinska Institutet, Stockholm, Sweden*
[2]*Clinical Memory Research Unit, Department of Clinical Sciences Malmö, Lund University, Lund, Sweden*
[3]*Memory Clinic, Skåne University Hospital, Malmö, Sweden*
[4]*Department of Neurology, Skåne University Hospital, Lund, Sweden*
[5]*Department of Physics, Göteborg University, Göteborg, Sweden*
[6]*Department of Clinical Sciences Lund, Diagnostic radiology, Lund, Sweden*
[7]*Imaging and Function, Skåne University Health Care, Lund, Sweden*

There is increasing evidence showing that the accumulation of the amyloid-β (Aβ) peptide into extracellular plaques is a central event in AD. These abnormalities can be detected as lowered levels of $A\beta_{42}$ in the cerebrospinal fluid (CSF) and are followed by increased amyloid burden on positron emission tomography (PET) several years before the onset of dementia. The aim of this study was to assess amyloid network topology in non-demented individuals with early stage Aβ accumulation, defined as abnormal CSF $A\beta_{42}$ levels and normal Florbetapir PET (CSF+/PET-), and more advanced Aβ accumulation, defined as both abnormal CSF $A\beta_{42}$ and Florbetapir PET (CSF+/PET+). The amyloid networks were built using correlations in the mean ^{18}F-florbetapir PET values between 72 brain regions and analyzed using graph theory analyses. Our findings showed an association between early amyloid stages and an increased covariance as well as shorter paths between several brain areas that overlapped with the default-mode network. Moreover, we found that individuals with more advanced amyloid accumulation showed more widespread changes in brain regions both within and outside the default-mode network. These findings suggest that amyloid network topology could potentially be used to assess disease progression in the pre-dementia stages of AD.

Keywords: Florbetapir PET, CSF Aβ42, graph theory, amyloid networks, AD

P75: In pre-clinical AD, subjective cognitive decline is associated with brain hyperactivation in conflict monitoring/control regions

Akiko Mizuno[1], Helmet Karim[1], Anusha Rangarajan[3], William Klunk[1,2], Howard Aizenstein[1,3], Beth Snitz[1,2]

[1]*Department of Psychiatry, University of Pittsburgh, Pittsburgh, PA, US*
[2]*Department of, Neurology of Pittsburgh, Pittsburgh, PA, US*
[3]*Department of Bioengineering, University of Pittsburgh, Pittsburgh, PA, US*

Subjective Cognitive Decline (SCD) is a pre-clinical state that refers to individuals with high subjective concern for cognitive decline (typically in memory) without objective cognitive impairment. SCD could represent the earliest stage of dementia; however, the risk for progression and underlying neural basis are not understood. There is evidence that education level moderates the degree of risk for cognitive decline among SCD participants. We measured beta-amyloid (Aβ) deposition and brain activation during a memory-encoding task among older individuals with no cognitive impairment and with various levels of subjective concern, examining education as a moderating factor.

We recruited 66 clinically unimpaired older individuals (mean age = 73±7). We used Pittsburgh compound B (PiB)-positron emission tomography imaging to measure Aβ deposition, and we used the "face-name" memory encoding fMRI task. We built a linear regression model of voxel-wise brain activation on 1) a subjective concern score, 2) education level, and 3) their interaction.

Aβ deposition was significantly correlated with subjective concern scores but not with objective memory scores (Figure 1). Aβ deposition was not directly associated with brain activation. The regions that showed a significant interaction between subjective concerns and education were conflict monitoring/control regions. The activations in these regions increased as subjective concern increased among participants with higher education; however, the activations decreased as subjective concern increased among participants with lower education (Figure 2A). This effect was more pronounced in participants with a high level of Aβ deposition (Figure 2B-C).

Our results on Aβ deposition suggested that self-evaluation of cognitive function may be more associated with Aβ than scores on objective memory tests in the pre-clinical state. Our fMRI results suggested that emerging dementia may affect conflict-monitoring/control regions (Figure 3). These may suggest that elevated internal conflict of prediction error may account for subjective concern. Education appeared to moderate these associations (i.e., cognitive reserve).

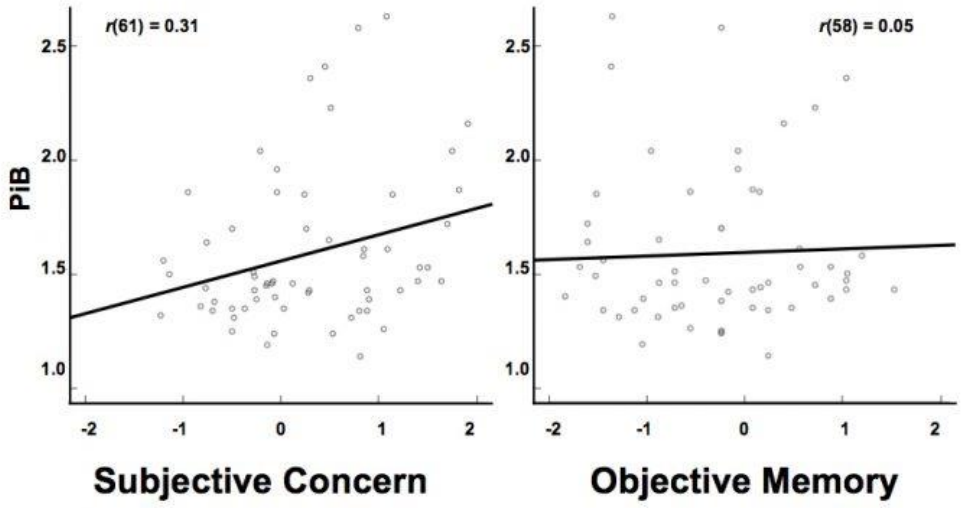

Figure 1. PiB was positively associated with subjective concern scores [left: p= $r(61)=0.31$, $p=0.01$], but not with objective scores [right: $r(58)=0.05$, $p=0.74$].

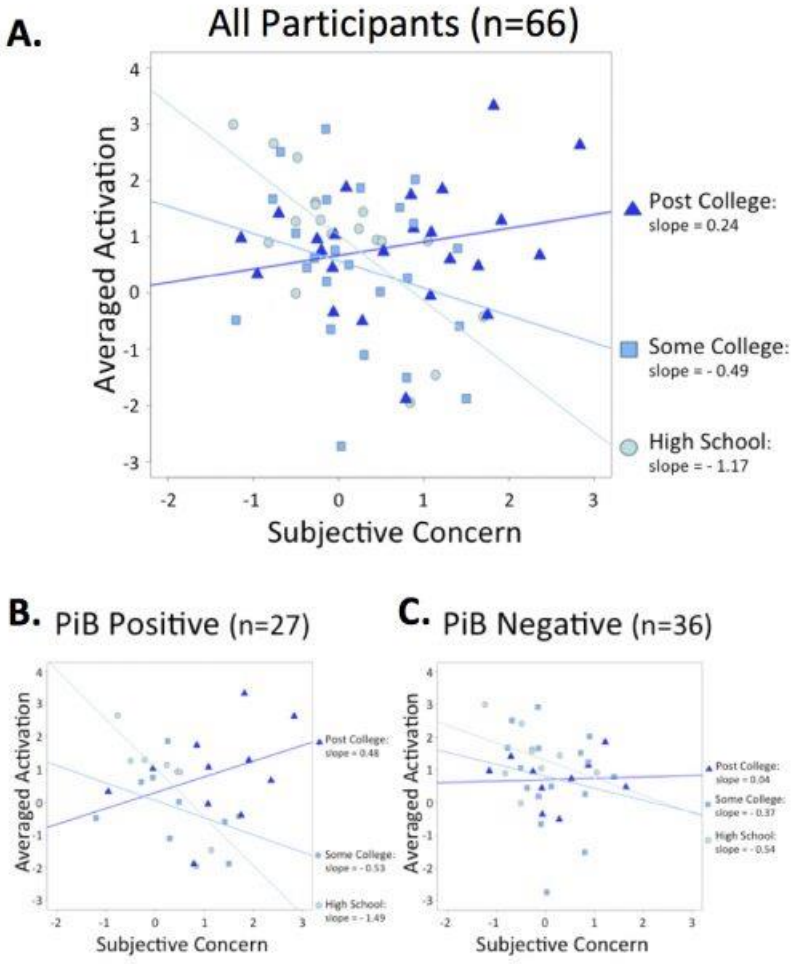

Figure 2. A) activations in conflict monitoring/control regions (salience networks and executive control networks) depended on the level of subjective concern and level of education. To visualize the interaction, we plotted the results by categorizing education levels into several groups using common educational stage cut-offs ("High School"=12, 12<"Some College"≤16, and "Post College">16). B-C) repeated the same analysis for PiB positive (B) and negative (C) participants separately. Significant interaction was found among participants in PiB positive (B) but not in PiB negative (C).

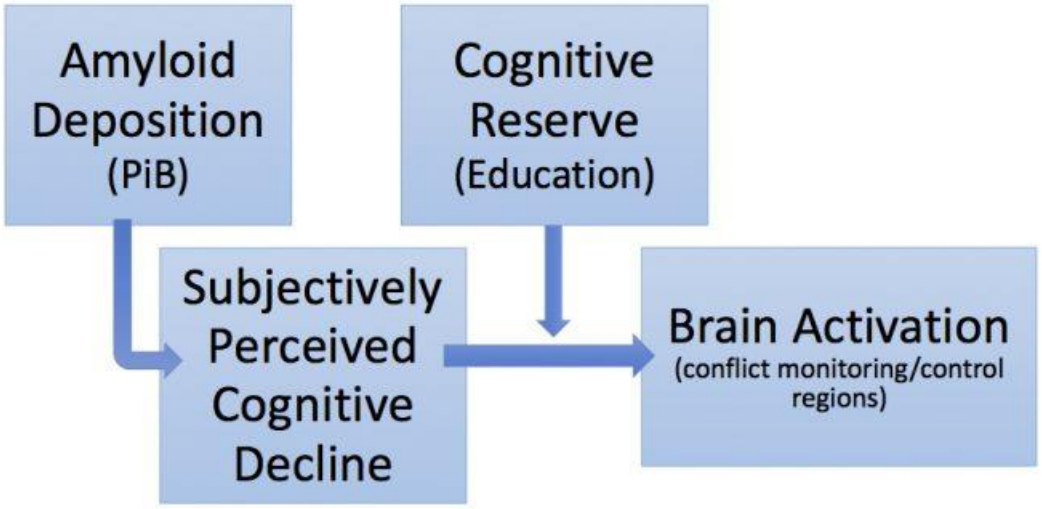

Figure 3. Schematic model of the overall results. From left: amyloid level was significantly associated with subjectively perceived cognitive decline (i.e., subjective concern). Amyloid level was not directly associated with brain activation. Right side: education level moderated the relationship between subjective concern level and activation in conflict monitoring/control regions. This moderation effect is consistent with the theory of cognitive reserve.

Keywords: Subjective Cognitive Concern, PiB, fMRI, Conflict Monitoring, Cognitive Reserve

P76: How useful is amyloid PET in clinical diagnosis? A systematic review and meta-analysis

Enrico Fantoni[1], Anastasia Chalkidou[2,3], John O'Brien[4], Gill Farrar[1], Alexander Hammers[2,3]

[1]*GE Healthcare, Life Sciences, Amersham, United Kingdom*
[2]*King's Imaging Technology Evaluation Centre, St Thomas' Hospital, London, United Kingdom*
[3]*Division of Imaging Sciences and Biomedical Engineering, King's College London, London, United Kingdom*
[4]*Department of Psychiatry, University of Cambridge, Cambridge, United Kingdom*

Background: With availability of five tracers for imaging amyloid with PET, this diagnostic modality has gained traction in the clinical evaluation of patients with cognitive impairment (CI). This work is the first comprehensive meta-analysis of the existing literature on aPET use as adjunct for AD diagnoses.

Methods: This systematic review and meta-analysis covers clinical and research studies published in English between 2000 and 2017, which conformed to predetermined inclusion criteria. The impact of visual aPET imaging on differential diagnosis of CI subjects without prior FDG-PET or CSF sampling was assessed with respect to change in diagnosis before and after aPET imaging.

Results: 1142 patients from 7 studies met the inclusion criteria [1–7]. Amyloid PET results discrepant from pre-aPET diagnoses were found in 31.5% of AD cases and 39.9% of non-AD cases, leading to, respectively, 86.4% and 74.1% average diagnostic change in these cases. Amyloid PET results concordant with pre-aPET diagnoses resulted in over 99% diagnostic confirmation rate and in diagnostic confidence increases. Overall, analysis suggests that 93.6% of final diagnoses reflect aPET outcomes and 31.3% of diagnoses are changed following aPET due to discrepant pre-aPET diagnosis.

Conclusion: This meta-analysis shows that aPET use significantly impacted diagnostic decision-making by helping physicians to ascertain or rule out AD in 93.6% of patients. The utility of aPET integrated with other imaging modalities and/or in selected populations and with respect to patient management is being explored as an extension of this analysis.

References:

[1] Zwan *et al.,* Alzheimers Res Ther 2017:1–8.
[2] Boccardi *et al*., JAMA Neurol 2016;73:1417.
[3] Mitsis *et al.,* Mol Neurodegener 2014;9:10.
[4] Pontecorvo *et al*., Br Nucl Med Soc Spring Meet 2016;1:P42.
[5] Sanchez-Juan *et al.,* Neurology 2014;82:230.
[6] Ishii *et al*., Alzheimer's Assoc Int Conf 2016:P4.
[7] Grundman *et al.*, Alzheimer Dis Assoc Disord 2013;27:4.

Keywords: utility, PET, positron emission tomography, diagnostic impact, meta-analysis

P77: [18F]AV-1451 binds to an unidentified white matter target in semantic dementia

Jennifer Whitwell, Peter Martin, Christopher Schwarz, Joseph Duffy, Heather Clark, Mary Machulda, Hugo Botha, Jonathan Graff-Radford, David Jones, Rene Utianski, David Knopman, Ronald Petersen, Val Lowe, Clifford Jack, Keith Josephs

Mayo Clinic, Rochester, MN, US

Background: Semantic dementia is a distinct neurodegenerative disease characterized clinically by the loss of conceptual knowledge pertaining to the meaning of words and objects. Semantic dementia is associated with focal atrophy of bilateral anterior medial temporal lobe structures and shows a distinct pathology related to the RNA binding protein, TDP-43. The relationship between semantic dementia and other proteins, such as beta-amyloid and paired helical filament tau, is unknown. We study beta-amyloid and paired helical filament tau in semantic dementia using molecular neuroimaging.

Methods: Eleven study participants with a clinical diagnosis, and neuroimaging characteristics, of semantic dementia were recruited into an NIH-funded study and underwent Pittsburgh Compound B (PiB) and [18F]AV-1451 PET scans. The presence of beta-amyloid deposition was assessed using a global PiB standard uptake value ratio and a cut-point of 1.42. Regional patterns of [18F]AV-1451 uptake were assessed in the whole cohort compared to 76 matched healthy controls, and patterns of uptake were compared between PiB positive and negative participants.

Results: Compared to controls, semantic dementia participants exhibited elevated [18F]AV-1451 uptake in the grey and white matter of the anterior medial temporal lobe regions including the temporal pole, inferior and middle temporal gyri, fusiform gyri, amygdala, parahippocampal gyri and entorhinal cortices (Figure 1). When beta-amyloid deposition was taken into account, we observed higher uptake in bilateral temporal pole, and entorhinal and lateral temporal cortices, in PiB-positive participants (n=5) compared to PiB-negative participants (n=6) (Figure 2). In PiB-negative participants, uptake was mainly located in white matter.

Conclusions: [18F]AV-1451 uptake in semantic dementia may be driven by two different processes. First, in the absence of beta-amyloid, [18F]AV-1451 uptake appears to be associated with an unidentified target in the white matter. Secondly, in the presence of beta-amyloid, a component of [18F]AV-1451 uptake may be related to binding to paired helical filament tau.

Figure 1: Patterns of [18F]AV-1451 uptake in semantic dementia compared to controls. Results cluster level corrected at p<0.05.

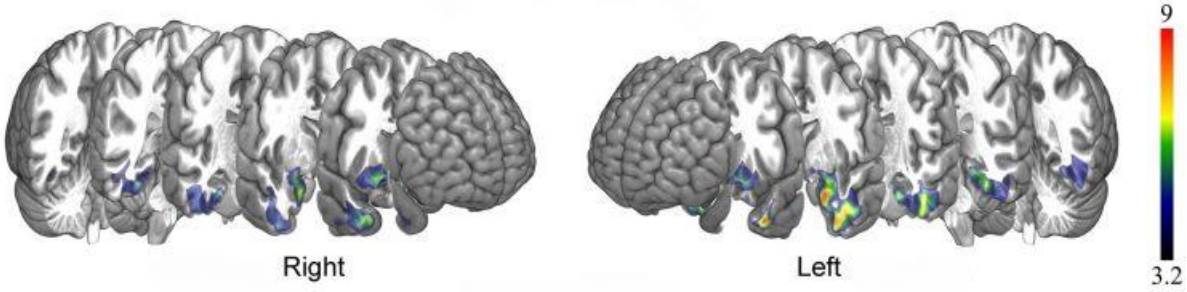

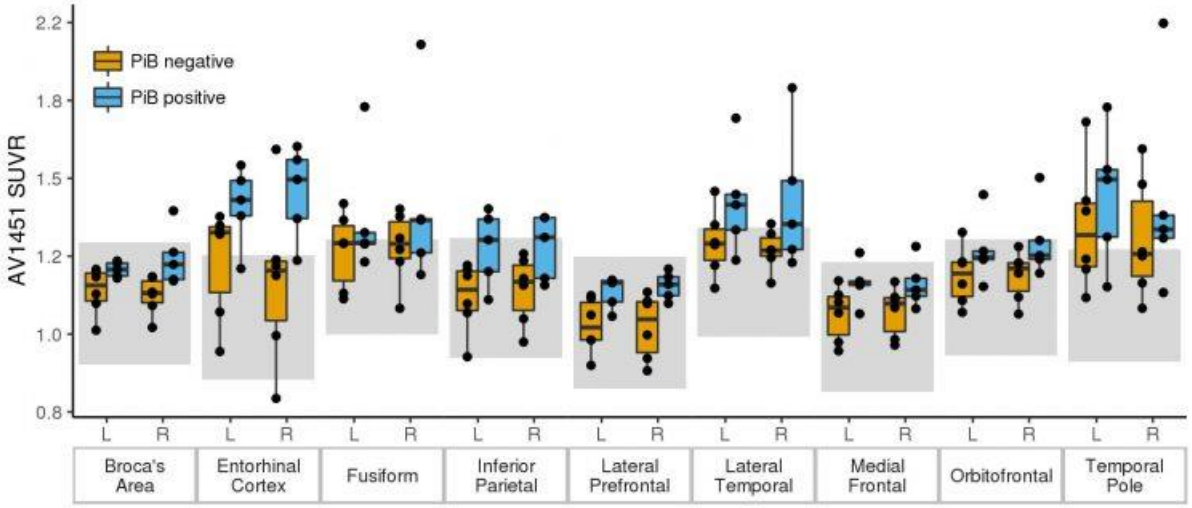

Figure 2: Boxplots of AV1451 uptake by region and hemisphere. Within each region, a grey blush is drawn to cover roughly 95% of a cognitively normal, PiB negative control population.

Keywords: AV-1451, tau, PET, semantic, primary progressive aphasia

P78: Quantifying stages of subtle memory impairment in clinically normal older adults

Kate Papp[1], Elizabeth Mormino[2], Ellen Grober[3], Reisa Sperling[1], Keith Johnson[4], Dorene Rentz[1]

[1]*Brigham and Women's Hospital, Boston, MA, US*
[2]*Stanford Medicine, Palo Alto, CA, US*
[3]*Albert Einstein College of Medicine, New York, NY, US*
[4]*Massachusetts General Hospital, Boston, MA, US*

Background: Quantifying the temporal unfolding of memory impairment in clinically normal (CN) is vital. The Free and Cued Selective Reminding Test (FCSRT) allows for the quantification of subtle retrieval difficulties to frank memory storage impairment, and may be useful to identify CN individuals at risk for future decline.

Methods: We examined 173 CN participants (CDR=0) with amyloid (Aβ) (PiB) and tau (Flortaucipir) PET. Participants were grouped into stages of objective memory impairment (SOMI) using FCSRT performance. SOMI Stage 0 was defined as Free Recall>30 and Total Recall>46, Stage 1 was Free Recall 25-30 and Total Recall>46, and Stage 2 was collapsed as either Free Recall 20-24 and Total Recall>44 or Total Recall 33-43 regardless of Free Recall score. SOMFig 1I group differences in PET markers were explored.

Results: A total of 65% were classified as SOMI Stage 0, 22% were Stage 1, 7% were Stage 2+ and 6% were unclassified (e.g., very low Free Recall with preserved Total Recall). A linear fit across Stage 0 to 2 was trend level for Aβ (p=0.060, Fig1) and significant for IT (p=0.001, Fig2) and Entorhinal Tau (p=0.006, Fig3). Post-hoc contrasts revealed that Stage 1 had significantly higher levels of IT Tau compared with Stage 0 (p=0.043), and that Stage 2 exhibited greater IT tau burden compared with Stage 0 (p=0.009). The unspecified group had IT tau levels comparable to Stage 2 and statistically greater than Stage 0 (p=0.000) and Stage 1 (p=0.025). A similar but less robust pattern was observed with entorhinal Tau whereby the Stage 2 (p=0.007) and unspecified groups (p=0.001) had high Tau compared with Stage 0.

Conclusions: Staging of memory impairment using SOMI categories amongst clinically normal individuals on the FCSRT can help identify those Aβ+ individuals at greatest risk for elevated tau, an ideal population for secondary prevention.

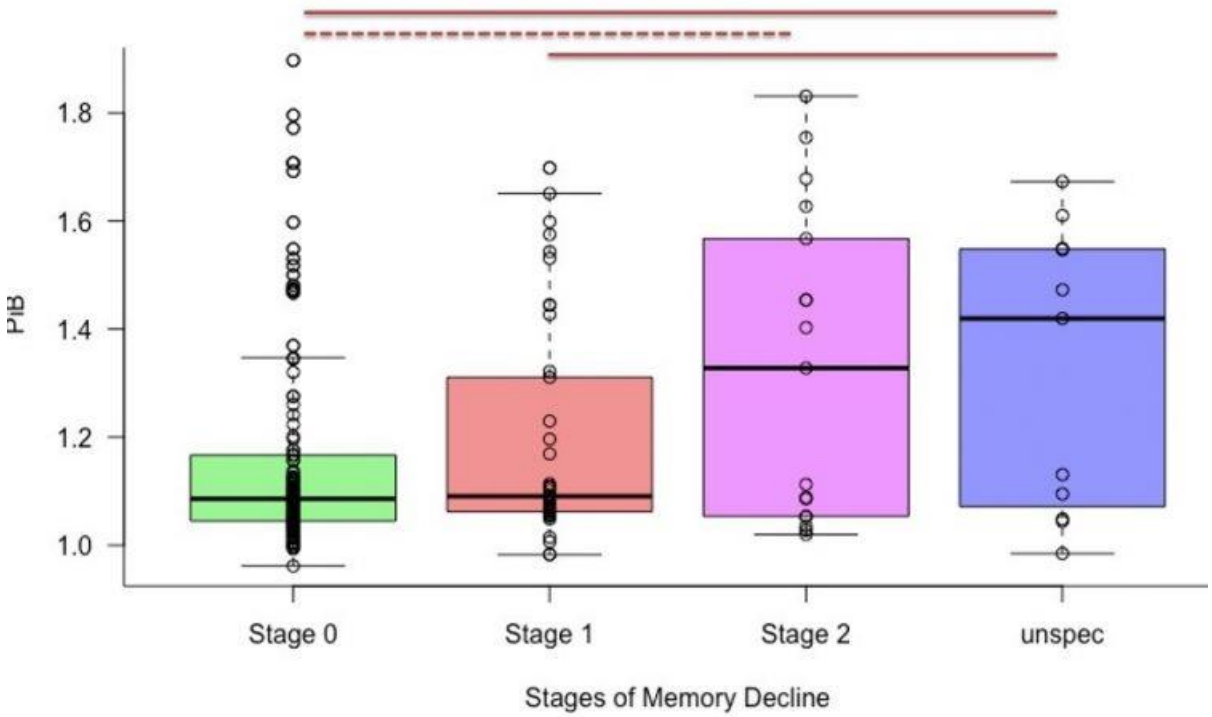
PiB
1.8
1.6
1.4
1.2
1.0
Stage 0
Stage 1
Stage 2
unspec
Stages of Memory Decline

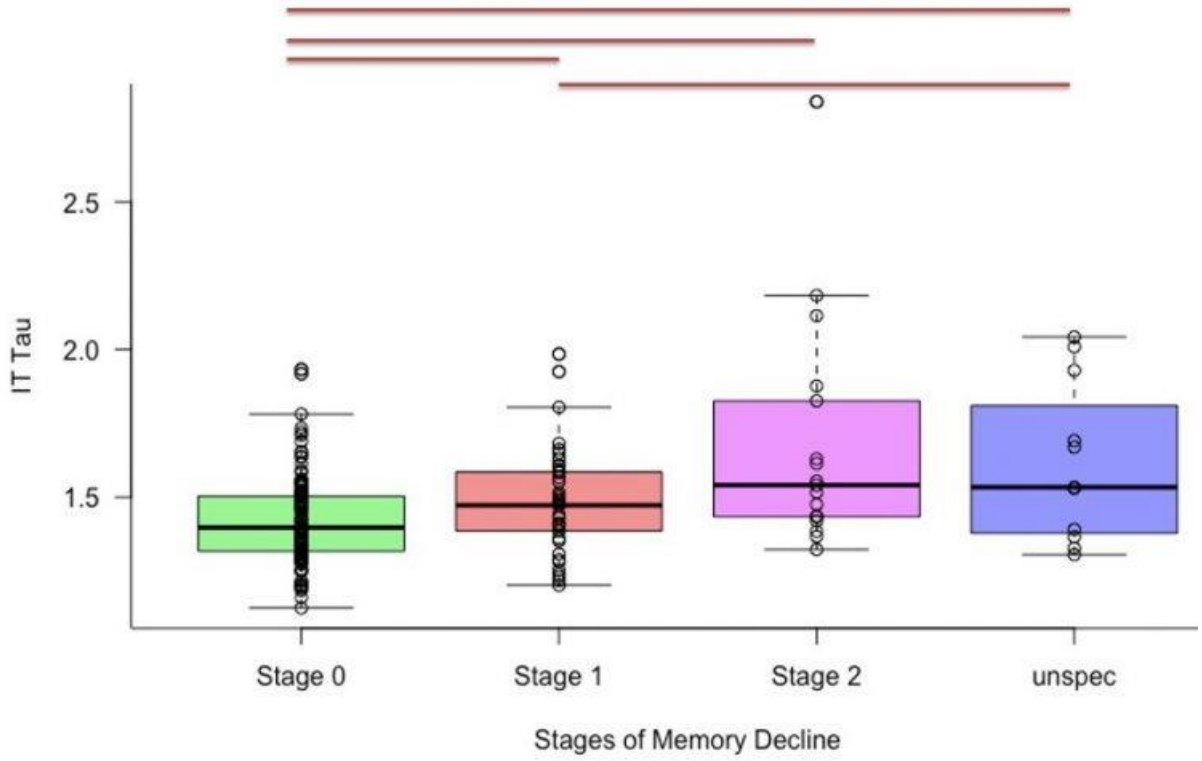
IT Tau
2.5
2.0
1.5
Stage 0
Stage 1
Stage 2
unspec
Stages of Memory Decline

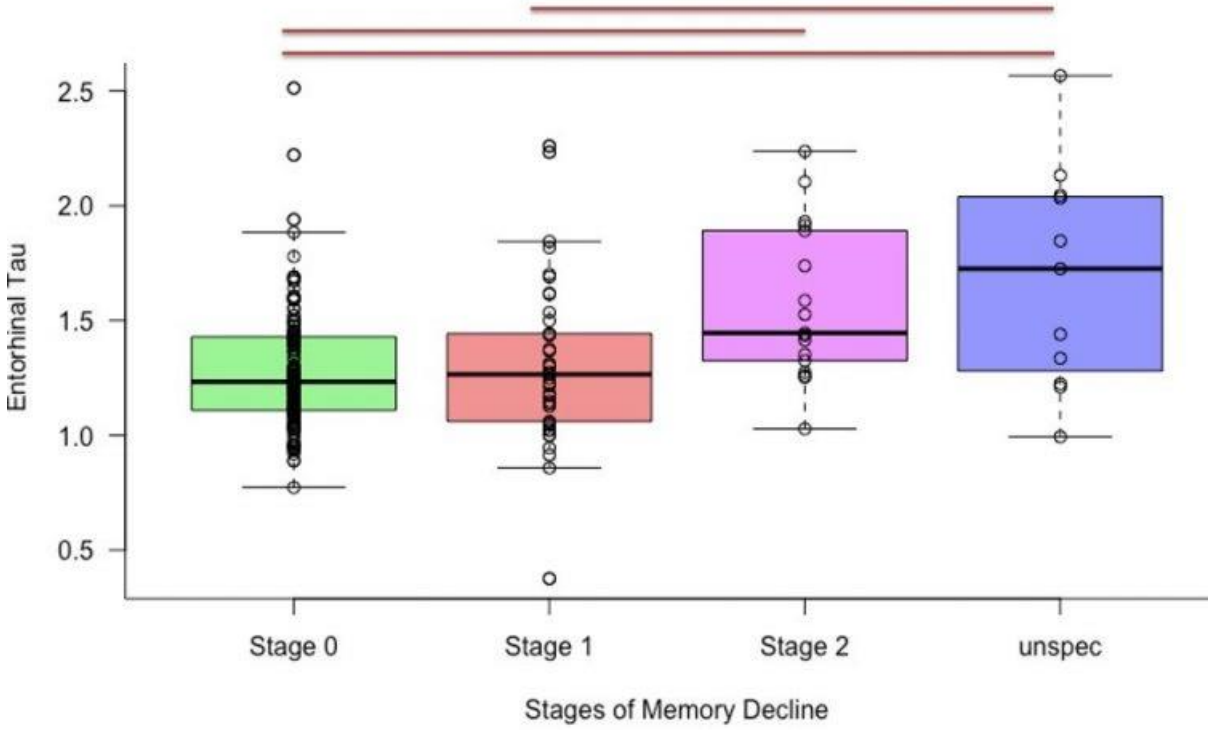

Keywords: memory, amyloid, tau

P79: The relationship between amyloid deposition and both global and hippocampal atrophy

Samantha Allison, Sara Berman, Lindsay Clark, Bradley Christian, Tobey Betthauser, Jennifer Oh, Sanjay Asthana, Barb Bendlin, Sterling Johnson

University of Wisconsin School of Medicine and Public Health, Madison, WI, US

During preclinical Alzheimer's disease (AD), initial elevations in amyloid levels lead to aggregated neurofibrillary tangles, causing neuronal death that cumulatively manifests as atrophy on MRI. Given this hypothesized time course, we may expect to see a relationship between initial levels of amyloid deposition and cerebral atrophy over time in cognitively healthy individuals in late mid-life. Therefore, the purpose of this study was to examine whether baseline amyloid deposition is associated with both global and hippocampal atrophy over time. Participants were 161 cognitively normal late middle-aged adults (mean age=61.42; SD=6.44). Amyloid deposition was imaged using Positron Emission Tomography (PET) with [C-11]Pittsburgh Compound B (PiB). Volumetric estimates for the hippocampus were obtained using FSL FIRST, and volumes of CSF and brain tissue were derived in SPM12. Each participant had two structural MRI scans (average time between scans=4.30 years, SD=1.67) and one PET-PiB scan at the time of the first MRI scan. To examine change over time, regression analyses with the most recent scan as the outcome variable, controlling for both age and baseline scan, were conducted in SPSS. Baseline amyloid deposition was associated with an increase in global atrophy defined as the ratio of CSF to brain volume (β=.079; p=.024; see figure below), but not hippocampal atrophy (β=.017; p=.638). These findings fit with the existing literature concerning the temporal course of AD with amyloid deposition occurring first and changes in brain structure occurring later. Interestingly, PiB was only associated with global, but not hippocampal, volumetric decline. That these findings were detectible at late middle-age may be particularly important for predicting cognitive outcome and for selecting participants for prevention trials.

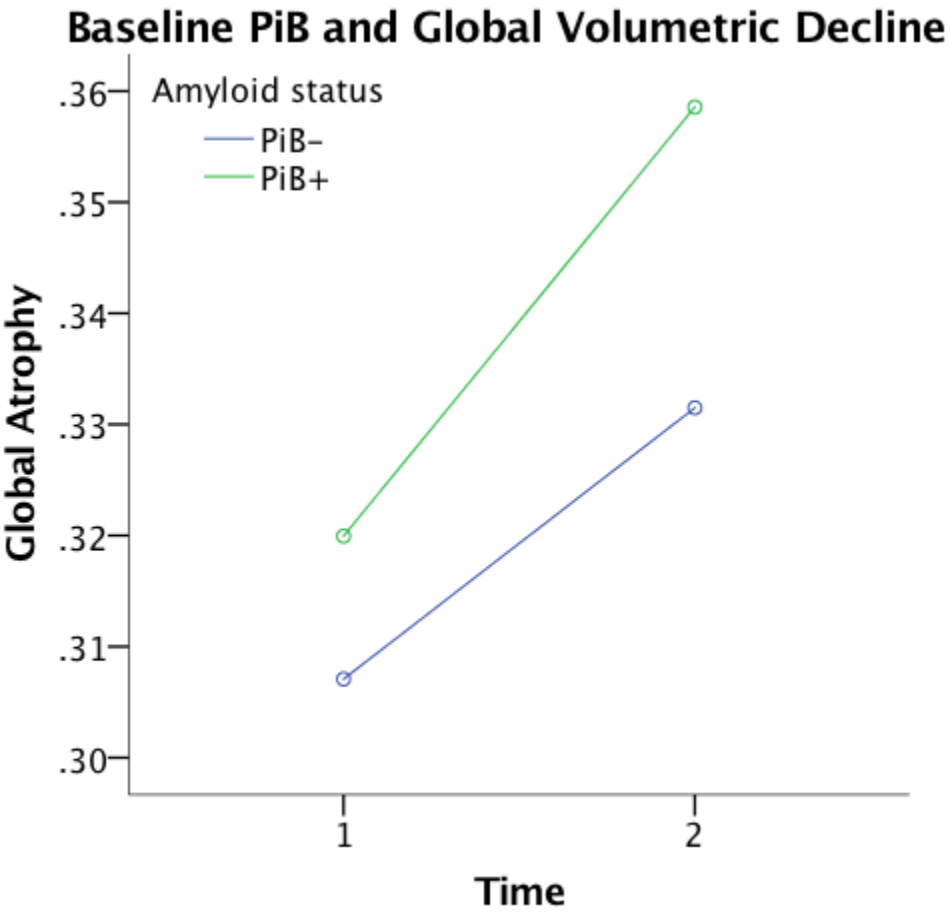

Keywords: PiB, amyloid, global atrophy, hippocampal atrophy

P80: AV1451-PET measurements show substantial overlap across diagnostic groups and amyloid status

Susan Landau[1,2], Deniz Korman[1,2], William Jagust[1,2]

[1]*University of California, Berkeley, Berkeley, CA, US*
[2]*Lawrence Berkeley National Laboratory, Berkeley, CA, US*

Objectives: Although tau is strongly linked to cognition, considerable overlap of tau-PET measurements across cognitively normal and AD subjects has been observed in limited samples. Here we examined this overlap as well as tau-cognition associations in a broad sample using several AV1451-PET quantification methods.

Methods: We examined 194 subjects from the Alzheimer's Disease Neuroimaging Initiative (106 cognitively normal, 34 early MCI, and 54 late MCI/AD) who had concurrent AV1451-PET and amyloid-PET scans, and a cognitive assessment. AV1451-PET images were quantified using mean uptake in medial temporal (MTL), inferolateral, and extra-temporal neocortical regions that approximate Braak staging, as well as a peak region approach designed to capture individual differences in the locations of maximum uptake.

Results: Across the entire sample, amyloid positivity and clinically impaired diagnosis (LMCI/AD) was associated with higher AV1451-PET. Examining diagnostic groups separately, however, we observed considerable variability in AV1451-PET such many EMCI and LMCI/AD subjects overlapped with amyloid-normals (Figure 1), particularly in neocortical regions. Specifically, 30-50% of amyloid+ MCI and AD patients had SUVRs at and below the 90th percentile of amyloid- cognitively normal subjects (Figure 2). Finally, although memory was strongly associated with MTL AV1451 across the entire sample, tau in the low to moderate range was minimally predictive of memory performance. For example, among subjects with MTL SUVR $\leq$ 1.42 (the 90th percentile of amyloid- normals), there was no relationship between AV1451 and AVLT Free Recall scores (Figure 3). We observed similar relationships using an individual peak region approach.

Conclusion: AV1451-PET SUVRs of one third to one half of amyloid+ MCI and AD patients overlap with amyloid- normals. Consistent with this, low to moderate AV1451-PET was not related to cognition. This overlap poses a challenge for dichotomous categorization and for understanding the role of tau in cognitive impairment.

Figure 1

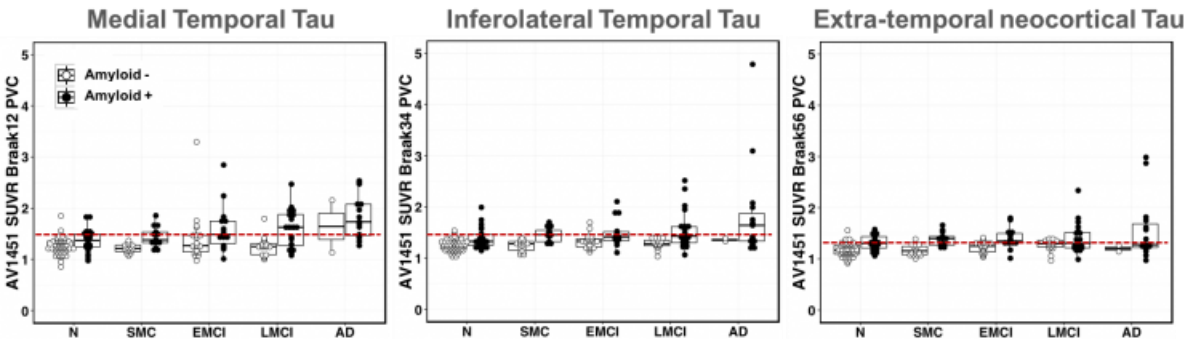

Figure 2

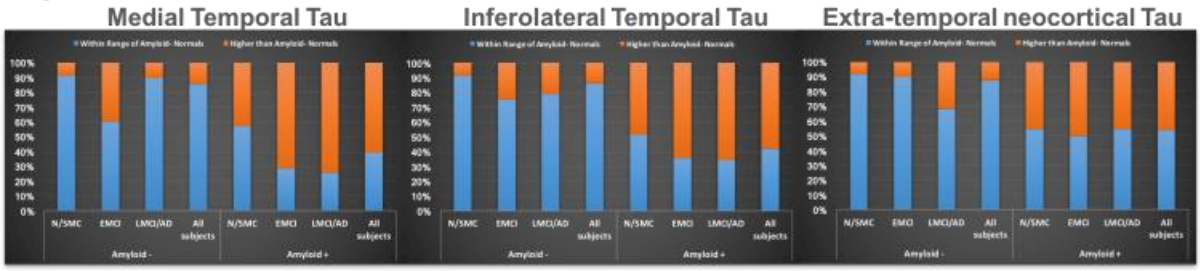

Figure 3

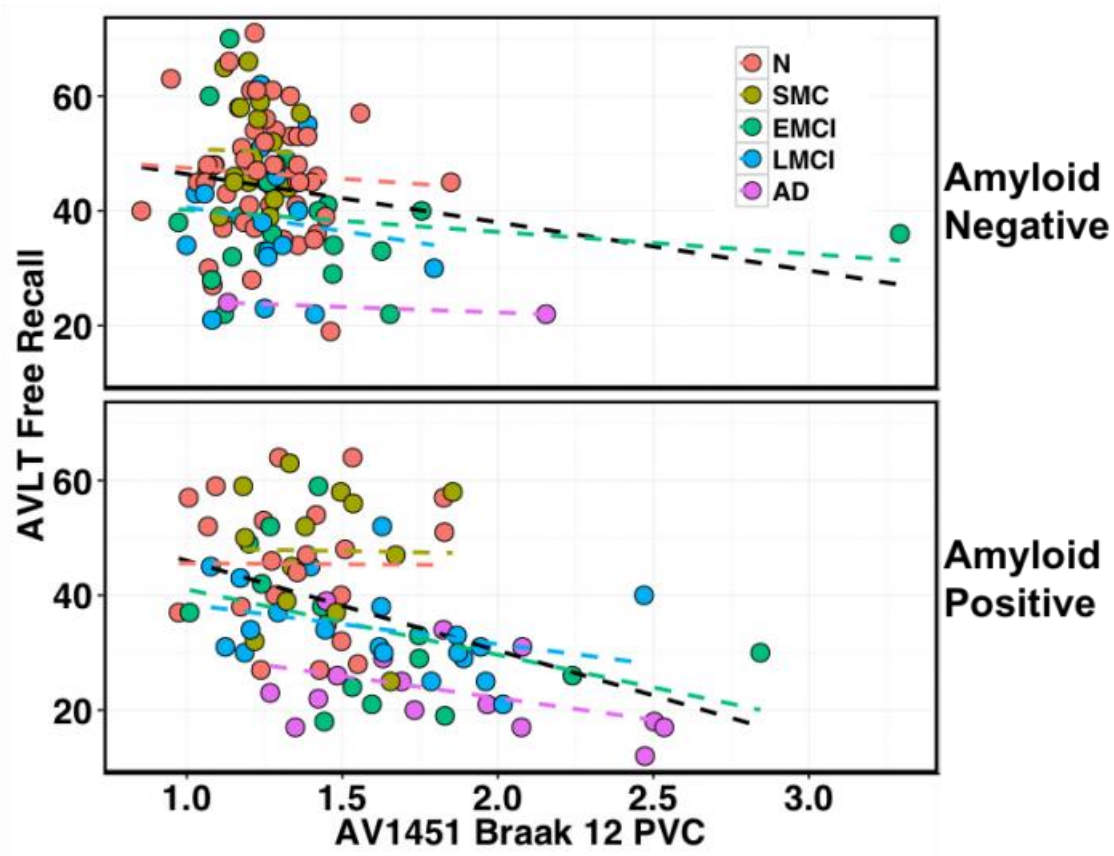

Keywords: tau, cognition, normal aging

P81: Shrinking cortex and tau burden in the aphasic variant of Alzheimer's disease

Adam Martersteck[1,2], Jaiashre Sridhar[2], Allison Rainford[2], M.-Marsel Mesulam[2,3], Emily Rogalski[2]

[1]*Department of Radiology, Northwestern University Feinberg School of Medicine, Chicago, IL, US*
[2]*Cognitive Neurology and Alzheimer's Disease Center, Northwestern University Feinberg School of Medicine, Chicago, IL, US*
[3]*Department of Neurology, Northwestern University Feinberg School of Medicine, Chicago, IL, US*

Background: Primary progressive aphasia (PPA) is a clinical dementia syndrome often characterized by asymmetric atrophy of the language-dominant (usually left) hemisphere. Common neuropathologies reported for PPA include Alzheimer disease (AD) or a form of frontotemporal lobar degeneration. In line with post-mortem studies of neurofibrillary tangles, early cross-sectional studies examining flortaucipir tau PET (^{18}F-AV-1451) in AD have reported a close relationship with atrophy.

Objective: Determine if elevated flortaucipir PET signal correlated with cross-sectional and longitudinal cortical atrophy in an atypical form of AD.

Methods: Seven participants with PPA and suspected underlying Alzheimer's disease pathology (PPA-AD^{bio+};^{18}F-florbetapir whole-cerebellar SUVR > 1.17) underwent flortaucipir PET imaging and structural MR imaging. Furthermore, four underwent longitudinal MRI (mean 2.04 years apart). Freesurfer (FS) v6.0.0 was used to reconstruct the T_1-weighted MRI scan, calculate atrophy (grey volume), and for Müller-Gärtner modified partial volume correction (PVC). Thirty-five normal controls were used to calculate atrophy z-scores. The annualized symmetrized percent change in atrophy, cross-sectional atrophy z-score, and cerebellar grey SUVR tau PET load was measured in 68 regions from the left and right hemisphere Desikan-Killiany atlas in subject native space.

Results: Cross-sectional atrophy and PVC flortaucipir in the 68 regions for seven PPA-AD^{bio+} was strongly correlated, r(474)=-0.450, $p < 0.0001$. The annualized percent change in cortical volume had a similar negative correlation with PVC tau PET signal in four PPA-AD^{bio+} participants, r(270)=-0.471, $p < 0.0001$. Correlations repeated using non-PVC tau PET data remained highly significant (r=-0.430 for cross-sectional atrophy and r=-0.468 for longitudinal, both $p < 0.0001$).

Conclusions: A preliminary study of flortaucipir tau PET and longitudinal atrophy in an atypical form of AD supports the close relationship found in previous cross-sectional studies. A more extensive evaluation with a larger sample will be required to determine the robustness of these early results.

Keywords: primary progressive aphasia, AV-1451, flortaucipir, structural MRI, atrophy

P82: Cross-sectional associations between tau pathology burden measured by [18F]GTP1 PET imaging and cognition in AD adjusting for amyloid PET and cortical atrophy

Michael Ward, Paul Manser, Edmond Teng, Sandra Sanabria-Bohorquez, Rebecca Ray, Suzanne Baker, Geoff Kerchner, Robby Weimer

Genentech, Inc., South San Francisco, CA, US

[^{18}F]GTP1 is a tau PET tracer being developed to assess tau pathology in Alzheimer's disease (AD). [^{18}F]GTP1 and Amyvid PET images, volumetric MRI and cognitive measures (MMSE, ADAS-Cog13, RBANS, CDR-SB) were collected in an ongoing natural history study from amyloid-positive prodromal (MMSE 24-30, CDR = 0.5), mild (MMSE 22-30, CDR 0.5 or 1) or moderate (MMSE 16-21, CDR 0.5 or 1 or 2) AD patients, aged 50-85. Using baseline data from 51 AD subjects, we evaluated cross-sectional associations among tau pathology burden [whole-cortical gray (WCG) [^{18}F]GTP1 SUVR], overall β-amyloid burden (composite amyloid SUVR), MRI-based atrophy, and cognitive performance.

Cross-sectional associations between WCG [^{18}F]GTP1 SUVR and cognitive performance were first modeled using simple linear regression. WCG [^{18}F]GTP1 SUVR explained a small-to-moderate amount of variance in cognitive measures (MMSE: Adj R^2=0.14, CDR-SB: Adj R^2=0.08, RBANS Total: Adj R^2= 0.24, ADAS-Cog13: Adj R^2=0.16). MRI-based cortical atrophy explained a similar amount of variance in cognitive measures: (MMSE: Adj R^2=0.16, CDR-SB: Adj R^2=0.12, RBANS Total: Adj R^2= 0.13, ADAS-Cog13: Adj R^2=0.15). All regression coefficients were nominally significant ($p<0.05$).

Multiple linear regression adjusting for overall β-amyloid burden, MRI-based cortical atrophy, and patient age was then performed to assess the relationship between cognitive performance and WCG [^{18}F]GTP1 SUVR after accounting for these covariates. Adjusted R^2 values from multiple regression were generally higher than those from simple linear regression: (MMSE: Adj R^2=0.19, CDR-SB: Adj R^2=0.17, RBANS Total: Adj R^2= 0.23, ADAS-Cog13: Adj R^2=0.28). Wald tests for WCG [^{18}F]GTP1 SUVR were nominally significant ($p<0.05$) for all cognitive measures. No other covariates were consistently significant, though increasing patient age was associated with higher CDR-SB and ADAS-Cog13 scores.

[^{18}F]GTP1 Imaging is significantly associated with broad-based cognitive performance measures, even after accounting for key biological covariates.

Keywords: [18F]GTP1, tau PET, Cognition, Atrophy, Alzheimer's disease

P83: Cognition and [18F]-Florbetaben PET imaging of amyloid in Parkinson's disease

Megan Stark[1,3], Tracy Melzer[1,2,3], Ross Keenan[3,6], Daniel Myall[3], Guneet Kaur[3], Leslie Livingston[1,3], Kyla Horne[3,4], Steven Marsh[5], Sophie Grenfell[3], Bob Young[3], Michael MacAskill[1,3], John Dalrymple-Alford[1,2,3,4], Tim Anderson[1,2,3,7]

[1]*Department of Medicine, University of Otago, Christchurch, New Zealand*
[2]*Brain Research New Zealand - Rangahau Roro Aotearoa, Centre of Research Excellence, Auckland, New Zealand*
[3]*New Zealand Brain Research Institute, Christchurch, New Zealand*
[4]*Department of Psychology, University of Canterbury, Christchurch, New Zealand*
[5]*Department of Physics and Astronomy, University of Canterbury, Christchurch, New Zealand*
[6]*Pacific Radiology, Christchurch, New Zealand*
[7]*Neurology Department, Christchurch Hospital, Christchurch, New Zealand*

Cognitive decline in Parkinson's disease (PD) leads to dementia (PDD) in over 80% of cases. Recent work suggests that misfolded beta-amyloid protein, a pathological hallmark of Alzheimer's disease (AD), may also contribute to the multifactorial neuropathology of PDD. We therefore examined cortical amyloid accumulation in 108 individuals with PD, using 18F-Florbetaben positron emission tomography. Patients with mild cognitive impairment (PD-MCI) were targeted, as they are known to be at high risk of developing PDD. Prior to scanning, cognitive status was determined using a comprehensive neuropsychological battery. Participants were classified as having PD with normal cognition (PD-N; n=20), PD-MCI (n=72), or PDD (n=16).

We found that clinical positivity for amyloid was higher in the PDD group (38% [6/16]) than in the PDN (20% [4/20]) and PD-MCI (15% [11/72]) groups. However, age was found to be the primary driving factor behind amyloid load, rather than any effect of amyloid on cognitive ability. Furthermore, voxel-wise analysis revealed no spatial association between amyloid deposition and global cognitive ability. Amyloid deposition may be a factor in some patients, however the low prevalence of amyloid in the PD-MCI and PDD groups compared with that seen in amnestic MCI (~50-70%) and in AD dementia (~80-95%) indicates that alternative pathologies, such as alphasynucleinopathy and tauopathy, predominate in cognitively impaired PD patients.

Keywords: Parkinson's disease, cognition, amyloid, positron emission tomography, florbetaben

P84: Increased central arterial stiffening relates to CSF markers of tau aggregation and neurodegeneration in the oldest-old

Francis E. Cambronero[1], Dandan Liu[2], Elizabeth E. Moore[1], Michelle Babicz[1], Timothy J. Hohman[1], Katherine A. Gifford[1], Susan P. Bell[3], Lealani M. Acosta[1], James G. Terry[4], Sangeeta Nair[4], Thomas J. Wang[3], John J. Carr[4], Kaj Blennow[5], Henrik Zetterberg[5,6], Angela L. Jefferson[1]

[1]*Vanderbilt Memory & Alzheimer's Center, Vanderbilt University Medical Center, Nashville, TN, US*
[2]*Department of Biostatistics, Vanderbilt University Medical Center, Nashville, TN, US*
[3]*Division of Cardiovascular Medicine, Department of Medicine, Vanderbilt University Medical Center, Nashville, TN, US*
[4]*Department of Radiology and Radiological Sciences, Vanderbilt University Medical Center, Nashville, TN, US*
[5]*Department of Psychiatry and Neurochemistry, Institute of Neuroscience and Physiology, The Sahlgrenska Academy at University of Gothenburg, Mölndal, Sweden*
[6]*Department of Molecular Neuroscience, UCL Institute of Neurology, Queen Square, London, United Kingdom*

Background: Age-related central arterial stiffening is increasingly associated with worse brain health, but most studies emphasize cerebrovascular mechanisms. Far less is known about arterial stiffness associations with Alzheimer's disease pathological mechanisms and whether these associations are affected by advanced aging. In this study, we relate a gold-standard measurement of arterial stiffening, aortic pulse wave velocity (PWV), to cerebrospinal fluid (CSF) markers of amyloid deposition (Ab_{42}), phosphorylated tau aggregation (p-tau), neurodegeneration (tau), and axonal injury (neurofilament light, NFL).

Methods: Using the Vanderbilt Memory & Aging Project (MAP) cohort, we examined 146 cognitively normal, at-risk, and mild cognitive impairment participants. PWV was quantified on cardiac magnetic resonance in the proximal aorta, where pulsatile flow is buffered. CSF was acquired via lumbar puncture. Linear regression models related PWV to CSF concentrations (ng/L) of Ab_{42}, p-tau, tau, and NFL adjusting for age, race/ethnicity, education, Framingham Stroke Risk Profile (including sex, systolic blood pressure, anti-hypertensive medication usage, diabetes, left ventricular hypertrophy, atrial fibrillation, and prevalent cardiovascular disease), body mass index, cognitive diagnosis, and apolipoprotein E e4 status. Secondary models tested a PWV x age interaction followed by stratification by age group (≤73 young-old, >73 oldest-old).

Results: PWV was unrelated to CSF biomarkers (p-values>0.30). However, there was an age interaction with PWV on tau (b=38.69, p=0.005) and p-tau (b=4.31, p=0.007). Age-stratified models revealed increased PWV related to more tau (b=19.34, p=0.045) and p-tau (b=2.38, p=0.036) pathology among the oldest-old.

Conclusions: Increased arterial stiffening is associated with *in vivo* biomarker evidence of tau aggregation and neurodegeneration in the oldest-old, perhaps due to accelerated vascular aging or increased cerebral vulnerability to worsening central compliance. Findings suggest management of arterial stiffness may have implications for abnormal tau aggregation with advancing age.

Keywords: arterial stiffness, tau, neurodegeneration, cerebrospinal fluid, Alzheimer's disease

P85: Alterations in memory self-appraisal are associated with elevated tau deposition in normal older adults

Federico d'Oleire Uquillas[1], Aaron P. Schultz[1,3], Heidi I.L. Jacobs[2,3], Bernard Hanseeuw[2,3,5], Rachel F. Buckley[2,3,6,7], Alvaro Pascual-Leone[8], Reisa A. Sperling[1,3,4], Keith A. Johnson[2,3,4], Patrizia Vannini[2,3,4]

[1]*Department of Neurology, Massachusetts General Hospital, Harvard Medical School, Boston, MA, US*
[2]*Department of Radiology, Massachusetts General Hospital, Harvard Medical School, Boston, MA, US*
[3]*Athinoula A. Martinos Center for Biomedical Imaging, Massachusetts General Hospital, Harvard Medical School, Charlestown, MA, US*
[4]*Department of Neurology, Brigham and Women's Hospital, Harvard Medical School, Boston, MA, US*
[5]*Department of Neurology, Saint-Luc University Hospital, Institute of Neuroscience, Université Catholique de Louvain, Brussels, Belgium*
[6]*Florey Institutes of Neuroscience and Mental Health, University of Melbourne, Melbourne, Australia*
[7]*Melbourne School of Psychological Science, University of Melbourne, Melbourne, Australia*
[8]*Berenson-Allen Center for Noninvasive Brain Stimulation, Beth Israel Deaconess Medical Center, Harvard Medical School, Boston, MA, US*

Introduction: Self-appraisal of memory performance is important for effective functioning. Patients with AD often overestimate their memory (also known as anosognosia). Previous work in young adults shows that regions susceptible to AD pathology are involved with memory self-appraisal. Here we investigated the association of *in-vivo* tau and amyloid with judgments-of-learning (JOL) measured in an fMRI face-name association task in normal older adults.

Methods: 91 adults (64%-Females; 65-92years-old; CDR=0) from the Harvard Aging Brain Study, underwent an fMRI experiment involving JOL ratings (JOL1: 'learned well', JOL2: 'learned not-so-well', JOL3: 'not-learned-at-all') immediately following encoding of face-name pairs. A measure of memory self-appraisal was calculated by subtracting percentage of JOL1 predictions from percentage of correct responses (0 indicates accurate memory self-appraisal, >0 indicates memory over-estimation, <0 indicates memory under-estimation). The JOL1>JOL3 fMRI contrast identified regions related with predicted learning success. Mean signal was extracted from 3mm-spheres around peaks of clusters qFDR<0.05 (uncorrected p=0.001), and used in linear regressions with fMRI activity as dependent, and entorhinal cortex Flortaucipir (EC-FTP, tau-PET) or neocortical PiB as continuous independent variables, separately. PET data was partial-volume corrected.

Results: Higher EC-FTP was related to overestimation of memory performance (β=17.38±8.25, p=0.038). Higher levels of activation (JOL1>JOL3) were found in prefrontal and temporo-parietal regions (Table1,Fig1). Associations were found between EC-FTP and activation in the anterior cingulate (β=-0.76±0.36, p=0.036), vmPFC (β=-1.41±0.46, p=0.003), precuneus (β=-1.44±0.42, p=0.0009), pallidum (β=-0.64±0.26, p=0.015), and insula (β=-0.47±0.21, p=0.027), such that higher levels of tau were related to lower neural activity during predicted learning success (Fig2). Neocortical PiB did not relate to behavioral or functional activity in any region.

Conclusions:
In normal older individuals, memory self-appraisal engages a brain network commonly affected in AD. Tau, but not amyloid pathology, is associated with behavioral and functional alterations of memory self-appraisal, suggesting incipient anosognosia building up in the preclinical AD stages.

Table 1. Brain regions associated with predicted learning success

Study Task	MNI coordinates x	y	z	T/F-Stat		Region
JOL1 > JOL3	-9	38	23	5.3093	L	Anterior cingulate
	12	44	14	4.2012	R	Anterior cingulate
	3	-64	32	5.2698	R	Precuneus
	-3	-44.5	17	4.6349	L	Post-cingulate
	-30	-22	-7	4.9218	L	Hippocampus
	21	-13	-7	4.3746	R	Hippocampus
	-6	53	-10	4.6175	L	vmPFC
	24	-4	-1	4.1966	R	Pallidum
	27	26	-4	4.3376	R	Insula

Only clusters of 30 or more voxels and a significance of qFDR<0.05 (uncorrected p=0.001) are reported. JOL1, Judgement-of-learning-1='learned well'; JOL3, Judgement-of-learning-3='not-learned-at-all'; vmPFC, ventromedial prefrontal cortex; L, left; R, right.

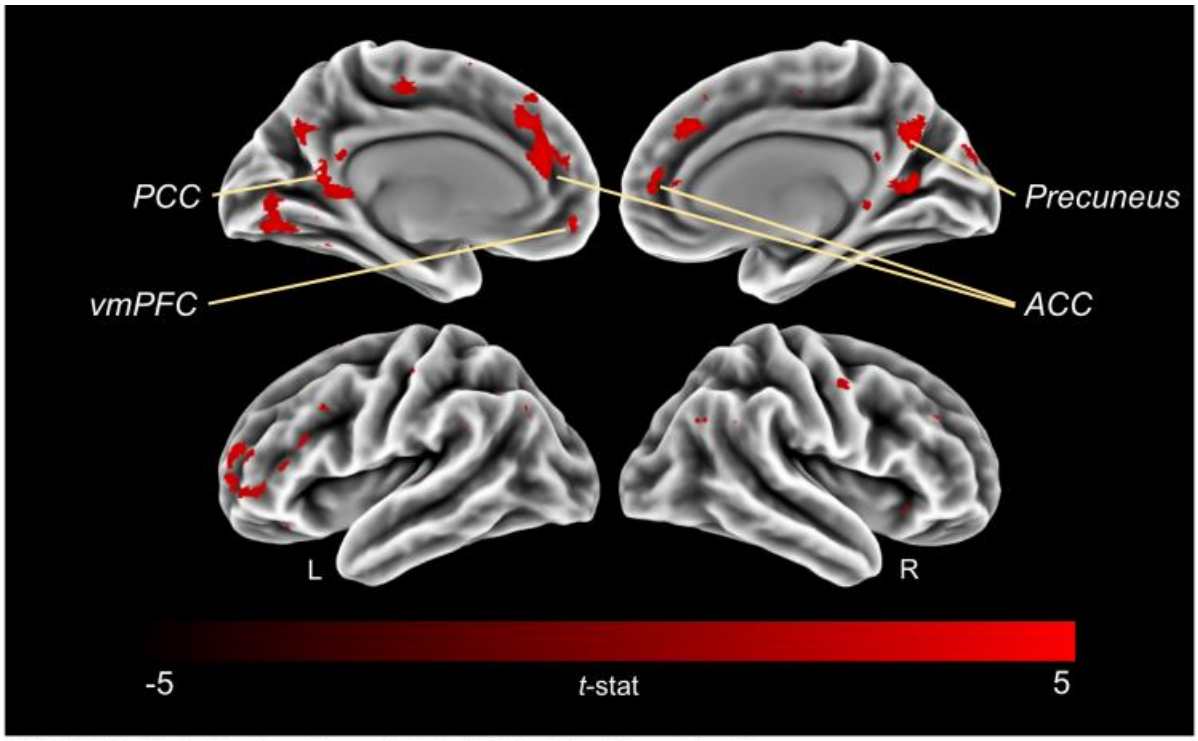

FIGURE 1: Brain Regions Associated with Predicted Learning Success
Regions showing greater responses for JOL1 than JOL3 (JOL1>JOL3, qFDR<0.05, uncorrected p=0.001). ACC, anterior cingulate cortex; PCC, posterior cingulate cortex; vmPFC, ventro-medial prefrontal cortex; L, left; R, right.

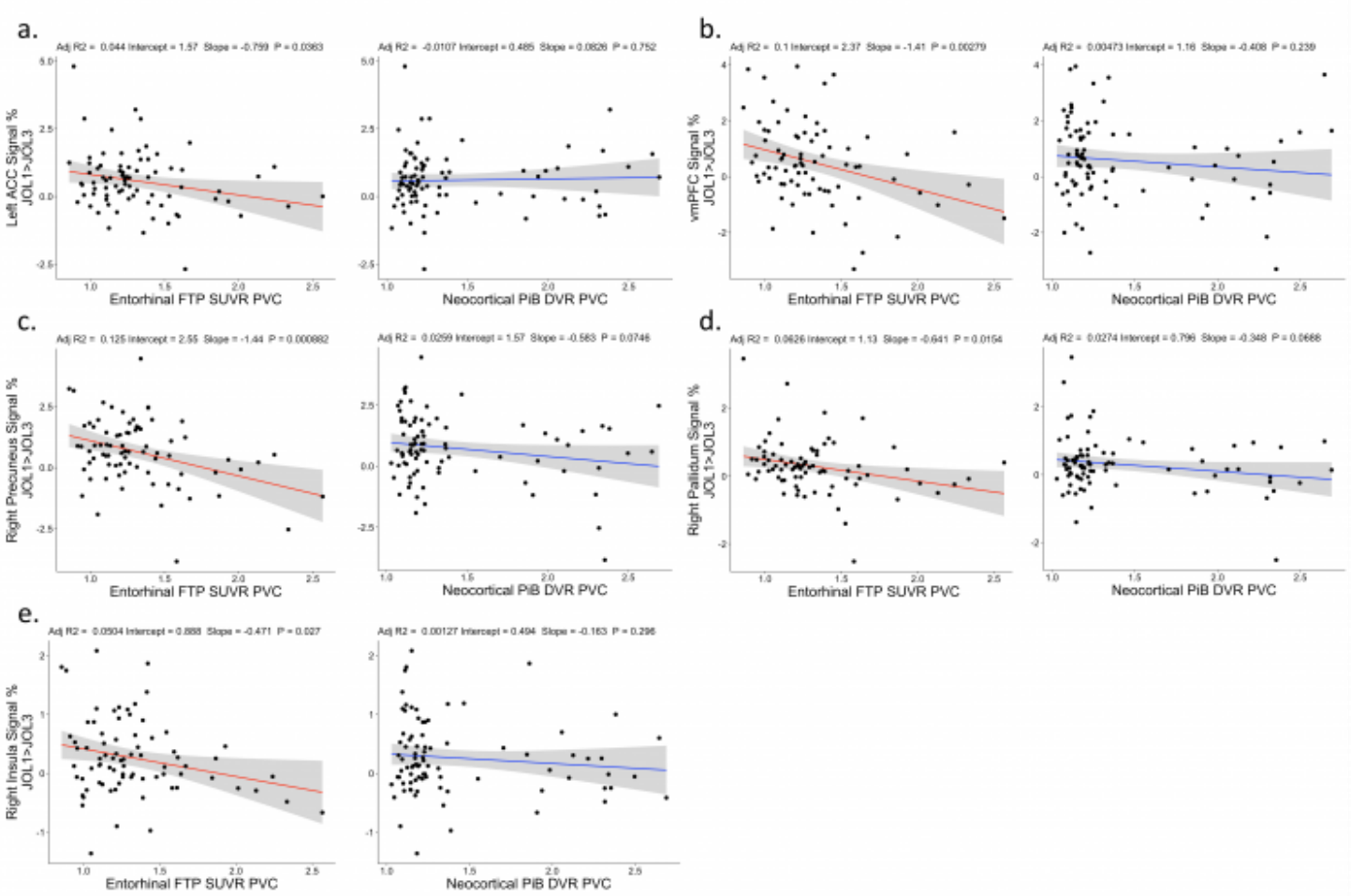

FIGURE 2: Investigating the Effect of Tau and Amyloid on Memory Self-Appraisal
Mean signal extracted from peaks of clusters that were found to increase in activation in a JOL1>JOL3 contrast (qFDR<0.05, uncorrected p=0.001) was entered linear regression models with activity as the dependent variable and entorhinal cortex Flortaucipir (EC-FTP) or amyloid (PiB) as independent continuous variables. EC-FTP, but not PiB, was related to neural activation in the (**a**) left anterior cingulate cortex (ACC), (**b**) ventromedial prefrontal cortex (vmPFC), (**c**) right precuneus, (**d**) right pallidum, and (**e**) right insula.

Keywords: Memory, fMRI, Flortaucipir, Amyloid

P86: Segregation of tau deposits across clinical stages provides the basis for pathophysiological staging in AD

Sulantha Mathotaarachchi[1], Tharick A. Pascoal[1], Andréa L. Benedet[1], Monica Shin[1], Min Su Kang[1], Hanne Struyfs[1], Joseph Therriault[1], Mira Chamoun[1], Kok Pin Ng[1], Melissa Savard[1], Ashley Knight[1], Serge Gauthier[1,2], Pedro Rosa-Neto[1,2]

[1]Translational Neuroimaging Laboratory, McGill University, Montreal, QC, Canada
[2]Alzheimer's Disease Research Unit, McGill University Research Centre for Studies in Aging, Montreal, QC, Canada

Introduction: The stages of neurofibrillary tangle (NFT) deposition during the course of Alzheimer's disease is well understood through the Braak stages; however, the underlying mechanism behind the NFT propagation remains unclear. Here we propose to identify the segregation of brain regions of tau deposition based on data-driven community identification of tau networks using tau PET imaging. We hypothesize the convergence of brain regions into communities sharing patterns of tau accumulation across specific disease stages.

Methods: [^{18}F]AV1451 images of 95 cognitively normal (CN), 66 mild cognitive impairment (MCI) individuals and 17 Alzheimer's disease (AD) individuals were acquired from the ADNI cohort and the standardized uptake value ratio (SUVr) maps were generated using the cerebellar grey matter as the reference region. The inter-regional correlation was created for 58 cortical brain regions and stochastic block model analysis was conducted to identify the communities in binarized correlation matrices (FDR threshold; 0.001, bootstrap threshold; 0.95).

Results: In CN the tau retention segregates into 5 distinct communities in the entire brain, in which the limbic community display the highest tau load (Figure 1, 2). In MCI, limbic and frontal communities' aggregates to a single community, while in AD, the entire brain behaves as a single community.

Conclusion: This data-driven method based on community identification of tau deposition networks identifies patterns of segregation that recapitulate disease stages based on pathological criteria. This method can be used as an unbiased method for staging and monitoring disease progression.

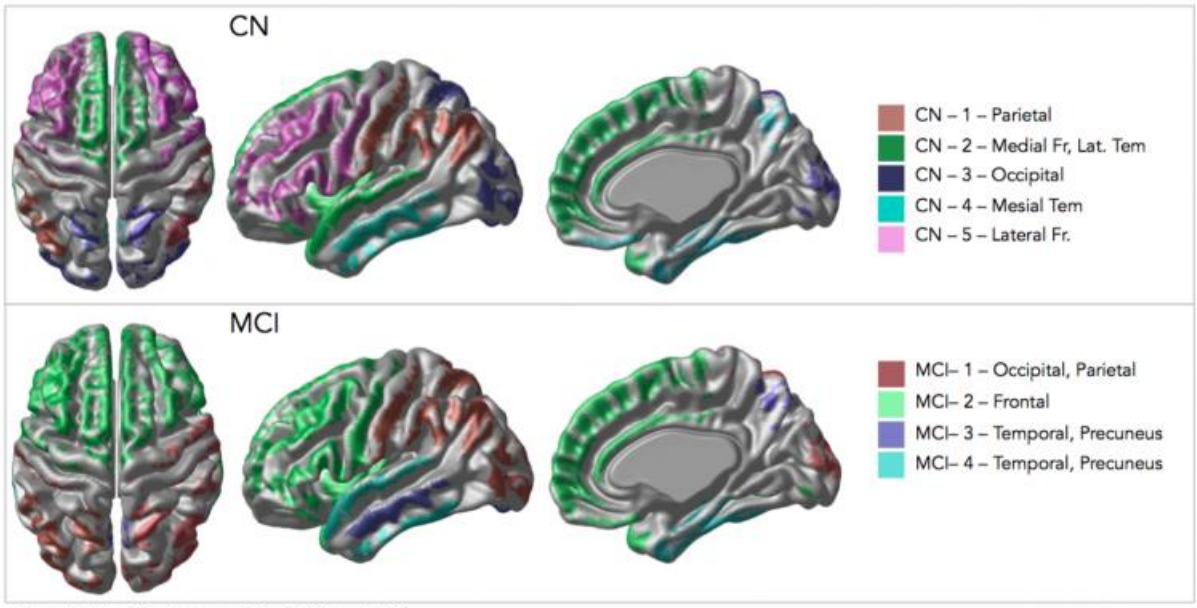

Figure 1. Identified communities in CN and MCI.

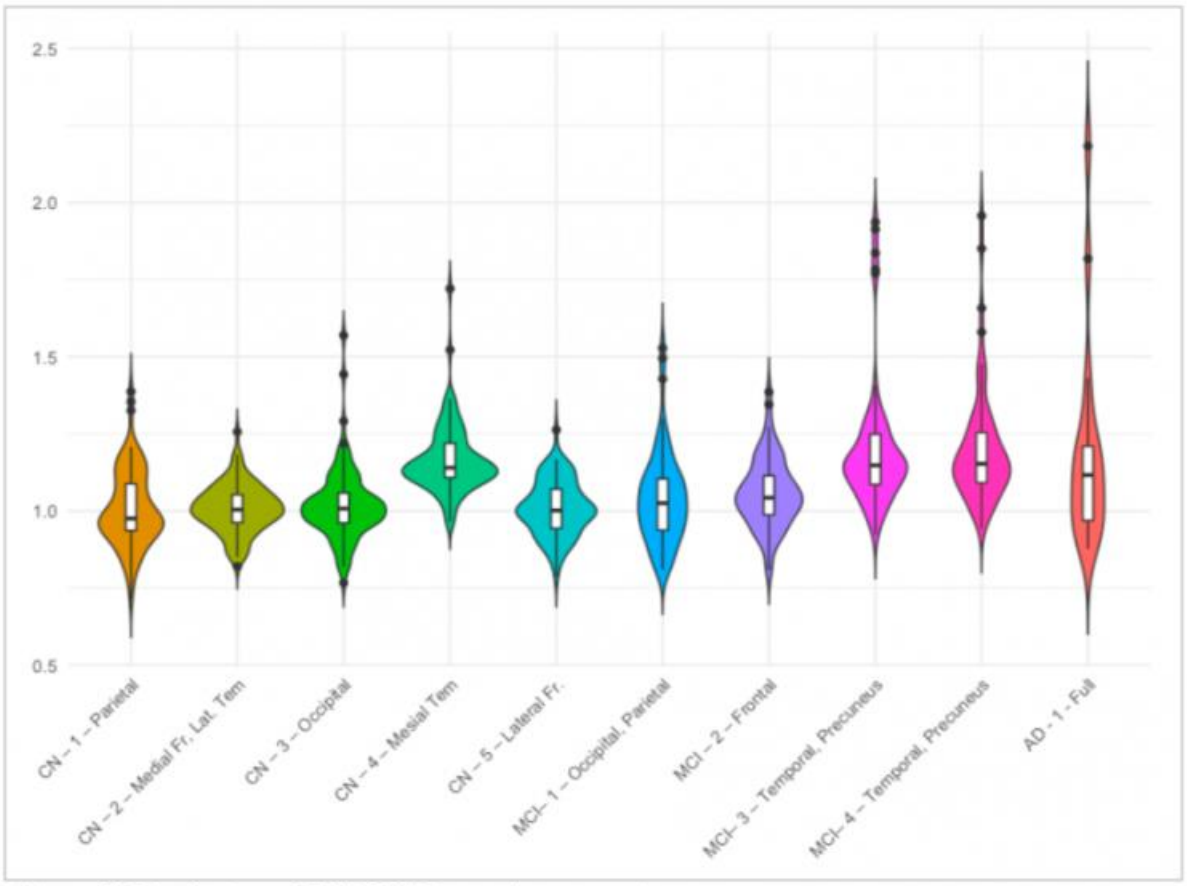

Figure 2. Distribution of TAU SUVR in each community

Keywords: tau, network analysis, Alzheimer's disease, staging

P87: Increasing Aβ is associated with nonlinear change in BOLD modulation to difficulty in cognitively normal middle-aged and older adults: further evidence from an n-back task

Chris Foster, Kristen M. Kennedy, Karen Rodrigue

Center for Vital Longevity - University of Texas at Dallas, Dallas, TX, US

Beta-amyloid (Aβ) positive individuals hyper-activate brain regions compared to those not at-risk; however, hyperactivation is then thought to diminish as Alzheimer's disease symptomatology begins, evidencing eventual hypoactivation. It remains unclear when in the disease staging this transition occurs. We recently showed that a non-linear trajectory of functional activation exists with Aβ SUVR, explaining both hyper- and hypo-activation on a spatial distance judgment task in bilateral angular and medial frontal cortices in a nondemented aging sample (Foster et al., 2017 *NeuroImage*). Here we sought to replicate this nonlinear effect in the same sample using a different functional task to test the generalizability of this phenomenon. Using an N-Back working memory task (0-, 2-, 3-, and 4-back), 68 healthy adults (51-94 years) underwent fMRI and ^{18}F-Florbetapir PET imaging. Mean cortical SUVR was calculated from several regions across the neocortex, normalized by whole cerebellum uptake. A linear contrast was used as the dependent variable in a model with age, Aβ, Aβ^2, and average task accuracy as predictors. Performance on both accuracy and response time declined as WM-load increased (*p*'s < .015). fMRI results revealed that Aβ^2 was a significant negative predictor of activation in two large inferior clusters: bilateral subcortical nuclei (figure panel A) and bilateral cerebellum/fusiform (B), regions strongly associated with working memory and dopaminergic pathways. Individuals with slightly elevated Aβ burden evidenced greater activation as compared to individuals with little or no Aβ burden whereas individuals with the greatest Aβ burden evidenced less activation as compared to individuals with slightly elevated Aβ (panels C, D). The current study extends prior findings by providing further evidence for a dose-response, nonlinear relationship between increasing Aβ burden and alteration in BOLD modulation. Results will be further discussed in light of Aβ ability to modulate presynaptic neurons and control dopamine release in animal models.

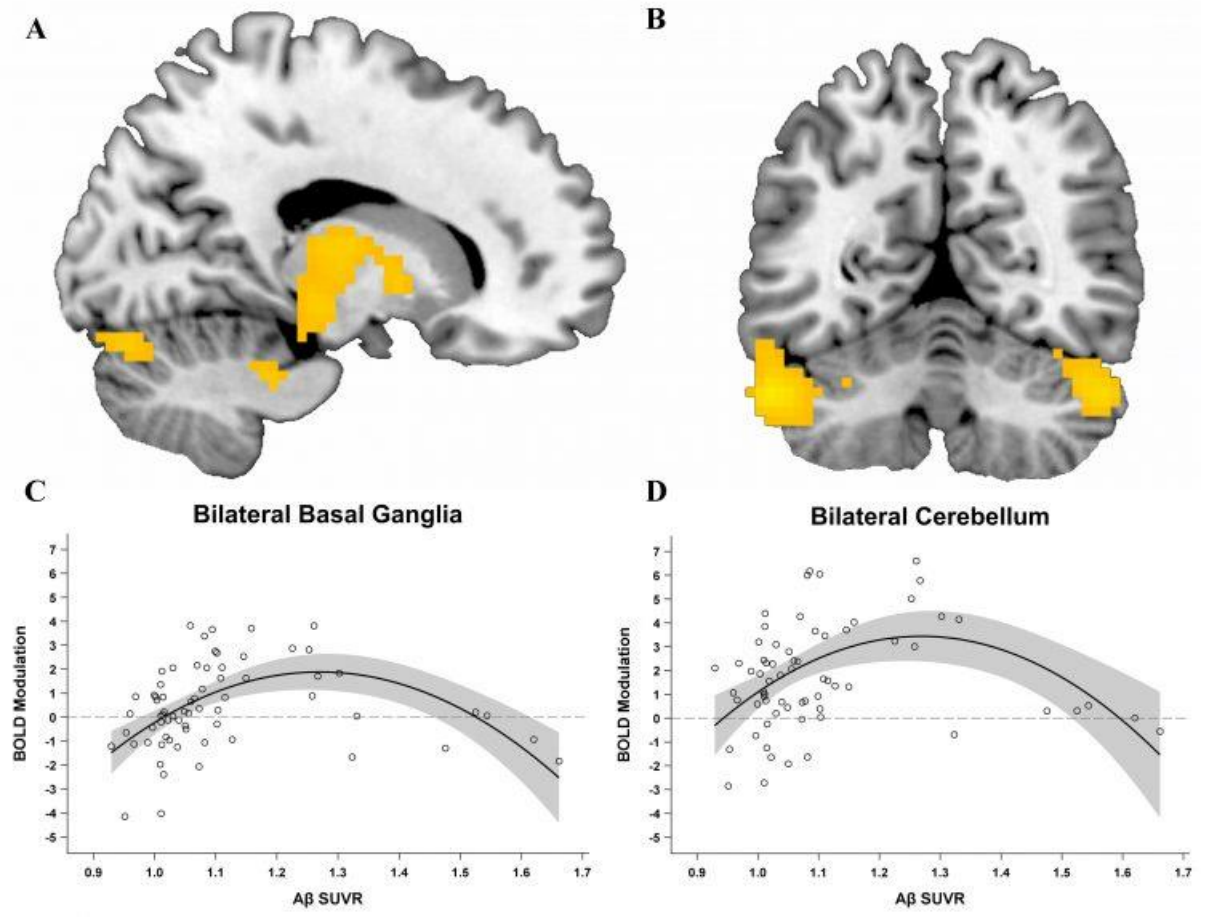

Keywords: normal aging, amyloid PET imaging, hyperactivation, hypoactivation, working memory

P88: Co-existence of deleterious and neuroprotective interaction between amyloid and neuroinflammation in late stage Alzheimer's disease

Ashley Knight[1,6], Min Su Kang[1], Maxime Parent[1,2], Tharick Pascoal[1], Sulantha Mathotaarachchi[1], Joseph Therriault[1], Andrea Benedet[1], Mira Camoun[1], Arturo Aliaga[1,2], Eduardo Zimmer[1,3,4], Monica Shin[1], Antonio Aliaga[5], Alexey Kostikov[5], Jean-Paul Soucy[5], Serge Gauthier[7], Claudio Cuello[6], Pedro Rosa-Neto[1,5,7]

[1]*Translational Neuroimaging Laboratory, McGill University Research Center for Studies in Aging, Montreal, QC, Canada*
[2]*Douglas Hospital Research Center, McGill University, Montreal, QC, Canada*
[3]*Department of Biochemistry, Federal University of Rio Grande do Sul, Porto Alegre, Brazil*
[4]*Brain Institute (BraIns) of Rio Grande do Sul, Porto Alegre, Brazil*
[5]*Montreal Neurological Institute, Montreal, QC, Canada*
[6]*Department of Pharmacology and Therapeutics, McGill University, Montreal, QC, Canada*
[7]*Alzheimer's Disease Research Unit, McGill University Research Centre for Studies in Aging, Montreal, QC, Canada*

Purpose: The role of neuroinflammation in cognitive functions in Alzheimer's disease(AD) is still elusive. Molecular imaging agents designed to track amyloid plaques, a hallmark of AD, and translocator protein (TSPO), a marker of neuroinflammation upregulated in reactive glial cells can be used to monitor regional differences in protein expression *in vivo*. We measured amyloid load and neuroinflammation in McGill-R-Thy1-APP transgenic(Tg) rats, which is an animal model expressing only amyloid pathology without neuro-fibrillary tangles or cell death. Here, we investigated the differential effects of amyloid pathology and neuro-inflammation on cognition. Although, amyloid has negligible association with behavioral measures, we predict that interaction between amyloid and neuroinflammation is associated with cognitive function in AD animals.

Procedures: A total of 15 (6 Wild type(WT) and 9 Tg) rats at 17 months of age underwent [^{18}F]PBR06 and [^{18}F]NAV4694 PET to image neuroinflammation and amyloid load, respectively, and Morris Water Maze for cognition. All PET images were transformed into a template space via affine transformation. The non-displaceable binding potential(BP_{ND}) parametric maps were generated using cerebellar grey as a reference region based on Simplified Reference Tissue Method (SRTM). For statistical analysis, we performed voxel-wise linear regression using the following models in VoxelStats: Cognition ~ PBR06*Genotype and Cognition ~ PBR06*AZD4694

Results: Interaction of TSPO and b-amyloid plaques(t=4.62) in the basal forebrain, indicated by increases in [^{18}F]PBR06 and [^{18}F]NAV4694 was associated with reduced memory performance as indicated by an increase in latency in the Morris Water Maze. Conversely, the same interaction(t=-7.59) in the hippocampal formation was associated with improved memory indicated by decrease in latency.

Conclusion: These results suggest that the role of neuroinflammation might depend on regional factors and cannot be easily generalized. In this animal model, interactions between amyloid and neuroinflammation can provide both neuroprotective and detrimental effects in a regionally specific manner.

Keywords: Amyloid, neuroinflammation, PET imaging, animal models

P89: Amyloid and tau deposition determine cognitive impairment through epigenetic changes in individuals across the AD spectrum

Tharick Pascoal, Monica Shin, Min Su Kang, Kok Pin Ng, Andrea Benedet, Sulantha Mathotaarachchi, Joseph Therriault, Mira Chamoun, Gassan Massarweh, Ashley Knight, Jean-Paul Soucy, Serge Gauthier, Pedro Rosa-Neto

McGill University, Montreal, QC, Canada

Background: Emerging literature on rheumatoid arthritis, asthma and other conditions has shown that faster clinical improvement is obtained when abnormal expression of Histone deacetylases (HDACs) class is rectified. However, the role of HDAC I in Alzheimer's disease (AD) remains elusive. [^{11}C]Martinostat is a novel Positron Emission Tomography (PET) agent that selectively binds to HDAC I. Here, we tested the hypothesis that HDAC I is reduced in patients with AD dementia. Also, we investigated whether HDAC I reduction links amyloid and tau with cognitive impairment.

Methods: We studied 25 individuals (9 cognitively normal elderly; 3 MCI; 13 AD) with PET amyloid obtained with [^{18}F]NAV4694, tau with [^{18}F]MK6240, and HDAC I with [^{11}C]Martinostat as well as cognitive assessment (Mini-Mental State Examination (MMSE)). Voxel-wise analysis of variance tested the difference of [^{11}C]Martinostat uptake between controls and AD patients. In significant regions, Pearson correlation tested the association between biomarkers and cognition. Structured equation modeling test whether [^{11}C]Martinostat mediates the effects of [^{18}F]NAV4694 and [^{18}F]MK624 on cognition. The models were adjusted for age, gender and diagnosis.

Results: We found reduced [^{11}C]Martinostat uptake in individuals with AD in the brain's posterior default mode network regions compared to controls(Fig.1). In the posterior DMN, [^{11}C]Martinostat strongly negatively correlated with [^{18}F]NAV4694 and [^{18}F]MK6240, while strongly positively correlated with MMSE(Fig.2). Finally, we found that [^{11}C]Martinostat uptake in the posterior DMN mediates the effect of [^{18}F]NAV4694 and [^{18}F]MK6240 on cognition(Fig.3).

Conclusions: In this preliminary analysis, we demonstrated for the first time that HDAC I levels are reduced in patients with AD. In addition, we showed that this reduction has significant clinical implications mediating the effects of amyloid and tau on cognition. Together, these results support previous observations suggesting that HDAC availability plays a role in cognition and suggests HDAC I reduction as a possible novel therapeutic target to AD with promising clinical implications.

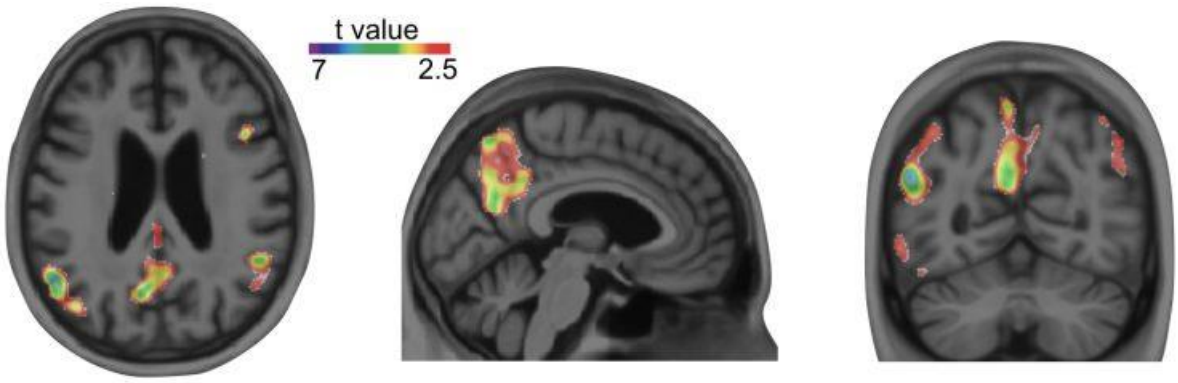

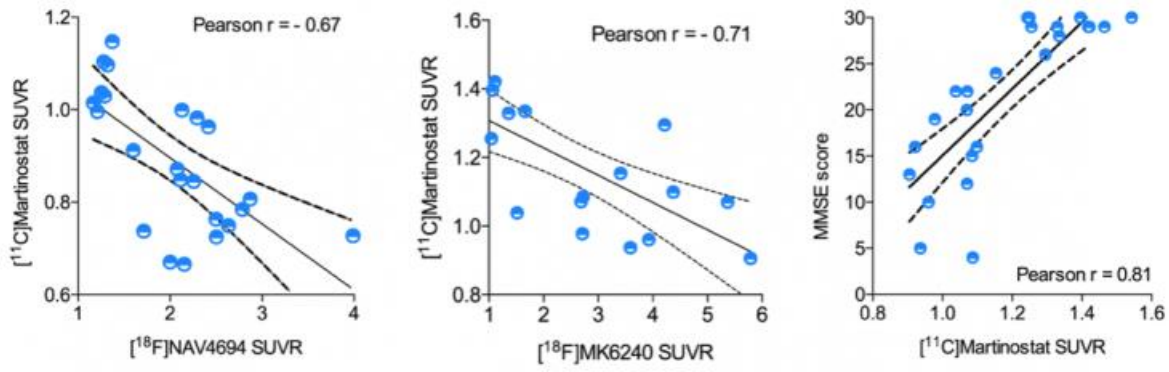

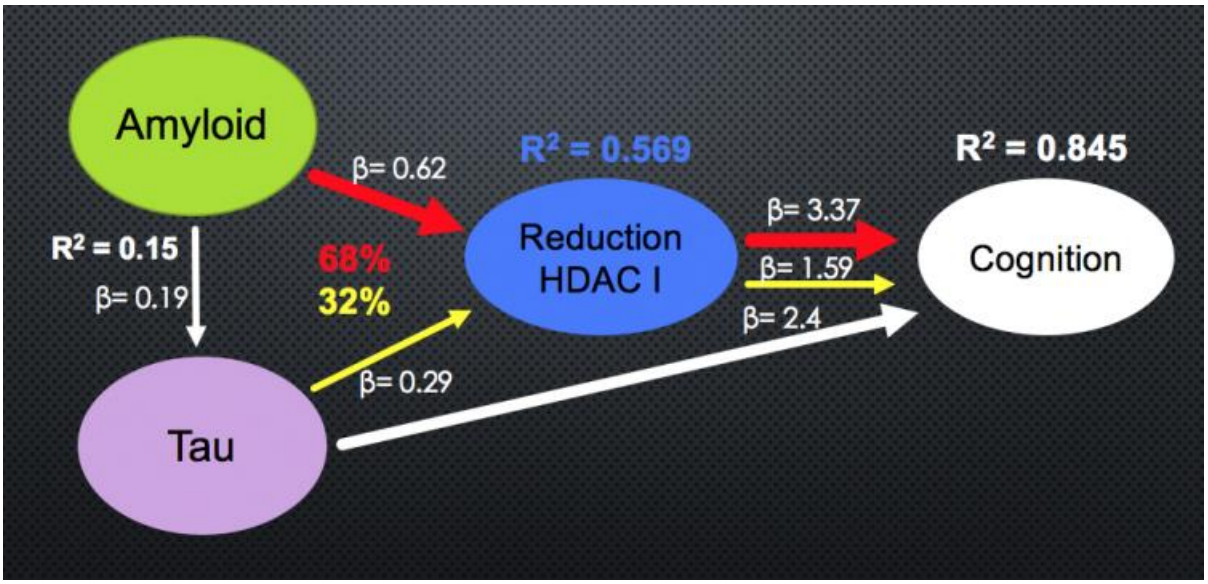

Keywords: Amyloid, tau, epigenetic

P90: 18F-AV-1451 uptake on tau PET differs between dementia with Lewy bodies and posterior cortical atrophy

Zuzana Nedelska[1], Keith Josephs[2], Jonathan Graff-radford[2], Scott Przybelski[3], Timothy Lesnick[3], Bradley Boeve[2], Val Lowe[1], Daniel Drubach[2], David Knopman[2], Ronald Petersen[2], Clifford Jack, Jr.[1], Jennifer Whitwell[1], Kejal Kantarci[1]

[1]*Department of Radiology, Mayo Clinic, Rochester, MN, US*
[2]*Department of Neurology, Mayo Clinic, Rochester, MN, US*
[3]*Department of Health Sciences, Rochester, MN, US*

Objective: Clinical patients with posterior cortical atrophy (PCA) and dementia with Lewy bodies (DLB) have both shown hypometabolism on FDG-PET and AV-1451 uptake on tau-PET in the occipital and posterior temporo-parietal cortices and visuo-spatial impairment. We investigated differences in distribution and magnitude of AV-1451 uptake between PCA and DLB.

Methods: Consecutive patients with DLB (n=30) and PCA (n=14) underwent ^{18}F-AV-1451 PET and MRI. For comparison, we included clinically normal adults (CN; n=100) from the Mayo Clinic Study of Aging. Differences in the distribution and magnitude of AV-1451 uptake between DLB and PCA were assessed using voxel-wise analysis with statistical parametric mapping and an atlas-based approach. Two-class partial volume correction was used. Regions which performed best in distinguishing between PCA and DLB patients were identified using the area under receiver operating curve statistics with Bonferroni correction and a "posterior composite" region of interest that reflected the largest differences in AV-1451 uptake.

Results: PCA and DLB patients were similar on clinical dementia rating, sum of boxes ($p>0.05$). Although both PCA and DLB had greater AV-1451 uptake in posterior temporo-parietal, occipital and frontal cortices than CN (figure), the magnitude of AV-1451 uptake was substantially greater in PCA than DLB in posterior temporo-parietal and occipital cortices. The posterior composite region combining AV-1451 uptake from occipital, lingual, fusiform, cuneus, parietal and calcarine cortex (figure) completely distinguished PCA from DLB (AUC=1.0; $p<0.001$).

Conclusions: Although the pattern of hypometabolism on FDG-PET and clinical symptoms can overlap between DLB and PCA patients with similar levels of impairments, and a subset of PCA patients may have Lewy body pathology in addition to AD, AV-1451 uptake is markedly greater in PCA. Because of the underlying AD pathophysiology in majority of PCA patients, this finding is expected and useful in the differential diagnosis in cases with overlapping DLB and PCA symptoms.

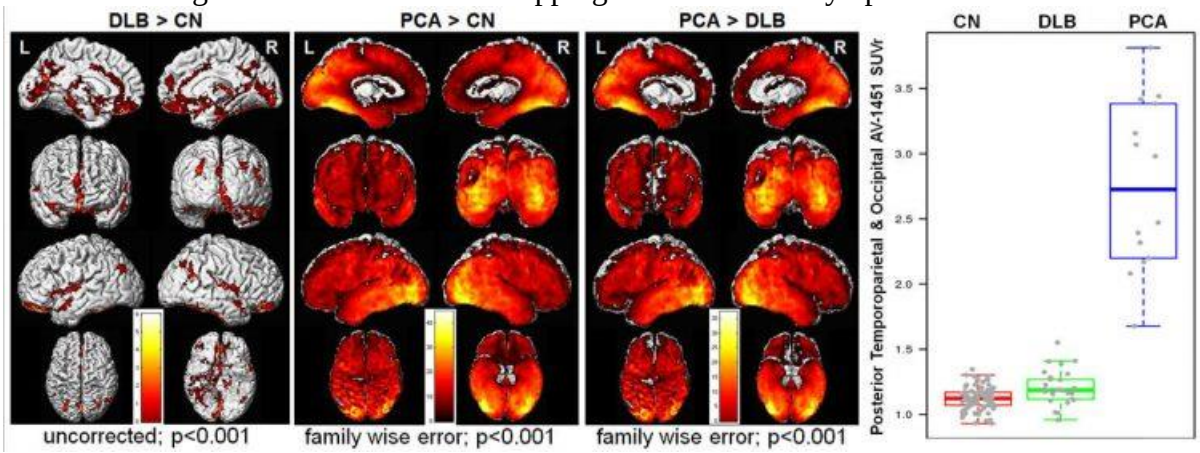

Keywords: dementia with Lewy bodies, posterior cortical atrophy, AV-1451 tau PET

P91: Finding ground zero: identifying the medial temporal origin of tau deposition during life

Justin Sanchez[1], Jean Augustinack[1,2], J. Alex Becker[1,2], Heidi Jacobs[1,2], David Jin[1], Samantha Katz[1], Evelyn Luner[1], Kirsten Moody[1], Dorene Rentz[3], Reisa Sperling[1,2,3], Julie Price[1,2], Keith Johnson[1,2,3]

[1]Departments of Radiology and Neurology, Massachusetts General Hospital, Boston, MA, US
[2]Athinoula A. Martinos Center, Harvard Medical School, Charlestown, MA, US
[3]Center for Alzheimer Research and Treatment, Department of Neurology, Brigham and Women's Hospital, Harvard Medical School, Boston, MA, US

Background: Post-mortem studies suggest that tau neurofibrillary pathologic deposition commonly begins in a region of medial temporal periallocortex that includes lateral entorhinal and perirhinal cortices, and spreads to adjacent cortices under the influence of beta–amyloid. We sought to identify and sample tau-PET signal reflecting this process, accounting for anatomic variability.

Methods: 18F-Flortaucipir (FTP) PET was acquired in 228 clinically-normal participants (Table 1) in the Harvard Aging Brain Study, surface-sampled using Freesurfer, and expressed as SUVR (WM-reference, modified MG partial-volume correction). Temporal cortical maps were evaluated vertex-wise with an automated process yielding location and surface curvature angle, permitting us to identify the fundus (depth) of the rhinal and/or anterior collateral sulci (Figure 1). A "rhinal cortex" (RC) region was sampled along the length of this fundus (~20mm) within a 6mm radius. RC was characterized and compared to inferior temporal (IT) FTP SUVR with respect to PiB DVR and age.

Results: Among low-amyloid (n=185), the RC tau SUVR distribution differed from IT in being positively skewed (Welch two-sample t=33.14; p<1e-15). In contrast, RC and IT were similar among high-amyloid (N=43) in having a positive association of tau SUVR with PiB DVR (Figure 2). Individuals with both low-amyloid and high-tau in RC (PVC SUVR > 1.4), were marginally more likely to carry the APOEe2 allele as compared to the other groups (Fisher's Exact, p=0.08; Figure 2c).

Conclusions: We assessed a rhinal cortex (RC) region, an anatomically-defined portion of the medial temporal cortex thought to be the initial site of tau tangle deposition. Individuals with low amyloid burden and PET evidence of elevated tau in RC may represent an earlier and relatively amyloid-independent tauopathy. However, longitudinal studies currently underway will be required for confirmation. These observations may be useful for defining a low-tau status as a basis to evaluate tau spread and its prevention.

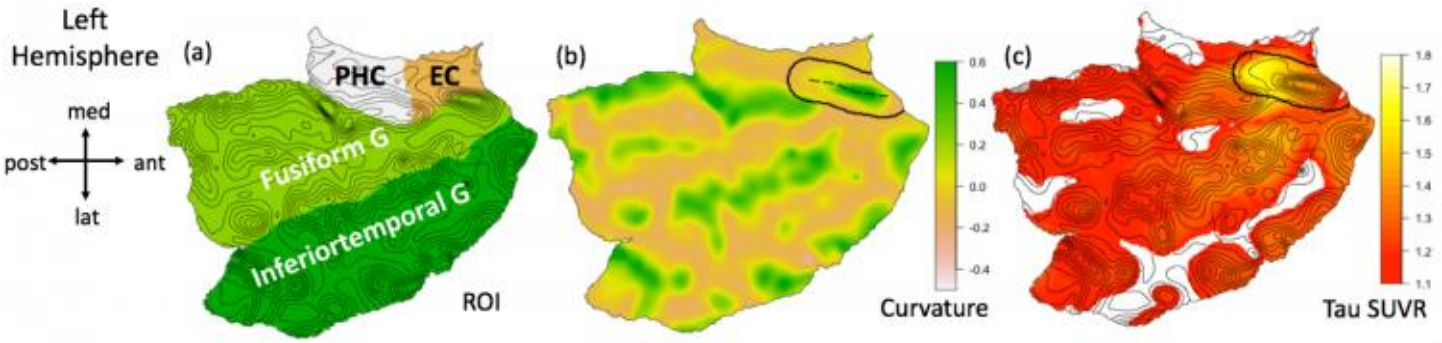

Figure 1: The automated procedure yielded a standardized and individualized sampling of "rhinal cortex" (RC), a portion of the lateral entorhinal that extended into perirhinal and ectorhinal cortices. Sample temporal cortical flatmaps shown are (a) FreeSurfer labeled regions (EC-entorhinal cortex; PHC-parahippocampal cortex) with curvature contour; (b) curvature map (sulci in green) with collateral fundus (dotted line) and RC perimeter; (c) FTP SUVR heat map with curvature contour, RC outlined.

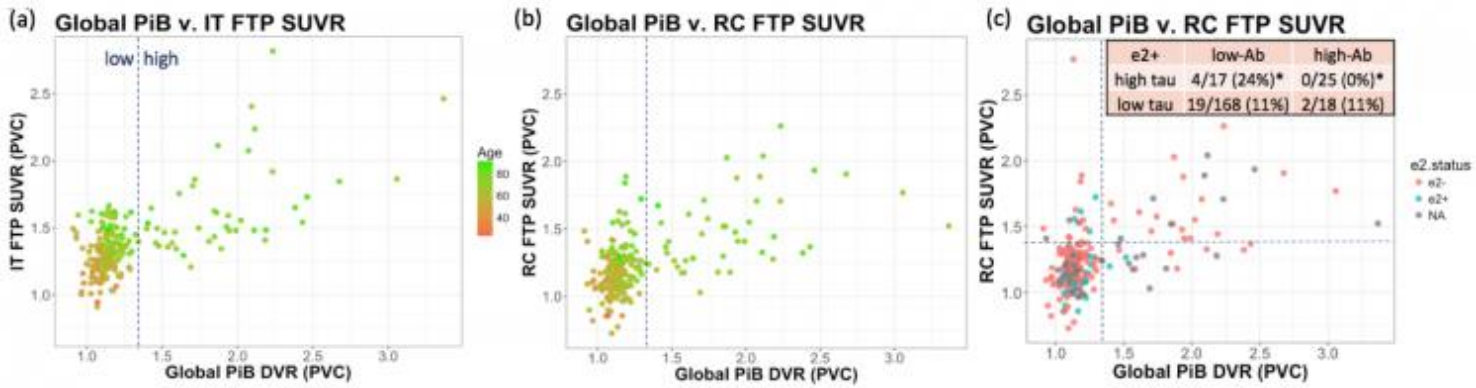

Figure 2: Global PiB DVR v. regional mean FTP SUVR in (a) IT and (b) RC. In low-Ab, tau is positively skewed in RC but not in IT (Table 2). In high-Ab, there is a positive association between global PiB and FTP SUVR in both regions ($p<.003$). (c) There was a marginally significant difference in the proportion of e2 carriage among individuals with high/low tau or high/low amyloid (Fisher's $p=0.08$). Posthoc comparisons showed that individuals with low amyloid/high tau were more likely to carry the e2 allele than individuals with high amyloid/high tau (unadjusted $p=0.02$)

	All (N=228)	High-Ab (N=43)	Low-Ab (N=185)
Age	63.2±13.5 (21-93)	76.1±7.6 (59-92)	63.2±13.5 (21-93)
Gender (F)	95 (43%)	27 (62.8%)	92 (49.7%)
Years of Education	16.0±2.6 (8-21)	16.8±2.5 (12-20)	15.9±2.8 (6-21)

Table 1: Demographics. All participants cognitively normal.

FTP PVC SUVR	All (N=228)	High-Ab (N=43)	Low-Ab (N=185)
RC			
mean	**1.2511	*1.4992	**1.1934
SD	0.2537	0.2820	0.2086
CV (SD/mean)	0.2028	0.1881	0.1748
skew	*1.8864	***0.7174	***2.7443
IT			
mean	**1.3789	*1.6473	**1.3165
SD	0.2601	0.3428	0.1895
CV (SD/mean)	0.1886	0.2081	0.1439
skew	*1.8018	***1.5294	***0.8410

Table 2: Tau PET descriptive statistics. * denotes statistically significant differences between RC and IT distributions: *p<.05; **p<.000001; ***p<1e-14

Keywords: Tau PET, medial temporal, pathology

P92: Age-related change of THK-5351 PET in amyloid-negative and non-demented elderly subjects

Takashi Kato[1], Kaori Iwata[1], Go Kizawa[1], Naohiko Fukaya[1], Izumi Kuratsubo[1], Yasuyuki Kimiura[1], Nobuyuki Okamura[2], Kazuhiko Yanai[2], Kengo Ito[1], Akinori Nakamura[1], MULNIAD Study Group[1]

[1]*National Center for Geriatrics and Gerontology, Obu-shi, Japan*
[2]*Tohoku University, Sendai, Japan*

Background and purpose: [F-18]THK-5351 is a PET imaging agent that has high affinity to tau of paired helical filaments and off-target such as monoamine oxidase B (MAO-B). The purpose of this study was to investigate age-related change of THK-5351 PET in amyloid-negative and non-demented elderly subjects.

Subjects and method: Subjects selected from in-house studies were 31 cognitively normal subjects (CN) (age: 70.1±4.2 (62-79) y.o., MMSE: 28.7±1.4 (26-30), CDR 0) whose PiB PET scans were visually rated as negative scans. PiB PET images of 50-70 min and the THK-5351 PET images of 40-60 min after the injections were spatially normalized using DARTEL and 3D-T1 weighted MR images. Regions of interest (ROIs) values were obtained on the basis of the Automated Anatomical Labeling Atlas for target and reference values for SUVR (standard uptake value ratio) calculation. Statistical analyses were performed using SPM8 and SPSS19.

Results: Age showed significant positive association with THK-5351 SUVR values in the precuneus, posterior cingulate, inferior and mid temporal, and inferior parietal cortices ($p<0.001$, FWEc-corr $p<0.05$) in a SPM analysis. Analyses on ROI basis also detected statistically significant correlations with age in widespread cerebral areas, especially in the posterior cingulate ($p<0.001$, $r>0.564$), mid and inferior temporal cortices ($p<0.003$, $r>0.520$), angular cortices ($p<0.005$, $r>0.489$), and precuneus ($p<0.007$, $r>0.475$), while the analyses did not detect any significant correlations in the hippocampus and parahippocampal cortices. No significant correlation was observed between each ROI SUVR value and each cognitive performance (MMSE, ADAS, WMS-R logical memory I/II).

Conclusion: Age-related increase of THK-5351 accumulation is observed in the widespread cerebral areas but not in the hippocampus and parahippocampal cortices. The elevation dose not significantly affect cognition. Those findings of THK-5351 PET might reflect MAO-B change. However, the pathophysiological mechanisms of this phenomenon is not clear because of limited evidence and methodologies.

Keywords: THK-5351 PET normal PiB age

P93: Human testing of non-selective alpha-synuclein PET tracers

Edilio Borroni[1], Michael Honer[1], Luca Gobbi[1], Chet Mathis[2], William Klunk[2], Paul Kotzbauer[3], Zhude Tu[3], Robert Mach[4], Dale Mitchell[5], Ken Marek[6], Jamie Eberling[7]

[1]*Neuroscience Department, Hoffmann-La Roche Ltd., Basel, Switzerland*
[2]*University of Pittsburgh, Pittsburgh, PA, US*
[3]*Washington University, St. Louis, MO, US*
[4]*University of Pennsylvania, Philadelphia, PA, US*
[5]*Charles River Laboratories, Cambridge, United Kingdom*
[6]*Invicro, New Haven, CT, US*
[7]*Michael J Fox Foundation for Parkinson's Research, New York, NY, US*

A PET tracer capable of imaging the distribution and rate of aggregated α-synuclein deposition in the brain would be an essential imaging biomarker for the understanding of the pathophysiology of Parkinson's disease (PD) and the development of novel treatments. The MJFF Alpha-synuclein Imaging Consortium identified compounds that bind with high affinity (1 to 10 nM) to native α-synuclein aggregates in brain sections of both PD patients and transgenic mice overexpressing human A30P α-synuclein. These compounds are not selective for α-synuclein and also bind to amyloid-beta plaques as demonstrated by autoradiographic studies in Alzheimer's disease (AD) brain sections. Two compounds were selected for testing first in nonhuman primates and then in humans. Both compounds were radiolabeled with ^{18}F to high specific activity and purity. PET scans in rhesus macaques indicated good brain entry, homogenous distribution across all brain regions, followed by rapid washout from the brain, low nonspecific binding and favorable pharmacokinetics. These radioligands have the potential to become PET radiotracers to visualize brain α-synuclein aggregates in subjects devoid of amyloid-beta deposits. Both PET tracer candidates were tested in three PD patients and three control subjects all of whom were negative for amyloid-beta as demonstrated by [^{18}F]florbetapir or [^{18}F]florbetaben PET. Although both tracers showed good brain penetration a similar pattern of uptake and retention was observed in the PD and control subjects with no obvious evidence of specific binding in the PD subjects. A more detailed analysis of these PET data as well as testing of both tracers in AD patients is currently being performed to assess whether the lack of evident specific binding in PD patients is due to unfavorable tracer properties or it may be related to the low density of α-synuclein pathology. The results of this study will help to define the tracer properties required to image α-synuclein.

Keywords: Parkinson's disease, Alzheimer's disease, synucleinopathies, Imaging biomarker

Thursday, January 18, 2018 - 11:00 am - 11:45 am

Podium Session

Keynote Lecture

Seeley, William

Network-based neurodegeneration

William Seeley

University of California, San Francisco, CA, US

The anatomy of neurodegenerative disease can be understood in terms of two key aspects: onset and progression.[1] Mechanisms controlling onset timing and location remain mysterious, and each disease features striking heterogeneity in its onset sites. Regarding progression, network analyses have revealed that each neurodegeneration syndrome reflects the targeting of a specific large-scale network.[2] Each vulnerable network, in turn, is anchored by a pivotal "epicenter" whose functional-anatomical connections govern the vulnerability of other regions, perhaps because prion-like corruptive templating begets trans-synaptic disease protein spread.[3] I will illustrate these principles across a range of neurodegenerative disorders linked to diverse molecular pathological substrates. I will also discuss more recent efforts to understand the pathological substrates of brain imaging biomarkers and to use connectomic data to predict disease progression.

1. Seeley WW. Mapping Neurodegenerative Disease Onset and Progression. Cold Spring Harb Perspect Biol 2017.
2. Seeley W, Crawford R, Zhou J, Miller B, Greicius M. Neurodegenerative diseases target large-scale human brain networks. Neuron 2009;62:42-52.
3. Zhou J, Gennatas ED, Kramer JH, Miller BL, Seeley WW. Predicting regional neurodegeneration from the healthy brain functional connectome. Neuron 2012;73:1216-1227.

Thursday, January 18, 2018 - 11:45 am - 01:30 pm

Podium Session

Session 5: Genetically Determined AD

CHAIRS: William Klunk, Eric McDade

Thursday, January 18, 2018		
11:45 - 01:30	**Session 5: GENETICALLY DETERMINED AD**	CHAIRS: William Klunk | Eric McDade
11:45	Autoradiographic Evaluation of MK-6240 compared to AV-1451	**Lowe** | Bruinsma | Sarma | Curran | Min | Fang | Pandey | Bennacef | Serie | Jones | Josephs | Parisi | Knopman | Boeve | Kantarci | Jack | Dickson | Petersen | Murray
12:00	In vivo and in vitro [18F]MK6240 show neurofibrillary tangles deposition heterogeneity in individuals with a wide range of cognitive symptoms	**Pascoal** | Chamoun | Shin | Mathotaarachchi | Kang | Therriault | Savard | Benedet | Knight | Chakravarty | Massarweh | bennacef | Soucy | Gauthier | Rosa-Neto
12:15	Multi-site study of PiB-PET imaging using the Centiloid method: relationships to pathological measures of β-amyloid pathology	**La Joie** | Ayakta | Borys | Boxer | deCarli | Dore | Grinberg | Huang | Jack | Jin | Klunk | Ikonomovic | Lockhart | Lowe | Masters | Miller | Mungas | Murray | O'Neil | Olichney | Petersen | Reed | Rowe | Seeley | Vemuri | Villemagne | Jagust | Rabinovici
12:30	[F-18]-AV-1451 binding profile in Chronic Traumatic Encephalopathy: a postmortem case series	Marquié | **Aguero** | Siao Tick Chong | Ramanan | Sáez-Calveras | Verwer | Kim | Bennett | Silva Amaral | Johnson | Frosch | Alvarez | McKee | Normandin | Gómez-Isla
12:45	Neuropathological and biochemical correlates of tau and amyloid PET imaging in two autopsy brains	**Ikonomovic** | Abrahamson | Kofler | Price | Becker | Mathis | Lopez | Klunk
01:00	Discussion	

Genetic and environmental factors are differentially related to Aβ burden in the presymptomatic phase of autosomal dominant and sporadic Alzheimer's disease

Julie Gonneaud[1,2], Christophe Bedetti[1,2], Alexa Pichet Binette[1,2,3], Tammie Benzinger[5,6], John Morris[5,7], Randall Bateman[5,7], Judes Poirier[1,2], John Breitner[1,2], Sylvia Villeneuve[1,2,3,4], The DIAN Study Group[5], PREVENT-AD Research Group[2]

[1]*Department of Psychiatry, McGill University, Montreal, QC, Canada*
[2]*Douglas Mental Health University Institute, StoP-AD Centre, Montreal, QC, Canada*
[3]*Integrated Program in Neuroscience, McGill University, Montreal, QC, Canada*
[4]*Department of Neurology and Neurosurgery, McGill University, Montreal, QC, Canada*
[5]*Knight Alzheimer's Disease Research Center, Washington University School of Medicine, St. Louis, MO, US*
[6]*Department of Radiology, Washington University School of Medicine, St. Louis, MO, US*
[7]*Department of Neurology, Washington University School of Medicine, St. Louis, MO, US*

Objective: To evaluate whether Aβ trajectories in presymptomatic ADAD mutation carriers and asymptomatic individuals with a parental history (PH) of sporadic (s)AD are similarly affected by genetic (apolipoproteinE4 [*APOE*4]) and environmental (education level) risk factors of sAD.

Methods: Aβ-PET scans were collected using ^{11}C-PIB in 132 presymptomatic ADAD mutation carriers from the DIAN study (age=48.13±7.38) and ^{18}F-NAV4694 in 62 asymptomatic individuals with a PH of sAD from the PREVENT-AD cohort (age=67.15±4.76). The mean neocortical SUVR (normalized by the whole cerebellum values) was computed for each individual. We tested the interaction between *APOE*4 status and education (i.e. years of schooling) on Aβ burden in each cohort using general linear models, controlling for age and gender. Using the same analytic approach, we performed exploratory analyses assessing whether *APOE*4 status and/or education influence the relationship between parental estimated years to onset (pEYO = 'affected parent's age at symptom onset' – 'participant's age at assessment') and Aβ burden.

Results: In presymptomatic ADAD, completing higher levels of education was associated with lower Aβ burden ($F_{1,113}$=4.61, p=.03) but not with *APOE*4 (Figure.1a). In asymptomatic individuals with a PH of sAD we found an *APOE*4*education interaction ($F_{1,55}$=4.03, p=.05), such that the protective effect of education was stronger in *APOE*4 carriers (Figure.1b). pEYO was related to increased Aβ burden in both cohorts (r=.21 and r=.26 respectively, ps<.05), but interaction with *APOE*4 and/or education did not reached significance (Figure.2).

Conclusion: Our results suggest that *APOE*4 has no impact on Aβ trajectory in ADAD, while it is highly associated with Aβ accumulation in people at risk of sAD. By contrast, environmental factors, approximated here using education, could affect biomarker progression in both variants of the disease. Furthermore, education was able to counteract the deleterious effect of *APOE*4 on Aβ burden in asymptomatic individuals with a PH of sAD.

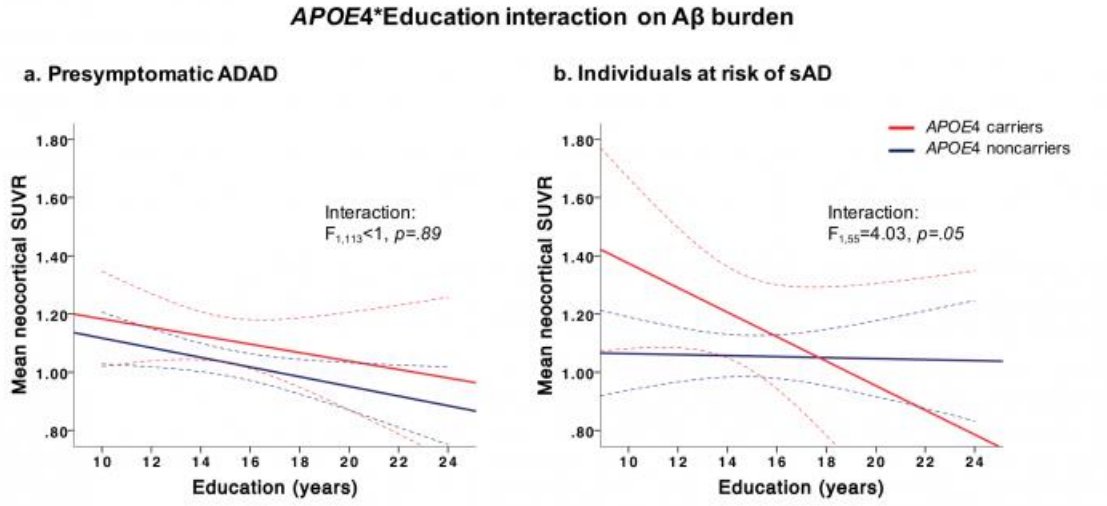

Figure 1. Apolipoprotein E (*APOE*)4 * Education interaction on Aβ burden in presymptomatic autosomal dominant AD (ADAD) mutation carriers (a) and asymptomatic individuals with a parental history of AD (b). Solid lines represent estimated regression lines, while dotted lines represent 95% confidence intervals.
Statistical values were obtained using general linear models, controlling for age and gender. *APOE*4 homozygous carriers (n=1 in each cohort) were removed from these analyses.

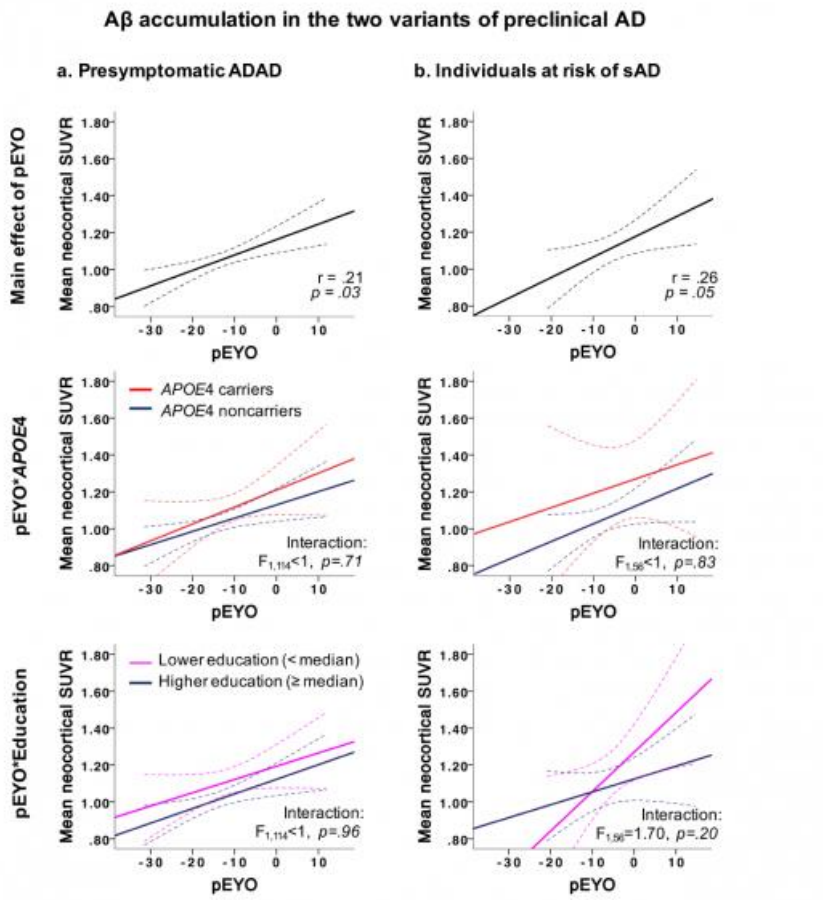

Figure 2. Aβ accumulation as a function of the parental estimated years to symptoms onset (pEYO) in presymptomatic autosomal dominant AD (ADAD) mutation carriers (a) and asymptomatic individuals with a parental history of AD (b). pEYO predict Aβ accumulation in the two cohorts (top panel), but do not interact with the *APOE*4 status (middle panel) or education level (bottom panel).
Solid lines represent estimated regression lines, while dotted lines represent 95% confidence intervals.
Statistical values were obtained using partial correlations (top panel) or general linear model (middle and bottom panels), controlling for age and gender. In the pEYO*Education model, education was entered as a continuous variable but, for illustration convenience, group was split in lower and higher education according to the cohorts' median.

Keywords: Amyloid, preclinical, Autosomal dominant Alzheimer's disease, sporadic Alzheimer's disease, education

In vivo measurements of cortical thickness, amyloid and tau pathology, and episodic memory in preclinical autosomal dominant Alzheimer's disease

Yakeel T. Quiroz[1], Cinthya Aguero[1], Francisco Lopera[2], Daniel Norton[1], Daniel Aguirre-Acevedo[2], Kewei Chen[3], Ana Baena[2], Edmarie Guzman-Velez[1], Enmanuelle Pardilla-Delgado[1], Sergio Alvarez[4], Brad Dickerson[1], Reisa Sperling[1], Eric Reiman[3], Keith Johnson[1]

[1]*Massachusetts General Hospital/Harvard Medical School, Boston, MA, US*
[2]*Universidad de Antioquia, Grupo de Neurociencias, Medellin, Colombia*
[3]*Banner Alzheimer's Institute, Phoenix, AZ, US*
[4]*Hospital Pablo Tobon Uribe, Medellin, Colombia*

Background: Cortical thinning has been reported in individuals with autosomal dominant Alzheimer's disease (AD), several years before anticipated clinical onset. Here we compared brain imaging measurements of cortical thickness, amyloid and tau pathology, and characterized associations with memory performance in cognitively unimpaired mutation carriers and non-carriers from the Colombian Presenilin-1 (*PSEN1*) E280A kindred.

Methods: We used structural MRIs, PiB and flortaucipir PET images of amyloid and tau burden, and CERAD word list learning memory scores in the assessment of 12 cognitively unimpaired 37±3 year-old mutation carriers, approximately 7 years before the kindred's median age at mild cognitive impairment (MCI) onset. Automated brain mapping algorithms were used to compute mean cortical PiB DVRs, entorhinal cortex (EC) and inferior temporal (IT) flortaucipir SUVRs, and cortical thickness in 9 regions-of-interest (ROIs) known to be affected by AD. Spearman's correlations were used to characterize relationships among these brain imaging and memory measurements.

Results: Compared to non-carriers, cognitively unimpaired *PSEN1* mutation carriers showed cortical thinning in the inferior temporal gyrus ($p<0.001$), middle temporal gyrus ($p=0.03$), superior temporal gyrus ($p<0.001$), and temporal pole ($p<0.001$). In the carrier group, amyloid burden was only associated with thinning in the superior parietal lobule ($r=-0.78$, $p<0.001$). EC and IT tau burden were associated with thinning in the anterior cingulate ($r= -0.87$, $p<0.001$ and $r= -0.76$, $p=0.04$, respectively) and precuneus ($r= -0.96$, $p<0.001$ and $r= -0.94$, $p<0.001$, respectively). Poorer memory performance was associated with thinning in the supramarginal gyrus ($r=0.57$, $p=0.05$), thinning in posterior cingulate cortex ($r=0.69$, $p=0.013$), and EC tau burden ($r=-0.67$, $p=0.01$).

Conclusions: This study provides preliminary information about the limited associations between amyloid burden and neurodegeneration, and the more extensive associations between tau burden, neurodegeneration and cognitive decline, several years before the estimated age of MCI onset in individuals at virtually certain risk for autosomal dominant AD.

Keywords: cortical thickness, tau pathology, amyloid pathology, autosomal dominant Alzheimer's disease

Comparison of striatal longitudinal changes in amyloid deposition in non-demented elderly and Down syndrome

Dana Tudorascu[1], Charles Laymon[1], Davneet Minhas[1], Brian Lopresti[1], Julie Price[2], Chester Mathis[1], Howard Aizenstein[1], William Klunk[1], Benjamin Handen[1], Bradley Christian[3], Ann Cohen[1]

[1]University of Pittsburgh, Pittsburgh, PA, US
[2]Massachusetts General Hospital, A. A. Martinos Center for Biomedical Imaging, Boston, MA, US
[3]University of Wisconsin, Madison, WI, US

Down syndrome (DS) predisposes individuals to early Alzheimer's disease (AD) and, using [^{11}C]PiB, a pattern of striatal amyloid (Ab) that is elevated relative to neocortical binding has been reported, similar to that of non-demented autosomal dominant AD mutation carriers. However, it is not known if change in striatal [^{11}C]PiB over time differs in a non-demented DS population when compared to change in a non-demented elderly (NDE) population.

Objective: To assess longitudinal changes in trajectories of Ab in a non-demented DS compared to an NDE cohort.

Methods: NDE (n=100, age=75 (6)) and DS (n=83, age=38(7)) who underwent [^{11}C]PiB -PET at baseline and over 2-5 years were included. The regional trajectories for striatum (AVS), frontal cortex (FRC) and precuneus (PRC) [^{11}C]PiB SUVR 50-70 (cerebellum reference, non-partial volume corrected) were explored over time using linear mixed effects models with fixed effects of time, cohort and time-by-cohort interactions and subject as random effect.

Results: Significant differences between DS and NDE cohort trajectories for all ROIs were observed ($p<0.05$), with DS showing a faster trajectory of accumulation in AVS compared to NDE as opposed to a slower trajectory of accumulation in FRC and PRC. The differences in amyloid deposition trajectories over time between DS and NDE were as follows (AVS: 0.15, 95%CI (0.03,0.28), FRC: -0.17, 95% CI (-0.27, -0.07), PRC -0.08, 95% CI (-0.18, 0.03)).

Discussion: DS and NDE participants differed significantly in longitudinal change in [^{11}C]PiB in both AVS and neocortical ROIs, with faster accumulation of Ab in DS relative to NDE in AVS and slower accumulation in neocortical regions. These data suggest that in addition to the previously reported distinct pattern of early striatal deposition not commonly seen in late onset AD, individuals with DS may also accumulate Ab at a rate faster in AVS than that seen in late onset disease.

Keywords: down syndrome, amyloid rates, normal aging amyloid deposition

[F-18]AV-1451 PET in non-demented adults with Down Syndrome is related to both amyloid and age

Ann Cohen[1], Charles Laymon[1], Davneet Minhas[1], Jeffery James[1], Cathy Wolfe[1], Patrick Lao[2], Chester Mathis[1], Marwan Sabbagh[3], Shahid Zaman[4], William Klunk[1], Benjamin Handen[1], Bradley Christian[2]

[1]*University of Pittsburgh School of Medicine, Pittsburgh, PA, US*
[2]*University of Wisconsin –Madison School of Medicine, Madison, WI, US*
[3]*Barrow Neurological Institute, Phoenix, AZ, US*
[4]*University of Cambridge, Cambridge, United Kingdom*

Background: Adults with Down syndrome (DS) are uniformly affected by AD pathology by their 30's and have a 70-80% chance of clinical dementia by their 60's. Yet, nowhere is it clearer than in DS that Aβ deposition is not sufficient to produce dementia, as individuals harbor this pathology for over a decade before cognitive decline is apparent. In the longitudinal study of Neurodegeneration in Aging DS (NiAD), we have begun to explore AD related biomarkers including both amyloid and tau PET in adults with DS.

Objective: In the present study, we examined tau pathology using [F-18]AV-1451 PET in non-demented adults with DS.

Methods: 17 participants with DS (mean age 40.4 years) underwent [F-18]AV-1451 PET. [F-18]AV-1451 80-100 min summed images were created and warped to a common space via FreeSurfer. Images were converted to SUVR by normalization to FreeSurfer cerebellar gray matter. We assessed the voxelwise relationship of [F-18]AV-1451 SUVR to DSMSE using SPM8. Additionally, we assessed the retention of [F-18]AV-1451 based on amyloid status, measured by PiB-PET in a subset (n=10) of participants.

Results: A significant positive relationship ($p<0.01$) was observed between [F-18]AV-1451 retention and age. Additionally, when examining the voxelwise difference in [F-18]AV-1451 between PiB(+) and PiB(-) participants, there was a significant ($p<0.05$) difference between groups (Fig 1).

Conclusions: Significant tau burden, measured by [F-18]AV-1451 PET is observed in non-demented adults with DS and is related to both amyloid status and age. Ongoing studies will examine these relationships in more detail, particularly the relationship of regional amyloid deposition in DS to tau burden. These data suggest that [F-18]AV-1451 may be a good marker of tau burden in DS.

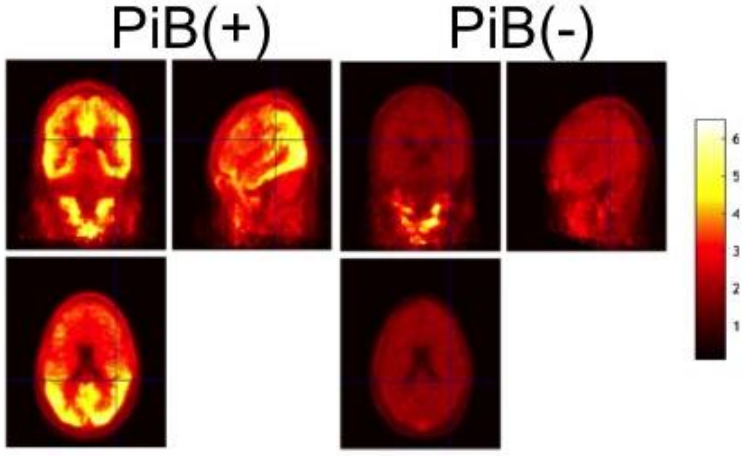

Keywords: tau, AV-1451, down syndrome

Baseline amyloid PET and longitudinal change in non-amyloid biomarkers from the DIAN Study

Eric McDade, Guoqiao Wang, Anne Fagan, Brian Gordon, Jason Hassenstab, John C Morris, Chengjie Xiong, Randall J Bateman

Washington University in St. Louis, St. Louis, MO, US

Background: Fibrillar amyloid-β (Aβ) plaques are one of the earliest detectable abnormalities of Alzheimer's disease (AD). Yet, the period of time from when Aβ-plaques are first detectable to the emergence of non-Aβ pathologies remains unclear. Identifying thresholds for Aβ-plaques that are related to the subsequent development of non-Aβ pathologies, rather than defining a disease/non-disease group could help in clarifying optimal points for intervention. In the Dominantly Inherited Alzheimer Network (DIAN) we explored the relationship between baseline PiB-PET and longitudinal changes in non- Aβ biomarkers and cognition.

Methods: 251 mutation carriers enrolled in DIAN with baseline PiB-PET and longitudinal follow-up in precuneus-FDG, hippocampal volumes (HV), CSF Tau/p-tau and cognitive evaluations (range 2-6, median 2 visits). We estimated the baseline PiB composite SUVR where the rate of change for each outcome became significantly different from zero by applying a linear mixed effects model to each outcome with fixed effects for time from baseline, baseline PiB, and the two-way interaction.

Results: The annual rate of increase of PiB-PET SUVR for mutation carriers was 0.08/year. The following PIB-SUVR levels were related to significant change over time for each measure: PiB-PET-1.2, HV 1.4, Cognition-1.5, p-tau-2.0. For p-tau, there was a negative change after the PiB-SUVR level identified, indicating a decline in soluble p-tau after this point, **Figure**.

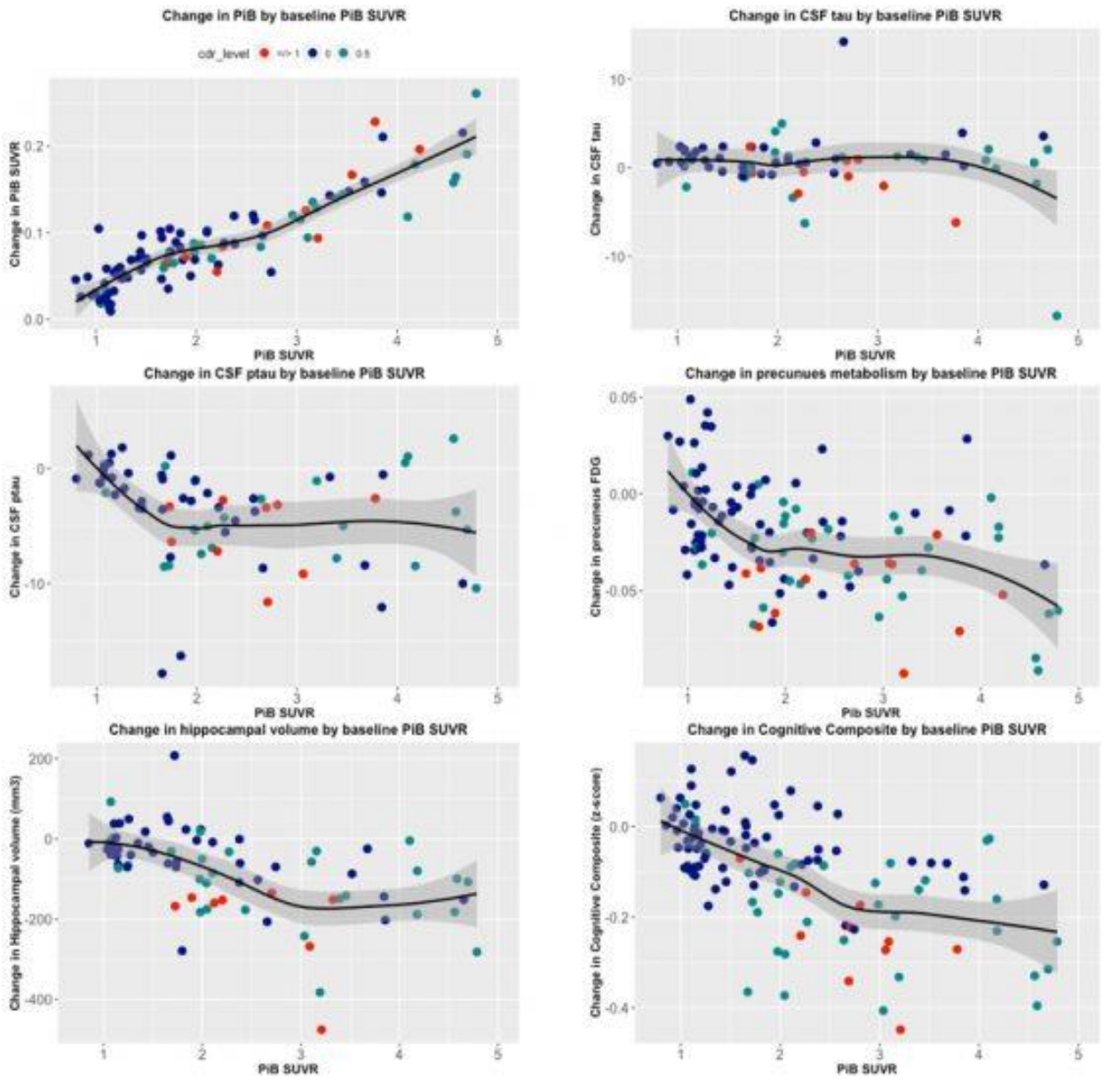

Conclusion: In autosomal dominant AD, we find that a cortical SUVR as low as 1.2 is associated with a significant acceleration in the accumulation of fibrillar Aβ-plaques. At an increase of 0.08 SUVR/year in PiB-PET, this suggests that within 3-5 years, the initial acceleration in hippocampal volume and cognition begin. Hence, interventions designed to maximally prevent the progression of AD may need to be introduced at the point of earliest Aβ-plaques level detection if exceeding this threshold triggers non-AD dependent changes and likelihood of response to Aβ therapies.

Keywords: Amyloid PET, dominantly inherited Alzheimer's disease,

Thursday, January 18, 2018 - 02:45 pm - 04:45 pm

Podium Session

Session 6: Amyloid and Tau: Correlations with Patient Characteristics and CSF

CHAIRS: Oskar Hansson, Agneta Nordberg

Thursday, January 18, 2018		
02:45 - 04:45	**Session 6: AMYLOID AND TAU: CORRELATIONS WITH PATIENT CHARACTERISTICS AND CSF**	CHAIRS: Oskar Hansson | Agneta Nordberg
02:45	Genotype-dependent longitudinal trajectories of brain metabolism and cognition in autosomal dominant AD	**Rodriguez-Vieitez** | Mazrina | Almkvist | Chiotis | Almeida | Carter | Schöll | Thordardottir | Axelman | Kinhult Ståhlbom | Viitanen | Lannfelt | Graff | Wall | Nordberg
03:00	Coupling between amyloid and tau occurs at a younger age in APOE E4 carriers than in non-carriers	**Jacobs** | Becker | Hanseeuw | Pase | Satizabal | Beiser | Demissie | Daniluk | Schafer | Peets | Killiany | Sperling | DeCarli | Seshadri* | Johnson*
03:15	Greater tau load and reduced cortical thickness in the parietal cortex of APOE ε4 negative AD patients	**Mattsson** | Ossenkoppele | Smith | Strandberg | Ohlsson | Jögi | Palmqvist | Stomrud | Hansson
03:30	Sex-specific effects on cognitive decline in preclinical Alzheimer's disease: findings from ADNI, AIBL and HABS	**Buckley** | Mormino | Rabin | Lim | Papp | Burnham | Hanseeuw | Dore | Dobson | Waller | Masters | Rowe | Maruff | Donohue | Rentz | Kirn | Properzi | Hedden | Schultz | Chhatwal | Johnson | Amariglio | Villemagne | Sperling
03:45	Distinct information from CSF Tau and AV1451 PET measures in nondemented individuals	Lim | Maruff | Johnson | Sperling | **Mormino**
04:00	Abnormal CSF Aβ changes do not reliably precede florbetapir-PET increases in Aβ-negative normals followed longitudinally	**Landau** | Shaw | Trojanowski | Jagust
04:15	Discussion	

Genotype-dependent longitudinal trajectories of brain metabolism and cognition in autosomal dominant AD

Elena Rodriguez-Vieitez[1], Mariam S. Mazrina[1], Ove Almkvist[1,2,3], Konstantinos Chiotis[1], Rita Almeida[4], Stephen F. Carter[1], Michael Schöll[1,5], Steinunn Thordardottir[2,6], Karin Axelman[2], Anne Kinhult Ståhlbom[2,6], Matti Viitanen[2,7,8,9], Lars Lannfelt[10], Caroline Graff[2,6], Anders Wall[11], Agneta Nordberg[1,2]

[1]*Department of Neurobiology, Care Sciences and Society, Division of Translational Alzheimer Neurobiology, Karolinska Institutet, Stockholm, Sweden*
[2]*Department of Geriatric Medicine, Karolinska University Hospital Huddinge, Stockholm, Sweden*
[3]*Department of Psychology, Stockholm University, Stockholm, Sweden*
[4]*Department of Neuroscience, Karolinska Institutet, Stockholm, Sweden*
[5]*Department of Psychiatry and Neurochemistry, University of Gothenburg, Gothenburg, Sweden*
[6]*Dept of Neurobiology, Care Sciences & Society, Div of Neurogeriatrics, Karolinska Institutet, Stockholm, Sweden*
[7]*Department of Neurobiology, Care Sciences and Society, Div.of Clinical Geriatrics, Karolinska Institutet, Stockholm, Sweden*
[8]*Department of Geriatrics, Turku City Hospital, Turku, Finland*
[9]*University of Turku, Turku, Finland*
[10]*Department of Public Health and Caring Sciences/Geriatrics, Uppsala University, Uppsala, Sweden*
[11]*Department of Surgical Sciences, Section of Nuclear Medicine & PET, Uppsala University, Uppsala, Sweden*

Background: Previous studies in autosomal-dominant AD (ADAD) reported discrepant times of earliest metabolic/cognitive decline, ranging from a decade before up to several years after clinical onset. Neuropathological and in-silico studies have revealed genotype differences in amyloid deposits and other pathological features of ADAD. Here we investigated genotype-dependent longitudinal metabolism and cognition in a Swedish ADAD cohort.
Methods: A cohort of five families harboring a mutation in *APP* (22 carriers, 22 non-carriers) or *PSEN1* genes (13 carriers, 21 non-carriers) (*APPswe, APParc, PSEN1* M146V, H163Y, I143 mutations) was followed with repeated clinical examinations including comprehensive cognitive assessments (2.6±1.7 assessments/participant, 206 total assessments; 7.2±5.4 years follow-up). From this cohort, 48 participants underwent ^{18}F-fluorodeoxyglucose PET imaging (~1-5 scans/participant, 112 total; 5.7±6.9 years follow-up), quantified as regional SUVR(/pons). Estimated years-to-onset (EYO) was defined as individual's age minus family-specific average age-of-onset (AAO). Mixed-effects models predicted metabolism vs. EYO, EYO^2, mutation status (carrier/non-carrier), genotype (*APP/PSEN1*), interaction terms, and possible mutation effects; age and education were covariates.
Results: Regional metabolism in *APP* carriers followed a linear trajectory vs. EYO with earliest decline from EYO≈-12 years in parieto-temporal cortex, while *PSEN1* carriers followed a curvilinear (EYO, EYO^2) model with earliest decline at EYO≈-5 years. Consistent with metabolic findings, *APP* carriers showed earlier cognitive decline first affecting episodic memory from EYO≈-14 years, while *PSEN1* carriers began deviating from non-carriers from EYO≈0 years affecting multiple domains. Regional metabolism was significantly associated to episodic memory alone in *APP* carriers, while to several cognitive domains (episodic memory, executive and visuospatial functions) in *PSEN1* carriers.
Conclusions: Few studies have yet addressed the effect of genotype on imaging biomarkers or cognition in ADAD. Our results suggest that genotype may partly explain the observed heterogeneity regarding time-point of earliest metabolic/cognitive decline, as well as the corresponding distinct associations between longitudinal regional metabolism and cognition.
Keywords: Metabolism; autosomal dominant AD; PSEN1; APP; cognition

Jacobs, Heidi

Coupling between amyloid and tau occurs at a younger age in APOE E4 carriers than in non-carriers

Heidi Jacobs[1], Alex Becker[1], Bernard Hanseeuw[1], Matthew Pase[2], Claudia Satizabal[2], Alexa Beiser[3], Serkalem Demissie[3], Dan Daniluk[2], Colin Schafer[2], Bryanne Peets[2], Ronald Killiany[4], Reisa Sperling[5], Charles DeCarli[6], Sudha Seshadri*[2], Keith Johnson*[1]

[1]*Division of Nuclear Medicine and Molecular Imaging, Department of Radiology, Massachusetts General Hospital/Harvard Medical School, Boston, MA, Boston, MA, US*
[2]*School of Medicine, Department of Neurology, Boston University, Boston, MA, US*
[3]*Boston University School of Public Health,Dept of Biostatistics, Boston, MA, US*
[4]*Boston University School of Medicine, Department of Anatomy & Neurobiology, Boston, MA, US*
[5]*Center for Alzheimer Research and Treatment, Department of Neurology, Brigham and Women's Hospital, Harvard Medical School, Boston, MA, Boston, MA, US*
[6]*UC Davis, Center for Neuroscience, Department of Neurology, Davis, CA, US*

Introduction: Neocortical tauopathy is hypothesized to be driven by rising amyloid burdens within an age-range that has not been well-defined. However, entorhinal tauopathy begins at a much younger age, occurring in ~50% of 50-year-olds. We evaluated cross-sectional age-associations between both proteinopathies, along with potential moderations by sex, and APOE-carrier status.

Methods: We included 213 individuals (20.75–91.50 years, CDR=0) from the Harvard Aging Brain Study and Framingham Study. Neocortical Aβ was quantified using PiB-DVR. Tau was measured in entorhinal (EC) and inferior temporal (IT) cortices (Flortaucipir-SUVR). Robust linear regression with floodlight analyses examined associations between age and Aβ (or tau) on tau (or Aβ), followed by interactions with APOE-status and sex. Estimates were bootstrapped (n=2000) generating BCA-confidence intervals. Covariates were sex, APOE, education and cohort.

Results: Figure 1: Aβ was positively associated with EC tau ($p<0.001$,[0.17,0.36]) and IT tau ($p<0.001$,[0.11,0.21]). Age was positively associated with Aβ, EC and IT tau ($p<0.001$). Aβ did not modify associations between age and EC ($p=0.19$) or IT tau ($p=0.35$).

Figure 2: EC tau modified the age – Aβ association, such that higher Aβ was positively associated with age in individuals with elevated EC tau. This relationship was significant in APOE-ε4 carriers older than 54 years, and in non-carriers after 65 years ($p=0.002$,[0.005,0.029], bottom row Figure 2). IT tau did not modify associations between age and Aβ; there were no sex interactions.

Figure 3: In the low-Aβ subsample (more inclusive threshold:<1.5 DVR;n=176), Aβ was associated with IT tau ($p=0.007$,[0.08,0.50], independent of age, while Aβ was associated with EC tau in a dose-response manner after 71 years ($p=0.032$,[0.002,0.063])

Discussion: Independent of age, Aβ was associated with allocortical and neocortical tau, even in clinically normal individuals with lower Aβ levels. In APOE- ε4 carriers, EC tau and Aβ are associated 12 years earlier in life than in non-carriers.

Figure 1: Aβ was positively associated with EC and IT tau, independent of age

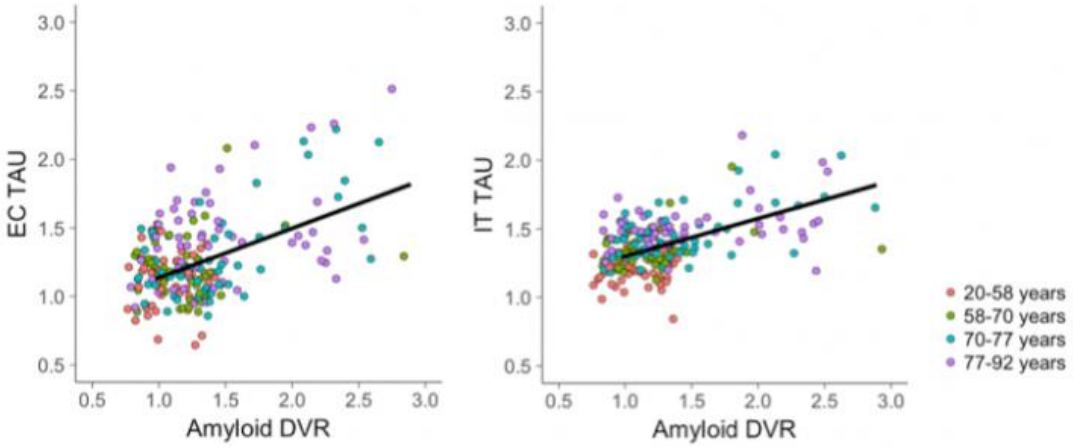

Note: There were no synergistic (p>0.05), but rather independent effects of age and Aβ on tau (p < 0.001). Age was investigated continuously, but for visualization purposes, we colored the points based on quartiles of age. Abbreviations: EC = Entorhinal, IT = inferior temporal, DVR = Distribution Volume Ratio.

Figure 2: EC tau modified the association between age and Aβ

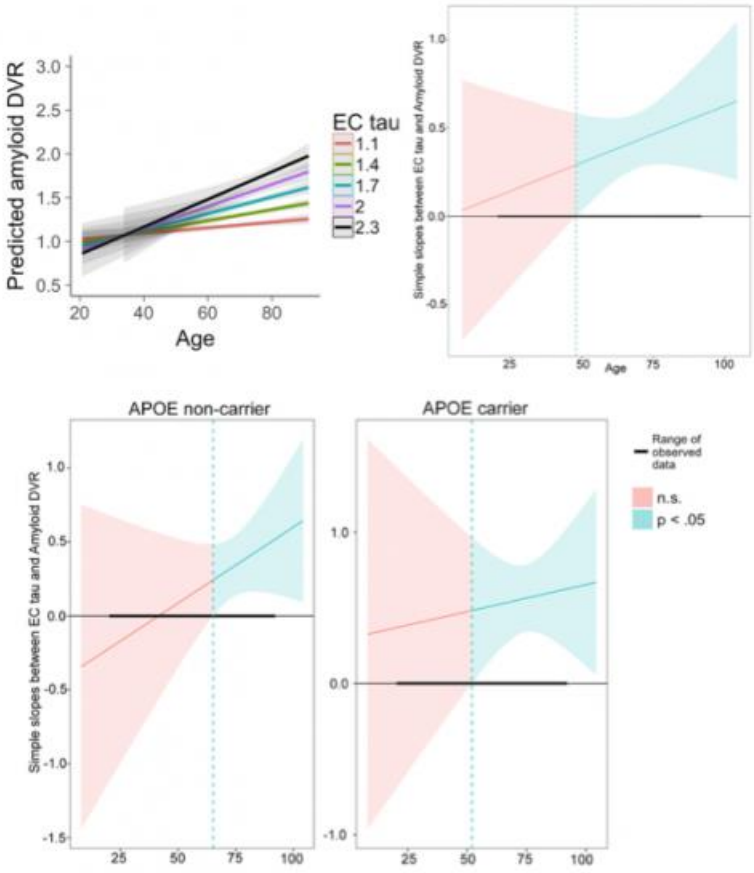

Note: Left top corner: the relationship between age and Aβ was positive when EC tau levels were higher. Right top corner: the robust floodlight analyses showed that the positive association between EC tau and Aβ was significant when individuals were older than 50 years. Bottom row: the positive association between EC tau and Aβ was significant at an earlier age in APOE ε 4 carriers (54 years, right) than in non-carriers (65 years, left). Abbreviations: EC = Entorhinal, DVR = Distribution Volume Ratio. Similar results were observed using logistic regression with Aβ dichotomous as outcome.

Figure 3: Dose-response associations between amyloid on EC tau in clinically normal individuals with lower levels of Aβ

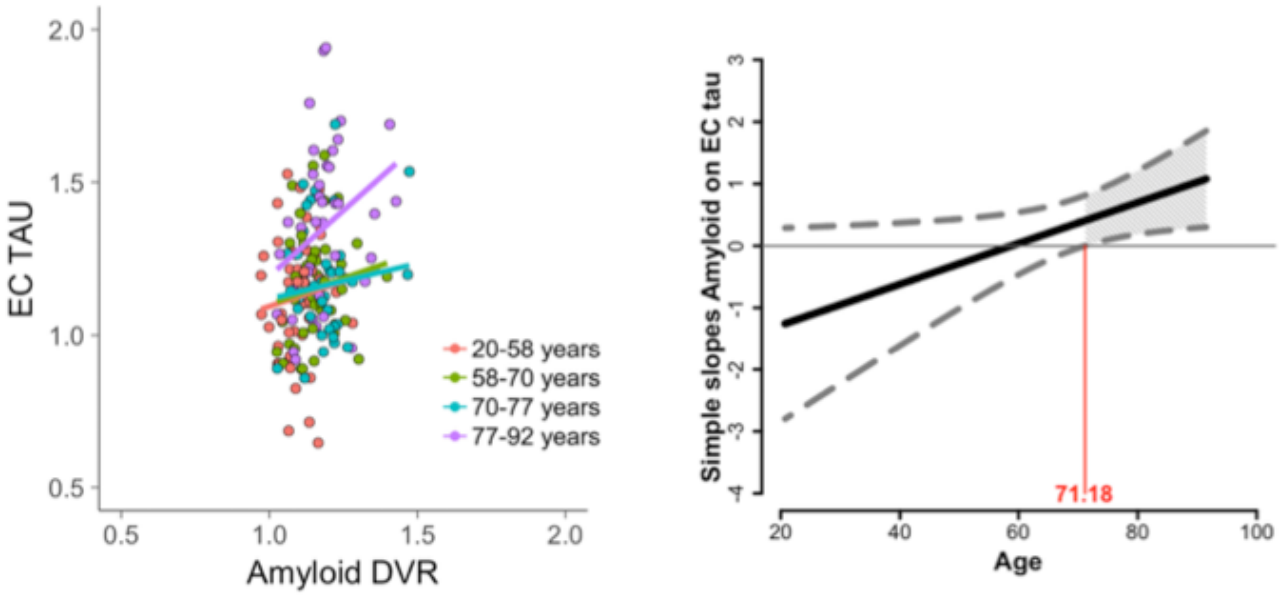

Note: Left: We observed synergistic effects between age and amyloid on EC tau. Age was investigated continuously, but for visualization purposes, we colored the points based on quartiles of age. Right: the positive association between Aβ and EC tau was significant when individuals were older than 71 years. Abbreviations: EC = Entorhinal, DVR = Distribution Volume Ratio.

Keywords: APOE, Flortaucipir, Age, Amyloid, lifespan

Greater tau load and reduced cortical thickness in the parietal cortex of APOE ε4 negative AD patients

Niklas Mattsson[1], Rik Ossenkoppele[1,2], Ruben Smith[1], Olof Strandberg[1], Tomas Ohlsson[3], Jonas Jögi[3], Sebastian Palmqvist[1], Erik Stomrud[1], Oskar Hansson[1]

[1]*Lund University, Lund, Sweden*
[2]*VU University medical center, Amsterdam, Netherlands*
[3]*Skåne University Hospital, Lund, Sweden*

Alzheimer's disease (AD) is a neurodegenerative disease, which is characterized by pathological accumulation of β-amyloid (Aβ) and tau proteins. The clinical presentations and brain changes vary among AD patients. Part of this heterogeneity may be linked to the risk allele *APOE* e4, which is present in 50-70% of patients with sporadic AD. Despite that AD patients may have largely similar amount and distribution of Aβ pathology independently of presence of APOE ε4, patients lacking APOE ε4 are more likely to have predominant non-amnestic rather than memory impairment, and more frontoparietal rather than hippocampal and lateral temporal lobe atrophy. Little data exists on the effects of *APOE* ε 4 on tau pathology in AD.

We therefore tested in 65 Aβ–positive patients at the prodromal and dementia stages of AD whether regional [^{18}F]AV1451 (tau) PET uptake and cortical thickness differed between *APOE* ε4 positive (n=46) and negative (n=19) groups. We found that, compared to their *APOE* ε4-positive counterparts, *APOE* ε4-negative patients had significantly greater tau load and reduced cortical thickness specifically in the parietal cortex.

This suggests that the differences in disease pathways as a function of *APOE* genotype may result in differential development and spread of tau pathology.

Keywords: tau, APOE, PET, atrophy

Sex-specific effects on cognitive decline in preclinical Alzheimer's disease: findings from ADNI, AIBL and HABS

Rachel Buckley[1,4], Elizabeth Mormino[3], Jennifer Rabin[1], Yen Ying Lim[4], Kathryn Papp[1,2], Samantha Burnham[5], Bernard Hanseeuw[1,6], Vincent Dore[5], Annette Dobson[8], Michael Waller[8], Colin Masters[4], Christopher Rowe[7], Paul Maruff[9], Michael Donohue[10], Dorene Rentz[1,2], Dylan Kirn[1,2], Michael Properzi[1], Trey Hedden[1], Aaron Schultz[1], Jasmeer Chhatwal[1], Keith Johnson[1,2], Rebecca Amariglio[1,2], Victor Villemagne[7], Reisa Sperling[1,2]

[1]*Massachusetts General Hospital/Harvard Medical School, Boston, MA, US*
[2]*Brigham and Women's Hospital, Boston, MA, US*
[3]*Stanford University, Stanford, CA, US*
[4]*Florey Institutes of Neuroscience and Mental Health, University of Melbourne, Melbourne, Australia*
[5]*eHealth, CSIRO Health & Biosecurity, Melbourne, Australia*
[6]*University of Louvain, Belgium, Belgium*
[7]*Austin Hospital, University of Melbourne, Melbourne, Australia*
[8]*University of Queensland, Brisbane, Australia*
[9]*Cogstate Ltd., Melbourne, Australia*
[10]*University of Southern California, Los Angeles, CA, US*

Background: A recent meta-analysis showed that female apolipoprotein ε4 (*APOEε*4) carriers between the ages of 65-75 exhibit greater risk for progression to Alzheimer's disease (AD) dementia than males. The influence of sex on cognitive decline in the context of biomarkers of preclinical AD is less clear and requires large sample sizes for statistical detection. We harmonized three datasets to investigate whether clinically-normal females exhibit faster cognitive decline within the context of Aβ-amyloid, *APOEε*4 and age.

Methods: We analyzed sex-specific effects on cognitive decline using the Preclinical Alzheimer Cognitive Composite (PACC) across three cohorts (n=755;CDR=0;Age(SD)=73.6(6.5);Female=55%): the Alzheimer's Disease Neuroimaging Initiative (ADNI;n=330), the Australian Imaging, Biomarker and Lifestyle (AIBL;n=161) study, and the Harvard Aging Brain Study (HABS;n=264). Mean follow-up was 4 years (range=3-7years). We fit mixed-effects models of cognitive change by sex controlling for age, education and baseline PACC with quadratic time effects. We then modeled separately the contributions of sex-by-Aβ-amyloid, sex-by-*APOEε*4, and three-way interactions.

Results: Sex alone did not influence cognitive decline (t=-1.29,*p*=.20), however, females with high Aβ-amyloid exhibited faster cognitive decline than males (t=-2.60,*p*=.009;Fig1). The sex-by-Aβ-amyloid model provided a better fit than one considering Aβ-amyloid alone (LogLikelihoodRatio=17.6,*p*=.002). Females over 80 with high Aβ-amyloid showed the greatest decline trajectories (t=-2.16,*p*=.03;Fig2). No interaction was found between sex and *APOE*e4 on decline (t=-0.45,*p*=.64). Neither did we find a three-way interaction between sex, Aβ-amyloid and APOEε4 (t=1.58,*p*=.11). *Post-hoc* contrasts, however, suggested that female *APOEε*4 carriers with high Aβ-amyloid exhibited a moderately steeper decline in cognition compared with their male counterparts (*p*=.04;Fig3).

Discussion: Harmonizing across datasets provides the statistical power to model sex-specific effects on cognitive change in preclinical AD. Our results suggest that females demonstrate greater cognitive decline than males, specifically in the setting of high Aβ-amyloid. These results highlight the need to explore biological or other mechanisms that confer sex-specific risks for AD.

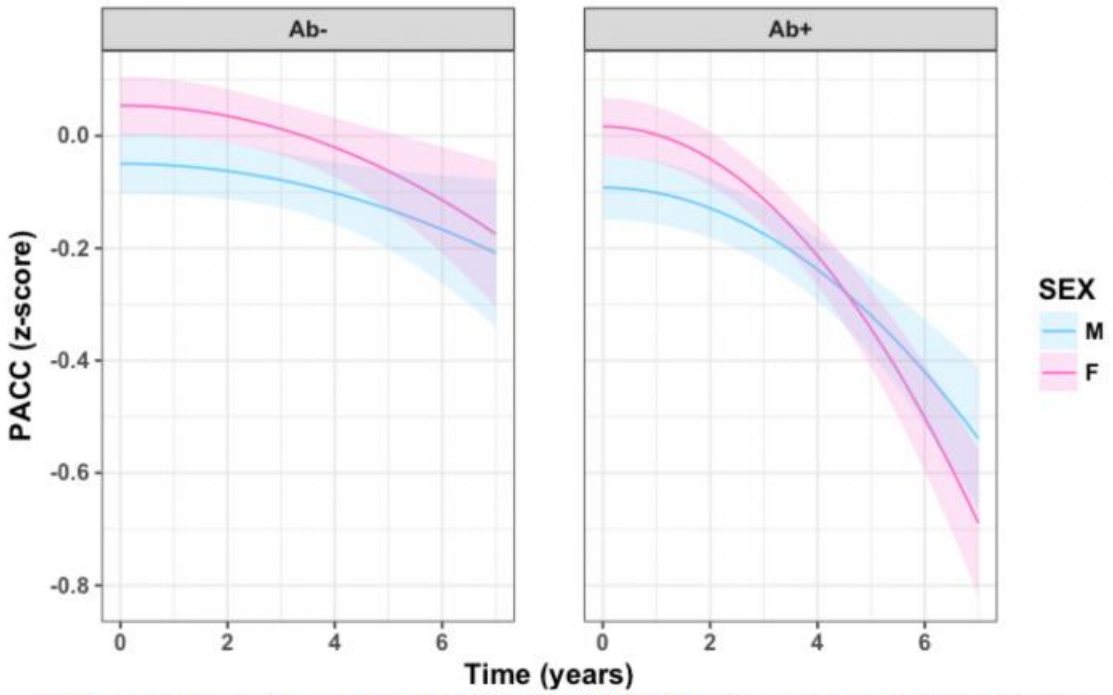

Fig1. Females with elevated amyloid exhibit the steepest cognitive decline

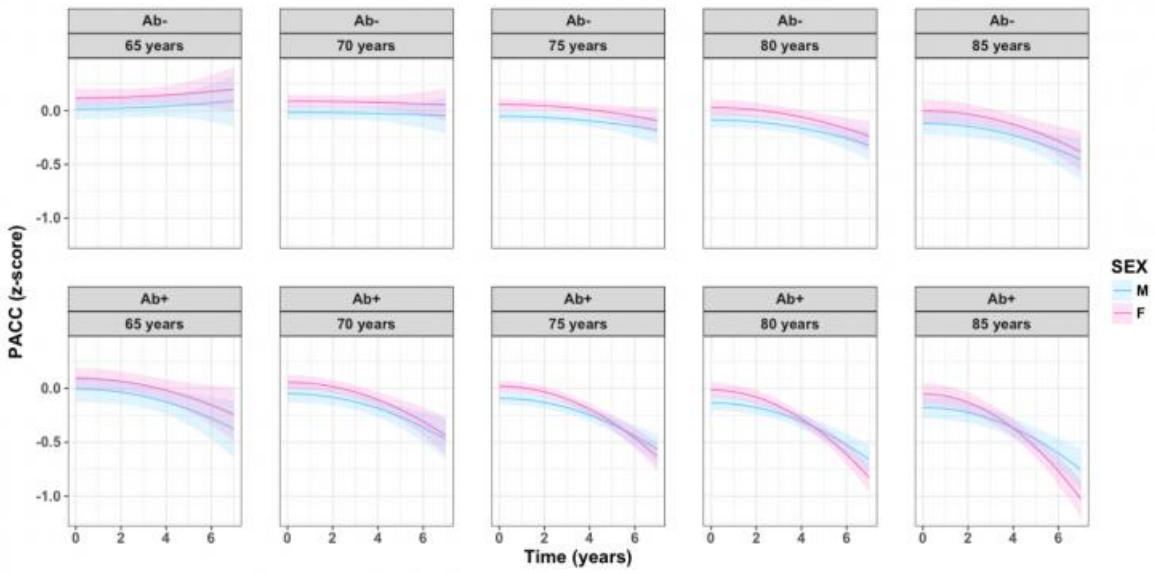

	Age 65-69	Age 70-74	Age 75-79	Age 80-94	Age 85+
Ab- (N)	183	115	118	64	16
Ab+ (N)	34	60	64	40	13

Fig2. Females over 80 with elevated amyloid are particularly vulnerable to cognitive decline

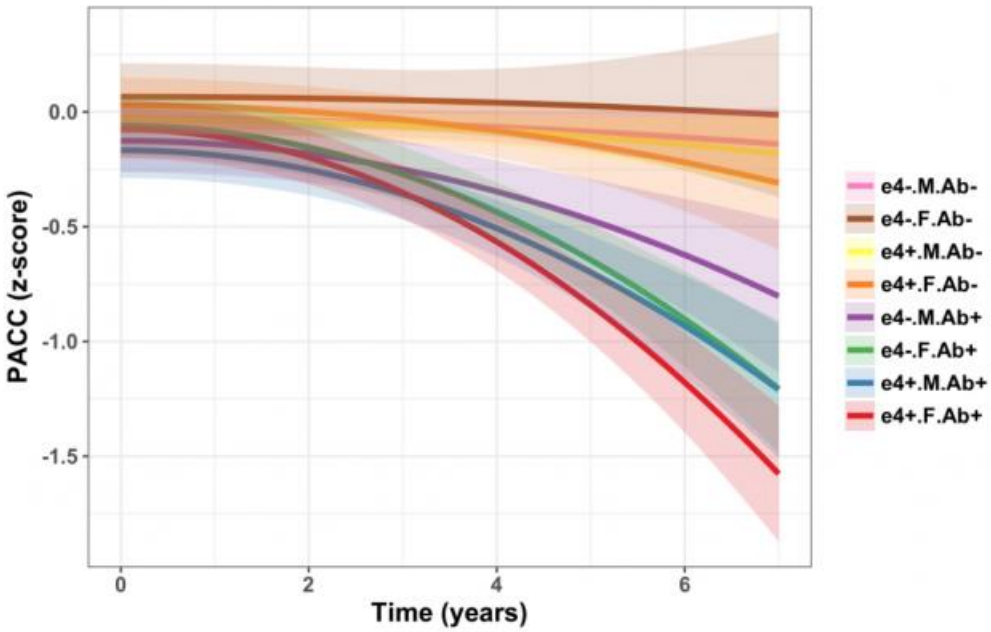

	APOEe4- M	APOEe4+ M	APOEe4- F	APOEe4+ F
Ab- (N)	191	41	220	62
Ab+ (N)	46	47	58	54

Fig3. Female APOEε4 carriers with elevated amyloid exhibit marginally greater cognitive decline than male counterparts

Keywords: Sex, Amyloid, Cognitive decline, APOE

Distinct information from CSF Tau and AV1451 PET measures in nondemented individuals

Yen Lim[1], Paul Maruff[1], Keith Johnson[2], Reisa Sperling[2], Elizabeth Mormino[3]

[1]*The Florey Institute of Neuroscience and Mental Health, Parkville, Australia*
[2]*Massachusetts General Hospital, Boston, MA, US*
[3]*Stanford University, Palo Alto, CA, US*

Background: Measurements of Amyloid and Tau become abnormal many years prior to the clinical presentation of Alzheimer's disease dementia. The complementary information gleaned from combining Amyloid and Tau during stages preceding dementia, especially across different Tau measurements (regional Tau PET v. CSF), remains unclear.

Methods: Nondemented participants from the Alzheimer's disease neuroimaging initiative (ADNI; N=33 normal and 38 MCI) were classified as Aβ- or Aβ+ using global cortical florbetapir PET values. As AV1451 Tau PET was introduced mid-study, florbetapir PET and CSF data closest to the AV1451 scan were used, as well as retrospective memory change that occurred prior to the AV1451 scan (mean=4 years). We examined associations between regional AV1451 PET (entorhinal, parahippocampal, hippocampus, and limbic), CSF Tau and pTau, and memory in each Aβ group, controlling for age and diagnosis.

Results: Across the entire group, AV1451 PET and CSF measures of Tau showed weak-to-moderate correlations, with the highest correlation between AV1451 Tau levels in entorhinal and CSF pTau ($r=0.57$, $p<.001$; Figure 1). Aβ+ individuals showed higher AV1451 PET values across all regions ($p<0.001$, Cohen's $d>1$), as well as higher levels of CSF total Tau and pTau ($p<0.001$, Cohen's $d>0.8$; Figure 2). Within the Aβ+ group, higher levels of continuous Aβ were associated with higher regional AV1451 values but not with CSF Tau. Regional AV1451 measures were associated with retrospective memory decline in the Aβ+ group only. CSF Tau or pTau were not related to memory in either Aβ group (Figure 3).

Conclusions: Tau measures are elevated among Aβ+ nondemented individuals. However, we observed only moderate associations between CSF and AV1451 Tau measures. Further, only AV1451 PET values relate to memory within Aβ+ individuals. CSF and PET measures of Tau capture different aspects of prodromal AD and should be examined simultaneously to improve our understanding of early pathology.

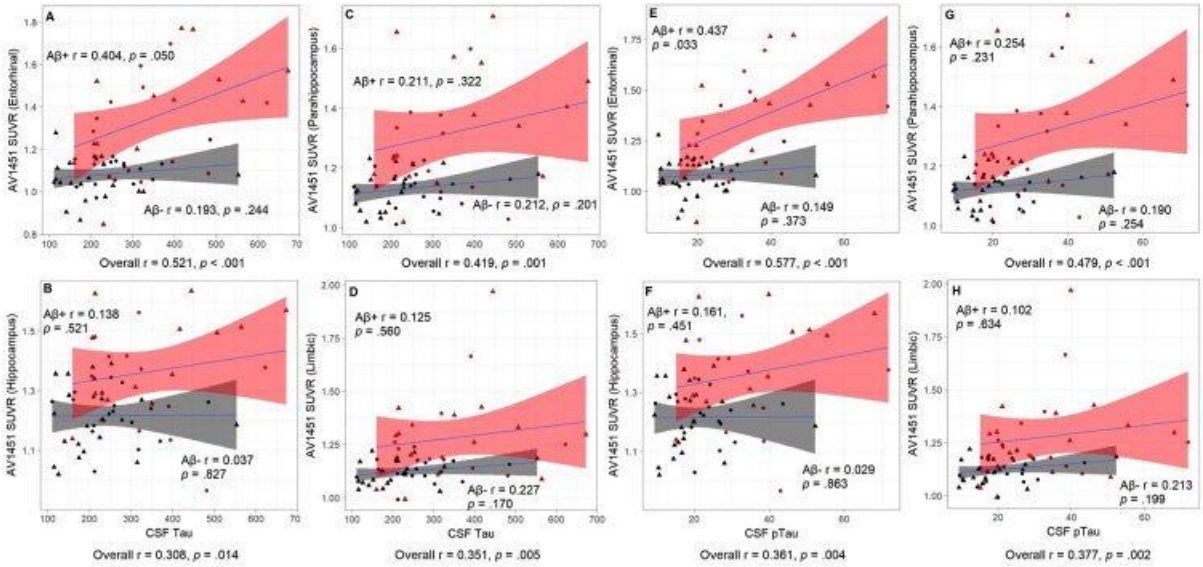

Figure 1: Association between Tau in each AV1451 region, and CSF tau and ptau.

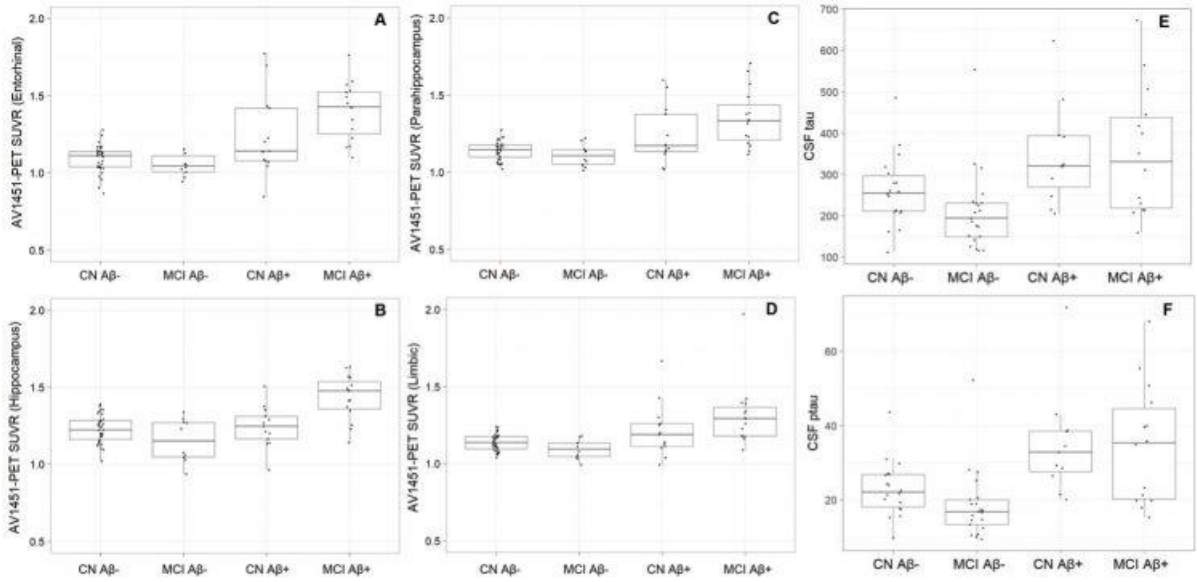

Figure 2: Measures of Tau from AV1451 (A-D) and CSF (E, F) by Aβ group.

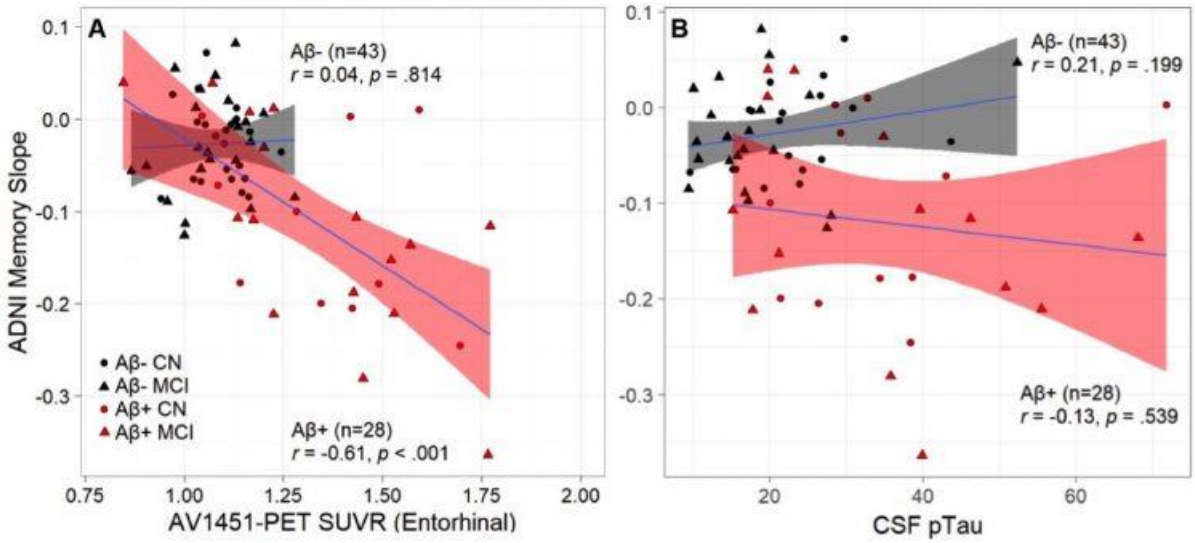

Figure 3: Association between memory and AV1451 from entorhinal (A) and CSF pTau (B). A similar pattern was seen across all examined AV1451 regions; the same lack of association with memory was observed for CSF total tau.

Keywords: CSF Tau, AV1451 PET, prodromal AD, memory

Abnormal CSF Aβ changes do not reliably precede florbetapir-PET increases in Aβ-negative normals followed longitudinally

Susan Landau[1,2], Lesley Shaw[3], John Trojanowski[3], William Jagust[1,2]

[1]*University of California, Berkeley, Berkeley, CA, US*
[2]*Lawrence Berkeley National Laboratory, Berkeley, CA, US*
[3]*Perelman School of Medicine, University of Pennsylvania, Philadelphia, PA, US*

Objectives: Low CSF Aβ is presumed to reflect Aβ deposition that is detectable prior to increasing amyloid PET. However, this widely-held view is based on small sample sizes, limited longitudinal followup, and poor CSF/PET measurement reliability. We used longitudinal florbetapir & CSF Aβ measurements in cognitively normal, Aβ-negative subjects from the Alzheimer's Disease Neuroimaging Initiative (ADNI) to determine whether the earliest subthreshold changes in Aβ are detectable with CSF before PET or vice versa.

Methods: Participants included 81 cognitively normal ADNI subjects who were unambiguously Aβ-negative at baseline (negative florbetapir-PET *and* negative CSF Aβ), and who had 2 or 3 concurrent florbetapir and CSF measurements over 2.7+/-1.0yrs. Measurements were optimized using recently developed strategies for longitudinal florbetapir analysis and the new Elecsys immunoassay platform. We examined CSF Aβ and florbetapir-PET annualized change for each subject to determine whether slopes were concordant (both CSF and PET indicating Aβ accumulation or both not indicating Aβ accumulation), or were discordant (CSF Aβ worsening but florbetapir was not; florbetapir worsening but CSF was not).

Results: Of Aβ-negative normals with at least 2 florbetapir-PET & CSF Aβ measurements, 45% of subjects had concordant CSF and PET slopes. Of the remaining individuals with discordant slopes, 25% worsened on florbetapir-PET only while 30% worsened on CSF Aβ only, indicating that early abnormal Aβ change was detectable with florbetapir-PET alone in nearly as many subjects as it was detectable with CSF Aβ alone. We also repeated the analysis using subjects with 3 florbetapir-PET & CSF Aβ measurements and found consistent results (of discordant subjects, 4/26 were worsening on PET only; 6/26 were worsening on CSF Aβ only).

Conclusion: Abnormal CSF Aβ changes are detectable prior to PET in some individuals, but the CSF-before-PET sequence of Aβ abnormality is not consistent. These findings challenge current assumptions about measurement of the earliest Aβ changes in late onset AD.

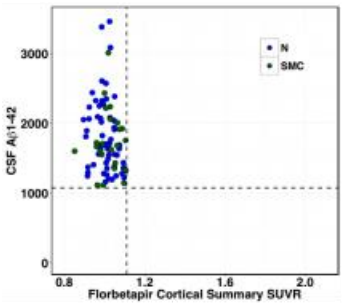

Fig A. N=81 Normal subjects with or without a subjective memory complaint who are negative on baseline florbetapir-PET and CSF Aβ and who had 2.7 +/- 1.0 yrs followup (2 or 3 concurrent longitudinal florbetapir-PET and CSF measurements over 2 to 4 years).

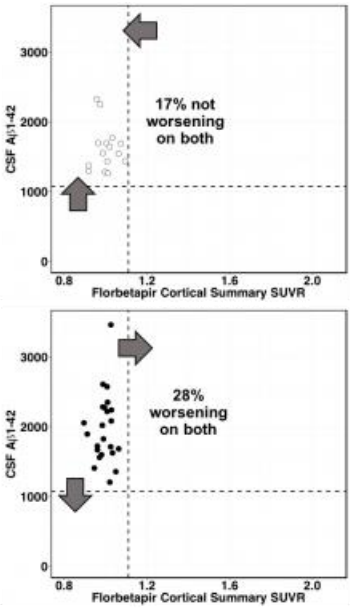

Fig B. 45% of these subjects had longitudinal CSF and PET slopes that were concordant in terms of Aβ worsening/not worsening: 17% of the group had longitudinal slopes consistent with worsening on both CSF & PET (top) while 28% had slopes that were consistent with not worsening on both (bottom).

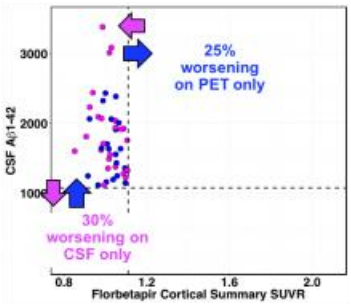

Fig C. Of the remaining subjects with discordant CSF & PET slopes, 25% were worsening on PET only while 30% were worsening on CSF only.

Keywords: CSF, PET, amyloid, normals

Thursday, January 18, 2018 - 04:50 pm - 05:35 pm

Podium Session

Poster Session 2B

See page 152.

Friday, January 19, 2018 - 08:30 am - 10:15 am

Podium Session

Session 7: Staging and Longitudinal Studies

CHAIRS: Keith Johnson, Reisa Sperling

Friday, January 19, 2018		
08:30 - 10:15	**Session 7: STAGING AND LONGITUDINAL STUDIES**	CHAIRS: Keith Johnson | Reisa Sperling
08:30	Longitudinal tau-PET in aging and Alzheimer's disease	**Jack** | Wiste | Schwarz | Lowe | Senjem | Vemuri | Weigand | Therneau | Knopman | Gunter | Jones | Graff-Radford | Kantarci | Roberts | Mielke | Machulda | Petersen
08:45	Longitudinal [18F]-AV-1451 Tau-PET scans in healthy older adults and Alzheimer's disease	**Harrison** | La Joie | Maass | Baker | Rabinovici | Jagust
09:00	"Where matters most": Regional amyloid deposition predict progression from preclinical to prodromal stages of Alzheimer's disease	**Bischof** | Hönig | Matusche | Hammes | Giehl | van Eimeren | Drzezga
09:15	In-vivo staging of regional amyloid deposition: evidence for validity and clinical significance from two independent cohort studies	**Grothe** | Sakr | Cavedo | Habert | Bertin | Locatelli | Lehericy | Dubois | Teipel | Hampel
09:30	Predictors of regional AV1451 uptake in non-demented older adults	Ziontz | **Bilgel** | Taylor | Shafer | Wong | Resnick
09:45	Discussion	

Longitudinal tau-PET in aging and Alzheimer's disease

Clifford Jack, Heather Wiste, Christopher Schwarz, Val Lowe, Matthew Senjem, Prashanthi Vemuri, Stephen Weigand, Terry Therneau, Dave Knopman, Jeff Gunter, Dave Jones, Jon Graff-Radford, Kejal Kantarci, Rosebud Roberts, Michelle Mielke, Mary Machulda, Ronald Petersen

Mayo Clinic, Rochester, MN, US

Objective: To compare different whole-brain and region-specific measurements of within-subject change on serial tau PET.

Methods: We studied 126 individuals: 59 cognitively unimpaired with normal amyloid (CUA-), 37 CU with abnormal amyloid (CUA+) and 30 cognitively impaired with amnestic phenotype and abnormal amyloid (CIA+). All had baseline PiB PET and two AV1451 tau-PET, MRI, and clinical assessments. We compared the topography (across all cortical ROIs) of tau-PET accumulation rates and the rates of four different whole-brain or region-specific meta-ROIs among the three clinical groups. We computed sample size estimates for change in tau-PET, cortical volume, and clinical/cognitive indices for use as outcome measures in clinical trials.

Results: The CUA- group had low rates of tau accumulation (near 0% per year) throughout the brain. Tau accumulation rates in CUA+ were low (0.5% per year) but greater than rates in CUA− in basal temporal and limbic areas. Tau accumulation rates in CIA+ were 3% per year and greater than rates in CUA+ in all cortical areas except medial temporal. Rates of accumulation in the four meta-ROIs differed but only slightly from one another. Among all tau-PET meta-ROIs, sample size estimates were smallest for a temporal lobe composite. The ordering of the sample size estimates by outcome measure was MRI < tau-PET < cognitive measures.

Conclusions: Once accumulation of pathologic tau has spread out of limbic areas, it accumulates throughout the brain, not in one area at a time in sequence or in clearly demarcated stages. The information captured by rate measures in different meta-ROIs, even those with no topographic overlap, was similar. The implication is that rate measurements based on granular Braak-like topographic staging or voxel-wise approaches may not provide significantly more information than simple meta-ROI rate measurements. Tau-PET SUVR measures should be an efficient outcome measure in disease modifying clinical trials.

Keywords: tau-PET, serial tau-PET, amyloid PET, clinical trials, Alzheimer’s disease

Longitudinal [18F]-AV-1451 Tau-PET scans in healthy older adults and Alzheimer's disease

Theresa Harrison[1], Renaud La Joie[2], Anne Maass[1,3], Suzanne Baker[4], Gil Rabinovici[2], William Jagust[1,4]

[1]*Helen Wills Neuroscience Institute, UC Berkeley, Berkeley, CA, US*
[2]*Memory and Aging Center, UCSF, San Francisco, CA, US*
[3]*German Center for Neurodegenerative Diseases, Magdeburg, Germany*
[4]*Lawrence Berkeley National Laboratory, Berkeley, CA, US*

Background: Tau accumulation is associated with normal aging and with Alzheimer's disease (AD). The rate at which tau accumulates in healthy older adults and patients with AD is not well described.

Methods: We used [^{18}F]-AV-1451-PET to interrogate tau accumulation over time in healthy older adults (OA; n=28) and patients with AD and MCI (n=8; Table 1). AV1451 images were normalized by cerebral white matter and preprocessed using a longitudinal pipeline that allowed for voxelwise analyses of change over time. ROI analyses were also performed using partial volume correction (PVC; Rousset method) and annual percent change (APC) was calculated for mean PVC SUVR values in regions corresponding to Braak stages. Linear mixed effects (LME) models were used to predict AV1451 change in Braak regions.

Results: Voxelwise analyses in OA revealed areas of bilateral temporal lobe including parahippocampal gyrus, temporal pole and inferior temporal gyrus where AV1451 significantly increased when controlling for age and time between AV1451 scans ($p<0.001$, cluster FWE $p<0.05$; Fig.1). There were no voxelwise differences related to sex, PiB status, *APOE* genotype or age. One sample t-tests on AV1451-APC in OA showed significant increases at follow-up in each Braak stage (Braak I/II mean AV1451-APC=3.58%, $p<0.001$; Braak III/IV mean AV1451-APC=3.01%, $p<0.001$; Braak V/VI mean AV1451-APC=2.69%, $p=0.002$). There were no differences in AV1451-APC based on PiB status in OA. LME models also showed no difference in rate of AV1451 change in PiB+ versus PiB- OA. In a model that included AD patients, there were significant differences in AV1451 change over time between AD and OA in Braak III/IV (mean AD AV1451-APC=6.44%, $p\leq0.01$; Fig.2) and Braak V/VI (mean AD AV1451-APC=7.45%, $p\leq0.001$), but not Braak I/II (mean AD AV1451-APC=2.39%, $p>0.3$).

Conclusions: Our findings provide evidence of in vivo tau accumulation in OA, and compare this to more severe pathological tau accumulation in AD.

Table 1: Cohort Demographics

	Healthy Older Adults (n=28)	AD/aMCI (n=8)
Age	78.4±5.6 (60-93)	61.6±8.8 (55-77)
Sex (M/F)	9/19	4/4
Edu	16.8±1.6 (13-20)	17.5±2.3 (16-22)
PiB +/- at Tau TP1	11+/17-	8+
APOE ε4 carriers	10 (1 missing)	5
Years Btwn Tau Scans	1.8±0.59 (1.04-3.19)	1.2±0.22 (1.02-1.73)

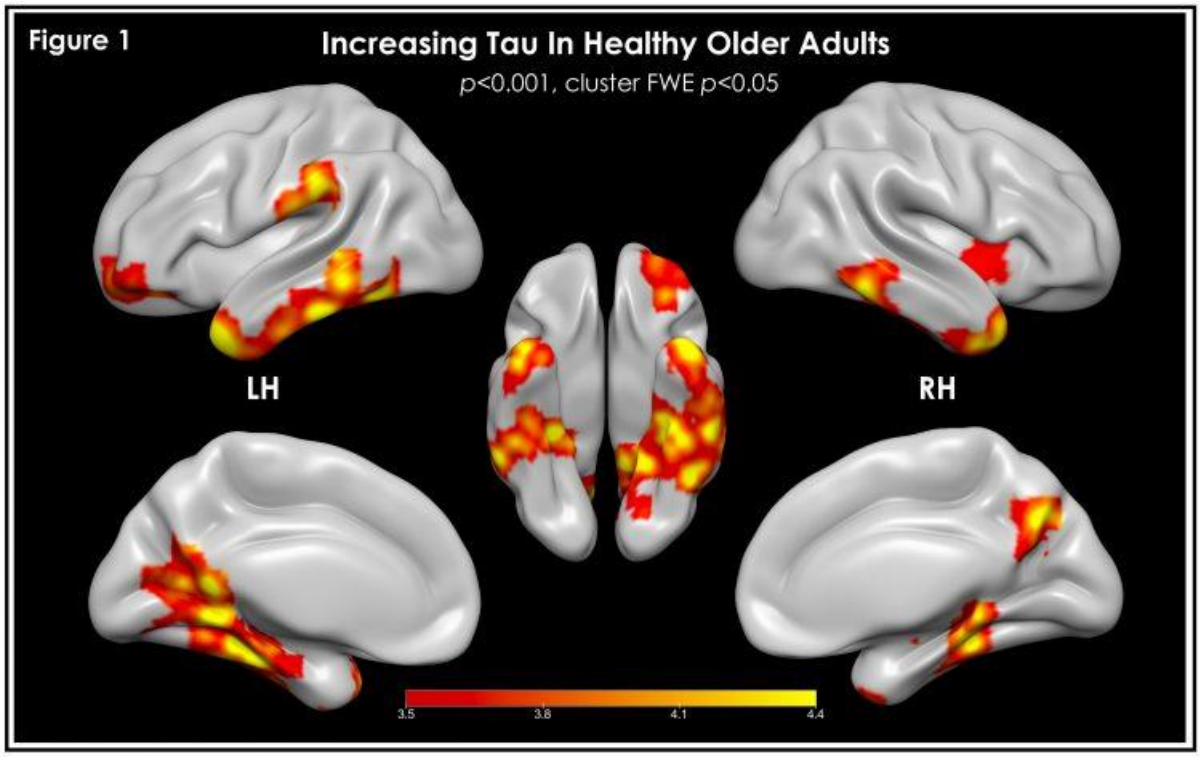

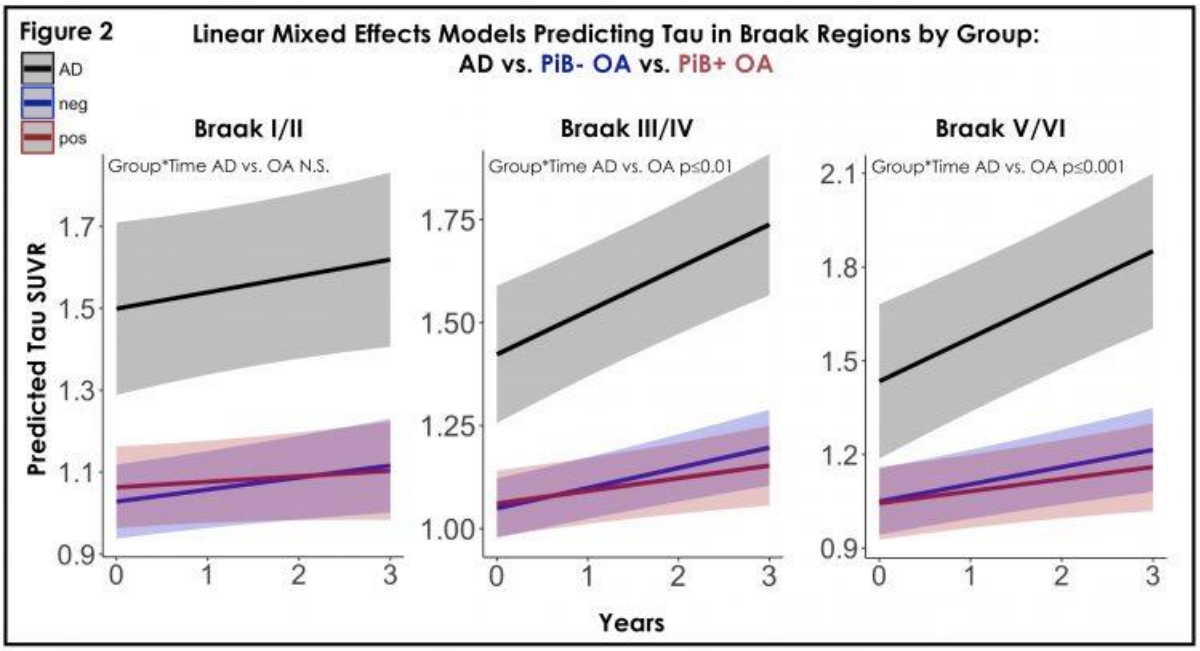

Keywords: PiB, linear mixed effects, partial volume correction

"Where matters most": Regional amyloid deposition predict progression from preclinical to prodromal stages of Alzheimer's disease

Gerard Bischof[1,2], Merle Hönig[1], Britta Matusche[1], Jochen Hammes[1], Kathrin Giehl[1], Thilo van Eimeren[1,2,3,4], Alexander Drzezga[1]

[1]*Multimodal Neuroimaging Group, Department of Nuclear Medicine, University Hospital Cologne, Cologne, Germany*
[2]*Cognitive Neuroscience, Institute of Neuroscience and Medicine (INM-3), Research Center Jülich, Jülich, Germany*
[3]*Department of Neurology, University Hospital Cologne, Cologne, Germany*
[4]*German Center for Dementia Research (DZNE), Bonn, Germany*

Beta-amyloid plaques (Aβ) a pathological hallmark of AD has been proposed to instigate the cascade of pathophysiological events that ultimately leads to AD. *In vivo* measurement of Aβ using PET have shown, that elevated cortical levels of amyloid burden (i.e., amyloid positivity) confer an increased risk to advance to prodromal stages of AD (MCI). However, not all amyloid-positive individuals progress to MCI, questioning the generalizability of overall cortical amyloid measures as an indicator of progression. Interestingly, very little is known about the contribution of regional amyloid accumulation to the advancement from preclinical to prodromal stages of AD.

Hence, we sought to test the hypothesis if regional amyloid accumulation differs in amyloid positive individuals who either continue to remain normal or progress to mild cognitive impairment over an observation period of up to five years. Individuals were matched for age, APOE status, education and sex. The resulting sample consisted of 44 individuals of amyloid-positive non-decliners and amyloid-positive decliners (*N*=22 each group). We examined a) differences in global amyloid burden b) assessed differences in regional amyloid accumulation and c) related amyloid deposition to temporal metrics of decline.

Whereas global amyloid did not differ between decliners and non-decliners, regional amyloid burden, primarily in the right hemisphere (e.g., angular gyrus, precuenus, inferior temporal and superior frontal cortex) was elevated in decliners compared to non-decliners. Importantly, in all amyloid-positive individuals, differing quantities of amyloid deposition in these particular regions was associated with the maintenance of cognitive status over time.

Our results underscore the role of regional amyloid accumulation to predict progression to prodromal stages of AD, whereas global amyloid levels may be less informative to predict decline within a certain time window. Together our results highlight the regional vulnerability of amyloid deposition and its contribution to the advancement from preclinical to prodromal stages of AD.

Keywords: Human Amyloid Imaging, Preclincal Alzheimer's Disease, MCI, Regional Amyloid Deposition, Amyloid Positivity

In-vivo staging of regional amyloid deposition: evidence for validity and clinical significance from two independent cohort studies

Michel Grothe[1], Fatemah Sakr[2], Enrica Cavedo[3], Marie Odille Habert[3], Hugo Bertin[3], Maxime Locatelli[3], Stephane Lehericy[3], Bruno Dubois[3], Stefan Teipel[1,2], Harald Hampel[3]

[1]*German Center for Neurodegenerative Diseases (DZNE), Rostock, Germany*
[2]*University Rostock Medical Center, Rostock, Germany*
[3]*Sorbonne Universités, Université Pierre et Marie Curie (UPMC) Paris 06, Inserm, CNRS, Hôpital de la Pitié-Salpêtrière, Paris, France*

Background: Neuropathologic studies suggest a distinct regional progression pattern of cerebral amyloid deposits that forms the basis of well-established amyloid staging schemes. We have recently adopted this neuropathologic approach to the analysis of florbetapir-PET data of cognitively normal (CN) older individuals from the ADNI cohort, and derived a 4-stage model of regional amyloid progression (Fig. 1) that resembled neuropathologic estimates and allowed to stage 96% of the individual deposition profiles (Grothe et al., Neurology, 2017). Here we evaluated the validity and clinical significance of this hierarchical staging scheme across large series of florbetapir-PET scans from individuals not originally involved in model determination.

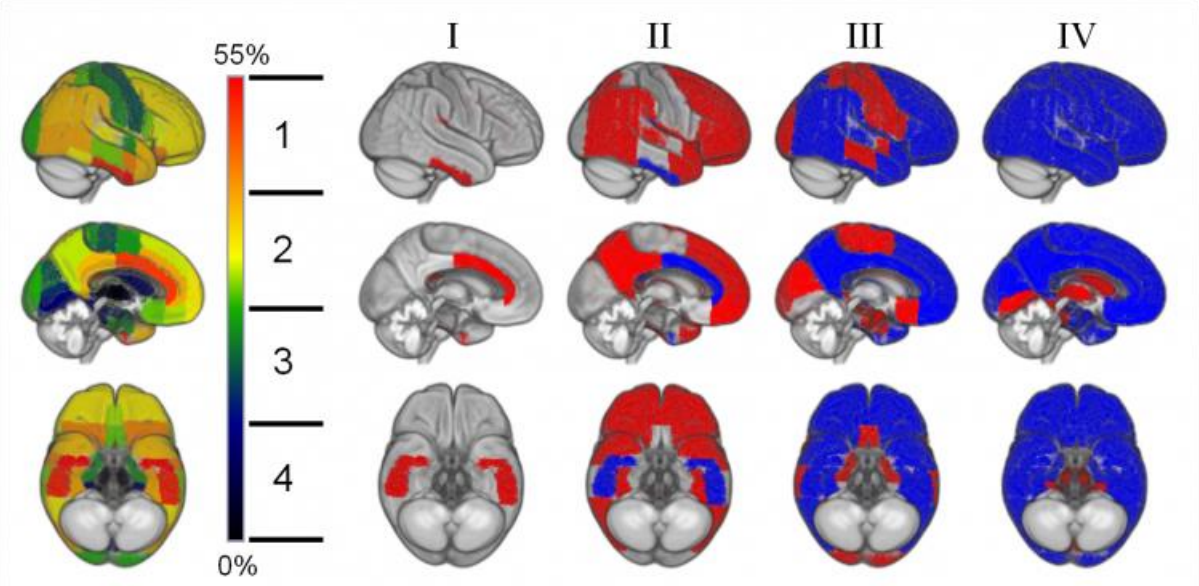

Figure 1. Model of regional amyloid progression and staging scheme. Brain renderings on the left illustrate the frequency of regional amyloid positivity across ADNI CN individuals. Brain regions are merged into 4 larger anatomic divisions based on equal partitions of the frequency range (1–4), and are used to define a 4-stage model of regional amyloid progression (I–IV) (Grothe et al. Neurology, 2017).

Methods: We analyzed florbetapir-PET and neuropsychologic data of patients with MCI (N=403) and AD dementia (N=85) from the ADNI cohort, as well as from an independent sample of CN individuals with subjective memory complaints (SMC) from the French INSIGHT-preAD study (N=318). Florbetapir-PET data was processed analogously to our original staging analysis and used to determine amyloid-positivity/negativity in the 4 anatomical divisions considered by the in-vivo staging scheme. We studied the prevalence of individual violations to the expected regional hierarchy, and assessed the association of amyloid stage with clinical diagnosis and delayed recall performance.

Results: Individual amyloid deposition profiles of all groups rarely deviated from the previously estimated regional hierarchy, allowing to stage 98% of ADNI-MCI, 99% of ADNI-AD, and 95% of INSIGHT-SMC with regional amyloid deposition into one of the 4 successive amyloid stages (Fig. 2). Advanced in-vivo amyloid stages (III/IV) were most frequently observed among cognitively impaired individuals (96% of ADNI-AD, 66% of ADNI-MCI, and 16% of INSIGHT-SMC with stageable amyloid deposition) and correlated with declining memory performance in nondemented individuals (ADNI-MCI: p<0.001; INSIGHT-SMC: p=0.03).

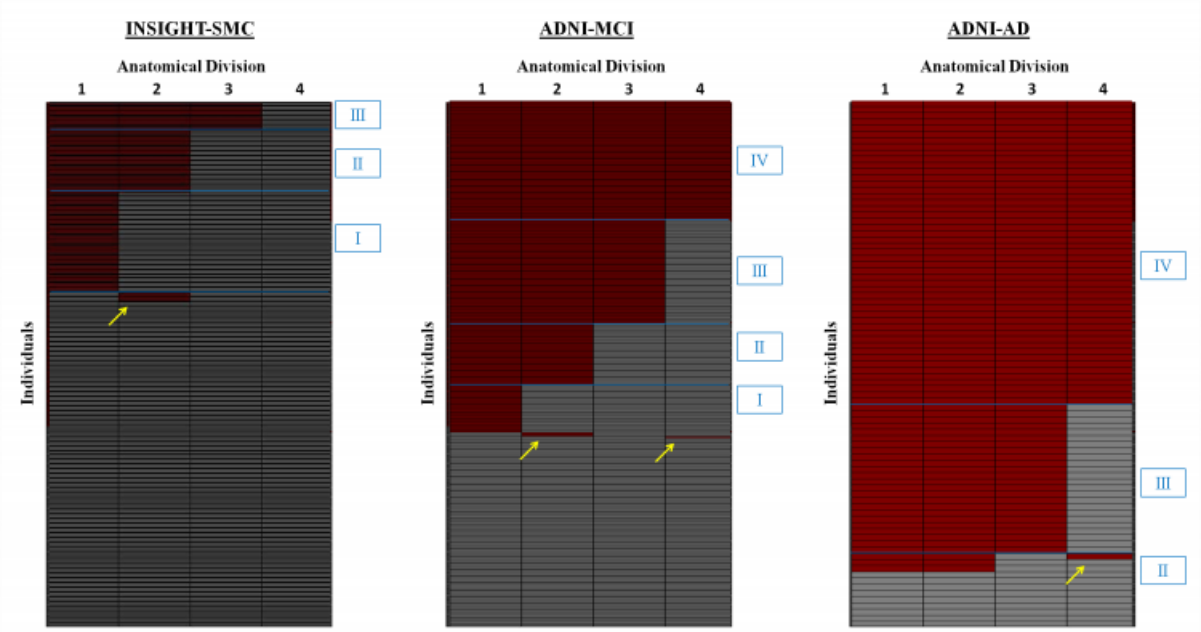

Figure 2. In-vivo staging of individual amyloid burden. Rows correspond to study participants and columns to the 4 anatomic divisions (1–4). Absence or presence of amyloid is denoted by gray and red, respectively. In each group, amyloid deposition shows a consistent hierarchical nesting across the 4 anatomic divisions considered by the staging scheme (blue boxes, I–IV). Deviations from the expected regional hierarchy (yellow arrows; 6 INSIGHT-SMC, 3 ADNI-MCI, 1 ADNI-AD) mainly affected order violations between the first two anatomical divisions.

Conclusions: The previously estimated hierarchical staging scheme of PET-evidenced amyloid deposition generalizes well to independent data and may provide a clinically-relevant stratification of prodromal AD.

Keywords: Amyloid, PET, Staging, Thal phases

Predictors of regional AV1451 uptake in non-demented older adults

Jacob Ziontz[1], Murat Bilgel[1], Jill Taylor[1], Andrea Shafer[1], Dean Wong[2], Susan Resnick[1]

[1]*Laboratory of Behavioral Neuroscience, National Institute on Aging, Baltimore, MD, US*
[2]*Department of Radiology and Radiological Science, Johns Hopkins University School of Medicine, Baltimore, MD, US*

Introduction: There is increasing interest in predictors of regional AV1451 uptake among non-demented older adults.

Methods: Cross-sectional PET data of 40 non-demented individuals (mean age 77.5 SD 8.6) from the Baltimore Longitudinal Study of Aging (BLSA) were analyzed using multiple regression models to explore associations between voxelwise AV1451 SUVR, age, and PiB group. This analysis identified regions of interest that, along with select areas based on Braak tau staging, were further examined for their correlations with age. We also examined the association of SUVR with regional PiB DVR and regional volume (residualized to account for intracranial volume), adjusting for age.

Results: The lentiform nucleus was identified as an area where both age and PiB positivity were associated with greater AV1451 uptake, confirmed by linear regression using regional SUVR as outcome. Age-adjusted SUVR was positively associated with continuous PiB DVR among PiB+ individuals in the fusiform gyrus (Braak III; p=0.02), inferior temporal gyrus (Braak IV; p=0.01), precuneus (Braak V; p=0.02), and postcentral gyrus (Braak VI; p=0.02). Age was correlated with SUVR only in the lentiform nucleus (p=0.035). Volume was negatively associated with age-adjusted SUVR in the inferior temporal gyrus (p=0.032), and positively associated in the postcentral gyrus (p=0.019).

Discussion: These are the first reported findings from the BLSA using the AV1451 tracer. In all analyzed regions in Braak III and beyond, AV1451 SUVR demonstrated a dose-dependent relationship with PiB DVR, indicating that data from our sample align with the current hypothesis that the spread of tau into the neocortex occurs in the presence of amyloid. The unexpected finding that both age and PiB positivity were associated with signal in the lentiform nucleus may be explained in part by previously-reported off-target binding of AV1451 in the putamen. Further investigation is necessary to better understand the factors influencing regional variation in AV1451 signal.

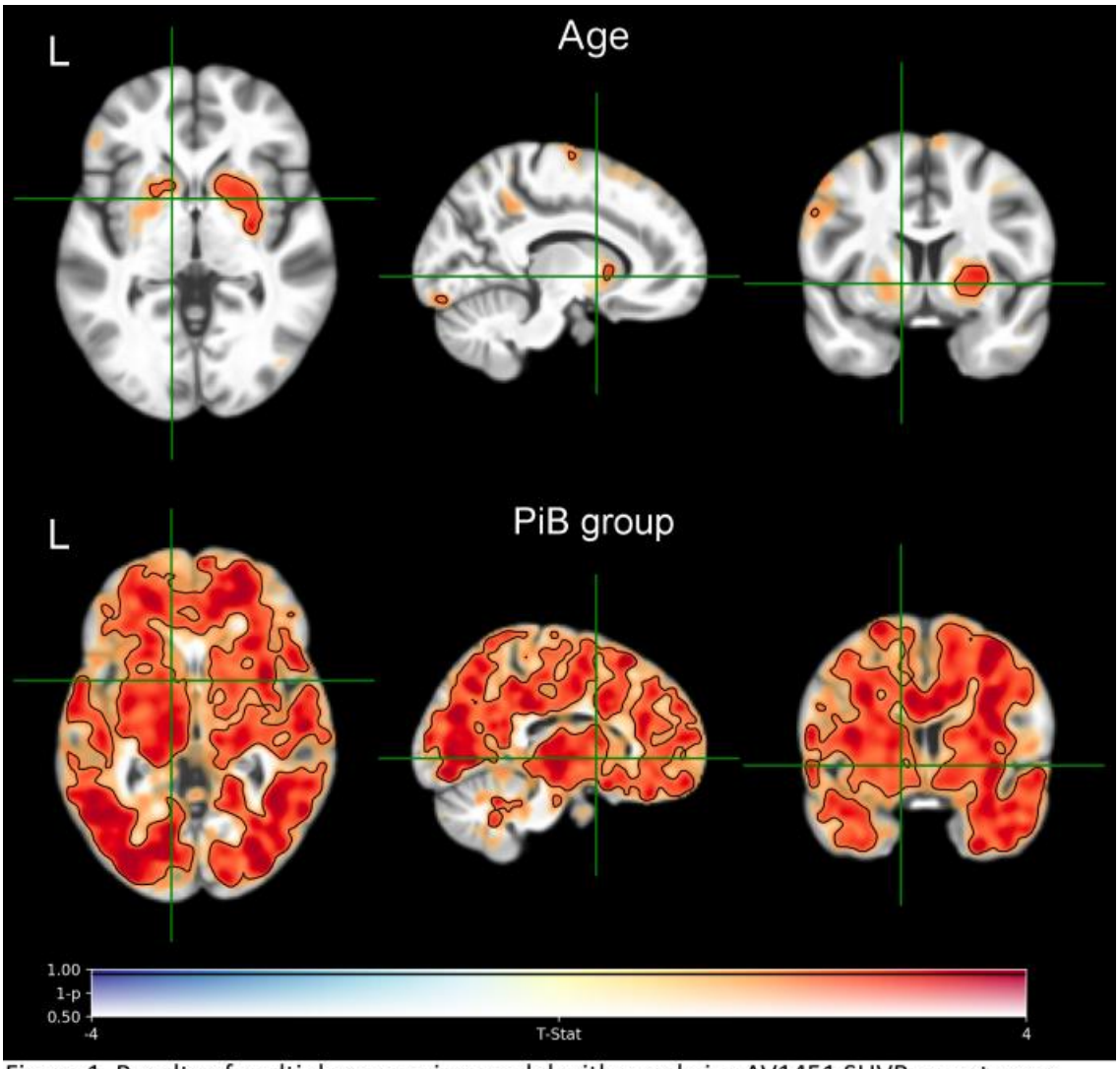

Figure 1. Results of multiple regression model with voxelwise AV1451 SUVR as outcome, and age and PiB group as predictors. T-statistics are mapped to color hue; (1-p) is mapped to transparency. Contours denote regression coefficients that are statistically different from 0 at $p<0.05$ (two-tailed t-tests, uncorrected).

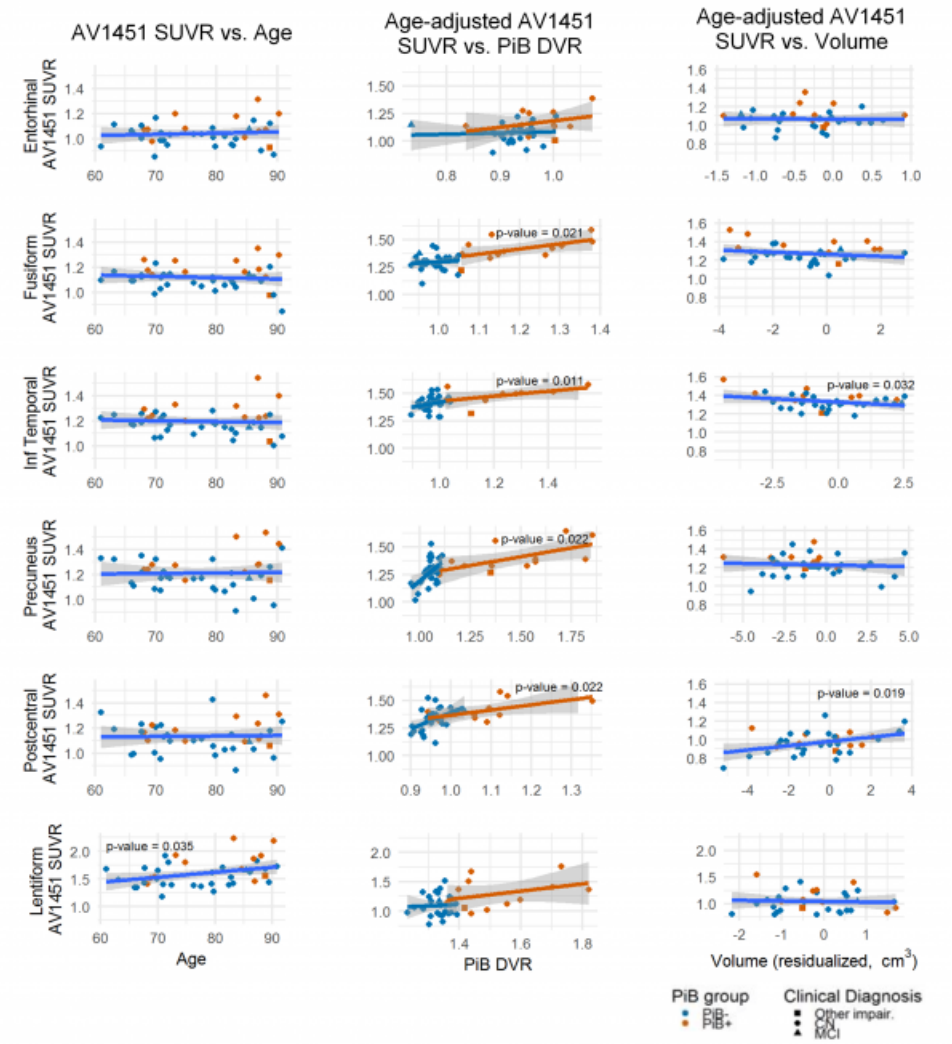

Figure 2. Left to right: (a) regional AV1451 SUVR vs. age, (b) age-adjusted regional AV1451 SUVR vs. regional PiB DVR, and (c) age-adjusted regional AV1451 SUVR vs. regional volume (residualized to account for intracranial volume). Top to bottom: Regions of interest: Entorhinal cortex (Braak I), fusiform gyrus (Braak III), inferior temporal gyrus (Braak IV), precuneus (Braak V), postcentral gyrus (Braak VI), and lentiform nucleus. Each marker indicates an individual. Blue = PiB-, orange = PiB+, circle = CN; triangle = MCI; square = other impairment.

Keywords: AV1451, PiB, volume, aging, PET

Friday, January 19, 2018 - 10:15 am - 11:00 am

Poster Session 3A *(3B will repeat at 4:15pm)*

Board #	Poster Title	Authors	Presenter
FRIDAY – POSTER SESSIONS 3A AND 3B			
115	[18F] AV-1451 uptake in corticobasal syndrome: the influence of beta-amyloid and clinical presentation	Ali | Whitwell | Martin | Senjen | Knopman | Jack | Lowe | Petersen | Boeve | Josephs	**Ali, Farwa**
116	Tau positron emission tomography is not elevated in HIV infected individuals	Ances | Beaumont | Cooley | Strain | Morris | Benzinger	**Ances, Beau**
141	Longitudinal relationships between brain amyloid deposition and glucose metabolism across the Alzheimer's disease spectrum	Bejanin | Arenaza-Urquijo | De Flores | Tomadesso | Chételat	**Bejanin, Alexandre**
104	Assessing the impact of beta-amyloid deposition in progressive supranuclear palsy	Boland | Ahlskog, PhD, MD | Tosakulwong, BS | Senjem, MS | Spychalla, BS | Petersen, MD | Jack Jr, MD | Lowe, MD | Josephs, MD, MST, MSc | Whitwell, PhD	**Boland, Sarah**
102	Application of the PredictND decision support system to cross-sectional imaging and psychometric data from an aMCI to probable AD three year outcomes clinical study	Buckley | Moreland | Urhemaa | van Gils | Wolber | lotjonen	**Buckley, Christopher**
121	Cerebrospinal fluid ratio of phosphorylated tau protein to beta-amyloid peptide 42 may improve the prediction of amyloid PET positivity: data from the Czech Brain Ageing Study	Cerman | Laczo | Vyhnalek | Sheradova | Ferda | Belohlavek | Hort	**Cerman, Jiri**
113	Twelve-month glucose metabolism declines in an empirically pre-defined statistical region-of-interest in amyloid-positive persons with Alzheimer's dementia and Mild Cognitive Impairment: updated ADNI findings	Chen | Lee | Kuang | Luo | Devadas | Thiyyagura | Chen | Bauer | Weiner | Jagust | Van Dyck | Reiman	**Chen, Kewei**
111	Effects of amyloid deposition and hippocampal activation on subjective memory complaints	Chen | Jingting | Farrell | Park	**Chen, Xi**
105	Flortaucipir imaging in primary progressive aphasia predicts variability in language impairment	Collins | Quimby | Makaretz | Sweeney | Wong | McGinnis | Dickerson	**Collins, Jessica**
112	Thresholds for amyloid positivity among normal, MCI and mild dementia subjects using [F-18] Florbetaben	Duara | Loewenstein | Lizzaraga | Adjouadi | Barker | Greig-Custo | Penate | Hanson | Marsiske | Vaillancourt | DeKosky | Golde	**Duara, Ranjan**
117	Left frontal hub connectivity delays cognitive decline in autosomal dominant and sporadic Alzheimer's disease	Franzmeier | Duezel | Jessen | Benzinger | Levin | Fagan | Morris | Bateman | Ewers	**Franzmeier, Nicolai**
136	[18F]-THK5351 binding patterns are associated with language deficits in primary progressive aphasia	Gabel | Schaeverbeke | Meersmans | Bruffaerts | Van Bouwel | Dries | Peeters | Van Laere | Dupont | Vandenberghe	**Gabel, Silvy**
109	Is there a local neurotoxic effect of regional amyloid deposits? A network-domain specific study of florbetapir-PET – cognition associations	Grothe | Sorg | Teipel	**Grothe, Michel**
118	Sex and e4 genotype influence the longitudinal association between amyloid and tau pathology in clinically normal older adults	Hanseeuw | Buckley | Mormino | Jacobs | Chhatwal | Gomez | Johnson | Sperling	**Hanseeuw, Bernard**
132	The BioFINDER-2 study: a longitudinal investigation on the role of tau and amyloid on cognitive function using 18F-RO6958948 and 18-Flutemetamol PET tracers	Hansson | Mattsson | Smith | Schöll | Klein | Farrar | Borroni | Coloma | Palmqvist | Stomrud	**Hansson, Oskar**
131	Multiple brain markers contribute to age-related changes in cognition	Hedden | Nierle | Perea | Rabin | Buckley | Schultz | Johnson | Sperling	**Hedden, Trey**

Board #	Poster Title	Authors	Presenter
FRIDAY – POSTER SESSIONS 3A AND 3B			
125	Tau pathology networks associated with functional connectivity networks and disease progression in Alzheimer's disease	Hönig | Bischof | Seemiller | Hammes | Fink | van Eimeren | Drzezga	**Hönig, Merle**
139	Long-term clinical stability in amyloid-positive subjects is predicted by negative FDG-PET scan	Iaccarino | Sala | Perani	**Iaccarino, Leonardo**
128	Nucleus basalis of Meynert volume predicts early tau pathology and memory performance when amyloid levels are elevated in cognitively normal older individuals	Jacobs | Hanseeuw | Schultz | Papp | Rentz | Sperling | Johnson	**Jacobs, Heidi**
127	Tau aggregates imaged with 18F-Flortaucipir PET contribute to core clinical features of the Lewy body dementias	Katz | Ye | Shirvan | Schultz | Makaretz | Dickerson | Sperling | Growdon | Johnson | Gomperts	**Katz, Samantha**
135	Effects of amyloid, tau, and hippocampal volume on normal and fast gait speeds in cognitively normal older adults: results from the Harvard Aging Brain study	Kirn | Buckley | Hanseeuw | Klein | Properzi | Sperling | Johnson	**Kirn, Dylan**
106	[18F]flutemetamol amyloid binding potential in relation to memory in cognitively normal subjects aged 80 years and older	Legdeur | Buslenko | Konijnenberg | ten Kate | Badissi | Tomassen | den Braber | Yaqub | Boomsma | Lammertsma | Maier | Scheltens | van Berckel | Visser	**Legdeur, Nienke**
123	18F-AV1451 tau PET in patients at risk for chronic traumatic encephalopathy	Lesman-Segev | La Joie | Tsai | Bourakova | Visani | Ayakta | P O'Neil | Maass | Baker | Perry | Kramer | Miller | Jagust | Rabinovici	**Lesman-Segev, Orit**
110	A similar prevalence and magnitude of amyloid positivity between cognitively normal elderly Japanese and Americans	Yu | Lopresti | Ihara | Cui | Aizenstein | Dodge | Minhas | Lopez | Klunk | Mathis | Kuller | Miyamoto | Sekikawa	**Lopresti, Brian**
124	Longitudinal [18F]THK5317 and [18F]FDG PET in relation to novel CSF tau fragments in Alzheimer's disease and related primary tauopathies	Leuzy | Chiotis | Cicognola | Saint-Aubert | Zetterberg | Blennow | Höglund | Nordberg	**Leuzy, Antoine**
138	Tau deposition in relation to verbal and phonemic fluency in the Framingham Heart Study	Luner | Jacobs | Papp | Becker | Beiser | Daniluk | Himali | Jin | Katz | Killiany | Moody | Pase | Peets | Raman | Sanchez | Satizabal | Schafer | Seshadri | Johnson	**Luner, Evelyn**
134	Effects of tau and amyloid deposition on domain-specific memory function in old age	Maass | Berron | Harrison | Baker | Mellinger | Swinnerton | Bell | Duezel | Jagust	**Maass, Anne**
100	Cross-sectional and longitudinal atrophy is preferentially associated with tau rather than Aβ PET pathology	McCullough | Gordon | Mishra | Blazey | Su | Christensen | Dincer | Jackson | Hornbeck | Morris | Ances | Benzinger	**McCullough, Austin**
129	Increased GM regions in association with SUVR are candidate to predict convergence to Preclinical AD	Monté-Rubio | Rodriguez-Gomez | Sanabria | Alegret | Perez-Cordon | Lomeña | Pavia | Gismondi | Bullich | Vivas-Larruy | Gomez-Chiari | Ruiz-Laza | Tárraga | Boada	**Monté-Rubio, Gemma**
140	Associations between tau, Aβ and cortical thickness with cognition in Alzheimer's disease	Ossenkoppele | Smith | Ohlsson | Mattsson | Strandberg | Palmqvist | Hansson	**Ossenkoppele, Rik**
120	Evidence for neuroinflammation in semantic dementia	Pascual | Zanotti-Fregonara | Pal | Rockers | Funk | Yu | Roman | Schultz | Masdeu	**Pascual, Belen**
137	Personality traits and neuropsychiatric factors are related to increased amyloid deposition in cognitively normal older adults	Pichet Binette | Vachon-Presseau | Gonneaud | Marchant | Bellec | Breitner | Villeneuve | Research Group	**Pichet Binette, Alexa**
114	Flortaucipir PET measurements and relationships with cognitive impairment	Protas | Ghisays | Luo | DeMarco | Thiyyagura | Devadas | Bauer | Landau | Weiner | Jagust | Reiman | Chen	**Protas, Hillary**
119	The DCTclockTM test captures subtle cognitive changes and biomarker evidence of preclinical Alzheimer's disease	Rentz | Papp | Orlovsky | Souillard-Mandar | Penney | Davis | Johnson	**Rentz, Dorene**

Board #	Poster Title	Authors	Presenter
FRIDAY – POSTER SESSIONS 3A AND 3B			
108	[18F]Flutemetamol imaging in the ALFA project: Cognitively healthy subjects enriched for Alzheimer's disease genetic risk factors	Salvadó | Brugulat | Falcon | Pavia | Lomeña | Molinuevo | Gispert	**Salvadó, Gemma**
103	Tau pathology detected by [18F]GTP1 negatively correlates with cortical volume in Alzheimer's disease	Ray | Baker | Manser | Ward | Teng | Weimer | Sanabria Bohórquez	**Sanabria Bohórquez, Sandra**
130	Distinct [18F]-THK5351 binding patterns in primary progressive aphasia variants	Schaeverbeke | Gabel | Bruffaerts | Meersmans | Van Bouwel | Dries | Peeters | Van Laere | Dupont | Vandenberghe	**Schaeverbeke, Jolien**
133	PiB PET as a biomarker for white matter integrity in aging and dementia	Su | Wang | Flores | Wang | Beau | Morris | Benzinger	**Su, Yi**
101	[18F]Florbetapir binding potential in relation to cognition in subjective cognitive decline	Timmers | Verfaillie | Wesselman | Slot | Prins | van der Weijden | Yaqub | Lammertsma | Boellaard | Ossenkoppele | van der Flier | van Berckel	**Timmers, Tessa**
126	Characterizing regional β-amyloid burden by magnetic susceptibility	Unschuld | van Bergen | Li | Quevenco | Gietl | Treyer | Meyer | Buck | Kaufmann | Nitsch | van Zijl | Hock	**Unschuld, Paul**
107	Amyloid-β load is related to worries in individuals with subjective cognitive decline	Verfaillie | Timmers | Slot | van der Weijden | Wesselman | Prins | Sikkes | Lammertsma | Scheltens | Ossenkoppele | van Berckel | van der Flier	**Verfaillie, Sander**
122	Relationships between self-reported sleep, tau, and Aβ in healthy older adults	Winer | Maass | Harrison | Mellinger | Baker | Walker | Jagust	**Winer, Joseph**

P100: Cross-sectional and longitudinal atrophy is preferentially associated with tau rather than Aβ PET pathology

Austin McCullough[1], Brian Gordon[1,2,3], Shruti Mishra[1], Tyler Blazey[1], Yi Su[1], Jon Christensen[1], Aylin Dincer[1], Kelley Jackson[1], Russ Hornbeck[1], John Morris[2,4], Beau Ances[2,4], Tammie Benzinger[1,2]

[1]*Mallinckrodt Institute of Radiology, Washington University in St. Louis, St. Louis, MO, US*
[2]*Knight Alzheimer's Disease Research Center, Washington University in St. Louis, Saint Louis, MO, US*
[3]*Department of Psychological and Brain Sciences, Washington University in St. Louis, St. Louis, MO, US*
[4]*Department of Neurology, Washington University in St. Louis, St. Louis, MO, US*

Introduction: Structural magnetic resonance imaging (MRI) is a marker of grey matter health and decline that is sensitive to impaired cognition and Alzheimer's disease pathology. Prior work has shown that both amyloid-beta (Aβ) and tau biomarkers are related to cortical thinning, but it is unclear what unique influences they have on the brain.

Methods: Aβ pathology was measured with [18F] AV-45 (florbetapir) positron emission tomography (PET) and tau was assessed with [18F] AV-1451 (flortaucipir) PET in a population of 183 older adults, of which 127 had longitudinal MRI assessments (average of 5.7 years) that preceded the PET acquisitions.

Results: In cross-sectional analyses greater tau PET pathology was associated with thinner cortices. When examined independently in longitudinal models, both Aβ and tau were associated with greater antecedent loss of grey matter. However when examined in a combined model levels of tau, but not Aβ, were still highly related to change in cortical thickness.

Discussion: Measures of tau PET are strongly related to grey matter and likely mediate relationships between Aβ and grey matter.

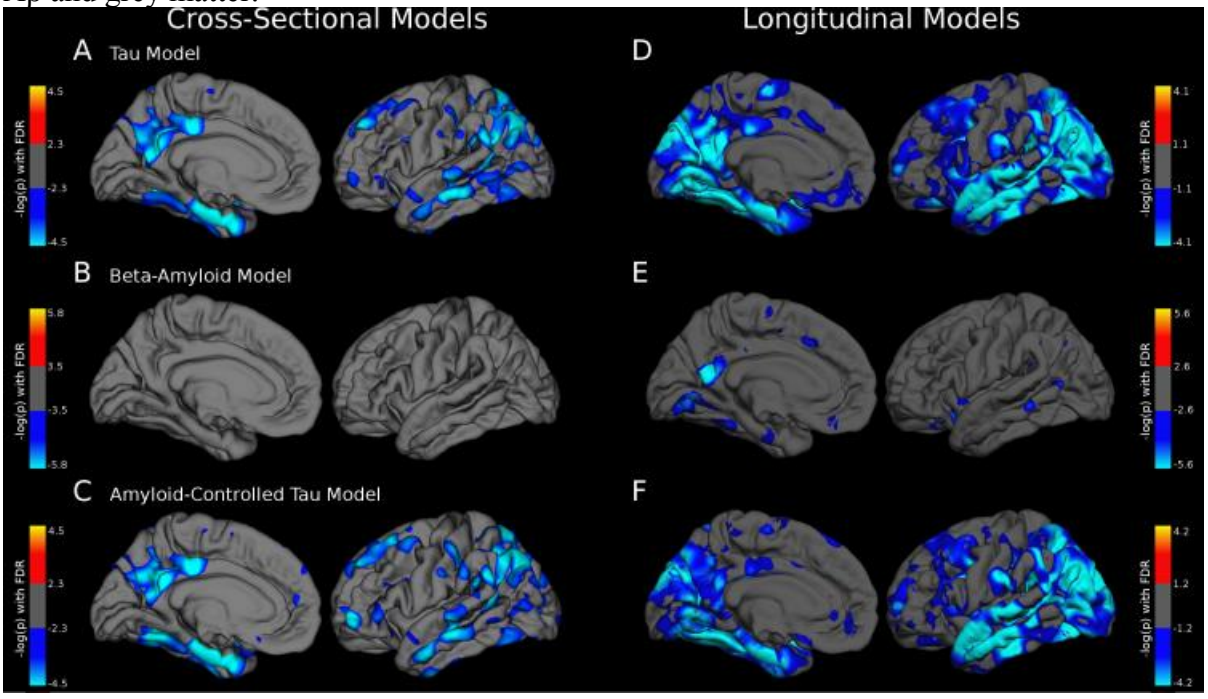

Figure 1. The relationship between global AD pathology and grey matter

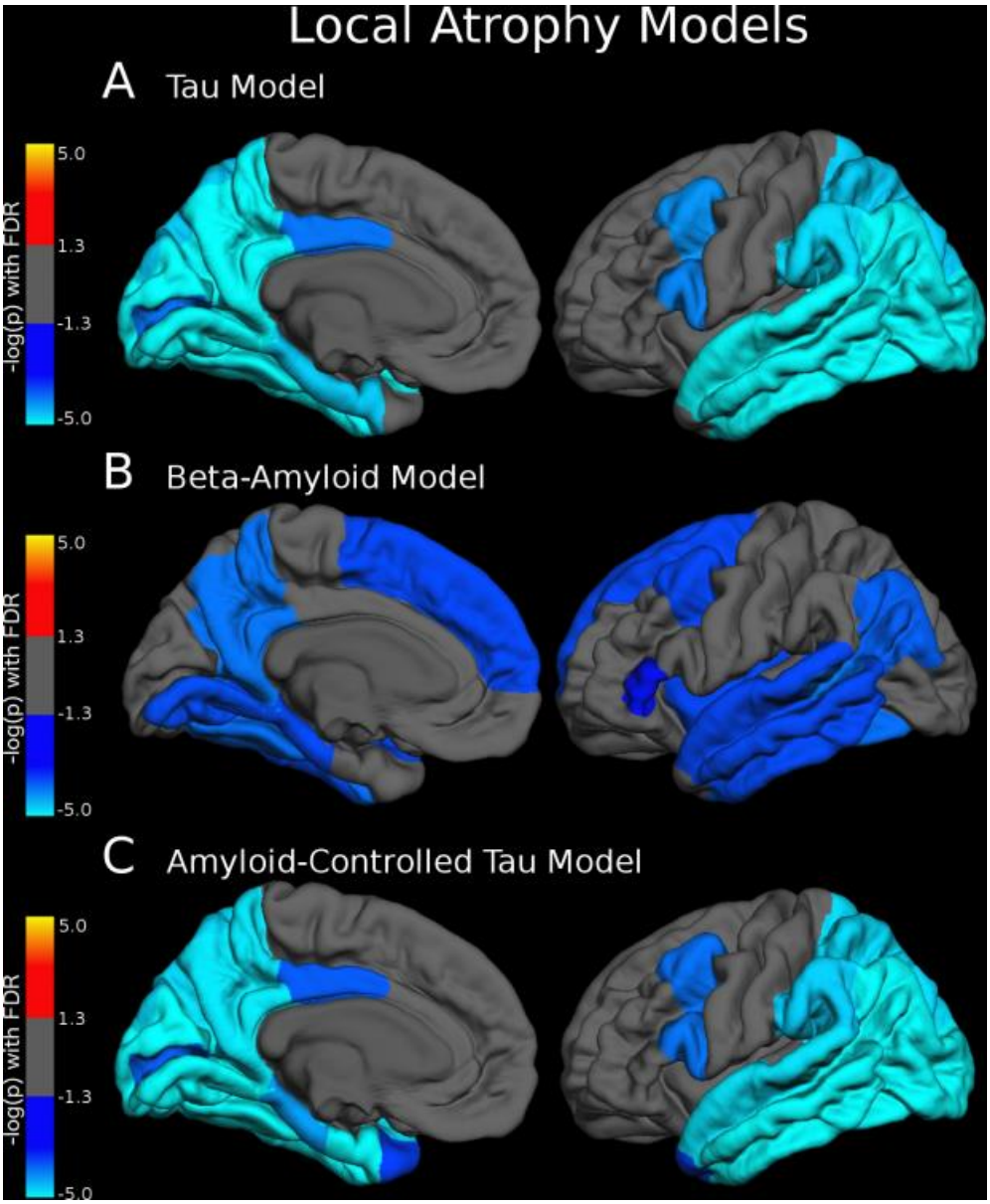

Figure 2. The relationship between local AD pathology and grey matter

Keywords: thickness, atrophy, tau, amyloid, PET, positron emission tomography, MRI

P101: [18F]Florbetapir binding potential in relation to cognition in subjective cognitive decline

Tessa Timmers[1,2], Sander C.J. Verfaillie[2], Linda M.P. Wesselman[2], Rosalinde E.R. Slot[2], Niels D. Prins[2], Chris W.J. van der Weijden[1], Maqsood M. Yaqub[1], Adriaan A. Lammertsma[1], Ronald Boellaard[1], Rik Ossenkoppele[2,3], Wiesje M. van der Flier[2,4], Bart N.M. van Berckel[1]

[1]Department of Radiology & Nuclear Medicine, Amsterdam Neuroscience, VU University Medical Center, Amsterdam, Netherlands
[2]Alzheimer Center, Department of Neurology, Amsterdam Neuroscience, VU University Medical Center, Amsterdam, Netherlands
[3]Clinical Memory Research Unit, Lund University, Lund, Sweden
[4]Department of Epidemiology and Biostatistics, VU University Medical Center, Amsterdam, Netherlands

Background: Subjective cognitive decline (SCD) is associated with an increased risk of dementia and might reflect the earliest changes related to Alzheimer's disease. The aim of this study was to investigate the relationships between specific [^{18}F]florbetapir binding at baseline and concurrent and longitudinal cognitive performance in SCD.

Methods: 98 subjects with SCD (age 64±8, 45% female, MMSE 29±1, 22% amyloid positive on visual assessment) were recruited from the SCIENCe study, an ongoing prospective memory clinic cohort study on SCD. All underwent 90 minute dynamic [^{18}F]florbetapir PET scans at baseline. Receptor parametric mapping (RPM) with cerebellar gray matter as reference tissue was used to calculate [^{18}F]florbetapir binding potential (BP_{ND}) in parietal, temporal, occipital, frontal and global regions. Neuropsychological tests covering, memory, language, executive function and attention domains, were performed at baseline and for a subset at follow up (n=65 at follow up year 1, n= 12 at follow up year 2). Linear mixed models, adjusting for age, sex and education, were used to assess the relationships between [^{18}F]florbetapir BP_{ND} and neuropsychological scores.

Results: Significant main effects of [^{18}F]florbetapir showed that higher BP_{ND} in global neocortex, and frontal, temporal and parietal regions were related to lower baseline MMSE ($p<0.05$, Table-1). Significant interactions with time indicated that higher [^{18}F]florbetapir BP_{ND} was associated with steeper annual decline on delayed recall of Rey Auditory Visual Learning Test, Visual Association Test, and Digit Span forward (Table-1).

Conclusion: SCD subjects with higher specific [^{18}F]florbetapir binding demonstrated somewhat lower global cognitive performance at baseline. Moreover, higher amyloid load predisposed for faster decline in memory and attention. These data are in line with the notion that amyloid positivity in cognitively normal individuals increases the risk of subsequent cognitive decline.

Table 1: Neuropsychological baseline data and annual change

	Global [^{18}F]florbetapir	Frontal [^{18}F]florbetapir	Parietal [^{18}F]florbetapir	Temporal [^{18}F]florbetapir	Occipital [^{18}F]florbetapir
Global cognition					
MMSE	**-2.2 ± 0.7***	**-1.9 ± 0.6***	**-2.0 ± 0.6***	**-2.6 ± 0.9***	-1.4 ± 0.8
Annual change	0.2 ± 0.8	0.1 ± 0.7	0.6 ± 0.7	-0.1 ± 0.9	0.3 ± 0.9
Memory					
VAT-B	-0.1 ± 0.8	-0.3 ± 0.7	-0.3 ± 0.7	-0.3 ± 1.0	0.7 ± 0.9
Annual change	-1.9 ± 1.0	**-2.2 ± 0.9***	-1.3 ± 0.8	-1.7 ± 1.2	-1.0 ± 1.1
RAVLT	-1.9 ± 1.0	-2.5 ± 5.3	-2.8 ± 5.2	-3.0 ± 7.1	3.3 ± 6.3
Annual change	-5.5 ± 4.4	-5.4 ± 3.9	-3.9 ± 3.6	-5.3 ± 4.8	-4.8 ± 4.8
RAVLT delayed recall	-2.2 ± 2.1	-2.4 ± 1.8	-2.2 ± 1.8	-2.4 ± 2.5	0.2 ± 2.1
Annual change	**-3.4 ± 1.7***	-2.7 ± 1.5	-2.6 ± 1.4	-3.5 ± 1.9	-3.0 ± 1.8
Rey figure delayed recall	3.0 ± 3.8	1.9 ± 3.3	2.9 ± 3.2	2.9 ± 4.4	3.6 ± 3.8
Annual change	-3.1 ± 3.2	-4.7 ± 2.8	-2.9 ± 2.5	-1.6 ± 3.8	1.2 ± 3.3
Attention					
Digit span forward	-0.8 ± 2.1	-1.3 ± 1.8	-0.5 ± 1.8	-0.6 ± 2.5	0.1 ± 2.1
Annual change	**-3.0 ± 1.4***	-2.1 ± 1.3	**-2.5 ± 1.1***	**-3.8 ± 1.5***	-2.9 ± 1.5
TMT-A	0.1 ± 0.1	0.1 ± 0.1	0.1 ± 0.1	0.1 ± 0.1	0.0 ± 0.1
Annual change	-0.6 ± 0.1	-0.0 ± 0.1	-0.0 ± 0.1	-0.7 ± 0.1	-0.1 ± 0.1
Stroop I	-0.3 ± 0.0	-0.0 ± 0.0	-0.0 ± 0.0	-0.0 ± 0.1	-0.1 ± 0.0
Annual change	-0.4 ± 0.0	-0.0 ± 0.0	-0.0 ± 0.0	-0.0 ± 0.3	-0.0 ± 0.0
Executive					
Digit span backwards	0.7 ± 1.8	0.4 ± 1.6	0.9 ± 1.5	0.7 ± 2.1	0.8 ± 1.8
Annual change	-1.4 ± 1.5	-0.9 ± 1.3	-1.4 ± 1.2	-2.0 ± 1.6	-0.7 ± 1.6
TMT-B	0.0 ± 0.1	0.0 ± 0.1	0.0 ± 0.1	-0.0 ± 0.1	-0.0 ± 0.1
Annual change	-0.1 ± 0.1*	-0.1 ± 0.1	-0.1 ± 0.1	-0.1 ± 0.1	-0.1 ± 0.1
Stroop III	-0.0 ± 0.1	-0.0 ± 0.1	-0.0 ± 0.1	-0.0 ± 0.1	-0.0 ± 0.1
Annual change	-0.0 ± 0.0	-0.0 ± 0.0	-0.0 ± 0.0	-0.0 ± 0.0	-0.0 ± 0.0
Letter fluency	4.5 ± 7.2	2.0 ± 6.2	3.0 ± 6.1	7.8 ± 8.4	6.7 ± 7.3
Annual change	-6.5 ± 4.8	-6.5 ± 4.3	-3.2 ± 3.9	-7.8 ± 5.3	-6.0 ± 5.2
Language					
Animal fluency	-0.9 ± 3.6	-2.3 ± 3.1	-1.4 ± 3.0	1.1 ± 4.2	1.7 ± 3.6
Annual change	-1.6 ± 2.5	-2.1 ± 2.2	-1.2 ± 2.0	-1.8 ± 2.7	0.2 ± 2.7
BNT	-2.2 ± 3.7	-2.1 ± 3.2	-2.0 ± 3.1	-0.9 ± 4.3	-2.2 ± 3.8
Annual change	-2.7 ± 2.0	-2.5 ± 1.8	-1.8 ± 1.6	-3.2 ± 2.2	-2.2 ± 2.3
Visuospatial functioning					
Rey figure copy	0.9 ± 1.2	1.1 ± 1.0	0.8 ± 1.0	0.5 ± 1.4	0.3 ± 1.2
Annual change	-0.7 ± 1.6	-1.5 ± 1.4	-0.3 ± 1.3	-1.0 ± 1.8	1.1 ± 1.6

Neuropsychological data are represented as β ± SE, as estimated by linear mixed models

* p<.05

Abbrevations: MMSE = Mini Mental State Examination, VAT = Visual Association Test, RAVLT = Rey Auditory Visual Learning Test, RBMT = Riverhead Behavioral Memory Test, TMT = Trail Making Test, BNT = Boston Naming Test. TMT and Stroop test scores are inversed and log transformed.

Keywords: subjective cognitive decline, preclinical AD, [18F]Florbetapir, amyloid

P102: Application of the PredictND decision support system to cross-sectional imaging and psychometric data from an aMCI to probable AD three year outcomes clinical study

Christopher Buckley[1], Jamie Moreland[1], Timo Urhemaa[2], Mark van Gils[2], Jan Wolber[1], Jyrki lotjonen[3]

[1]GE Healthcare, Amersham, United Kingdom
[2]VTT Technical Research Centre of Finland Ltd., Tampere, Finland
[3]Combonostics, Tampere, Finland

Objectives: The objective of this work was to use PredictND with baseline cross-sectional PET and MRI imaging with psychometrics to predict the cognitive trajectory of 222 subjects categorized as amnestic mild cognitive impairment (aMCI). The prognostic indication was tested against known outcomes from a 3-year aMCI to probable AD over three years in GE Healthcare's GE067-005 study.

Methods: The algorithm in the decision support system computes a disease state index (DSI) for an individual by comparing the similarity of his/her biomarkers to those from previously diagnosed cases (training data). In this use case DSI's of 0 and 1 are associated with low and high progression probabilities respectively.

Here, the system was trained with MRI images, amyloid PET derived SUVRs and MMSE data from ADNI and GE Healthcare's phase II studies with 244 cognitively normal and 241 AD subjects.

The aMCI validation dataset used 222 baseline MRI images, SUVR from the [^{18}F]flutemetamol PET images and MMSE scores from the GE067-005 study. Subjects were assessed every 6 months to test for conversion to probable AD. The baseline image data were stratified into four groups where their study amyloid status (A-, A+) and neuronal injury status (N-,N+) - determined in a post-hoc analysis. The four possible groupings were compared against a Kaplan-Meier survival (non-conversion to AD) analysis.

Results: Figure 1 shows the Kaplan-Meier survival data aMCI study for the four (A,N) baseline status groups. Table 1. Shows the PredictND DSI scores from the imaging and psychometric data for these groups together with their survival fractions. The computed DSIs when low predict a high survival fraction (A-,N- group) and when high they predict a low survival fraction (A+,N+ group). The DSIs were also concordant with the (A+,N-) and (A-,N+) outcomes.

Conclusions: This study demonstrates that the predictive system provides accurate and useful prognostic information for patients at risk of AD dementia.

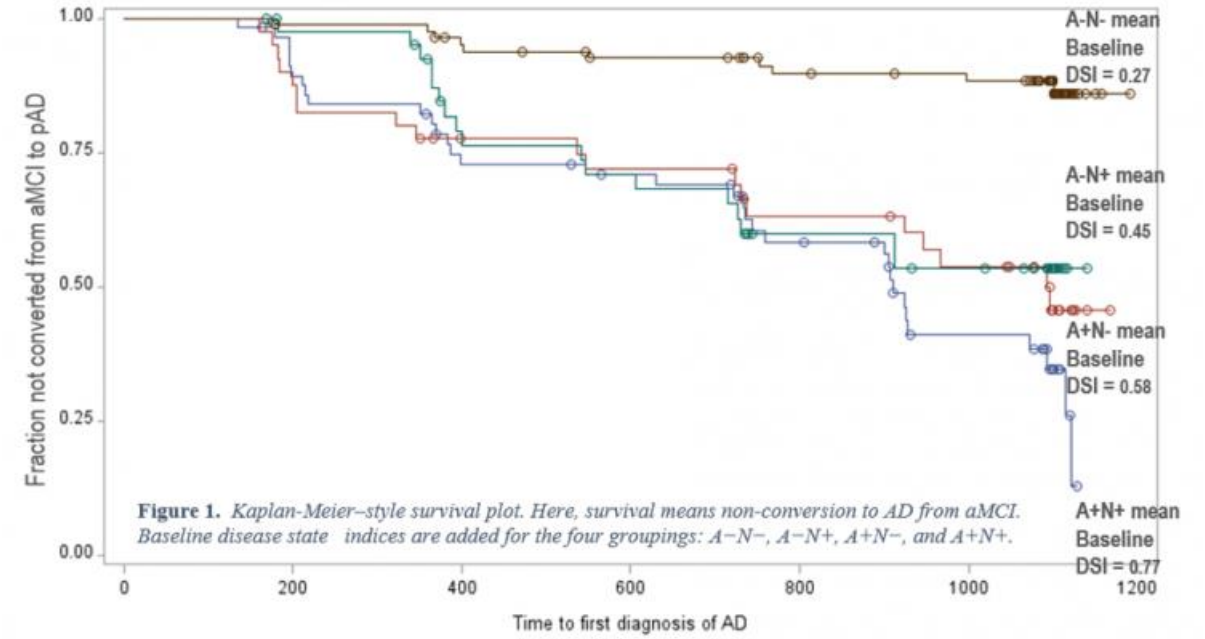

Figure 1. *Kaplan-Meier–style survival plot. Here, survival means non-conversion to AD from aMCI. Baseline disease state indices are added for the four groupings: A−N−, A−N+, A+N−, and A+N+.*

Study status	Number of subjects	Median DSI	Kaplan-Meier Survival Fraction (95% CI) after 36 months
A– N–	83	0.16	0.86 (0.75, 0.92)
A– N+	42	0.43	0.53 (0.36, 0.68)
A+ N–	40	0.50	0.46 (0.28, 0.62)
A+ N+	57	0.91	0.12 (0.13, 0.39)

Figure 2. *Comparison of the predictive DSIs with survival fraction from a 3-year aMCI to pAD outcomes study*

Keywords: PredictND, progression, aMCI, predictive, SUVR

P103: Tau pathology detected by [18F]GTP1 negatively correlates with cortical volume in Alzheimer's disease

Rebecca Ray, Suzanne Baker, Paul Manser, Michael Ward, Edmond Teng, Robby Weimer, Sandra Sanabria Bohórquez

Genentech, Inc., South San Francisco, CA, US

Cortical atrophy, and cerebral tau and amyloid accumulation are signatures of Alzheimer's Disease (AD). Understanding the relationship between cortical volume and tau accumulation may provide insights into disease pathophysiology. Volumetric MRI and [^{18}F]GTP1 tau PET images were collected as part of [^{18}F]GTP1 reproducibility and natural history studies in healthy volunteers (HV, amyloid positive and negative, n=15) and amyloid-positive AD subjects (MMSE 16-30, CDR 0.5-2, n=56).

FreeSurfer was used to perform cortical segmentation on MRIs. [^{18}F]GTP1 SUVR was calculated using cerebellar gray as reference. Regional volumes and [^{18}F]GTP1 SUVR in whole cortical gray matter (WCG), in vivo Braak regions (Schöll et al. Neuron 2016) and an AD meta-ROI (Jack et al. Alzheimer's & Dementia 2017) were measured.

ANCOVA analyses of regional volumes on diagnosis controlling for intracranial volume were performed. The analysis showed that AD subjects' Braak 1/2 and 3/4 regions were smaller than in HV (adjusted R^2=0.40, p=1.6-08 and adjusted R^2=0.33, p=4.8e-07, respectively); HV and AD subjects did not differ in Braak 5/6 volume (adjusted R^2=0.17, p>0.05). Analyses of [^{18}F]GTP1 SUVR in Braak 1/2, 3/4, and 5/6, showed group differences with AD subjects showing greater SUVR than HV (p<.001).

The relationship between volume and [^{18}F]GTP1 SUVR was assessed using partial Pearson correlations, controlling for intracranial volume. [^{18}F]GTP1 SUVR negatively correlated with cortical volume. Moderately strong correlations were observed in the AD meta-ROI (r=-0.56, p<1e-7), WCG (r=-0.45, p<.001) and Braak ROIs 1/2 and 3/4 (r=-0.44, p<.001). The correlation was weaker in Braak 5/6 (r=-0.26, p=0.03). AD subjects' Braak 1/2 volumes were smaller than those of HV and this corresponded with greater [^{18}F]GTP1 SUVR. In contrast, Braak 5/6 did not show volume group differences but displayed higher [^{18}F]GTP1 SUVR in AD subjects.

Ongoing analysis of longitudinal data will provide further insights of the association between tau burden and volumetric changes in AD.

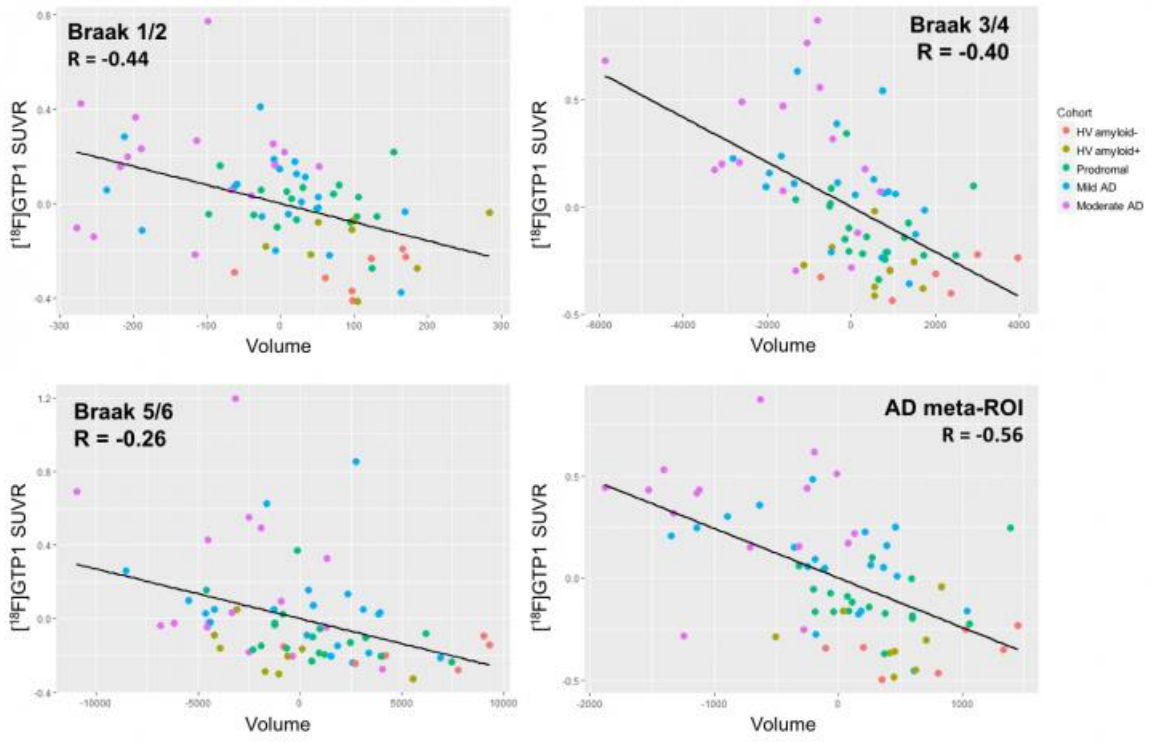

Figure 1. Scatterplot of [^{18}F] GTP1 SUVR and cortical volume residuals in *in vivo* Braak 1/2, 3/4 and 5/6 and AD meta-ROI controlling for total intracranial volume

Keywords: Tau imaging, [18F]GTP1, cortical atrophy

P104: Assessing the impact of beta-amyloid deposition in progressive supranuclear palsy

Sarah M. Boland, J. Eric Ahlskog, PhD, Nirubol Tosakulwong, Matthew L. Senjem, Anthony J. Spychalla, Ronald C. Petersen, Clifford R. Jack, Jr, Val Lowe, Keith Josephs, Jennifer L. Whitwell

Mayo Clinic, Rochester, MN, US

Introduction: Progressive supranuclear palsy (PSP) is a primary 4R tauopathy. However, concomitant Alzheimer's disease has been observed at autopsy in PSP. We utilized molecular neuroimaging to determine the frequency of beta-amyloid deposition in PSP, and to determine whether beta-amyloid deposition in PSP is associated with differences in [18F]AV-1451 uptake or clinical features.

Methods: Thirty PSP participants underwent MRI, Pittsburgh compound B (PiB) PET, [18F]AV-1451 PET and apolipoprotein allele E4 determination. A global PiB standard-uptake value ratio (SUVR) was calculated and participants were considered PiB(+) using a cut-point of 1.42. A voxel-level analysis was conducted to assess for differences in [18F]AV-1451 uptake patterns between PiB(+) and PiB(-) cases and compared to 64 normal PiB(-) controls. Clinical features were also compared between PiB(+) and PiB(-) cases.

Results: Twelve subjects (40%) showed beta-amyloid deposition and were considered PiB(+). Higher PiB SUVR correlated with older age. The proportion of APOE e4 carriers was 40% in the PiB(+) subjects compared to 14% in the PiB(-) subjects. Similar patterns of elevated [18F]AV-1451 uptake were observed in the PiB(-) and PiB(+) groups compared to controls, predominantly involving the midbrain, thalamus, putamen, and pallidum. After adjusting for age at scan, we did not find any differences in clinical testing between groups.

Conclusion: Beta-amyloid deposition occurs in a relatively high proportion of PSP subjects. However, there is little evidence that beta-amyloid plays a significant role in neurodegeneration in PSP.

Keywords: Progressive Supranuclear Palsy, PSP

P105: Flortaucipir imaging in primary progressive aphasia predicts variability in language impairment

Jessica Collins, Megan Quimby, Sara Makaretz, Kristen Sweeney, Bonnie Wong, Scott McGinnis, Brad Dickerson

Frontotemporal Disorders Unit, Department of Neurology, Massachusetts General Hospital and Harvard Medical School, Boston, MA, US

Background: The primary goal of this study was to investigate the utility of Flortaucipir (aka AV1451) PET imaging for discriminating between patients with different variants of primary progressive aphasia (PPA): semantic (svPPA), logopenic (lvPPA) and non-fluent (nfvPPA). We tested the following hypotheses: 1) The magnitude of Flortaucipir binding within the language network would distinguish between patients with PPA likely due to Alzheimer's pathology versus those with PPA likely due to different pathology. 2) Variability in the presentation of language symptoms amongst patients with non-Alzheimer's PPA (svPPA and nfvPPA) would be predicted by the magnitude of Flortaucipir binding within distinct nodes of the language network.

Methods: 7 svPPA patients, 5 lvPPA patients, and 6 nfvPPA patients underwent ^{18}F-Flortaucipir PET imaging and comprehensive language testing. Flortaucipir SUVR values (partial volume corrected) were calculated for six left-hemisphere regions within the language network (Figure 1), and a control region in early visual cortex.

Results: 5/5 lvPPA, 1/7 svPPA, and 1/6 nfvPPA patients were amyloid positive. Relative to the other two PPA subtypes, lvPPA was associated with significantly elevated Flortaucipir signal in the IFG [F(1,16) 8.05, p=.012], cMFG [F(1,16)=17.56, p=.001], and pSTS [F(1,16)=4.93, p=.041]. When comparing svPPA and nfvPPA, svPPA was associated with greater signal in the temporal pole [F(1,11)=6.28, p=.029], whereas nfvPPA was associated with greater signal in the cMFG [F(1,11)=11.55, p=.006]. Amongst the svPPA and nfvPPA patients, auditory verbal working memory impairment (percent correct on the WAB repetition task) was predicted by Flortaucipir signal in the MTG [r(10)=-.604, p=.032], whereas verbal fluency impairment (number of words generated on the FAS task) was predicted by Flortaucipir signal in the IFG [r(7)=-.702, p=.039].

Conclusions: Our results suggest that Flortaucipir imaging is useful for distinguishing between PPA patients with and without Alzheimer's pathology; and that Flortaucipir signal in PPA patients without Alzheimer's pathology is behaviorally relevant.

Figure 1.

A. Language Network ROIs

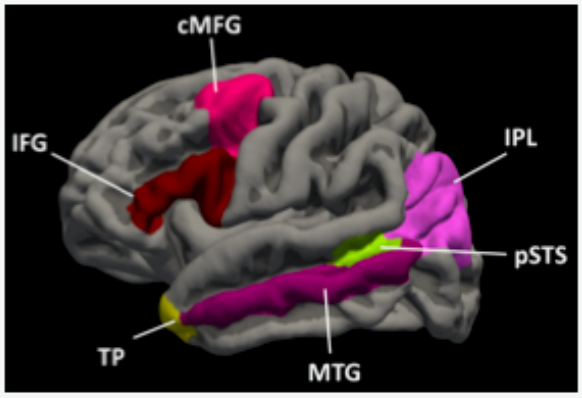

IFG = inferior frontal gyrus, cMFG = caudal middle frontal gyrus, TP = temporal pole, , MTG = middle temporal gyrus, pSTS = posterior superior temporal sulcus, IPL = Inferior parietal lobule,

B. Flortaucipir in PPA subtypes

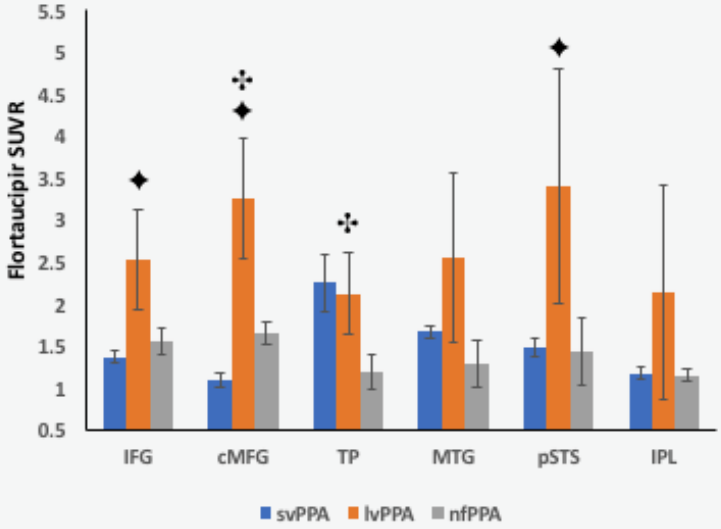

✦ = Significant difference for the contrast of lvPPA > svPPA & nfPPA.
✣ = Significant difference between the nfPPA and svPPA groups.
Error bars reflect standard error of the mean.

Figure 2. Relationship between focal Flortaucipir SUVR and language performance in svPPA and nfPPA patients

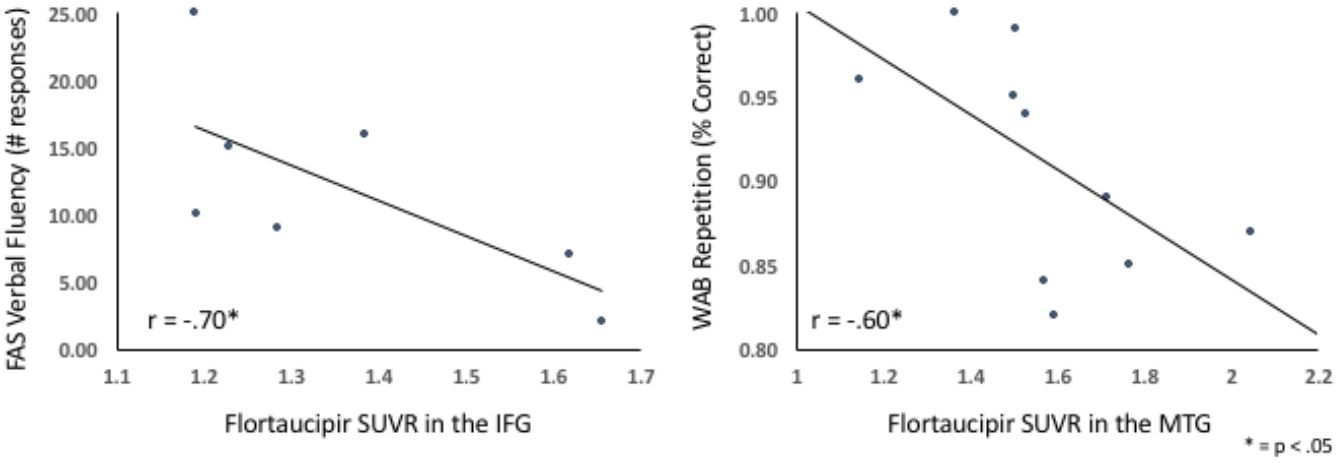

Keywords: Flortaucipir, Primary Progressive Aphasia, Language

P106: [18F]flutemetamol amyloid binding potential in relation to memory in cognitively normal subjects aged 80 years and older

Nienke Legdeur[1], Olga Buslenko[1], Elles Konijnenberg[1], Mara ten Kate[1], Maryam Badissi[1], Jori Tomassen[1], Anouk den Braber[1,2], Maqsood Yaqub[3], Dorret I Boomsma[2], Adriaan A Lammertsma[3], Andrea B Maier[4,5], Philip Scheltens[1], Bart NM van Berckel[3], Pieter Jelle Visser[1,6]

[1]Alzheimer Center & Department of Neurology, Amsterdam Neuroscience, VU University Medical Center, Amsterdam, Netherlands
[2]Department of Biological Psychology, VU University Amsterdam, Amsterdam, Netherlands
[3]Department of Radiology & Nuclear Medicine, VU University Medical Center, Amsterdam Neuroscience, Amsterdam, Netherlands
[4]Department of Medicine and Aged Care, Royal Melbourne Hospital, University of Melbourne, Melbourne, Australia
[5]MOVE Research Institute Amsterdam, Faculty of Human Movement Sciences, VU University Amsterdam, Amsterdam, Netherlands
[6]Department of Psychiatry & Neuropsychology, School for Mental Health and Neuroscience, Maastricht University, Maastricht, Netherlands

Introduction: This study investigated the relation of amyloid load and memory in cognitively normal subjects aged 80 years and older.

Methods: We selected 44 cognitively normal subjects (CDR = 0) ≥80 years from the PreclinAD study (including monozygotic twins) and the 90+ Study at the VU University Medical Center. The following (working) memory tests were used: CERAD 10 words test immediate and delayed recall, Visual Association Test (VAT), Rey Complex Figure Test 3 minute recall and Digit Span Forward (DSF). Dynamic [18F]flutemetamol (FMM) scans were acquired using a "coffee-break" protocol, i.e. acquiring data 0-30 and 90-110 minutes post injection. The FMM scans were made on a Philips Ingenuity Time-of-Flight PET-MRI camera. After co-registering both parts of the scan, parametric FMM non-displaceable binding potential (BP_{ND}) images were generated using the basis function implementation of the simplified reference tissue model (RPM) with cerebellar grey matter as reference tissue. Associations between FMM BP_{ND} and memory were examined using generalized estimated equation models correcting for twin status, age, gender and education.

Results: Subjects had a mean age of 89.2±4.8 years and 70.5% was female. FMM BP_{ND} was related to lower scores on the CERAD 10 words test delayed recall (ß = -2.3, p = 0.01).

Discussion: Amyloid load in cognitively healthy subjects aged 80 years and older is not a harmless feature of aging but is related to lower memory function.

Keywords: [18F]flutemetamol amyloid binding potential, oldest old, memory function

P107: Amyloid-β load is related to worries in individuals with subjective cognitive decline

Sander C.J. Verfaillie[1,2], Tessa Timmers[1,2], Rosalinde E.R. Slot[2], Chris W.J. van der Weijden[1], Linda Wesselman[1], Niels D. Prins[1], Sietske A.M. Sikkes[2], Adriaan A. Lammertsma[1], Philip Scheltens[1], Rik Ossenkoppele[2], Bart N.M. van Berckel[1], Wiesje M. van der Flier[1]

[1]Neurology & Alzheimer Center, VU University Medical Center, Amsterdam, Netherlands
[2]Radiology & Nuclear Medicine, VU University Medical Center, Amsterdam, Netherlands

Background. Self-perceived cognitive decline is associated with an increased risk of AD. The majority of individuals with subjective cognitive decline (SCD), however, do not harbor preclinical AD. The aim of this study was to investigate whether amyloid load is associated with a specific pattern of cognitive complaints.

Methods. We included 106 SCD memory-clinic patients (mean±SD age: 64±8, 45%F) with [^{18}F]florbetapir PET scans from the ongoing SCIENCe study. Mean cortical amyloid binding potential (BPnd) was derived from 90-minutes dynamic PET scans using optimized receptor parametric mapping (RPM). We used following questionnaires to assess SCD: cognitive change index (CCI, self&informant-reported; 2x20 items), subjective cognitive functioning (SCF), and the two closed questions "What complaints do you report?", and "Does this worry you?". We used the Rivermead Behavioral Memory Test (RBMT)-Stories (delayed recall) to assess objective memory functioning. Additionally, we calculated a self-awareness index (Z-transformed RBMT minus self-reported CCI), and a self-proxy index (self- minus informant-reported CCI). We used linear regression analyses, adjusted for age, sex and education, to investigate associations between amyloid BPnd (independent variable) with measures of SCD (dependent variables). Because education level could have a differential impact on these associations,[5] we additionally tested for education*amyloid interactions. Standardized betas were reported if $p<0.05$.

Results. Increased amyloid-β load was associated with worries (Beta=0.23, p=0.02), but not with the CCI (informant and self-reported, total scores or individual items) or SCF. Additionally, we found that increased amyloid-β load was associated with an increased self-awareness index (i.e. complaint severity>memory performance; Beta=0.41, p=0.007), but not with the self-proxy index.

Conclusions. Our results suggest that amyloid-β load is associated with worries and higher degree of insight, but not with severity or specific pattern of cognitive complaints. These findings suggest that worries about self-perceived cognitive decline is the strongest indicator of preclinical AD, while other items seem less sensitive.

Keywords: subjective cognitive decline, memory clinic based cohort, quantitative amyloid

P108: [18F]Flutemetamol imaging in the ALFA project: Cognitively healthy subjects enriched for Alzheimer's disease genetic risk factors

Gemma Salvadó[1], Anna Brugulat[1], Carles Falcon[1,2], Javier Pavia[2,3], Francisco Lomeña[3], José Luís Molinuevo[1], Juan Domingo Gispert[1,2]

[1]*BarcelonaBeta Brain Research Center, Barcelona, Spain*
[2]*CIBER de Bioengeniería, Biomateriales y Nanomedicina, Barcelona, Spain*
[3]*Nuclear Medicine Department, Hospital Clínic. Instititut d'Investigacions Biomèdiques August Pi i Sunyer, Barcelona, Spain*

Background: The ALFAplus study, nested in the ALFA project, [1] aims to define Alzheimer's disease (AD) early pathophysiological events, to understand risk-modifying factors and to characterize progression markers. For this purpose, a cohort of healthy cognitive (HC) participants, enriched for AD risk factors, was recruited. Here, we show preliminary results on amyloid (Aβ) deposition in this HC middle-aged population along with associations with cognition.

Methods: 440 participants, aged 45-71, will undertake [18F]Flutemetamol and FDG PET imaging, CSF sampling, an advanced MRI protocol, clinical history, cognition, genetics and environmental and lifestyle questionnaires. [18F]Flutemetamol images are assessed both by visual read and quantification in Centiloid scale (CL) [2]. Participants are categorized as 'Positive' (>50CL), 'Gray Zone' ([GZ], 20<CL<50) and 'Negative' (<20CL). The cut-off points defining the GZ are meant to reliably identify avid amyloid accumulators [3]. Neuropsychological evaluation includes the Memory Binding Test (MBT) for episodic memory and WAIS-IV subtests. Subjective cognitive decline (SCD) and SCD+ features were assessed following international guidelines [4]. A general linear model was conducted to assess the effect of Aβ-load (both by visual read and continuous CL values) on each cognitive test, covariating by age, education, gender and APOE.

Results: Descriptive statistical analysis of the initial 107 ALFAplus participants is shown in Table 1. Cognition correlates are depicted in Table 2. Matrix Reasoning subtest show a significant association with amyloid positivity by visual read ($F(1,90)=6.088$, $p=0.016$).

Conclusion: [18F]flutemetamol PET imaging is being used to characterize ALFAplus participants. Preliminary results show worse executive performance in amyloid positive individuals.

Acknowledgements: Authors would like to acknowledge GE Healthcare for kindly providing [18F]flutemetamol for this study.

References:

[1] Molinuevo et al. Alz. & Dement. TRCI 2016
[2] Klunk et al. Alz. & Dement. 2014
[3] Jack et al. Alz. & Dement. 2017
[4] Jessen et al. Alz. & Dement. 2014

	Visual Read (n=91)			Centiloid Quantification (=107)			
	Negative (n=80)	Positive (n=11)	p	Negative (n=88)	Gray zone (n=11)	Positive (n=8)	p
Age (years), Mean (SD) [range]	58.5 (4.9) [46-65]	63.6 (2.7) [61-71]	**0.001***	58.0 (5.1) [46-65]	61.9 (2.5) [56-65]	63.3 (3.5) [60-71]	**0.002***
Education (years), Mean (SD)	13.7 (3.6)	12.5 (4.1)	0.647	13.7 (3.6)	13.5 (4.0)	11.5 (3.5)	0.601
Female sex, n (%)	49 (53.85)	5 (5.49)	0.317	55 (82.1)	7 (10.4)	5 (7.5)	0.997
Number of APOE-e4 alleles, n (%)*			0.301				0.190
None	42 (85.71)	7 (14.28)		53 (85.4)	5 (8.06)	4 (6.45)	
One	22 (84.61)	4 (15.38)		19 (67.8)	5 (17.8)	4 (14.3)	
Two	16 (100)	0 (0)		15 (93.7)	1 (6.25)	0	
Family history of AD, n (%)			0.152				0.972
AD onset <75	58 (92.06)	5 (7.93)		62 (82.6)	8 (10.6)	5 (6.6)	
AD onset ≥75	21 (77.77)	6 (22.22)		25 (80.6)	3 (9.6)	3 (9.6)	
No history of AD	1 (100)	0 (0)		1	0	0	
Subjective Cognitive Decline, n (%)*			0.622				0.125
SCD-more	7 (77.77)	2 (22.22)		7 (63.6)	1 (9.1)	3 (27.3)	
SCD-less	7 (87.5)	1 (12.5)		7 (87.5)	1 (12.5)	0	
None SCD	65 (89.04)	8 (11.11)		73 (83.9)	9 (10.3)	5 (5.7)	

Table 1: Characteristics of participants according to their amyloid load by visual read classification (n=91) and Centiloid quantification (n=107).
* Depict statistical significant differences by groups.

	Visual read (n=91)		Centiloid Quantification (n=107)	
	F	*p*	*F*	*p*
Memory Binding Test (MBT)				
Total Paired Recall (TPR)	0.152	0.70	0.161	0.69
Total Free Recall (TFR)	0.008	0.93	0.981	0.32
Total Delayed Paired Recall (TDPR)	0.177	0.66	0.504	0.48
Total Delayed Free Recall (TDFR)	0.021	0.89	0.715	0.40
WAIS-IV				
Visual Puzzles	1.907	0.17	0.056	0.81
Digit Span (Forward)	0.000	0.99	0.040	0.84
Digit Span (Backward)	0.004	0.95	0.145	0.70
Digit Span (Sequencing)	0.233	0.63	0.035	0.85
Matrix	**6.088**	**0.02***	**3.001**	**0.09**
Similarities	0.011	0.92	0.923	0.34
Coding	0.027	0.87	0.035	0.85

Table 2: *F* statistics and *p* values for cognition correlations with amyloid load, both by visual read classification and Centiloid quantification. Age, education, gender and APOE status (number of APOE-e4 alleles) were used as covariates.
*Show statistical significant correlation with amyloid load.

Keywords: Flutemetamol, Centiloid, Healthy cognitive, Gray Zone, Cognition

P109: Is there a local neurotoxic effect of regional amyloid deposits? A network-domain specific study of florbetapir-PET – cognition associations

Michel Grothe[1], Christian Sorg[2], Stefan Teipel[1,3]

[1]*German Center for Neurodegenerative Diseases (DZNE), Rostock, Germany*
[2]*Department of Psychiatry, Neuroradiology, and TUM-Neuroimaging Center, Klinikum Rechts der Isar, Technische Universität München, Munich, Germany*
[3]*University Rostock Medical Center, Rostock, Germany*

Background: A recent molecular imaging study indicated that regional amyloid deposits do not generally link to glucose hypometabolism of the affected brain region, arguing against a local neurotoxic effect of accumulated amyloid-β protein. However, accumulated amyloid may also result in functional derangements not associated with decreased glucose utilization, such as dysfunctional neuronal hyperactivity. We aimed to study the functional consequences of regional amyloid accumulation by using sensitive performance measures in domain-specific neuropsychologic tests as markers of regional brain dysfunction.

Methods: We investigated Florbetapir-PET and neuropsychologic test data of 577 nondemented elderly subjects (cognitively normal and MCI) participating in the ADNI study. Specifically, partial correlation analyses controlled for age, sex, education, and diagnosis examined amyloid-cognition associations within "posterior medial" (PM) and "anterior temporal" (AT) brain networks known to specifically subserve episodic (delayed recall, DR) and semantic memory (Boston Naming Test, BNT) processes, respectively. The regional specificity of the associations was assessed by additional control for global cortical amyloid load. Analogous analyses assessed network-specific cognition correlates of regional glucose hypometabolism measured by FDG-PET.

Results: Amyloid load in the PM network correlated with worse DR ($r=-0.17$, $p<0.001$), but not with worse BNT performance. Amyloid load in the AT network correlated with worse BNT ($r=-0.13$, $p=0.001$) performance, but even more so with worse DR ($r=-0.22$, $p<0.001$). Moreover, after controlling for global cortical amyloid burden, none of the regional associations remained significant. By contrast, globally controlled glucose hypometabolism correlated with cognitive dysfunction in a network-specific manner, correlating with DR in the PM ($p<0.001$) and with BNT in the AT ($p<0.001$), but not vice versa (both $p>0.05$).

Conclusions: In contrast to FDG-PET measured hypometabolism, network-specific amyloid load does not specifically associate with dysfunction in the respective cognitive domain, corroborating recent evidence of negligible local neurotoxicity of accumulated amyloid-β protein.

Keywords: Amyloid, PET, regional analysis, cognitive domains, memory networks

P110: A similar prevalence and magnitude of amyloid positivity between cognitively normal elderly Japanese and Americans

Zheming Yu[1], Brian Lopresti[1], Masafumi Ihara[5], Chendi Cui[4], Howard Aizenstein[2], Hiroko Dodge[4,6], Davneet Minhas[1], Oscar Lopez[3], William Klunk[2], Chester Mathis[1], Lewis Kuller[4], Yoshihiro Miyamoto[5], Akira Sekikawa[4]

[1]*University of Pittsburgh School of Medicine, Department of Radiology, Pittsburgh, PA, US*
[2]*University of Pittsburgh School of Medicine, Department of Psychiatry, Pittsburgh, PA, US*
[3]*University of Pittsburgh School of Medicine, Department of Neurology, Pittsburgh, PA, US*
[4]*University of Pittsburgh Graduate School of Public Health, Dept. of Epidemiology, Pittsburgh, PA, US*
[5]*National Cerebral and Cardiovascular Center, Suita, Osaka, Japan*
[6]*University of Michigan School of Medicine, Dept. of Neurology, Ann Arbor, MI, US*

Background: Epidemiological studies imply a 20-50% lower prevalence of Alzheimer's Disease (AD) in Japan compared to the U.S. and Europe despite the Japanese having the greatest longevity. Interestingly, the prevalence of AD in Japanese Americans is reported to be comparable to Caucasian Americans, suggesting that genetic factors alone are unlikely to explain this observation. These factors led us to hypothesize that cognitively normal (CN) elderly Japanese have significantly lower prevalence of brain amyloidosis than a comparable American population.

Methods: 24 CN elderly Japanese participants (12 Male, 12 Female) aged 80-89 were recruited from the Suita study cohort and underwent PiB imaging in Japan. Regional and global indices of PiB retention were determined using a Freesurfer-based analysis. For each Japanese participant, a CN American counterpart was identified from within Pittsburgh study cohorts that matched in terms of age, gender, and education. To exclude MCI and dementia, all participants were administered a neuropsychological test battery and evaluated by experienced neuropsychologists.

Results: The Japanese and American cohorts have a similar number of PiB positive subjects (7/24 vs. 6/24). No significant differences in regional or global PiB SUVR were observed [Global median (quantiles) 1.16 (1.11, 1.52) vs 1.18 (1.11, 1.31), $P = 0.70$] based on a nonparametric paired test. There were also no significant differences in cognitive performance between the cohorts ($P > 0.6$). However, among PiB negative subjects, the Japanese population showed significantly lower PiB retention in the precuneus [Median(quantiles) 1.15 (1.11, 1.21) vs 1.24 (1.18, 1.28), $P = 0.01$] using a nonparametric test.

Conclusion: The current study suggests a similar prevalence of brain amyloidosis between Japanese and American CN elderly, although a larger sample size could reveal subtle differences in amyloid trajectories.

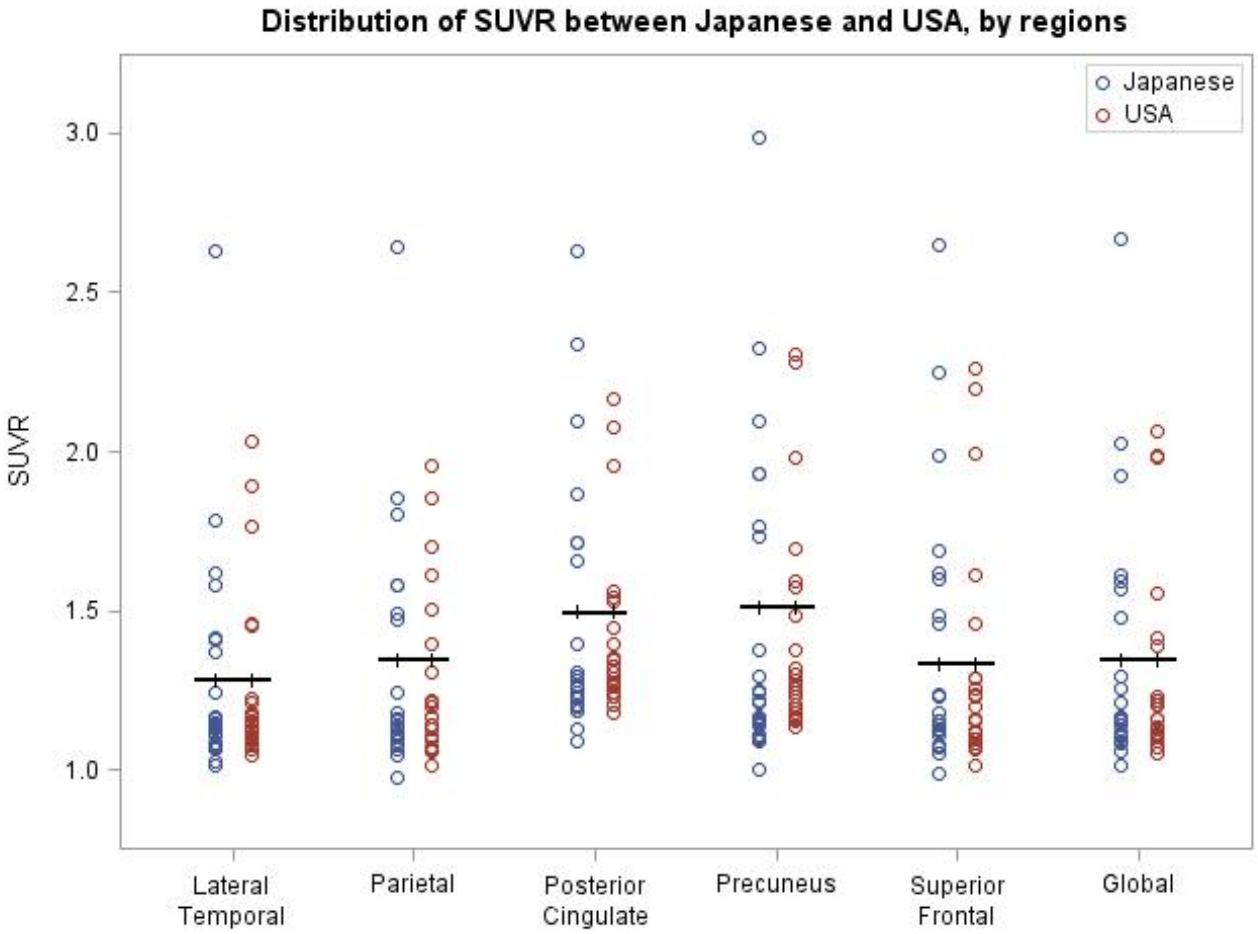

Figure: Distribution of regional PiB retention measures (SUVR50-70) for Japanese (n=24) and American (n=24) cohorts. Horizontal lines indicate positivity thresholds for regional and composite (Global) index of PiB retention. There were no significant differences observed between cohorts for any region (p>0.16)

Keywords: amyloid, aging, Japanese, PiB,

P111: Effects of amyloid deposition and hippocampal activation on subjective memory complaints

Xi Chen, Zhang Jingting, Michelle Farrell, Denise Park

Center for Vital Longevity, University of Texas at Dallas, Dallas, TX, US

Introduction: There is growing evidence that amyloid deposition in cognitively-normal adults is associated with increased memory complaints, suggesting an awareness of decline before there is measurable cognitive change. In the present study, we considered whether low hippocampal activation might also be associated with SMC and, if so, whether amyloid and hippocampal activity independently contributed to SMC or interacted, such that the effect of low hippocampal activation was uniquely associated with higher levels of amyloid, resulting in an interaction.

Methods: Fifty-eight older adults (aged 60-88) from the Dallas Lifespan Brain Study reported their perceived capacity and stability in memory on two subscales from Metamemory in Adulthood questionnaire (Dixon et al., 1988). Amyloid burden was measured with mean SUVR from seven regions using florbetapir PET imaging. Hippocampal activation was measured using an fMRI scene-encoding subsequent memory task. Analyses focused on hippocampal activity during subsequently high-confidence remembered versus forgotten items.

Results: Using multiple regressions and controlling for age, we found significant independent effects of amyloid deposition (p=.041 for perceived memory capacity; and p=.024 for perceived memory stability), but no significant interaction between amyloid and hippocampus activation. Amyloid deposition predicted beliefs of lower capacity and lower stability in memory (Fig.1). Moreover, lower hippocampal activation was associated with perceived poorer memory capacity and stability for younger-old adults (aged 60-70 for perceived capacity; 60-72 for perceived stability), but not the older adults (Fig. 2).

Conclusions: Consistent with previous findings, cognitively-normal individuals with elevated amyloid burden are more likely to complain about their memory functioning. Memory complaints also reflect deficits in hippocampus function, particularly in younger-older adults. The concurring but independent effects of amyloid and hippocampal activation on SMC may suggest that functional deficits in the hippocampus may be one of the earliest brain markers contributing to SMC in normal aging and preclinical AD.

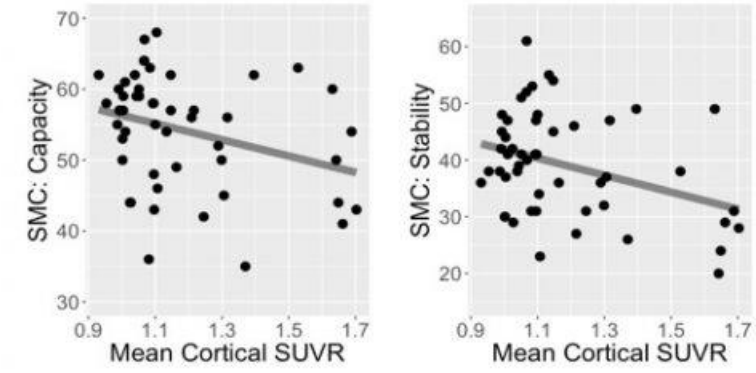

Figure 1. Higher amyloid deposition is associated with lower memory capacity and lower stability in memory.

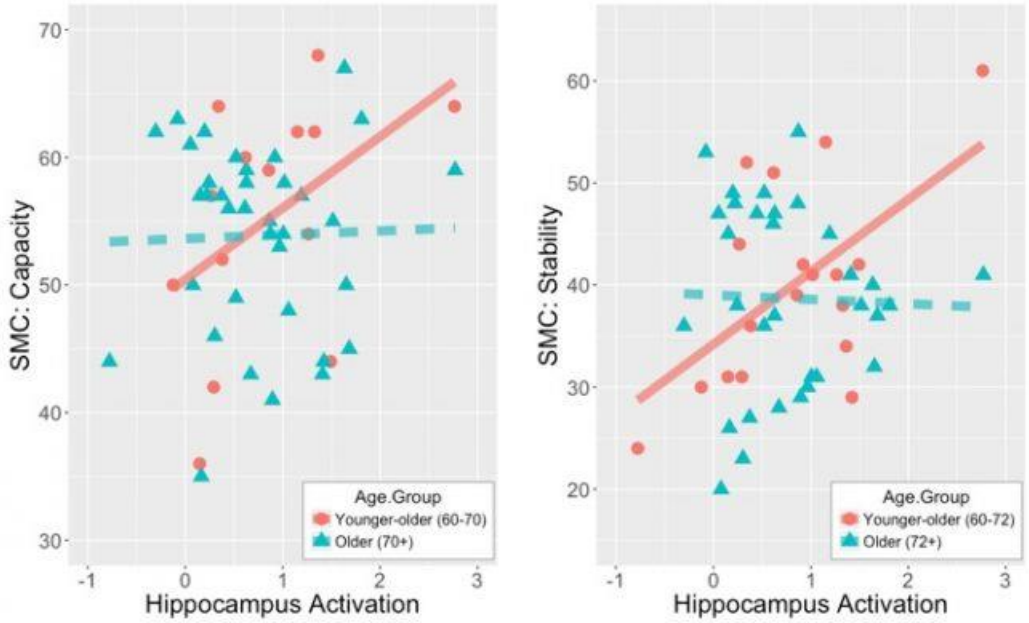

Figure 2. Failures in activating hippocampus during successful encoding is associated with lower self-report memory capacity and lower stability in memory in younger-older individuals.

Keywords: subjective memory complaints, amyloid, hippocampal activation, subsequent memory

P112: Thresholds for amyloid positivity among normal, MCI and mild dementia subjects using [F-18] Florbetaben

Ranjan Duara[1], David Loewenstein[2], Gabriel Lizzaraga[3], Malek Adjouadi[3], Warren Barker[1], Maria Greig-Custo[1], Ailyn Penate[1], Kevin Hanson[4], Michael Marsiske[4], David Vaillancourt[4], Steven DeKosky[4], Todd Golde[4]

[1]*Wien Center, Mount Sinai Medical Center, Miami Beach, FL, US*
[2]*University of Miami, Miami, FL, US*
[3]*Florida International University, Miami, FL, US*
[4]*University of Florida, Gainesville, FL, US*

Introduction: Validation of binary visual readings of antemortem amyloid PET scans in terminal patients was accomplished by correspondence to beta-amyloid deposits at post mortem. In this study we used visual ratings of amyloid PET scans to determine thresholds for amyloid positivity, using quantitative measures of amyloid load in the brain.

Methods: Two raters performed binary reads on 95 [F-18] Florbetaben PET scans (concordance was 100% for amyloid negative; 93.2% for positive) in a longitudinal study (1Florida ADRC). Subject diagnoses were: CN (n=35), MCI (n=52) and Mild Dementia (n= 29) (mean age 71.6 ±7.7 years). Optimal discrimination of visually rated PET scans, using Standardized Uptake Value Ratios (SUVRs) referenced to the cerebellar gray matter, were determined by ROC analyses.

Results: Visual ratings were amyloid positive for 6.7% of CN, 39.3% of MCI and 66.7% of dementia subjects. An optimal SUVR threshold of 1.24 for amyloid positivity, which was not different for CN, MCI or dementia cases, was obtained on 102 scans (92.3 % sensitivity; 92.1 % specificity; AUC=.974; SE=.01). Mean SUVR was 1.04 ±0.14 for CN, 1.23 ±0.23 for MCI and 1.34 ±0.30 for Dementia. Age-adjusted correlations were: r=.51 (p<.001) with semantic intrusions in a word-list learning test, r =-.32; p <.006 with hippocampal volumes and r=-.39 (p=.001) with entorhinal cortex volume.

Conclusion: The optimal SUVR threshold for amyloid positivity in this study (1.24) is substantially lower than the value (1.48) using the same ligand and validated by postmortem amyloid status (Sabri et al., 2015). The lower SUVR threshold we obtained may be attributed to the use of visual ratings (which can identify ligand binding in limited neocortical regions), and the use of a mildly impaired, more representative, community-based population. Application of the current findings in Alzheimer prevention and treatment trials will increase the number of eligible subjects.

Keywords: Amyloid, threshold, Florbetaben

P113: Twelve-month glucose metabolism declines in an empirically pre-defined statistical region-of-interest in amyloid-positive persons with Alzheimer's dementia and Mild Cognitive Impairment: updated ADNI findings

Kewei Chen[1,2,6,8], Wendy Lee[1,2], Xiaoying Kuang[1,2], Ji Luo[1,2], Vivek Devadas[1,2], Pradeep Thiyyagura[1,2], Yinghua Chen[1,2], Robert Bauer[1,2], Michael Weiner[3], William Jagust[4], Christopher Van Dyck[5], Eric Reiman[1,2,6,7,8]

[1]*Banner Alzheimer's Institute, Phoenix, AZ, US*
[2]*Arizona Alzheimer's Consortium, Phoenix, AZ, US*
[3]*University of California, San Francisco, San Francisco, CA, US*
[4]*University of California, Berkeley, Berkeley, CA, US*
[5]*Yale University, New Haven, CT, US*
[6]*University of Arizona, Tucson, AZ, US*
[7]*Translational Genomics Research Institute, Phoenix, AZ, US*
[8]*Arizona State University, Tempe, AZ, US*

Background: We previously used data from the ADNI to track AD-related cerebral metabolic rate for glucose (CMRgl) declines and evaluate disease-modifying treatments in persons with mild-to-moderate AD and MCI with improved power and freedom from the inflated Type I error associated with multiple comparisons in an empirically prespecified statistical region of interest (sROI) (Chen, NeuroImage 2010). We now extend our sROI approach to those mild-to-moderate AD dementia and MCI patients who are amyloid-positive (Aβ+).

Methods: Baseline and 12-month follow-up FDG PET scans from 31 persons with mild-to-moderate AD dementia and 44 Aβ+ persons with mild cognitive impairment (MCI), all with florbetapir SUVRs ≥ 1.18 (Fleisher, JAMA Neurol 2011), served as a training set to establish AD-dementia and MCI-related SROIs as previously described. Baseline and 12-month follow-up scans from 23 other persons with AD dementia and 40 other persons with MCI, all with florbetapir SUVRs ≥ 1.18, served as a test to estimate the respective number of persons with AD dementia or MCI per group needed to detect a 25% treatment effect on sROI CMRgl declines in a 12-month placebo-controlled randomized clinical trial (RCT) with 80% power and two-tailed P=0.05.

Results: Using the relevant Aβ+ sROI, we estimate the need for 126 Aβ+ persons with mild-to-moderate AD dementia or 320 Aβ+ persons with MCI per group to detect a 25% treatment effect on sROI CMRgl declines in a 12-month placebo-controlled RCT with 80% power and two-tailed P=0.05. Power estimates were similar to the number of persons with AD dementia or MCI we had estimated to detect treatment effects prior to the availability of Aβ PET scans.

Conclusions: This study provides sROIs and 12-month sample size estimates for the evaluation of AD-modifying treatments in Aβ+ persons with mild-to-moderate AD dementia or MCI.

Keywords: FDG PET, statistical region of interest (sROI), amyloid positivity (Aβ+), sample size estimation, clinical trial design

P114: Flortaucipir PET measurements and relationships with cognitive impairment

Hillary Protas[1,2], Valentina Ghisays[1,2], Ji Luo[1,2], Eric DeMarco[1,2], Pradeep Thiyyagura[1,2], Vivek Devadas[1,2], Robert Bauer[1,2], Susan Landau[7], Michael Weiner[6], William Jagust[7], Eric Reiman[1,2,3,4,5], Kewei Chen[1,2,3,5]

[1]*Banner Alzheimer's Institute, Phoenix, AZ, US*
[2]*Arizona Alzheimer's Consortium, Phoenix, AZ, US*
[3]*University of Arizona, Tucson, AZ, US*
[4]*Translational Genomics Research Institute, Phoenix, AZ, US*
[5]*Arizona State University, Tempe, AZ, US*
[6]*University of California, San Francisco, San Francisco, CA, US*
[7]*University of California, Berkley, CA, US*

Background: We used a voxel-based analysis technique to investigate the magnitude and spatial extent of flortaucipir PET measurements of paired helical filament (PHF) tau burden. We then used pre-specified regions-of-interest (ROIs) to investigate relationships between regional PHF tau burden and cognitive impairment in amyloid-β positive (Aβ+) or negative (Aβ-) persons with MCI from ADNI-3.

Methods: Flortaucipir PET scans were acquired in 20 Aβ+ and 39 Aβ- persons with MCI and in 57 Aβ- cognitively unimpaired older adults. Aβ positivity was defined using mean cerebral-to-cerebellar florbetapir SUVRs ≥1.18 (Fleisher, JAMA Neurol2011). SPM12 was used to compare regional flortaucipir SUVRs in the three subject groups. Pre-specified entorhinal, precuneus, parahippocampal and inferior temporal regions were used to characterize relationships between regional flortaucipir SUVRs and magnitude of cognitive impairment using the MMSE, ADAS-cog, CDR-SB and AVLT long-term memory scores in the Aβ+ and/or Aβ- MCI groups.

Results: In comparison with the Aβ- unimpaired controls, the Aβ+ and Aβ- MCI groups each had significantly higher flortaucipir SUVRs in a number of locations, including in the preselected Braak ROIs that are preferentially affected by AD. In comparison with the Aβ- MCI group, the Aβ+ MCI group had significantly higher flortaucipir SUVRs in the same locations. In Aβ- MCI group, higher entorhinal cortex, parahippcampus, precuneus and inferior temporal flortaucipir SUVRs were significantly associated MMSE, ADAS-cog and CDR-SB measures of cognitive impairment, but not with lower memory scores. We failed to detect significant correlations in the Aβ+ MCI subjects, perhaps due to limited statistical power.

Conclusion: This study finds a characteristic pattern of PHF tau deposition in persons with Aβ+ and Aβ- MCI--as well as relationships between regional PHF tau burden and severity of cognitive impairment in persons with MCI who do not have florbetapir PET evidence of moderate-to-frequent Aβ plaques.

Keywords: Flortaucipir PET, Amyloid Positivity, Cognitive Decline, MCI, Tau/Cognition Correlation

P115: [18F] AV-1451 uptake in corticobasal syndrome: the influence of beta-amyloid and clinical presentation

Farwa Ali, Jennifer Whitwell, Peter Martin, Matthew Senjen, David Knopman, Clifford Jack Jr., Val Lowe, Ronald Petersen, Bradley Boeve, Keith Josephs

Mayo Clinic, Rochester, MN, US

Corticobasal syndrome (CBS) is a phenotypic manifestation of diverse pathologies affecting the supplementary motor, premotor, parietal and superior frontal cortex, characterized by dystonia, apraxia, parkinsonism and cortical sensory neglect. Same cortical regions are implicated in apraxia of speech (AOS). Newly described 18F-AV1451 is a tau protein ligand that has variable binding to different tau-isoforms. We compared AV1451 tau-PET standardized uptake value ratios (SUVRs) in specific brain regions of interest (ROIs) between cases with corticobasal syndrome who presented with apraxia of speech with those who presented with motor symptoms. PiB-PET positive and negative patients in both groups were compared to distinguish Alzheimer's disease pathology. We compared 13 patients with CBS, of whom 6 presented with AOS, and remaining 7 presented with motor symptoms. 6 patients had positive PiB-PET scans of whom two presented with AOS. According to our study, only those CBS patients who presented with AOS had AV1451 tau-PET SUVRs higher than 476 normal amyloid negative controls. This was observed in supplementary motor area, superior frontal and parietal cortices bilaterally. In contrast, patients who presented with motor symptoms, did not have elevated tau-PET SUVRs as compared to normal controls. When comparing PiB positive to PiB negative patients; 2 cases without AOS and positive PiB-PET were found to have higher tau-PET SUVRs, in a distribution suggestive of Alzheimer's disease pathology (Fig 1). In our study, only patients with AOS were found to have AV-1451 uptake as compared to controls, this may indicate higher tau burden or greater neurodegeneration. AOS is also unlikely to be related to Alzheimer's disease as only two patients had elevated amyloid, one of whom had elevated tau uptake expected in AD. These results have important implications on the use of AV-1451 PET scans in the study of tauopathies.

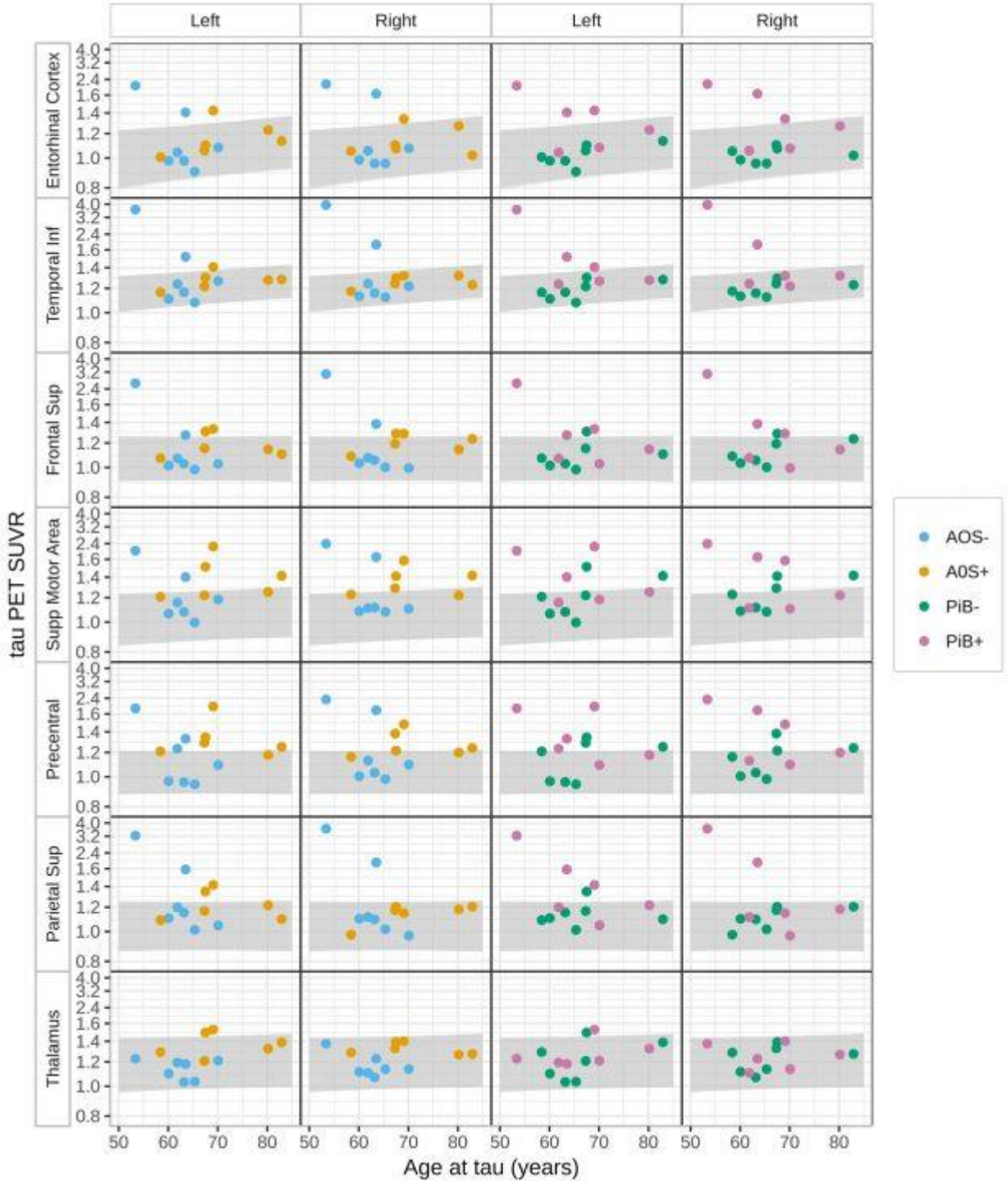
Left
Right
Left
Right
Entorhinal Cortex
Temporal Inf
Frontal Sup
Supp Motor Area
Precentral
Parietal Sup
Thalamus
tau PET SUVR
4.0
3.2
2.4
1.6
1.4
1.2
1.0
0.8
50
60
70
80
Age at tau (years)
AOS-
A0S+
PiB-
PiB+

Figure 1

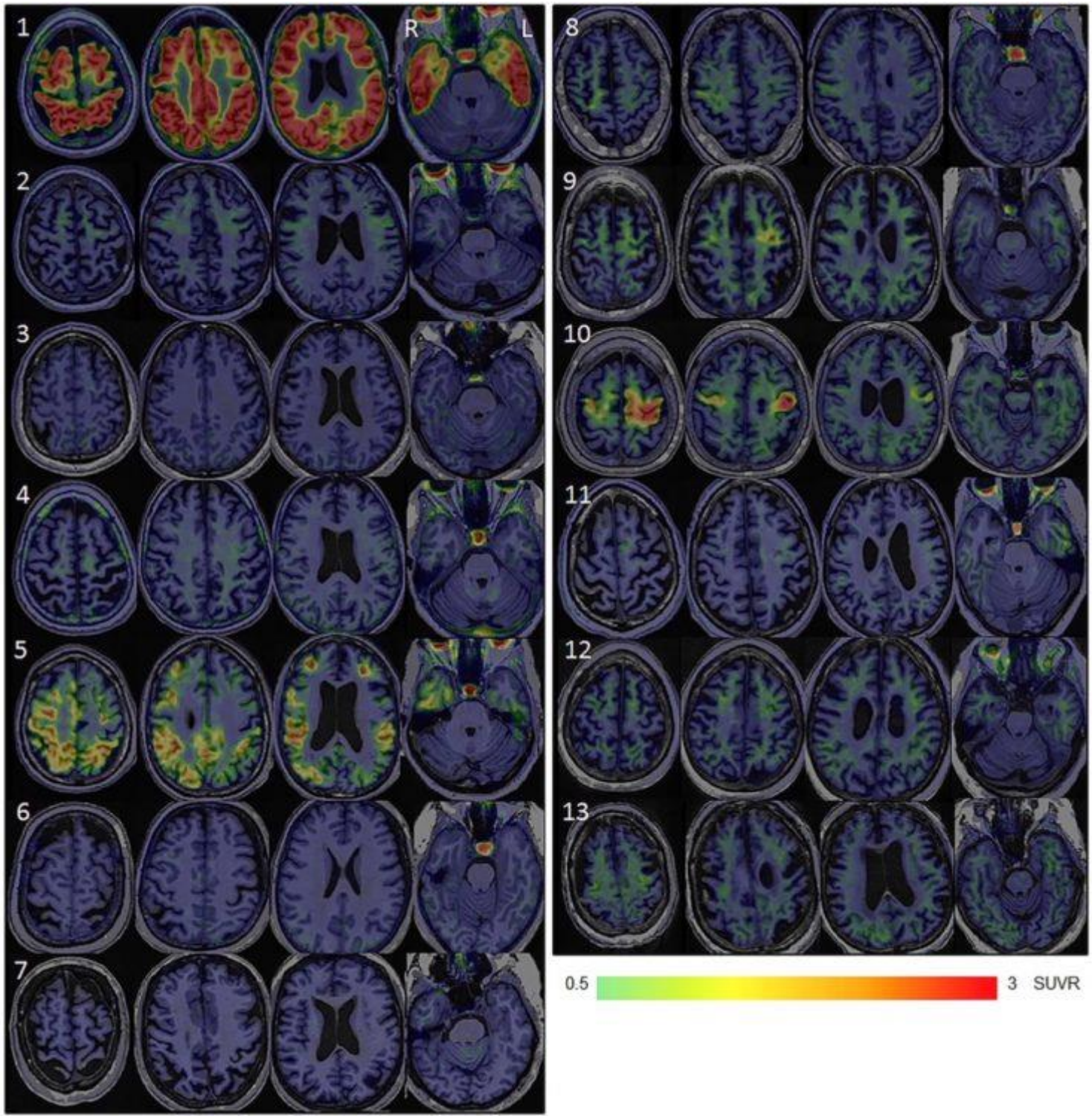

Figure 2
Keywords: AV-1451, corticobasal syndrome, amyloid PiB-PET

P116: Tau positron emission tomography is not elevated in HIV infected individuals

Beau Ances, Helen Beaumont, Sarah Cooley, Jeremy Strain, John Morris, Tammie Benzinger

Washington University in Saint Louis, Saint Louis, MO, US

Objectives: As the HIV infected (HIV+) population continues to age, challenges remain concerning differentiating cognitive impairment due to HIV from Alzheimer's disease (AD) in these older HIV+ individuals. Tau mediated neurodegeneration may occur in both conditions. Tau positron emission tomography (PET) using ^{18}F-AV-1451 was performed in 26 HIV+ participants (cognitively normal (n=21) and impaired (n=5)) and 26 cognitively normal community controls.

Methods: In this case-control study, all participants had tau PET and neuropsychometric testing. Regional standardized uptake value ratios (SUVRs) for tau PET were determined with the cerebellar cortex serving as a reference region. Statistical differences in tau PET SUVR in regions of interest were compared amongst community controls, HIV+ cognitively normal (HIVn), and HIV+ impaired (HIVi) using the Kruskal-Wallis test. Within the HIV+ participants, tau PET SUVR was compared to standard clinical measures including viral load (VL) and CD4 cell count (recent and nadir).

Results: HIV infection was not associated with increased tau PET SUVR. The degree of cognitive impairment due to HIV was not associated with tau PET SUVR with HIVn and HIVi having similar values. In addition, tau PET SUVRs did not correlate with standard clinical markers of disease (VL or CD4 cell count).

Conclusions: These results suggest that older HIV+ individuals are not at increased risk of tau mediated neurodegeneration. Tau PET was not elevated in patients with cognitive impairment due to HIV compared to elevated tau PET typically seen in AD. Observed Tau PET imaging may therefore assist in differentiating various neurodegenerative processes that can occur in older HIV+ individuals.

Keywords: HIV, tau PET, Alzheimer's disease, viral load

P117: Left frontal hub connectivity delays cognitive decline in autosomal dominant and sporadic Alzheimer's disease

Nicolai Franzmeier[1], Emrah Duezel[2], Frank Jessen[3,4], Tammie Benzinger[5,6], Johannes Levin[7,8], Anne M Fagan[5,6,9], John C Morris[5,6,9], Randall Bateman[5,6,9], Michael Ewers[1]

[1]*Institute for Stroke and Dementia Research, Ludwig Maximilians University, Munich, Germany*
[2]*German Center for Neurodegenerative Diseases, Magdeburg, Germany*
[3]*German Center for Neurodegenerative Diseases, Bonn, Germany*
[4]*Department of Psychiatry, University of Cologne, Cologne, Germany*
[5]*Department of Radiology, Washington University, St. Louis, MO, US*
[6]*Knight Alzheimer's Disease Research Center, Washington University, St. Louis, MO, US*
[7]*German Center for Neurodegenerative Diseases, Munich, Germany*
[8]*Department of Neurology, Ludwig Maximilians University, Munich, Germany*
[9]*Hope Center for Neurological Disorders, Washington University, St. Louis, MO, US*

Background: Alzheimer's disease (AD) patients vary in their ability to sustain cognition while developing brain pathology. A major question is which brain differences support higher reserve, i.e. relatively preserved cognition despite AD pathology. Higher fMRI-assessed global connectivity of a left frontal cortex (gLFC, Brodmann Area 6/44) hub is a core candidate underlying reserve as it is associated with education (i.e. a protective factor associated with reserve) and attenuated cognitive impairment in prodromal AD. Here, we asked whether such higher gLFC-connectivity supports reserve within the course of AD, including the preclinical stage when cognitive decline is subtle.

Methods: We obtained resting-state fMRI in 74 autosomal dominant AD (ADAD) cases and 55 non-carrier controls from the DIAN cohort. In addition, 75 amyloid-positive elderly subjects plus 41 amyloid-negative normal controls from the German DELCODE study were included. Subject-specific gLFC-connectivity was obtained by seed-based resting-state connectivity analysis, with the LFC as the seed. As a proxy of disease severity, we used estimated years from symptom onset (EYO) in ADAD and cerebrospinal-fluid tau (CSF-Tau) levels in sporadic AD. Using linear mixed models, we tested the interaction effect (gLFC-connectivity x disease severity) on global cognition (MMSE) and episodic memory (delayed recall).

Results: For ADAD, a significant gLFC-connectivity x EYO interaction was found, indicating an alleviated effect of EYO on delayed recall ($p=0.012$) and MMSE ($p=0.008$) at higher levels of gLFC-connectivity. Similarly, in sporadic AD, effects of CSF-tau on delayed recall ($p=0.011$) and MMSE ($p=0.002$) were attenuated at higher gLFC-connectivity levels (Figure 1). gLFC-connectivity was not correlated with AD severity. Polynomial regression analysis showed that relative to AD-biomarker trajectories, cognitive decline was shifted towards later AD stages in subjects with high gLFC-connectivity (Figure 2).

Conclusion: Our findings suggest that higher resilience against the development of cognitive impairment throughout AD is at least partially attributable to higher gLFC-hub connectivity.

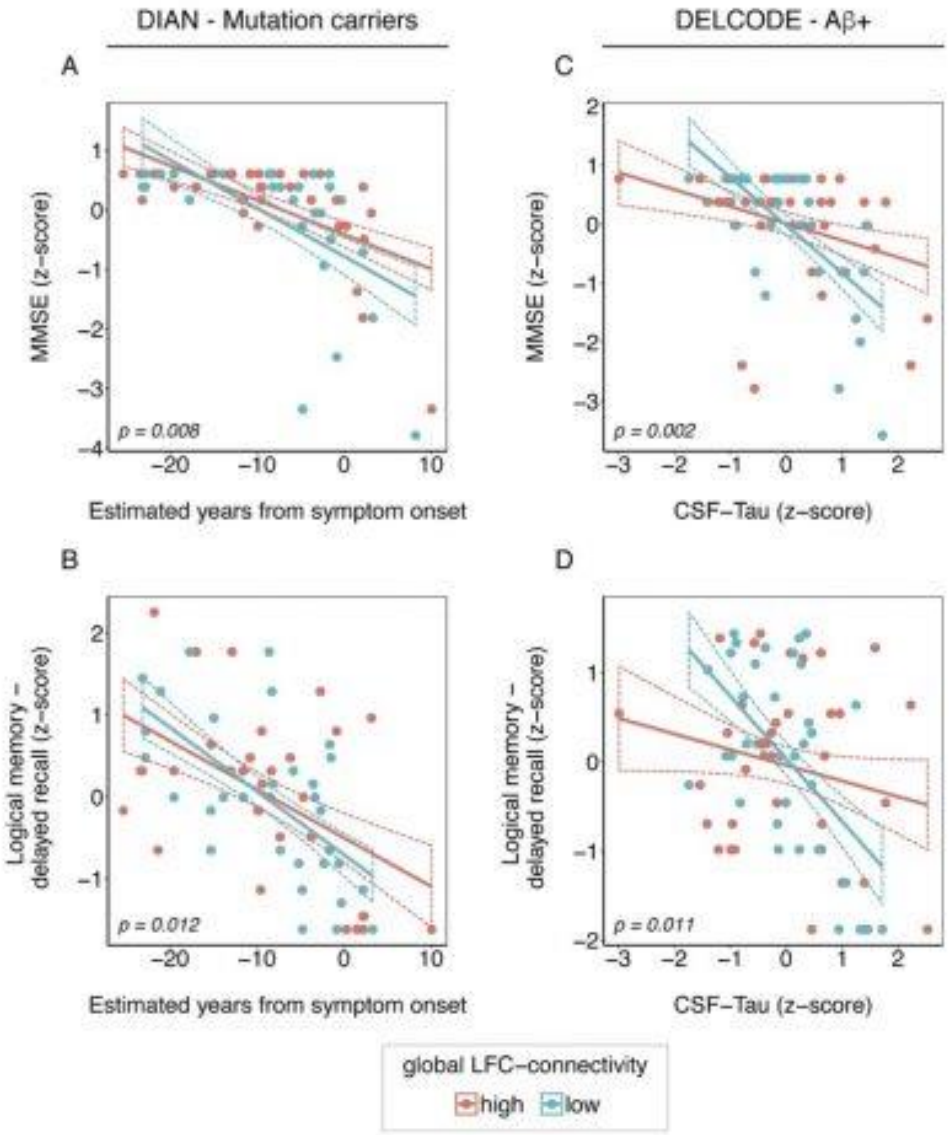

Figure 1: Interaction gLFC-connectivity x AD severity on cognition
Scatterplots of the interaction gLFC-connectivity x AD severity on cognitive performance in the ADAD (DIAN) and sporadic AD (DELCODE) sample. For DIAN, the estimated years from symptom onset (EYO) are plotted against the MMSE score (A) and the delayed free recall score of the logical memory scale (B). For DELCODE, CSF-Tau levels are plotted against MMSE (C) and logical memory delayed free recall (D). For illustrational purposes groups of high and low gLFC-connectivity (defined via median split) are plotted separately, statistical interactions were calculated using continuous measures. Dashed lines indicate 95% Confidence intervals. P-values of the interaction terms are displayed for each graph.

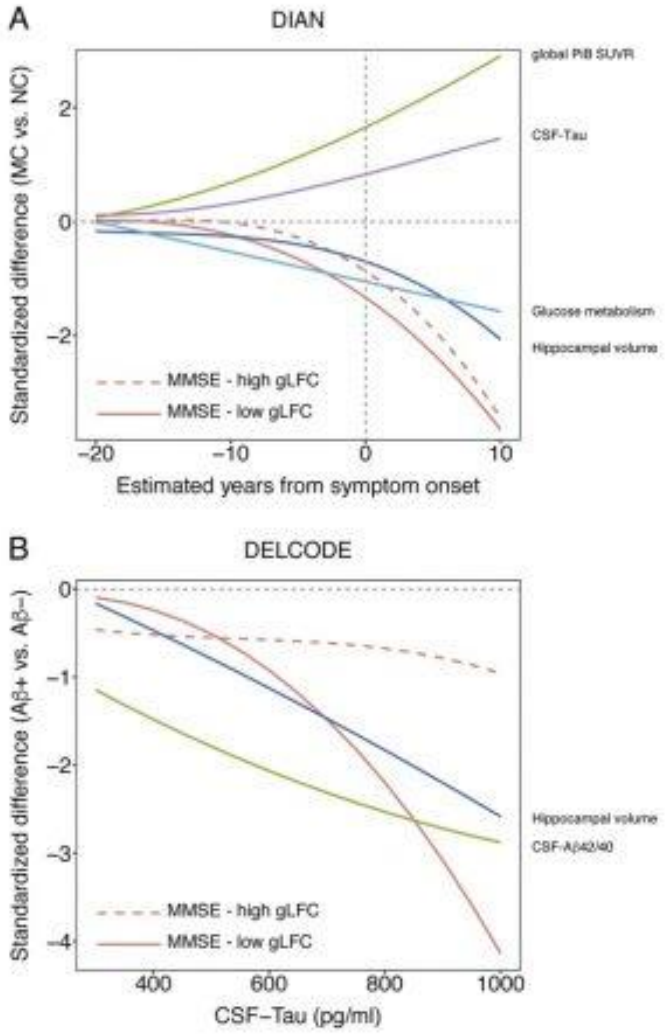

Figure 2: Cognitive & biomarker changes

Cognitive and biomarker changes as a function of AD severity. MMSE is plotted separately for individuals with high vs. low gLFC-connectivity (as defined via median split). For the DIAN sample (A) we plotted the standardized difference between MC and NC against the EYO based on the polynomial linear mixed models that best fit each marker. The plot suggests that high gLFC-connectivity is associated with a delay of cognitive decline towards a later timepoint with more progressed levels of AD pathology. For the DELCODE sample (B) we plotted the standardized difference between CSF-Aβ+ and CSF-Aβ- subjects against CSF-Tau levels. Congruent with the DIAN sample, the plot suggests that cognitive decline is shifted to a later timepoint in individuals with high levels of gLFC-connectivity.

Keywords: Reserve, Resilience, autosomal dominant Alzheimer's disease, sporadic Alzheimer's disease, fMRI

P118: Sex and e4 genotype influence the longitudinal association between amyloid and tau pathology in clinically normal older adults

Bernard Hanseeuw[1,2], Rachel Buckley[1], Elizabeth Mormino[3], Heidi Jacobs[1], Jasmeer Chhatwal[1], Teresa Gomez[1], Keith Johnson[1], Reisa Sperling[1]

[1]*Massachusetts General Hospital, Boston, MA, US*
[2]*Cliniques Universitaires Saint-Luc, Brussels, Belgium*
[3]*Stanford University, Palo Alto, CA, US*

Background: Women are at greater risk for AD dementia than men, but the biological mechanisms underlying sex differences in AD are largely unknown. Previous reports suggest that women with MCI have greater tau, but clinically normal (CN) women have similar tau levels as men (Altmann, 2014). We thus hypothesized that CN women might accumulate tau faster than men, specifically women at-risk for AD (e4 carriers with Aβ pathology).

Methods: We analyzed baseline and longitudinal CSF data from 240ADNI CN participants, using Roche Elecsys® assays (2.8observations per participant [min=2, max=8], follow-up duration=3.1±2.1years). We used linear regressions to predict baseline data. We used mixed-models with random intercepts and slopes to predict change in total and phosphorylated tau (t-tau/p-tau) with sex, e4 status, age, and baseline Aβ levels.

Results: Fig.1: Women (n=125, age=74.0±5.7, e4+=21.6%) and men (n=115, age=74.5±6.0, e4+=27.0%) had similar Aβ, t-tau, and p-tau levels. Age and e4+ predicted lower Aβ. Age, e4+, and Aβ levels predicted higher tau. Sex did not modify these associations.

Fig.2: Faster rates of t-tau and p-tau accumulation were predicted by lower Aβ levels (+0.03±0.01pg/mL/year of p-tau per -100pg/mL of baseline Aβ, p=0.01), but not by sex, e4+, or age. The association between baseline Aβ levels and longitudinal tau accumulation was stronger in e4 carriers than in non-carriers, specifically in women e4+ (+0.13±0.04pg/mL/year of p-tau per -100pg/mL of Aβ compared to women non-carriers, p=0.002). Aβ explained 33% of the variance in p-tau accumulation in women e4+ (p=0.002), 11% in men e4+ (p=0.07), and <3% in non-carriers.

Conclusion: In CN, age, e4 status, and Aβ are associated with higher tau levels, regardless of sex. Baseline Aβ levels are associated with faster tau accumulation in women e4 carriers. Taken together, these findings may account for the observation that CN women at-risk for AD progress faster to symptomatic AD, with higher tau levels detectable at the MCI stage.

Fig.1 Baseline CSF data

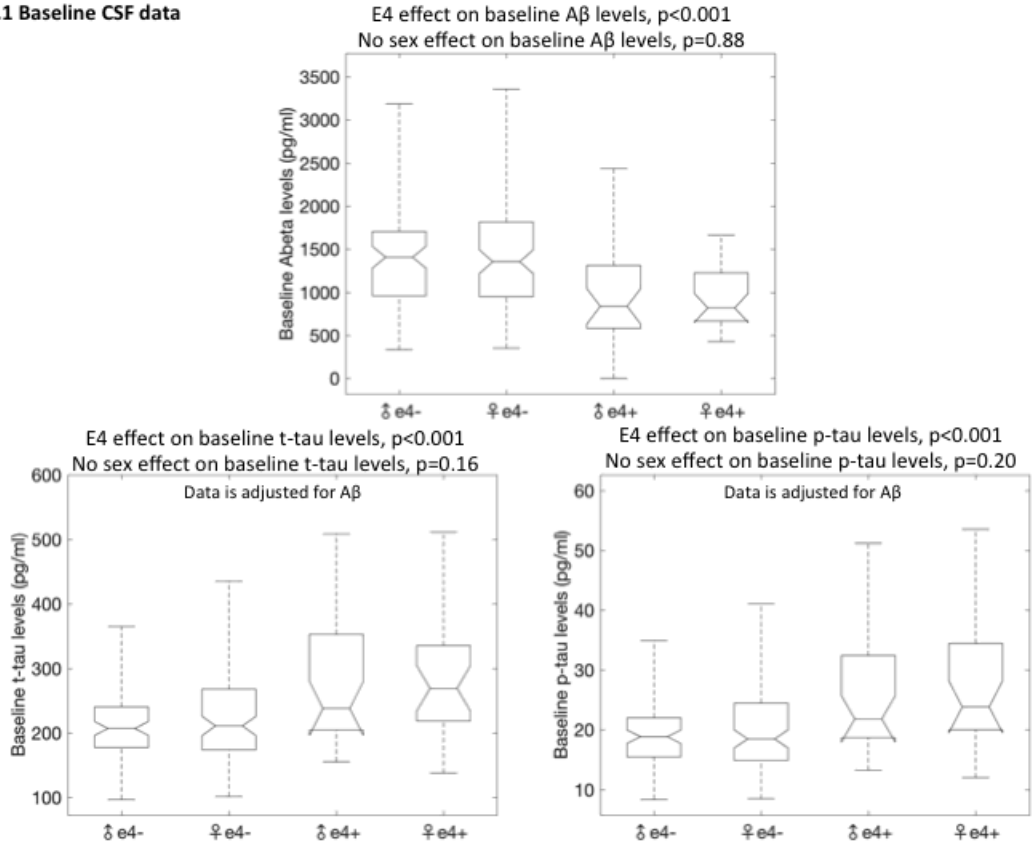

Fig.2 Longitudinal CSF data

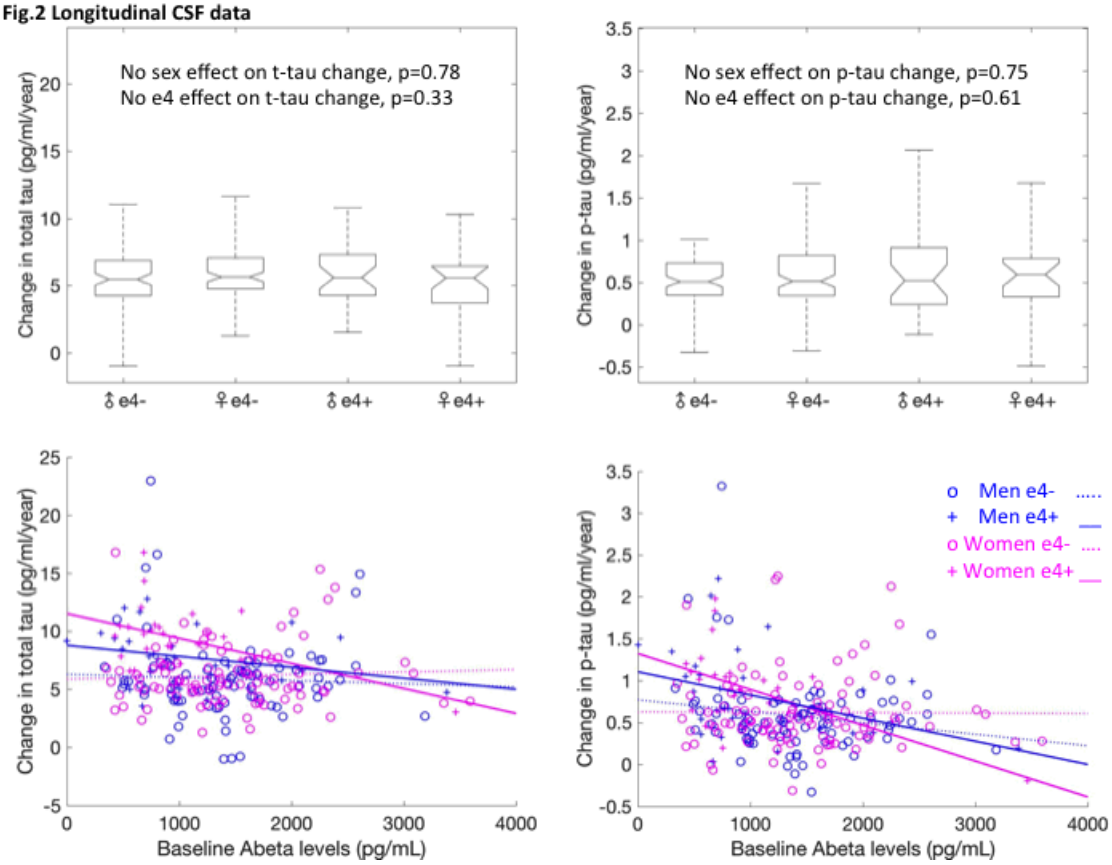

Keywords: CSF, follow-up, tau accumulation, sex, E4

P119: The DCTclockTM test captures subtle cognitive changes and biomarker evidence of preclinical Alzheimer's disease

Dorene Rentz[1,2], Kathryn Papp[1,2], Irina Orlovsky[3], William Souillard-Mandar[3,4,5], Dana Penney[3,6], Randall Davis[1,2,7], Keith Johnson[7]

[1]*Department of Neurology, Brigham and Women's Hospital, Harvard Medical School, Boston, MA, US*
[2]*Department of Neurology, Massachusetts General Hospital, Harvard Medical School, Boston, MA, US*
[3]*Digital Cognition Technologies, Waltham, MA, US*
[4]*Department of Neurology, Lahey Hospital and Medical Center, Burlington, MA, US*
[5]*Department of Neurology, Tufts University School of Medicine, Boston, MA, US*
[6]*CSAIL, Massachusetts Institute of Technology, Cambridge, MA, US*
[7]*Department of Radiology, Massachusetts General Hospital, Harvard Medical School, Boston, MA, US*

Background: Measuring cognitive change in clinically normal (CN) older adults is challenging. The DCTclock (from Digital Cognition Technologies) radically revises a familiar drawing test by combining digitizing pen technology with novel software to precisely measure nuances in cognitive performance beyond just correct completion of the task. We sought to determine whether DCTclock was associated with AD biomarkers and could thus serve as a sensitive marker of preclinical cognitive changes.

Methods: We studied 63 CN participants from the Harvard Aging Brain Study (HABS). All subjects were administered neuropsychological (NP) tests and the DCTclock. All subjects underwent (a) PIB PET imaging to measure amyloid accumulation in an aggregate of frontal, lateral and retrosplenial cortices, and in frontal lobes; (b) Flortaucipir (a.k.a. AV-1451) PET imaging to measure tau accumulation in inferior temporal and entorhinal regions and (c) FDG PET to measure glucose metabolism in association cortices. Linear regression models and effect sizes were used to explore the relationships between DCTclock variables, NP tests and AD biomarkers.

Results: The DCTclock score was highly correlated with NP tests for Executive Function ($r=0.40$, $p=0.001$) and Processing Speed ($r=0.56$, $p<0.001$) suggesting construct validity for frontal network processing. An inverse relationship between DCTclock and amyloid burden was noted in whole brain ($B=-0.004$, $p=0.001$) and frontal regions ($B=-0.005$, $p=0.001$), and a positive relationship noted with parietal FDG ($B=0.002$, $p=0.012$). Furthermore, the DCTclock score revealed non-significant trends with inferior temporal tau ($B=-0.002$, $p=0.054$) and entorhinal tau ($B=-0.001$, $p=0.089$). The DCTclock test was better overall at correlating with AD biomarkers compared with traditional NP tests.

Conclusion: Measuring cognitive performance with the DCTclock is a revolutionary approach to standard NP assessments. The results of this study suggest that the development and validation of such measures would allow for more automated assessments of cognition that might be sensitive to subtle changes related to preclinical AD.

Keywords: Novel cognitive tests, preclinical Alzheimer's disease, PET imaging

P120: Evidence for neuroinflammation in semantic dementia

Belen Pascual[1], Paolo Zanotti-Fregonara[1,2], Neha Pal[1], Elijah Rockers[1], Quentin Funk[1], Meixiang Yu[3], Gustavo C Roman[1], Paul E Schultz[4], Joseph C Masdeu[1]

[1]Nantz National Alzheimer Center, Houston Methodist Neurological Institute, Houston Methodist Research Institute, Weill Cornell Medicine, Houston, TX, US
[2]PET Core, Houston Methodist Research Institute, Weill Cornell Medicine, Houston, TX, US
[3]Cyclotron and Radiopharmaceutical Core, Houston Methodist Research Institute, Weill Cornell Medicine, Houston, TX, US
[4]Department of Neurology, McGovern Medical School at UTHealth, Houston, TX, US

Background: Semantic dementia (SD) is a progressive naming disorder with atrophy in the anterior portion of the left temporal lobe. It is associated with a propensity for autoimmune disease and increased inflammation in peripheral blood; however, brain inflammation has not been assessed *in vivo.* Our main objective was to measure brain inflammation in SD using the PET translocator protein (TSPO) radioligand ^{11}C-PBR28.

Methods: We performed ^{11}C-PBR28 PET in five SD patients and six healthy controls. Patients (3/5 women, mean age 71.2±4.6 years) were amyloid-negative, and did not differ significantly in age from the controls (2/6 women, mean age 67±5.8 years). The V_T values for ^{11}C-PBR28 were calculated at the regional level with a Logan plot and a metabolite-corrected arterial input function, with and without correction for partial volume effect.

Results: Compared to controls, patients with SD had increased V_T mainly in the anterior portion of left temporal cortex, but also in the tip of the right temporal pole. After partial volume correction, patients showed increased V_T in left temporal cortex from the tip to the posterior portion of the temporal lobe, and in the right temporal pole. An increased V_T was also found in regions of the orbitofrontal cortex adjoining anterior temporal cortex.

Conclusions: This study provides the first direct *in vivo* evidence for neuroinflammation in SD. It was greatest in regions known to be associated with loss of volume, namely the temporal poles and, to a lesser extent, orbitofrontal cortex. TSPO imaging can be used to follow disease progression and determine the association between inflammation and other features of the neurodegenerative process, such as the accumulation of misfolded proteins or neuronal loss.

Keywords: Semantic dementia, neuroinflammation, 11C-PBR28, translocator protein, TSPO

P121: Cerebrospinal fluid ratio of phosphorylated tau protein to beta-amyloid peptide 42 may improve the prediction of amyloid PET positivity: data from the Czech Brain Ageing Study

Jiri Cerman[1], Jan Laczo[1], Martin Vyhnalek[1], Katerina Sheradova[2], Jiri Ferda[3], Otakar Belohlavek[4], Jakub Hort[1]

[1]2nd Faculty of Medicine, Charles University in Prague and Motol University Hospital, Department of Neurology, Prague, Czech Republic
[2]International Clinical Research Center, St. Anne's University Hospital Brno, Brno, Czech Republic
[3]Faculty of Medicine in Pilsen, Charles university, Department of Medical Imaging, Pilsen, Czech Republic
[4]Na Homolce Hospital, Department of Nuclear Medicine and PET Center, Prague, Czech Republic

Background: Current guidelines for Alzheimer's disease (AD) shift the focus from clinical findings to biomarkers. Most widely used metabolic biomarkers are cerebrospinal fluid (CSF) levels of amyloid-β1-42 (Aβ1-42), total-tau (t-tau), and phosphorylated tau 181 (p-tau181), as well as amyloid positron emission tomography (PET). However, the concordance between amyloid PET and CSF biomarkers is not well established and interpretation of biomarkers in clinical settings may also be challenged by analytical procedures and cut-off values.

We present pilot clinical data from the Czech Brain Ageing Study. Our aim was to investigate the use CSF biomarkers in prediction of amyloid PET positivity and propose cut off values in clinical settings.

Method: 44 patients with mild cognitive impairment or mild dementia classified as possible AD (National Institute on Aging–Alzheimer's Association criteria) underwent volumetric MRI, neuropsychological assessment, flutemetamol PET and CSF sampling. PET results were evaluated visually and dichotomized. AUCs of individual ROC curves for Aβ1-42, p-tau and p-tau181/Aβ1-42 ratios were compared. Optimal cutoff points were based on the highest Youden's J indices.

Results: P-tau181/Aβ1-42 ratio (AUC=0.975, 95% CI=0.938–0.999, P<0.001), followed by Aβ1-42 (AUC=0.905, 95% CI=0.812–0.999, P=0.001) and p-tau181 (AUC=0.797, 95% CI=0.666–0.972, P=0.001) levels were found to discriminate PET positive and negative patients. A p-tau181/Aβ1-42 ratio of 0.098 provided 88,0% sensitivity and 100% specificity.

Conclusion: In our cohort, we propose P-tau181/Aβ1-42 ratio with good sensitivity and specificity for identification of amyloid PET positive patients. Its use in amyloid PET positivity prediction for broader clinical population should be exploited in future studies.

Keywords: CSF, amyloid PET, concordance

P122: Relationships between self-reported sleep, tau, and Aβ in healthy older adults

Joseph Winer[1], Anne Maass[2,3], Theresa Harrison[3], Taylor Mellinger[3], Suzanne Baker[4], Matthew Walker[1,3], William Jagust[3,4]

[1]*Department of Psychology, University of California, Berkeley, Berkeley, CA, US*
[2]*German Center for Neurodegenerative Diseases, Magdeburg, Germany*
[3]*Helen Wills Neuroscience Institute, University of California, Berkeley, Berkeley, CA, US*
[4]*Molecular Biophysics and Integrated Bioimaging, Lawrence Berkeley National Lab, Berkeley, CA, US*

Background: Worsening sleep quality is likely both a risk factor for and result of Alzheimer's disease. Both objective and subjective measures of sleep have been linked to increased β-amyloid (Aβ) burden in healthy older adults, but the relationship between tau pathology and sleep disruption remains unexplored.

Methods: Here we compared subjective ratings of current and lifespan sleep quality, using the Pittsburgh Sleep Quality Index (PSQI) and a retrospective questionnaire, to *in vivo* [18]F-AV1451 and [11]C-PIB retention in healthy older adults (N=65, age 78 ± 7.6). [18]F-AV1451 SUVRs (80-100 min, inferior cerebellar gray reference) were calculated for each subject and regions of interest (ROIs) paralleling transentorhinal and limbic Braak stages were created in native space using FreeSurfer. A global cortical [11]C-PIB DVR index was calculated for each subject.

Results: Global PSQI scores (indicating worse sleep quality) were associated with cortical [11]C-PIB DVR (**Figure 1**) but not with [18]F-AV1451 SUVR in transentorhinal or limbic Braak stage ROIs. T-tests revealed subjects with significant sleep disruption had higher cortical [11]C-PIB (**Figure 1**; 1.07 ± 0.12; 1.19 ± 0.24; p=0.01). Separately, subjects who reported their sleep quality had worsened with aging had higher cortical 11C-PIB (1.07 ± 0.14; 1.17 ± 0.22; p=0.049). These group differences were not significant for 18F-AV1451 in any brain region (**Figure 2**).

Conclusions: This confirms findings that Aβ accumulation is associated with subjective reports of poor sleep quality, extending them to include retrospective reports of age-related decline in sleep quality. In addition, tau is not associated with measures of self-reported sleep quality. These results suggest that Aβ pathology, but not tau, may be linked to subjective sleep decline. Thus, subjective sleep report may serve as an informative and pathology-specific tool for indicating abnormal Aβ burden in healthy older adults

.

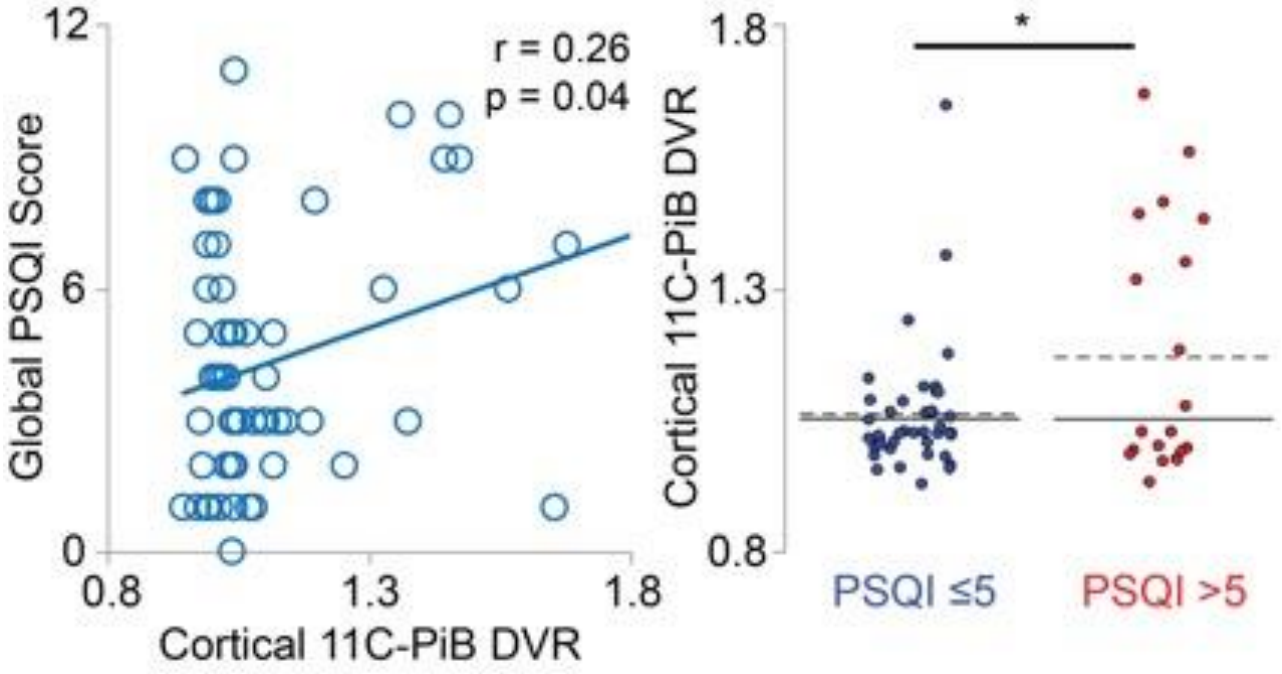

Relationships between subjective sleep quality and amyloid

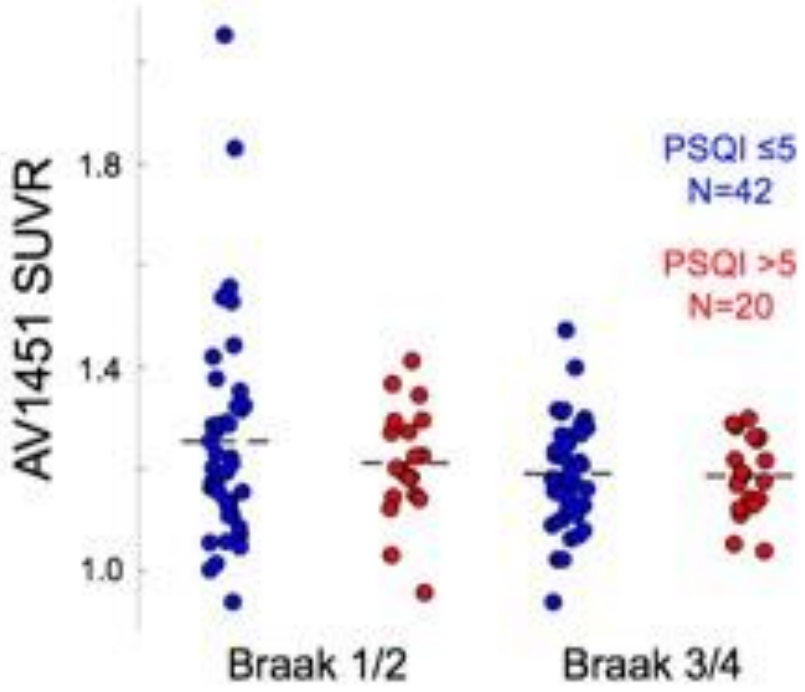

Relationships between subjective sleep quality and tau

Keywords: sleep, tau, amyloid, aging

P123: 18F-AV1451 tau PET in patients at risk for chronic traumatic encephalopathy

Orit Lesman-Segev[1], Renaud La Joie[1], Richard Tsai[1], Viktoriya Bourakova[1], Adrienne Visani[1], Nagehan Ayakta[1], James P O'Neil[2], Anne Maass[3], Suzanne Baker[2], David Perry[1], Joel Kramer[1], Bruce Miller[1], William Jagust[2,3], Gil Rabinovici[1]

[1]*Memory and Aging Center, University of California San Francisco, San Francisco, CA, US*
[2]*Life Sciences Division, Lawrence Berkeley National Laboratory, Berkeley, CA, US*
[3]*Helen Wills Neuroscience Institute, University of California Berkeley, Berkeley, CA, US*

Background: Chronic traumatic encephalopathy (CTE) is a neurodegenerative tauopathy that can only be diagnosed post-mortem. Here we describe preliminary findings of ^{18}F-AV1451 PET in a series of patients at risk for CTE.

Methods: Eleven males with a history of repetitive mild TBI and cognitive/behavioral complaints (table 1), underwent detailed cognitive assessment, 3T-MRI, and PET with ^{18}F-AV1451 (tau, acquisition: 80-100min post injection, reference: inferior-cerebellum GM), ^{11}C-PIB (β-amyloid, 50-70min, reference: cerebellum-GM). SUVR images were calculated. Patients were rated as β-amyloid positive/negative based on visual interpretation of ^{11}C-PIB SUVR images. ^{18}F-AV1451 SUVR images were inspected visually, individual age-adjusted Z-score (w-score) maps were created, patterns of abnormality were assessed qualitatively, and global cortical uptake and inferomedial temporal lobe SUVRs were extracted and compared to healthy-controls (n=67) and AD patients (n=22) (table 1).

Results: Three patients met criteria for dementia and eight had mild cognitive impairment. Two patients were β-amyloid positive – one showed a diffusely positive PIB scan (cortical ^{11}C-PIB SUVR=1.68) while the other showed focal uptake in left frontal cortex and precuneus (cortical SUVR=1.28). As expected, these patients showed highest ^{18}F-AV1451 retention values (Figure 1). In the nine PIB-negative patients, ^{18}F-AV1451 PET ranged from normal to mildly elevated binding, predominantly in the temporal and to a lesser extent in the frontal lobes. Global cortical binding was mostly in range of controls while inferomedial temporal binding was slightly above it in a subset of patients (Figure 2).

Conclusions: ^{18}F-AV1451 uptake in β-amyloid-positive patients may be explained by AD, CTE (stages III-IV) or both. In the PIB-negative sub-group we found modest ^{18}F-AV1451 retention in a subset of patients, predominantly in the temporal lobes, potentially consistent with pathologic stages III-IV. ^{18}F-AV1451 may detect imaging signature of CTE processes in later stages of disease. Correlation with post-mortem findings are needed to validate these findings.

Table 1: Patient and Control Groups Characteristics

	Sex	Age	Head Injury Exposure	CDR total	CDR SB	MMSE	[C^{11}]PIB Status
Pt1	M	64	NFL	1	7	4	Diffuse positive
Pt2	M	77	NFL	1	4.5	24	Focal positive
Pt3	M	46	College football, car racing	0.5	4	22	Negative
Pt4	M	47	Rugby, HS football	0.5	0.5	29	Negative
Pt5	M	50	NFL	1	4.5	27	Negative
Pt6	M	72	NFL	0.5	1	27	Negative
Pt7	M	65	Rodeo	0.5	3.5	25	Negative
Pt8	M	68	NFL	0.5	3.5	28	Negative
Pt 9	M	68	NFL	0.5	2	28	Negative
Pt10	M	63	Baseball, College football	0.5	2	27	Negative
Pt11	M	32	NFL	0.5	2.5	27	Negative
All sCTE Patients, n=11	100% M	60 (32-77)	7 retired NFL 4 other contact sports	3 CDR of 1 8 CDR 0.5	3 (0.5-7)	24 (4-29)	2 Positive 9 Negative
Healthy Controls, n=67	55% M 45% F	66 (20-93)	-	-	-	27 (25-30)	All negative
AD Patients (Patient control group), n=22	23% M 77% F	64 (48-82)	-	10 CDR of 0.5 12 CDR of 1	4.5 (1.5-6)	21 (8-28)	All positive

- AD – Alzheimer's Disease; sCTE – suspected CTE; CDR – Clinical Dementia Rating; SB – Sum of Boxes; CDR of 0.5 – mild cognitive impairment; CDR of 1 – mild dementia ; Continuous variables are presented as mean (range)

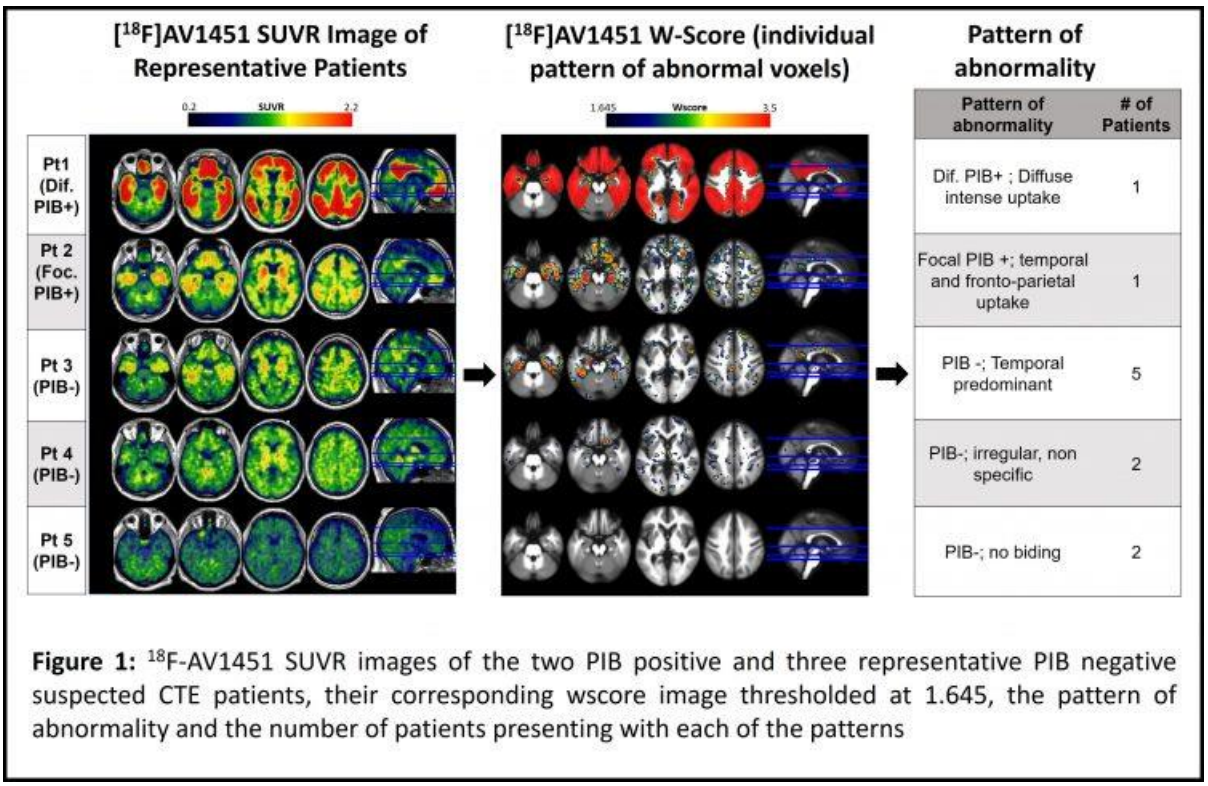

Figure 1: ^{18}F-AV1451 SUVR images of the two PIB positive and three representative PIB negative suspected CTE patients, their corresponding wscore image thresholded at 1.645, the pattern of abnormality and the number of patients presenting with each of the patterns

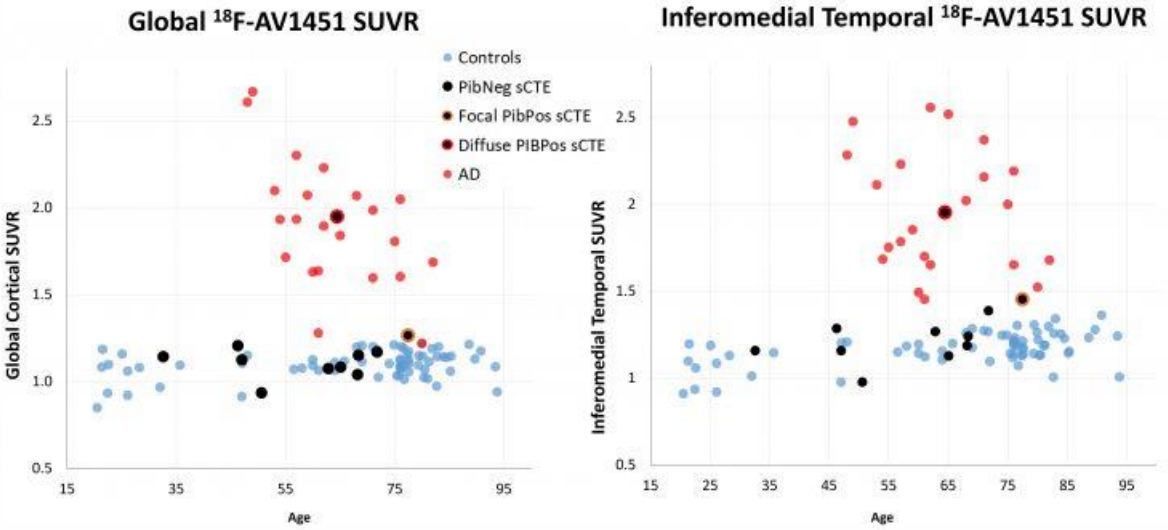

Figure 2: Global cortical (A) and inferomedial temporal (B) ^{18}F-AV1451 uptake (extracted in native space) in diffuse and focal PIB positive and PIB negative suspected CTE patients compared to healthy controls and AD patients

Keywords: Chronic traumatic encephalopathy, Imaging, Positron-emission tomography, 18F-AV1451, Tau

P124: Longitudinal [18F]THK5317 and [18F]FDG PET in relation to novel CSF tau fragments in Alzheimer's disease and related primary tauopathies

Antoine Leuzy[1], Konstantinos Chiotis[1], Claudia Cicognola[2], Laure Saint-Aubert[1], Henrik Zetterberg[2,3], Kaj Blennow[2], Kina Höglund[2], Agneta Nordberg[1,4]

[1]Department NVS, Centre for Alzheimer Research, Division of Translational Alzheimer Neurobiology, Karolinska Institutet, Stockholm, Sweden
[2]Department of Psychiatry and Neurochemistry, Institute of Neuroscience and Physiology, The Sahlgrenska Academy, University of Gothenburg, Mölndal, Sweden
[3]Department of Molecular Neuroscience, UCL Institute of Neurology, Queen Square, London, United Kingdom
[4]Department of Geriatric Medicine, Karolinska University Hospital Huddinge, Stockholm, Sweden

Introduction: CSF and PET-based biomarkers of tau pathology have been shown to correlate overall. These studies, however, have used commercial assays targeting mid-domain or specific phosphorylation sites of tau. Evidence for the presence of tau fragments spanning both mid-domain and terminus regions, however, suggests that additional assays may be required to more fully understand the relationship between tau biomarkers.

Aims: To investigate the cross-sectional and longitudinal relationships between different forms of pathological tau in CSF and uptake of the tau tracer [^{18}F]THK5317 and [^{18}F]FDG, in a cohort of patients with AD and related primary tauopathies.

Methods: Twenty patients (fourteen AD; six non-AD) who previously completed baseline [^{18}F]THK5317 and [^{18}F]FDG studies were included. Follow-up PET data was acquired for twelve subjects (ten AD; two corticobasal) after 17-months (median). CSF tau (sampled prior to baseline PET) was measured using commercial INNOTEST (mid-domain; total tau, T-tau), ELISA (N-terminus plus mid-domain; N-Mid) and SIMOA (C-terminus; Tau-368). PET measures included DVR ([^{18}F]THK5317), SUVR ([^{18}F]FDG), and rate of change.

Results: The relationship between [^{18}F]THK5317 and CSF tau (all measures) was found to vary by levels of amyloid pathology, with differing slopes noted between those that had high, intermediate, and low levels of CSF A$\beta_{1\text{-}42}$. Longitudinally, [^{18}F]THK5317 uptake related only to Tau-368 and N-Mid (follow-up) as well as to Tau-368/N-Mid and Tau-368/T-tau ratios (rate of change). When looking at the relationship between [^{18}F]FDG and CSF tau, findings were more extensive in comparison to [^{18}F]THK5317. The interaction effect noted for [^{18}F]THK5317, however, was absent.

Conclusion: These findings suggest that CSF tau may better reflect neurodegenerative changes ([^{18}F]FDG PET), relative to tau pathology, with its association to tau PET modulated by CSF A$\beta_{1\text{-}42}$ levels; and that measures capturing C-terminus and N-terminus/mid-domain forms of pathological tau may better predict longitudinal tau PET findings.

Keywords: CSF, tau, [18F]HK5317, PET, Alzheimer's

P125: Tau pathology networks associated with functional connectivity networks and disease progression in Alzheimer's disease

Merle Hönig[1], Gérard Bischof[1,2], Joseph Seemiller[3], Jochen Hammes[1], Gereon R. Fink[2,4], Thilo van Eimeren[1,2,4,5], Alexander Drzezga[1,5]

[1]*Multimodal Neuroimaging Group, Department of Nuclear Medicine, University Hospital Cologne, Cologne, Germany*
[2]*Cognitive Neuroscience, Institute of Neuroscience and Medicine (INM-3), Research Center Juelich, Juelich, Germany*
[3]*Geisinger Commonwealth School of Medicine, Scranton, PA, US*
[4]*Department of Neurology, University Hospital Cologne, Cologne, Germany*
[5]*German Center for Neurodegenerative Diseases (DZNE), Bonn, Germany*

A stereotypical propagation pattern of tau pathology has been described in Alzheimer's disease (AD). According to the network degeneration hypothesis, this distribution pattern could be indicative of tau pathology spreading across functional networks. Here, we examined whether independent components could be identified in the distribution pattern of *in vivo* tau pathology and whether these components correspond with specific functional connectivity networks. To identify independent tau pathology networks (TPNs), we employed an independent component analysis (ICA) on [^{18}F]AV-1451 tau-PET imaging data of 22 patients with AD. Next, to investigate if regions of high tau burden are associated with functional connectivity networks, we extracted the region of maximum tau burden in each of the generated TPNs and adopted them as seeds in a subsequent resting-state functional MRI analysis, conducted in a group of healthy adults derived from the 1000 Functional Connectomes Project. Third, to examine if the TPNs correspond with functional connectivity networks, we quantified the spatial overlap between the seed-based networks and the corresponding TPN using the dice similarity coefficient. Additionally, we assessed if the seed-based networks spatially co-localize with known functional resting-state networks. Finally, we examined the relevance of the identified TPNs in relation to the neuropathological Braak stages. We identified 10 independently coherent TPNs with the majority showing a symmetrical distribution pattern and coinciding with highly functionally connected brain regions. A fair to moderate overlap was observed between the TPNs and corresponding seed-based networks, which in turn resembled known resting-state networks, particularly the default mode network. Moreover, greater tau burden in the TPNs was associated with more advanced Braak stages. Using the data-driven approach of ICA, we observed a set of independently coherent TPNs in AD which were associated with disease progression and partly coincided with functional networks previously reported to be impaired in AD.

Keywords: Alzheimer's disease, tau pathology, PET, independent component analysis, functional connectivity networks

P126: Characterizing regional β-amyloid burden by magnetic susceptibility

Paul G. Unschuld[1,2], Jiri M.G. van Bergen[2], Xu Li[3,4], Frances Quevenco[2], Anton F. Gietl[1,2], Valerie Treyer[2,5], Rafael Meyer[1,2], Alfred Buck[5], Philipp A. Kaufmann[5], Roger M. Nitsch[1,2], Peter C.M. van Zijl[3,4], Christoph Hock[1,2]

[1]*Hospital for Psychogeriatric Medicine, University of Zurich,, Zurich, Switzerland*
[2]*Institute for Regenerative Medicine (IREM), University of Zurich, Schlieren, Switzerland*
[3]*The Russell H. Morgan Department of Radiology and Radiological Science, Division of MR Research, Johns Hopkins University School of Medicine, Baltimore, MD, US*
[4]*F.M. Kirby Research Center for Functional Brain Imaging, Kennedy Krieger Institute, Baltimore, MD, US*
[5]*Department of Nuclear Medicine, University Hospital Zurich and University of Zurich, Zurich, Switzerland*

The accumulation of β-amyloid is a pathological hallmark of Alzheimer's disease (AD) that precedes the manifestation of the clinical syndrome by years. Recently published data suggest that elevated magnetic susceptibility may represent a risk factor for β-amyloid associated cognitive decline. We hypothesized that regional β-amyloid plaques with increased magnetic susceptibility may define brain regions with particular liability to β-amyloid related impairment, as indicated by an association with cognitive performance levels in non-demented old aged adults

116 elderly individuals (mean age 75±7.4 years) received neuropsychological testing to calculate a global cognitive performance score, incorporating major cognitive domains. All participants were scanned on a combined PET-MRI for contemporaneous T1-sequences for anatomic mapping, quantitative magnetic susceptibility mapping (QSM), and 18F-Flutemetamol-PET for estimating β-amyloid plaque load. Biological parametric mapping (BPM) was used to generate masks indicating voxels with significant ($p\text{-}FDR<0.05$) correlation between susceptibility and 18F-Flutemetamol-SUVR.

We found a bilateral pattern of clusters with significant regional correlations between magnetic susceptibility and 18F-Flutemetamol-SUVR, indicating co-localized paramagnetic properties and β-amyloid plaques. For two bilateral clusters, located in the frontal and temporal cortex, significant relationships ($p\text{-}FDR<0.05$) between local β-amyloid and cognitive performance could be observed.

Our data suggest that magnetic susceptibility, as measured by QSM, may complement PET data on regional β-amyloid for stratification of preclinical study populations. Further preclinical and translational research is needed to clarify pathophysiological correlates of this finding, including the impact of paramagnetic tissue-deposits such as iron on the risk for β-amyloid related cognitive decline.

Keywords: PET-MRI,18F-Flutemetamol, QSM, iron, β-amyloid

P127: Tau aggregates imaged with 18F-Flortaucipir PET contribute to core clinical features of the Lewy body dementias

Samantha Katz[1,2], Rong Ye[1], Julia Shirvan[1], Aaron Schultz[2], Sara Makaretz[1], Bradford Dickerson[1], Reisa Sperling[3], John Growdon[1], Keith Johnson[1,2], Stephen Gomperts[1]

[1]Department of Neurology, Massachusetts General Hospital, Harvard Medical School, Boston, MA, US
[2]Department of Radiology, Massachusetts General Hospital, Harvard Medical School, Boston, MA, US
[3]Center for Alzheimer's Research and Treatment, Brigham and Women's Hospital, Harvard Medical School, Boston, MA, US

Background: Neuropathological substrates of the hallmark clinical features of dementia with Lewy bodies (DLB) and Parkinson disease dementia (PDD) are unknown. At autopsy, neurofibrillary tangles in brain regions including inferior temporal (IT), posterior cingulate (PC), frontal, and occipital cortices and amyloid deposits often accompany alpha-synuclein pathology. We sought to relate regional tau burden to characteristic features of these diseases: slowed cognitive processing, parkinsonism, cognitive fluctuations, and hallucinations.

Methods: Thirty-one Lewy body disease (LBD) subjects underwent 18F-Flortaucipir (FTP) PET, 11C-PIB-PET, MRI, neurologic and neuropsychological testing – 9 cognitively-normal PD (CDR 0, 66.9 ± 7.6 years), 11 cognitively-impaired PD (74.7 ± 7.1), 11 DLB (70.8 ± 7.5). Evaluation included Mayo fluctuations scale, NPIQ hallucinations subscale, tests of language processing (letter fluency, semantic fluency), and UPDRS. PET and cognitive measures were compared to 180 normal controls (NC, 74.0 ± 7.4 years). We restricted analyses to ROIs based on specific hypotheses relating cingulate (posterior and anterior (AC)) uptake to processing speed and fluctuations; lateral frontal uptake to UPDRS; and occipital uptake to hallucinations, and we included IT in each analysis. Regional PET measures (SUVRs, partial volume corrected, cerebellum referenced) were entered into linear regression models accounting for age, gender and education, predicting severity of clinical features.

Results: FTP retention differed among diagnostic groups in IT, PC, and occipital cortices. In LBD but not NC, FTP binding in PC and IT was associated with slowed processing. FTP retention in frontal cortex but not IT was associated with greater motor impairment. AC retention was associated with greater fluctuations of cognition. FTP binding in occipital and IT regions in PD-impaired and DLB was not associated with hallucinations. These results persisted in subjects with low amyloid burden.

Discussion: Regional tau pathology contributes to LBD clinical features that accompany dementia, including bradyphrenia, motor manifestations of parkinsonism, and cognitive fluctuations.

Keywords: Tau, Flortaucipir, DLB, Parkinson's disease

P128: Nucleus basalis of Meynert volume predicts early tau pathology and memory performance when amyloid levels are elevated in cognitively normal older individuals

Heidi Jacobs[1], Bernard Hanseeuw[1], Aaron Schultz[1], Kathryn Papp[2], Dorene Rentz[2], Reisa Sperling[2], Keith Johnson[1]

[1]Division of Nuclear Medicine and Molecular Imaging, Department of Radiology, Massachusetts General Hospital/Harvard Medical School, Boston, MA, Boston, MA, US
[2]Center for Alzheimer Research and Treatment, Department of Neurology, Brigham and Women's Hospital, Harvard Medical School, Boston, MA, Boston, MA, US

Background: Neuropathology studies suggest that accumulation of pretangle material occurs in the nucleus basalis of Meynert (NBM) before neurofibrillary tangles in the entorhinal cortex or amyloid depositions in the neocortex can be observed. Neuroimaging studies reported a negative association between amyloid deposition and NBM volume in older individuals and prodromal Alzheimer's disease (AD) patients. Imaging techniques do not allow us to visualize early tau lesions. Therefore, we sought to examine the relationship between NBM volume and regional tau pathology in the preclinical AD stages.

Methods: 179 older individuals (mean age: 75.29 ±7.75; 111 females (62%)) were enrolled from the Harvard Aging Brain Study. The NBM was defined using a stereotaxic probabilistic map from postmortem brains and registered to each native T1-scan using diffeomorphic normalization tools (ANTs). Amyloid status was determined based on an aggregate of neocortical regions (PVC cut-off: 1.32 PiB-DVR). Associations with tau pathology (Flortaucipir-PET) were assessed with voxel-wise regression analyses and confirmed using region-of-interest analyses. Age, sex and education were included as covariates. Memory was a composite score derived from a factor analysis on the complete cohort. Mediation analyses were performed to understand to relationships between NBM volume (ICV-corrected), tau, amyloid and memory.

Results: NBM volume was negatively associated with tau deposition in the right entorhinal cortex, hippocampus, amygdala, inferior temporal cortex and fusiform gyrus in individuals with elevated amyloid (all $p<0.05$, Figure 1-2).

Figure 1: Voxel-wise analyses between nucleus basalis of Meynert volume and Tau binding in individuals with low and elevated amyloid burden

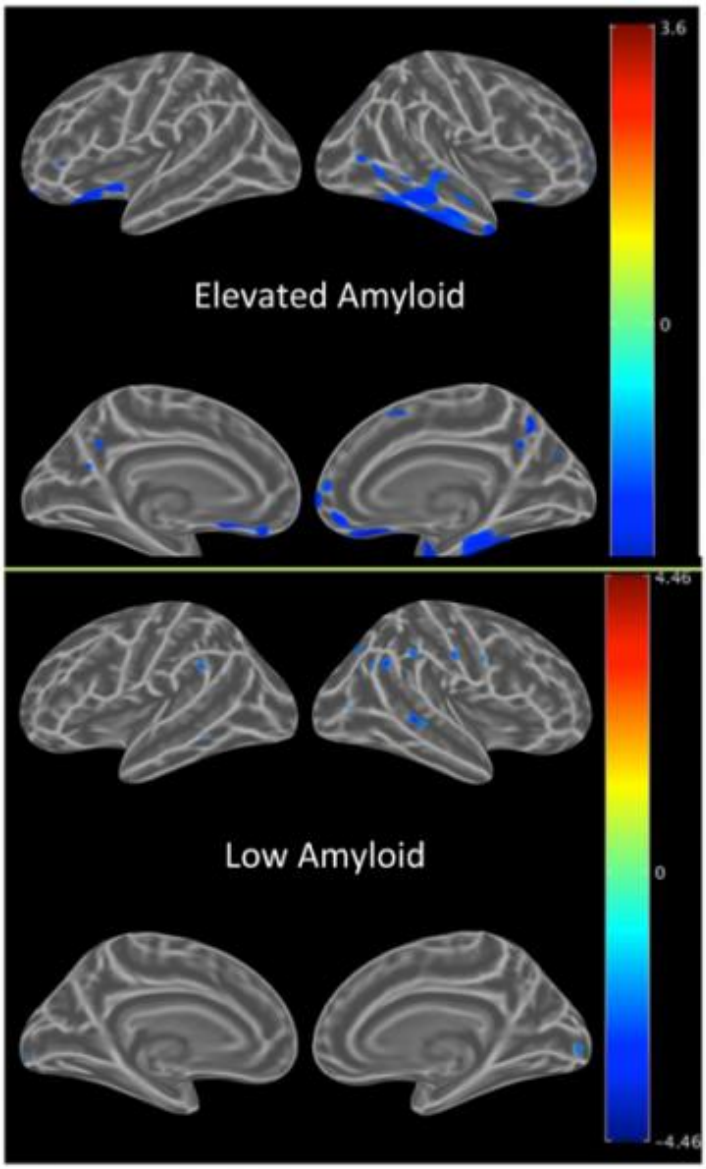

Note: Negative correlation maps thresholded at p<0.05 (t-value=2.00), corrected for age, education and sex.

Figure 2: FreeSurfer-based ROI analyses: the associations between nucleus basalis of Meynert volume and tau binding is different between individuals with elevated amyloid and low amyloid levels.

Tau ROI ~ amyloid * NBM volume	B-coeff	t-value	P-value
Entorhinal, right	-0.0019	-2.001	0.047*
Entorhinal, left	-0.0001	-0.135	0.89
Inferior temporal, right	-0.0022	-3.119	0.002**
Inferior temporal, left	-0.0005	-0.738	0.46
Fusiform, right	-0.0018	-2.669	0.008**
Fusiform, left	-0.0006	-1.176	0.24
Hippocampus, right	-0.0013	-2.517	0.013*
Hippocampus, left	-0.0009	-1.611	0.11
Amygdala, right	-0.0013	-1.844	0.067
Amygdala, left	-0.0014	-1.940	0.054

Note: statistics (unstandardized beta-coefficient, t-value and p-value) are shown for the interaction effect. Linear regression analyses were corrected for age, education and sex. *: p-value < 0.05, **: p-value < 0.01

NBM volume did not predict memory performance by itself, but did when moderated by amyloid pathology (t=2.83, p=0.005). Regional tau deposition mediated the relationship between NBM volume and memory when amyloid levels were elevated (Indirect effect: z=2.20, p=0.028; Figure 2).

Figure 3: Mediation of tau on the relationship between nucleus basalis of Meynert volume and memory is moderated by amyloid burden

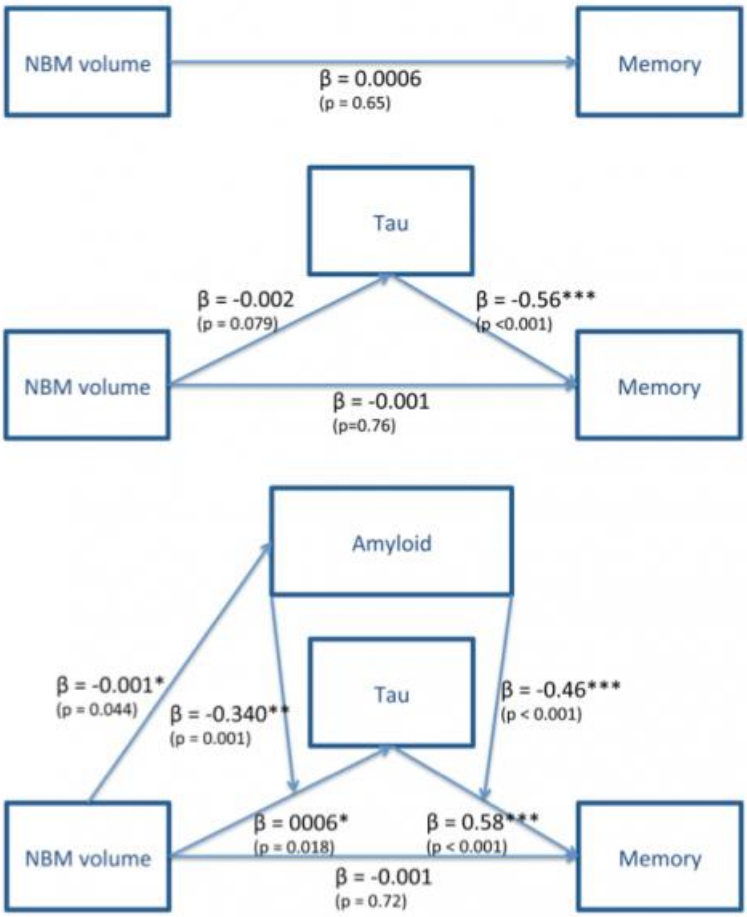

Note: The unstandardized beta-coefficients are displayed in the figure. NBM volume did not predict memory (top part) and tau does not mediate this relationship (middle part). Under levels of high amyloid, tau does mediate the relationship between NBM volume and memory. Abbreviations: NBM=nucleus basalis of Meynert. Tau in the model is an aggregate of right entorhinal, right inferior temporal and right fusiform.

Discussion: NBM volume is associated with tau pathology in clinically normal older individuals. However, the link between NBM and memory is dependent on AD pathology, suggesting that NBM volume changes may precede AD-related symptomatology.

Keywords: forebrain, Flortaucipir, amyloid, memory, mediation

P129: Increased GM regions in association with SUVR are candidate to predict convergence to Preclinical AD

Gemma Monté-Rubio[1], Octavio Rodriguez-Gomez[1], Angela Sanabria[1], Montse Alegret[1], Alba Perez-Cordon[1], Francisco Lomeña[2], Javier Pavia[2], Rossella Gismondi[3], Santi Bullich[3], Assumpta Vivas-Larruy[4], Marta Gomez-Chiari[4], Agustín Ruiz-Laza[1], Lluis Tárraga[1], Mercè Boada[1]

[1]*Fundació ACE. Institut Català de Neurociències Aplicades., Barcelona, Spain*
[2]*Hospital Clinic de Barcelona, Barcelona, Spain*
[3]*PIRAMAL, Berlin, Germany*
[4]*Clinica Corachan, Barcelona, Spain*

Diagnosis of AD requires of lumbar puncture or PET, as these are the best strategies for this purpose. Finding additional biomarkers is a field of interest to detect Preclinical-AD. SUVR is a quantitative measure from 18F-Florbetaben (FBB-)PET to determine amyloidosis. The current work explores the association of SUVR with MRI data as a potential biomarker.

Methods: 195 participants with subjective cognitive decline (SCD) from the FACEHBI study (description in Rodriguez-Gomez et al. 2016), underwent a FBB-PET and a MR protocol. SUVR was estimated using Freesurfer and FSL. Only 16 participants overcame the threshold of amyloidosis (1.45). VBM technique was conducted with the MRI data according Dartel, in SPM12. Modulated GM images were smooth with 8mm FWHM. A regression analysis with SUVR was driven. Additionally, a Ridge Regression, Pattern Recognition (PR) approach implemented in PRONTO, was applied. FBB-PET images were used to quantify highest predictive power of SUVR. To test predictive capacity, the regions found in the VBM, as well as whole brain modulated GM and WM, were tested.

Results: In the VBM, only increased GM volume was associated to SUVR in areas described in early stages of AD (Table1; Fig.1). Regarding PR, PET images predicted SUVR with a correlation- coeff.=0.84, MSE=0.01, R2=0.70 (p = 0.01) (Fig.2). As expected according SCD subjects, GM and WM provided poor features. Regions from VBM provided efficient features instead, correlation- coeff.=-0.72, MSE=0.02, R2=0.52 (p=0.01).

Conclusions: VBM shows that areas associated with AD appear increased with higher SUVR values. The PR analysis shows that these areas are key regions to focus at the onset of the disease, as they have increased predictive value. Further studies are in process to state if this is due to an anatomical feature or inflammation at the onset of the disease, in association with genetics and other demographic factors.

	location	cluster size (k)	coordinates		
			x	y	z
Cluster 1	Temporal_Inf_R	816	40.5	-43.5	-16.5
	Fusiform_R				
Cluster 2	Calcarine_R	1506	9	-79.5	30
	Cuneus_R				
	Lingual_R				
	Cuneus_L				
	Precuneus_L				
	Precuneus_R				
	Cerebelum_6_R				
	Vermis_6				
Cluster 3	Occipital_Inf_L	328	-36	-82.5	-12
	Fusiform_L				
Cluster 4	Lingual_L	250	-16.5	-73.5	-7.5
Cluster 5	Temporal_Inf_L	188	-58.5	-66	-7.5
Cluster 6	Occipital_Mid_L	215	-54	-79.5	1.5
Cluster 7	Occipital_Mid_R	161	43.5	-79.5	3
Cluster 8	Occipital_Mid_L	160	-18	-90	16.5
	Occipital_Sup_L				
Cluster 9	Frontal_Mid_L	100	-33	19.5	31.5
	Frontal_Inf_Oper_L				
	Frontal_Inf_Tri_L				
Cluster 10	Angular_L	250	-39	-64.5	43.5
	Parietal_Inf_L				

Table 1. VBM. Locations where subjects with SCD show increased volume in association with higher SUVR.

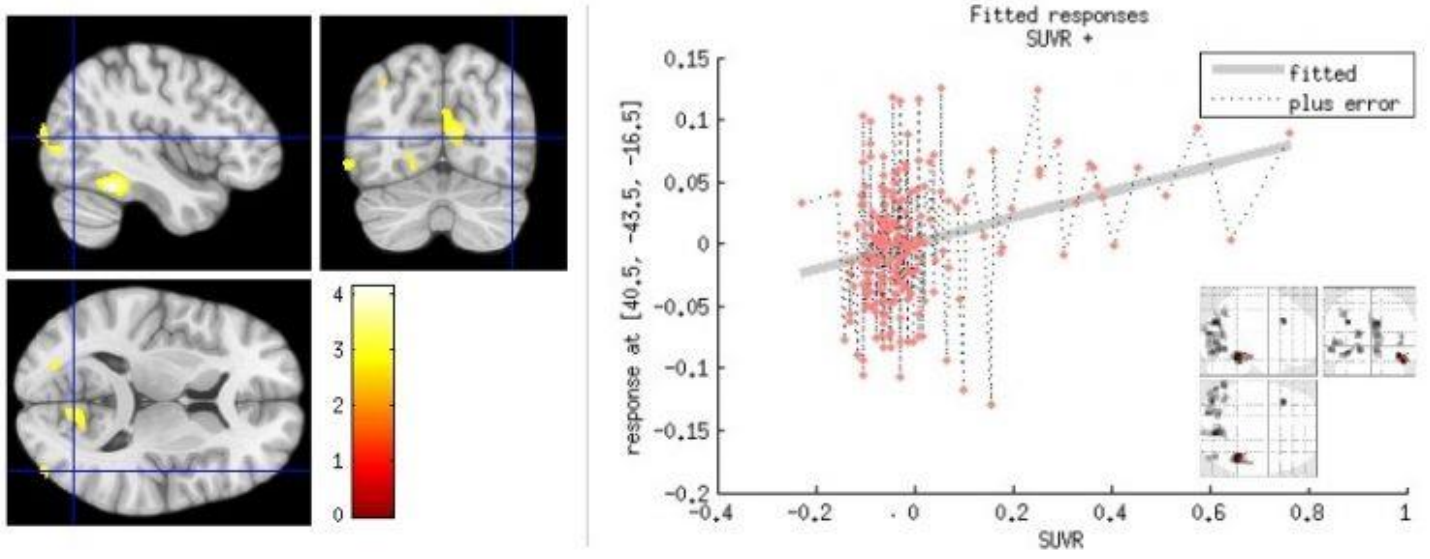

Fig.1. VBM - Statistical map with the areas of increased GM volume in the regression with the SUVR, desing accounted for age and sex (unc. p<0.005, k=100).

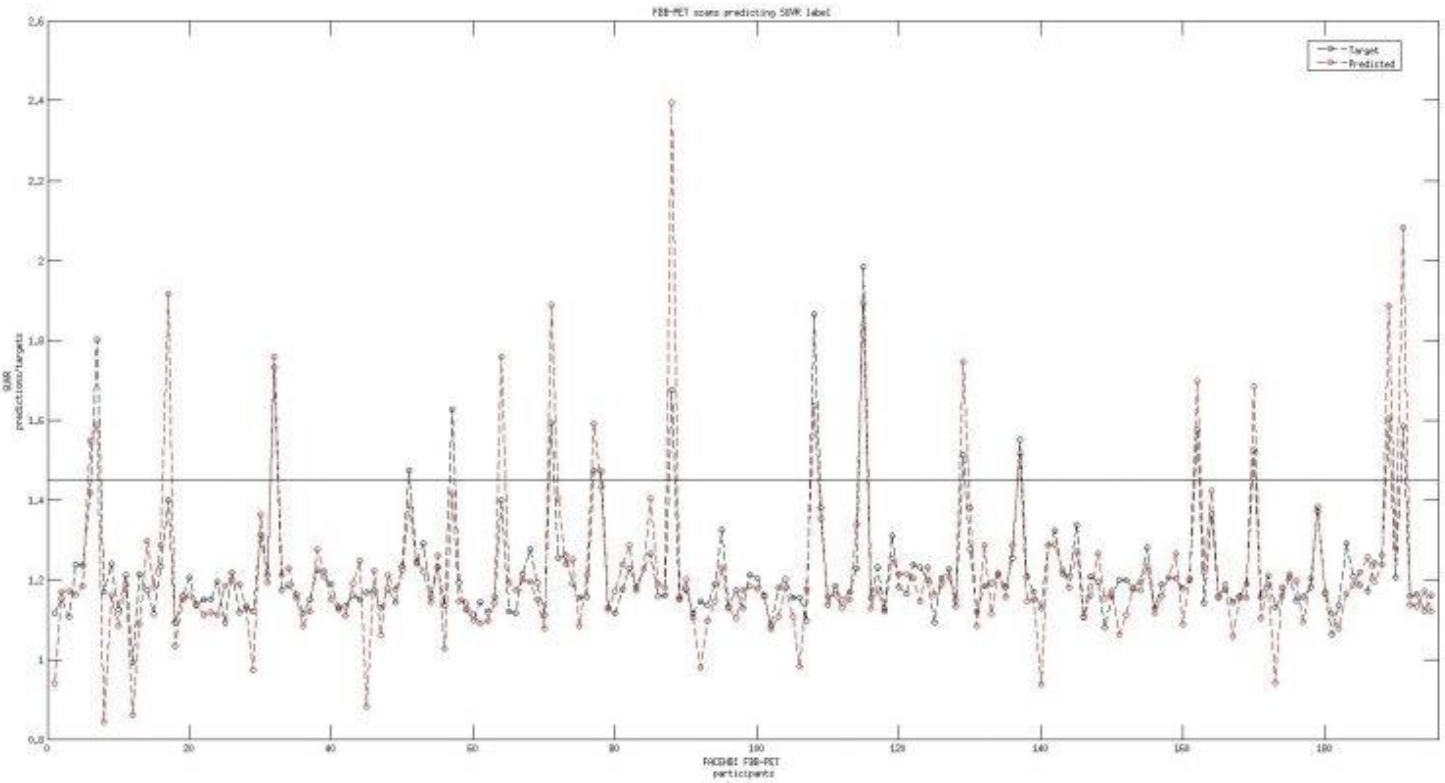

Fig.2. PR - Performance from the Ridge Regression using PET images and SUVR as label. SUVR appears to be a conservative but efficient measure. In many subjects, predicted SUVR values are upper than the real, their PET images were found closer to the amyloidosis pattern.

Keywords: Preclinical-AD, FBB-PET (SUVR), MRI, VBM, Pattern Recognition

P130: Distinct [18F]-THK5351 binding patterns in primary progressive aphasia variants

Jolien Schaeverbeke[1,2,3], Silvy Gabel[1,2,3], Rose Bruffaerts[1,4], Karen Meersmans[1], Karen Van Bouwel[4], Eva Dries[4], Ronald Peeters[5], Koen Van Laere[3,6], Patrick Dupont[1], Rik Vandenberghe[1,2,3,4]

[1]*Laboratory for Cognitive Neurology, KU Leuven, Leuven, Belgium*
[2]*Alzheimer Research Centre, KU Leuven, Leuven, Belgium*
[3]*Leuven Institute of Neuroscience and Disease, KU Leuven, Leuven, Belgium*
[4]*Neurology Department, UZ Leuven, Leuven, Belgium*
[5]*Radiology Department, UZ Leuven, Leuven, Belgium*
[6]*Nuclear Medicine and Molecular Imaging, KU Leuven and UZ Leuven, Leuven, Belgium*

Primary Progressive Aphasia (PPA) has a heterogeneous underlying pathology.

We evaluated whether [^{18}F]-THK5351-PET is able to identify different patterns between PPA variants. Twenty PPA patients participated (three with logopenic variant (LV), 12 with non-fluent variant (NFV), and five with semantic variant (SV) PPA), as well as 20 age- and gender-matched healthy controls. Subjects received a static [^{18}F]-THK535-PET-scan (50-80 min *post* injection) and a T_1-weighted structural, volumetric MRI-scan. Standardized Uptake Value Ratio (SUVR) images were calculated with cerebellar gray matter as reference and SUVR-images were partial-volume-corrected (Muller-Gartner, 1992). Voxelwise ANOVA was performed with group as between-subject factor and [^{18}F]-THK5351-SUVR-images as within-subject factor, corrected for age and gender at a significance threshold of voxel-level uncorrected $p<0.001$ and cluster-level family wise error-corrected $p<0.05$.

Compared to controls, NFV showed significantly increased binding in the left premotor cortex, pars triangularis, pars opercularis, insula, supplementary motor area (SMA) bilaterally, thalamus, basal ganglia, and in midbrain nuclei. SV showed significantly increased binding in the anterior temporal poles and right orbitofrontal cortex while LV showed significantly increased binding in the right angular gyrus. Contrasts between PPA variants revealed that in comparison to SV, NFV showed increased binding in the left premotor cortex, in the SMA bilaterally, and in the basal ganglia, thalamus, and midbrain. Compared to LV, NFV had increased binding in the thalamus and midbrain nuclei. SV showed increased binding in the anterior temporal lobe compared to NFV and LV and additionally in the right orbitofrontal cortex compared to NFV. LV demonstrated increased binding in the angular gyrus bilaterally compared to SV and compared to NFV, LV had additionally increased binding in the occipital cortex and in the inferior parietal lobule bilaterally.

[^{18}F]-THK5351 imaging reveals characteristic binding patterns in the three PPA variants, with a topography closely matching the anatomical distribution of predicted underlying pathology.

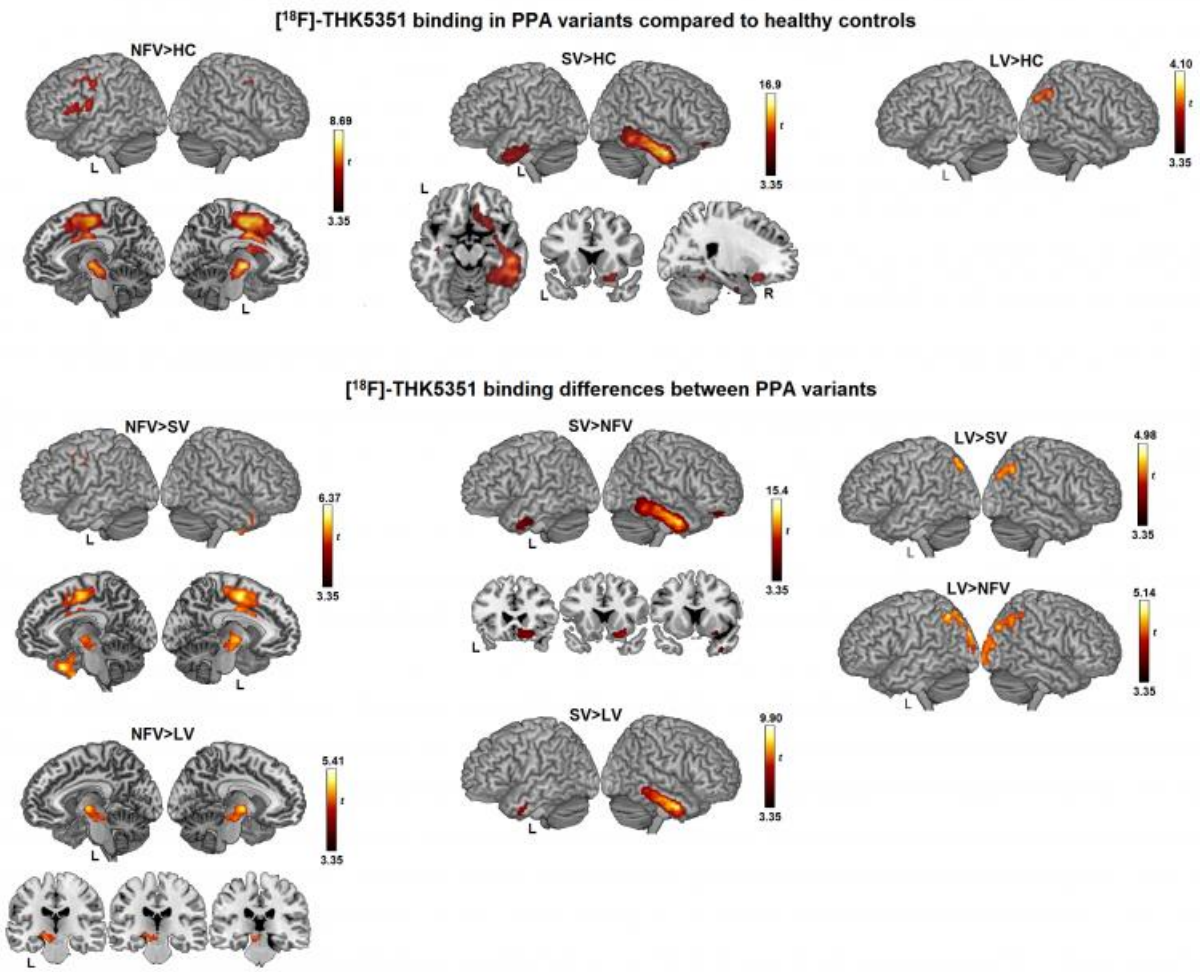

Keywords: PPA, THK5351, PET, tau, imaging

P131: Multiple brain markers contribute to age-related changes in cognition

Trey Hedden[1,2], Hannah Nierle[1], Rodrigo Perea[1,2], Jennifer Rabin[1,2], Rachel Buckley[1,4,5], Aaron Schultz[1,2], Keith Johnson[1,2,3], Reisa Sperling[1,2,3]

[1]*Massachusetts General Hospital, Boston, MA, US*
[2]*Harvard Medical School, Boston, MA, US*
[3]*Brigham and Women's Hospital, Boston, MA, US*
[4]*Florey Institute of Neuroscience & Mental Health, Melbourne, Australia*
[5]*University of Melbourne, Melbourne, Australia*

How do age-related changes in cognitive function follow from differences in brain morphometry, function, and disease-related biomarkers? Here, we extended cross-sectional findings (Hedden et al, 2016) by examining shared and selective contributions of multiple brain markers to age-related longitudinal changes in cognition across cognitive domains.

Methods: Cognitively normal older adults aged 62-90 from the Harvard Aging Brain Study (N=254) were characterized at baseline on MRI markers of gray matter thickness and volume, white matter lesions (WML), fractional anisotropy (FA), and resting state functional connectivity, and PET markers of glucose metabolism (FDG) and amyloid burden. Longitudinal change in processing speed, executive function, and episodic memory were assessed with follow-up of 1-6 years (mean=4.2 years). Linear mixed models estimated subject-specific slopes. Partial correlations examined the age-related variance in slope of cognition shared with each brain marker, and the unique age-related variance contributed by each marker controlling for all other markers. Mediation models examined the minimal set of brain markers significantly mediating age-related variance in cognitive change.

Results: The largest shared relationships to all cognitive factors involved hippocampal volume, FA, and WML. Amyloid burden shared ~20% of age-related variance, but only 2-4% was unique to amyloid. Approximately 80% of the age-related variance in cognitive change was shared when all brain markers were combined (but only <=34% of total variance). Cortical thickness, FA, and FDG were significant mediators of age-related change in processing speed. Hippocampal volume and amyloid were significant mediators of age-related change in executive function. Hippocampal volume, amyloid, entorhinal thickness, and FDG were significant mediators of age-related change in episodic memory.

Conclusion: These results suggest that the majority of age-related variation in cognitive change is shared among multiple brain markers, and that brain markers reflective of Alzheimer's disease pathology are among the most important mediators of cognitive change during aging.

Keywords: aging, amyloid, MRI, cognition, memory

P132: The BioFINDER-2 study: a longitudinal investigation on the role of Tau and amyloid on cognitive function using 18F-RO6958948 and 18-Flutemetamol PET tracers

Oskar Hansson[1,2], Niklas Mattsson[1,2], Ruben Smith[1], Michael Schöll[1], Gregory Klein[4], Gill Farrar[3], Edilio Borroni[4], Preciosa Coloma[4], Sebastian Palmqvist[1,2], Erik Stomrud[1,2]

[1]*The Clinical Memory Research Unit, Department of Clinical Sciences Malmö, Lund University, Lund, Sweden*
[2]*Memory Clinic, Skåne University Hospital, Malmö, Sweden*
[3]*GE Healthcare, London, United Kingdom*
[4]*Hoffmann La-Roche, Basel, Switzerland*

The prospective and longitudinal BioFINDER-2 study aims to study the roles of amyloid and tau pathologies on synaptic cognitive function during different stages of Alzheimer's and Parkinson's disease-related disorders.

The BioFINDER study will during a three-year period (started in May 2017) recruit more than 1500 subjects, who will all undergo detailed cognitive, neurological and psychiatric assessments, an extensive MRI protocol, CSF and plasma sampling and 18F-RO6958948 PET imaging. Further, non-demented cases will also undergo 18F-flutemetamol imaging. Examinations will be repeated over a period up to 8 years. In a subset of cases we will also perform high-field (7T) functional MRI and PET imaging using 11C-UCB-J.

In the BioFinder-2 study we will recruit 540 cognitively healthy cases (n=40, 20-39 y; n=250, 40-65 y; n=250, 66-100 y) from a longitudinal population-based study in the city of Malmö, stratified on both *APOE4* genotype and family history of AD. Further, 150 patients with SCD and 150 patients with MCI with evidence of an incipient neurodegenerative disease (including prodromal AD) will be included, as well and 150 patients with SCD/MCI without evidence of ongoing neurodegenerative disease. Finally, we are recruiting demented cases with early and late-onset AD (n=175), FTD/PPA/PSP/CBS (n=140), VaD (n=50), PD/PDD/DLB (n=150).

We will present initial finding when it comes the initial Tau and Amyloid PET imaging results using the new digital GE Discovery MI scanners. Results obtained in different diagnostic groups will be presented.

Keywords: Neurodegenerative diseases, PET, MR, biomarkers, cohort

P133: PiB PET as a biomarker for white matter integrity in aging and dementia

Yi Su[1,4], Qing Wang[1,4], Shaney Flores[1], Yong Wang[2,4], Ances Beau[3,4], John Morris[3,4], Tammie Benzinger[1,4]

[1]Department of Radiology, Washington University School of Medicine, St. Louis, MO, US
[2]Department of Obstetrics and Gynecology, Washington University School of Medicine, St. Louis, MO, US
[3]Department of Neurology, Washington University School of Medicine, St. Louis, MO, US
[4]Knight Alzheimer's Disease Research Center, Washington University School of Medicine, St. Louis, MO, US

Background: White matter (WM) damage is common in aging populations and patients with Alzheimer disease (AD). WM damage is directly associated with cognitive dysfunction and is an important factor in the complex etiology of AD. Currently, magnetic resonance (MR) imaging is the main technique for the in vivo assessment of WM damage, while emerging research suggests amyloid PET tracers may bind to myelin and serve as a sensitive imaging biomarker of WM integrity.

Methods: In this study, we quantify WM uptake of the [^{11}C]-Pittsburgh compound B (PiB) in a memory and aging study cohort with 591 cross-sectional and 253 longitudinal PiB scans to examine its longitudinal changes and relationship with other biomarkers. A mean cortical standard uptake value ratio with regional spread function based partial volume correction (MCSUVRRSF) is used to measure amyloid burden. WM PiB uptake is assessed distribution volume ratio (DVR), and an R1 index is estimated to quantify regional perfusion. WM hypointensity (WMH) volume was defined based on MR. Paired *t*-test was used to assess longitudinal changes of biomarkers. Partial correlation analysis was also performed to control for interdependencies among various biomarkers.

Results: A significant longitudinal decrease ($p<0.01$) in WM PiB uptake can be observed for the entire cohort as well as for the normal control (NC, CDR=0) group and symptomatic AD group (amyloid+ and CDR>0). Partial correlation analysis revealed that WM PiB uptake is independently associated with age ($p<0.01$), amyloid burden ($p<0.05$), relative perfusion ($p<0.0001$), and WMH volume ($p<0.0001$).

Conclusion: Our data provide compelling evidence that amyloid PET imaging may serve as a sensitive WM integrity marker for the investigation of AD progression and disease monitoring. This finding also indicates that WM is unsuitable for use as a reference region in the quantification of brain amyloid burden in either cross-sectional or longitudinal study.

Figure 1. Summary of study cohorts

Cohort		N	Age (SD)	N_Male (%)	APOE4+ (%)	MMSE (SD)	Interval years (SD)
Cross-sectional		591	67.7 (10.0)	246 (41.6)	222 (37.6)	28.6 (2.0)	--
	Normal Control	398	64.8 (9.8)	141 (35.4)	104 (26.1)	29.2 (1.1)	--
	Preclinical	101	72.6 (7.0)	48 (47.5)	63 (62.3)	29.0 (1.3)	--
	A+CDR+	64	76.6 (7.4)	39 (60.1)	44 (68.8)	25.2 (3.4)	--
	A-CDR+	28	71.3 (8.3)	18 (64.3)	11 (39.3)	28.0 (1.7)	--
Longitudinal		253	65.8 (9.4)	90 (35.6)	85 (33.6)	29.1 (1.3)	3.2 (1.5)
	Normal Control	185	64.2 (9.6)	60 (32.4)	48 (25.9)	29.2 (1.0)	3.2 (1.5)
	Preclinical	41	69.6 (6.4)	15 (36.6)	26 (63.4)	29.2 (0.9)	2.9 (1.3)
	A+CDR+	18	73.6 (6.6)	13 (72.2)	9 (50.0)	27.3 (2.9)	2.5 (1.0)
	A-CDR+	9	67.2 (11.0)	2 (22.2)	2 (22.2)	29.3 (1.3)	4.0 (1.6)

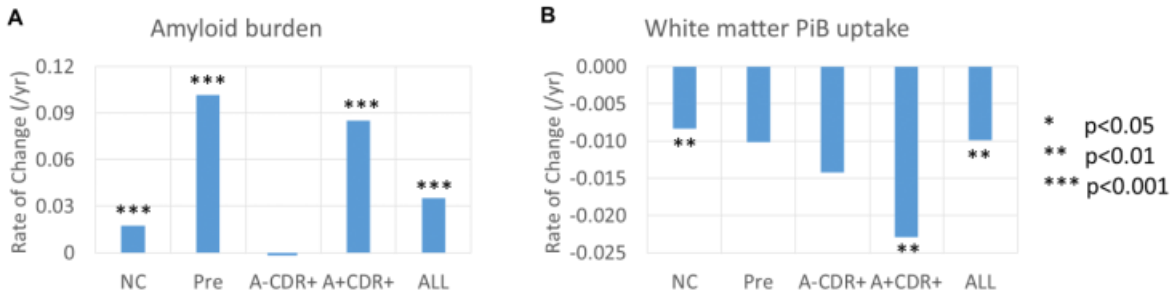

Figure 2. The rate of biomarker longitudinal changes. NC: normal control; Pre: preclinical AD; A-CDR+: cognitively impaired while amyloid negative; A+CDR+: symptomatic AD; ALL: the entire cohort.

	e4	Gender	Age	MCSUVRRSF	DVRUWMRSF	R1UWMRSF	WMHV	mmse
e4				7.90E-18	2.15E-01	5.21E-01	5.06E-01	6.85E-01
Gender				3.70E-01	9.91E-01	3.09E-01	9.45E-02	9.47E-02
Age				4.22E-13	3.68E-03	3.24E-06	2.49E-13	9.98E-02
MCSUVRRSF	7.90E-18	3.70E-01	4.22E-13	1.00E+00	1.19E-02	5.32E-01	5.27E-01	8.51E-19
DVRUWMRSF	2.15E-01	9.91E-01	3.68E-03	1.19E-02	1.00E+00	3.24E-05	3.48E-18	5.25E-01
R1UWMRSF	5.21E-01	3.09E-01	3.24E-06	5.32E-01	3.24E-05	1.00E+00	3.00E-07	4.16E-01
WMHV	5.06E-01	9.45E-02	2.49E-13	5.27E-01	3.48E-18	3.00E-07	1.00E+00	9.78E-05
mmse	6.85E-01	9.47E-02	9.98E-02	8.51E-19	5.25E-01	4.16E-01	9.78E-05	1.00E+00

p<0.001

0.001<p<0.05

p>0.05

Figure 3. Partial correlation structure (p-values) among different biomarkers. E4: APOE e4 status; MCSUVRRSF: global amyloid burden measured as mean cortical standard uptake value ratio (SUVR) with regional spread function (RSF) based partial volume correction (PVC); DVRUWMRSF: deep white matter PiB uptake measured as distribution volume ratio (DVR) with RSF PVC; R1UWMRSF: relative perfusion of deep white matter region estimated using simplified reference tissue model (SRTM); WMHV: white matter T1-hypointensity volume; mmse: mini-mental-state exam score

Keywords: amyloid, PET, white matter, Alzheimer's disease, aging

P134: Effects of tau and amyloid deposition on domain-specific memory function in old age

Anne Maass[1,2], David Berron[2,3], Theresa Harrison[1], Suzanne Baker[4], Taylor Mellinger[1], Kaitlin Swinnerton[1], Rachel Bell[1], Emrah Duezel[2,3], William Jagust[1,4]

[1]*University of California, Berkeley, Berkeley, CA, US*
[2]*German Center for Neurodegenerative Diseases (DZNE), Magdeburg, Germany*
[3]*Institute of Cognitive Neurology and Dementia Research, Magdeburg, Germany*
[4]*Lawrence Berkeley National Lab, Berkeley, CA, US*

Objectives: Processing of spatial and object information relies on posterior-medial and anterior-temporal systems, respectively. This suggests that tau accumulation in the temporal lobe might affect domain-specific memory function differentially. We tested how in vivo measures of tau and Aβ relate to object vs. scene memory function in cognitively normal older adults (OA).

Methods: Forty-seven OA (78±6yrs) and 20 young adults (YA; 26±4yrs) performed a continuous recognition memory task that poses high demands on memory precision and dissociates object vs. scene memory (Fig.1). Subjects discriminated between repeated images and novel but similar images. Domain-specificity was assessed as the difference in corrected hit rates between objects and scenes. High-resolution fMRI data was acquired at 3T while subjects performed the task (1.5mm^3 isotropic resolution, whole brain; Fig.2). In OA, global cortical Aβ burden was measured with [^{11}C]PiB PET (23 PIB$^-$, 24 PIB$^+$) and tau accumulation with [^{18}F]AV-1451 PET. AV-1451 SUVRs (80-100min post-injection, inferior cerebellar gray reference) were derived in native-space after partial volume correction using FreeSurfer-defined regions. Effects of age, Aβ and tau measures in Braak composite regions on domain-specific memory were tested by means of ANOVAs (group x domain) and correlational analyses (Fig.3).

Results: OA performed worse than YA ($p<.001$) across both domains (n.s. group x domain interaction; $p>.80$). Scenes were more difficult than objects across groups ($p<.01$). There was no relationship between Aβ and domain-specific memory performance. However, higher AV-1451 SUVRs in Braak I/II ($r=0.33$, $p=.03$) and III/IV ($r=0.27$, $p=.06$) regions were related to relatively worse object than scene memory.

Conclusions: Our data suggest that OA with tau accumulation in the temporal lobe show a tendency towards worse object recognition memory relative to scenes. While our data did not reveal evidence for a specific effect of Aβ on scene memory performance, this could be present in later stages of AD.

Fig. 1 Continuous domain-specific recognition memory task

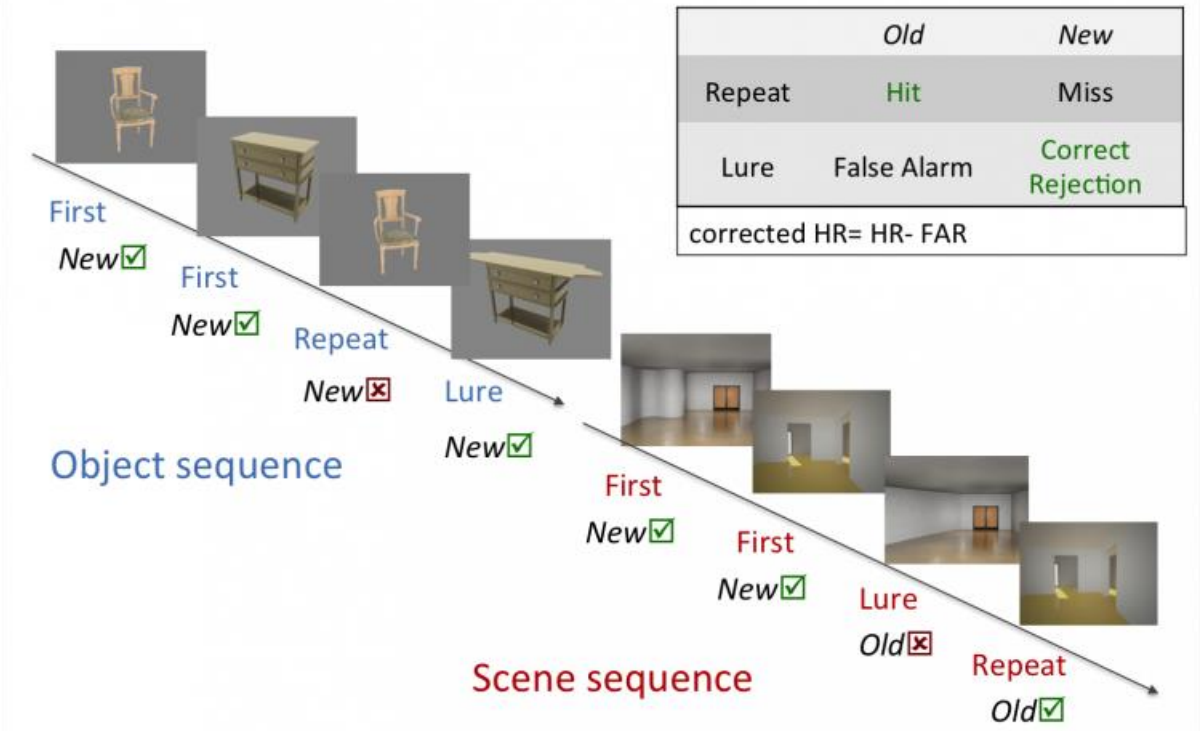

Figure adapted from Berron et al. (in revision)

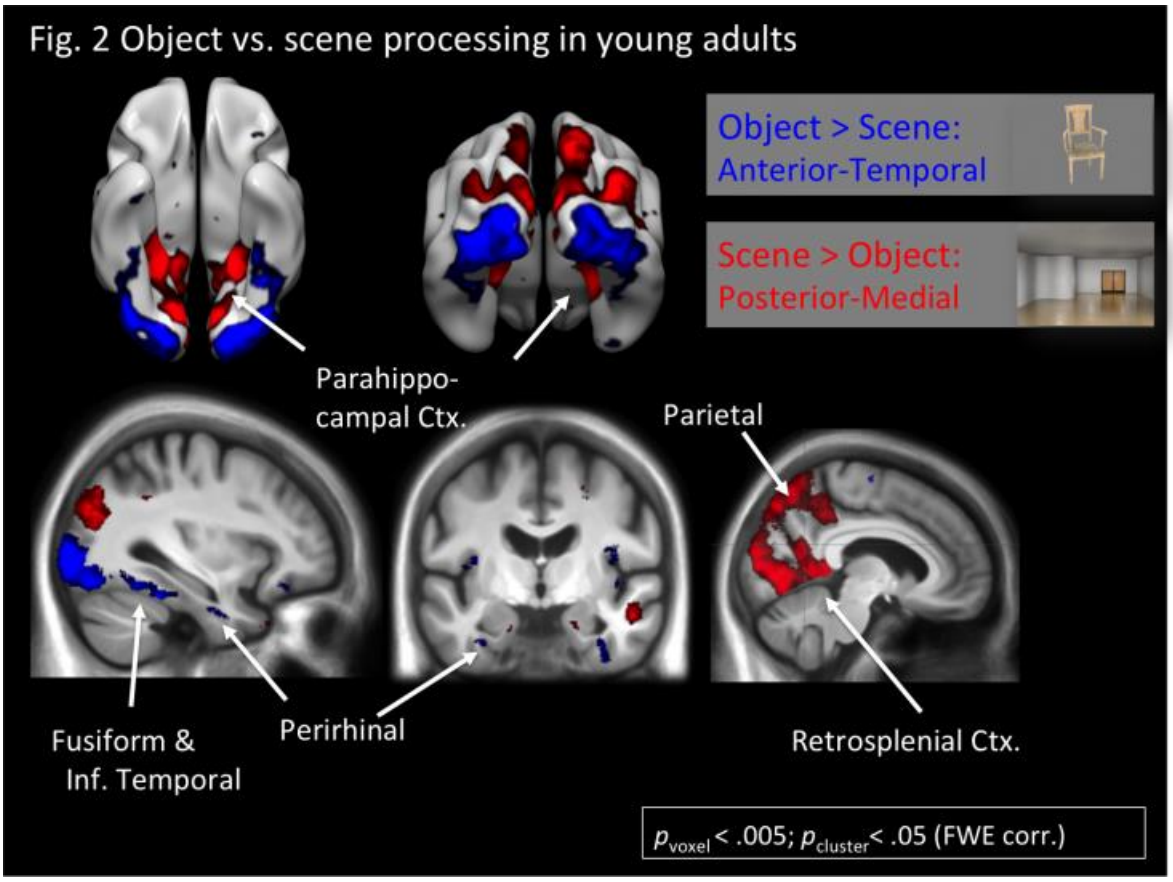

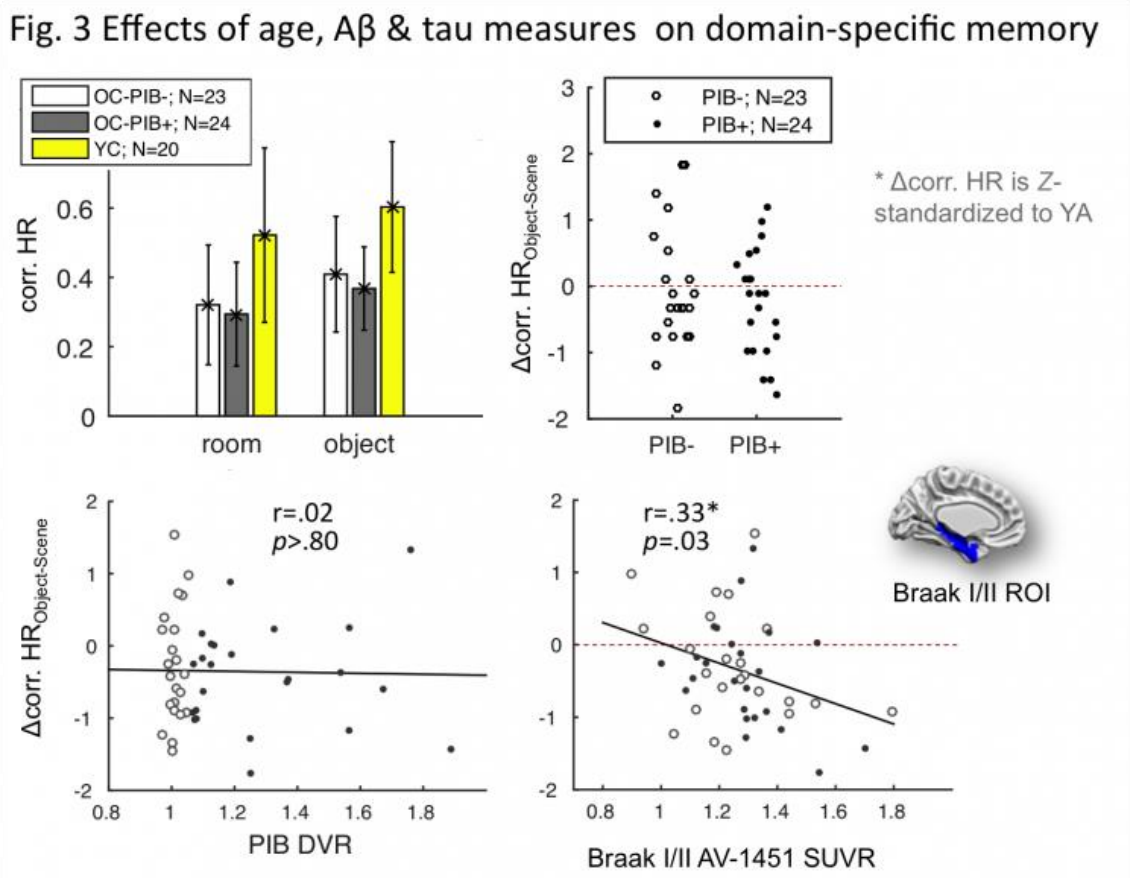

Keywords: AV-1451, memory, object, scene, temporal tau

P135: Effects of amyloid, tau, and hippocampal volume on normal and fast gait speeds in cognitively normal older adults: results from the Harvard Aging Brain study

Dylan Kirn[1], Rachel Buckley[1,3,4,5], Bernard Hanseeuw[1], Hannah Klein[1], Michael Properzi[1], Reisa Sperling[1,2,3], Keith Johnson[1,2,3]

[1]*Department of Neurology, Massachusetts General Hospital, Boston, MA, US*
[2]*Department of Neurology, Brigham and Women's Hospital, Boston, MA, US*
[3]*Harvard Medical School, Boston, MA, US*
[4]*Florey Institutes of Neuroscience and Mental Health, Melbourne, Australia*
[5]*Melbourne School of Psychological Science, University of Melbourne, Melbourne, Australia*

Background: Evidence from post-mortem studies suggest that AD pathology may influence physical functioning. Fast gait speed (fGS) has rarely been used as an outcome measure in relation to AD biomarkers, although it may serve as a more sensitive measure of physical-functioning in a clinically-asymptomatic cohort. This study examines the relationships between AD biomarkers (ß-amyloid(Aß), hippocampal volume(HV), and inferiortemporal/entorhinal tau(IT/EC, respectively)) and both normal(nGS) and fGS.

Methods: 76 older adults(78.4±5.9yrs) underwent PiB-PET, structural MRI, and Tau-PET(n=57) imaging. Global Aß burden was represented by a summary distribution volume ratio(DVR). HV was measured bilaterally and adjusted for intracranial volume. IT/EC were measured using 18F-Flortaucipir. nGS(normal pace) and fGS(walk as quickly as possible) were measured using a straight 7-meter course. Correlations were used to examine unadjusted relationships between our nGS/fGS and AD biomarkers. Linear regression analyses were run to determine whether nGS and fGS were associated with AD biomarkers, accounting for age and gender.

Results: Aß and IT/EC tau were not associated with nGS or fGS. These results were unchanged when controlling for age and gender in linear regression models. Significant associations were observed with HV and nGS(R_{76}=0.23,p=0.04) and fGS(R_{76}=0.32,p=0.004). The association with HV and nGS was no longer significant when controlling for age and gender(ß=0.15,p=0.28), and fGS reduced to trend-level(ß=0.23,p=0.09). A *post-hoc* analysis revealed the interaction of HV and Aß status predicts fGS at trend-level(ß=1.52,p=0.07),but not nGS.

Conclusion: These preliminary analyses did not reveal a cross-sectional association between gait and Aß or IT/EC Tau. Our results suggest a relationship with HV, which we found to be slightly stronger with fGS. When adding the interaction of HV and Aß status to our model, a trend-level association existed for fGS, suggesting that the relationship between fGS and HV may be strengthened by elevated amyloid. These analyses are preliminary, and a larger sample is required to investigate these relationships further.

Figure 1: Normal Gait Speed and HV by Aß Status

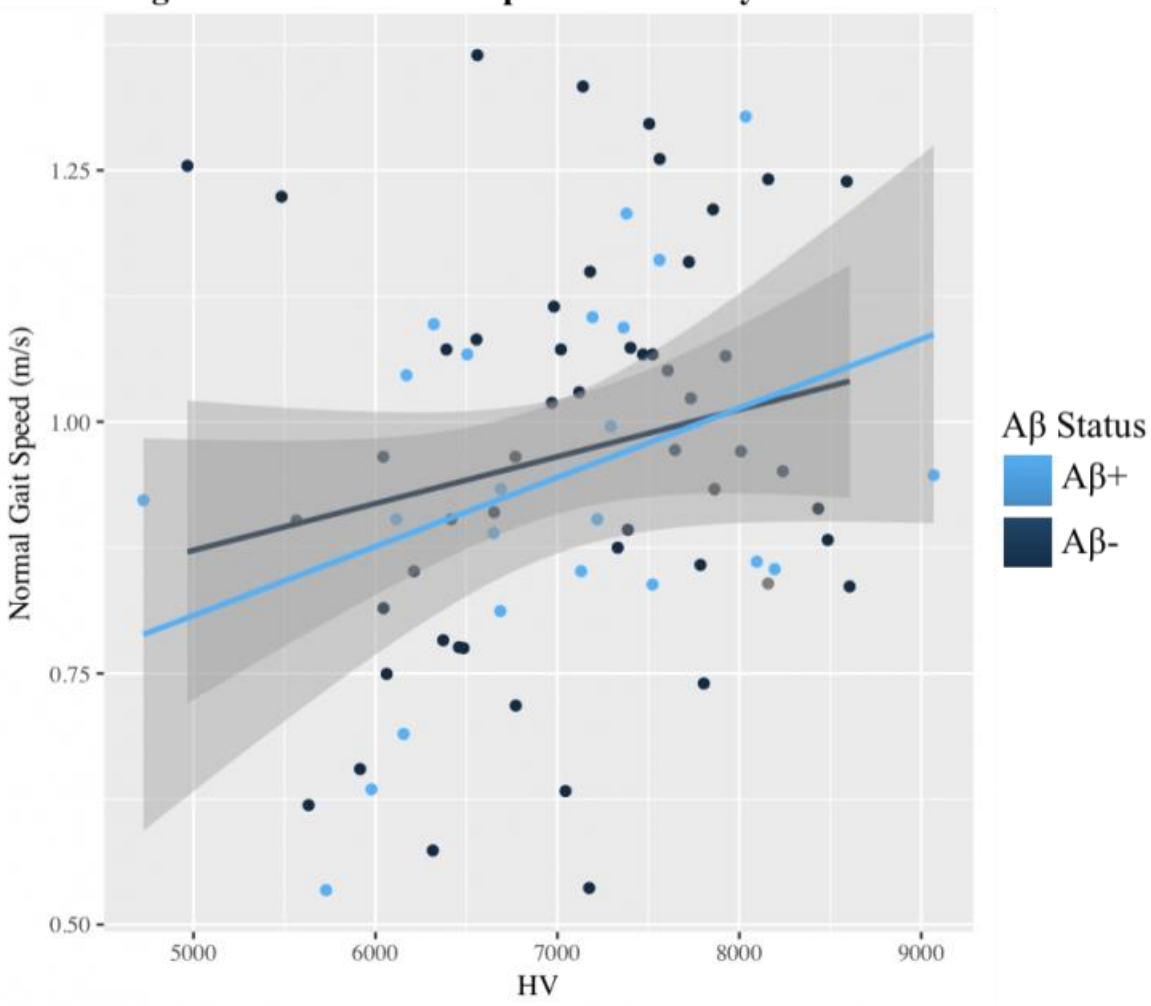

Figure 2: Fast Gait Speed and HV by Aß Status

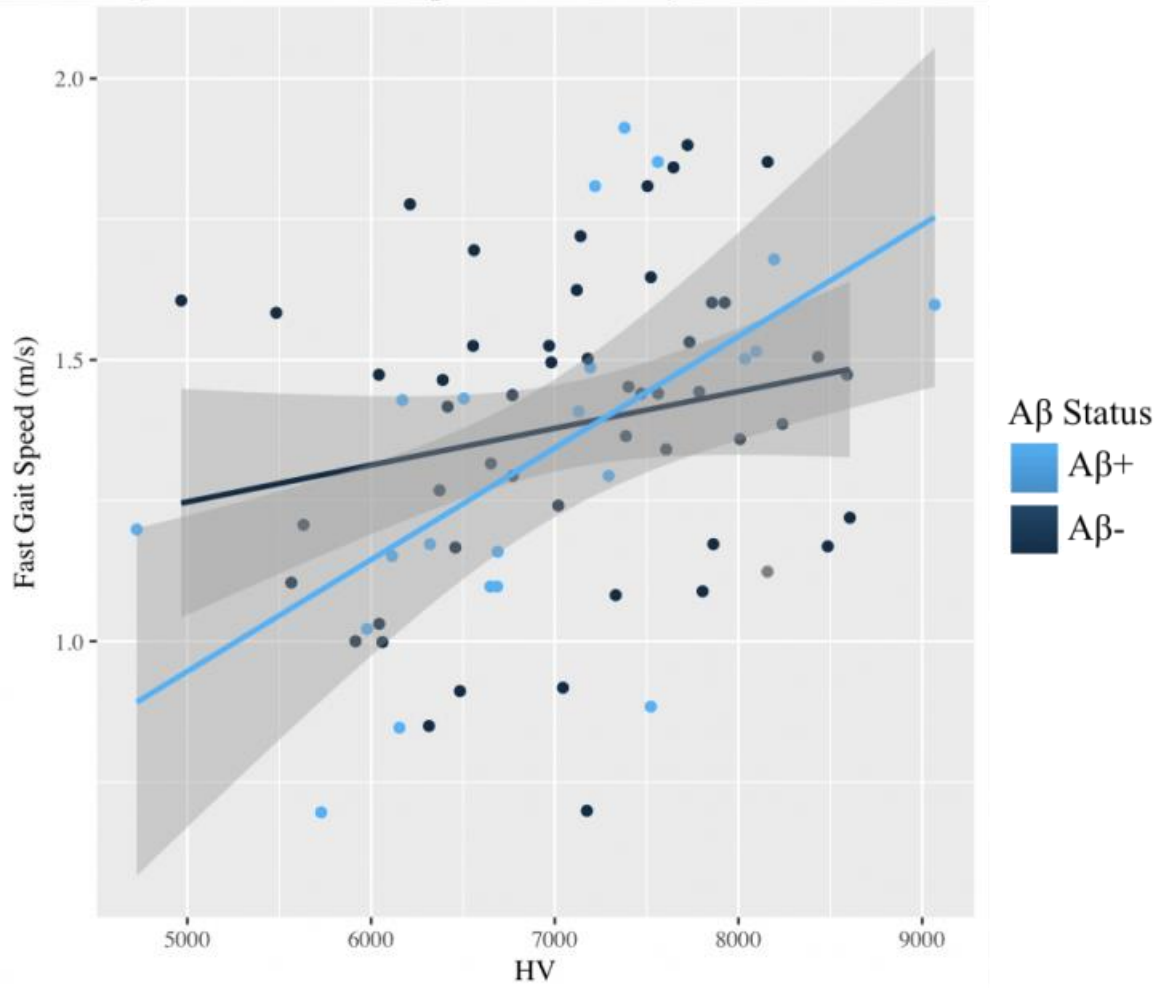

Keywords: gait speed, amyloid, tau, hippocampal volume

P136: [18F]-THK5351 binding patterns are associated with language deficits in primary progressive aphasia

Silvy Gabel[1,2], Jolien Schaeverbeke[1,2], Karen Meersmans[1], Rose Bruffaerts[1,4], Karen Van Bouwel[4], Eva Dries[4], Ronald Peeters[5], Koen Van Laere[3,6], Patrick Dupont[1], Rik Vandenberghe[1,3,5]

[1]*Laboratory for Cognitive Neurology, KU Leuven, Leuven, Belgium*
[2]*Alzheimer Research Centre, KU Leuven, Leuven, Belgium*
[3]*Leuven Institute of Neuroscience and Disease, Leuven, Belgium*
[4]*Neurology Department, UZ Leuven, Leuven, Belgium*
[5]*Radiology Department, UZ Leuven, Leuven, Belgium*
[6]*Nuclear Medicine and Molecular Imaging, Leuven, Belgium*

Neurolinguistic tests of repetition of vowels, consonant-vowel combinations, simple and complex words and sentences of increasing length are core components in subtyping primary progressive aphasia (PPA) patients with the nonfluent (NFV) and with the logopenic variant (LV). PPA-NFV patients, in whom predominantly premotor and inferior frontal cortex are affected, are more impaired on phoneme repetition than PPA-LV. Inversely, PPA-LV patients, in whom predominantly left temporoparietal cortex is affected, are more impaired on sentence repetition. We examined to which degree repetition scores for these materials correlate with [^{18}F]-THK5351 binding distribution in comparison to volumetric changes.

Twelve PPA-NFV and three PPA-LV patients received neuropsychological testing, a static [^{18}F]-THK5351-PET scan (acquisition-window: 50-80 min *post*-injection) and T1-weighted structural MRI (used for voxel-based morphometry). Standardized Uptake Value Ratio (SUVR) images were calculated with cerebellar gray matter as reference and partial-volume corrected (PVC) (Muller-Gartner, 1992). We administered five Aachener Aphasia (AAT) repetition subtests, including phoneme, single word, cognate word, compound word and sentence repetition. Voxelwise linear regressions were performed between PVC [^{18}F]-THK5351 SUVR as dependent variable and AAT subtest scores as independent variable, corrected for age and gender at significance threshold of voxel-level uncorrected $p<0.001$ and Bonferroni-corrected for the number of tests (n=5). Across the entire group, lower scores on phoneme repetition correlated with elevated [^{18}F]-THK5351 binding in left premotor cortex. Lower scores on compound word and sentence repetition correlated with [^{18}F]-THK5351 binding in temporoparietal regions, including inferior temporal gyrus, angular gyrus, superior temporal gyrus and inferior parietal gyrus. No significant correlations were obtained for single and cognate word repetition. No correlations were found between repetition subtests and atrophy.

The anatomical distribution of the correlations is in agreement with the preferential involvement of premotor and temporoparietal cortex in phoneme and sentence repetition, respectively. [^{18}F]-THK5351 binding is more sensitive for detecting these correlations with language scores than brain volumetry.

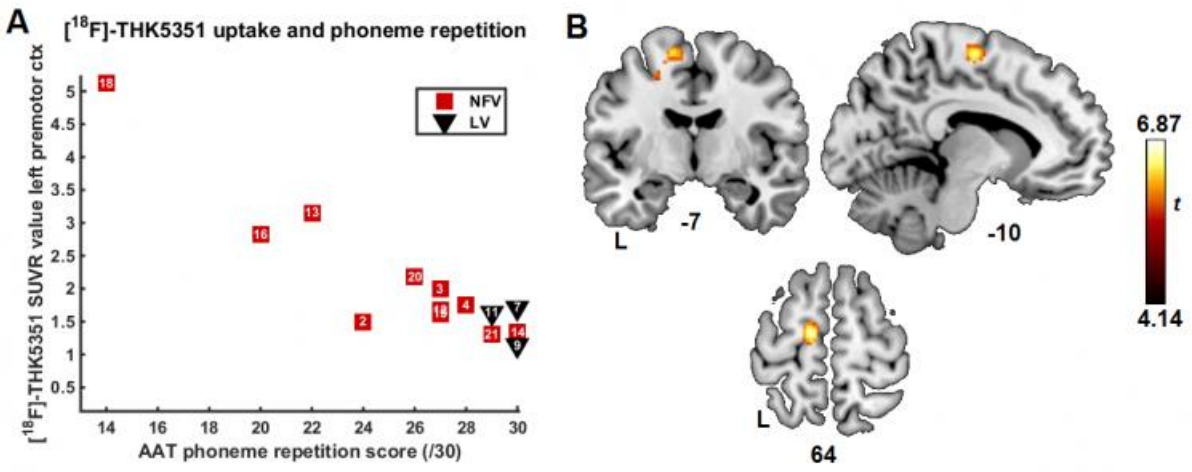

Keywords: primary progressive aphasia, [18F]-THK5351, language deficits, atrophy

P137: Personality traits and neuropsychiatric factors are related to increased amyloid deposition in cognitively normal older adults

Alexa Pichet Binette[1,2], Etienne Vachon-Presseau[3], Julie Gonneaud[1,2], Natalie Marchant[4], Pierre Bellec[5], John Breitner[1,2], Sylvia Villeneuve[1,2], PREVENT-AD Research Group[2]

[1]*Department of Psychiatry, McGill University, Montreal, QC, Canada*
[2]*Douglas Mental Health Research Institute, Montreal, QC, Canada*
[3]*Department of Physiology, Northwestern University, Chicago, IL, US*
[4]*Department of Psychiatry, University College London, London, United Kingdom*
[5]*Department of Computer Science and Operations Research, Université de Montréal, Montreal, QC, Canada*

Introduction: Neuropsychiatric factors (NPF), such as anxiety, depression and apathy, are highly prevalent in older adults and are associated with an increased risk of Alzheimer's disease (AD). Recent evidence has also linked personality traits, such as neuroticism, with progression to AD. The effects of such factors on AD biomarkers, however, still need to be better understood, especially in the preclinical phase of the disease. In cognitively normal older adults with a family history of sporadic AD, we investigated whether combined personality traits and NPF are related to AD pathology (amyloid [Aβ] and tau deposition) and brain function.

Methods: Fifty-six subjects (PREVENT-AD study, mean age=67±5) answered questionnaires assessing personality, depression, anxiety, stress, apathy, perseverative thinking, and had Aβ ([^{18}F]NAV4694) and tau ([^{18}F]AV1451) PET scans. SUVR were calculated bilaterally from 33 FreeSurfer Desikan cortical regions. We used a multivariate approach (partial least squares correlation with permutation tests) to assess which, if any, combination of factors are related to Aβ and tau deposition separately in the cortical regions. Then, we investigated whether this combination of factors was related to within-network functional connectivity in subjects with high and low levels of pathology.

Results: A latent variable (LV) with high loadings on anxiety, perseverative thinking, neuroticism and low extraversion was related to a higher Aβ burden, predominantly in the AD signature regions ($p=0.03$, Fig. 1). Higher scores on this LV were further related to higher connectivity in the dorsal attention and frontoparietal networks in Aβ+ subjects when compared to Aβ- subjects ($p_{Aβ\ status*Connectivity}=0.002$ and 0.03 respectively, Fig. 2). We did not find similar results with tau.

Conclusions: Our multivariate approach revealed that Aβ burden was increased in cognitively normal individuals at risk of AD with high neuroticism, low extraversion and negative NPF scores, which were in turn related to altered brain connectivity.

Figure 1

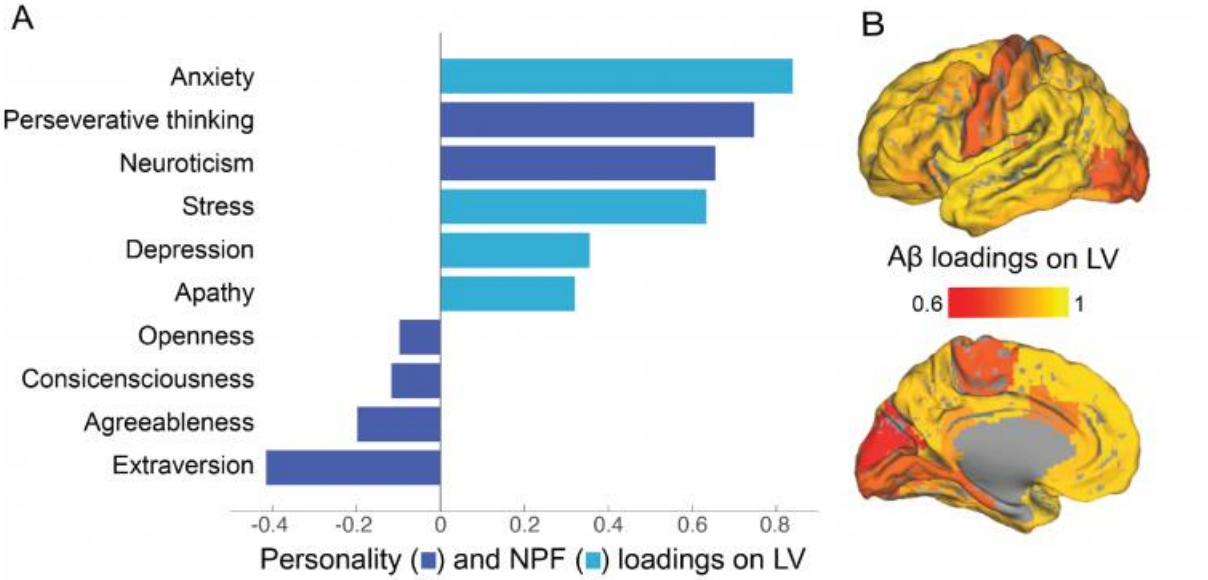

1A. Loadings from personality traits and neuropsychiatric factors (NPF) of the significant latent variable (LV). 1B. Loadings of Aβ SUVR in the different cortical regions from LV. Overall, having higher scores on NPF, neuroticism and lower score on extraversion is associated with more Aβ burden throughout the cortex.

Figure 2

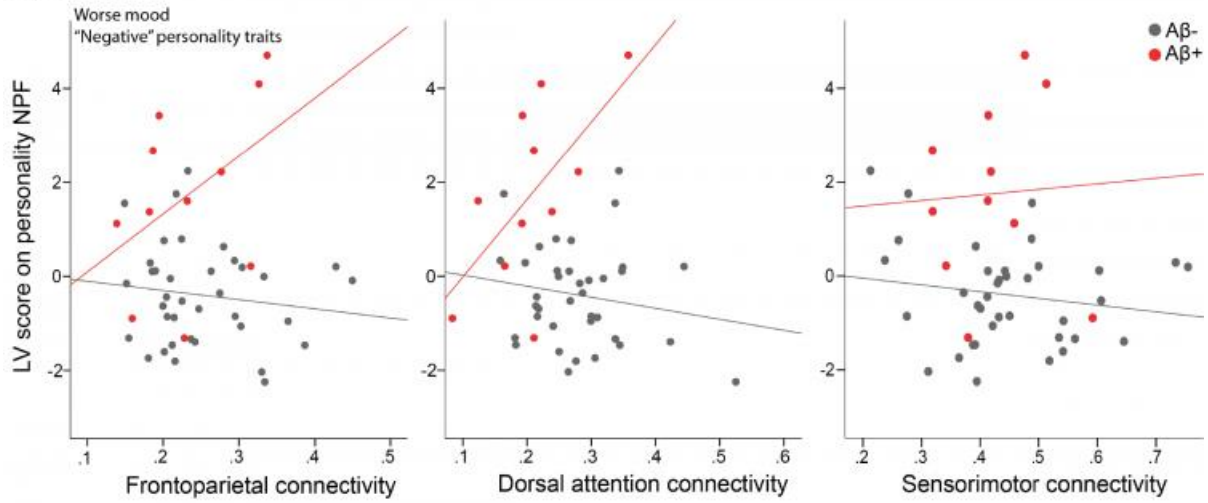

Aβ status * functional connectivity interaction suggesting that in Aβ+ cognitively normal individuals, more neuroticism, less extraversion and higher NPF (=higher score on latent variable, LV) is related with higher connectivity in associative networks when compared to Aβ- subjects.

Keywords: personality traits, amyloid, neuropsychiatric factors, functional connectivity

P138: Tau deposition in relation to verbal and phonemic fluency in the Framingham Heart Study

Evelyn Luner[1], Heidi Jacobs[1], Kathryn Papp[1,2], Alex Becker[1], Alexa Beiser[3], Dan Daniluk[3], Jayandra Himali[3,4], David Jin[1], Samantha Katz[1], Ron Killiany[7], Kirsten Moody[1], Matthew Pase[3,5], Bryanne Peets[3], Mekala Raman[9], Justin Sanchez[3], Claudia Satizabal[3,4], Colin Schafer[3], Sudha Seshadri[1,2], Keith Johnson[1,2]

[1]Departments of Neurology, Radiology, and the Athinoula A. Martinos Center for Biomedical Imaging, Massachusetts General Hospital, Harvard Medical School, Boston, MA, US
[2]Center for Alzheimer's Research and Treatment, Department of Neurology, Brigham and Women's Hospital, Harvard Medical School, Boston, MA, US
[3]The Framingham Heart Study, Framingham, MA, US
[4]Department of Neurology, Boston University School of Medicine, Boston, MA, US
[5]Centre for Human Psychopharmacology, Swinburne University of Technology, Hawthorn, Australia
[6]Department for Biostatistics, Boston University School of Public Health, Boston, MA, US
[7]Center for Biomedical Imaging, Boston University School of Medicine, Boston, MA, US
[8]University of California at Davis, Sacramento, CA, US
[9]Section of Preventive Medicine, Department of Medicine, Boston University School of Medicine, Boston, MA, US

Objective: Tau deposition is commonly observed at autopsy by age 50 years, however, the association of tau PET with cognitive function in this age group has not been reported. To explore this issue, we acquired tau and amyloid PET in a group of Framingham Heart Study (FHS) participants with a median age of 55 years.

Methods: A total of 86 clinically normal participants in the FHS, 32 F and 54 M (Age range: 39-72 years, SD: 7.11, Table 1), underwent 11C-PiB amyloid and 18F-Flortaucipir (FTP) tau PET imaging at the Massachusetts General Hospital. FTP PET measures (SUVR, cerebellar reference) were evaluated with linear regression models co-varying age, sex, and education, predicting test scores for phonemic fluency (FAS), category fluency (CAT), memory (SRT-total), and mental status (MMSE). SUVRs, corrected for partial volume effect, were sampled in seven cortical and subcortical regions of interest: entorhinal, fusiform, inferior temporal, parahippocampal, posterior cingulate, amygdala, and hippocampus (adjusted for choroid plexus). Additionally, interactions between tau and sex on cognition were investigated.

Results: Lower performance on FAS and CAT was associated with FTP SUVR in amygdala and fusiform ($p<0.05$, Fig. 1), with marginal associations for FAS in inferior temporal and entorhinal ($p< 0.08$) and for CAT in the inferior temporal and hippocampus ($p<0.1$). After multiple comparison correction, the associations remained at trend level ($p = 0.07 - 0.11$). There was a significant interaction with sex, so that for a given amount of tau in the inferior temporal cortex, women performed better than men on the SRT-total ($p<.01$, Fig. 2), similar marginal associations were observed in the fusiform ($p<0.06$).

Conclusions: Tau deposition was associated with reduced phonemic and category fluency in several brain regions in this sample. In this younger cohort, sex was an important moderator of the association between tau and memory.

Table 1: Demographic, PET and Cognitive Variables. Mean ± SD (Range)

	All	Female	Male
Total N (%)	86	32 (37)	54 (63)
AGE	54.9 ± 7.1 (39.0-72)	55.6 ± 6.7 (40.3-71)	54.6 ± 7.3 (39.0-72)
YRS EDUCATION	15.2 ± 2.3 (12-22)	15.7 ± 2.0 (12-19)	15.0 ± 2.5 (12-22)
	TAU SUVR (PVC)		
AMYGDALA	1.23 ± 0.18 (0.80-1.73)	1.17 ± 0.15 (.89-1.42)	1.26 ± 0.19 (0.80-1.73)
ENTORHINAL	1.15 ± 0.22 (0.65-2.08)	1.09 ± 0.17 (.69-1.03)	1.18 ± 0.24 (0.65-2.08)
FUSIFORM	1.26 ± 0.12 (0.97-1.59)	1.23 ± 0.09 (1.02-1.40)	1.27 ± 0.13 (0.97-1.59)
HIPPOCAMPUS (residual)	1.03 ± 0.13 (0.73-1.45)	1.00 ± 0.12 (0.74-1.26)	1.04 ± 0.14 (0.73-1.45)
INFERIOTEMPORAL	1.28 ± 0.15 (0.84-1.95)	1.25 ± 0.11 (1.04-1.53)	1.30 ± 0.17 (0.84-1.95)
PARAHIPPOCAMPAL	1.03 ± 0.14 (0.66-1.42)	0.97 ± 0.11 (0.66-1.23)	1.06 ± 0.14 (0.67-1.42)
POSTERIOR CINGULATE	1.09 ± 0.11 (0.78-1.36)	1.06 ± 0.09 (0.86-1.24)	1.10 ± 0.12 (0.78-1.36)
	AMYLOID DVR (PVC)		
GLOBAL NEOCORTICAL	1.05 ± 0.08 (0.90-1.38)	1.07 ± 0.08 (0.99-1.32)	1.04 ± 0.07 (0.90-1.38)
	NP TEST SCORES		
MMSE	29.3 ± 1.0 (26-30)	29.4 ± 1.0 (26-30)	29.2 ± 1.0 (26-30)
SRT TR	46.1 ± 8.7 (26-62)	50.3 ± 6.5 (36-62)	43.6 ± 8.9 (26-62)
FAS	40.7 ± 11.9 (17-68)	41.8 ± 11.3 (17-62)	40.0 ± 12.4 (19-68)
CAT	45.5 ± 9.7 (23-72)	47.6 ± 8.5 (32-70)	44.3 ± 8.5 (23-72)

Figure 1: Increased FTP PVC SUVR in both hemispheres of the fusiform and amygdala regions correlates with decreased CAT and FAS performance among FHS subjects. These plots show uncorrected data, however, these correlations were still observed when correcting for age, sex, and years of education. PiB DVR is represented on a scale by the color of each point.

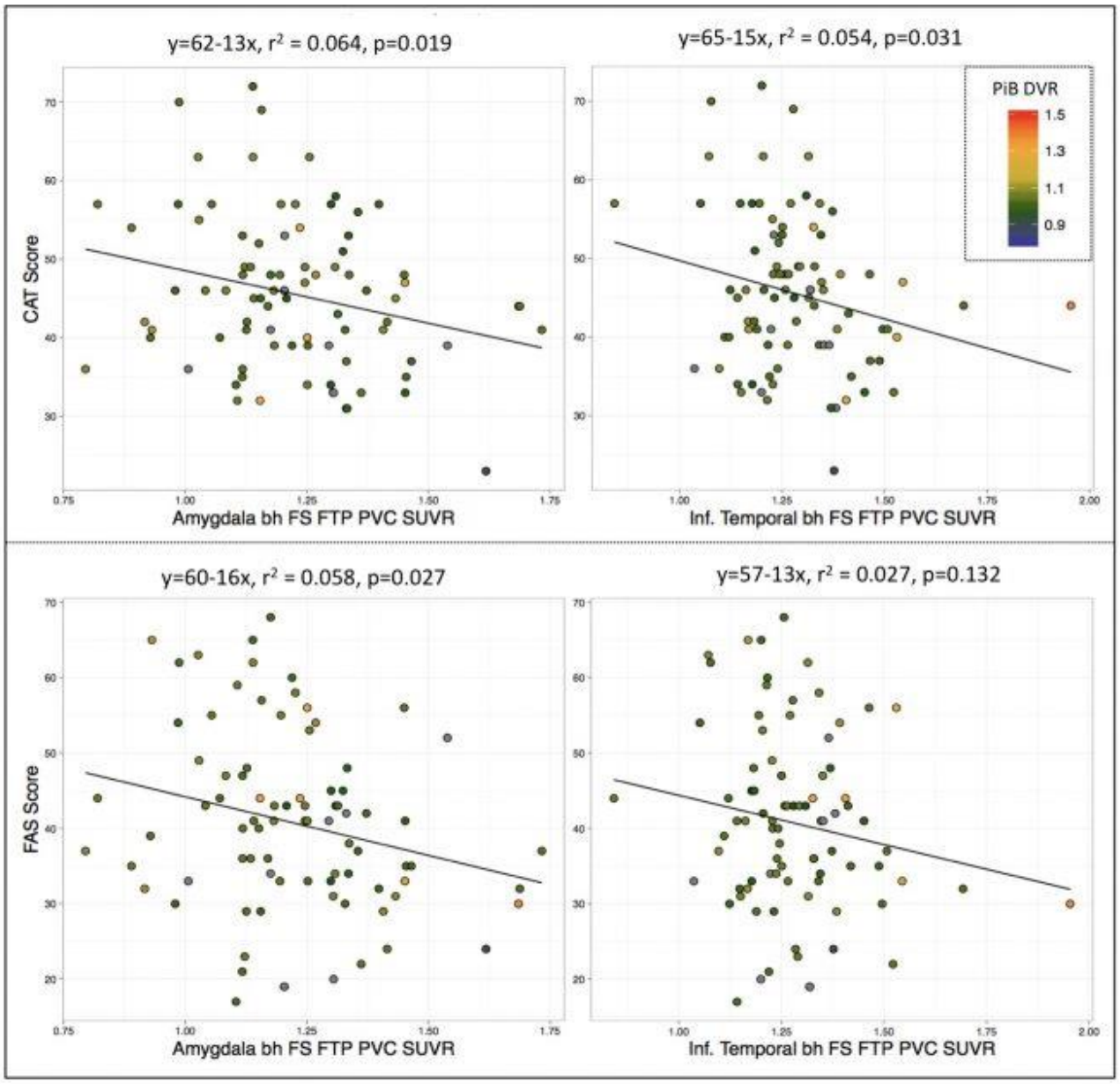

Figure 2: Interaction between sex and inferior temporal FTP SUVR in relation to SRT Total Recall performance (p<0.01). For a given amount of IT tau, females performed better on the SRT TR while males performed worse. Uncorrected data. PiB DVR is represented on a scale by the color of each point. Separate male and female correlations are represented by the color line.

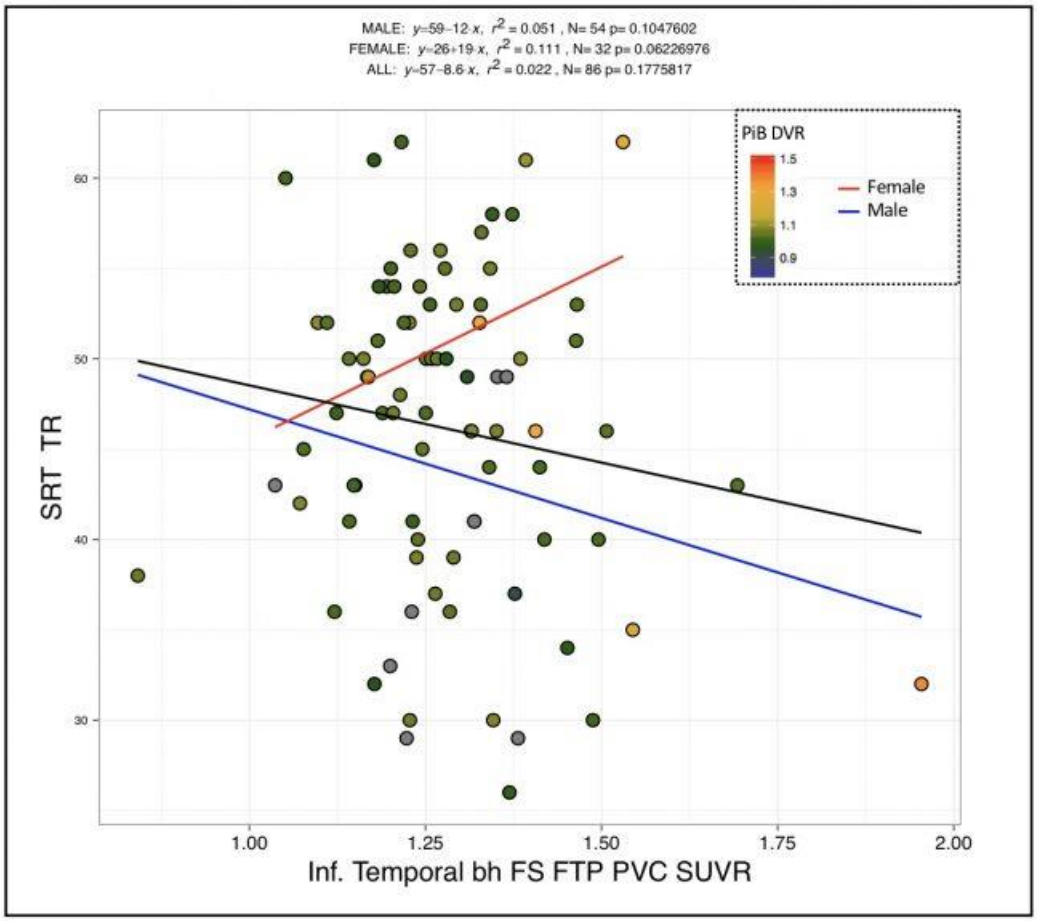

Keywords: Flortaucipir, cognition, clinically normal, PET, tau imaging

P139: Long-term clinical stability in amyloid-positive subjects is predicted by negative FDG-PET scan

Leonardo Iaccarino[1,2], Arianna Sala[1,2], Daniela Perani[1,2,3]

[1]*Vita-Salute San Raffaele University, Milan, Italy*
[2]*In vivo human molecular and structural neuroimaging Unit, Division of Neuroscience, IRCCS San Raffaele Scientific Institute, Milan, Italy*
[3]*Nuclear Medicine Unit, IRCCS San Raffaele Hospital, Milan, Italy*

The measure of brain amyloid burden by PET has fueled the design of prevention trials in Alzheimer's Disease (AD), enabling the screening of amyloid-positivity in mild cognitive impairment (MCI) subjects and even in healthy controls (HC) at risk for AD. However, incidental amyloidosis or brain amyloid deposition associated with non-AD conditions could lead to misclassification at baseline, with a subsequent pointless exposure to potentially harmful therapies' side effects.

We selected N=787 subjects (N=268HC, N=519MCI) from the ADNI database, all with Amyloid-PET and average follow-up of 45.65±22.03 months. Following the standard screening strategy of amyloid positivity for clinical trials, we first considered Amyloid-PET alone as the biomarker for AD pathology. We confirmed that amyloid positivity was associated with a significantly increased risk of clinical progression in both HC and MCI (log-rank tests, $p<0.001$), with a similar rate of conversion ($p=.371$). Crucially, however, a large amount of amyloid-positive participants (HC=55/83[66%]; MCI=175/291[60%]), remained clinically stable during the follow-up period.

In order to investigate whether FDG-PET brain metabolism, as biomarker of neurodegeneration, would have been able to identify stable cases at baseline, we selected the cases with an FDG-PET scan within 6-months from Amyloid-PET (N=73HC; N=259MCI) and used a validated voxel-wise FDG-PET method to assess individual brain metabolism. We found that a normal FDG-PET metabolic pattern strongly excluded clinical progression, with high negative predictive values (NPV) for both HC (NPV=0.83) and MCI (NPV=0.81) subjects. Further subject stratification by age additionally showed the highest NPVs in younger participants (NPVs=.91/.90 in HC and MCI, respectively).

Our results suggest that measures of neurodegeneration, such as FDG-PET brain metabolism, should be coupled to Amyloid-PET for a more robust screening in clinical trials. This seems to be particularly effective for trials including young subjects at pre-symptomatic or earliest clinical disease phases.

Keywords: amyloid-PET, FDG-PET, survival analysis, dementia, early diagnosis

P140: Associations between tau, Aβ and cortical thickness with cognition in Alzheimer's disease

Rik Ossenkoppele, Ruben Smith, Tomas Ohlsson, Niklas Mattsson, Olof Strandberg, Sebastian Palmqvist, Oskar Hansson

Lund University, Clinical Memory Research Unit, Malmö, Sweden

Objective: To examine the associations between tau, amyloid-β (Aβ) and cortical thickness on neuropsychological function across the preclinical and clinical spectrum of Alzheimer's disease (AD).

Methods: We included 106 participants (29 preclinical AD [Aβ-positive cognitively normal controls], 25 prodromal AD [Aβ-positive mild cognitive impairment] and 48 probable AD dementia) who underwent [^{18}F]AV1451 (tau) and [^{18}F]flutemetamol PET and structural MRI (cortical thickness) in the Swedish BioFINDER study (Table 1). Linear regression models adjusting for age, sex and education, were performed to assess associations between seven regions-of-interest and eight neuropsychological tests for each of the three imaging modalities.

Results: In preclinical AD, [^{18}F]AV1451 – but not [^{18}F]flutemetamol or cortical thickness – was associated with decreased global cognition, memory and processing speed ($p<0.05$, Table 2). In the combined prodromal AD and AD dementia group, both increased [^{18}F]AV1451 uptake and reduced cortical thickness were associated with worse performance on a variety of neuropsychological tests, while [^{18}F]flutemetamol was specifically associated with lower scores on a delayed memory task ($p<0.05$, Table 3). The strongest effects for both [^{18}F]AV1451 and cortical thickness on cognition were found in lateral and medial parietal cortex and in lateral temporal cortex.

Conclusions: Our findings suggest that [^{18}F]AV1451 PET is the most sensitive marker for detecting early changes in cognitive function and that temporoparietal [^{18}F]AV1451 PET and cortical thickness both have potential clinical utility in the prodromal and dementia stage of AD.

Table 1. Demographic and clinical characteristics according to diagnostic group

	Preclinical AD	Prodromal AD	AD dementia
N	33	25	48
Age	74.4±7.3	73.1±7.2	71.5±7.3
Sex (male/female)	13/20	16/9	26/22
Education (years)	11.8±3.8	12.7±3.5	12.5±3.8
Amyloid status (% positive)	100	100	100
CSF Aβ42	507±91	435±102	397±110
CSF t-tau	449±147	627±186	739±326
CSF p-tau	57±14	77±19	89±37
Global [^{18}F]AV1451 SUVr	1.07±0.07	1.29±0.28	1.52±0.37
Global [^{18}F]flutemetamol SUVr	0.82±0.14	0.96±0.08	1.02±0.15
Global cortical thickness	2.21±0.12	2.13±0.11	2.09±0.12
MMSE	29.1±1.1	25.6±2.8	21.4±4.9
ADAS Immediate recall	7.3±1.4	4.6±1.1	3.9±1.6
ADAS delayed recall	7.5±2.0	3.7±2.3	2.0±2.2
TMT-A	52.8±19.7	68.7±39.5	104.8±82.1
AQT-CS	65.5±15.5	89.1±34.1	102.9±34.9
SDMT	34.4±8.0	27.2±8.7	23.1±10.2
ADAS naming	11.2±1.9	10.8±1.9	9.9±2.8
Fluency – Animals (1 min)	20.8±5.7	13.9±4.8	11.0±5.7

Differences in baseline characteristics between groups were assessed using ANOVA with *post hoc* Bonferroni tests for continuous variables and X^2 and Kruskal-Wallis with *post hoc* Mann-Whitney U tests for dichotomous or categorical data.

Table 2. Associations between [^{18}F]AV1451, [^{18}F]flutemetamol and cortical thickness with cognition in preclinical AD

	MMSE	ADAS – Immediate recall	ADAS – Delayed recall	TMT-A	AQT-CS	SDMT	ADAS – Naming	Animal fluency
[^{18}F]AV1451 (n=33)								
Lateral parietal	-0.08	-0.51**	-0.39*	0.23	-0.08	0.04	-0.06	-0.22
Medial parietal	-0.19	-0.52**	-0.30	0.37*	0.09	-0.04	0.02	0.10
Lateral temporal	-0.23	-0.40*	0.26	0.35*	0.17	0.07	-0.05	-0.20
Medial temporal	-0.45*	-0.22	-0.16	0.28	0.29	0.03	0.04	-0.09
Frontal	-0.05	-0.36	-0.33	0.39*	-0.07	0.10	-0.13	-0.21
Occipital	-0.22	-0.28	-0.25	0.29	0.02	-0.02	-0.16	0.05
Whole brain	-0.15	-0.42*	-0.32	0.38*	0.03	0.07	-0.10	-0.16
[^{18}F]flutemetamol (n=30)								
Lateral parietal	-0.11	-0.14	0.04	0.01	0.25	-0.13	-0.12	-0.04
Medial parietal	-0.14	-0.15	0.06	-0.12	0.16	-0.08	-0.09	-0.07
Lateral temporal	-0.15	-0.12	0.08	0.01	0.28	-0.08	0.02	-0.08
Medial temporal	0.01	-0.19	0.07	0.06	0.32	-0.09	-0.07	-0.07
Frontal	-0.26	-0.13	0.01	-0.16	0.20	-0.04	-0.03	-0.04
Occipital	0.05	-0.13	0.13	0.12	0.32	0.03	-0.09	-0.14
Whole brain	-0.15	-0.14	0.06	-0.05	0.23	-0.06	-0.05	-0.06
Cortical thickness (n=33)								
Lateral parietal	0.26	0.21	0.03	0.00	-0.17	0.09	-0.25	0.02
Medial parietal	0.16	0.19	-0.08	-0.24	-0.32	0.11	-0.20	0.01
Lateral temporal	0.07	0.12	-0.03	-0.12	0.01	0.06	-0.31	-0.02
Medial temporal	-0.14	0.07	0.09	-0.07	0.22	-0.02	0.01	0.06
Frontal	0.15	0.15	-0.03	0.13	-0.01	0.10	0.26	0.08
Occipital	0.20	0.21	0.13	-0.18	-0.03	-0.09	-0.18	0.04
Whole brain	0.18	0.18	0.03	-0.06	-0.06	0.08	-0.25	0.02

Data presented are standardized β-coefficients derived from linear regression models, adjusting for age, sex and education: * p<0.05, ** p<0.01, *** p<0.001.

Table 3. Associations between [^{18}F]AV1451, [^{18}F]flutemetamol and cortical thickness with cognition in prodromal AD and AD dementia

	MMSE	ADAS – Immediate recall	ADAS – Delayed recall	TMT-A	AQT-CS	SDMT	ADAS – Naming	Animal fluency
[^{18}F]AV1451 (n=73)								
Lateral parietal	-0.32*	-0.12	-0.22	0.44**	0.36**	-0.65***	-0.20	-0.41**
Medial parietal	-0.28*	-0.26	-0.30*	0.37**	0.30*	-0.43**	-0.31*	-0.48**
Lateral temporal	-0.34*	-0.31*	-0.35**	0.28*	0.17	-0.38**	-0.38**	-0.45**
Medial temporal	-0.25*	-0.31*	-0.32*	0.01	-0.03	-0.13	-0.22	-0.25*
Frontal	-0.37**	-0.46**	-0.33*	0.05	0.06	-0.34*	-0.51***	-0.53***
Occipital	-0.20	-0.07	-0.27*	0.41**	0.27	-0.45***	0.05	-0.29*
Whole brain	-0.36*	-0.33*	-0.33*	0.30*	0.22	-0.51***	-0.36*	-0.50***
[^{18}F]flutemetamol (n=58)								
Lateral parietal	-0.21	-0.02	-0.33*	0.20	0.21	-0.21	-0.05	-0.02
Medial parietal	-0.15	-0.10	-0.35**	0.07	0.07	-0.11	-0.09	0.02
Lateral temporal	-0.24	-0.09	-0.37**	0.07	0.13	-0.07	-0.07	0.03
Medial temporal	-0.26	-0.03	-0.30*	0.01	0.00	0.06	-0.04	-0.01
Frontal	-0.23	-0.09	-0.29*	0.08	0.10	-0.13	-0.07	0.03
Occipital	-0.15	-0.05	-0.25	0.31*	0.30*	-0.28*	0.08	-0.08
Whole brain	-0.23	-0.08	-0.33*	0.13	0.16	-0.15	-0.05	0.01
Cortical thickness (n=73)								
Lateral parietal	0.31*	0.00	0.16	-0.31**	-0.43***	0.40**	0.00	0.24
Medial parietal	0.21	-0.08	0.06	-0.28*	-0.45***	0.27*	-0.02	0.16
Lateral temporal	0.32**	0.14	0.25*	-0.21	-0.32**	0.33**	0.25*	0.38**
Medial temporal	0.40**	0.28*	0.37**	-0.02	-0.20	0.32*	0.16	0.37**
Frontal	0.25*	0.15	0.07	0.01	-0.07	0.15	0.14	0.35**
Occipital	0.13	-0.16	0.13	-0.28*	-0.36**	0.37**	-0.10	0.06
Whole brain	0.32**	0.09	0.18	-0.18	-0.31**	0.35**	0.13	0.34**

Data presented are standardized β-coefficients derived from linear regression models, adjusting for age, sex and education: * p<0.05, ** p<0.01, *** p<0.001.

Keywords: Tau, Amyloid, Cortical thickness, Cognition, Alzheimer's disease

P141: Longitudinal relationships between brain amyloid deposition and glucose metabolism across the Alzheimer's disease spectrum

Alexandre Bejanin, Eider Arenaza-Urquijo, Robin De Flores, Clémence Tomadesso, Gaël Chételat

Inserm, Inserm UMR-S U1237, Université de Caen-Normandie, Caen, France

Objective: To assess the longitudinal change of glucose metabolism and amyloid deposition across the Alzheimer's disease (AD) spectrum and explore their relationships over time.

Methods: 103 participants (39 normal older adults, 15 patients with subjective cognitive decline [SCD], 35 with MCI and 14 with AD dementia) underwent 2-to-3 ^{18}F-FDG-PET and ^{18}F-AV45-PET scans. PET images were spatially normalized and scaled using the brain stem and the cerebral white matter respectively. For each subject, the mean SUVR of 106 brain regions defined in the Harvard–Oxford structural atlas was converted to Z-scores using a sample of 45 young healthy subjects. Mixed-effects models were performed i) to determine brain regions showing decreased metabolism and/or increased amyloid deposition over time in patients compared to normal older adults, and ii) to perform inter-modality analyses within each group and across all brain regions to test for a link between baseline ^{18}F-FDG and longitudinal ^{18}F-AV45 changes and reversely.

Results: Patients with AD showed decreased ^{18}F-FDG-SUVR over time in temporo-parietal and lateral frontal regions, and increased ^{18}F-AV45-SUVR in the putamen and frontal areas (Fig. 1-2). In MCI, decreased ^{18}F-FDG-SUVR predominated in lateral and medial temporal regions while ^{18}F-AV45-SUVR increased in most cortical regions. Patients with SCD showed decreased ^{18}F-FDG-SUVR in medial and lateral anterior temporal regions but no increased ^{18}F-AV45-SUVR compared to controls. Inter-modality analyses revealed that baseline ^{18}F-AV45 was associated with increased metabolism over time in parietal and frontal lobe in normal older adults but to decreased metabolism in patients (Fig. 3).

Conclusions: This study highlighted specific patterns of metabolic and amyloid deposition changes over time in the different clinical groups, with AD and MCI showing the most widespread changes in metabolism and amyloid deposition respectively. Further, inter-modality analyses suggested a differential association of amyloid pathology with glucose metabolism over the course of the disease.

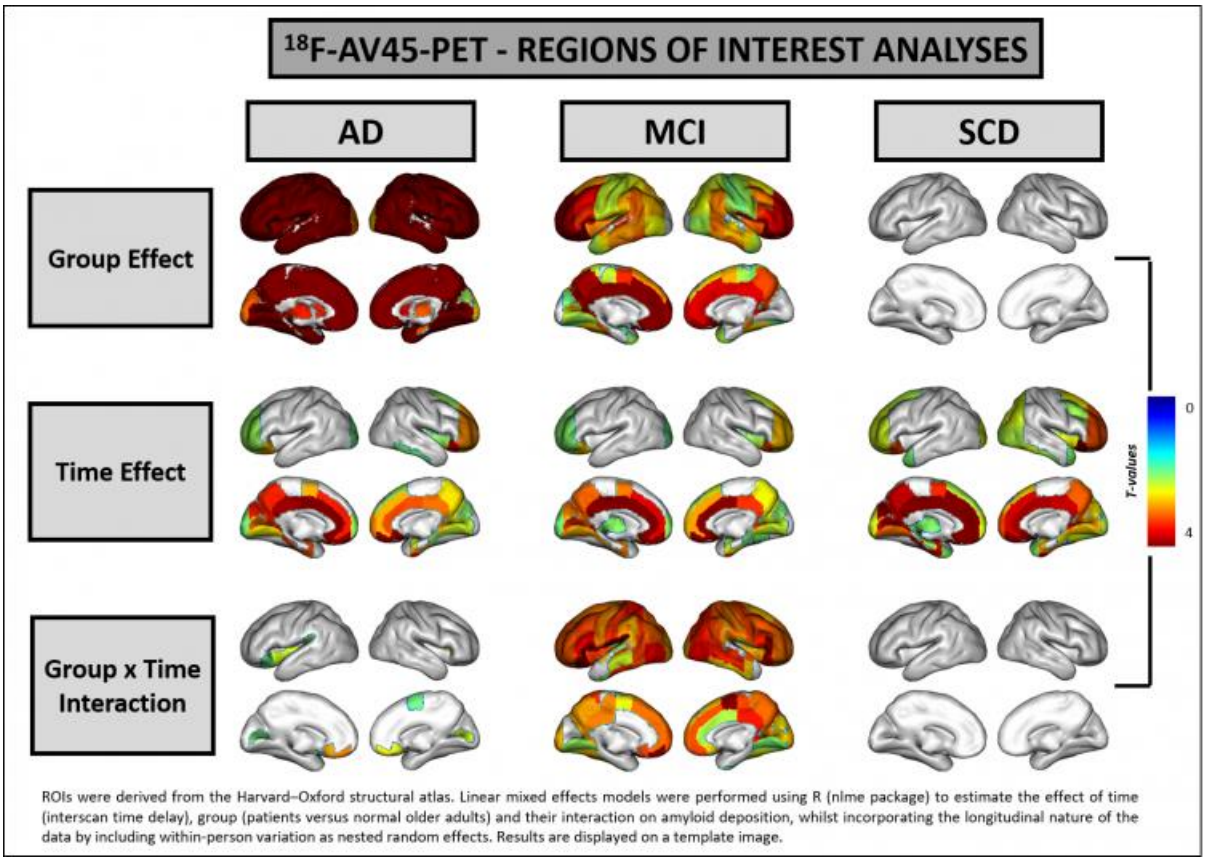

ROIs were derived from the Harvard–Oxford structural atlas. Linear mixed effects models were performed using R (nlme package) to estimate the effect of time (interscan time delay), group (patients versus normal older adults) and their interaction on amyloid deposition, whilst incorporating the longitudinal nature of the data by including within-person variation as nested random effects. Results are displayed on a template image.

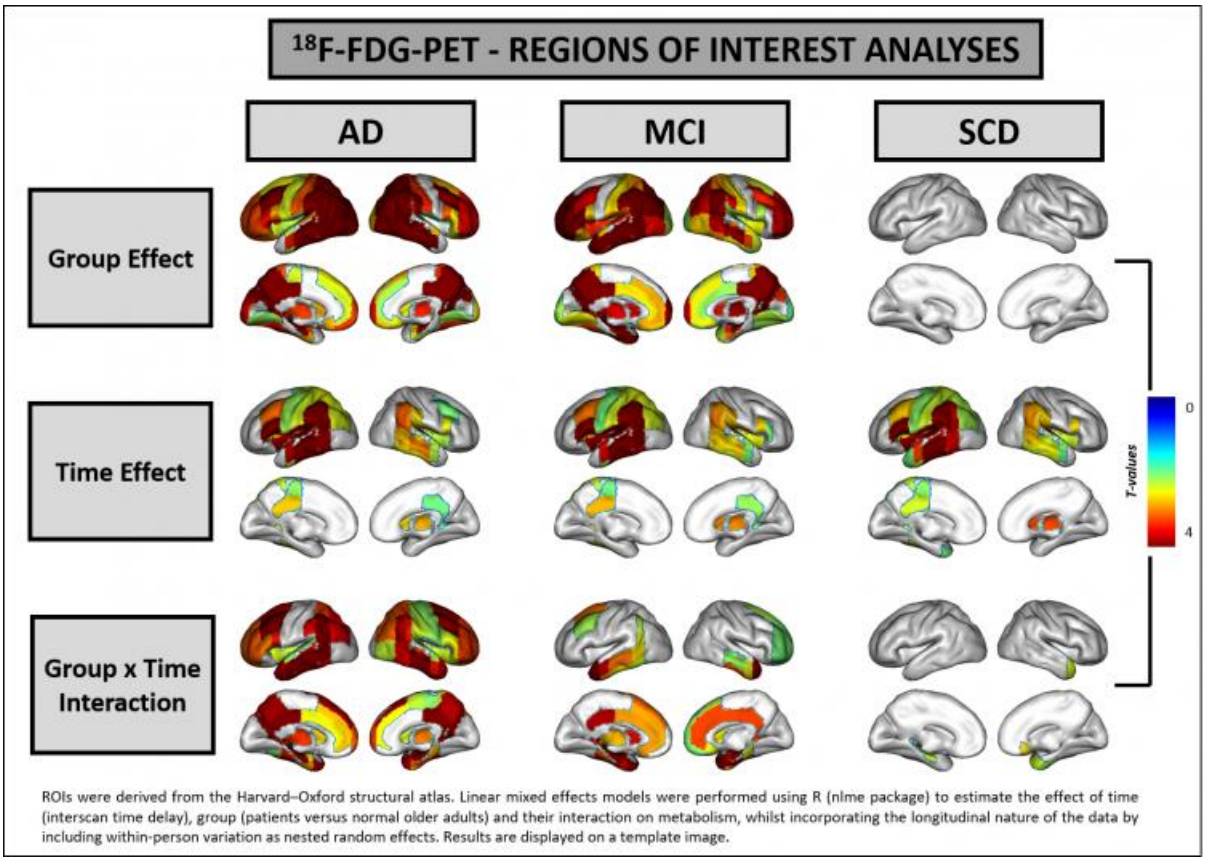

ROIs were derived from the Harvard–Oxford structural atlas. Linear mixed effects models were performed using R (nlme package) to estimate the effect of time (interscan time delay), group (patients versus normal older adults) and their interaction on metabolism, whilst incorporating the longitudinal nature of the data by including within-person variation as nested random effects. Results are displayed on a template image.

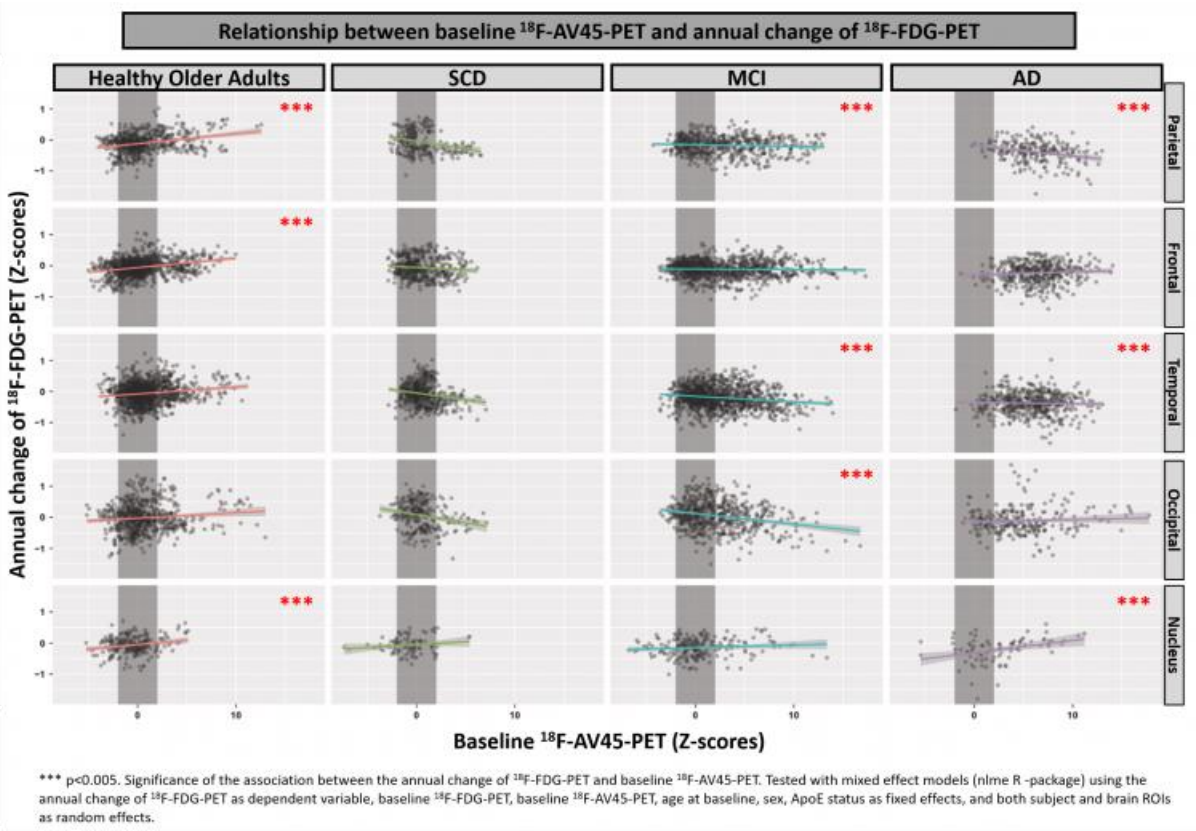

*** p<0.005. Significance of the association between the annual change of ^{18}F-FDG-PET and baseline ^{18}F-AV45-PET. Tested with mixed effect models (nlme R -package) using the annual change of ^{18}F-FDG-PET as dependent variable, baseline ^{18}F-FDG-PET, baseline ^{18}F-AV45-PET, age at baseline, sex, ApoE status as fixed effects, and both subject and brain ROIs as random effects.

Keywords: Longitudinal changes, AV45-PET, FDG-PET, SCD, MCI, AD

Friday, January 19, 2018 - 11:00 am - 12:45 pm

Podium Session

Session 8: Applications in Clinical Populations

CHAIRS: Rik Ossenkoppele, Gil Rabinovici

Friday, January 19, 2018		
11:00 - 12:15	**Session 8: APPLICATIONS IN CLINICAL POPULATIONS**	CHAIRS: Rik Ossenkoppele | Gil Rabinovici
11:00	Impact of the appropriate use criteria: effect of amyloid imaging on diagnosis and patient management in an unselected memory clinic cohort: the ABIDE project	**de Wilde** | Ossenkoppele | Pelkmans | Bouwman | Groot | Zwan | Yaqub | Barkhof | Lammertsma | van der Flier | van Berckel | Scheltens
11:15	The influence of age at onset on regional [18F]AV-1451 uptake in atypical Alzheimer's disease	**Whitwell** | Graff-Radford | Martin | Senjem | Spychalla | Machulda | Weigand | Drubach | Jack | Lowe | Josephs
11:30	Hemispheric asymmetry on structural MRI, [18F]AV-1451-PET, and [11C]PIB-PET across clinical phenotypes of Alzheimer's disease	**Visani** | La Joie | Baker | Bourakova | Pham | Miller | Jagust | Rabinovici
11:45	Detection of tau pathology in Gerstmann-Sträussler-Scheinker Disease (PRNP F198S) by [18F]Flortaucipir PET	**Risacher** | Farlow | Bateman | Quaid | Epperson | Tallman | Richarson | Murrell | Unverzagt | Apostolova | Bonnin | Ghetti | Saykin
12:00	FDG-PET in tau-negative amnestic dementia resembles that of autopsy proven hippocampal sclerosis	**Botha** | Mantyh | Graff-Radford | Murray | Josephs | Parisi | Dickson | Machulda | Przybelski | Wiste | Senjem | Petersen | Boeve | Lowe | Knopman | Jack | Jones
12:15	Discussion	

Impact of the appropriate use criteria: effect of amyloid imaging on diagnosis and patient management in an unselected memory clinic cohort: the ABIDE project

Arno de Wilde[1], Rik Ossenkoppele[1,2,3], Wiesje Pelkmans[1], Femke Bouwman[1], Colin Groot[1,2], Marissa Zwan[1], Maqsood Yaqub[2], Frederik Barkhof[2,4], Adriaan Lammertsma[2], Wiesje van der Flier[1,5], Bart van Berckel[2], Philip Scheltens[1]

[1]*Department of Neurology & Alzheimer Center, Amsterdam Neuroscience, VU University Medical Center, Amsterdam, Netherlands*
[2]*Department of Radiology & Nuclear Medicine, Amsterdam Neuroscience, VU University Medical Center, Amsterdam, Netherlands*
[3]*Lund University, Clinical Memory Research Unit, Malmö, Sweden*
[4]*Institutes of Neurology and Healthcare Engineering, UCL, London, United Kingdom*
[5]*Department of Epidemiology & Biostatistics, Amsterdam Neuroscience, VU University, Amsterdam, Netherlands*

Background: Appropriate use criteria (AUC) for amyloid imaging have been developed to provide guidance for its clinical implementation. To date, these criteria have not been evaluated in an unselected memory clinic cohort. The current study compared the impact of amyloid PET on diagnosis and patient management in patients that are consistent or inconsistent with the AUC.

Methods: A total of 507 patients underwent static [^{18}F]florbetaben PET scans after routine diagnostic work-up for dementia, including medical history, neurological examinations, neuropsychological testing, laboratory testing and MRI. Neurologists determined syndrome diagnosis, suspected etiology and patient management plans, both before and after PET. We classified patients as either "AUC-like" ([A] unexplained/persistent MCI, [B] atypical AD dementia or [C] early-onset dementia) or "non-AUC".

Results: 250 (49%) patients were classified as AUC-like and 257 (51%) as non-AUC (Table 1). Of AUC-like patients, 89 (36%) were classified as unexplained/persistent MCI, 82 (33%) as atypical AD dementia, and 79 (31%) as early-onset dementia. After [^{18}F]florbetaben PET, suspected etiological diagnosis changed in 71 (28%) AUC-like and 37 (23%) non-AUC patients (p=0.054). There was a change in management plan in 80 (32%) AUC-like and 43 (17%) non-AUC patients (p<0.001). Especially amongst demented patients with a suspected AD etiology, changes in suspected etiology and patient management were comparable in AUC-like and non-AUC. Even in SCD patients, which are by definition non-AUC, amyloid PET led to changes in suspected etiology in 23% and changes in patient management in 11%.

Conclusions: In this unselected memory clinic cohort, half of patients were AUC-like. Amyloid imaging had substantial impact on changes in etiological diagnosis in both AUC-like and non-AUC patients, while AUC-like patients showed an almost twofold increased change in management compared to non-AUC.

Keywords: Alzheimer's, amyloid PET, clinical utility, Appropriate Use Criteria

The influence of age at onset on regional [18F]AV-1451 uptake in atypical Alzheimer's disease

Jennifer Whitwell, Jonathan Graff-Radford, Peter Martin, Matthew Senjem, Anthony Spychalla, Mary Machulda, Stephen Weigand, Daniel Drubach, Clifford Jack, Val Lowe, Keith Josephs

Mayo Clinic, Rochester, MN, US

Introduction: [18F]AV-1451 characteristics in Alzheimer's disease (AD) have been shown to differ according to age-at-onset, driven largely by late-onset patients that show focal medial temporal uptake with little cortical involvement. Other comorbidities are likely to contribute to impairment in these late-onset patients. It is unclear whether age-at-onset influences [18F]AV-1451 uptake, or clinical phenotype, in patients with atypical variants of AD who typically present at a younger age with predominant deficits in cognitive domains other than memory.

Methods: Thirty-seven PiB-positive atypical AD subjects were recruited and underwent [18F]AV-1451 PET, Pittsburgh Compound B (PiB) PET and volumetric MRI. The 37 subjects included 18 with posterior cortical atrophy and 19 with logopenic aphasia. [18F]AV-1451 uptake was calculated for ten regions-of-interest covering cortical and medial temporal regions. Regional values were divided by uptake in cerebellar crus to generate standard uptake value ratios, which were then compared between subjects with age at onset <65 (n=22, median age=56, IQR=55-60) and ≥65 years (n=15, median age=69, IQR=65-72). The relationship between SUVR and age as a continuous variable was also modelled.

Results: Young-onset subjects were more likely to have a diagnosis of posterior cortical atrophy compared to late-onset subjects (64% versus 27%, p=0.05). Early-onset subjects showed higher SUVRs in inferior and superior parietal, precuneus, posterior cingulate, lateral temporal, lateral frontal and medial and lateral occipital lobe compared to late-onset subjects. No differences were observed in medial temporal lobe or fusiform cortex. A 2% decrease in [18F]AV-1451 uptake was observed per 1-year increase in age-of-onset across all cortical regions-of-interest.

Conclusion: Although atypical AD is considered a young-onset disease, there is significant heterogeneity in age at onset. Subjects with young age at onset are more likely to show widespread and severe cortical tau uptake and present with posterior cortical atrophy. These findings increase understanding of the clinical heterogeneity underlying AD.

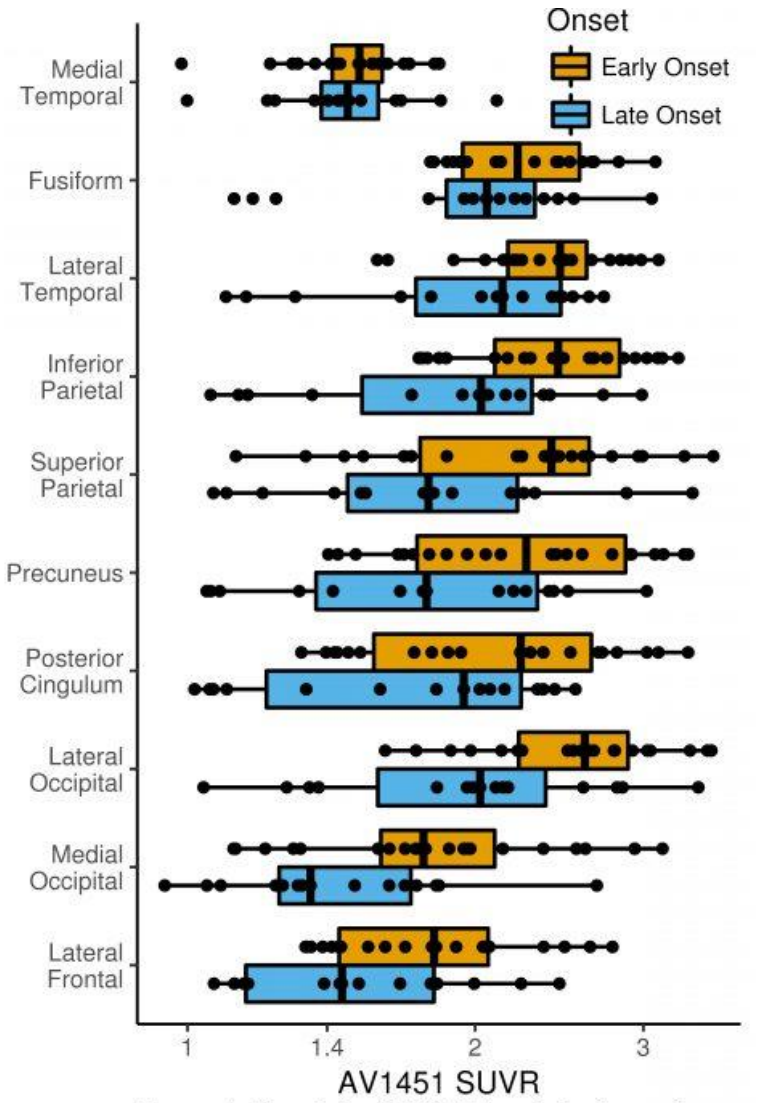

Figure 1: Boxplots of AV1451 uptake by region and early versus late onset in a cohort of 37 cases of atypical Alzheimer's disease.

Keywords: AV-1451, tau, logopenic, posterior cortical atrophy, age

Hemispheric asymmetry on structural MRI, [18F]AV-1451-PET, and [11C]PIB-PET across clinical phenotypes of Alzheimer's disease

Adrienne Visani[1], Renaud La Joie[1], Suzanne Baker[2], Viktoriya Bourakova[1], Julie Pham[1], Bruce Miller[1], William Jagust[2,3], Gil Rabinovici[1,3]

[1]UCSF Memory and Aging Center, San Francisco, CA, US
[2]Life Sciences Division, Lawrence Berkeley National Laboratory, Berkeley, CA, US
[3]Helen Wills Neuroscience Institute, University of California Berkeley, Berkeley, CA, US

Objective: To examine variations in hemispheric asymmetry of neurodegeneration (structural MRI), tau ([18F]AV-1451-PET) and beta-amyloid ([11C]PIB-PET) across clinical phenotypes of Alzheimer's Disease.

Methods: We studied 64 patients with 3T T1-MRI, [18F]AV-1451-PET and [11C]PIB-PET (demographics in Table 1). All patients were [11C]PIB-PET-positive, including 36 memory/executive-predominant AD, 13 posterior cortical atrophy (PCA), and 15 logopenic variant primary progressive aphasia (lvPPA). FreeSurfer 5.3 and SPM12 were used to obtain SUVR images ([11C]PIB: 50-70 min, ref: cerebellar gray; [18F]AV-1451: 80-100min, ref: inferior cerebellar gray). We examined group differences using 1) asymmetry index (Fig1A) on cortical volume and PET SUVR and 2) w-maps for PET images (age-adjusted z-score maps compared to 87 Aβ-PET-negative controls, Table 1).

Results: Many amnestic/dysexecutive AD patients were symmetric across modalities (Fig1B). All PCA patients were asymmetric on cortical [18F]AV-1451-PET and volume, but there was no hemispheric preference across the group. lvPPA showed left-lateralized asymmetry ([18F]AV-1451-PET>volume>[11C]PIB-PET). Figure 1C shows absolute (de-lateralized) asymmetry in each lobe/diagnosis. In frontal areas, [18F]AV-1451-PET asymmetry exceeded other modalities across all diagnostic groups. In occipital/parietal lobes, volumetric asymmetry was more prominent for PCA only (Fig1C). Post-hoc analyses showed no difference between [18F]AV-1451-PET and volume asymmetries in the temporal lobe. [11C]PIB-PET patterns were largely symmetric across lobes/diagnoses (Fig1C, 2B). Finally, volumetric asymmetry correlated with [18F]AV-1451-PET ($r=0.781$, $p<0.001$), but not [11C]PIB-PET asymmetry (Fig1D).

Conclusions: Variations in asymmetry among diagnoses and lobes were found for [18F]AV-1451-PET and volume, but not for [11C]PIB-PET. In regions that are generally relatively spared (e.g. the frontal lobe in AD/PCA/lvPPA, the occipital lobe in AD/lvPPA), [18F]AV-1451-PET asymmetry was more pronounced than volumetric asymmetry. In regions with advanced pathology (e.g. temporal regions in AD/PCA/lvPPA, occipitoparietal regions in PCA), volumetric asymmetry matched or exceeded [18F]AV-1451-PET, suggesting asymmetry might be a feature of early stages of biomarker abnormality, with a pattern that becomes more symmetric over time.

	Controls n=87	Patients n=64	Patients vs. Controls	AD n=36	PCA n=13	lvPPA n=15	Among Patient Groups
Age	60.4 ± 22.8 [20.5, 84.5]	63.9 ± 8.4 [48, 83]	*H=2.478, p=0.115*	64.6 ± 9.7 [48, 83]	62.1 ± 6.2 [53.2, 73.7]	65.0 ± 6.8 [54.5, 77.8]	*H=1.172, p=0.557*
F / M	41 / 46	34 / 30	*p=0.512*	16 / 20	7 / 6	7 / 8	*p=0.941*
Education years	16.6 ± 1.9 [12, 20] (1)	17.1 ± 2.8 [12, 25] (12)	*H=0.504, p=0.478*	17.7 ± 2.6 [12, 22] (7)	16.8 ± 4.0 [12, 25] (1)	17.4 ± 2.0 [14, 21] (4)	*H=1.326, p=0.515*
MMSE	28.9 ± 1.1 [25, 30] (28)	21.5 ± 5.5 [8, 30] (3)	***H=69.24, p<0.001***	22.2 ± 5.5 [8, 30] (2)	20.8 ± 5.1 [9, 28]	20.4 ± 6.1 [11, 29] (1)	*H=1.207, p=0.547*
CDR sum of boxes	N/A	4.2 ± 2.0 [0, 11] (5)	N/A	4.4 ± 1.8 [1, 8] (3)	4.8 ± 2.8 [0, 11]	3.1 ± 1.4 [0.5, 6] (2)	***H=6.031, p=0.049*** **32.5 / 33.9 / 19.8**
% ApoE4 carriers	9.5% (45)	51% (13)	***p<0.001***	58% (5)	46%	29% (8)	*p=0.180*
[^{11}C]PIB DVR (cortical ROI)	1.00 ± 0.03 [0.92, 1.06] (9)	1.61 ± 0.24 [1.02, 2.18] (3) *(pt with DVR=1.02 had focal cortical uptake)*	***H=99.06, p<0.001***	1.58 ± 0.27 [1.02, 2.09] (1)	1.71 ± 0.17 [1.48, 2.0]	1.61 ± 0.23 [1.23, 2.18] (2)	*H=1.881, p=0.391*

Table 1. Patient and control demographics, with continuous variables presented as mean ± standard deviation [min, max] and missing data in parentheses. Patients and controls were significantly different on MMSE, %ApoE4 carriers, and [^{11}C]PIB DVR. Diagnostic groups were not significantly different for any variable except CDR. Kruskal-Wallis test was used for continuous variables (adjusted H), with mean ranks presented for CDR among patient groups. Fisher's Exact test was used for categorical variables. For patients, median months between PET scans = 0; between PET and clinical diagnosis = 2, between PET and MRI = 1.

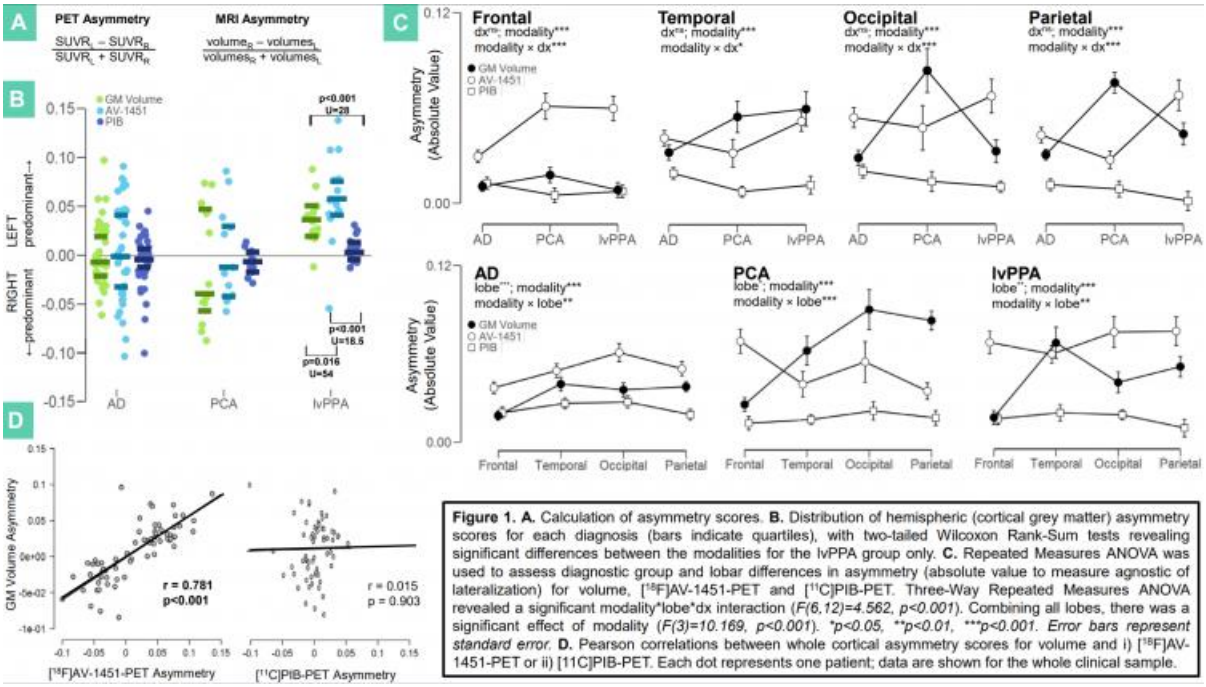

Figure 1. A. Calculation of asymmetry scores. **B.** Distribution of hemispheric (cortical grey matter) asymmetry scores for each diagnosis (bars indicate quartiles), with two-tailed Wilcoxon Rank-Sum tests revealing significant differences between the modalities for the lvPPA group only. **C.** Repeated Measures ANOVA was used to assess diagnostic group and lobar differences in asymmetry (absolute value to measure agnostic of lateralization) for volume, [^{18}F]AV-1451-PET and [^{11}C]PIB-PET. Three-Way Repeated Measures ANOVA revealed a significant modality*lobe*dx interaction (*F(6,12)=4.562, p<0.001*). Combining all lobes, there was a significant effect of modality (*F(3)=10.169, p<0.001*). *p<0.05, **p<0.01, ***p<0.001. *Error bars represent standard error.* **D.** Pearson correlations between whole cortical asymmetry scores for volume and i) [^{18}F]AV-1451-PET or ii) [11C]PIB-PET. Each dot represents one patient; data are shown for the whole clinical sample.

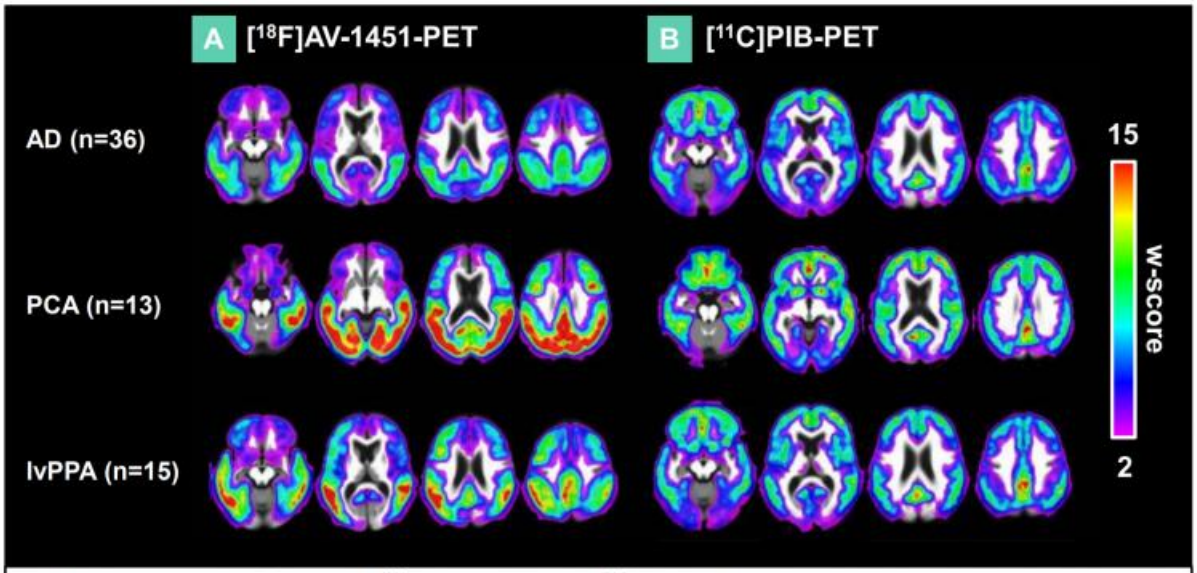

Figure 2. Average patterns of abnormal **A.** [^{18}F]AV-1451-PET and **B.** [^{11}C]PIB-PET uptake in each clinical group. We calculated voxelwise w-scores (age-adjusted z-scores) using a control group of 87 Aß-PET-negative healthy older adults (subsample of n=60 used for [^{18}F]AV-1451, subsample of n=62 for [^{11}C]PIB) and generated mean maps for each patient group. Note that group mean images may not capture hemispheric asymmetry in phenotypes without a consistent left/right preference across the group.

Keywords: Alzheimer's, [18F]AV-1451, [11C]PIB, posterior cortical atrophy, logopenic variant primary progressive aphasia

Detection of tau pathology in Gerstmann-Sträussler-Scheinker Disease (PRNP F198S) by [18F]Flortaucipir PET

Shannon Risacher[1,6], Martin Farlow[2,6], Daniel Bateman[3,6], Kimberly Quaid[4,6], Francine Epperson[5,6], Eileen Tallman[1,6], Rose Richarson[5], Jill Murrell[7], Fredrick Unverzagt[3,6], Liana Apostolova[1,2,6], Jose Bonnin[5], Bernardino Ghetti[5,6], Andrew Saykin[1,6]

[1]*Department of Radiology and Imaging Sciences, Indiana University School of Medicine, Indianapolis, IN, US*
[2]*Department of Neurology, Indiana University School of Medicine, Indianapolis, IN, US*
[3]*Department of Psychiatry, Indiana University School of Medicine, Indianapolis, IN, US*
[4]*Department of Medical and Molecular Genetics, Indiana University School of Medicine, Indianapolis, IN, US*
[5]*Department of Pathology and Laboratory Medicine, Indiana University School of Medicine, Indianapolis, IN, US*
[6]*Indiana Alzheimer Disease Center, Indiana University School of Medicine, Indianapolis, IN, US*
[7]*Department of Pathology and Laboratory Medicine, The Children's Hospital of Philadelphia, Philadelphia, PA, US*

Objective: To investigate the uptake pattern of [^{18}F]flortaucipir (^{18}F-AV1451) PET in individuals affected by a dominantly inherited prion amyloidosis called Gerstmann-Sträussler-Scheinker disease (GSS). This disorder is associated with a *PRNP* gene mutation resulting in a serine for phenylalanine amino acid change (F198S) in the Prion protein (PrP).

Methods: Two individuals from a single pedigree underwent [^{18}F]flortaucipir PET. Scans were processed using standard methods, intensity-normalized using cerebellar crus uptake to create SUVR images, and viewed for qualitative analysis. [^{18}F]flortaucipir images and quantitative SUVR values from the GSS patients were compared to two cognitively normal (CN) older adults and two early onset Alzheimer's disease (AD) patients.

Results: Patients were at different stages of disease progression. One (Patient A) was mildly symptomatic with motor and cognitive symptoms and a history of psychiatric disorder. Patient B was neurologically severely symptomatic and had a history of psychosis. The [^{18}F]flortaucipir PET scans showed uptake in the basal ganglia, thalamus, frontal lobe, cingulate, sensorimotor cortex, and insula of the GSS patients (Figure 1). PET scans of Patient B show greater [^{18}F]flortaucipir uptake than in Patient A and both showed a dramatically different pattern of [^{18}F]flortaucipir uptake from that in the early onset AD and CN (Figure 2). Patient B expired nine months after the [^{18}F]flortaucipir PET scan and underwent a study aimed at correlating imaging findings with neuropathology (Figure 3). Immunohistochemistry demonstrates tau deposition not only in the regions that show uptake on the [^{18}F]flortaucipir PET scan, but also in regions that did not reveal uptake by PET.

Conclusion: In F198S GSS patients, tau deposition is detectable *in vivo* by [^{18}F]flortaucipir PET; however, tau appears to accumulates with a pattern that is strikingly different from that seen in AD. These results suggest that tau pathology contributes significantly to both psychiatric and motor symptoms observed in GSS.

Figure 1. [18F]Flortaucipir PET GSS F198S Patients

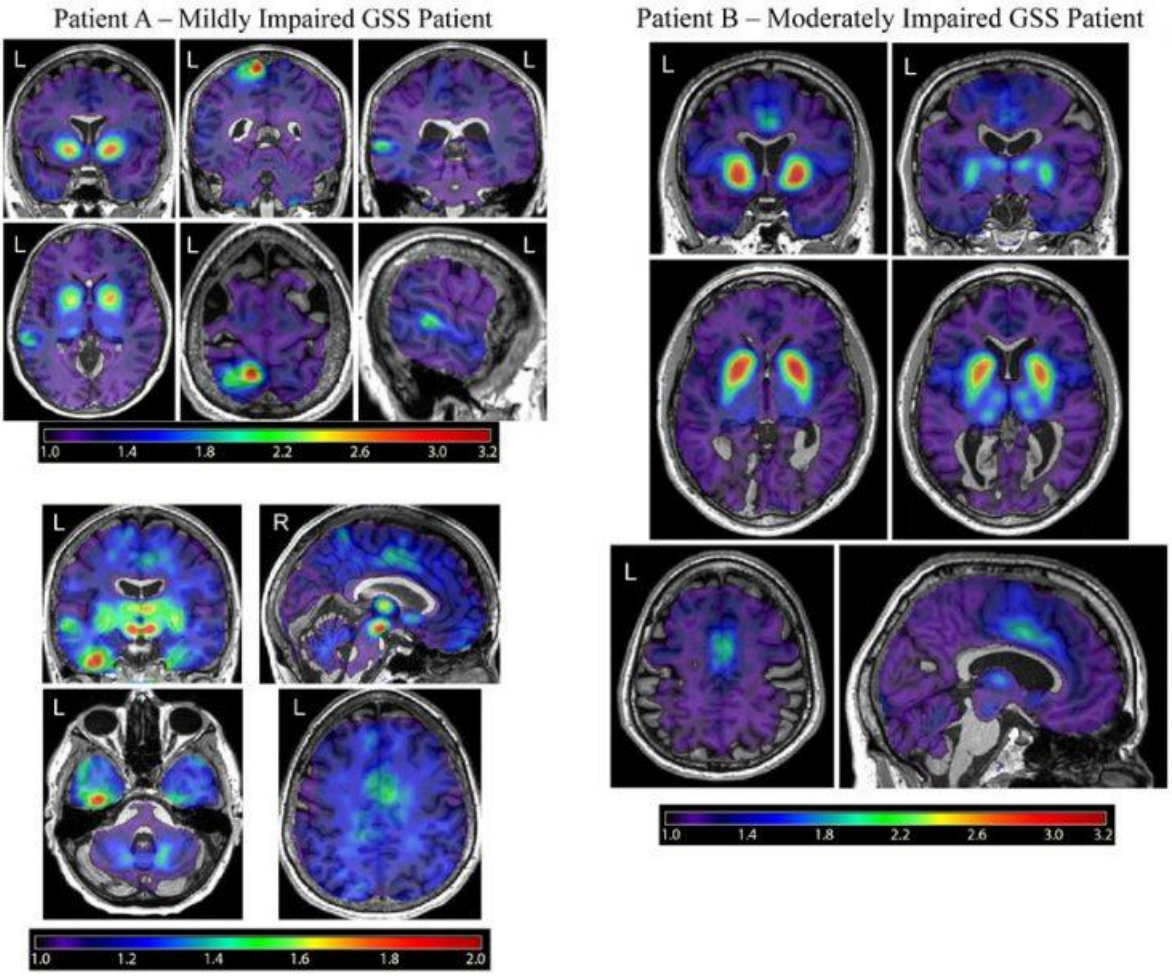

Figure 2. Qualitative Comparison of [18F]Flortaucipir in GSS F198S Patients Relative to Early Onset AD and CN

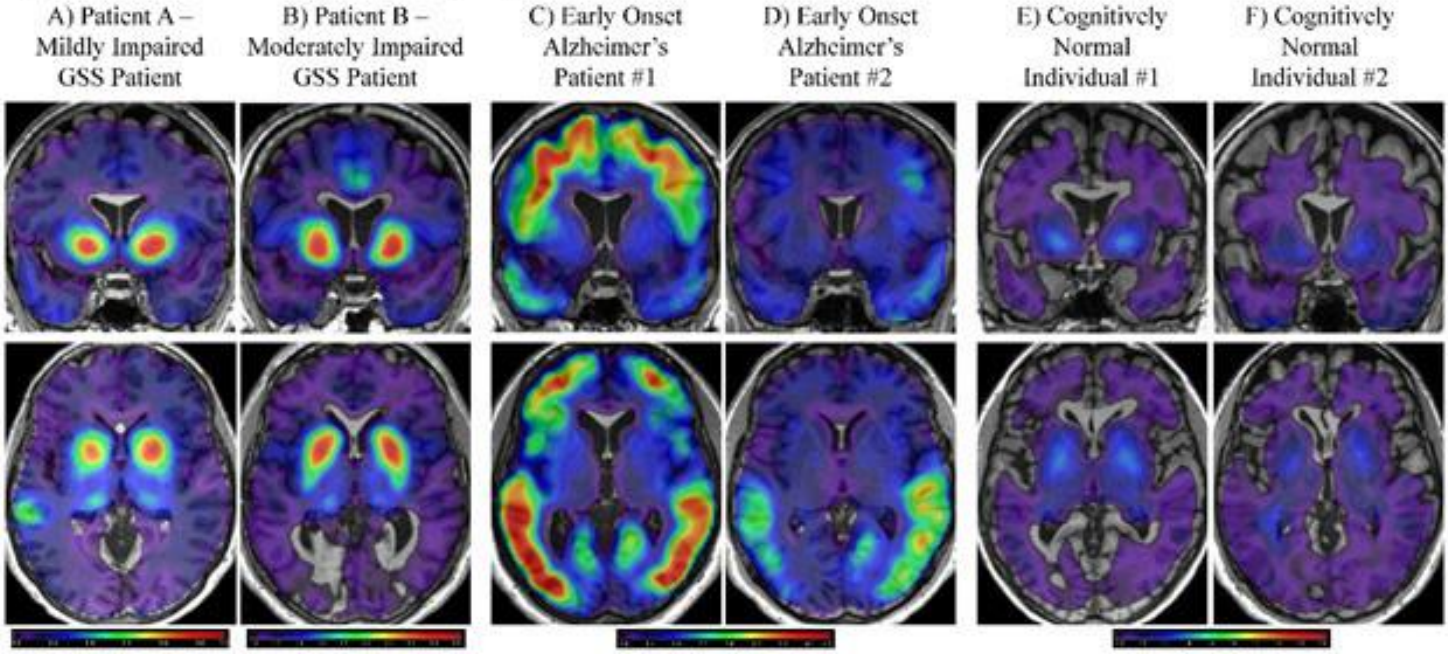

Figure 3. Neuropathologic analysis of the moderately impaired GSS patient B

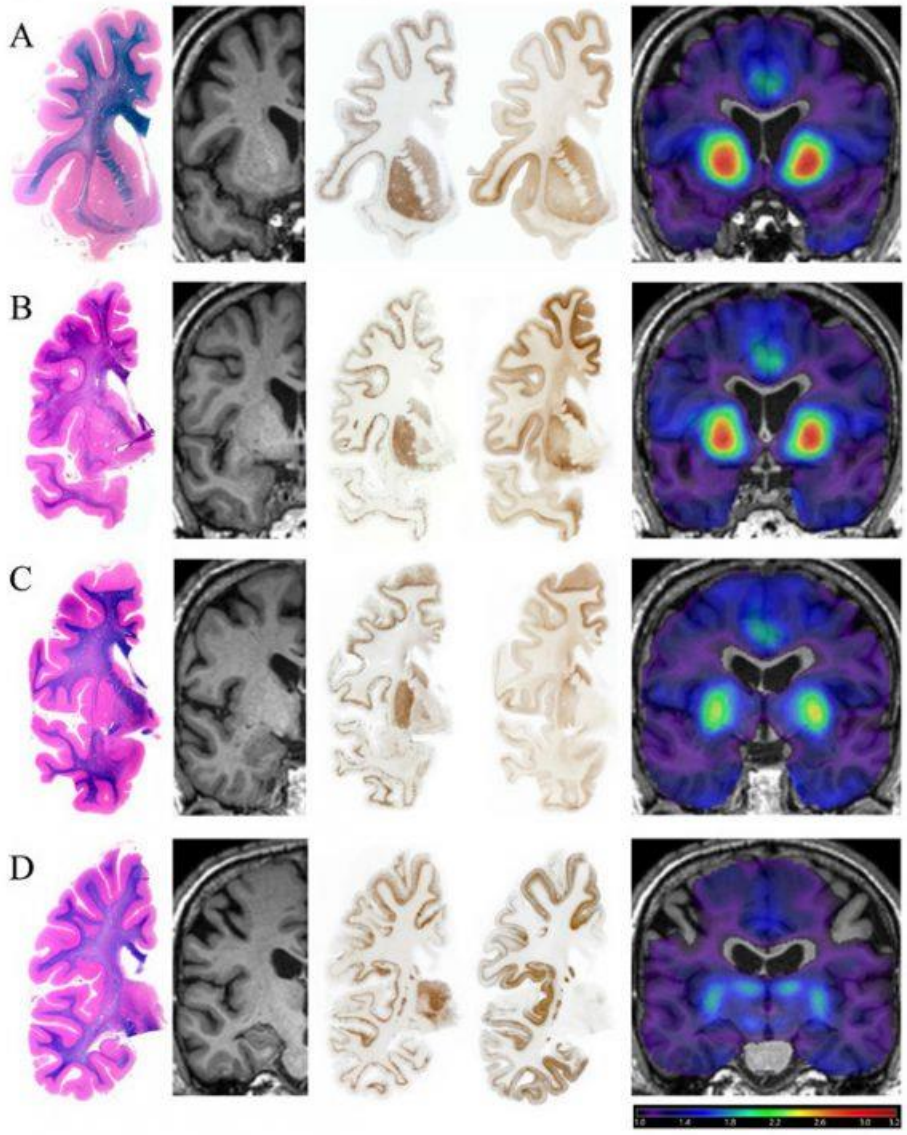

Keywords: [18F]flortaucipir/AV-1451/T-807; Gerstmann-Sträussler-Scheinker Disease (GSS); Tau; Prion protein

FDG-PET in tau-negative amnestic dementia resembles that of autopsy proven hippocampal sclerosis

Hugo Botha[1], William Mantyh[1], Jonathan Graff-Radford[1], Melissa Murray[2], Keith Josephs[1], Joseph Parisi[1], Dennis Dickson[2], Mary Machulda[1], Scott Przybelski[1], Heather Wiste[1], Matthew Senjem[1], Ronald Petersen[1], Bradley Boeve[1], Val Lowe[1], David Knopman[1], Clifford Jack[1], David Jones[1]

[1]Mayo Clinic, Rochester, MN, US
[2]Mayo Clinic, Jacksonville, FL, US

Background: Age-related hippocampal sclerosis may account for a significant proportion of elderly participants with amnestic dementia. We evaluated the utility of FDG-PET to differentiate tau PET negative from tau PET positive amnestic MCI and dementia, and used an autopsy confirmed cohort to test the hypothesis that hippocampal sclerosis might account for the observed PET pattern.

Methods: We identified impaired participants with amnestic presentations ≥ 75 years who had MRI, FDG-PET, amyloid PET and tau PET imaging performed. For the FDG-PET analysis we compared each group to controls and to each other in a voxel based analysis, and supplemented this with an ROI-based analysis comparing inferior to medial temporal metabolism. A separate autopsy confirmed cohort of TDP-43 negative Alzheimer's disease cases and TDP-43 positive hippocampal sclerosis cases was constructed and underwent the same FDG-PET analysis.

Results: Fifteen amyloid and tau positive participants and nine tau negative participants (five of whom were amyloid positive) were included. FDG-PET analyses revealed focal medial temporal and posterior cingulate/retrosplenial hypometabolism in tau-negative cases, regardless of amyloid status, whereas tau positive cases had additional lateral parietal and temporal involvement (Figure 1). The ratio between temporal ROIs was significantly different between the groups with the tau negative group having a higher ratio (Figure 2). In the autopsy series, hippocampal sclerosis cases had greater medial temporal and orbitofrontal hypometabolism than Alzheimer's disease cases, who had more parietal and lateral/inferior temporal hypometabolism. Again, the ratio between temporal ROIs differed significantly between groups (Figure 3).

Conclusions: Tau-negative amnestic MCI and dementia, clinically mimicking Alzheimer's disease, is associated with focal medial temporal and posterior cingulate hypometabolism regardless of amyloid status. The inferior/medial temporal metabolism ratio and focal posterior cingulate hypometabolism with sparing of association cortex can help identify tau-negative cases of amnestic dementia and may serve as a hippocampal sclerosis biomarker.

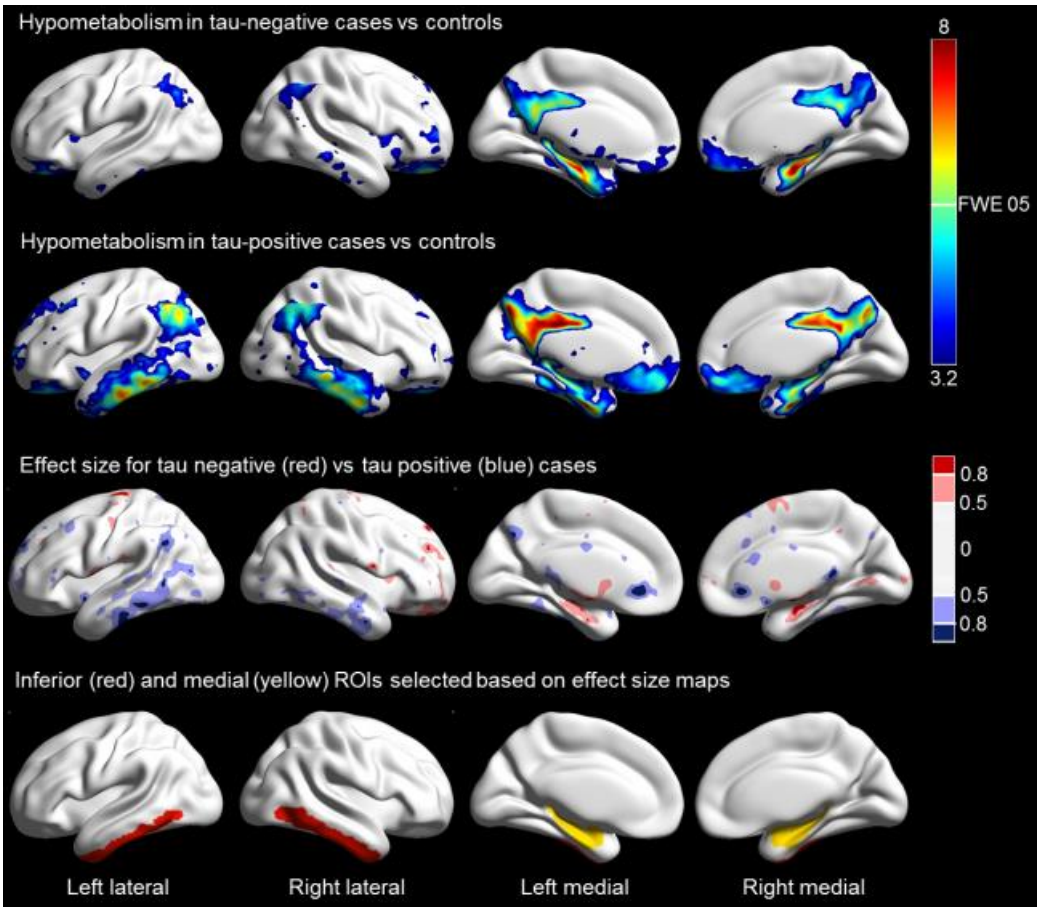

Figure 1: Three-dimensional brain renderings showing results of FDG-PET analysis for the clinical cohort

Compared to controls, tau-negative participants had hypometabolism in the posterior and middle cingulate, the inferior precuneus and the mesial temporal lobe. Tau-positive participants also had hypometabolism in the posterior and middle cingulate and the precuneus, but there was more widespread cortical involvement including inferior and middle temporal gyri and the angular gyri bilaterally. In addition, mesial temporal lobe involvement was less pronounced. Effect size (Cohen's d) maps for the direct comparison revealed moderate (0.5-0.8) to large (>0.8) effect sizes for the medial temporal (more involved in tau-negative cases) and inferior temporal (more involved in tau-positive cases) gyri. Based on the effect size maps, inferior and medial temporal ROIs were chosen from the AAL atlas.

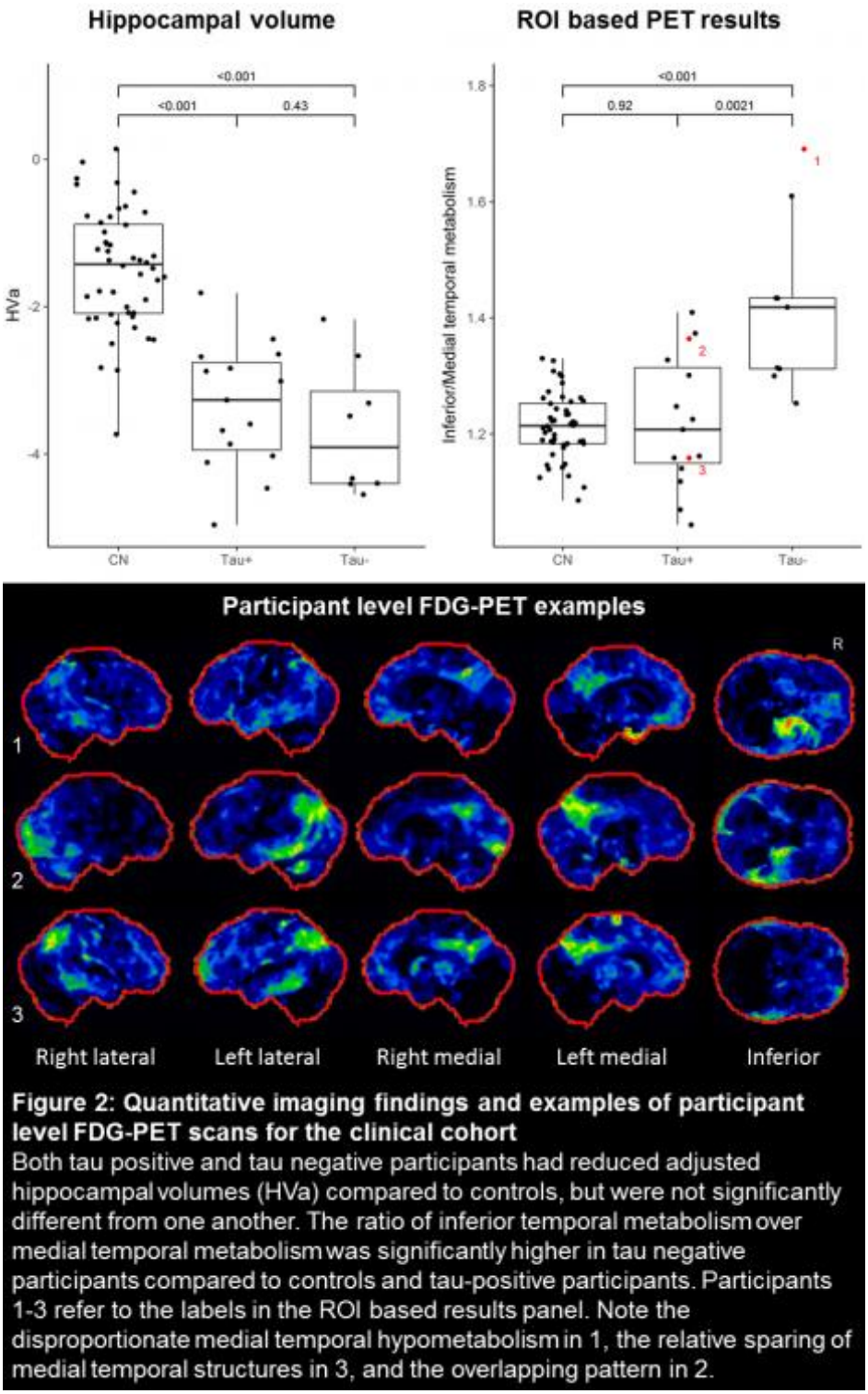

Figure 2: Quantitative imaging findings and examples of participant level FDG-PET scans for the clinical cohort

Both tau positive and tau negative participants had reduced adjusted hippocampal volumes (HVa) compared to controls, but were not significantly different from one another. The ratio of inferior temporal metabolism over medial temporal metabolism was significantly higher in tau negative participants compared to controls and tau-positive participants. Participants 1-3 refer to the labels in the ROI based results panel. Note the disproportionate medial temporal hypometabolism in 1, the relative sparing of medial temporal structures in 3, and the overlapping pattern in 2.

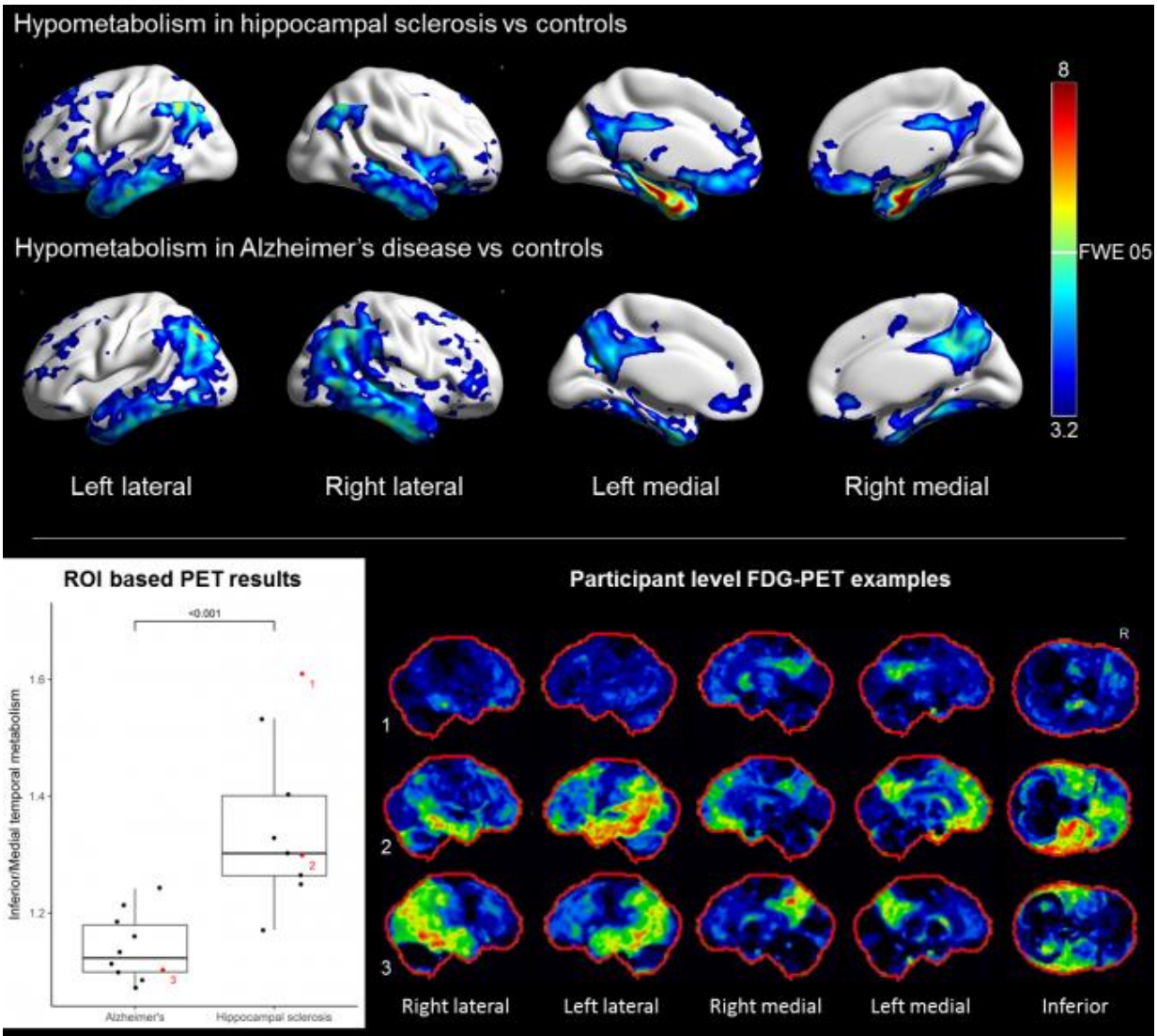

Figure 3: Imaging results in the autopsy cohort
Compared to controls, hippocampal sclerosis was associated with hypometabolism predominantly in the medial temporal lobe, with additional involvement of the middle and inferior temporal, lateral parietal and insular regions. Pure Alzheimer's disease was associated with hypometabolism of the posterior cingulate, middle and inferior temporal and lateral and medial parietal regions including the precuneus. The ratio of inferior temporal metabolism over medial temporal metabolism was significantly higher in hippocampal sclerosis positive cases compared to Alzheimer's disease. Again, this pattern was often present on the single subject level. Note the disproportionate medial temporal hypometabolism in 1, the relative sparing of medial temporal structures in 3, and the overlapping pattern in 2.

Keywords: Alzheimer's disease, hippocampal sclerosis, FDG-PET, biomarkers

Friday, January 19, 2018 - 02:00 pm - 02:45 pm

Podium Session

Keynote Lecture

Davies, Peter

Molecular, temporal and spatial aspects of tau pathology

Peter Davies

Litwin-Zucker Center for Research on Alzheimer's Disease, Feinstein Institute for Medical Research, Northwell Health, Manhasset, NY, US

There is a great deal of excitement at the prospect of PET imaging of tau pathology in living individuals with Alzheimer's disease (AD) or other conditions involving neurofibrillary tangles formation. These efforts will have to consider both the molecular evolution of this pathology in each distinct disease, and the differences in this evolution in different regions of brain. The earliest detectable signs of development of tau pathology are changes in tau conformation, coincident with phosphorylation at serine 202 and threonine 231. It appears that initially this abnormal tau is diffusely present throughout the neuron – dendrites, cell bodies and axons and is not aggregated into the filamentous masses we call neurofibrillary tangles. This type of early pathology will later co-exist with more heavily phosphorylated, filamentous tau aggregates as the disease progresses, although the numbers of neurons showing early verses late pathology will vary across different brain regions. The precise nature of the filamentous aggregates does appear to be different in different tauopathies, and is currently a topic of very active investigation. The challenge for PET imaging is to determine what types of tau pathology are binding ligand and the relative contribution of each type of pathology to the final images.

Friday, January 19, 2018 - 02:45 pm - 04:15 pm

Podium Session

Session 9: Early Detection and Prediction

CHAIRS: William Jagust, Elizabeth Mormino

Friday, January 19, 2018		
02:45 - 04:15	**Session 9: EARLY DETECTION AND PREDICTION**	CHAIRS: William Jagust | Elizabeth Mormino
02:45	Early detection of longitudinal amyloid-related cognitive decline in middle-aged and initially amyloid-negative adults	**Farrell** | Chen | Rundle | Chan | Wig | Park
03:00	Prediction of incident sporadic Alzheimer dementia: longitudinal biomarkers and clinical changes	**Ances** | Roe | Head | Babula | Stout | Xiong | Holtzman | Fagan | Benzinger | Morris
03:15	Multiple brain markers contribute to risk of progression on the Clinical Dementia Rating Scale in clinically normal older adults	**Neal** | Rabin | Schultz | Johnson | Sperling | Hedden
03:30	Low levels of brain beta-amyloid predict tau deposition and memory decline in aging	**Leal** | Lockhart | Maass | Bell | Jagust
03:45	Discussion	

Early detection of longitudinal amyloid-related cognitive decline in middle-aged and initially amyloid-negative adults

Michelle Farrell, Xi Chen, Melissa Rundle, Micaela Chan, Gagan Wig, Denise Park

University of Texas at Dallas, Dallas, TX, US

Introduction: The recent failures of anti-amyloid clinical trials have led to a shift towards trials aimed at earlier intervention, underscoring the need for information about the earliest stages of amyloid accumulation and its impact on cognition. In the present longitudinal study, we focused on two overlapping groups of individuals in whom the earliest signs of amyloid pathology are likely to be detected: initially amyloid-negative adults (aged 30-89) and middle-aged adults (including amyloid negative and positive adults). Within these groups, we assessed whether regional changes in amyloid over 4 years were related to early declines in episodic memory and MMSE performance.

Methods: 142 cognitively normal participants (age 30-89) were included from the Dallas Lifespan Brain Study who completed florbetapir PET and a cognitive battery at baseline and 4-year follow-up. Change in SUVR was computed across 23 bilateral FreeSurfer ROIs from the Desikan-Killiany atlas. We examined the relationship between change in regional amyloid burden and change in cognition (episodic memory and MMSE) using partial correlations, controlling for baseline global amyloid burden, baseline cognitive performance, age, sex, education and APOE.

Results: In both initially amyloid-negative adults and middle-aged adults, we detected a regionally-specific relationship between declining episodic memory and increasing amyloid accumulation across multiple posterior cortical regions, see Figure 1. In contrast, a global relationship was detected between mean cortical amyloid accumulation and MMSE decline.

Conclusion: Our results indicate that assessing regional and global changes in amyloid can aid in early detection of amyloid-related cognitive decline in low-risk groups (e.g., amyloid-negative adults, middle-aged adults). Furthermore, posterior cortical regions may be particularly useful in isolating an early footprint of AD-risk. Future research is needed to assess whether amyloid may have direct effects on cognitive decline at this early stage, or if the observed effects are mediated by tau or other pathologies.

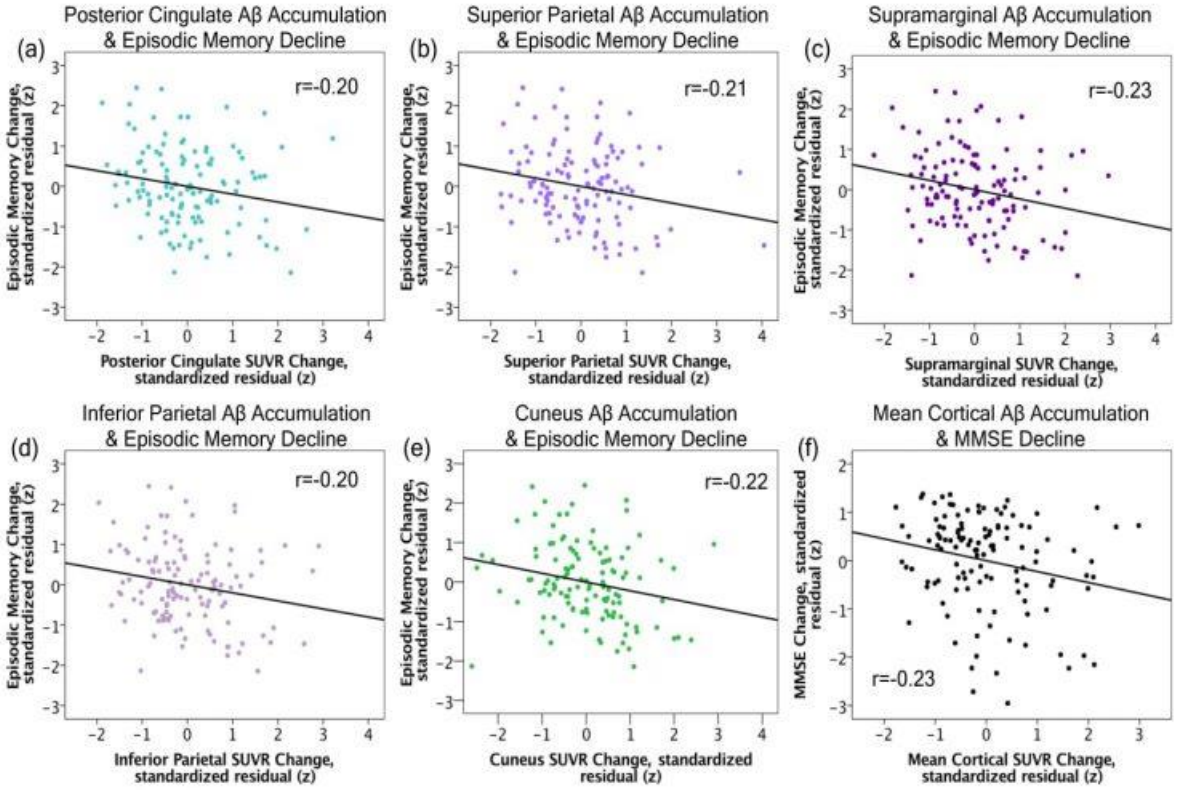

Figure 1. Early Relationships between Regional Amyloid Accumulation and Cognitive Decline in Initially Amyloid Negative Adults. (a-e) Increasing rate of accumulation across multiple posterior cortical regions was related to greater episodic memory decline in initially amyloid negative adults. (f) Increasing global amyloid accumulation was associated with declining MMSE performance.

Keywords: amyloid, cognition, longitudinal, early detection, middle age

Prediction of incident sporadic Alzheimer dementia: longitudinal biomarkers and clinical changes

Beau Ances, Catherine Roe, Denise Head, Ganesh Babula, Sarah Stout, Chengjie Xiong, David Holtzman, Anne Fagan, Tammie Benzinger, John Morris

Washington University in Saint Louis, Saint Louis, MO, US

Objective: To test the ability of molecular (cerebrospinal fluid [CSF] and amyloid PET imaging), structural MRI, and cognitive biomarkers to predict incident sporadic Alzheimer disease (AD) dementia and examine longitudinal biomarker changes before and after symptomatic onset.

Methods: Cognitively normal (CDR 0) participants at baseline, had amyloid PET and/or CSF, and had ≥2 clinical assessments. Stepwise Cox proportional hazards models tested for associations of molecular (PIB; CSF: $A\beta_{42}$, tau, $ptau_{181}$, tau/$A\beta_{42}$), structural (normalized hippocampal volume [nHV] and whole brain volume), and cognitive (Animal Naming, Trailmaking A, Trailmaking B, Selective Reminding Test - Free Recall [SRTFREE]) biomarkers with first time to developing symptomatic impairment (CDR >0). Differences in the rate of biomarker change across time for symptomatic and cognitively normal groups were tested using linear mixed models.

Results: From 664 cognitively normal participants at baseline (mean age=71.4 ±9.2 years) followed for up to 16.9 years (mean=6.2±3.5 years), 145 (21.8%) became symptomatic. SRTFREE scores, nHV, and molecular biomarkers predicted time to symptomatic impairment. The rate of decline for cognitive biomarkers and nHV was significantly faster for participants who became symptomatic compared to those remaining cognitively normal, while the rate of change of molecular biomarkers was similar (**Figure 1**). The overall magnitude of each biomarker (y-intercept) was more abnormal for participants who became symptomatic compared to those who remained cognitively normal. Within participants who became symptomatic, a significant separation existed according to amount and rate of amyloid accumulation. Apolipoprotein ε4 (APOE4) genotype was associated with higher PIB and greater rate of increase while APOE2 was protective (**Figure 2**).

Conclusion: Conversion from cognitively normal to impaired is characterized by not only magnitude of molecular biomarkers but also rate of change in cognitive and structural biomarkers. Each of these groups of biomarkers provide different, non-redundant, information, and combine to predict onset of symptomatic AD.

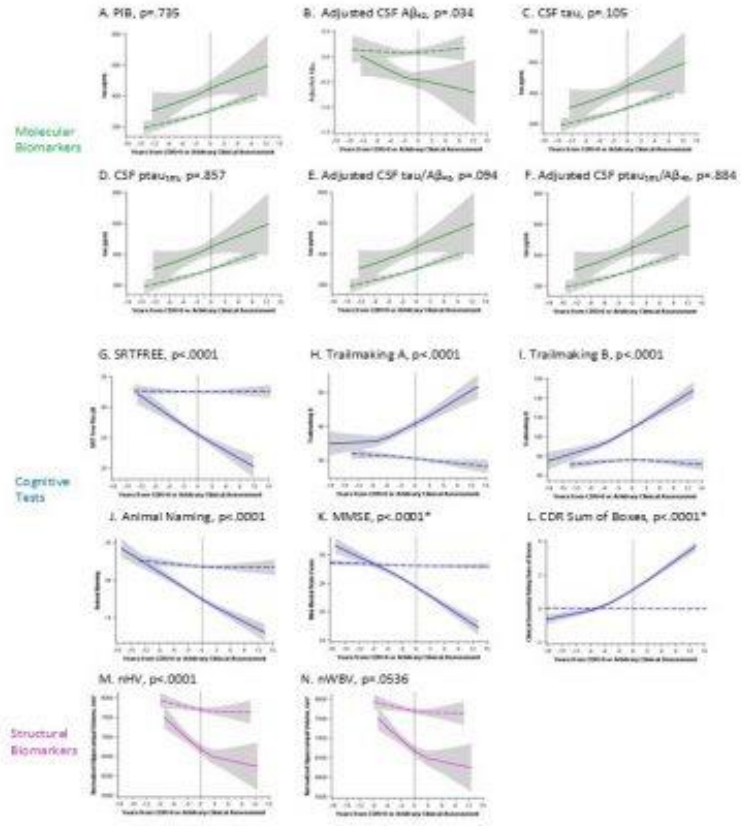

Figure 1.

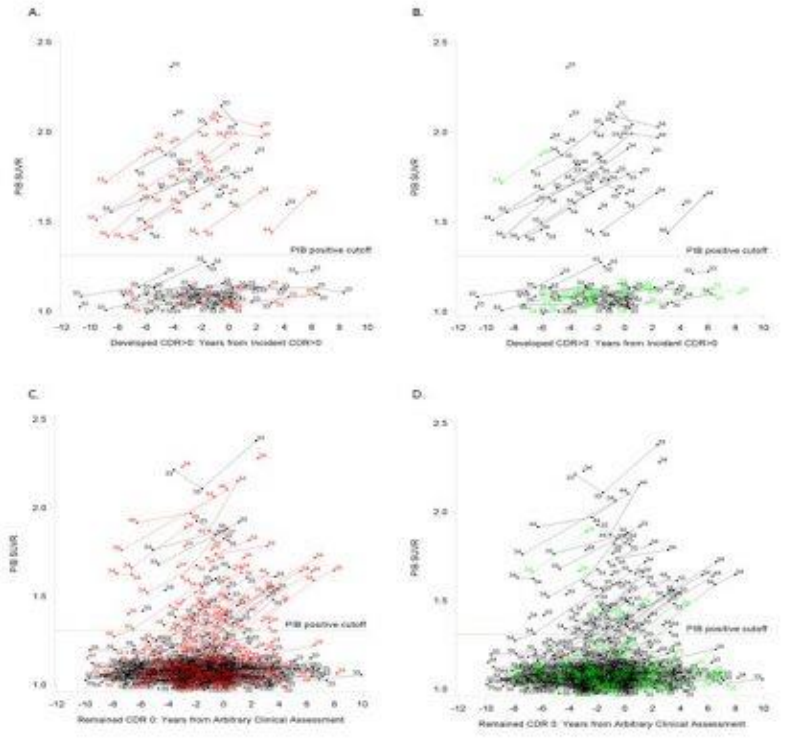

Figure 2.

Keywords: Alzheimer's disease, amyloid PET, APOE4, structural imaging, biomarkers

Multiple brain markers contribute to risk of progression on the Clinical Dementia Rating Scale in clinically normal older adults

Taylor Neal[1], Jennifer Rabin[1,2], Aaron Schultz[1,2], Keith Johnson[1,2,3], Reisa Sperling[1,2,3], Trey Hedden[1,2]

[1]*Massachusetts General Hospital, Boston, MA, US*
[2]*Harvard Medical School, Boston, MA, US*
[3]*Brigham and Women's Hospital, Boston, MA, US*

How do brain markers associated with age-related changes in cognition influence the rate at which cognitively normal individuals (Clinical Dementia Rating=0) progress to mild functional impairment as indicated by a CDR of 0.5? Prior findings indicate that individuals with high amyloid burden and either low hippocampal volume or poor memory function progress at the fastest rate (Rowe et al, 2014). Here, we simultaneously examined multiple brain markers and cognitive domains as predictors of progression.

Methods: Participants included 254 clinically normal older adults (M=73.5 years old) from the Harvard Aging Brain Study with at least one follow-up neuropsychological assessment and all imaging measures at baseline. Participants were assessed at baseline on magnetic resonance imaging markers of gray matter thickness and volume, white matter lesions (WML), fractional anisotropy (FA), and resting state functional connectivity; positron emission tomography markers of glucose metabolism (FDG) and amyloid burden (PiB); cognitive factor scores of episodic memory, executive function, and processing speed performance, and change over time in these cognitive scores. Cox regression models were used to assess the time to progression to CDR of 0.5 as predicted by baseline brain markers and cognition. All models included covariates for age, sex and education.

Results: Sixty-three participants (24.8%) progressed to CDR=0.5 over an average follow-up of 3.75 years (range: 1-6). Low hippocampal volume, decreased functional connectivity of the default and salience networks, high amyloid burden, and lower baseline memory performance all significantly contributed to the rate of progression while controlling for contributions of other biomarkers, cognitive measures, and covariates.

Conclusions: Consistent with prior findings, amyloid burden and hippocampal volume influenced progression to a CDR global score of 0.5. Resting state functional connectivity of the default and salience networks additionally influenced progression. These brain markers independently influenced progression beyond the predictive value of baseline or change in cognitive performance.

Keywords: clinical progression, MRI, amyloid, connectivity, memory

Low levels of brain beta-amyloid predict tau deposition and memory decline in aging

Stephanie Leal[1], Samuel Lockhart[1,2], Anne Maass[1,3], Rachel Bell[1], William Jagust[1,4]

[1]*Helen Wills Neuroscience Institute, University of California, Berkeley, Berkeley, CA, US*
[2]*Department of Internal Medicine, Division of Gerontology and Geriatric Medicine, Wake Forest School of Medicine, Winston-Salem, NC, US*
[3]*German Center for Neurodegenerative Diseases, Magdeburg, Germany*
[4]*Molecular Biophysics and Integrated Bioimaging, Lawrence Berkeley National Laboratory, Berkeley, CA, US*

Current approaches to the early detection of Alzheimer's disease (AD) rely upon classifying individuals as "positive" or "negative" for biomarkers related to the core pathology of beta-amyloid (Aβ). However, the accumulation of Aβ begins slowly, years before biomarkers become abnormal. The goal of this study was to investigate the relationships between the earliest stages of Aβ deposition, tau aggregation, and memory decline in cognitively normal older adults with low and nominally negative measurements of brain Aβ. We measured Aβ longitudinally (average follow-up time 4.5 years) with [^{11}C] Pittsburgh Compound B (PIB) PET imaging in a sample of older adults (N = 71, mean age 75 years), while tau was measured in a subset with [^{18}F] AV-1451 PET imaging at the end of the observation period. Cognitive testing was also conducted longitudinally. First, we found evidence for an inverted-U relationship between baseline Aβ and Aβ slope in asymptomatic older adults, suggesting a slowing of Aβ accumulation even in cognitively normal individuals. Second, we found evidence that Aβ measures predict subsequent tau deposition in cortical Braak regions associated with AD even in those who are Aβ- (Figure 1). Finally, we found that memory decline begins as baseline levels of Aβ increase, suggesting a late stage of preclinical disease. These findings strongly support the necessity of early intervention with amyloid lowering therapies even in those who are amyloid negative.

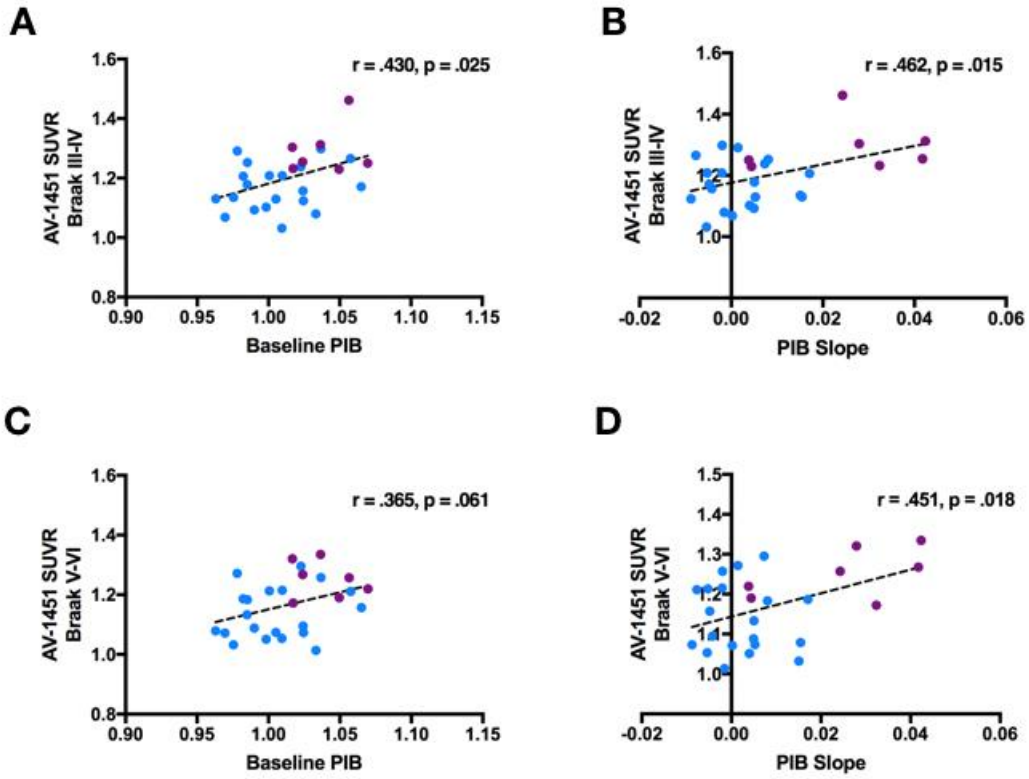

Figure 1. Relationship between PIB measures and AV-1451 uptake in cortical Braak ROIs in PIB- individuals. Participants (N = 27) were identified as PIB- (blue) and PIB+ converters (purple) based on a standard threshold of 1.07 PIB DVR. A) Correlation between baseline PIB and AV-1451 uptake in Braak III-IV in PIB- participants, B) Correlation between PIB slope and AV-1451 uptake in Braak III-IV in PIB- participants, C) Correlation between baseline PIB and AV-1451 uptake in Braak V-VI in PIB- participants, D) Correlation between PIB slope and AV-1451 uptake in Braak V-VI in PIB- participants.

Keywords: preclinical, tau, amyloid, longitudinal, memory

Friday, January 19, 2018 - 04:15 pm - 05:00 pm

Poster Session 3B

See page 275.

Friday, January 19, 2018 - 05:00 pm - 06:05 pm

Podium Session

Session 10: AD—Vascular Interactions

CHAIRS: Tammie Benzinger, Sylvia Villeneuve

Friday, January 19, 2018		
05:00 - 06:05	**Session 10: AD—VASCULAR INTERACTIONS**	CHAIRS: Tammie Benzinger | Sylvia Villeneuve
05:00	Amyloid deposition, small-vessel disease accrual and neurodegeneration, and progression to Mild Cognitive Impairment (MCI) in cognitively normal older adults	**Nadkarni** | Tudorascu | Snitz | Cohen | Lopez | Halligan | Campbell | Aizenstein | Klunk
05:15	The association of mid- and late-life systemic inflammation with brain amyloid deposition: atherosclerosis risk in communities-PET Study	**Walker** | Windham | Brown | Knopman | Jack | Mosley | Selvin | Wong | Hughes | Zhou | Gross | Gottesman
05:30	β-amyloid burden and vascular risk interact to predict neocortical tau PET signal in clinically normal older individuals	**Rabin** | Yang | Schultz | Hanseeuw | Hedden | Marshall | Kilpatrick | Klein | Buckley | Properzi | Rao | Papp | Kirn | Rentz | Johnson | Sperling | Chhatwal
05:45	Discussion	

Amyloid deposition, small-vessel disease accrual and neurodegeneration, and progression to Mild Cognitive Impairment (MCI) in cognitively normal older adults

Neelesh Nadkarni[1,2], Dana Tudorascu[1,2], Beth Snitz[1,2], Annie Cohen[1,2], Oscar Lopez[1,2], Edye Halligan[1], Elizabeth Campbell[1], Howard Aizenstein[1,2], William Klunk[1,2]

[1]*University of Pittsburgh, Pittsburgh, PA, US*
[2]*Pittsburgh Alzheimer's Disease Research Center, Pittsburgh, PA, US*

Background: Neuroimaging indices of amyloid deposition (**A**), small-vessel disease accrual (**V**) and neurodegeneration (**N**) are associated with AD in cross-sectional independent mixed samples; however, their association with the development of MCI in longitudinal samples of cognitively normal older adults (CN) remains unclear.

Aim: To determine the association between baseline and longitudinal **A**, **V** and **N** biomarker positivity and MCI outcomes in CN.

Methods: In 99 CN, 75 of whom had two or more assessments over 10 years, we adjudicated MCI outcomes using clinical assessments. Participants underwent PiB-PET to assess **A**, MRI to assess **V** and, FDG-PET to assess **N** at baseline and follow-up. Using established cutoffs, we designated individuals as having high or low amyloid ($\mathbf{A}^+/\mathbf{A}^-$) on PiB-PET, greater or lower white matter hyperintensities burden ($\mathbf{V}^+/\mathbf{V}^-$) on FLAIR and, diminished or undiminished cortical metabolism on FDG-PET ($\mathbf{N}^+/\mathbf{N}^-$). We examined the association between $\mathbf{A}^+/\mathbf{A}^-$, $\mathbf{V}^+/\mathbf{V}^-$ and $\mathbf{N}^+/\mathbf{N}^-$ at baseline and, an "ever positive" scan on follow-up, with MCI outcomes using Cox proportional hazards and Kaplan Meier analyses adjusted for age and APOE-e4 carrier status.

Results: Sample characteristics are summarized in Table 1. At baseline, an $\mathbf{A}^+$, $\mathbf{V}^+$ or $\mathbf{N}^+$ scan was not associated with progression to MCI in univariate or multivariate models. However, an $\mathbf{A}^+$ scan (HR=2.3, p=0.05), not a $\mathbf{V}^+$ (p=0.8) or $\mathbf{N}^+$ (p=0.4) scan, over the study period was associated with development of MCI in univariate but not in multivariate models. Amongst the **A, V** and **N** groups, the ever-$\mathbf{A}^+$ group had a higher probability of progression to MCI over the study period compared to the never-$\mathbf{A}^+$ group (Figure 1).

Conclusion: A subthreshold level of amyloid accumulation at any single time-point can pose a challenge in predicting progression to MCI as compared to an $\mathbf{A}^+$ PiB-PET scan determined longitudinally. The relationship of disease non-specific biomarkers (**V** and **N**) with MCI progression remains unclear.

Table 1: Participant characteristics

	N=99
Age (mean, range)	73.6 years (65-90 years)
Gender (female, N, %)	64 (65%)
Education (mean)	15 years
Race (White)	83%
APOE-e4 carrier status (%)	21.3%
Imaging follow-up (mean, range)	3.5 years (1-10 years)
Clinical follow-up (mean, range)	4.3 years (1-10 years)
MMSE score (mean, SD)	28.6 (1.5)

Figure 1: Relationship between an 'ever-' vs a 'never-' positive amyloid (A^+), small-vessel disease (V^+) and neurodegeneration (N^+) scan, and progression to MCI over the study period.

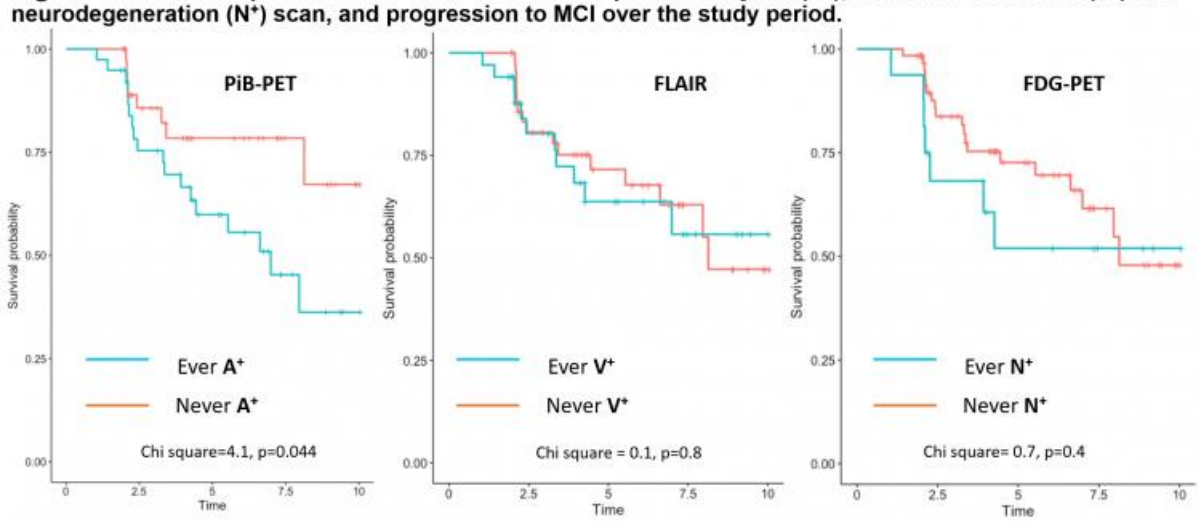

Keywords: PiB-PET, FDG-PET, WMH, Cognitively normal, MCI

The association of mid- and late-life systemic inflammation with brain amyloid deposition: atherosclerosis risk in communities-PET Study

Keenan Walker[1], B. Gwen Windham[2], Charles Brown[3], David Knopman[4], Clifford Jack[5], Thomas Mosley[6], Elizabeth Selvin[7], Dean Wong[8], Timothy Hughes[9], Yun Zhou[10], Alden Gross[7], Rebecca Gottesman[1,7]

[1]Department of Neurology, Johns Hopkins University, Baltimore, MD, US
[2]Department of Medicine, Division of Geriatrics, University of Mississippi Medical Center, Jackson, MS, US
[3]Department of Anesthesiology and Critical Care Medicine, Johns Hopkins University, Baltimore, MD, US
[4]Department of Neurology, Mayo Clinic, Rochester, MN, US
[5]Department of Radiology, Mayo Clinic, Rochester, MN, US
[6]Departments of Neurology and Geriatrics/Gerontology, University of Mississippi Medical Center, Jackson, MS, US
[7]Department of Epidemiology, Johns Hopkins Bloomberg School of Public Health, Baltimore, MD, US
[8]Departments Radiology and Neuroscience, Johns Hopkins University School of Medicine, Baltimore, MD, US
[9]Department of Internal Medicine, Section on Gerontology and Geriatric Medicine, Wake Forest School of Medicine, Winston-Salem, NC, US
[10]Department of Radiology, Section of High Resolution Brain PET Imaging, Johns Hopkins University School of Medicine, Baltimore, MD, US

Introduction: Although inflammation has been implicated in the pathogenesis of Alzheimer's disease, the effects of systemic inflammation on human brain amyloid deposition remain unclear. We examined the association of midlife and late-life systemic inflammation with late-life brain amyloid levels in a community sample of non-demented older adults from the Atherosclerosis Risk in Communities (ARIC) – PET Study.

Methods: Non-demented older adults were recruited from the ARIC study to undergo florbetapir PET (amyloid) imaging. Blood levels of high sensitivity C-reactive protein (CRP), a non-specific marker of systemic inflammation, were measured 22 years (Visit 2) and 16 years (Visit 4) before, and concurrent with PET imaging (Visit 5). The primary outcome was elevated (>1.2) global cortex standardized uptake value ratio.

Results: We included 339 older adults (age: 75[SD 5]; 56% female; 42% African American). In the full sample, Visit 2 CRP was not associated with brain amyloid after adjusting for demographic and vascular risk factors using multivariable logistic regression. However, a higher Visit 2 CRP was associated with increased odds of brain amyloid among white participants in race-stratified analyses (OR 1.32, 95% CI: 1.01, 1.72; figure 1). In sex-stratified analyses, higher Visit 2 CRP was associated with increased odds of elevated brain amyloid among male participants (OR 1.78, 95% CI: 1.20, 2.64; figure 2). Sex and race interaction terms were statistically significant ($p < .05$). Higher CRP at Visits 4 and 5 was not associated with elevated brain amyloid. Among male participants, those who had high CRP levels (≥3 mg/L) at all three visits were most likely to have elevated brain amyloid (OR, 7.69; 95% CI: 1.44, 41.00).

Discussion: Systemic inflammation during midlife and chronic systemic inflammation may each be associated with brain amyloid deposition in a subset of the population. However, findings based on subgroup analyses should be interpreted with caution.

Figure 1

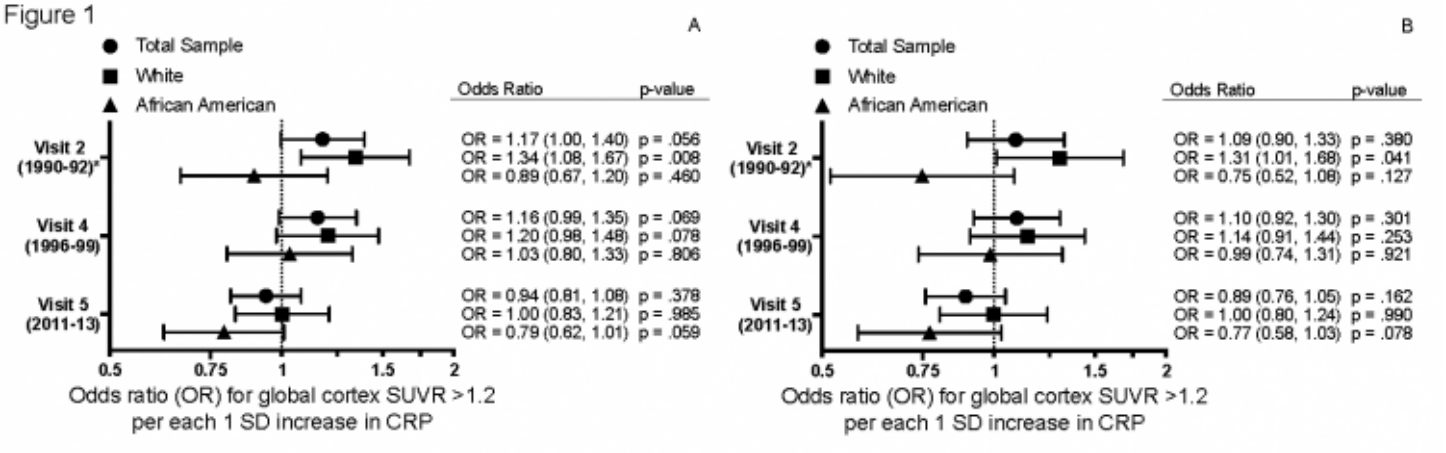

Figure 2

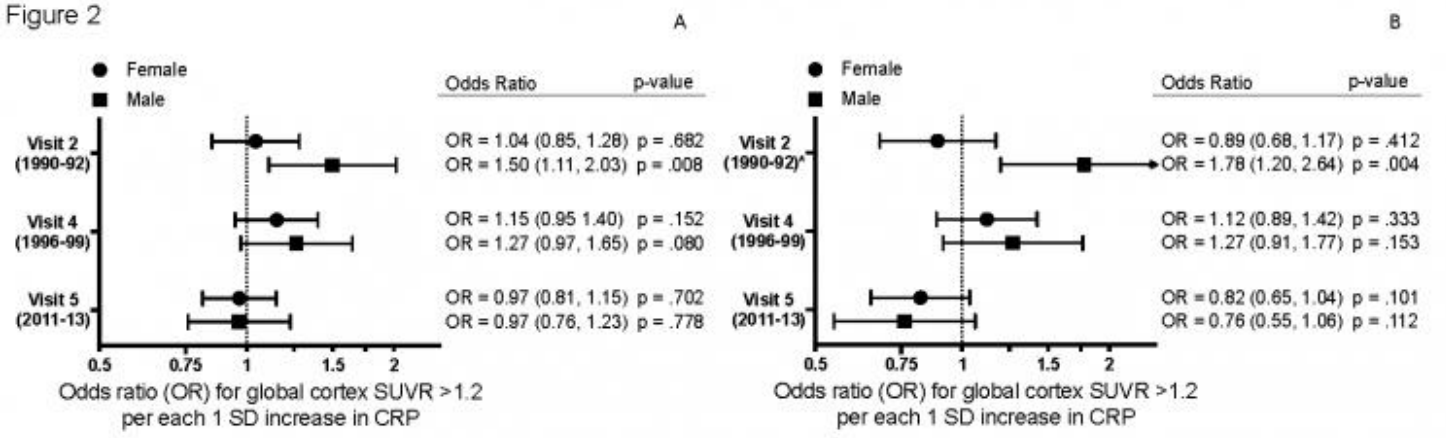

Keywords: Amyloid, Inflammation, Alzheimer's disease, C-reactive protein, Immune

β-amyloid burden and vascular risk interact to predict neocortical tau PET signal in clinically normal older individuals

Jennifer Rabin[1], Hyun-Sik Yang[1,2], Aaron Schultz[1], Bernard Hanseeuw[1], Trey Hedden[1], Gad Marshall[1,2], Emily Kilpatrick[1], Hannah Klein[1], Rachel Buckley[1,3,4], Michael Properzi[1], Vaishnavi Rao[1], Kathryn Papp[1,2], Dylan Kirn[1,2], Dorene Rentz[1,2], Keith Johnson[1,2], Reisa Sperling[1,2], Jasmeer Chhatwal[1]

[1]*Massachusetts General Hospital, Boston, MA, US*
[2]*Brigham and Women's Hospital, Boston, MA, US*
[3]*Florey Institutes of Neuroscience and Mental Health, Melbourne, Australia*
[4]*Melbourne School of Psychological Science, University of Melbourne, Melbourne, Australia*

We recently demonstrated a synergism between amyloid burden and vascular risk, whereby the combination of high vascular risk and elevated amyloid predicted steeper rates of cognitive decline in elderly participants in the Harvard Aging Brain Study (HABS; Rabin et al., under review). Given the close linkage of tau pathology to cognitive decline, we examined whether higher levels of vascular risk are associated with higher PET measures of tau pathology.

Objective: To examine whether a well-validated measure of systemic vascular risk predicts regional tau PET signal, alone or in combination with amyloid burden. Two ROIs were chosen: (1) entorhinal cortex (ENT), an early site of age-related tau deposition; and (2) inferior temporal cortex (ITC), an early site of Alzheimer's disease-related tau deposition.

Methods: 152 clinically normal older adults from HABS (mean age of 73.6±6.2 years) underwent amyloid (^{11}C Pittsburgh Compound B) and tau (^{18}F Flortaucipir) PET. Vascular risk was quantified via the Framingham Heart Study cardiovascular disease risk algorithm (FHS-CVD). Amyloid imaging and FHS-CVD were performed at baseline; tau PET was acquired 3.0 (*SD*±1.1) years later. Amyloid and FHS-CVD were examined as independent and interactive predictors of tau PET in separate linear regression models, controlling for age, sex, APOE e4 status, and interval between baseline and tau PET.

Results: There was no relationship between FHS-CVD and amyloid ($p=0.37$). Higher FHS-CVD was associated with higher tau PET signal in ITC ($p=0.009$), but not ENT ($p=0.22$). Higher amyloid was associated with elevated ENT and ITC tau PET signal (all $p<0.001$). In separate models, amyloid and FHS-CVD significantly interacted to predict tau PET signal in ITC ($p=0.004$), but not ENT ($p=0.44$; Figures 1, 2).

Conclusions: Higher amyloid and FHS-CVD may synergistically promote neocortical tau deposition, representing a possible mechanism to account for the accelerated cognitive decline observed in individuals with both elevated amyloid and high vascular risk.

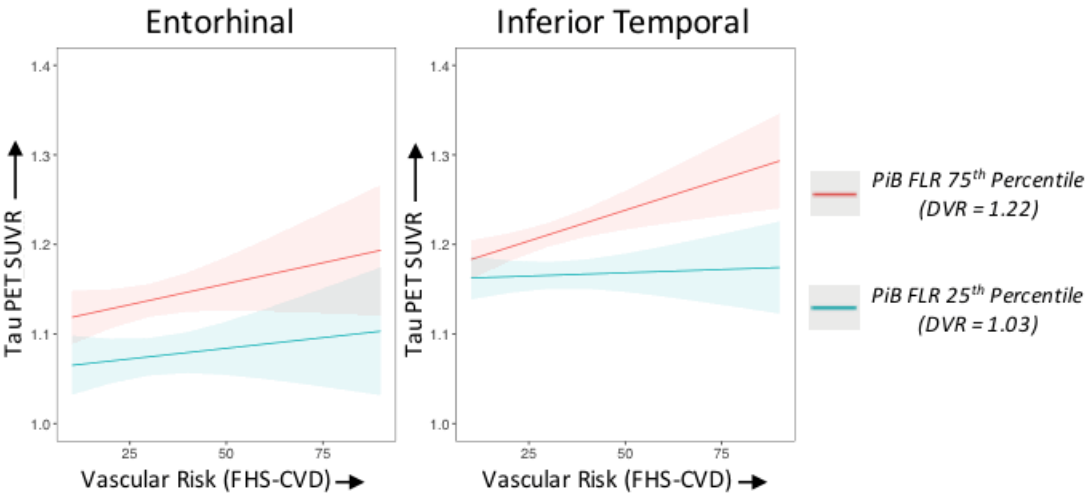

Figure 1. The interaction between FHS-CVD and amyloid burden in relation to tau PET signal. The interaction is significantly associated with tau PET signal in inferior temporal cortex, p = 0.004 (right), but not in entorhinal cortex, p = 0.44 (left). FHS-CVD = Framingham Heart Study General cardiovascular disease risk score.

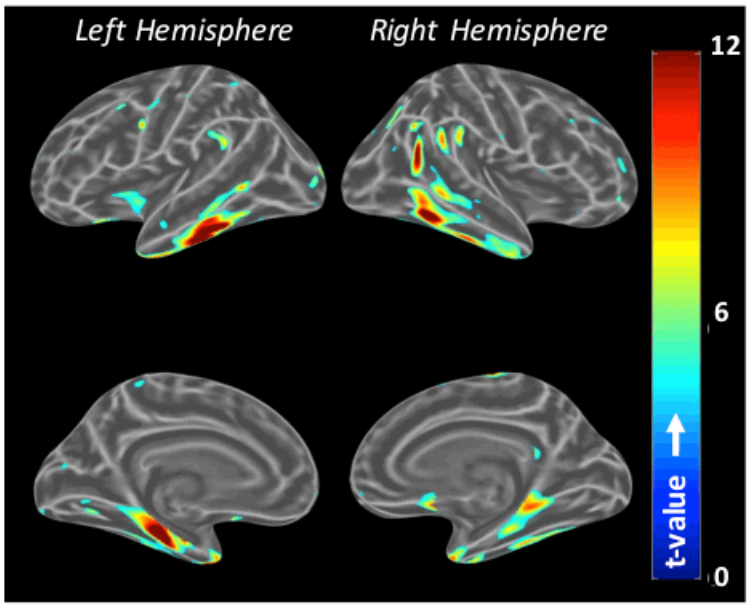

Figure 2. Whole brain voxel-wise map of tau PET signal demonstrating the interaction between amyloid burden and FHS-CVD, adjusted for age and sex. Maps are presented at $p < 0.05$, uncorrected. Color bar represents *t* values. FHS-CVD = Framingham Heart Study General cardiovascular disease risk score.

Keywords: Amyloid PET, tau PET, vascular risk, preclinical AD

Funding for this conference was made possible in part by grant R13 AG042201 from the National Institute on Aging.

The 12th Human Amyloid Imaging Conference is supported through educational grants and sponsorships from:

GOLD

Biogen

Lilly

For further information concerning Lilly grant funding visit www.lillygrantoffice.com

Tau Consortium

Silver

MERCK

GE Healthcare

Janssen Pharmaceutical Companies of Johnson & Johnson

Pfizer

CERESEAU technologies

Piramal knowledge action care

Bronze

abbvie

BIOCLINICA SEE MORE CLEARLY

www.worldeventsforum.com/hai or mobile app: https://my.yapp.us/HAICONF